RIGA TECHNICAL UNIVERSITY

Artemijs Ščeglovs

INJICĒJAMO ANTIBAKTERIĀLO HIDROGELU IZSTRĀDE AUDU INŽENIERIJAI

Promocijas darbs

DEVELOPMENT OF INJECTABLE ANTIBACTERIAL HYDROGELS FOR TISSUE ENGINEERING

Doctoral Thesis

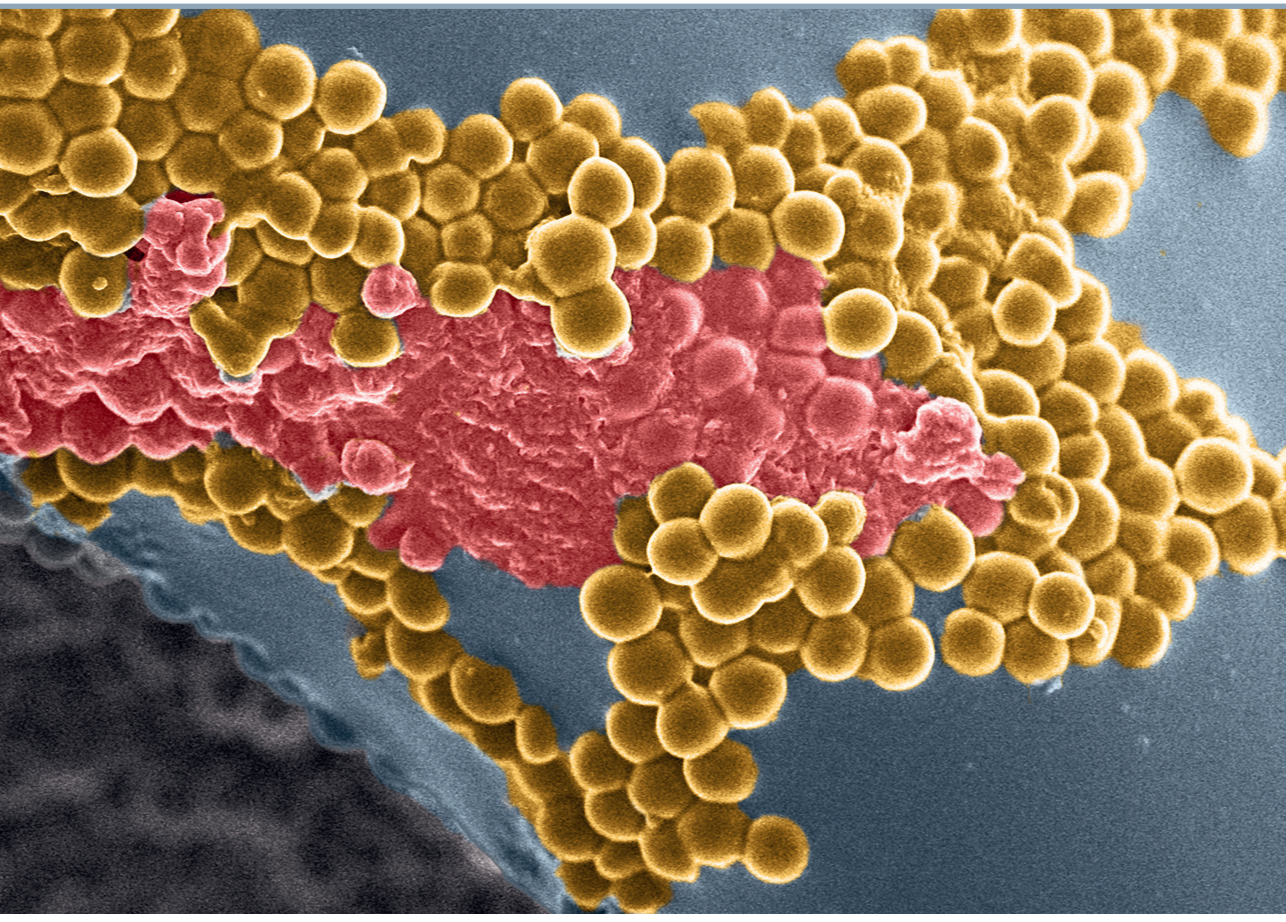

RTU Izdevniecība
RTU Press
Rīga 2026

RĪGAS TEHNISKĀ UNIVERSITĀTE

Dabaszinātņu un tehnoloģiju fakultāte

Biomateriālu un bioinženierijas institūts

RIGA TECHNICAL UNIVERSITY

Faculty of Natural Sciences and Technology

Institute of Biomaterials and Bioengineering

Artemijs Ščeglovs

Doktora studiju programmas "Ķīmija, materiālzinātne un tehnoloģijas" doktorants

Doctoral Student of the Study Programme "Chemistry, Material Science and Engineering"

INJICĒJAMU ANTIBAKTERIĀLU HIDROGELU IZSTRĀDE AUDU INŽENIERIJAI

Promocijas darbs

DEVELOPMENT OF INJECTABLE ANTIBACTERIAL HYDROGELS FOR TISSUE ENGINEERING

Doctoral Thesis

Zinātniskās vadītājas / Scientific supervisors

profesore / Professor *Dr. sc. ing.*

KRISTĪNE ŠALMA-ANCĀNE

profesore / Professor *Dr. med.*

JUTA KROIČA

RTU Izdevniecība / RTU Press

Rīga 2026 / Riga 2026

Ščeglovs, A. Injicējamo antibakteriālo hidrogelu izstrāde audu inženierijai. Promocijas darbs. Rīga: RTU Izdevniecība, 2026. 174 lpp.

Ščeglovs, A. Development of Injectable Antibacterial Hydrogels for Tissue Engineering. Summary of the Doctoral Thesis. Riga: RTU Press, 2026. 174 pages.

Publicēts saskaņā ar promocijas padomes "RTU P-02" 2025. gada 13. oktobra lēmumu, protokols Nr. 04030-9.2/8.

Published in accordance with the decision of the Promotion Council "P-02" of 13 October 2025, Minutes No. 04030-9.2/8.

Promocijas darba pētījumi izstrādāti, pateicoties Latvijas Zinātnes padomes pētniecības projektam Nr. lzp-2020/1-0072 "Injicējami bioaktīvi biokompozītmateriāli osteoporotisku kaulaudu reģenerācijai (*inBioBone*)" un Eiropas Savienības pētniecības un inovāciju programmai "Apvārsnis 2020", granta līgums Nr. 857287. Baltijas Biomateriālu ekselences centrs (*BBCE*). Promocijas darbu atbalstīja arī Eiropas Savienības pētniecības un inovāciju programma "Apvārsnis 2020", granta līgums Nr. 952347 (*RISEus2*), kā arī Konsolidācijas un pārvaldības izmaiņu ieviešana Rīgas Tehniskajā universitātē, LiepU, RTA, LJA un LJK virzībai uz izcilību augstākajā izglītībā, zinātnē un inovācijās C4835.Dok.1025 Projekta Nr. 5.2.1.1.i.0/2/24/I/CFLA/003.

The research conducted within the Doctoral Thesis has been supported by the Latvian Council of Science research project No. lzp-2020/1-0072 "Injectable Bioactive Biocomposites for Osteoporotic Bone Tissue Regeneration (inBioBone)" and European Union's Horizon 2020 research and innovation programme under grant agreement No. 857287, Baltic Biomaterials Centre of Excellence (BBCE). The Doctoral Thesis has also been supported by the European Union's Horizon 2020 research and innovation programme under grant agreement No. 952347 (RISEus2) and Ph.D. grant (C4835.Dok.1025) from the project No 5.2.1.1.i.0/2/24/I/CFLA/003 "Implementation of Consolidation and Management Changes at Riga Technical University, Liepaja University, Rezekne Academy of Technology, Latvian Maritime Academy and Liepaja Maritime College for the Progress towards Excellence in Higher Education, Science and Innovation" funded by the EU Recovery and Resilience Facility.

PATEICĪBAS

Liels paldies visai manai ģimenei un draugiem, kuru saraksts ir tik liels, ka bezgalība nestāv blakus, par atbalstu! Jūs vienmēr esat mana galvenā motivācija, laime un mīlestība, pozitīvo emociju avots un veids, kā uz mirkli aizmirst par visu, kas notiek apkārt! Pateicos arī par to, ka vienmēr esat blakus jebkuros dzīves momentos!

Paldies arī manam vecajam labajam kolektīvam – Sofjai, Karīnai, Elīzai, Kristīnei A., Kristīnei I., Andai, Signei, Janai, Līgai, Kristapam R., Agnesei, Lāsmai, Valentīnai un Vitai, kā arī jaunajam labajam kolektīvam – Annai R., Anastasijai T., Ilijanai, Terezai, Laumai, *Jingzhi*, *Oznur*, Viktoram par palīdzību darbā, idejām un sarunām, kad vajadzēja atpūsties no darba rutīnas!

Pateicos visiem, ar kuriem man bija iespēja strādāt/mācīties kopā un par ieguldījumu šī darba izstrādē un paveikto promocijas darba aizstāvēšanai – *Jacek K. Wychowaniec*, *Claudia Siverino*, *Marco Chitto*, Ingus Skadiņš, Inese Čakstiņa-Dzērve, Valdis Pirsko, *Matteo D'Este*, *Fintan T. Moriarty* un *Charlotte Edwards-Gayle*!

Pieredzējušie zinātnieki un mani mentori – profesors Jānis Ločs, profesore Dagnija Loča, asociētā profesore Arita Dubņika un mana promocijas darba vadītāja profesore Juta Kroiča – milzīgs paldies jums par ieteikumiem, par kopā pavadīto laiku, par spēju atrast momentu, kad uzslavēt un kad aizrādīt, kad palīdzēt un kad ļaut patstāvīgi tikt galā!

No visa sirds vēlētos pateikties manai darba vadītājai profesorei *Dr. sc. ing.* Kristīnei Šalmai-Ancānei par kopā pastrādāto un pārdzīvoto, kā arī par spēju tajā vai citā mērā apvienot visu to, kas iepriekš tika minēts!

ACKNOWLEDGEMENTS

Heartfelt thanks to my family members and friends – I am so fortunate to have you, and I am proud of this! Thanks for your motivation, happiness, and love; for being an endless source of positive emotions; for giving me a way to step away from everything around me; and for always being there!

Thanks to my old band colleagues – Sofja, Karina, Eliza, Kristine A., Kristine I., Anda, Signe, Jana, Liga, Kristaps R., Agnese P., Lasma, Valentina, and Vita –, and colleagues from the new band – Anna R., Anastasia T., Ilijana, Theresa, Lauma, Jingzhi, Oznur, and Viktors – for your help, ideas, the off-work conversations, and jokes!

My immense gratitude to the people I worked and studied with for their invaluable input in the Doctoral Thesis – Jacek K. Wychowaniec, Claudia Siverino, Marco Chitto, Ingus Skadiņš, Inese Čakstiņa-Dzērve, Valdis Pirsko, Matteo D'Este, Fintan T. Moriarty, and Charlotte Edwards-Gayle!

Experienced scientists and my mentors – Prof. Jānis Ločs, Prof. Dagnija Loča, Assist. Prof. Arita Dubnika – and my supervisor – Prof. Juta Kroiča – Huge thanks to you for your advice, the time we spent together, and your wisdom in knowing when to praise and when to scold, when to help and when to step back and let me manage on my own.

From the bottom of my heart, I would like to express gratitude to my supervisor Prof. Kristīne Šalma-Ancāne for the work we have done together and experience we have gained, as well as for your ability to combine all of the above!

"……*Where there is desire, there is gonna be a flame*
Where there is a flame, someone's bound to get burned
But just because it burns doesn't mean you're gonna die
You've gotta get up and try, try, try……"

(Alecia Beth Moore, also known as Pink)

PROMOCIJAS DARBS IZVIRZĪTS ZINĀTNES DOKTORA GRĀDA IEGUŠANAI RĪGAS TEHNISKAJĀ UNIVERSITĀTĒ

Promocijas darbs zinātnes doktora (*Ph. D.*) grāda iegūšanai tiek publiski aizstāvēts 2026. gada 20.februārī plkst. 11 Rīgas Tehniskās universitātes Dabaszinātņu un tehnoloģiju fakultātē, Paula Valdena ielā 3, 272. auditorijā.

OFICIĀLIE RECENZENTI

Tenūrprofesors *Dr. sc. ing.* Sergejs Gaidukovs,
Rīgas Tehniskā universitāte

MD Ph. D. nefrologs Kārlis Rācenis,
Rīgas Stradiņa universitāte, Latvija

Ph. D. Nihal Engin Vrana,
uzņēmums "*SPARTHA MEDICAL*", Francija

APSTIPRINĀJUMS

Apstiprinu, ka esmu izstrādājis šo promocijas darbu, kas iesniegts izskatīšanai Rīgas Tehniskajā universitātē zinātnes doktora (*Ph. D.*) grāda iegūšanai. Promocijas darbs zinātniskā grāda iegūšanai nav iesniegts nevienā citā universitātē.

Artemijs Ščeglovs (paraksts)
Datums: ……

Promocijas darbs sagatavots kā tematiski vienota zinātnisko publikāciju kopa. Tajā ir kopsavilkums latviešu un angļu valodā un piecas *SCI* publikācijas. Publikācijas uzrakstītas angļu valodā, to kopējais apjoms ir 174 lpp.

ANOTĀCIJA

Šajā promocijas darbā tika veikta jaunu ķīmiski šķērssaistītu hidrogelu sintēze uz divu dabiskas izcelsmes biopolimēru, antimikrobiālā polipeptīda – ε-polilizīna (ε-PL) – un bioloģiski aktīvas hialuronskābes (HA), bāzes un šo hidrogelu visaptverošs raksturojums. Šī pētījuma galvenais mērķis bija izstrādāt antibiotikas nesaturošus, dabiski antibakteriālus biomateriālus uz hidrogelu bāzes inficēto audu atjaunošanai un dzīšanai. Šis darbs tika sadalīts divos galvenajos posmos, kas ietvēra kovalenti šķērssaistītas hidrogela matricas sintēzi ar turpmāku fizikālķīmisko īpašību, tādu kā molekulārās struktūras, morfoloģijas, gela frakcijas, uzbriešanas pakāpes, reoloģisko īpašību raksturošanu un analīzi. Pirmajā posmā tika pētīta arī tvaika sterilizācijas ietekme uz izstrādāto hidrogelu fizikālķīmiskajām īpašībām. Turklāt tika novērtēta tīra antimikrobiālā polipeptīda ε-PL, kā arī sintezēto ε-PL/HA hidrogelu antibakteriālā aktivitāte un citotoksicitātes profils *in vitro*. Minimālās inhibējošās koncentrācijas (*MIC*), minimālās baktericīdās koncentrācijas (*MBC*) vērtības un rezistences veidošanās pētījumi tīram ε-polilizīnam (ε-PL), kā arī sintezēto hidrogelu antibakteriālā aktivitāte tika novērtēta gan īstermiņā (pēc 24 stundām), gan ilgtermiņā (līdz pat 168 stundām) pret plaši pazīstamiem gramnegatīviem un grampozitīviem patogēno baktēriju celmiem, tostarp *ATCC* references *Escherichia coli* un *Staphylococcus aureus (E. coli* un *S. aureus*), klīniski izolētām *Pseudomonas aeruginosa* (*P. aeruginosa)*, kā arī multirezistentām, grūti ārstējamām meticilīna rezistentām *S. aureus* (MRSA*)* un paplašināta spektra β-laktamāzes producējošo *E. coli (ESBL E. coli*) baktērijām. Citotoksicitātes profils tika novērtēts, izmantojot Balb/c 3T3 peļu fibroblastu (tiešais kontakta tests) un cilvēka ādas fibroblastu (netiešais/ekstrakta tests) šūnu līnijas. Otrajā posmā antibakteriālā ε-PL/HA hidrogela matrica tika funkcionalizēta ar bioaktīvām stroncija aizvietotām hidroksilapatīta (Sr-HAp) nanodaļiņām, lai izstrādātu antibakteriālus un bioaktīvos injicējamus hidrogelus kaulaudu reģenerācijai. Lai izvērtētu lietojumam specifisko veiktspēju, tika novērtētas fizikālķīmiskās un bioloģiskās īpašības, tostarp ilgstoša (līdz 168 h) antibakteriālā aktivitāte pret *E. coli*, *S. aureus*, MRSA un *ESBL E. coli* baktērijām.

Promocijas darbs ir izstrādāts kā zinātnisko rakstu kopa. Zinātnisko rakstu kopsavilkums uzrakstīts latviešu un angļu valodā. Tas ietver četras zinātniskās oriģinālpublikācijas un vienu apskatrakstu. Katrs kopsavilkums ietver 10 attēlus un vienu tabulu, tā apjoms – 46 lappuses.

IZMANTOTIE SAĪSINĀJUMI

3D	trīsdimensionāls
AMP	antimikrobiālie peptīdi
AMR	antimikrobiālā rezistence
ATCC	Amerikas Kultūru tipa kolekcija
Balb/c 3T3	fibroblastu šūnas, izolētas no BALB/c peļu embrijiem
BSA	liellopu seruma albumīns
CLSI	Klīnisko un laboratorijas standartu institūts
CaP	kalcija fosfāti
CDC	Slimību kontroles un profilakses centrs
CRAB	pret karbapenēmu rezistents *Acinetobacter baumannii*
CRPA	pret karbapenēmu rezistents *Pseudomonas aeruginosa*
E'/E"	saspiešanas krājuma/zuduma modulis
E. coli	*Escherichia coli*
ECM	ekstracelulāra matrice
EDC	1-etil-3-(3-dimetilamīnpropil) karbodiimīds
ε-PL	ε-polilizīns
EPS	eksopolisaharīdi
ESBL	paplašināta spektra β-laktamāzi producējošs baktēriju celms
ES *MDR*	Eiropas Savienības Medicīnisko ierīču regula
EU-CAST	Eiropas Antimikrobiālās jutības noteikšanas komiteja
FDA	ASV Pārtikas un zāļu pārvalde
FTIR	Furjē transformācijas infrasarkanā spektroskopija
G'/G"	krājuma/zuduma modulis
GAG	glikozaminoglikāni
GEN	gentamicīns
HA	hialuronskābe
HAp	hidroksilapatīts
HCl	sālsskābe
HDF	cilvēka ādas fibroblasti
in vitro	eksperimentāli pētījumi ārpus dzīvā organisma
LVR	lineārais viskoelastības reģions
M. tuberculosis	*Mycobacterium tuberculosis*
MBC	minimālā baktericīdā koncentrācija
MIC	minimālā inhibējošā koncentrācija

MRSA	pret meticilīnu rezistents *Staphylococcus aureus*.
NaCl	nātrija hlorīds
NaOH	nātrija hidroksīds
NDB	dabiskas izcelsmes biopolimērs
aNDB	antibakteriāls dabiskas izcelsmes biopolimērs
NHS	N-hidroksisukcinimīds
P. aeruginosa	*Pseudomonas aeruginosa*
PRSP	pret penicilīnu rezistents *Streptococcus pneumoniae*
PVA	polivinilspirts
RGD	arginīna-glicīna-asparagīnskābe
S. aureus	*Staphylococcus aureus*
S. epidermidis	*Staphylococcus epidermidis*
SAXS	mazo leņķu rentgenstaru izkliedēšanas analīze
SCI	recenzēti zinātniski žurnāli
SEM	skenējošā elektronu mikroskopija
Sr-HAp	stroncija aizvietots hidroksilapatīts
USD	Amerikas Savienoto Valstu dolārs
VAN	vankomicīns
VRE	pret vankomicīnu rezistenti *enterokoki*
PVO	Pasaules Veselības organizācija

SATURS

PROMOCIJAS DARBA VISPĀRĒJS RAKSTUROJUMS 9
Ievads un literatūras apskats 9
Mērķis un uzdevumi 12
Aizstāvēšanai izvirzītas tēzes 13
Zinātniskā novitāte 13
Praktiskā nozīme 14
Darba struktūra un apjoms 14
Publikācijas un promocijas darba aprobācija 14
PROMOCIJAS DARBA GALVENIE REZULTĀTI 18
Dabiskas izcelsmes biopolimēru (*NDB*) potenciāls kā alternatīva antibakteriāliem līdzekļiem audu inženierijas lietojumiem (1. publikācija) 18
Jaunas dabiski antibakteriālās ķīmiski šķērssaistītas hidrogela matricas izstrāde (2. publikācija) 19
Ķīmiski šķērssaistītu ε-PL/HA hidrogelu sintēzes metodes optimizācija, topoloģijas novērtēšana un tvaika sterilizācijas ietekme uz fizikālķīmiskajām un antibakteriālajām īpašībām (3. publikācija) 24
ε-PL/HA hidrogelu antibakteriālā potenciāla un citotoksicitātes novērtēšana *in vitro* (4. publikācija) 29
Antibakteriālu Sr-HAp funkcionalizētu ε-PL/HA hidrogelu sintēze un raksturošana (5. publikācija) 33
SECINĀJUMI 38
ATSAUCES 39
PIELIKUMI 90

1.Pielikums **A. Sceglovs**, I. Skadins, M. Chitto, J. Kroica, K. Salma-Ancane. Failure or future? Exploring alternative antibacterials: a comparative analysis of antibiotics and naturally-derived biopolymers, *Front. Microbiol.*, 2025, 16: 1526250. doi: 10.3389/fmicb.2025.1526250

2.Pielikums K. Salma-Ancane, **A. Sceglovs**, E. Tracuma, J. K. Wychowaniec, K. Aunina, A. Ramata-Stunda, V. Nikolajeva, D. Loca. Effect of crosslinking strategy on the biological, antibacterial and physicochemical performance of hyaluronic acid and ε-polylysine based hydrogels, *Int. J. Biol. Macromol.*, 2022, 208, 995–1008. https://doi.org/10.1016/J.IJBIOMAC.2022.03.207.

3.Pielikums **A. Sceglovs**, J.K. Wychowaniec, I. Skadins, A. Reinis, C.J.C. Edwards-Gayle, M. D'Este, K. Salma-Ancane, Effect of steam sterilisation on physico-chemical properties of antibacterial covalently cross-linked ε-polylysine/hyaluronic acid hydrogels, *Carbohydr. Polym. Technol. Appl.,* 2023, 6: 100363. https://doi.org/10.1016/J.CARPTA.2023.100363.

4.Pielikums **A. Sceglovs**, C. Siverino, I. Skadins, V. Pirsko, M. Sceglova, J. Kroica, F. T. Moriarty, K. Salma-Ancane. Injectable ε-polylysine/hyaluronic acid hydrogels with resistance-preventing antibacterial activity for treating wound infections, ACS Appl. Bio Mater., 2025, 8 (11), 9916–9930. https://doi.org/10.1021/acsabm.5c01252.

5.Pielikums A. Rubina, **A. Sceglovs**, A. Ramata-Stunda, I. Pugajeva, A. R. Boyd, A. Tumilovica, L. Stipniece and K. Salma-Ancane. Injectable mineralized Sr-hydroxyapatite nanoparticles-loaded ε-polylysine-hyaluronic acid composite hydrogels for bone regeneration, *Int. J. Biol. Macromol.,* 2024, 280: 135703. https://doi.org/10.1016/j.ijbiomac.2024.135703.

PROMOCIJAS DARBA VISPĀRĒJS RAKSTUROJUMS

Ievads un literatūras apskats

Saskaņā ar Pasaules Veselības organizācijas (PVO) datiem bakteriālas infekcijas izraisa 13,6 % no cilvēku mirstības, kas ir aptuveni katrs astotais nāves gadījums pasaulē [1]. Vienīgā stratēģija bakteriālo infekciju ārstēšanai un profilaksei veselības aprūpē joprojām ir antibiotikas, jo alternatīvas neantibiotiskas ārstēšanas iespējas ir ierobežotas, izņemot "pēdējās izvēles" baktēriofāgu terapiju. Šādi "pēdējās izvēles" apstākļi ir cieši saistīti ar baktēriju rezistences pret antibiotikām pieaugumu. PVO un Slimību kontroles un profilakses centrs (*CDC*) atzīst, ka antimikrobiālā rezistence (AMR) ir globāla krīze, ko veicina pret "pēdējās izvēles" antibiotikām rezistento patogēnu pieaugošā izplatība. Jau gadu desmitiem pieaug ar AMR saistīto patogēnu saraksts, kas ir izraisījuši simtiem tūkstošu nāves gadījumu. To vidū ir pret penicilīnu rezistentās *Streptococcus pneumoniae* (PRSP), pret karbapenēmiem rezistentās *Pseudomonas aeruginosa* un *Acinetobacter baumannii* (CRPA un CRAB), pret meticilīnu rezistentās *Staphylococcus aureus* (MRSA), pret vankomicīnu rezistentās *enterokoki* (VRE) un paplašināta spektra β-laktamāzes (ESBL) producējošas *Escherichia coli (E. coli)* baktērijas. Turklāt tiek lēsts, ka līdz 2050. gadam ar AMR saistīto nāves gadījumu skaits varētu pārsniegt 10 miljonus gadā. Lai cīnītos ar šo pieaugošo krīzi, PVO Globālajā rīcības plānā ir uzsvērta steidzama nepieciešamība izstrādāt alternatīvas antibiotikas nesaturošas stratēģijas [2].

Lai gan antibakteriālie dabiskas izcelsmes biopolimēri (*aNDB*) [3]–[5] jau sen tiek izmantoti biomedicīnā, to pētniecība pēdējā desmitgadē ir strauji attīstījusies. Atšķirībā no citiem biomedicīnā izmantotajiem biopolimēriem, kas var būt gan dabiskas (hialuronskābe, želatīns utt.), gan sintētiskas (polivinilspirts (*PVA*), polietilēnglikols (PEG) u. c.) izcelsmes, *aNDB* iegūst no dabiskiem avotiem (augiem, sēnēm, mikroorganismiem, aļģēm un dzīvniekiem), un tiem piemīt biosaderība un dabiska antibakteriāla aktivitāte bez papildu ķīmiskās modifikācijas [4]. Interese par *aNDB* kā antibakteriāliem līdzekļiem biomateriālu izstrādē ir strauji pieaugusi, un kopš 2015. gada publikāciju skaits par to izmantošanu ir palielinājies par gandrīz 400 %. Šo pieaugošo tendenci galvenokārt nosaka *aNDB* atzīšana par daudzsološām antibakteriālām molekulām lokālas piegādes lietojumiem, kas piedāvā gan biosaderību, gan antibakteriālo iedarbību pret patogēnajām baktērijām. Turklāt tiek uzsvērts, ka baktēriju spēja attīstīt rezistenci pret šādām vielām ir ievērojami mazāka, jo aNDB antibakteriālās aktivitātes mehānisms un mērķa specifiskums būtiski atšķiras no tradicionālajām antibiotikām [4]. Vairāki pētījumi apliecina, ka ir izstrādāti dažādi biomateriāli

ar ievērojamu antibakteriālo aktivitāti, kuru pamatā ir dabīgas izcelsmes antibakteriālie biopolimēri (aNDB), tostarp zāļu piegādes sistēmas, oftalmoloģiskās kontaktlēcas, injicējami kaulu cementi, medicīnisko ierīču un implantu pārklājumi, mikrošķiedru plāksteri, brūču pārsēji, nanodaļiņas, nanošķiedras un hidrogeli [2], [6]–[8]. Šādi *aNDB* ir hitozāns, κ-karaginānss, algināts, pektīns, o-pullulāns, fukoidāns, hondroitīna sulfāts, baktēriju ražotie eksopolisaharīdi, kā arī antimikrobiālie peptīdi (AMP) [2], [6]–[12].

Hidrogeli ir kļuvuši par daudzsološu biomateriālu klasi biomedicīnā, pateicoties to augstajai biosaderībai, pielāgojamām mehāniskajām īpašībām un spējai imitēt cilvēka audu ekstracelulāro matricu (ECM). Šīs īpašības padara hidrogelus īpaši piemērotus audu inženierijā un reģeneratīvajā medicīnā, jo tie spēj atbalstīt šūnu adhēziju, proliferāciju un diferencēšanu, tādējādi veicinot audu reģenerāciju. Pēdējās desmitgades laikā pētījumi arvien vairāk koncentrējas uz hidrogelu izstrādi ar antibakteriālo funkcionalitāti, lai risinātu kritisko klīnisko problēmu, kas saistīta ar inficētu audu atjaunošanu un dzīšanu. Viena no visefektīvākajām stratēģijām ietver antibakteriālu hidrogelu izstrādi uz *aNDB* bāzes. Šiem dabiski antibakteriālajiem hidrogeliem piemīt vairākas priekšrocības, tostarp pārmērīgas antibakteriālo līdzekļu vai antibiotiku lietošanas riska mazināšana, vienkāršots sastāvs, augsta biosaderība un ilgstoša antibakteriālā efektivitāte [13]. Papildus audu infekciju kontrolei tiek pētītas arī hidrogelu lietošanas iespējas kaulaudu reģenerācijā. Kaulu defekti un lūzumi, ko izraisa tādas slimības kā osteoporoze, osteosarkoma un smagu traumu izraisīti kaulu lūzumi, ir nozīmīgs globāls slogs veselībai, kas skar vairāk nekā 200 miljonus cilvēku visā pasaulē un rada ekonomiskas izmaksas, kas pārsniedz 100 miljonus ASV dolāru gadā [14], [15]. Šos stāvokļus bieži vien sarežģī paaugstināts infekcijas risks, īpaši atvērtu lūzumu, ķirurģisku iejaukšanos un imūnsupresētu pacientu gadījumos. Posttraumatiskais osteomielīts, periprostētisko locītavu infekcijas un ar implantiem saistītās infekcijas joprojām ir būtiskas klīniskās problēmas, kas bieži izraisa aizkavētu kaulu dzīšanu, implantu atgrūšanu un pat letālu iznākumu. Tāpēc daudzfunkcionālu, uz kaulaudiem vērstu antibakteriālu biomateriālu ar reģeneratīvu potenciālu izstrāde ir kļuvusi par vienu no vadošajiem pētniecības virzieniem ar mērķi uzlabot ārstēšanas efektivitāti un novērst ar infekcijām saistītās komplikācijas kaulu dzīšanas un reģenerācijas procesā.

Daudzsološa pieeja šajā jomā ir hidrogela matricas biofunkcionalizēšana ar bioaktīvām un osteogēnām neorganiskām sastāvdaļām, piemēram, kalcija fosfāta (CaP) savienojumiem. CaP biomateriāli, piemēram, hidroksilapatīts (HAp), uzrāda augstu biosaderību un bioaktivitāti fizioloģiskos apstākļos, jo tie strukturāli un ķīmiski līdzinās kaula ECM galvenajai minerālajai sastāvdaļai [16], [17]. Šī strukturālā līdzība ļauj šiem biomateriāliem veidot ciešas funkcionālas saites ar kaulaudiem, tādējādi veicinot osteointegrāciju un kaulaudu remodelēšanos. Tomēr, neskatoties uz šīm priekšrocībām, CaP biomateriāliem raksturīgi vairāki ierobežojumi, tādi kā zema mehāniskā izturība, nenoteikts biodegradācijas ātrums un nepietiekama strukturālā integritāte. Turklāt komerciāli pieejamie kaulu biomateriāli joprojām nespēj pilnībā atdarināt dabisko kaulaudu hierarhisko kompozītstruktūru, kas savukārt būtiski ierobežo to reģeneratīvo potenciālu kaulaudu defektu un lūzumu ārstēšanā [18]. Hidrogela matricas funkcionalizēšana ar CaP ļauj izstrādāt kompozīthidrogelus ar uzlabotām funkcionālajām īpašībām, tostarp paaugstinātu biosaderību un bioloģisko aktivitāti, uzlabotu strukturālo integritāti, optimizētu porainību, regulējamu mehānisko stingrību un bioloģiskās noārdīšanās ātrumu. Šīs īpašības padara ar CaP-funkcionalizētus hidrogelus par daudzsološiem biomateriāliem kaulaudu reģenerācijai, nodrošinot bioaktīvu un mehāniski atbalstošu vidi šūnu augšanai un audu

integrācijai [17]. Pašreizējais klīniskais "zelta standarts" inficēto kaulaudu ārstēšanā ietver sistēmisku vai lokālu antibiotiku lietošanu, kā arī atsevišķu ķirurģisku iejaukšanos, lai implantētu kaula biomateriālu kaulaudu atjaunošanai [19]. Vietējai antibiotiku piegādei bieži tiek izmantotas sintētiskā poli(metilmetakrilāta) (PMMA) kaulu cementa lodītes un starplikas, kas ļauj lokāli piegādāt augstu antibiotiku koncentrāciju, piemēram, vankomicīnu (VAN) vai gentamicīnu (GENTA) [20]. Tomēr PMMA biomateriāliem kā bioinertiem un bioloģiski nenoārdāmiem antibiotiku nesējiem ir būtiski trūkumi, tostarp slikta zāļu izdalīšanās kinētika [20], kas var veicināt rezistences attīstību pret antibiotikām, patogēnu kolonizāciju un biofilmu veidošanos, kā arī izraisīt toksicitāti un nepieciešamību pēc papildu ķirurģiskas operācijas biomateriāla izņemšanai. Viena soļa pieeju demonstrē bioaktīvie GENTA vai VAN saturošie hidroksilapatīta (HAp)/kalcija sulfāta biomateriāli, kas ir jauni komerciāli pieejami injicējami sintētiskie kaulu implanti *CERAMENT® G* un *CERAMENT® V (BONESUPPORT*, Zviedrija). Šiem komerciālajiem produktiem ir būtiska priekšrocība, jo tie vienlaikus nodrošina lokālu antibiotiku terapiju un veicina jaunu kaulaudu veidošanos [21]. Tomēr hroniska osteomielīta ārstēšanas laikā ir ziņots par lokālām brūču komplikācijām, noturīgām infekcijām un noturīgu bioplēves klātbūtni. Tāpēc dabiskas izcelsmes, ar CaP uzlādēti, dabiski antibakteriāli kompozīthidrogeli ir ārkārtīgi nozīmīgs pētniecības virziens, kas var piedāvāt potenciālu risinājumu divām izplatītām veselības aprūpes problēmām – bakteriālām infekcijām un kaulu slimībām. Lai risinātu AMR krīzi, kā arī uzlabotu bakteriālu infekciju ārstēšanu un kaulu rekonstrukcijas efektivitāti, šajā promocijas darbā ir izstrādāti un pētīti antibakteriāli hidrogeli, uz antimikrobiāla polipeptīda ε-polilizīns (ε-PL) un bioloģiski aktīvās hialuronskābes (HA) bāzes, kā arī ε-PL/HA kompozīthidrogeli. ε-PL/HA kompozīthidrogeli ir izstrādāti, funkcionalizējot antibakteriālo hidrogela matricu ar bioaktīvām Sr-HAp nanodaļiņām. Šīs pieejas mērķis bija piešķirt specializētas funkcionālās īpašības, piemēram, veicināt mezenhimālo cilmes šūnu diferenciāciju, ietekmēt ECM proteīnu adsorbciju, kā arī uzlabot šūnu adhēziju un audu veidošanos, vienlaikus imitējot dabisko kaulaudu nanostruktūru un sastāvu, lai uzlabotu kaulaudu reģenerācijas spēju.

Pirmkārt, svarīgākie parametri antibakteriālo hidrogelu izstrādē ir piemērotu komponentu izvēle un piemērota šķērssaistīšanas stratēģija. Šajā pētījumā tika izvēlētas ε-PL un HA, pamatojoties uz šo komponentu izcilām funkcionālajām īpašībām, vienlaikus nodrošinot antibakteriālo aktivitāti un spēju imitēt dabisko ECM. HA ir nozīmīgs vairāku audu ECM polisaharīds, kam piemīt lieliska biosaderība un kam ir svarīga bioķīmiska nozīme dažādos fizioloģiskos procesos [22], [23]. Turklāt HA ir vairākas funkcionālās grupas, kas ļauj veikt daudzveidīgas turpmākas ķīmiskas modifikācijas [13], [24]. Starp tipiskiem īsas ķēdes antimikrobiālajiem peptīdiem (AMP), ε-PL tiek klasificēts kā garas ķēdes antimikrobiāls polipeptīds, kas pazīstams arī kā poliaminoskābe. ε-PL piemīt vairākas unikālās īpašības, to ir atzinusi par drošu lietošanai (*GRAS – Generally Recognized As Safe*) ASV Pārtikas un zāļu pārvalde (*FDA*). Salīdzinot ar citiem AMP, tam ir vairākas priekšrocības, tostarp dabiska izcelsme, vienkārša struktūra, zema imunogenitāte, zema toksicitāte, biosaderība, antibakteriāls darbības mehānisms caur šūnu membrānas bojāšanu, stabilitāte dažādos pH un temperatūras apstākļos, kā arī izmaksu efektivitāte. Līdz šim tikai dažos pētījumos ir aprakstīta ε-PL saturošu antibakteriālu hidrogelu pagatavošana un antibakteriālās aktivitātes novērtēšana, tostarp ķīmiski šķērssaistītu poliglutamīnskābes/ε-PL kompozīthidrogeli, ε-PL saturoši liellopu seruma albumīna (*BSA*) un polivinilspirta (*PVA*) divu tīklu hidrogeli, fotopolimerizēti zīda fibrīna/ε-PL

hidrogeli, poliakrilamīda, želatīna un ε-PL hidrogeli, ε-PL stabilizēti agarozes/polidopamīna hidrogeli un dinamiski arginīna-glicīna-asparagīnskābes (*RGD*)/ε-PL hidrogeli [2], [24].

Lai saglabātu abu komponentu īpašības, tos apvienojot vienā vienotā hidrogela matricā, tika izvēlēta ķīmiskā šķērssaistīšana metode, izmantojot 1-etil-3-(3-dimetilamīnpropil) karbodiimīdu (EDC)/ N-hidroksisukcinimīda (NHS). EDC/NHS šķērssaistīšana nodrošina maigus reakcijas apstākļus, abu reaģentu šķīdību ūdenī, zemāku toksiskumu, salīdzinot ar citiem šķērssaistītājiem, kā arī nodrošina uzlabotas iegūtas hidrogela matricas mehāniskās īpašības, pateicoties stabilu kovalento saišu izveidei [25].

Otrkārt, lai izstrādātu kompozīthidrogelus, ir būtiski izvēlēties atbilstošu un zinātniski pamatotu *CaP* atvasinājumu. Kaulu ECM galvenā neorganiskā sastāvdaļa ir nanoizmēra karbonātus saturošs kalcija deficīta apatīts, kas satur tādus mikroelementus kā Mg, Zn, Sr u. c. Sintētiskās hidroksilapatīta (HAp) nanodaļiņas ir līdzīgas dabiskajam kaula apatītam gan pēc ķīmiskā sastāva, gan struktūras, gan izmēra. Tāpēc sintētiskajam nanokristāliskajam HAp piemīt izcilas osteokonduktīvās īpašības. Dažādi materiāli uz HAp bāzes ir plaši pētīti kā nesēji bioloģiski aktīvu savienojumu piegādei, jo tiem ir liels īpatnējais virsmas laukums, unikāla bioaktivitāte un adsorbcijas kapacitāte pāri bioloģiskajām barjerām [26]. Nesen ir pētīti nesēji uz HAp bāzes mērķtiecīgai pretosteoporotisko zāļu, pretvēža zāļu, antibiotiku, proteīnu, gēnu, radionuklīdu un neorganisko jonu, piemēram, Mg^{2+}, Zn^{2+}, Sr^{2+}u. c., piegādei. Ar joniem aizvietoti HAp biomateriāli tiek uzskatīti par daudzsološām sistēmām biomimetisko kaulu ECM mikroelementu ilgtspējīgai, lokālai piegādei [27]–[29]. Šādus funkcionalizētus HAp biomateriālus var izmantot, lai izstrādātu nākamās paaudzes biomateriālus kaulu slimību (tostarp osteoporotisku kaulu lūzumu) ārstēšanai un rekonstrukcijai, kontrolēti piegādājot bioloģiski aktīvus neorganiskos jonus vai zāles tieši kaulu defektu vietās [30]. No dažādiem kandidātiem ar joniem aizvietotu HAp izstrādei plašu interesi ir izraisījuši Sr^{2+} joni, jo tie darbojas kā kaulu terapeitiskie aģenti ar unikālu divējāda iedarbības mehānismu, t. i., vienlaikus veicinot kaulaudu veidošanos, aktivizējot Ca jutīgos receptorus un kavējot kaulaudu noārdīšanos [31], [32]. Sr^{2+} joni tiek iekļauti kaulaudos, izmantojot divus galvenos mehānismus: 1) ātras uzsūkšanās mehānismu, kas atkarīgs no osteoblastu aktivitātes, kad Sr^{2+} joni tiek absorbēti jonu apmaiņas procesā ar Ca^{2+} joniem vai saistoties ar osteoīdu proteīniem; 2) Sr^{2+} joni tiek iekļauti kaulu minerāla kristālrežģī. Sr^{2+} joniem piemīt osteogēns potenciāls, un ir pierādīts, ka Sr-saturoši HAp biomateriāli spēj piegādāt Sr^{2+} jonus kaula defekta vietā, kur tie veicina kaulu reģenerāciju, stimulējot osteoblastu proliferāciju un diferenciāciju, vienlaikus nomācot osteoklastu aktivitāti.

Ņemot vērā izvēlēto komponentu un šķērssaistīšanas stratēģijas pierādīto potenciālu, šī promocijas darba mērķis bija izstrādāt un vispusīgi raksturot injicējamus hidrogelus, apvienojot ε-PL dabiskās antibakteriālās īpašības, HA ECM imitējošās un bioloģiskās saderības īpašības, kā arī Sr-HAp nanodaļiņu osteogēno iedarbību. Šī daudzfunkcionālā hidrogela sistēma izstrādāta ar mērķi vienlaikus cīnīties pret baktēriālajām infekcijām un veicināt kaulaudu reģenerāciju, tādējādi risinot iepriekš minētos kritiskos veselības aprūpes izaicinājumus.

Mērķis un uzdevumi

Promocijas darba mērķis ir izmantot antimikrobiālo polipeptīdu ε-PL, lai izstrādātu kovalenti šķērssaistītus antibakteriālus hidrogelus audu inženierijas lietojumiem. Lai sasniegtu

definēto mērķi, promocijas darba eksperimentālais plāns tika sadalīts četrās daļās, aptverot hidrogelu un Sr-HAp funkcionalizētu hidrogelu sintēzes metodoloģijas izstrādi, un šo biomateriālu turpmāko izpēti. Šīs daļas atbilst promocijas darba uzdevumiem.

1. Izstrādāt ķīmiski šķērssaistītas ε-PL/HA hidrogela matricas sintēzes metodoloģiju, izmantojot EDC/NHS šķērssaistīšanas reakciju.
2. Izpētīt iegūto ε-PL/HA hidrogelu fizikālķīmiskās un *in vitro* bioloģiskās īpašības.
3. Izstrādāt ar Sr-HAp funkcionalizētu ε-PL/HA (Sr-HAp/ε-PL/HA) hidrogelu sintēzes metodoloģiju.
4. Izpētīt iegūto Sr-HAp/ε-PL/HA kompozīthidrogelu fizikālķīmiskās un *in vitro* bioloģiskās īpašības.

Aizstāvēšanai izvirzītas tēzes

1. *EDC*/NHS ierosinātas ķīmiskās šķērssaistīšanas metode ir izmantojama ε-PL/HA hidrogelu izstrādei, lai sasniegtu vēlamas fizikālķīmiskās un bioloģiskās īpašības audu inženierijas jomai: stingrību, injicējamību, šļircējamību, pašatjaunošanās kapacitāti, sterilizācijas spēju, antibakteriālo aktivitāti un šūnu dzīvotspēju.
2. Kovalenti šķērssaistītus ε-PL/HA hidrogelus var sterilizēt ar konvencionālu tvaika sterilizāciju, minimāli ietekmējot to fizikālķīmiskās un *in vitro* antibakteriālās īpašības.
3. ε-PL/HA hidrogeli uzrāda spēcīgu antibakteriālo aktivitāti pret gramnegatīviem un grampozitīviem baktēriju celmiem, tostarp ATCC references un klīniski izolētiem grūti ārstējamiem multirezistentiem celmiem.
4. ε-PL/HA hidrogela matricas funkcionalizēšana ar Sr-HAp nanodaļiņām nemaina sākotnējās hidrogela matricas īpašības, saglabājot injicējamību, antibakteriālo aktivitāti, vienlaikus piešķirot regulējamu biodegradācijas profilu, kas ir būtiski kaulaudu reģenerācijas lietojumiem.

Zinātniskā novitāte

1. Pirmo reizi ir izstrādāta bioloģiski saderīga un antibakteriāla hidrogela matrica, izmantojot divus dabiskas izcelsmes biopolimērus ε-PL un HA, izmantojot EDC/NHS ierosinātu ķīmisko šķērssaistīšanu.
2. Tika sistemātiski novērtēta tvaika sterilizācijas ietekme uz izstrādāto ε-PL/HA hidrogelu fizikālķīmiskajām īpašībām un antibakteriālo aktivitāti *in vitro* apstākļos, demonstrējot minimālu ietekmi uz to funkcionālajām īpašībām un potenciālu klīniskai lietošanai.
3. Tika pētīts potenciāls baktēriju rezistences attīstībai pret ε-PL, izmantojot gan ATCC references celmus, gan klīniski izolētus multirezistentiem grampozitīvos un gramnegatīvos baktēriju celmus.
4. Ir izstrādāti injicējami ε-PL/HA hidrogeli, funkcionalizēti ar Sr-HAp nanodaļiņām, un novērtēta to dubultā funkcionalitāte – antibakteriālā aktivitāte un osteogēnais potenciāls, uzsverot to lietojuma potenciālu kaulu infekciju ārstēšanā.
5. Tika pētīta ε-PL/HA hidrogelu un ar Sr-HAp funkcionalizētu ε-PL/HA hidrogelu antibakteriālā aktivitāte gan ātras iedarbības (24 h), gan ilgstošas iedarbības (168 h) režīmos pret plašu baktēriju celmu spektru, apstiprinot izstrādāto hidrogelu sistēmu ilgstošo un plaša spektra antibakteriālo efektivitāti.

Praktiskā nozīme

Šī promocijas darba ietvaros tika sasniegti šādi praktiskie rezultāti:

1) izstrādāta efektīva un reproducējama sintēzes metodoloģija injicējamu, antibakteriālu un autoklāvējamu hidrogelu iegūšanai uz ε-PL un HA bāzes, izmantojot *EDC*/NHS ierosinātu ķīmisko šķērssaistīšanu biomedicīniskiem lietojumiem;
2) izstrādāti standartizēti darbības protokoli, lai novērtētu izstrādāto hidrogelu viskoelastīgās īpašības, antibakteriālo aktivitāti *in vitro* un citotoksicitāti, tostarp detalizētas paraugu sagatavošanas procedūras pēc sintēzes un testēšanas reproducējamības validācija;
3) izstrādāta *in situ* funkcionalizācijas metodoloģija, lai iegūtu ar Sr-HAp funkcionalizētus ε-PL/HA hidrogelus kā dubultas funkcionalitātes biomateriālus, apvienojot antibakteriālo aktivitāti ar osteogēnu potenciālu inficētu kaulu defektu ārstēšanai;
4) izstrādātās hidrogela matricas sintēzes, sterilizācijas un funkcionalizācijas vienkāršība liecina par augstu translācijas potenciālu mērķtiecīgai antibakteriālai terapijai, nākamās paaudzes implantu pārklājumu, zāļu piegādes sistēmu vai kompozīthidrogelu izstrādē.

Darba struktūra un apjoms

Promocijas darbs izstrādāts kā zinātnisko publikāciju kopa, tas veltīts ķīmiski šķērssaistītas ε-PL/HA hidrogela matricas un ar Sr-HAp funkcionalizētu ε-PL/HA hidrogelu izstrādei un visaptverošai izpētei. Darbs ietver četras oriģinālās zinātniskās publikācijas, publicētas recenzētos zinātniskos (*SCI*) žurnālos, kā arī vienu apskatrakstu.

Publikācijas un promocijas darba aprobācija

Promocijas darbā iegūtie rezultāti un sasniegumi publicēti četrās oriģinālās zinātniskās publikācijās. Turklāt tika publicēts arī apskatraksts, kurā aplūkota ar promocijas darbu saistīta tēma. Promocijas darba izstrādes laikā galvenie rezultāti tika prezentēti 16 zinātniskās konferencēs.

SCI publikācijas

1. **A. Sceglovs**, I. Skadins, M. Chitto, J. Kroica, K. Salma-Ancane. Failure or future? Exploring alternative antibacterials: a comparative analysis of antibiotics and naturally-derived biopolymers, Front. Microbiol., 2025, 16: 1526250. doi: 10.3389/fmicb.2025.1526250 (*IF 4,5, Q1, CiteScore 7,7*).
   A. Ščeglova ieguldījums (85/100 %): konceptualizācija, resursi, rakstīšana – sākotnējā versija, rakstīšana – pārskatīšana un rediģēšana.
2. K. Salma-Ancane, **A. Sceglovs**, E. Tracuma, J. K. Wychowaniec, K. Aunina, A. Ramata-Stunda, V. Nikolajeva, D. Loca. Effect of crosslinking strategy on the biological, antibacterial and physicochemical performance of hyaluronic acid and ε-polylysine based hydrogels, *Int. J. Biol. Macromol.*, 2022, 208, 995–1008. https://doi.org/10.1016/J.IJBIOMAC.2022.03.207 (*IF 8,5, Q1, CiteScore 13,7*).
   A. Ščeglova ieguldījums (35/100 %): metodoloģija, validācija, formālā analīze, izpēte.

3. **A. Sceglovs**, J. K. Wychowaniec, I. Skadins, A. Reinis, C. J. C. Edwards-Gayle, M. D'Este, K. Salma-Ancane, Effect of steam sterilisation on physico-chemical properties of antibacterial covalently cross-linked ε-polylysine/hyaluronic acid hydrogels, Carbohydr. *Polym. Technol. Appl*., 2023, 6: 100363. https://doi.org/10.1016/J.CARPTA.2023.100363 (*IF 6,5, Q1, CiteScore 8,7*).
   A. Ščeglova ieguldījums (70/100 %): konceptualizācija, resursi, rakstīšana – sākotnējais variants, metodoloģija, validācija, rakstīšana – pārskatīšana un rediģēšana.
4. **A. Sceglovs**, C. Siverino, I. Skadins, V. Pirsko, M. Sceglova, J. Kroica, F. T. Moriarty, K. Salma-Ancane. Injectable ε-polylysine/hyaluronic acid hydrogels with resistance-preventing antibacterial activity for treating wound infections, *ACS Appl. Bio Mater*., 2025, 8 (11), 9916–9930. https://doi.org/10.1021/acsabm.5c01252.
   A. Ščeglova ieguldījums (75/100 %): konceptualizācija, resursi, metodoloģija, validācija, rakstīšana – pārskatīšana un rediģēšana.
5. A. Rubina, **A. Sceglovs**, A. Ramata-Stunda, I. Pugajeva, A. R. Boyd, A. Tumilovica, L. Stipniece and K. Salma-Ancane. Injectable mineralized Sr-hydroxyapatite nanoparticles-loaded ε-polylysine-hyaluronic acid composite hydrogels for bone regeneration, *Int. J. Biol. Macromol.,* 2024, 280: 135703. https://doi.org/10.1016/j.ijbiomac.2024.135703 (*IF 8,57, Q1, CiteScore 13,7*).
   A. Ščeglova ieguldījums (35/100 %): rakstīšana – pārskatīšana un rediģēšana, rakstīšana – sākotnējā versija, vizualizācija, izpēte, formālā analīze, konceptualizācija.

Zinātniskās konferences:

1. **A.Sceglovs**, A.Reinis, K.Salma-Ancane. Natural biopolymer-based antibacterial hydrogels for tissue engineering. *European Society for biomaterials (ESB 2021),* 5–9 September 2021, virtual event, virtual poster presentation.
2. **A. Sceglovs**, A. Reinis, K. Salma-Ancane. Synthesis and characterization of chemically cross-linked hydrogels based on ε-polylysine and hyaluronic acid. *Materials Science and Applied Chemistry conference of RTU (MSAC 2021)*, 22nd of October 2021, virtual event, virtual poster presentation.
3. **A. Sceglovs**, C. Siverino, F. T. Moriarty, K. Salma-Ancane. Covalently bonded ε-polylysine/hyaluronic acid hydrogels with enhanced antibacterial action. *Scandinavian Society for biomaterials conference (ScSB 2022)*, 13–15 June 2022, Jurmala, Latvia, poster presentation.
4. **A. Sceglovs**, C. Siverino, J. K. Wychowaniec, F. T. Moriarty, M. D'Este, K. Salma-Ancane. Functional ε-polylysine/hyaluronic acid hydrogels with antibacterial activity. *Tissue engineering and Regenerative Medicine International Society conference (TERMIS EU 22)*, 28th of June – 1st of July 2022, Krakow, Poland, poster presentation.
5. **A. Sceglovs**, K. Salma-Ancane. Effect of Steam Sterilization Strategy on ε-Polylysine/Hyaluronic Acid Hydrogel Properties. *European Society for biomaterials (ESB 2022)*, 4–8 September 2022, Bordo, France, poster presentation.
6. A. Rubina, I. Kreicberga, **A. Sceglovs**, K. Salma-Ancane. Development of Functional Composite Hydrogels for Bone Regeneration. *European Society for biomaterials (ESB 2022)*, 4–8 September 2022, Bordo, France, poster presentation.
7. **A. Sceglovs**, K. Salma-Ancane. Investigation of Impact of Steam Sterilization on ε-Polylysine/Hyaluronic Acid Hydrogel Properties. *Materials Science and Applied*

Chemistry conference of RTU (MSAC 2022), 21st of October 2022, Riga, Latvia, poster presentation.

8. A. Rubina, I. Kreicberga, **A. Sceglovs**, K. Salma-Ancane. Development of Functional Composite Hydrogels for Bone Regeneration. *Materials Science and Applied Chemistry conference of RTU (MSAC 2022)*, 21st of October 2022, Riga, Latvia, poster presentation.
9. **A. Sceglovs**, I. Skadins, V. Pirsko, J. Kroica, K. Salma-Ancane. Injectable Polypeptide-Based Hydrogels for Local Antibacterial Therapy. *European Society for biomaterials (ESB 2023),* 4–8 September 2023, Davos, Switzerland, poster presentation.
10. A. Rubina, A. Tumilovica, **A. Sceglovs**, L. Stipniece, K. Salma-Ancane. Injectable Hyaluronic Acid/ε-Polylysine Hydrogels Loaded with Strontium Hydroxyapatite Nanoparticles For Osteoporotic Bone Fracture Healing. *European Society for biomaterials (ESB 2023)*, 4–8 September 2023, Davos, Switzerland, poster presentation.
11. **A. Sceglovs**, I. Skadins, V. Pirsko, J. Kroica, K. Salma-Ancane. Revealing Physicochemical and Antibacterial Properties of Chemically Coupled ε-Polylysine/Hyaluronic Acid Hydrogel. *Materials Science and Applied Chemistry conference of RTU (MSAC 2023)*, 6th of October 2023, Riga, Latvia, oral presentation.
12. A. Rubina, A. Tumilovica, **A. Sceglovs**, L. Stipniece, K. Salma-Ancane. Injectable nanoparticle-hydrogel composites for bone regeneration. *Materials Science and Applied Chemistry conference of RTU (MSAC 2023)*, 6th of October 2023, Riga, Latvia, oral presentation.
13. **A. Sceglovs**, I. Skadins, J. Kroica, K. Salma-Ancane. Injectable hydrogels based on antimicrobial polypeptide exhibit enhanced in vitro antibacterial activity. *4th International Biennial BioMaH Conference*, 15–18 October 2024, Rome, Italy, poster presentation.
14. A. Rubina, **A. Sceglovs**, A. Ramata-Stunda, A. Tumilovica, L. Stipniece, K. Salma-Ancane. Injectable mineralized Sr-hydroxyapatite nanoparticles-loaded composite hydrogels for bone regeneration. *4th International Biennial BioMaH Conference*, 15–18 October 2024, Rome, Italy, oral presentation.
15. **A. Sceglovs**, I. Skadins, J. Kroica, K. Salma-Ancane. Advanced hydrogel platforms: cross-linked polypeptide for non-antibiotic antibacterial applications. *RSU Research Week Biennial conference (RW 2025)*, 24–28 March 2025, Riga, Latvia, oral presentation.
16. **A. Sceglovs**, A. Rubina, I. Skadins, J. K. Wychowaniec, A. Ramata-Stunda, J. Kroica, K. Salma-Ancane. Attaining non-antibiotic antibacterial hydrogels: from ε-polylysine networks to composite platforms. *Tissue engineering and Regenerative Medicine International Society conference (TERMIS EU 25)*, 19–23 May 2025, Freiburg, Germany, oral presentation.

Citas zinātniskās publikācijas, kas tapušas promocijas darba izstrādes laikā

1. M. Mosina, C. Severino, L. Stipniece, **A. Sceglovs**, R. Vasiļjevs, F. T. Moriarty, J. Locs. Gallium-Doped Hydroxyapatite Shows Antibacterial Activity against Pseudomonas aeruginosa without Affecting Cell Metabolic Activity. *J. Funct Biomater*., 2023, 14 (51). https://doi.org/10.3390/jfb14020051.
2. L. Stipniece, A. Ramata-Stunda, J. Vecstaudza, I. Kreicberga, D. Livkisa, A. Rubina, **A. Sceglovs**, K. Salma-Ancane. A Comparative Study on Physicochemical Properties and In Vitro Biocompatibility of Sr-Substituted and Sr Ranelate-Loaded Hydroxyapatite

Nanoparticles. *ACS Appl. Bio Mater*., 2023, 6, 5264–5281. https://doi.org/10.1021/acsabm.3c00539.

3. A. Rubina, A. Tumilovica, **A. Sceglovs**, K. Klavins, A. Vaska, L. Stipniece, A. Sizovs, I. Novosjolova, K. Salma-Ancane. Injectable hyaluronic acid/nanohydroxyapatite composite hydrogels for localized drug delivery and bone repair. *Carbohydr. Polym. Technol. Appl.*, 2025, 12: 101030. https://doi.org/10.1016/j.carpta.2025.101030 (*IF 6.5, Q1, CiteScore 11.0*).

Citas zinātnisko konferenču prezentācijas

1. A. Tumilovica, A. Rubina, **A. Sceglovs**, L. Stipniece, K. Salma-Ancane. Development of injectable composite hydrogels containing hydroxyapatite nanoparticles and hyaluronic acid, *Materials Science and Applied Chemistry conference of RTU (MSAC 2023)*, 6th of October 2023, Riga, Latvia, poster presentation.
2. A. Tumilovica, A. Rubina, **A. Sceglovs**, K. Klavins, L. Stipniece, K. Salma-Ancane. Development of injectable bioactive composite hydrogels for bone regeneration. *4th International Biennial BioMaH Conference*, 15–18 October 2024, Rome, Italy, poster presentation.

PROMOCIJAS DARBA GALVENIE REZULTĀTI

Dabiskas izcelsmes biopolimēru (*NDB*) potenciāls kā alternatīva antibakteriāliem līdzekļiem audu inženierijas lietojumiem (1. publikācija)

Bakteriālās infekcijas ir bijušas nozīmīga problēma visā cilvēces vēsturē. Lai gan antibiotiku izstrāde 20. gadsimtā radīja revolūciju infekciju ārstēšanā, tā vienlaikus aizsāka arī nepārtrauktu evolūcijas cīņu ar patogēnajiem mikroorganismiem. Šo dzīvību glābjošo antibiotiku pārmērīga un nepareiza lietošana ir veicinājusi globālas sabiedrības veselības krīzes, ko dēvē par antimikrobiālo rezistenci (AMR), izplatību visā pasaulē [33]. PVO dramatiskais ziņojums liecina, ka līdz 2050. gadam rezistence pret antibiotikām var kļūt tikpat nāvējoša kā vēzis un radīt ievērojamus ekonomiskos zaudējumus, ja netiks veikti preventīvi pasākumi [34]. Antibiotiku efektivitātes samazināšanās un alternatīvu ārstēšanas līdzekļu ierobežotā pieejamība uzsver steidzamu nepieciešamību ieviest jaunas antibakteriālās terapijas klases. Ideālajām alternatīvām būtu jādarbojas kā mehānismiem, kas mazina rezistences attīstības risku.

Šajā kontekstā **antibakteriāli dabiskas izcelsmes biopolimēri (*aNDB*)** ir piesaistījuši ievērojamu uzmanību to unikālo antibakteriālo īpašību dēļ. Aptuveni pirms 20 gadiem *aNDB* ar pierādītu antibakteriālo aktivitāti pirmo reizi tika ierosināti kā alternatīva antibiotikām bakteriālu infekciju ārstēšanai [35]. Mūsdienās *aNDB* balstītas stratēģijas tiek uzskatītas par perspektīvu risinājumu lokālai, antibiotiku nesaturošai antibakteriālai terapijai, kas vienlaikus atbalsta imūnsistēmas darbību un samazina ietekmi uz dabisko mikrobiotu. Šādas pieejas varētu kļūt par ilgtspējīgas inovācijas pamatu mūsdienu veselības aprūpē.

Saistībā ar *aNDB* ir būtiski izprast to antibakteriālās darbības mehānismu pret baktērijām (1. att.). Pirmkārt, jāņem vērā tas, ka baktēriju šūnu sienas ārējās struktūras (adhēzijas un patogenitātes faktori) ir negatīvi lādētas. Pie šādām struktūrām pieder gramnegatīvo baktēriju lipopolisaharīdi un fosfolipīdi, kā arī grampozitīvo baktēriju teihonskābes un lipoteihonskābes. Otrkārt, *aNDB* sastāv no molekulām (hondroitīnsulfāts, o-pullulāns, ε-polilizīns, hitozāns, antimikrobiālie peptīdi, piemēram, magainīns-2 u. c.), kas satur katjonu grupas, piemēram, primārās amīnu, kvartārās amonija, kvartārās fosfonija, guanidīnija vai terciārās sulfonija grupas [36], kas nodrošina to kopējo pozitīvo lādiņu fizioloģiska pH apstākļos. Rezultātā *aNDB* un baktēriju mijiedarbība sākas ar savstarpēju pieķeršanos, ko izraisa elektrostatiskie spēki [37] (1. att.). Elektrostatiskā mijiedarbība ir pirmais solis ceļā uz *aNDB* baktericīdo iedarbību. Treškārt, lai panāktu multivalences efektu, ir jāsasniedz noteikta *aNDB* katjonu koncentrācija [38], kas nodrošina *aNDB* molekulu vienlaikus piesaisti baktēriju šūnu struktūrām. Turpmākie mehānismi ietver poru vai micelu veidošanās posmus (1. att.), kas raksturo baktēriju strukturālās integritātes izjaukšanu, kā rezultātā palielinās caurlaidība, rodas fizikāli bojājumi, notiek tālāka iekļūšana citoplazmā un baktēriju līze.

Turklāt vairāki pētījumi ir pierādījuši, ka dažādiem *aNDB* piemīt arī antibioplēves aktivitāte. Antibioplēves darbības mehānismi ir saistīti ar bioplēves eksopolisaharīdu (EPS), būtiska komponente bioplēves stabilitātei, izjaukšanu, kas izraisa baktēriju šūnu atdalīšanos, vai baktēriju adhēzijas novēršanu jau sākotnējā stadijā [39], [40]. Turklāt ir konstatēts, ka dažādi *aNDB*, piemēram, laktoferīna atvasinātie peptīdi, neitrofilu peptīdi, antimikrobiālie peptīdi (protegrīns-1), uzrāda antibakteriālu aktivitāti pret intracelulārajām baktērijām –

M. tuberculosis. Antibakteriālās darbības mehānisms ir balstīts mikobaktēriju šūnas sieniņas izjaukšanā un membrānas caurlaidības pastiprināšanā [9–11].

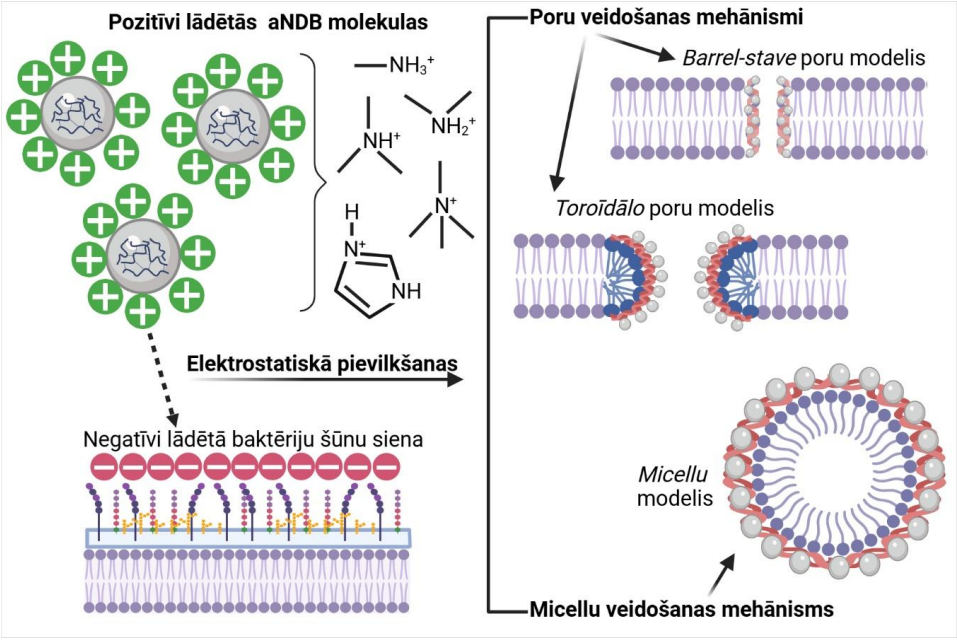

1. att. Biopolimēru (*aNDB*) – baktēriju šūnu mijiedarbība (pa kreisi) un baktericīdie mehānismi (pa labi) (Izveidots ar *Biorender* palīdzību).

Vēl viens būtisks aspekts ir iespējamība, ka baktērijas varētu attīstīt rezistenci pret *aNDB*. Rezistences mehānismi ir dažādi un parasti specifiski konkrētai antibiotiku klasei un tās darbības mehānismam. Tomēr biežākie mehānismi ietver specifisku enzīmu ražošanu, mērķmolekulu zudumu vai modifikāciju, efluksa sūkņu aktivizēšanu, izmaiņas mērķa vietās mutāciju rezultātā, kā arī izmaiņas šūnu membrānas caurlaidībā [12], [41]–[43]. Tradicionāli tiek uzskatīts, ka rezistences attīstība ir raksturīga tikai antibiotikām un ka – teorētiski – baktērijas nevar attīstīt rezistenci pret *aNDB*. No vienas puses, elektrostatiskā pievilkšanās starp *aNDB* un baktēriju ārējām struktūrām šķiet neizbēgama. Turklāt *aNDB* iedarbības mehānisms nav stingri mērķēts. Pat pēc nokļūšanas intracelulārājā vidē *aNDB* var traucēt vairākus vielmaiņas norises [44]–[46]. Ņemot vērā minēto, tiek uzskatīts, ka baktērijām ir grūti traucēt elektrostatisko mijiedarbību un attīstīt rezistenci, jo šāds process bioloģiski ir ļoti resursietilpīgs.

Jaunas dabiski antibakteriālās ķīmiski šķērssaistītas hidrogela matricas izstrāde (2. publikācija)

Hidrogeli ir inovatīvi biomateriāli audu inženierijas, reģeneratīvās medicīnas un zāļu piegādes lietojumiem, pateicoties to unikālajām īpašībām, tādām kā spējai iekapsulēt un kontrolēti pēc pieprasījuma izdalīt bioaktīvos savienojumus (piemēram, zāles vai augšanas faktorus), kā arī atbalstīt šūnu proliferāciju un augšanu [47]–[49]. Pēdējos gados īpašu interesi ir izraisījuši hidrogeli uz dabiskas izcelsmes antibakteriālu biopolimēru (*aNDB*) bāzes ar dabisku antibakteriālu aktivitāti, kas tiek pētīti kā daudzsološi antibiotikas nesaturoši

antibakteriāli līdzekļi infekciju ārstēšanai dažādos biomedicīnas lietojumos, piemēram, brūču dzīšanā un audu infekciju profilaksē [24], [50], [51]. Īsās ķēdes antimikrobiālo peptīdu (AMP) vidū īpašu uzmanību ir ieguvuši garās ķēdes AMP vai poli(aminoskābes), piemēram, **ε-polilizīns (ε-PL**), kas ir augstas veiktspējas *aNDB* ar lielu potenciālu antibakteriālu biomateriālu izstrādē [2], [52]–[55]. ε-PL ir dabā sastopams, lineārs katjonu polipeptīds, ko producē *Streptomyces albulus*. Tas ir iekļauts ASV Pārtikas un zāļu pārvalde klasifikatorā kā "*Generally Recognised as Safe*" (*GRAS* Nr. 000135) un nodrošina plaša spektra antimikrobiālo iedarbību gan pret grampozitīvām, gan gramnegatīvām baktērijām. Papildus tā antibakteriālajam mehānismam ar membrānas izjaukšanu ε-PL ir vairākas priekšrocības, salīdzinot ar citiem *aNDB*, tostarp augsta brīvo ε-aminogrupu (-NH_2) koncentrācija ε pozīcijā, vienkārša struktūra, zema imunogenitāte, zems toksiskuma profils, vienkārša ražošana un zemas izmaksas [2], [45], [55]–[57]. Līdz šim tikai nedaudzi pētījumi ir veikti antibakteriālu ε-PL saturošu hidrogelu izstrādei un antibakteriālo īpašību novērtējumam. Savukārt **hialuronskābe (HA)** ir anjonu, nesulfatēts glikozaminoglikāns (GAG) ar unikālām fizikālķīmiskām īpašībām un specifiskām bioloģiskām funkcijām. HA ir būtiska dabiskā ekstracelulāra matricas (ECM) sastāvdaļa, tāpēc tā ir pievilcīga izejviela biomimetisku, šūnu funkciju atbalstošu hidrogelu izstrādei audu inženierijas lietojumiem [58]–[60]. Hidrogelus galvenokārt izstrādā, izmantojot fizikālo vai ķīmisko šķērssaistīšanu vai kombinējot abas pieejas, lai izveidotu trīsdimensionālu (3D) šķērssaistītu polimēru tīklu [61]. Lai gan fizikāli šķērssaistītiem hidrogeliem raksturīga biomedicīniskā drošība un vienkārša izgatavošana, tiem piemīt zemas mehāniskās īpašības un ierobežota regulējama bionoārdīšanās, kas saistīta ar atgriezenisku starpmolekulāru mijiedarbību un vāju sekundāro spēku, piemēram, jonu/elektrostatisko mijiedarbību, ūdeņraža saišu u. c., veidošanos [61]–[63]. Tomēr ķīmiski šķērssaistītie hidrogeli parasti tiek veidoti ar ķīmiski stabilu kovalento šķērssaistīšanos, kas nodrošina labākas mehāniskās īpašības, stabilitāti fizioloģiskā vidē un regulējamu bioloģisko noārdīšanās dinamiku, salīdzinot ar fizikāli šķērssaistītiem hidrogeliem.

Promocijas darba pirmajā daļā tika sagatavoti jauni ķīmiski šķērssaistītie hidrogeli uz ε-PL un HA bāzes, izmantojot ūdenī šķīstošus 1-etil-3-(3-dimetilaminopropil) karbodiimīdu (EDC)/N-hidroksisukcinimīdu (NHS) šķērssaistīšanas aģentus, nodrošinot ķīmisko reakciju starp HA karboksilgrupām (-COOH) un ε-PL primārām ε-amino (-NH_2) grupām izmantojot nemainīgu EDC/NHS aģentu molāro attiecību (1 : 1). Šajā pētījumā izmantotā EDC/NHS koncentrācija (0,24 M) tika izvēlēta, pamatojoties uz literatūras datiem, kas liecina par tās efektivitāti hidrogelu šķērssaistīšanā, vienlaikus saglabājot biosaderību šūnu kultūru pētījumos [64]. Hidrogeli tika sintezēti ar dažādu ε-PL un HA masas attiecību 40 : 60, 50 : 50 un 60 : 40 masas%, tādējādi nodrošinot ε-PL nešķērssaistīto primāro ε-amino grupu klātbūtni (2. att.). Kā aprakstīts iepriekš, nešķērssaistītas brīvas ε-amino grupas galvenokārt ir atbildīgas par ε-PL antibakteriālo aktivitāti, pateicoties to elektrostatiskai mijiedarbībai ar baktēriju ārējo virsmu. Tomēr pārāk augsta brīvā ε-PL koncentrācija var palielināt citotoksicitātes risku. Tādēļ galvenā izstrādes stratēģija bija apvienot antibakteriālo polipeptīdu ε-PL ar bioloģiski aktīvo HA, lai iegūtu kovalenti saistītu hidrogela matricu, kas nodrošina ne tikai strukturālo stabilitāti, labas mehāniskās īpašības un viskoelastīgās īpašības, bet arī dabisku antibakteriālo aktivitāti, vienlaikus saglabājot šūnu dzīvotspēju [24]. Lai novērstu priekšlaicīgu želēšanu un nodrošinātu efektīvu EDC/NHS ierosinātu šķērssaistīšanu, visi reaģenti pirms sintēzes tika atdzesēti līdz 0–4 °C (2. att.).

Sākotnējie rezultāti par izstrādāto ε-PL/HA hidrogelu fizikālķīmiskajām īpašībām, *in vitro* citotoksicitāti un antibakteriālo aktivitāti tika publicēti *Salma-Ancane et al.* (2022) [24] kopīgajā pētījumā. Šī pētījuma mērķis bija izpētīt mainīgās ε-PL masas attiecības ietekmi ε-PL/HA hidrogelos uz to fizikālķīmiskajām (3. att.) un *in vitro* bioloģiskajām īpašībām. Tas ietvēra arī antibakteriālās aktivitātes novērtējumu pret gramnegatīvo *E. coli* MSCL 332 (4. A att.), kā arī un tiešā kontakta citotoksicitātes testu, lai noteiktu tīra ε-PL citotoksicitātes profilu (IC50) ar Balb/c 3T3 šūnu līniju (4. B–C att.).

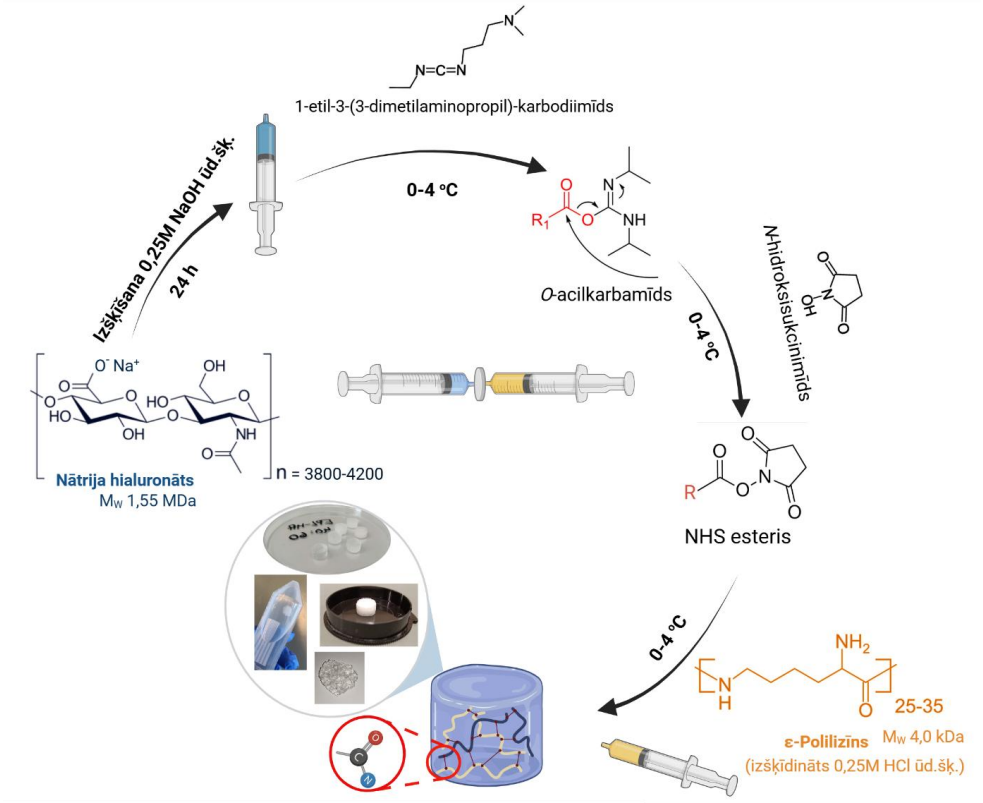

2. att. Ķīmiski šķērssaistītu ε-PL/HA hidrogelu sintēzes shēma.

Tika veikta fizikālķīmiskā raksturošana, lai novērtētu izstrādāto ķīmiski saistīto ε-PL/HA hidrogelu strukturālās un funkcionālās īpašības (3. A–D att.). Rentgenstaru difrakcijas (*XRD*) ainas (3. A att.) atklāja visu sagatavoto ε-PL/HA hidrogelu sēriju amorfu struktūru ar raksturīgu amorfās difrakcijas maksimumu 2θ 20–23° robežās. Papildus tika novēroti difrakcijas maksimumi pie 2θ 32°, 45° un 52°, kas raksturīgi NaCl kristāliskās fāzes maksimumiem. NaCl veidojās neitralizācijas reakcijas laikā starp 0,25M NaOH un 0,25M HCl, kas tika izmantoti sintēzē (2. att.). Sagatavoto ε-PL/HA hidrogelu Furjē transformācijas infrasarkanās spektroskopijas (*FTIR*) spektros (3. B att.) tika konstatēti raksturīgi absorbcijas maksimumi, kas atbilst tīro komponentu ε-PL un HA funkcionālajām grupām. Tādējādi absorbcijas maksimumi pie 1633 cm^{-1}, 1555 cm^{-1}un 1377 cm^{-1} tika attiecināti uz C=O stiepes vibrāciju (Amīds I), C=O-NH saites vibrāciju (Amīds II) un C-N saites vibrāciju (Amīds II). Salīdzinot ar tīra ε-PL un HA *FTIR* spektriem, neliela Amīda I, Amīda II un Amīda III joslu nobīde varētu liecināt par sintēzes laikā notikušo mijiedarbību starp ε-PL brīvajām aminogrupām un HA

karboksilgrupām, kā rezultātā veidojas jaunas kovalentās amīdu saites. Turklāt arī aprēķinātā Amīda I/Amīda II attiecība, kas iegūta no normalizētajiem ε-PL/HA hidrogela un tīrās komponentes spektriem, atklāja, ka šīs attiecības vērtības ir augstākas, salīdzinot ar tīro ε-PL, jo trīs hidrogela sastāviem šī vērtība bija aptuveni 0,87, savukārt ε-PL tā pati joslu attiecība bija 0,69. Absorbcijas joslas pie 3246 cm^{-1} un 3081 cm^{-1} atbilst neprotonētām $-NH_2$ un protonētām $-NH_3^+$ grupām. Kā iepriekš aprēķināts, NH_3^+ /NH_2 attiecību vērtības tika iegūtas kā 0,65, 0,73 un 0,89, kas attiecīgi atbilst 40 : 60, 50 : 50 un 60 : 40 masas% sastāviem. Tās liecina par pieejamām brīvām aminogrupām, kas nodrošina antibakteriālo aktivitāti. Analizējot gela frakciju testa rezultātus (3. C att.), redzams, ka līdzīgās gela frakcijas vērtības (51–57 %, statistiski nenozīmīgas, $p > 0,05$) sagatavotajos hidrogelos liecina par matricas nemainīgu šķērssaites blīvumu pie nemainīgiem parametriem: HA masa un EDC/NHS molārās koncentrācijas.

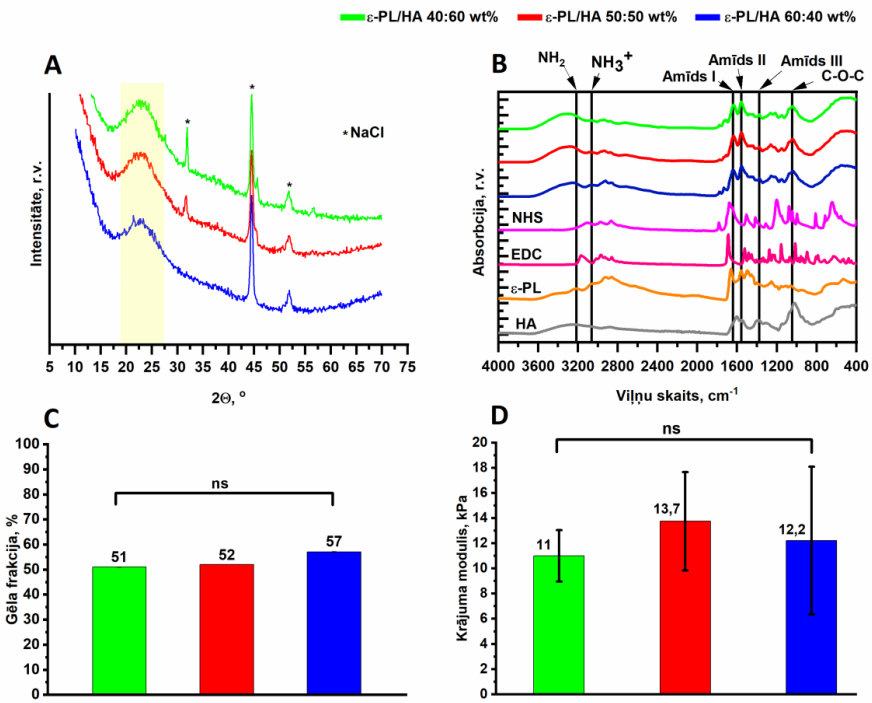

3. att. Sintezēto ε-PL/HA hidrogēlu fizikālķīmisko īpašību pētījumu galveno rezultātu kopsavilkums [24]. (A) Sagatavoto ε-PL/HA hidrogēlu rentgenstaru difrakcijas (XRD) ainas, kas iegūtas 2θ diapazonā no 10 līdz 70. (B) Sagatavoto ε-PL/HA hidrogēlu un to sagatavošanā izmantoto tīro komponentu - ε-PL, HA, EDC un NHS - Furjē transformācijas infrasarkanās spektroskopijas (*FTIR*) spektri 400-4000 cm-1 diapazonā. (C) Gēla frakcijas vērtības trim dažādām ε-PL/HA hidrogēlu sērijām, vērtības attēlotas kā vidējā vērtība ± SD. (D) ε-PL/HA hidrogēlu sēriju mehāniskā stingrība, kas iegūta no amplitūdas svārstību līknēm pie 1 Hz un 0,2 % deformācijas (LVR). No katras eksperimentālās grupas tika izmantoti trīs atkārtojumi.

No *in vitro* antibakteriālas aktivitātes pētījumiem tika konstatēts, ka sagatavotie ķīmiski šķērssaistītie ε-PL/HA hidrogeli nodrošina antibakteriālu iedarbību pret gramnegatīvo *E. coli* MSCL 332 (4. A att.). Antibakteriālā aktivitāte tika izvērtēta, izmantojot gan inhibīcijas zonas

testu (24 h kontakta laiks), gan buljona atšķaidījuma testu (1 h kontakta laiks), liecinot gan par ātru antibakteriālu aktivitāti tiešā kontaktā, gan par noteiktu daudzumu nešķērssaistītu ε-PL molekulu izdalīšanos agara vidē, kā novērots difūzijas pētījumā. Turklāt *in vitro* tiešie pētījumi uz fibroblastu šūnām parādīja, ka pēc 24 h iedarbības saglabājas šūnu dzīvotspēja un šūnu saplūšanu (4. B–C att.).

A

Kompozīcija	*Inhibīcijas zonas diametrs* ± SD [mm]*	*Log10 baktēriju reducēšana***
ε-PL/HA 40:60 wt%	11,5 ± 0,6	1,8
ε-PL/HA 50:50 wt%	13,0 ± 1,2	2,7
ε-PL/HA 60:40 wt%	15,0 ± 0,0	3,3
Gentamicīns, 10 mg/mL	30,7 ± 0,6	-

* Inhibīcijas zonas tests **24 h** pret *E.coli* MSCL 332
** Buljona atšķaidīšanas metode **1 h** pret *E.coli* MSCL 332

B

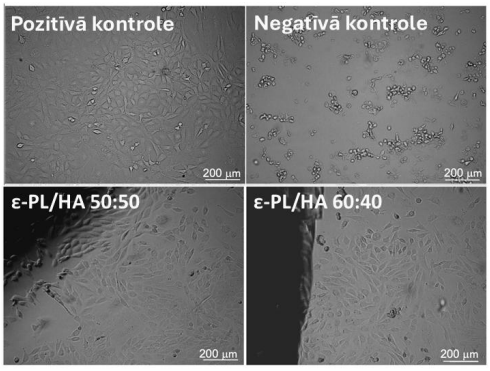

C

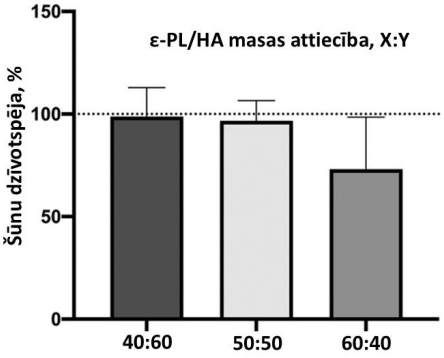

4. att. (A) Kvantitatīvie rezultāti, kas iegūti, veicot inhibīcijas zonas pētījumus pēc 24 h ilgas iedarbības pret gramnegatīvo *E. coli* MSCL 332 celmu, un buljona atšķaidījuma pētījumi pēc 1 h ilgas iedarbības ar to pašu baktēriju celmu. (B) Mikroskopiskie šūnu dzīvotspējas attēli pēc tieša kontakta (24 h) ar BALB/c 3T3 šūnu līniju. (C) Kvantitatīvie rezultāti par šūnu dzīvotspēju, kas atspoguļoti %, sagatavotajiem ε-PL/HA hidrogelu sērijām pēc tieša kontakta ar BALB/c 3T3 šūnām.

Promocijas darba pirmajā daļā tika pierādīts, ka *in situ* veidojošos, ķīmiski šķērssaistītus ε-PL/HA hidrogelus var veiksmīgi izstrādāt, izmantojot EDC/NHS mediētu polimerizācijas mehānismu. Jaunu kovalento saišu veidošanos starp ε-PL un HA atklāja raksturīgie *FTIR* spektri, salīdzinot absorbcijas maksimumus, nobīdes un Amīda I, Amīda II un Amīda III joslu attiecības ar tīrām sastāvdaļām ε-PL un HA. Aprēķinātās NH_3^+/NH_2 attiecības vērtības palielinājās ar augstāku ε-PL saturu hidrogelos, liecinot par augstāku protonētu ε-amino grupu klātbūtni, kas saistītas ar antibakteriālo aktivitāti. Šo tendenci papildus apstiprināja antibakteriālie testi. Tīra ε-PL citotoksicitātes profils uzrādīja IC_{50} koncentrāciju 4,21 mg/mL, liecinot par potenciālu citotoksicitāti augstākās koncentrācijās. Tomēr visi trīs hidrogela sastāvi neuzrādīja citotoksisku iedarbību, tieši iedarbojoties uz BALB/c 3T3 šūnu līniju fibroblastiem, kas uzsver izstrādāto hidrogelu bioloģisko drošību. Ķīmiskā šķērssaistīšana izrādījās piemērota stratēģija, kā rezultātā tika iegūti ε-PL/HA hidrogeli ar uzlabotu strukturālo integritāti un stabilu

stingrības moduli diapazonā no 10 kPa līdz 15 kPa, kas ir piemērots muskuļu un skeleta reģenerācijas lietojumiem (3. D att.) [63]. Stabilais kovalento saišu tīklojums arī veicināja ilgstošu antibakteriālu iedarbību, vienlaikus saglabājot zemu citotoksicitāti. Turklāt provizoriski tika atklāts, ka ķīmiski šķērssaistītus ε-PL/HA hidrogelus var sterilizēt ar tvaika sterilizāciju (121 °C 20 min), neietekmējot to integritāti.

Promocijas darba otrajā daļā tika īstenoti šādi pētījumu uzdevumi: (a) sintēzes optimizācija, lai samazinātu HA degradācijas risku; (b) ε-PL un HA masas attiecības optimizācija, lai panāktu optimālas mehāniskās īpašības, augstu antibakteriālo aktivitāti, vienlaikus nodrošinot šūnu dzīvotspēju; (c) hidrogelu topoloģijas novērtēšana; (d) hidrogelu viskoelastīgo īpašību novērtēšana; (e) tvaika sterilizācijas ietekmes izpēte uz hidrogelu fizikālķīmiskajām īpašībām; (f) *in vitro* antibakteriālās aktivitātes un šūnu dzīvotspējas novērtēšana.

Ķīmiski šķērssaistītu ε-PL/HA hidrogelu sintēzes metodes optimizācija, topoloģijas novērtēšana un tvaika sterilizācijas ietekme uz fizikālķīmiskajām un antibakteriālajām īpašībām (3. publikācija)

Pirmkārt, tika modificēta ε-PL/HA hidrogelu sintēzes metode *in situ,* izmantojot EDC/NHS mediētu karboksil-amīna šķērssaiti, aizstājot 0,25M NaOH (HA gadījumā) un 0,25M HCl (ε-PL gadījumā) ūdens šķīdumus ar dejonizētu ūdeni (2. att.). Šīs modifikācijas mērķis bija novērst HA degradācijas risku sārmainos apstākļos sintēzes laikā. Paplašinot eksperimenta dizainu, tika sagatavoti ε-PL/HA hidrogeli ar ε-PL un HA masas attiecību 40 : 60, 50 : 50, 60 : 40, 70 : 30 un 80 : 20 masas%.

Otrkārt, tika veikta mazo leņķu rentgenstaru izkliedes (*SAXS*) analīze, lai izpētītu visu izgatavoto hidrogelu iekšējo struktūru un tīkla topoloģiju [13]. Topoloģiskajām īpašībām ir būtiska nozīme biomedicīniskos lietojumos, jo tās ietekmē hidrogelu viskoelastīgo uzvedību, mehānisko integritāti, uzbriešanu un bioloģisko mijiedarbību. Īpaši būtiska ir hidrogela iekšējā virsmas struktūra, jo tā ietekmē biomateriāla mijiedarbību ar dzīvajiem audiem, tostarp šūnu adhēziju, migrāciju, mehānisko transdukciju, proliferāciju un antibakteriālo aktivitāti. *SAXS* analīze tika veikta q diapazonā (0,045 nm^{-1}–0,233 nm^{-1}), kas atbilst reālās telpas izmēriem 27–140 nm. Šis diapazons ietver hidrogelam līdzīgo struktūru *Porod* reģionu (reālajā d telpā), tādējādi sniedzot galvenokārt informāciju par hidrogela tīkla virsmas īpašībām, t. sk. gludumu. Iegūtie izkliedes dati tika analizēti, izmantojot spēka likumsakarību pielāgošanu, lai iegūtu novirzes eksponentu (*n*), kas sniedz ieskatu virsmas topoloģijā. Iegūtie ķīmiski šķērssaistīto ε-PL/HA hidrogelu rezultāti ir attēloti kā dubultlogaritmiskie q grafiki (5. A att.). Kā kontroles paraugs tika izmantots augsti koncentrēts HA šķīdums, kas uzrādīja samazinātu izkliedes intensitāti $\sim q^{-3,9} \approx q^{-4}$, liecinot par tipiski gludām virsmām, kas veidojušās no lieliem polielektrolītu kompleksiem (5. B att.) [65]. Ķīmiski šķērssaistītie ε-PL/HA hidrogeli uzrādīja līdzīgu samazinātu izkliedes intensitāti $\sim q^{(-3,6 \pm 0,4)}$, kas liecina par gludu un izturīgu tīkla topoloģiju *Porod* reģionā (5. B att.). Šis rezultāts ir saskaņā ar sagaidāmo topoloģiju ķīmiski šķērssaistītos tīklos, kuros gludu virsmu veidošanos nodrošina robustas kovalentās saites. Vienīgais izņēmums – ε-PL/HA hidrogelu sērija ar masas attiecību 40 : 60 masas% uzrādīja ievērojami atšķirīgu izkliedes intensitāti $\sim q^{-2,9}$ (5. B att.), kas pārsvarā raksturīga fizikāli šķērssaistītiem agregātu klasteriem ar raupjām virsmām [13]. Līdz ar to turpmākajos pētījumos

tika izmantoti ε-PL/HA hidrogeli ar ε-PL un HA masas attiecību 50 : 50, 60 : 40, 70 : 30 un 80 : 20 masas%.

Biomateriālu, īpaši hidrogelu, spēja izturēt konvencionālu tvaika sterilizāciju ir būtiska priekšrocība agrīnas izstrādes stadijās un klīniskās translācijas procesā. Tvaika sterilizācija ir ļoti efektīva, vienkārši lietojama un plaši pieejama sterilizācijas metode. Nākamajā posmā tika pētīta tvaika sterilizācijas ietekme uz iepriekš izvēlētajām hidrogelu sērijām, lai atklātu padziļinātas fizikālķīmiskās īpašības. Pēc tam tika veikta topoloģiskā izvērtēšana, kam sekoja skenējošās elektronu mikroskopijas (SEM) analīze. SEM tika izmantota, lai novērotu sagatavoto liofilizēto hidrogelu paraugu morfoloģiju (5. C att.). Gan nesterilizētie, gan sterilizētie paraugi uzrādīja homogēnu trīsdimensiju tīklu ar savstarpēji saistītu porainību, un pēc sterilizācijas visiem hidrogeliem tika konstatēta tikai minimāla ietekme. Turklāt poru izmēru sadalījums pēc sterilizācijas katrai attiecībai saglabājās līdzīgā makroizmēru diapazonā no 66,7 ± 34,2 μm līdz 193,35 ± 103,05 μm.

Nesterilizētu ε-PL/HA hidrogela paraugu gela frakcijas vērtības pie ε-PL un HA masas attiecības 50 : 50, 60 : 40, 70 : 30 un 80 : 20 masas% bija attiecīgi 55,6 ± 0,1 %, 56,2 ± 0,2 %, 54,7 ± 1,6 % un 44,2± 2,9 % (5. D att.). Šīs vērtības labi sakrita ar gela frakcijas vērtībām, kas iegūtas pirmajā publikācijā (~ 55 %) [24], izņemot 80 : 20 masas% paraugu, kuram bija ievērojami mazāka gela frakcija. Šis samazinājums tika skaidrots ar mazāku šķērssaistīšanās pakāpi konkrētajā attiecībā. Acīmredzot lielāks daudzums brīvā, nešķērssaistīta ε-PL difundēja, iegremdējot hidrogela paraugu ūdenī, rezultātā samazinot gela frakciju, jo lielāka ε-PL daļa izšķīda, salīdzinot ar sākotnējo polimēra masu hidrogelā. Starp nesterilizētiem un sterilizētiem hidrogelu paraugiem ar vienādu ε-PL un HA masas attiecību netika novērotas būtiskas atšķirības gela frakcijas vērtībās ($p > 0,05$). Tas liecina, ka tvaika sterilizācija neietekmēja kopējo šķērssaistīšanās pakāpi ε-PL/HA hidrogelu paraugos, tādējādi saglabājot sintēzes gaitā izveidoto tīkla topoloģiju.

Uzbriešanas uzvedības pētījumos gan nesterilizēti (ε-PL/HA), gan sterilizēti (ster ε-PL/HA) hidrogeli demonstrēja uzbriešanas pakāpi > 100 % pēc 2 h inkubācijas, saglabājot plato vērtības visā pētījuma laikā (24 h, 5. E att.). Nesterilizēto paraugu gadījumā uzbriešanas spēja palielinājās, palielinoties ε-PL masas attiecībai hidrogela paraugos 2 h laikā, attiecīgi 50 : 50 masas% sastāvam no 116 % (50 : 50 masas% attiecība) līdz 340 % (80 : 20 masas% attiecība). Visām trim sērijām ar attiecību 50 : 50, 60 : 40 un 80 : 20 masas% līdz 24 h netika novērotas būtiskas uzbriešanas spējas atšķirības ($p > 0,05$). Turpretī ster ε-PL/HA hidrogelu ar ε-PL un HA masas attiecību 70 : 30 masas% uzbriešanas spēja palielinājās no ~ 215 % līdz ~ 290 % ($p < 0,05$), kas, iespējams, liecina par mehāniski aktīvo šķērssaišu samazināšanos. Neraugoties uz šo novēroto atšķirību, visi ster ε-PL/HA hidrogeli uzbrieda 116–350 % robežās (atkarībā no ε-PL masas attiecības) pēc 4 h inkubācijas fizioloģiskos apstākļos (37 °C), demonstrējot atbilstošu strukturālo stabilitāti un kohēzijas īpašības potenciālai lietošanai audu inženierijā.

A

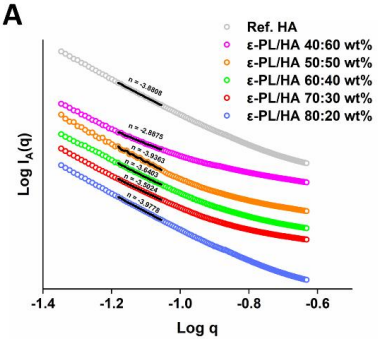

B

Parauga nosaukums	Spēka likuma pielāgošana (q^{-n}), kur *n* indekss atspoguļots zemāk
Ref. HA	3,9
ε-PL/HA 40:60 wt%	2,9
ε-PL/HA 50:50 wt%	3,9
ε-PL/HA 60:40 wt%	3,6
ε-PL/HA 70:30 wt%	3,5
ε-PL/HA 80:20 wt%	4,0

C

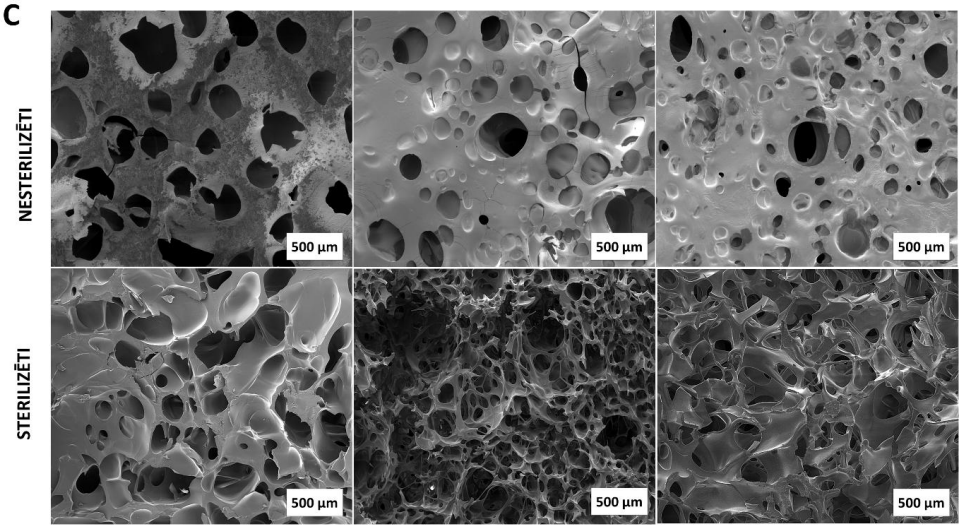

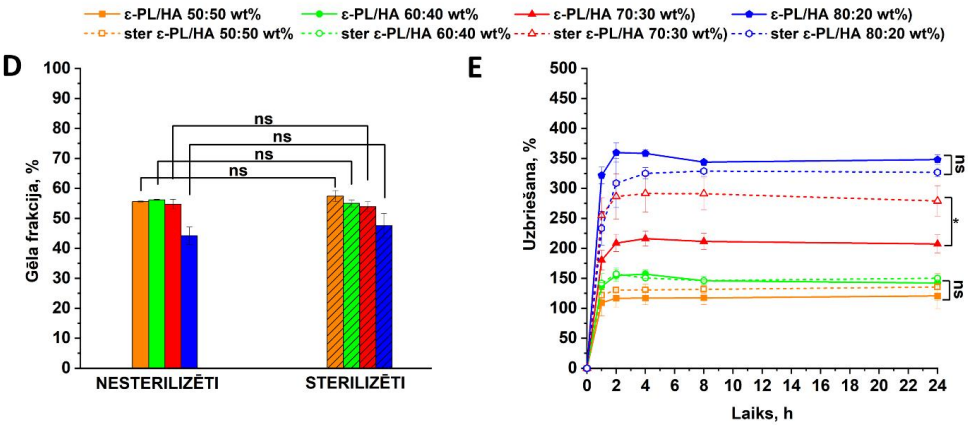

5. att. ε-PL/HA hidrogelu fizikālķīmisko īpašību izpēte [13]. (A) *SAXS* līknes ε-PL/HA hidrogeliem ar masas attiecību 40 : 60, 50 : 50, 60 : 40, 70 : 30 un 80 : 20 masas%. (B) Aprēķinātās spēka likuma atbilstības indeksa n aprēķinātās vērtības no q izkliedes samazinājuma (q^{-n}). (C) SEM mikrofotogrāfijas nesterilizētiem (augšā) un sterilizētiem hidrogeliem (apakšā), no kreisās uz labo pusi: 60 : 40, 70 : 30 un 80 : 20 masas% attiecīgi.

(D) Nesterilizētu un sterilizētu ε-PL/HA hidrogelu paraugu gela frakcijas vērtības. (E) Nesterilizēto un sterilizēto paraugu uzbriešanas līknes. D–E) Dati attēloti kā vidējā vērtība ± SD (n = 3).

Tika veiktas dažādas reoloģiskās analīzes, lai izpētītu sagatavoto ε-PL/HA hidrogelu viskoelastīgās īpašības (6. att.). Vispirms reoloģiskās īpašības tika vērtētas atkarībā no hidrogelu masas attiecībām un sterilizācijas. Amplitūdas svārstību pētījumi (6. A–B att.) tika veikti oscilācijas režīmā deformācijas diapazonā no 0,01 % līdz 1000 % (ε), pie konstantas frekvences 1 Hz , kas atbilst fizioloģiskajiem apstākļiem un 25 °C. No iegūtajām nesterilizētu hidrogelu līknēm (6. A att.) tika secināts, ka hidrogeliem piemīt mīksta cietai vielai līdzīga uzvedība ar krājuma moduļa (G') pārsvaru pār zudumu moduli (G") lineārās viskoelastības reģionā (LVR). Tomēr ε-PL/HA hidrogeliem tika novērots ierobežots LVR ~ 0,1–1 % svārstību deformācijas diapazonā. Turklāt novērotā G" uzvedība attiecībā pret G' uzrādīja lielāku G'/G" attiecību pie zemākām deformācijām, bet diezgan strauji samazinājās līdz krustošanās punktam G' = G". Visām kompozīcijām šis krustošanās punkts saglabājās pie ε ≈ 100 %, kas uzsvēra hidrogela matricas noturību pret pāreju no cietas uz šķidru fāzi galvenokārt stabilāku un elastīgāku ķīmisko šķērssaišu dēļ. Sterilizēto paraugu gadījumā (6. B att.) tika novērotas nelielas atšķirības: (i) visu kompozīciju krustošanās punkts (G' = G") mainījās no iepriekš identificētā ε ≈ 100 % uz ε ≈ 70 %; (ii) G" uzvedība pie zemākām svārstību deformācijas vērtībām (~ 0,01–1 %) kļuva identiska visām kompozīcijām, salīdzinot ar nesterilizētiem paraugiem tajā pašā svārstību deformācijas vērtību diapazonā. To varētu izskaidrot ar faktu, ka sterilizācijas rezultātā daļēji zūd fizikālās mijiedarbības hidrogela matricā, ko rada nesasaistītās ε-PL molekulas un negatīvi uzlādētās HA funkcionālās grupas. Nākamajā posmā krājuma moduļa (G') vērtības tika iegūtas no nesterilizētu un sterilizētu hidrogela paraugu amplitūdas svārstību līknēm pie ε = 0,2 % LVR (6. C att.). Krājuma moduļa vērtības sniedz ieskatu par hidrogelu mehānisko stingrību. Tika secināts, ka hidrogelu kompozīcijām ar masas attiecību 50 : 50, 60 : 40 un 80 : 20 masas% stingrības modulis būtiski neatšķīras pirms un pēc sterilizācijas (p > 0,05). Savukārt 70 : 30 masas% hidrogeliem tika konstatēta statistiski nozīmīga atšķirība (p < 0,05), liecinot, ka sterilizācija būtiskāk ietekmē šīs kompozīcijas struktūru un topoloģiju. Neskatoties uz to, ε-PL/HA hidrogelu stingrība ar 50 : 50, 60 : 40 un 70 : 30 masas% kompozīcijām pirms un pēc sterilizācijas saglabājās ap 10 kPa, savukārt 80 : 20 masas% kompozīcijai tā bija zemāka – 8,6 kPa pirms sterilizācijas un samazinājās līdz 6,9 kPa pēc apstrādes. Apkopojot iepriekš teikto, var secināt, ka stinguma vērtības liecina, ka šie hidrogeli pēc sterilizācijas joprojām atbilst stingruma prasībām (5–15 kPa), piemēram, kombinētiem antibakteriāliem un muskuļu un skeleta reģenerācijas lietojumiem [24].

Turpmākā reoloģiskā izpēte tika veikta plūsmas režīmā, un tās mērķis bija novērtēt sagatavoto hidrogela paraugu injicējamības īpašības. No bīdes ātruma atkarīgās viskozitātes līknēm (6. D att.) varēja redzēt, ka visiem sagatavotajiem paraugiem, palielinoties bīdes ātrumam, viskozitāte strauji samazinās. Šī tendence liecina, ka sagatavotajiem hidrogeliem piemīt injicējamības/šļircejāmības. Lai precīzāk atbildētu uz šo jautājumu, nākamajā posmā tika veikti atjaunošanas cikla pētījumi. Atjaunošanās cikli tika veikti, lai simulētu bīdes spriegumu, kas rodas hidrogela ekstrūzijas laikā no šļirces/ adatas, un novērotu matricas atjaunošanos, balstoties viskozitātes vērtībās (6. E att.).

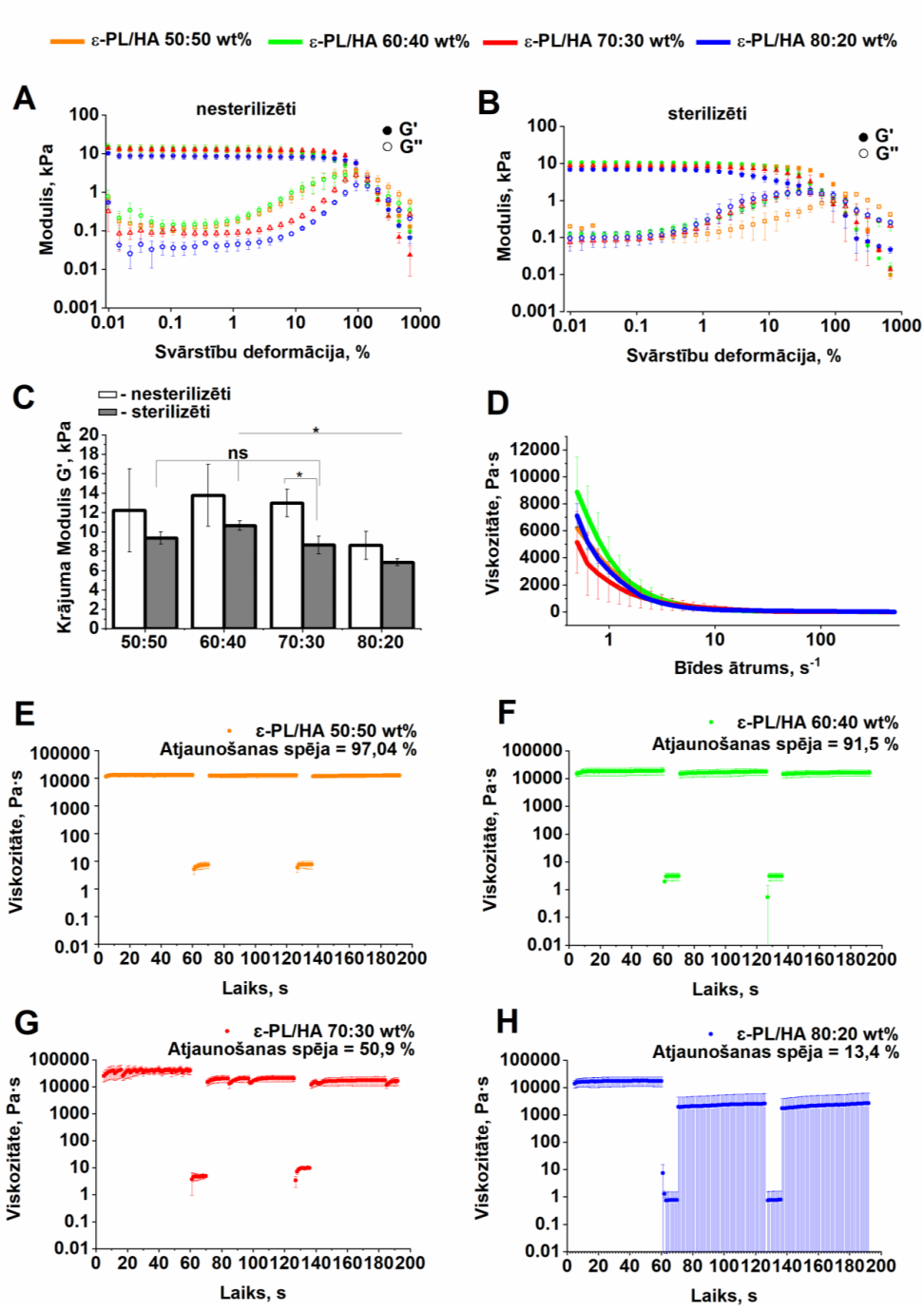

6. att. Sagatavoto ε-PL/HA hidrogelu reoloģiskie pētījumi [2], [13]. (A–B) Amplitūdas svārstību testa līknes nesterilizētiem (A) un sterilizētiem (B) dažāda sastāva hidrogelu paraugiem. (C) Ekstrahētais krājuma modulis (G') no amplitūdas testiem pie ε = 0,2 % deformācijas (LVR). (D) Līknes viskozitātes atkarībai no bīdes ātruma. (E–H) Atjaunošanas cikla tests, kas veikts 5 (3 + 2) ciklu laikā, kas atbilst trīs cikliem bez stresa – 0,1 s^{-1} bīdes

ātrums 60 s un dieviem stresa izraisītiem cikliem – 10 s pie 200 s^{-1}. Visi reoloģiskie mērījumi tika veikti trīs atkārtojumos, lai nodrošinātu reproducējamību un datu ticamību.

Kopumā līknes uzrādīja izjauktu starpmolekulāro saišu atjaunošanās iezīmes pēc inducētas slodzes apstākļiem, t. i., pie augstām bīdes ātruma vērtībām. Tika konstatēts, ka 50 : 50 un 60 : 40 masas% kompozīcijas ir vispiemērotākās injicējamiem biomateriāliem, jo tām bija stabila atjaunošanās pakāpe, kas pārsniedza 90 % pēc vairākiem slodzes cikliem. Zemākas atjaunošanās vērtības tika konstatētas 70 : 30 masas% sastāvam, kas liecina par zemāku matricas integritāti un elastīgāku ķēžu klātbūtni. Savukārt ε-PL/HA hidrogeli ar 80 : 20 masas% sastāvu uzrādīja ļoti zemas atjaunošanās īpašības, jo tika atjaunoti tikai 13,4 % viskozitātes, salīdzinot ar sākotnējām viskozitātes vērtībām, un, iespējams, tikai atsevišķu klasteru klātbūtnes dēļ sadalītā hidrogela paraugā. Rezultātā trīs sastāvi – 50 : 50, 60 : 40 un 70 : 30 masas% – spēja demonstrēt atjaunošanās īpašības. Vērtību atšķirības starp šīm kompozīcijām var skaidrot ar matricas strukturālo integritāti, jo, palielinoties ε-PL masas attiecībai, vairāk nešķērssaistītu ε-PL molekulu savienojas ar HA funkcionālajām grupām sintēzes laikā, tādējādi traucējot ķīmiskā šķērssaistīšanās tīkla veidošanos un organizāciju. Apkopojot iepriekšminēto, tika veikta fizikālķīmiskā raksturošana sēriju ε-PL/HA hidrogelu sērijām ar dažādām ε-PL un HA masas attiecībām. Hidrogeli uzrādīja gela frakcijas vērtības, kā arī uzbriešanas īpašības, kas raksturīgas audu inženierijas lietojumiem Turklāt tika apstiprināts, ka hidrogeli var tikt pakļauti tvaika sterilizācijai, būtiski neietekmējot šīs galvenās īpašības. Tomēr reoloģiskā analīze atklāja, ka 80 : 20 masas% kompozīcija neatbilst vēlamajām viskoelastīgajām prasībām attiecībā uz injicējamību un mehānisko stingrību. Pamatojoties uz šiem rezultātiem, turpmākajai *in vitro* bioloģiskajai novērtēšanai šī promocijas darba ietvaros tika izvēlētas tikai ε-PL/HA hidrogeli ar 50 : 50, 60 : 40 un 70 : 30 masas%.

ε-PL/HA hidrogelu antibakteriālā potenciāla un citotoksicitātes novērtēšana *in vitro* (4. publikācija)

Promocijas darba pirmajā daļā aprakstītie iepriekšējie pētījumi apstiprināja izstrādāto ε-PL/HA hidrogelu antibakteriālo potenciālu pret *E. coli* MSCL 332, izmantojot inhibīcijas zonas un buljona atšķaidīšanas testus gan īstermiņa (1 h), gan ilgtermiņa (24 h) ekspozīcijā. Tomēr vispirms bija būtiski izpētīt tīrā ε-PL antibakteriālo profilu, nosakot tā minimālo inhibējošo un baktericīdo koncentrāciju (MIC/MBC), kā arī novērtējot iespējamo rezistences attīstību kontaktā ar baktērijām. Tīra ε-PL un ε-PL/HA hidrogelu antibakteriālā aktivitāte tika raksturota ar buljona atšķaidīšanas metodi, izmantojot tiešu/netiešu kontaktu testus saskaņā ar modificētajiem *CLSI* un *EU-CAST* standartiem [66]. Antibakteriālie pētījumi tika veikti pret dažādiem gramnegatīviem un grampozitīviem baktēriju celmiem, tostarp *ATCC* references *Escherichia coli* (*E. coli*), *Staphylococcus aureus* (*S. aureus*) un *Staphylococcus epidermidis* (*S. epidermidis*), klīniski izolētām *Pseudomonas aeruginosa* (*P. aeruginosa*) un grūti ārstējamām klīniski izolētām multirezistentām baktērijām – meticilīnrezistentu *Staphylococcus aureus* (MRSA), paplašinātā spektra β-laktamāzes producējošo *Escherichia coli (ESBL E. coli*). Tīrā ε-PL MIC un MBC vērtības norādītas 1. tabulā. Rezultāti uzrādīja inhibējošu (*MIC*) un baktericīdu (*MBC*) aktivitāti pret visiem iepriekš minētajiem baktēriju celmiem mikrogramu diapazonā, savukārt IC_{50}, kā iepriekš noteikts, bija 4,21 mg/mL peļu fibroblastu šūnu līnijā Balb/c 3T3. Šie rezultāti liecina, ka iespējams modulēt ε-PL masas attiecību hidrogelu

paraugos, lai nodrošinātu augstu antibakteriālo aktivitāti, vienlaikus saglabājot šūnu dzīvotspēju.

1. tabula

Iegūtās tīrā ε-PL MIC/MBC koncentrāciju vērtības

Baktēriju celms	ε-PL MIC, μg/ml	ε-PL MBC, μg/ml
E. coli	37	75
P. aeruginosa	75	350
ESBL E. coli	18	37
S. aureus	37	75
S. epidermidis	18	37
MRSA	37	75

Turklāt tika pierādīts, ka ne references celmi *E. coli un S. aureus*, ne arī klīniski izolētie multirezistentie celmi *ESBL E. coli* un MRSA baktēriju celmi neattīstīja rezistenci pret ε-PL 1 mēneša eksperimentālā perioda laikā (10 uzsējumi), kas liecina par ε-PL/HA hidrogelu spēcīgu potenciālu nākotnes antibakteriālajos lietojumos (7. att.).

Rezultāti ar ε-PL/HA hidrogeliem uzrādīja statistiski nozīmīgu baktēriju koloniju augšanas inhibīciju pēc 24 h kontakta ($p < 0,05$), salīdzinot ar kontroles paraugiem, visos testētajos baktēriju celmos un hidrogelu kompozīcijās (8. A att.).

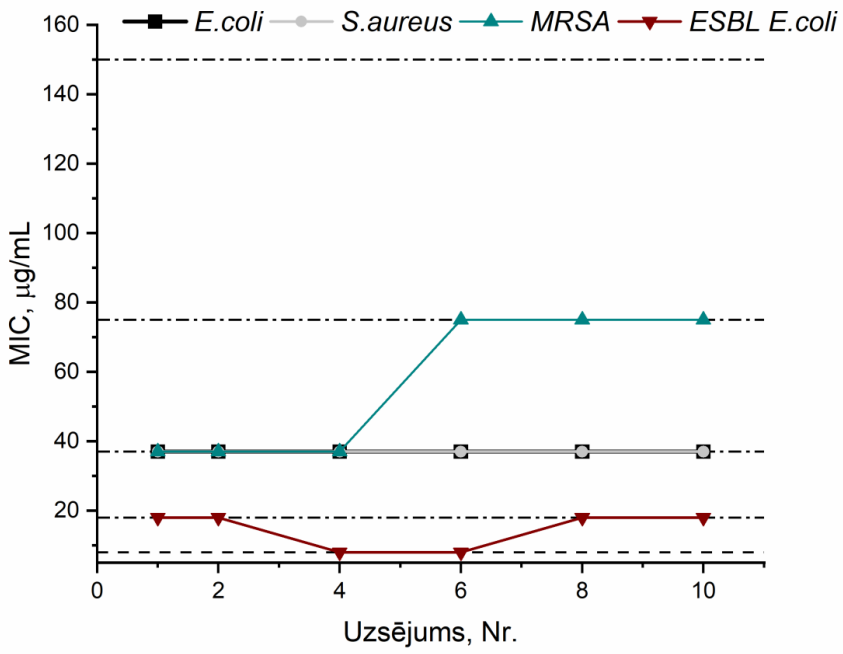

7. att. Tīru ε-PL rezistences attīstības pētījumi tika veikti pret *E. coli*, *S. aureus*, MRSA un *ESBL E. coli* . Eksperiments tika veikts 10 uzsējumu garumā, katrā solī pārkultivējot baktēriju kultūras no sub-MIC koncentrācijām.

Tomēr tika novēroti vairāki būtiski rezultāti: (i) inhibīcijas pakāpe, kas tika izteikta kā Log_{10} samazinājums, bija atkarīga no ε-PL masas attiecības hidrogela sastāvā, īpaši izceļas 70 : 30 masas% ε-PL/HA kompozīcija, kas uzrādīja visaugstāko inhibīcijas pakāpi. *S. epidermidis*, *P. aeruginosa* un MRSA baktēriju celmu gadījumā tika panākta pilnīga baktēriju izskaušana; ii) hidrogelu kompozīcijām ar 50 : 50 un 60 : 40 masas% tika novērota skaidra efektīvas inhibīcijas tendence pret grampozitīviem celmiem, tostarp references *S. aureus* un *S. epidermidis*, kā arī klīniski izolēto multirezistentu MRSA. Pretēji tam zemāka inhibīcijas aktivitāte tika konstatēta pret gramnegatīviem celmiem *(E. coli*, *P. aeruginosa* un *ESBL E. coli*). Šīs atšķirības var skaidrot ar gramnegatīvo baktēriju šūnu sienas unikālajām strukturālajām īpatnībām, piemēram, ārējās membrānas klātbūtni, kas darbojas kā papildu barjera polipeptīdu molekulu iekļūšanai, un eflukss sūkņu aktivitāti, kas var samazināt antibakteriālo aģentu intracelulāro uzkrāšanos.

Tika pētīts ε-PL/HA hidrogelu antibakteriālais potenciāls ilgstošā laika periodā (līdz 168 h). Hidrogelu paraugi tika inkubēti vienu nedēļu, veicot barotnes nomaiņas ciklus pēc 1 h un 24 h inkubācijas. Šāda pieeja tika izvēlēta, lai izvērtētu, vai pēc sākotnējās straujās nešķērssaistītā ε-PL izdalīšanās, kas sagaidāma pirmajās 24 h, ε-PL/HA hidrogela matrica spēj nodrošināt pakāpenisku ε-PL izdalīšanos saistībā ar matricas degradāciju. Pēc 168 h tika veikti gan tiešā kontakta, gan netiešā (supernatants) kontakta antibakteriālie testi, izmantojot 24 h ekspozīciju pret gramnegatīvo *E. coli* un grampozitīvo *S. aureus* (8. B att.). Rezultāti parādīja, ka visi hidrogelu sastāvi joprojām spēja veikt statistiski nozīmīgu antibakteriālo aktivitāti ($p < 0,05$) abos ekspozīcijas veidos: gan tiešā baktēriju kontaktā ar hidrogela matricu, gan netiešā kontaktā ar supernatantiem, kas iegūti pēc 168 h. Ievērojami, ka 50 : 50 masas% ε-PL/HA hidrogela kompozīcija uzrādīja zemāko inhibīcijas pakāpi, salīdzinot ar citām kompozīcijām abos ekspozīcijas veidos pret *S. aureus*, kas varētu tikt skaidrots ar tā blīvāku un kompaktāku matricu, kuras dēļ samazinās degradācijas ātrums un ierobežojas pozitīvi lādēto funkcionālo grupu pieejamība hidrogela virsmā.

Citotoksicitāte tika izvērtēta, izmantojot gan tiešā, gan netiešā kontakta testus (8. C–D att.). Netiešajā testā (8. D att.), izmantojot cilvēka dermas fibroblastus (HDF), visas ε-PL/HA hidrogelu sērijas neuzrādīja citotoksicitāti pie ekstrakta koncentrācijām līdz 4,35 mg/mL, jo šūnu dzīvotspēja pēc 48 h ekspozīcijas saglabājās virs 70 % (*ISO 10993-5:2009* [67] noteiktais slieksnis citotoksicitātes neesamībai). Ievērojami, ka pie ekstrakta koncentrācijas 2,025 mg/mL šūnu dzīvotspēja bija būtiski augstāka nekā kontroles paraugos, kas liecina, ka ε-PL atbilstošās koncentrācijās var veicināt šūnu proliferāciju. Interesanti, ka 50 : 50 masas% ε-PL/HA kompozīcija neuzrādīja citotoksicitāti (šūnu dzīvotspēja > 70 %) HDF šūnām līdz pat 93,023 mg/mL [2]. Šis rezultāts korelē ar ilgtermiņa antibakteriālajiem pētījumiem, kuros tā pati kompozīcija demonstrēja zemāku antibakteriālo aktivitāti, iespējams, blīvākas un kompaktākas šķērssaistītās matricas dēļ, kas samazināja ε-PL izdalīšanos un virsmas lādiņu. Savukārt 60 : 40 masas% kompozīcijai tika novērota citotoksiskā iedarbība jau pie 20,12 mg/mL, savukārt 70 : 30 masas% kompozīcijai – pie tik zemas koncentrācijas kā 9,36 mg/mL, kas liecina par korelāciju starp pieaugošo ε-PL saturu hidrogelu paraugos un samazinātu šūnu dzīvotspēju. Pie koncentrācijas ≥ 93,023 mg/mL visas kompozīcijas uzrādīja būtisku citotoksicitāti [2]. Tiešā kontakta pētījumos ar Balb/c 3T3 šūnām (8. C att.) pēc 24 h ekspozīcijas tika konstatēta viegla citotoksicitāte visās ε-PL/HA hidrogelu sērijās, šūnu dzīvotspējai saglabājoties tuvu pieļaujamajam slieksnim (~ 70 %): 69,5 ± 16,8; 65,3 ± 17,4 un

71,5 ± 7,9 attiecīgi 50 : 50, 60 : 40 un 70 : 30 masas% hidrogelu kompozīcijām. Statistiski nozīmīgas atšķirības starp kompozīcijām netika konstatētas.

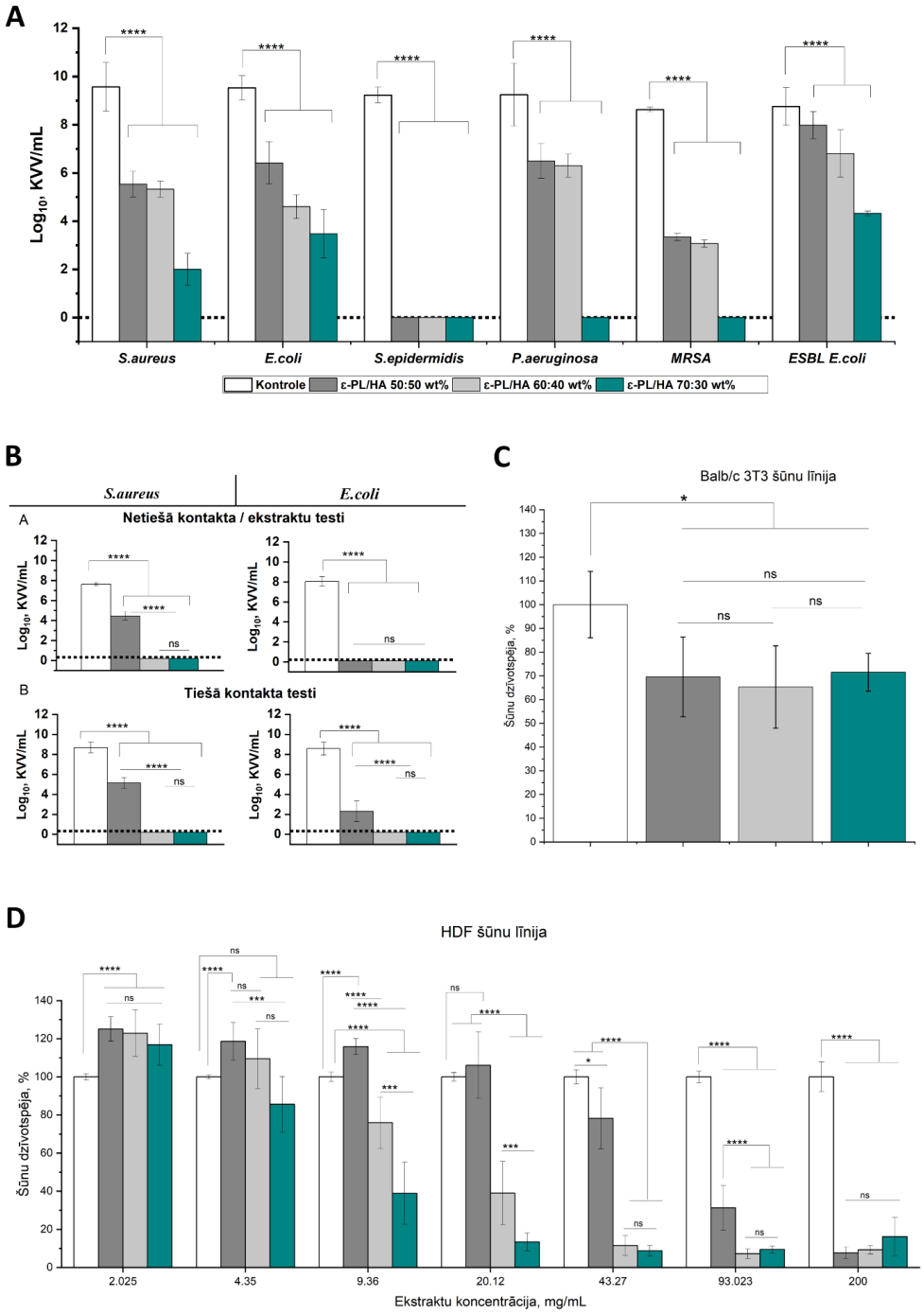

8. att. Sagatavoto ε-PL/HA hidrogelu *in vitro* pētījumi [2]. Visām ε-PL/HA hidrogelu kompozīcijām grafikos tika izmantota vienota krāsu palete, kas norādīta leģendā zem A grafika. (A) Tiešā kontakta pētījumi, izmantojot buljona atšķaidīšanas metodi pret dažādiem

gramnegatīviem un grampozitīviem baktēriju celmiem. Inhibīcijas rezultāti attēloti kā Log_{10} baktēriju skaita samazinājums. (B) Tiešā kontakta un netiešie (uz supernatanta bāzes) antibakteriālie pētījumi pēc 168 h inkubācijas ar barotnes nomaiņu 1 h un 24 h laikā pret *E. coli* un *S. aureus*. (C) Tiešā šūnu dzīvotspējas noteikšana, izmantojot Balb/c šūnu līniju pēc 24 h ekspozīcijas. (D) Netiešā šūnu dzīvotspējas noteikšana, izmantojot HDF šūnu līniju pēc 48 h ekspozīcijas dažādās ekstraktu koncentrācijās. Katrā eksperimentā tika veikti trīs atkārtojumi, un rezultāti attēloti kā vidējā vērtība ± SD.

Apkopojot iepriekš teikto, antibakteriālo īpašību izpēte parādīja, ka ε-PL/HA hidrogeliem piemīt inhibējošā aktivitāte pret plašu grampozitīvo un gramnegatīvo baktēriju spektru, tostarp klīniski nozīmīgiem un multirezistentiem celmiem. Turklāt *in vitro* netiešais citotoksicitātes tests (48 h) atklāja ε-PL devas atkarību no šūnu dzīvotspējas. Šie rezultāti nepārprotami liecina, ka gan antibakteriālo aktivitāti, gan šūnu dzīvotspēju ε-PL/HA hidrogelos iespējams modulēt, mainot ε-PL koncentrāciju hidrogela matricā. Starp testētajām kompozīcijām visdaudzsološākā izrādījās ε-PL/HA 50 : 50 masas% kompozīcija, kas nodrošināja nozīmīgu un noturīgu antibakteriālo aktivitāti pret dažādiem baktēriju celmiem, vienlaikus saglabājot pozitīvu šūnu dzīvotspēju, tādējādi panākot labvēlīgu līdzsvaru starp antibakteriālo efektivitāti un bioloģisko saderību.

Antibakteriālu Sr-HAp funkcionalizētu ε-PL/HA hidrogelu sintēze un raksturošana (5. publikācija)

Iepriekš izstrādātā ε-PL/HA hidrogela kompozīcija ar 50 : 50 masas% masas attiecību uzrādīja ātras iedarbības (līdz 24 h) un ilgstošu (līdz 168 h) antibakteriālo aktivitāti pret plašu patogēnu spektru, vienlaikus demonstrējot labvēlīgu šūnu dzīvotspēju, piemērotību tvaika sterilizācijai, injicējamību un vienmērīgu virsmas topoloģiju. Balstoties šajās īpašībās, 50 : 50 masas% ε-PL/HA hidrogela kompozīcija tika izvēlēta tālākai kompozītsistēmas izstrādei, funkcionālajai modifikācijai ar stronciju aizvietota hidroksilapatīta (Sr-HAp) nanodaļiņām. Šīs funkcionālās modifikācijas mērķis bija apvienot abu komponentu priekšrocības: izstrādātās ε-PL/HA hidrogela matricas viskoelastīgās un dabiski antibakteriālās īpašības ar Sr-HAp nanodaļiņu kaulaudu reģenerāciju veicinošo iedarbību, izstrādājot antibakteriālus un bioaktīvus hidrogelus kaulaudu inženierijas lietojumiem. Šajā pētījumā izstrādātas vairākas kompozīcijas, tostarp tīra ε-PL/HA hidrogela matrica ar 50 : 50 masas% attiecību un Sr-HAp/ε-PL/HA kompozīthidrogeli ar dažādām neorganiskās (Sr-HAp) un organiskās (ε-PL/HA 50 : 50 masas%) fāzes masas attiecību – 40 %, 50 % un 60 % (9. A att.).

Injicējamība ir nozīmīga biomateriālu īpašība, jo īpaši kaulu reģenerācijas lietojumos, tāpēc tika pētīts sagatavoto hidrogelu injekcijas spēks (9. B att.). Rezultāti parādīja, ka visas kompozīcijas, ieskaitot tīru ε-PL/HA hidrogelu , var injicēt caur šļirci ar uzgaļa iekšējo diametru 1,8 mm, lietojot 3 N injekcijas spēku. Saskaņā ar literatūras datiem, adatu izmēri diapazonā no 10 mm (iekšējais diametrs 2,69 mm) līdz 16 mm (iekšējais diametrs 1,19 mm) tiek uzskatīti par piemērotiem ortopēdiskām procedūrām, piemēram, kaula defektu un plaisu aizpildīšanai [68]. Turklāt injekcijas spēkam jāpaliek zem 30 N, kas tiek definēts kā manuālās injicējamības augšējā robeža [69]. Balstoties šajos kritērijos, izstrādātie hidrogeli klasificējami kā manuāli injicējami un potenciāli piemēroti klīniskām lietojuma vajadzībām.

Lai turpmāk izvērtētu Sr-HAp/ε-PL/HA hidrogelu viskoelastīgās īpašības, tika veikti spiedes testi kā daļa no to reoloģiskās raksturošanas. Spiedes testu rezultāti (9. C att.) atklāja līdzīgu uzvedību un kompresijas krājuma moduļa (E') vērtības ~ 1000 kPa visām testētajām sērijām frekvences diapazonā, kas attiecas uz fizioloģiskajiem apstākļiem (0,1–10 Hz). Saskaņā ar literatūras datiem, parasti kaulaudu reģenerācijai paredzēto kompozīthidrogelu kompresijas krājuma modulis (E') ir robežās no 100 kPa līdz vairākiem MPa [70], [71]. Tādējādi var secināt, ka izstrādāto Sr-HAp/ε-PL/HA hidrogelu kompresijas krājuma moduļa vērtības atbilst šim diapazonam un tos var izmantot kā biomateriālus kaulaudu reģenerācijai. Tomēr jāatzīmē, ka šie pētījumi nesniedz visaptverošu mehānisko īpašību novērtējumu, jo īpaši dinamiskas slodzes vai nestspējas apstākļos. Tāpēc Sr-HAp/ε-PL/HA hidrogelus nevar uzskatīt par piemērotiem lietojumaslodzi nesošās vietās. Neskatoties uz to, tie var kalpot kā daudzsološi biomateriāli, kas nodrošina labvēlīgus apstākļus dabiskajam kaula pārveidošanās procesam, saglabājot barības vielu transportu, nodrošinot porainību šūnu migrācijai, strukturālo integritāti un imitējot galvenās ekstracelulāras matricas īpašības [72].

Lai papildinātu iepriekš definēto praktisko funkcionalitāti, turpmākajos pētījumos tika veikta enzīmatiskās degradācijas un jonu izdalīšanās (Ca^{2+} un Sr^{2+}) kinētisko profilu analīze. Enzīmatiskās degradācijas līknes (9. D att.) parādīja, ka Sr-HAp/ε-PL/HA hidrogeli degradējas hialuronidāzi saturošā PBS vidē 20 nedēļu laikā. Savukārt 0% Sr-HAp kompozīcijas uzrādīja pakāpenisku degradācijas gaitu, sasniedzot pilnīgu degradāciju 20 nedēļās, 40 %, 50 % un 60 % Sr-HAp kompozīcijas degradējās straujāk, attiecīgi pilnībā noārdoties jau pēc 5, 10 un 16 nedēļām. Šie rezultāti liecina, ka Sr-HAp/ε-PL/HA hidrogelu biodegradācijas profils ir atkarīgs no Sr-HAp satura un to iespējams regulēt, lai pielāgotu konkrētām kaulaudu reģenerācijas lietojuma prasībām. Attiecībā uz jonu izdalīšanās līknēm tika novērots, ka Ca^{2+} un Sr^{2+} joni no hidrogelu matricas tika izdalīti strauji (*burst release*), salīdzinot ar tīra Sr-HAp izdalīšanās profilu (9. E–F att.). Iespējamais iemesls ir ε-PL/HA hidrogelu matricas skābā daba, kas var veicināt Sr-HAp šķīšanu un izraisīt straujo jonu izdalīšanos pirmajās eksperimenta dienās. Pēc tam Ca^{2+} un Sr^{2+} jonu izdalīšanās no Sr-HAp/ε-PL/HA hidrogeliem turpinājās lēni un nepārtraukti visa trīs mēnešu eksperimentālā perioda laikā. Būtiski, ka Sr^{2+} jonu koncentrācija nepārsniedza 20–30 μM, savukārt Ca^{2+} jonu izdalīšanās bija 200–350 μM diapazonā. Iepriekšējie pētījumi ir parādījuši, ka Sr^{2+} jonu koncentrācijas līdz 40 μM veicina osteoblastu proliferāciju šūnu kultūrās [73], savukārt paaugstināta Ca^{2+} jonu koncentrācija līdz 900 μM var vēl vairāk pastiprināt Sr^{2+} jonu kaulaudu reģeneratīvo efektu [74].

A

Apzīmējums	Kompozīcija
0 % Sr-HAp	100% ε-PL-HA (ε-PL:HA 50:50 wt%)
40 % Sr-HAp	Sr-HAp 40 wt%, ε-PL/HA 60 wt%
50 % Sr-HAp	Sr-HAp 50 wt%, ε-PL/HA 50 wt%
60 % Sr-HAp	Sr-HAp 60 wt%, ε-PL/HA 40 wt%

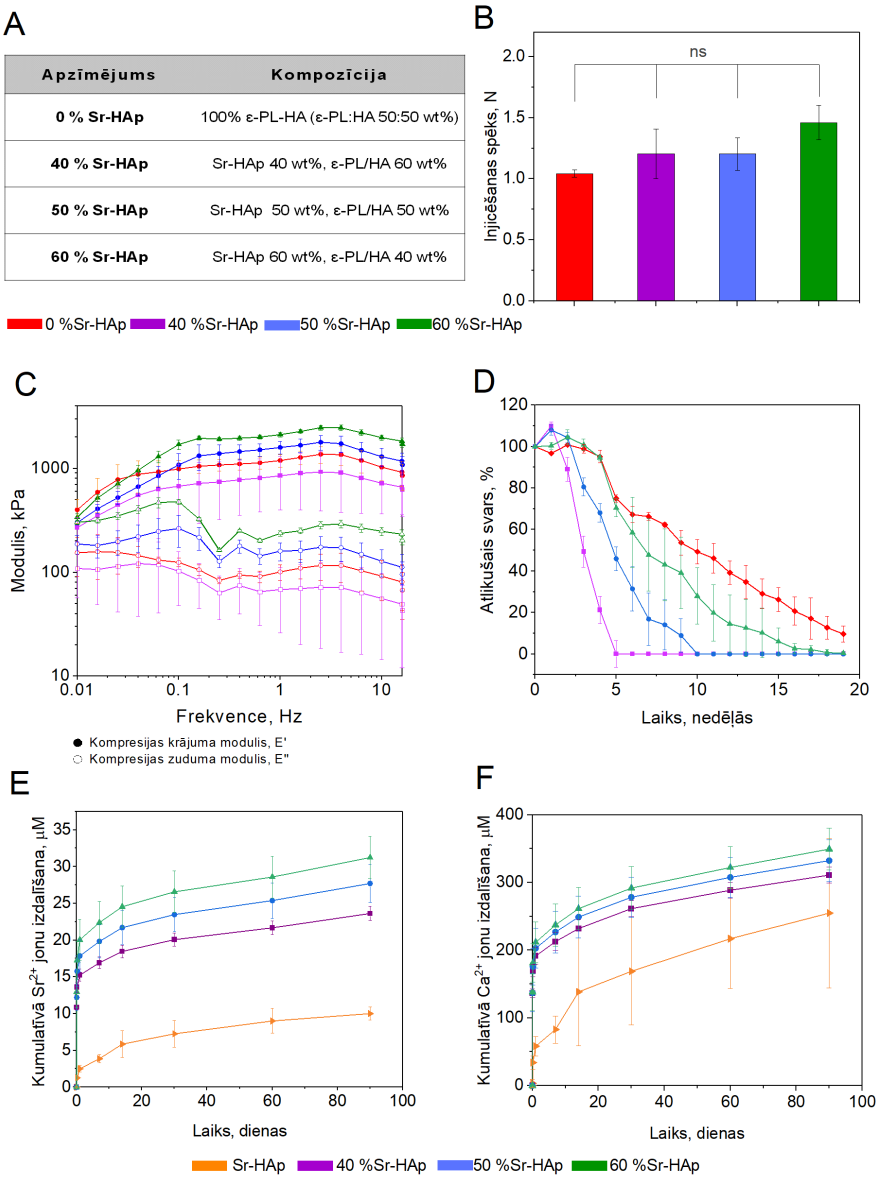

9. att. Sr-HAp/ε-PL/HA hidrogelu fizikālķīmisko īpašību pētījumi [72]. (A) Sr-HAp/ε-PL/HA hidrogelu apzīmējumi un sastāvs, kas izmantoti turpmākajos eksperimentālajos pētījumos. (B) Injekcijas spēku pētījumi. Starp izmantotajām kompozīcijām netika konstatētas statistiski nozīmīgas injekcijas spēka vērtību atšķirības (ns, $p > 0,05$). (C) Kompresijas pētījumi hidrogelu reoloģiskās izpētes ietvaros. Spiedes testi tika veikti pie 8 N aksiālā spēka (aksiālais spēks > dinamiskais spēks = 30 %), ar 30 µm aksiālo pārvietojumu frekvenču diapazonā no 0,01 Hz līdz 16 Hz. Tika monitorēts kompresijas krājuma modulis (E') un kompresijas zuduma modulis (E"). (D) Sr-HAp/ε-PL/HA hidrogelu enzīmatiskās degradācijas līknes hialuronidāzi saturošā PBS vidē 20 nedēļu periodā. (E) Sr^{2+} jonu izdalīšanās pētījumi. (F) Ca^{2+} jonu izdalīšanās pētījumi. (E–F) Sr-HAp/ε-PL/HA hidrogelu jonu izdalīšanās

pētījumi veikti 90 dienu periodā, rezultāti attēloti μM koncentrācijā. Katrā eksperimentā tika veikti trīs atkārtojumi, un rezultāti attēloti kā vidējā vērtība ± SD.

Noslēgumā tika izvērtēta Sr-HAp/ε-PL/HA hidrogelu antibakteriālā aktivitāte gan īstermiņa (24 h), gan ilgtermiņa (līdz 168 h) laika periodā (10. att.). Eksperimentālie laika punkti tika noteikti 24 h, 48 h, 72 h un 168 h, un pētījumi tika veikti pret grampozitīvajiem *S. aureus* (*Staphylococcus aureus*, *ATCC* 25923, references celms), MRSA (pret meticilīnu rezistents *Staphylococcus aureus*, klīniski izolēts multirezistents celms), kā arī pret gramnegatīvām baktērijām *E. coli* (*Escherichia coli*, *ATCC* 25922, references celms), *ESBL E. coli* (paplašināta spektra β-laktamāzi producējošs *Escherichia coli*, klīniski izolēts multirezistents celms). Iegūtie rezultāti atklāja, ka Sr-HAp/ε-PL/HA hidrogelu eksperimentālās sērijas spēj inhibēt gan references, gan klīniski izolētos multirezistentos gramnegatīvos un grampozitīvos baktēriju celmus. Tomēr jāuzsver vairākas tendences un nianses. Pirmkārt, tika novērota augstāka inhibīcijas pakāpe pret grampozitīvajām baktērijām, tostarp gan references, gan rezistentajiem celmiem. Šie rezultāti saskan ar iepriekšējiem tīro ε-PL/HA hidrogelu pētījumu rezultātiem (8. A att.), un līdzīgi tika atkārtoti novēroti arī 0 % Sr-HAp gadījumā. Kopumā relatīvi augsta inhibīcijas pakāpe saglabājās visām Sr-HAp/ε-PL/HA hidrogelu sērijām visa eksperimentālā perioda laikā. Otrkārt, salīdzinoši zemāka inhibīcijas pakāpe, salīdzinot ar grampozitīvajām baktērijām, tika novērota pret gramnegatīvajām baktērijām (gan references, gan klīniskajiem izolātiem). Pie 24 h laika punkta 0 % Sr-HAp kompozīcijas antibakteriālā aktivitāte sakrita ar ε-PL/HA hidrogelu ar 50 : 50 masas% iegūtajiem rezultātiem (8. A att.). Turklāt statistiski nozīmīga *E. coli* un *ESBL E. coli* inhibīcija visām eksperimentālajām sērijām tika novērota tikai īstermiņa laikā periodā (24 h).

Kā jau iepriekš tika pieņemts, iespējams, šo rezultātu var skaidrot ar gramnegatīvo baktēriju unikālo šūnu sieniņu struktūru un efektīvāku efluksa sūkņu sistēmām. Treškārt, tika skaidri novērots, ka 0 % Sr-HAp hidrogela kompozīcija vairākos laika punktos (*E. coli*: 24 h; MRSA: 72 h) uzrāda salīdzinoši augstāku inhibīcijas līmeni un dažos gadījumos ir vienīgā, kas uzrāda statistiski nozīmīgu inhibīciju (*E. coli*: 48 h un 72 h; *ESBL E. coli*: 48 h un 72 h). Šādus rezultātus varētu izskaidrot ar Sr-HAp neorganiskās fāzes klātbūtni hidrogela matricā 40 %, 50 % un 60 % Sr-HAp hidrogelu kompozīcijās. Funkcionalizācija ar Sr-HAp nanodaļiņām palielina fizikālo saišu skaitu starp ε-PL/HA hidrogela matricu un pozitīvi lādētajiem Ca^{2+}/Sr^{2+} joniem, veidojot fizisku barjeru un veicinot tīkla pārkārtošanos kompaktākā konfigurācijā. Tas negatīvi ietekmē antibakteriālo ε-PL molekulu atbrīvošanās kinētiku un samazina hidrogelu antibakteriālo potenciālu [75]. Visbeidzot, starp 40 %, 50 % un 60 % Sr-HAp hidrogeliem nevienā no pārbaudītajiem laika punktiem netika novērotas statistiski nozīmīgas atšķirības ($p > 0,05$), kas liecina, ka Sr-HAp klātbūtne būtiski neietekmē izstrādāto Sr-HAp/ε-PL/HA hidrogelu antibakteriālo aktivitāti.

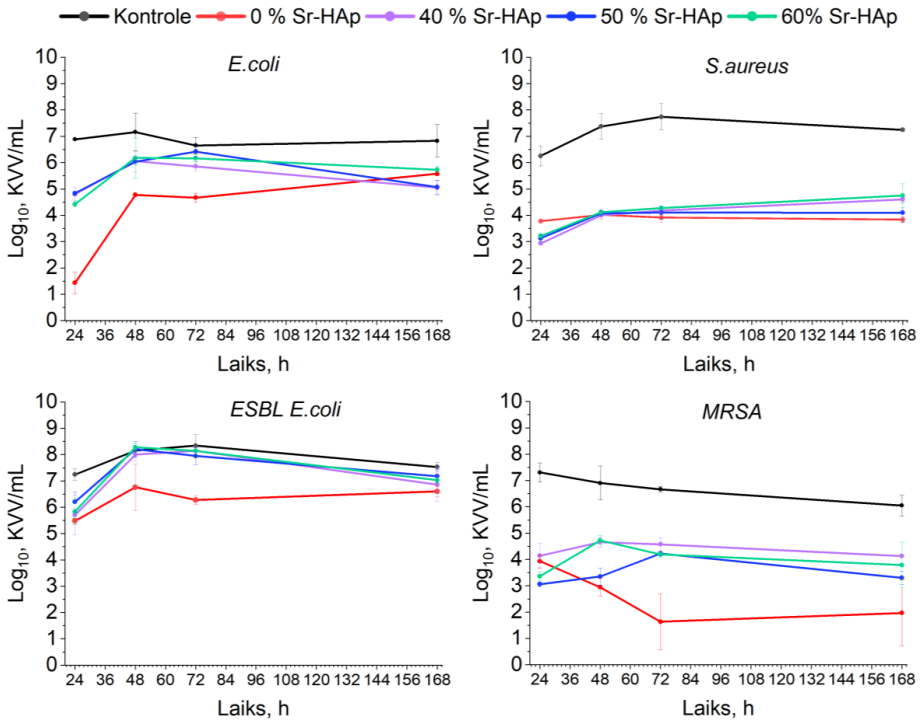

10. att. Sagatavoto Sr-HAp/ε-PL/HA hidrogelu antibakteriālā aktivitāte (24–168 h) pret *E. coli*, *S. aureus*, *ESBL E. coli* un MRSA baktēriju celmiem (n = 3) [72].

SECINĀJUMI

1. Izstrādāta reproducējama sintēzes metodoloģija ķīmiski šķērssaistītu, injicējamu ε-PL/HA hidrogelu iegūšanai, izmantojot *EDC*/NHS (0,24:0,24 mol) ķīmiju, ar ε-PL un HA masas attiecību 40 : 60, 50 : 50, 60 : 40, 70 : 30 un 80 : 20 masas%,
2. Izstrādātie ε-PL/HA hidrogeli uzrādīja īpašības, kas ir nozīmīgas antibakteriāliem lietojumiem audu inženierijā, tostarp: regulējams brīvo ε-grupu saturs (mainot ε-PL masas attiecību); stabila gela frakcija (50–60 %); (c) mehāniskā stingrība 5–15 kPa diapazonā, gluda virsmas topoloģija; injicējamība caur 19 G adatu; augsta atjaunošanās spēja pēc injekcijas (85–95 %) un autoklāvējamība 121 °C / 20 min. Šīs īpašības nodrošina ε-PL devas atkarīgu antibakteriālo aktivitāti, uzrādot 2–3 Log_{10} *E. coli* MSCL 332 samazinājumu jau pēc 1 h kontakta.
3. Tvaika sterilizācija (121 °C, 20 min) būtiski neietekmēja gela frakciju ($p > 0,05$), poru izmēru sadalījumu (66–200 μm); uzbriešanu (150–300 % pēc 2 h, līdzsvars pēc 4 h) un mehānisko stingrību, vienlaikus saglabājot antibakteriālo aktivitāti ar 4–9 Log_{10} baktēriju samazinājumu pēc sterilizācijas.
4. ε-PL/HA hidrogeli uzrādīja ε-PL devas atkarīgu antibakteriālo aktivitāti han īstermiņā (līdz 24 h), gan ilgtermiņā (līdz 168 h), tiešā un netiešā kontaktā pret *E. coli*, *S. aureus*, *P. aeruginosa*, kā arī klīniski nozīmīgiem multirezistentiem celmiem – MRSA, ESBL *E. coli*. Viena mēneša laikā (10 uzsējumi) references un multirezistentajos celmos netika novērota rezistences attīstība pret ε-PL.
5. Citotoksicitātes testi parādīja 70–90 % šūnu dzīvotspēju ε-PL/HA hidrogelos ar peļu fibroblastu šūnu līniju Balb/c 3T3, savukārt tīra ε-PL IC_{50} tika noteikts ar vērtību 4,21 mg/mL. Netiešie ekstraktu citotoksicitātes testi ar cilvēka ādas fibroblastiem (HDF) apstiprināja necitotoksisku iedarbību koncentrācijās ≤ 4,35 mg/mL, kas atbilst ε-PL devas atkarīgai izstrādāto hidrogelu bioloģiskai saderībai.
6. Sr-HAp/ε-PL/HA hidrogeli tika veiksmīgi izstrādāti un demonstrēja sinerģisku efektu starp ε-PL/HA hidrogeliem un Sr-HAp nanodaļiņām, nodrošinot ilgstošu Sr^{2+} (20–30 μM) un Ca^{2+} (200–350 μM) jonu izdalīšanos 90 dienu laikā, saglabātu injicējamību un regulējamu enzimātisko degradāciju atkarībā no Sr-HAp satura (pilnīga degradācija 5–20 nedēļās). Kompozīthidrogeli uzrādīja ātru antibakteriālo iedarbību (pēc 24 h) gan pret references, gan multirezistentiem baktēriju celmiem, kā arī ilgstošu antibakteriālo aktivitāti (līdz 168 h), īpaši pret *S. aureus* un klīniski izolēto multirezistentu MRSA.

ATSAUCES

[1] *7.7 million people die from bacterial infections every year – 2022 – ReAct*. https://www.reactgroup.org/news-and-views/news-and-opinions/year-2022/7-7-million-people-die-from-bacterial-infections-every-year/ (accessed 2025-02-19).

[2] Sceglovs, A.; Skadins, I.; Siverino, C.; Pirsko, V.; Sceglova, M.; Moriarty, F. T.; Kroica, J.; Salma-Ancane, K. Injectable ε-Polylysine/Hyaluronic Acid Hydrogels with Resistance-Preventing Antibacterial Activity for Treating Wound Infections. *ACS Appl. Bio Mater.*, **2025**, *8* (11), 9916–9930. https://doi.org/10.1021/acsabm.5c01252.

[3] Bilal, M.; Iqbal, H. M. N. Naturally-Derived Biopolymers: Potential Platforms for Enzyme Immobilization. *Int. J. Biol. Macromol.* **2019**, *130*, 462–482. https://doi.org/10.1016/J.IJBIOMAC.2019.02.152.

[4] Sceglovs, A.; Skadins, I.; Chitto, M.; Kroica, J.; Salma-Ancane, K. Failure or Future? Exploring Alternative Antibacterials: A Comparative Analysis of Antibiotics and Naturally Derived Biopolymers. *Front. Microbiol.* **2025**, *16*, 1526250. https://doi.org/10.3389/FMICB.2025.1526250.

[5] Sun, Y.; Bai, Y.; Yang, W.; Bu, K.; Tanveer, S. K.; Hai, J. Global Trends in Natural Biopolymers in the 21st Century: A Scientometric Review. *Front. Chem.* **2022**, *10*, 915648. https://doi.org/10.3389/FCHEM.2022.915648.

[6] Pahlevanzadeh, F.; Setayeshmehr, M.; Bakhsheshi-Rad, H. R.; Emadi, R.; Kharaziha, M.; Poursamar, S. A.; Ismail, A. F.; Sharif, S.; Chen, X.; Berto, F. A Review on Antibacterial Biomaterials in Biomedical Applications: From Materials Perspective to Bioinks Design. *Polym. 2022,* **2022**, *14* (11), 2238. https://doi.org/10.3390/POLYM14112238.

[7] Sam, S.; Joseph, B.; Thomas, S. Exploring the Antimicrobial Features of Biomaterials for Biomedical Applications. *Results Eng.* **2023**, *17*, 100979. https://doi.org/10.1016/J.RINENG.2023.100979.

[8] Coma, V. Polysaccharide-Based Biomaterials with Antimicrobial and Antioxidant Properties. *Polimeros* **2013**, *23* (3), 287–297. https://doi.org/10.4322/POLIMEROS020OV002.

[9] Khara, J. S.; Mojsoska, B.; Mukherjee, D.; Langford, P. R.; Robertson, B. D.; Jenssen, H.; Ee, P. L. R.; Newton, S. M. Ultra-Short Antimicrobial Peptoids Show Propensity for Membrane Activity Against Multi-Drug Resistant Mycobacterium Tuberculosis. *Front. Microbiol.* **2020**, *11*, 515317. https://doi.org/10.3389/FMICB.2020.00417.

[10] Jacobo-Delgado, Y. M.; Rodríguez-Carlos, A.; Serrano, C. J.; Rivas-Santiago, B. Mycobacterium Tuberculosis Cell-Wall and Antimicrobial Peptides: A Mission Impossible? *Front. Immunol.* **2023**, *14*, 1194923.

https://doi.org/10.3389/FIMMU.2023.1194923.

[11] Intorasoot, S.; Intorasoot, A.; Tawteamwong, A.; Butr-Indr, B.; Phunpae, P.; Tharinjaroen, C. S.; Wattananandkul, U.; Sangboonruang, S.; Khantipongse, J. In Vitro Antimycobacterial Activity of Human Lactoferrin-Derived Peptide, D-HLF 1-11, against Susceptible and Drug-Resistant Mycobacterium Tuberculosis and Its Synergistic Effect with Rifampicin. *Antibiot. 2022,* **2022**, *11* (12), 1785. https://doi.org/10.3390/ANTIBIOTICS11121785.

[12] C Reygaert, W. An Overview of the Antimicrobial Resistance Mechanisms of Bacteria. *AIMS Microbiol.* **2018**, *4* (3), 482–501. https://doi.org/10.3934/MICROBIOL.2018.3.482.

[13] Sceglovs, A.; Wychowaniec, J. K.; Skadins, I.; Reinis, A.; Edwards-Gayle, C. J. C.; D'Este, M.; Salma-Ancane, K. Effect of Steam Sterilisation on Physico-Chemical Properties of Antibacterial Covalently Cross-Linked ε-Polylysine/Hyaluronic Acid Hydrogels. *Carbohydr. Polym. Technol. Appl.* **2023**, *6*, 100363. https://doi.org/10.1016/J.CARPTA.2023.100363.

[14] Harvey, N.; Dennison, E.; Cooper, C. Osteoporosis: Impact on Health and Economics. *Nat. Rev. Rheumatol. 2010 62* **2010**, *6* (2), 99–105. https://doi.org/10.1038/nrrheum.2009.260.

[15] Sozen, T.; Ozisik, L.; Calik Basaran, N. An Overview and Management of Osteoporosis. *Eur. J. Rheumatol.* **2017**, *4* (1), 46–56. https://doi.org/10.5152/EURJRHEUM.2016.048.

[16] Hou, X.; Zhang, L.; Zhou, Z.; Luo, X.; Wang, T.; Zhao, X.; Lu, B.; Chen, F.; Zheng, L. Calcium Phosphate-Based Biomaterials for Bone Repair. *J. Funct. Biomater. 2022, Vol. 13, Page 187* **2022**, *13* (4), 187. https://doi.org/10.3390/JFB13040187.

[17] Tozzi, G.; De Mori, A.; Oliveira, A.; Roldo, M. Composite Hydrogels for Bone Regeneration. *Mater. 2016,* **2016**, *9* (4), 267. https://doi.org/10.3390/MA9040267.

[18] Zhang, Y.; Shu, T.; Wang, S.; Liu, Z.; Cheng, Y.; Li, A.; Pei, D. The Osteoinductivity of Calcium Phosphate-Based Biomaterials: A Tight Interaction With Bone Healing. *Front. Bioeng. Biotechnol.* **2022**, *10*, 911180. https://doi.org/10.3389/FBIOE.2022.911180.

[19] Inzana, J. A.; Schwarz, E. M.; Kates, S. L.; Awad, H. A. Biomaterials Approaches to Treating Implant-Associated Osteomyelitis. *Biomaterials* **2016**, *81*, 58–71. https://doi.org/10.1016/J.BIOMATERIALS.2015.12.012.

[20] van Vugt, T. A. G.; Arts, J. J.; Geurts, J. A. P. Antibiotic-Loaded Polymethylmethacrylate Beads and Spacers in Treatment of Orthopedic Infections and the Role of Biofilm Formation. *Front. Microbiol.* **2019**, *10*. https://doi.org/10.3389/FMICB.2019.01626.

[21] Freischmidt, H.; Armbruster, J.; Reiter, G.; Grützner, P. A.; Helbig, L.; Guehring, T. Individualized Techniques of Implant Coating with an Antibiotic-Loaded, Hydroxyapatite/Calcium Sulphate Bone Graft Substitute. *Ther. Clin. Risk Manag.* **2020**, *16*, 689–694. https://doi.org/10.2147/TCRM.S242088.

[22] Dovedytis, M.; Liu, Z. J.; Bartlett, S. Hyaluronic Acid and Its Biomedical Applications: A Review. *Eng. Regen.* **2020**, *1*, 102–113. https://doi.org/10.1016/J.ENGREG.2020.10.001.

[23] Wang, M.; Deng, Z.; Guo, Y.; Xu, P. Designing Functional Hyaluronic Acid-Based Hydrogels for Cartilage Tissue Engineering. *Mater. Today Bio* **2022**, *17*, 100495. https://doi.org/10.1016/J.MTBIO.2022.100495.

[24] Salma-Ancane, K.; Sceglovs, A.; Tracuma, E.; Wychowaniec, J. K.; Aunina, K.; Ramata-Stunda, A.; Nikolajeva, V.; Loca, D. Effect of Crosslinking Strategy on the Biological, Antibacterial and Physicochemical Performance of Hyaluronic Acid and ε-Polylysine Based Hydrogels. *Int. J. Biol. Macromol.* **2022**, *208*, 995–1008. https://doi.org/10.1016/J.IJBIOMAC.2022.03.207.

[25] Sionkowska, A.; Kulka-Kamińska, K.; Brudzyńska, P.; Lewandowska, K.; Piwowarski, Ł. The Influence of Various Crosslinking Conditions of EDC/NHS on the Properties of Fish Collagen Film. *Mar. Drugs 2024,* **2024**, *22* (5), 194. https://doi.org/10.3390/MD22050194.

[26] Munir, M. U.; Salman, S.; Javed, I.; Bukhari, S. N. A.; Ahmad, N.; Shad, N. A.; Aziz, F. Nano-Hydroxyapatite as a Delivery System: Overview and Advancements. *Artif. Cells, Nanomedicine, Biotechnol.* **2021**, *49* (1), 717–727. https://doi.org/10.1080/21691401.2021.2016785.

[27] Lee, N. H.; Kang, M. S.; Kim, T. H.; Yoon, D. S.; Mandakhbayar, N.; Jo, S. Bin; Kim, H. S.; Knowles, J. C.; Lee, J. H.; Kim, H. W. Dual Actions of Osteoclastic-Inhibition and Osteogenic-Stimulation through Strontium-Releasing Bioactive Nanoscale Cement Imply Biomaterial-Enabled Osteoporosis Therapy. *Biomaterials* **2021**, *276*, 121025. https://doi.org/10.1016/J.BIOMATERIALS.2021.121025.

[28] Pan, H. B.; Li, Z. Y.; Lam, W. M.; Wong, J. C.; Darvell, B. W.; Luk, K. D. K.; Lu, W. W. Solubility of Strontium-Substituted Apatite by Solid Titration. *Acta Biomater.* **2009**, *5* (5), 1678–1685. https://doi.org/10.1016/J.ACTBIO.2008.11.032.

[29] Stipniece, L.; Wilson, S.; Curran, J. M.; Chen, R.; Salma-Ancane, K.; Sharma, P. K.; Meenan, B. J.; Boyd, A. R. Strontium Substituted Hydroxyapatite Promotes Direct Primary Human Osteoblast Maturation. *Ceram. Int.* **2021**, *47* (3), 3368–3379. https://doi.org/10.1016/J.CERAMINT.2020.09.182.

[30] Stipniece, L.; Ramata-Stunda, A.; Vecstaudza, J.; Kreicberga, I.; Livkisa, D.; Rubina,

A.; Sceglovs, A.; Salma-Ancane, K. A Comparative Study on Physicochemical Properties and In Vitro Biocompatibility of Sr-Substituted and Sr Ranelate-Loaded Hydroxyapatite Nanoparticles. *ACS Appl. Bio Mater.* **2023**, *6* (12), 5264–5281. https://doi.org/10.1021/ACSABM.3C00539.

[31] Kołodziejska, B.; Stępień, N.; Kolmas, J. The Influence of Strontium on Bone Tissue Metabolism and Its Application in Osteoporosis Treatment. *Int. J. Mol. Sci. 2021,* **2021**, *22* (12), 6564. https://doi.org/10.3390/IJMS22126564.

[32] Rocha Scardueli, C.; Bizelli-Silveira, C.; Adriana Marcantonio, R. C.; Marcantonio Jr, E.; Stavropoulos, A.; Spin-Neto, R. Systemic Administration of Strontium Ranelate to Enhance the Osseointegration of Implants: Systematic Review of Animal Studies. *Int. J. Implant Dent. 2018 41* **2018**, *4* (1), 1–9. https://doi.org/10.1186/S40729-018-0132-8.

[33] Akram, F.; Imtiaz, M.; Haq, I. ul. Emergent Crisis of Antibiotic Resistance: A Silent Pandemic Threat to 21st Century. *Microb. Pathog.* **2023**, *174*, 105923. https://doi.org/10.1016/J.MICPATH.2022.105923.

[34] *New report calls for urgent action to avert antimicrobial resistance crisis*. https://www.who.int/news/item/29-04-2019-new-report-calls-for-urgent-action-to-avert-antimicrobial-resistance-crisis (accessed 2024-04-02).

[35] Muñoz-Bonilla, A.; Fernández-García, M. Polymeric Materials with Antimicrobial Activity. *Prog. Polym. Sci.* **2012**, *37* (2), 281–339. https://doi.org/10.1016/J.PROGPOLYMSCI.2011.08.005.

[36] Santos, M. R. E.; Fonseca, A. C.; Mendonça, P. V.; Branco, R.; Serra, A. C.; Morais, P. V.; Coelho, J. F. J. Recent Developments in Antimicrobial Polymers: A Review. *Mater. 2016,* **2016**, *9* (7), 599. https://doi.org/10.3390/MA9070599.

[37] Haktaniyan, M.; Bradley, M. Polymers Showing Intrinsic Antimicrobial Activity. *Chem. Soc. Rev.* **2022**, *51* (20), 8584–8611. https://doi.org/10.1039/D2CS00558A.

[38] Smola-Dmochowska, A.; Lewicka, K.; Macyk, A.; Rychter, P.; Pamuła, E.; Dobrzyński, P. Biodegradable Polymers and Polymer Composites with Antibacterial Properties. *Int. J. Mol. Sci. 2023,* **2023**, *24* (8), 7473. https://doi.org/10.3390/IJMS24087473.

[39] Mishra, R.; Panda, A. K.; De Mandal, S.; Shakeel, M.; Bisht, S. S.; Khan, J. Natural Anti-Biofilm Agents: Strategies to Control Biofilm-Forming Pathogens. *Front. Microbiol.* **2020**, *11*, 566325. https://doi.org/10.3389/FMICB.2020.566325.

[40] Melander, R. J.; Basak, A. K.; Melander, C. Natural Products as Inspiration for the Development of Bacterial Antibiofilm Agents. *Nat. Prod. Rep.* **2020**, *37* (11), 1454–1477. https://doi.org/10.1039/D0NP00022A.

[41] Munita, J. M.; Arias, C. A. Mechanisms of Antibiotic Resistance. *Microbiol. Spectr.* **2016**, *4* (2). https://doi.org/10.1128/MICROBIOLSPEC.VMBF-0016-2015.

[42] Peterson, E.; Kaur, P. Antibiotic Resistance Mechanisms in Bacteria: Relationships between Resistance Determinants of Antibiotic Producers, Environmental Bacteria, and Clinical Pathogens. *Front. Microbiol.* **2018**, *9* (NOV), 426686. https://doi.org/10.3389/FMICB.2018.02928.

[43] Abushaheen, M. A.; Muzaheed; Fatani, A. J.; Alosaimi, M.; Mansy, W.; George, M.; Acharya, S.; Rathod, S.; Divakar, D. D.; Jhugroo, C.; Vellappally, S.; Khan, A. A.; Shaik, J.; Jhugroo, P. Antimicrobial Resistance, Mechanisms and Its Clinical Significance. *Dis. Mon.* **2020**, *66* (6). https://doi.org/10.1016/J.DISAMONTH.2020.100971.

[44] Chamidah, A.; Hardoko; Prihanto, A. A. Antibacterial Activities of β-Glucan (Laminaran) against Gram-Negative and Gram-Positive Bacteria. *AIP Conf. Proc.* **2017**, *1844* (1), 20011. https://doi.org/10.1063/1.4983422/748336.

[45] Hyldgaard, M.; Mygind, T.; Vad, B. S.; Stenvang, M.; Otzen, D. E.; Meyer, R. L. The Antimicrobial Mechanism of Action of Epsilon-Poly-L-Lysine. *Appl. Environ. Microbiol.* **2014**, *80* (24), 7758–7770. https://doi.org/10.1128/AEM.02204-14.

[46] Jenssen, H.; Hancock, R. E. W. Antimicrobial Properties of Lactoferrin. *Biochimie* **2009**, *91* (1), 19–29. https://doi.org/10.1016/J.BIOCHI.2008.05.015.

[47] Vedadghavami, A.; Minooei, F.; Mohammadi, M. H.; Khetani, S.; Rezaei Kolahchi, A.; Mashayekhan, S.; Sanati-Nezhad, A. Manufacturing of Hydrogel Biomaterials with Controlled Mechanical Properties for Tissue Engineering Applications. *Acta Biomater.* **2017**, *62*, 42–63. https://doi.org/10.1016/J.ACTBIO.2017.07.028.

[48] Bai, X.; Gao, M.; Syed, S.; Zhuang, J.; Xu, X.; Zhang, X. Q. Bioactive Hydrogels for Bone Regeneration. *Bioact. Mater.* **2018**, *3* (4), 401–417. https://doi.org/10.1016/J.BIOACTMAT.2018.05.006.

[49] Moreira, C. D. F.; Carvalho, S. M.; Florentino, R. M.; França, A.; Okano, B. S.; Rezende, C. M. F.; Mansur, H. S.; Pereira, M. M. Injectable Chitosan/Gelatin/Bioactive Glass Nanocomposite Hydrogels for Potential Bone Regeneration: In Vitro and in Vivo Analyses. *Int. J. Biol. Macromol.* **2019**, *132*, 811–821. https://doi.org/10.1016/J.IJBIOMAC.2019.03.237.

[50] Cross, E. R.; Coulter, S. M.; Pentlavalli, S.; Laverty, G. Unravelling the Antimicrobial Activity of Peptide Hydrogel Systems: Current and Future Perspectives. *Soft Matter* **2021**, *17* (35), 8001–8021. https://doi.org/10.1039/D1SM00839K.

[51] Qu, H.; Yao, Q.; Chen, T.; Wu, H.; Liu, Y.; Wang, C.; Dong, A. Current Status of Development and Biomedical Applications of Peptide-Based Antimicrobial Hydrogels. *Adv. Colloid Interface Sci.* **2024**, *325*, 103099. https://doi.org/10.1016/J.CIS.2024.103099.

[52] Wang, R.; Xu, D.; Liang, L.; Xu, T.; Liu, W.; Ouyang, P.; Chi, B.; Xu, H. Enzymatically

Crosslinked Epsilon-Poly-l-Lysine Hydrogels with Inherent Antibacterial Properties for Wound Infection Prevention. *RSC Adv.* **2016**, *6* (11), 8620–8627. https://doi.org/10.1039/C5RA15616E.

[53] Zou, Y. J.; He, S. S.; Du, J. Z. ε-Poly(L-Lysine)-Based Hydrogels with Fast-Acting and Prolonged Antibacterial Activities. *Chinese J. Polym. Sci. (English Ed.* **2018**, *36* (11), 1239–1250. https://doi.org/10.1007/S10118-018-2156-1.

[54] Kennedy, S. M.; Deshpande, P.; Gallagher, A. G.; Horsburgh, M. J.; Allison, H. E.; Kaye, S. B.; Wellings, D. A.; Williams, R. L. Antimicrobial Activity of Poly-Epsilon-Lysine Peptide Hydrogels Against Pseudomonas Aeruginosa. *Invest. Ophthalmol. Vis. Sci.* **2020**, *61* (10), 18–18. https://doi.org/10.1167/IOVS.61.10.18.

[55] Wang, L.; Zhang, C.; Zhang, J.; Rao, Z.; Xu, X.; Mao, Z.; Chen, X. Epsilon-Poly-L-Lysine: Recent Advances in Biomanufacturing and Applications. *Front. Bioeng. Biotechnol.* **2021**, *9*, 895. https://doi.org/10.3389/FBIOE.2021.748976.

[56] Tan, Z.; Shi, Y.; Xing, B.; Hou, Y.; Cui, J.; Jia, S. The Antimicrobial Effects and Mechanism of ε-Poly-Lysine against Staphylococcus Aureus. *Bioresour. Bioprocess.* **2019**, *6* (1). https://doi.org/10.1186/s40643-019-0246-8.

[57] Li, Y.; Wang, Y.; Li, J. Antibacterial Activity of Polyvinyl Alcohol (PVA)/ε-Polylysine Packaging Films and the Effect on Longan Fruit. *Food Sci. Technol.* **2020**, *40* (4), 838–843. https://doi.org/10.1590/FST.19919.

[58] Amorim, S.; Reis, C. A.; Reis, R. L.; Pires, R. A. Extracellular Matrix Mimics Using Hyaluronan-Based Biomaterials. *Trends Biotechnol.* **2021**, *39* (1), 90–104. https://doi.org/10.1016/J.TIBTECH.2020.06.003.

[59] Harrer, D.; Sanchez Armengol, E.; Friedl, J. D.; Jalil, A.; Jelkmann, M.; Leichner, C.; Laffleur, F. Is Hyaluronic Acid the Perfect Excipient for the Pharmaceutical Need? *Int. J. Pharm.* **2021**, *601*, 120589. https://doi.org/10.1016/J.IJPHARM.2021.120589.

[60] Guo, W.; Douma, L.; Hu, M. H.; Eglin, D.; Alini, M.; Šećerović, A.; Grad, S.; Peng, X.; Zou, X.; D'Este, M.; Peroglio, M. Hyaluronic Acid-Based Interpenetrating Network Hydrogel as a Cell Carrier for Nucleus Pulposus Repair. *Carbohydr. Polym.* **2022**, *277*, 118828. https://doi.org/10.1016/J.CARBPOL.2021.118828.

[61] Hu, W.; Wang, Z.; Xiao, Y.; Zhang, S.; Wang, J. Advances in Crosslinking Strategies of Biomedical Hydrogels. *Biomater. Sci.* **2019**, *7* (3), 843–855. https://doi.org/10.1039/c8bm01246f.

[62] Cui, H.; Zhuang, X.; He, C.; Wei, Y.; Chen, X. High Performance and Reversible Ionic Polypeptide Hydrogel Based on Charge-Driven Assembly for Biomedical Applications. *Acta Biomater.* **2015**, *11* (1), 183–190. https://doi.org/10.1016/J.ACTBIO.2014.09.017.

[63] Xue, X.; Hu, Y.; Wang, S.; Chen, X.; Jiang, Y.; Su, J. Fabrication of Physical and

Chemical Crosslinked Hydrogels for Bone Tissue Engineering. *Bioact. Mater.* **2022**, *12*, 327–339. https://doi.org/10.1016/J.BIOACTMAT.2021.10.029.

[64] Hua, J.; Li, Z.; Xia, W.; Yang, N.; Gong, J.; Zhang, J.; Qiao, C. *Preparation and Properties of EDC/NHS Mediated Crosslinking Poly (Gamma-Glutamic Acid)/Epsilon-Polylysine Hydrogels*; Elsevier B.V., 2016; Vol. 61. https://doi.org/10.1016/j.msec.2016.01.001.

[65] Porod, G. *General Theory – Small Angle X-Ray Scattering*; Glatter, O. K. O., Ed.; Academic Press: London, 1982.

[66] *M07 Ed12 | Methods for Dilution Antimicrobial Susceptibility Tests for Bacteria That Grow Aerobically, 12th Edition*. https://clsi.org/standards/products/microbiology/documents/m07/ (accessed 2025-02-19).

[67] *ISO 10993-5:2009 – Biological evaluation of medical devices – Part 5: Tests for in vitro cytotoxicity*. https://www.iso.org/standard/36406.html (accessed 2025-02-27).

[68] Burguera, E. F.; Xu, H. H. K.; Sun, L. Injectable Calcium Phosphate Cement: Effects of Powder-to-Liquid Ratio and Needle Size. *J. Biomed. Mater. Res. Part B Appl. Biomater.* **2008**, *84B* (2), 493–502. https://doi.org/10.1002/JBM.B.30896.

[69] Jacquart, S.; Girod-Fullana, S.; Brouillet, F.; Pigasse, C.; Siadous, R.; Fatnassi, M.; Grimoud, J.; Rey, C.; Roques, C.; Combes, C. Injectable Bone Cement Containing Carboxymethyl Cellulose Microparticles as a Silver Delivery System Able to Reduce Implant-Associated Infection Risk. *Acta Biomater.* **2022**, *145*, 342–357. https://doi.org/10.1016/J.ACTBIO.2022.04.015.

[70] Baniasadi, M.; Minary-Jolandan, M.; Editor, A.; Zadpoor, A. A. Alginate-Collagen Fibril Composite Hydrogel. *Mater. 2015,* **2015**, *8* (2), 799–814. https://doi.org/10.3390/MA8020799.

[71] Liu, L.; Cooke, P. H.; Coffin, D. R.; Fishman, M. L.; Hicks, K. B. Pectin and Polyacrylamide Composite Hydrogels: Effect of Pectin on Structural and Dynamic Mechanical Properties. *J. Appl. Polym. Sci.* **2004**, *92* (3), 1893–1901. https://doi.org/10.1002/APP.20174.

[72] Rubina, A.; Sceglovs, A.; Ramata-Stunda, A.; Pugajeva, I.; Skadins, I.; Boyd, A. R.; Tumilovica, A.; Stipniece, L.; Salma-Ancane, K. Injectable Mineralized Sr-Hydroxyapatite Nanoparticles-Loaded ε-Polylysine-Hyaluronic Acid Composite Hydrogels for Bone Regeneration. *Int. J. Biol. Macromol.* **2024**, *280*, 135703. https://doi.org/10.1016/J.IJBIOMAC.2024.135703.

[73] Karvinen, J.; Kellomäki, M. Characterization of Self-Healing Hydrogels for Biomedical Applications. *Eur. Polym. J.* **2022**, *181*, 111641.

https://doi.org/10.1016/J.EURPOLYMJ.2022.111641.

[74] Murugesan, V.; Vaiyapuri, M.; Murugeasan, A. Fabrication and Characterization of Strontium Substituted Chitosan Modify Hydroxyapatite for Biomedical Applications. *Inorg. Chem. Commun.* **2022**, *142*, 109653. https://doi.org/10.1016/J.INOCHE.2022.109653.

DOCTORAL THESIS PROPOSED TO RIGA TECHNICAL UNIVERSITY FOR THE PROMOTION TO THE SCIENTIFIC DEGREE OF DOCTOR OF SCIENCE

To be granted the scientific degree of Doctor of Science (Ph. D.), the present Doctoral Thesis has been submitted for defence at the open meeting of RTU Promotion Council on 20 February 2026, at 11:00 at the Faculty of Natural Sciences and Technology of Riga Technical University, 3 Paula Valdena Street, Room 272.

OFFICIAL REVIEWERS

Tenured Professor Dr. sc. ing. Sergejs Gaidukovs
Riga Technical University, Latvia

Vice-Dean of Sciences, Nephrologist, MD Ph. D. Karlis Racenis
Riga Stradins University, Latvia

Ph. D. in Engineering Nihal Engin Vrana
CEO at SPARTHA MEDICAL, France

DECLARATION OF ACADEMIC INTEGRITY

I hereby declare that the Doctoral Thesis submitted for review to Riga Technical University for promotion to the scientific degree of Doctor of Science (Ph. D.) is my own. I confirm that this Doctoral Thesis has not been submitted to any other university for promotion to a scientific degree.

Artemijs Ščeglovs (signature)
Date: ……

The Doctoral Thesis has been elaborated as a collection of thematically related scientific publications completed by summaries in Latvian and English. The Doctoral Thesis unites four scientific publications. The scientific publications have been written in English, with a total volume of 174 pages, including supplementary data.

ABSTRACT

Within the current Doctoral Thesis, synthesis and comprehensive characterisation of a novel hydrogel matrix of two chemically crosslinked, naturally derived biopolymers, antimicrobial polypeptide ε-polylysine (ε-PL) and biologically active hyaluronic acid (HA), have been performed. The main aim of the study is to develop non-antibiotic, inherently antibacterial hydrogel-based biomaterials for the repair and healing of infected tissue. The research has been carried out two main stages, involving the synthesis of covalently crosslinked ε-PL/HA hydrogel matrix with further investigation of physicochemical properties such as molecular structure, morphology, gel fraction, swelling behaviour, as well as viscoelastic properties via rheological studies. Also, in the first stage, the effect of steam sterilisation on the physicochemical properties of the developed hydrogels has been investigated. Moreover, the *in vitro* antibacterial activity and cytotoxicity profile of the pure antimicrobial polypeptide ε-PL and furtherly ε-PL/HA hydrogels have been evaluated. Minimum inhibitory concentration (MIC), minimum bactericidal concentration (MBC) values and resistance development studies of pure ε-PL, as well as antibacterial activity of the fabricated hydrogels have been evaluated in both fast-acting (at 24 h) and sustained (up to 168 h) timeframes against widely known Gram-negative and Gram-positive pathogenic bacterial strains, including ATCC reference *Escherichia coli* and *Staphylococcus aureus* (*E. coli* and *S. aureus*), clinically isolated *Pseudomonas aeruginosa* (*P. aeruginosa*), as well as multidrug-resistant hard-to-treat methicillin-resistant *S. aureus* (MRSA*)* and extended spectrum β-lactamase *E. coli* (ESBL *E. coli*). The cytotoxicity profile has been evaluated using Balb/c 3T3 mouse fibroblasts via a direct contact assay, and Human dermal fibroblasts via an indirect (extract-based) assay. In the second stage, the antibacterial ε-PL/HA hydrogel matrix has been functionalised with bioactive strontium-substituted hydroxyapatite (Sr-HAp) nanoparticles to develop antibacterial and bioactive injectable hydrogels for bone tissue regeneration. To evaluate application-specific performance, further physicochemical and biological characterisation has been performed, including sustained (up to 168 h) antibacterial activity against *E. coli*, *S. aureus*, MRSA, and ESBL *E. coli*.

The Doctoral Thesis has been elaborated as a summary of scientific articles. The summary of scientific articles is written in Latvian and English. It includes four scientific publications and one review article. Each summary contains 10 figures and one table, totalling 44 pages.

USED ABBREVIATIONS

AMP	antimicrobial peptides
AMR	antimicrobial resistance
ATCC	American Type Culture Collection
Balb/c 3T3	fibroblast cells isolated from BALB/c mouse embryos
BSA	bovine serum albumin
CLSI	Clinical and Laboratory Standard Institute
CaP	calcium phosphates
CDC	Centers for Disease Control and Prevention
CRAB	carbapenem-resistant *Pseudomonas aeruginosa*
CRPA	carbapenem-resistant *Acinetobacter baumannii*
E'/E''	compression storage/loss modulus
E. coli	*Escherichia coli*
ECM	extracellular matrix
EDC	1-ethyl-3-(3-dimethyl aminopropyl) carbodiimide
ε-PL	ε-polylysine
EPS	exopolysaccharides
ESBL	extended spectrum β-lactamase producing bacteria strain
EU MDR	EU Medical Device Regulations
EUCAST	European Committee on Antimicrobial Susceptibility Testing
FDA	Food and Drug Administration
FTIR	Fourier transform infrared spectroscopy
G'/G''	storage/loss modulus
GAG	glycosaminoglycans
GEN	gentamicin
HA	hyaluronic acid
HAp	hydroxyapatite
HCl	hydrochloric acid
HDF	human dermal fibroblasts
in vitro	experimental studies outside a living organism
LVR	linear viscoelastic region
M. tuberculosis	*Mycobacterium tuberculosis*
MBC	minimum bactericidal concentration
MIC	minimum inhibitory concentration
MRSA	methicillin-resistant *Staphylococcus aureus*

NaCl	sodium chloride
NaOH	sodium hydroxide
NDB	naturally derived biopolymer
aNDB	antibacterial naturally derived biopolymer
NHS	*N*-hydroxysuccinimide
P. aeruginosa	*Pseudomonas aeruginosa*
PRSP	penicillin-resistant *Streptococcus pneumoniae*
PVA	polyvinyl alcohol
RGD	arginine-glycine-aspartic acid
S. aureus	*Staphylococcus aureus*
S. epidermidis	*Staphylococcus epidermidis*
SAXS	small-angle X-ray scattering
SCI	scientific
SEM	scanning electron microscopy
Sr-HAp	strontium-substituted hydroxyapatite
USD	United States dollar
VAN	vancomycin
VRE	vancomycin-resistant *Enterococci*
WHO	World Health Organization

TABLE OF CONTENTS

GENERAL DESCRIPTION OF THE RESEARCH 52
Introduction to the State-of-the-Art 52
Aim and Tasks 55
Thesis Statements to be Defended 56
Scientific Novelty 56
Practical Significance 57
Structure and Volume of the Doctoral Thesis 57
Publications and Approbation of the Doctoral Thesis 57
MAIN RESULTS OF THE DOCTORAL THESIS 61
Potential of Naturally Derived Biopolymers (NDBs) as Alternative Antibacterials for Tissue Engineering Applications (1st Publication) 61
Development of a Novel Inherently Antibacterial Chemically Crosslinked Hydrogel Matrix (2nd Publication) 62
Optimisation of Synthesis Method, Evaluation of Topology and Impact of Steam Sterilisation on physicochemical and Antibacterial Properties of Chemically Crosslinked ε-PL/HA Hydrogels (3rd Publication) 67
In Vitro Evaluation of Antibacterial Potential and Cytotoxicity of ε-PL/HA Hydrogels (4th Publication) 72
Synthesis and Characterisation of Antibacterial Sr-HAp Functionalised ε-PL/HA Hydrogels (5th Publication) 76
CONCLUSIONS 81
REFERENCES 82
APPENDICES 90

Appendix I. **A. Sceglovs**, I. Skadins, M. Chitto, J. Kroica, K. Salma-Ancane. Failure or future? Exploring alternative antibacterials: a comparative analysis of antibiotics and naturally-derived biopolymers, *Front. Microbiol.*, 2025, 16: 1526250. doi: 10.3389/fmicb.2025.1526250

Appendix II. K. Salma-Ancane, **A. Sceglovs**, E. Tracuma, J. K. Wychowaniec, K. Aunina, A. Ramata-Stunda, V. Nikolajeva, D. Loca. Effect of crosslinking strategy on the biological, antibacterial and physicochemical performance of hyaluronic acid and ε-polylysine based hydrogels, *Int. J. Biol. Macromol.*, 2022, 208, 995–1008. https://doi.org/10.1016/J.IJBIOMAC.2022.03.207.

Appendix III. **A. Sceglovs**, J.K. Wychowaniec, I. Skadins, A. Reinis, C.J.C. Edwards-Gayle, M. D'Este, K. Salma-Ancane, Effect of steam sterilisation on physico-chemical properties of antibacterial covalently cross-linked ε-polylysine/hyaluronic acid hydrogels, *Carbohydr. Polym. Technol. Appl.,* 2023, 6: 100363. https://doi.org/10.1016/J.CARPTA.2023.100363.

Appendix IV. **A. Sceglovs**, C. Siverino, I. Skadins, V. Pirsko, M. Sceglova, J. Kroica, F. T. Moriarty, K. Salma-Ancane. Injectable ε-polylysine/hyaluronic acid hydrogels with resistance-preventing antibacterial activity for treating wound infections, ACS Appl. Bio Mater., 2025, 8 (11), 9916–9930. https://doi.org/10.1021/acsabm.5c01252.

Appendix V. Rubina, **A. Sceglovs**, A. Ramata-Stunda, I. Pugajeva, A. R. Boyd, A. Tumilovica, L. Stipniece and K. Salma-Ancane. Injectable mineralized Sr-hydroxyapatite nanoparticles-loaded ε-polylysine-hyaluronic acid composite hydrogels for bone regeneration, *Int. J. Biol. Macromol.,* 2024, 280: 135703. https://doi.org/10.1016/j.ijbiomac.2024.135703.

GENERAL DESCRIPTION OF THE RESEARCH

Introduction to the State-of-the-Art

According to data from the World Health Organization (WHO), bacterial infections account for 13.6 % of human mortality, equating to approximately one in every eight deaths worldwide [1]. The only widely used strategy for treating and preventing bacterial infections in healthcare remains antibiotics, with few non-antibiotic alternatives available, except for "last resort" bacteriophage therapy. Such "last resort" use is closely linked to the growing problem of antibiotic resistance among bacterial pathogens. The WHO and the Centers for Disease Control and Prevention (CDC) recognise antimicrobial resistance (AMR) as a global crisis due to the increased prevalence of pathogens resistant to last-resort antibiotics. For decades, a growing list of AMR-associated pathogens has been responsible for hundreds of thousands of deaths. These include penicillin-resistant *Streptococcus pneumoniae* (PRSP), carbapenem-resistant *Pseudomonas aeruginosa* and *Acinetobacter baumannii* (CRPA and CRAB), methicillin-resistant *Staphylococcus aureus* (MRSA), v*ancomycin-resistant Enterococci* (VRE), and extended-spectrum β-lactamase (ESBL) producing *Escherichia coli* (*E. coli)*. Moreover, it is estimated that by 2050, AMR-related deaths could exceed 10 million annually. To combat this growing crisis, the WHO Global Action Plan has underlined the urgent need to develop alternative non-antibiotic strategies [2].

Although naturally derived antibacterial biopolymers (aNDBs) [3]–[5] have long been used in biomedical applications, their study has expanded significantly in recent years. Unlike the others biopolymers that are used in biomedicine and could be both of natural (hyaluronic acid, gelatin etc.) and synthetic (polyvinyl alcohol (PVA), polyethylene glycol (PEG), etc.) origin, aNDBs are obtained from natural sources (plants, fungi, microorganisms, algae, and animals) and exhibit biocompatability and intrinsic antibacterial activity without a need for additional chemical modifications [4]. Interest in aNDBs as non-antibiotic antibacterial agents has surged, with publications on their use increasing by nearly 400 % since 2015. This growing trend is primarily driven by recognising aNDBs as promising antibacterial molecules for local delivery applications, offering biocompatibility and antibacterial efficacy against pathogenic bacteria. Furthermore, it has been highlighted that bacteria are less likely to develop resistance against such material, as the antibacterial activity of aNDB differs from conventional antibiotics in both target specificity and mechanism of action [4]. Several studies have demonstrated the development of various biomaterials, such as drug delivery systems, ophthalmic contact lenses,

injectable cements, medical device and implant coatings, microneedle patches, wound dressings, nanoparticles and nanofibers, and hydrogels based on aNDB with significant antibacterial activity [2], [6]–[8]. These aNDB include chitosan, κ-carrageenan, alginate, pectin, o-pullulan, fucoidan, chondroitin sulphate, bacterial-produced exopolysaccharides, as well as antimicrobial peptides (AMP) [2], [6]–[12].

Hydrogels have emerged as a promising class of biomaterials in biomedicine due to their high biocompatibility, tuneable mechanical properties, and ability to mimic the extracellular matrix (ECM) of human tissues. These properties make hydrogels particularly advantageous for tissue engineering and regenerative medicine, as they can support cell adhesion, proliferation, and differentiation, thereby promoting tissue regeneration. Over the past decade, research has increasingly focused on developing hydrogels with antibacterial functionality to address the critical clinical challenge of infected tissue repair and healing. One of the most effective strategies involves the development of hydrogels based on aNDBs. These intrinsic antibacterial hydrogels offer several advantages, including eliminating additional antibacterial agents or antibiotics, a simplified composition, enhanced biocompatibility, and sustained antibacterial efficacy [13]. Beyond infection control, hydrogels are also being explored for applications in bone tissue regeneration. Bone defects and fractures resulting from diseases such as osteoporosis, osteosarcoma, and high-impact injuries represent a significant global health burden, affecting over 200 million people worldwide and incurring an economic cost exceeding $100 million annually [14], [15]. These conditions are frequently complicated by a high risk of infection, especially in cases of open fractures, surgical interventions, and immunocompromised patients. Post-traumatic osteomyelitis, periprosthetic joint infections, and implant-associated infections remain significant clinical challenges, often leading to delayed bone healing, implant failure, and increased mortality rates. Consequently, developing multifunctional, bone-targeted antibacterial biomaterials with regenerative potential has become a key research focus to improve treatment outcomes and prevent infection-related complications in bone healing and regeneration.

A promising approach in this field involves the biofunctionalisation of the hydrogel matrix with bioactive and osteogenic inorganic components, such as calcium phosphate (CaP) particles. CaP bone biomaterials, such as hydroxyapatite (HAp), demonstrate excellent biocompatibility and bioactivity in physiological conditions, as they closely resemble the primary mineral component of bone extracellular matrix (ECM) [16], [17]. This similarity allows CaP-based biomaterials to form intimate functional interfaces with bone tissue, enhancing osseointegration and bone remodelling. However, despite their advantages, CaP biomaterials exhibit limitations such as low mechanical strength, uncertain biodegradation rate, and lack of cohesiveness. Moreover, commercially available bone biomaterials still fail to fully replicate the hierarchical composite structure of native bone tissue and exhibit limited regenerative potential for the treatment bone-related diseases [18]. Combining CaP with a hydrogel matrix enables the development of composite hydrogels with enhanced functionalities, including superior biocompatibility and bioactivity, improved structural integrity, optimised porosity, tuneable mechanical stiffness, and biodegradation rates. These properties make the composite hydrogel a promising biomaterial for bone regeneration, providing a bioactive and mechanically supportive environment for cell growth and tissue integration [17]. The current clinical gold standard for infected bone tissue treatment includes administration of systemic or local antibiotics, as well as a separate surgery to implant a bone

graft for the reconstruction of bone tissue [19]. For local antibiotic therapy, synthetic poly (methyl methacrylate) (PMMA) bone cement beads and spacers are used to deliver a high concentration of antibiotics, for example, vancomycin (VAN), gentamicin (GENTA) [20]. However, bioinert non-biodegradable PMMA biomaterials as antibiotic carriers have substantial drawbacks, such as poor drug release kinetics [20], inducing the development of antibiotic resistance, providing a site for pathogen colonisation and biofilm formation, causing toxicity, and requiring additional surgery for removal. A one-step approach is demonstrated by bioactive GENTA or VAN loaded hydroxyapatite (HAp)/calcium sulphate biomaterials, a new commercially available injectable synthetic bone graft substitute, CERAMENT® G and CERAMENT® V (BONESUPPORT, Lund, Sweden). These commercial products have a significant advantage as they simultaneously provide local antibiotic therapy and promote new bone formation [21]. However, local wound complications, persistent infection, and residual mature biofilm have been reported in treating chronic osteomyelitis. This is why naturally-derived CaP-loaded inherently antibacterial composite hydrogels are a tremendously important research direction to provide a potential solution for two common problems in the healthcare sector – bacterial infections and bone disorders. To address the AMR crisis and the challenges associated with bacterial infection treatment and bone reconstruction, the Doctoral Thesis focuses on the development and investigation of antibacterial hydrogels based on antimicrobial polypeptide ε-polylysine (ε-PL) and biologically active hyaluronic acid (HA), and ε-PL/HA composite hydrogels. ε-PL/HA composite hydrogels have been developed by functionalising the antibacterial hydrogel matrix with bioactive Sr-HAp nanoparticles. This approach aims to introduce specialised functional properties, such as supporting mesenchymal stem cell differentiation, influencing ECM protein adsorption, and enhancing cell adhesion and tissue formation, while mimicking the nanostructure and composition of native bone tissue to improve bone regeneration capability.

Firstly, the most important parameters in designing antibacterial hydrogels include the selection of suitable components and an appropriate crosslinking strategy. In this study, ε-PL and HA have been selected based on the superior functional properties, providing both antibacterial activity and the ability to mimic the native ECM. HA is an essential polysaccharide of the ECM in many tissues, which demonstrates excellent biocompatibility and plays an important biochemical role in different physiological processes [22], [23]. Moreover, HA contains multiple functional groups that allow for numerous subsequent chemical modifications [13], [24]. Among typical short-chain antimicrobial peptides (AMPs), ε-PL is classified as a long-chain antimicrobial polypeptide, also known as a poly(amino acid). ε-PL has many unique characteristics and is generally recognised as safe by the Food and Drug Administration (FDA). It has several advantages compared to other AMPs, including natural origin, simple structure, low immunogenicity, low toxicity profile, biocompatibility, antibacterial mechanism through membrane disruption, stability under a range of pH and temperature, and cost-effectiveness. Until now, only a few studies have addressed the preparation and antibacterial evaluation of antibacterial hydrogels containing ε-PL, including chemically crosslinked polyglutamic acid/ ε-PL composite hydrogels, bovine serum albumin (BSA) and polyvinyl alcohol (PVA) dual-network hydrogels with embedded ε-PL, photo crosslinkable silk fibroin/ε-PL hydrogels, polyacrylamide, gelatin, and ε-PL hydrogels, ε-PL-stabilized agarose/polydopamine hydrogels and dynamic arginine-glycine-aspartic acid (RGD)/ ε-PL hydrogels [2], [24].

To preserve properties of both components while combining them into a single integral hydrogel matrix, a chemical crosslinking approach using 1-ethyl-3-(3-dimethylaminopropyl) carbodiimide (EDC) and *N*-hydroxysuccinimide (NHS) has been selected. EDC/NHS crosslinking offers mild reaction conditions, water solubility of both reagents, lower toxicity compared to conventional crosslinkers, and improved mechanical properties of the resulting hydrogel matrix due to the formation of stable covalent bonds [25].

Secondly, the development of composite hydrogels requires the selection of an appropriate and well-justified CaP derivative. The main inorganic component of the bone extracellular matrix (ECM) is nanosized carbonated calcium-deficient apatite containing trace elements such as Mg, Zn, Sr, etc. Synthetic hydroxyapatite (HAp) nanoparticles have similarities to bone apatite in terms of chemical composition, structure, and size. Therefore, synthetic nanocrystalline HAp exhibits excellent osteoconductive properties. Various HAp-based biomaterials have been extensively explored as carriers for the delivery of biologically active compounds due to their high specific surface area, unique bioactivity, and adsorption capacity across biological barriers [26]. Recently, HAp-based carriers for targeted delivery of antiosteoporotic drugs, anticancer drugs, antibiotics, proteins, genes, radionuclides, and inorganic ions, such as Mg^{2+}, Zn^{2+}, and Sr^{2+}, have been investigated. Ion-substituted HAp biomaterials are considered advantageous systems for the sustainable, local delivery of the biomimetic bone ECM trace elements [27]–[29]. These functionalised HAp can be applied for developing next-generation biomaterials to treat and reconstruct bone disorders (including osteoporotic bone fractures) through the controlled delivery of biologically active inorganic ions or drugs directly to bone defect sites [30]. Among different candidates for the development of ion-substituted HAp, Sr^{2+} ions have been of wide interest since they act as a bone therapeutic agent by a unique dual-acting mechanism, that is, simultaneously promoting bone formation by activating Ca-sensing receptors and inhibiting bone resorption [31], [32]. Sr^{2+} ions are incorporated into bone by two main mechanisms: (1) a rapid uptake mechanism dependent on osteoblast activity, whereby Sr^{2+} ions are absorbed via ion exchange processes with Ca^{2+} ions or binding to osteoid proteins, and (2) Sr^{2+} ions are incorporated into the crystal lattice of the bone mineral. Sr^{2+} ions have osteogenic potential, and it has been reported that Sr-containing HAp biomaterials can deliver Sr^{2+} ions to the site of a bone defect, where they assist in bone regeneration by promoting osteoblasts' proliferation and differentiation and suppressing osteoclast activity.

Considering the demonstrated potential of the selected components and crosslinking strategy, the Doctoral Thesis focuses on the development and comprehensive characterisation of injectable hydrogels combining the inherent antibacterial properties of ε-PL, the ECM-mimicking and biocompatible properties of HA, and the osteogenic effect of Sr-HAp nanoparticles. This multifunctional hydrogel system has been designed to simultaneously combat bacterial infections and support bone tissue regeneration, addressing the abovementioned critical healthcare challenges.

Aim and Tasks

The aim of the Doctoral Thesis is to use antimicrobial polypeptide ε-PL to develop covalently crosslinked antibacterial hydrogels for tissue engineering applications. To achieve the set aim, the experimental plan of the Doctoral Thesis has been divided into four parts related

to the synthesis methodology development of the hydrogels and Sr-HAp functionalised hydrogels and their further investigation. These parts correspond to the tasks set up in the Doctoral Thesis:

1. to develop a synthesis methodology of the chemically crosslinked ε-PL/HA hydrogel matrix via EDC/NHS crosslinking agent-mediated reaction;
2. to investigate physicochemical and *in vitro* biological properties of prepared ε-PL/HA hydrogels;
3. to develop a synthesis methodology of Sr-HAp nanoparticles functionalised ε-PL/HA (Sr-HAp/ε-PL/HA) hydrogels;
4. to investigate physicochemical and *in vitro* biological properties of the prepared Sr-HAp/ε-PL/HA composite hydrogels.

Thesis Statements to be Defended

1. An EDC/NHS-mediated chemical crosslinking approach has been used for the development of ε-PL/HA hydrogels, enabling key physicochemical and biological properties relevant to tissue engineering applications, including stiffness, injectability, syringeability, self-recovery, sterilisation ability, antibacterial activity, and cell viability.
2. Covalently crosslinked ε-PL/HA hydrogels can be sterilised using conventional steam sterilisation with minimal impact on their physicochemical and *in vitro* antibacterial performance.
3. ε-PL/HA hydrogels demonstrate potent antibacterial activity against both Gram-negative and Gram-positive bacterial strains, including ATCC reference strains and clinically isolated hard-to-treat multidrug-resistant bacterial strains.
4. Functionalisation of ε-PL/HA hydrogel matrix with Sr-HAp nanoparticles preserves the initial hydrogel matrix properties, including injectability and antibacterial activity, while introducing a tuneable biodegradation profile essential for bone tissue regeneration applications.

Scientific Novelty

1. For the first time, a biocompatible and antibacterial hydrogel matrix has been developed using a combination of two naturally derived biopolymers, ε-PL and HA, via EDC/NHS-mediated chemical crosslinking.
2. The impact of steam sterilisation on physicochemical properties and *in vitro* antibacterial activity of the developed ε-PL/HA hydrogels has been systematically evaluated, demonstrating minimal impact on their functional properties and potential for clinical translation.
3. The potential for bacterial resistance development against ε-PL has been investigated using both ATCC reference and clinically isolated multidrug-resistant Gram-negative and Gram-positive bacterial strains.
4. Injectable ε-PL/HA hydrogels functionalised with Sr-HAp nanoparticles have been developed and evaluated for their dual functionality – antibacterial activity and osteogenesis capacity, highlighting their potential for application in bone infection treatment.

5. The time-dependent antibacterial activity of the ε-PL/HA hydrogels and Sr-HAp functionalised ε-PL/HA hydrogels has been investigated over fast-acting (24 h) and sustained (168 h) durations against a wide spectrum of bacterial strains, confirming a prolonged and broad-spectrum antibacterial activity of the developed hydrogel systems.

Practical Significance

Within the Doctoral Thesis, the following practical outcomes have been achieved.

1. A robust and reproducible fabrication methodology has been developed for injectable, antibacterial, and autoclavable hydrogels based on ε-PL and HA, using EDC/NHS-mediated chemical crosslinking for biomedical applications.
2. Standardised operating protocols have been developed for the investigation of viscoelastic properties, *in vitro* antibacterial activity, and cytocompatibility of the prepared hydrogels, including detailed post-synthesis sample preparation procedures and validation of testing reproducibility.
3. An *in situ* functionalisation strategy has been developed to produce Sr-HAp functionalised ε-PL/HA hydrogels as dual-functionality biomaterials, combining antibacterial activity with osteogenic capacity for the treatment of infected bone defects.
4. The simplicity of synthesis, sterilisation and modification ability of the developed hydrogel matrix suggest a strong translational potential for targeted antibacterial therapy, next-generation implant coatings, drug delivery vehicles, or composite materials.

Structure and Volume of the Doctoral Thesis

The Doctoral Thesis has been elaborated as a summary of scientific publications dedicated to research on the development and comprehensive investigation of chemically crosslinked ε-PL/HA hydrogel matrix and Sr-HAp functionalised ε-PL/HA hydrogels. The Thesis includes four original research publications, published in scientific (SCI) journals, and one review article.

Publications and Approbation of the Doctoral Thesis

Results and achievements obtained within the Doctoral Thesis have been published in four original scientific publications. In addition, a review article has been published, covering a related topic of the Thesis. During the development period of the Doctoral Thesis, the main results have been presented at 16 international scientific conferences.

SCI publications:

1. **Sceglovs**, **A.,** Skadins, I., Chitto, M., Kroica, J., Salma-Ancane, K. (2025). Failure or Future? Exploring Alternative Antibacterials: A Comparative Analysis of Antibiotics and Naturally-Derived Biopolymers. *Front. Microbiol., 16*, 1526250. doi: 10.3389/fmicb.2025.1526250 (*IF 4.5, Q1, CiteScore 8.5*).
   Contribution of A. Sceglovs (85/100 %): Conceptualisation, Writing – original draft, Writing – review & editing.
2. Salma-Ancane, K., **Sceglovs**, **A**., Tracuma, E., Wychowaniec, J. K., Aunina, K., Ramata-Stunda, A., Nikolajeva, V., Loca, D. (2022). Effect of Crosslinking Strategy on the Biological, Antibacterial and Physicochemical Performance of Hyaluronic Acid and ε-

Polylysine Based Hydrogels. *Int. J. Biol. Macromol, 208*, 995–1008. https://doi.org/10.1016/J.IJBIOMAC.2022.03.207 (*IF 8.5, Q1, CiteScore 10.3*).
Contribution of A. Sceglovs (35/100 %): Methodology, Validation, Formal analysis, Investigation.

3. **Sceglovs**, **A**., Wychowaniec, J. K., Skadins, I., Reinis, A., Edwards-Gayle, C. J. C., D'Este, M., Salma-Ancane, K. (2023). Effect of Steam Sterilisation on Physico-Chemical Properties of Antibacterial Covalently Cross-Linked ε-Polylysine/Hyaluronic Acid Hydrogels. *Carbohydr. Polym. Technol. Appl., 6*, 100363. https://doi.org/10.1016/J.CARPTA.2023.100363 (*IF 6.5, Q1, CiteScore 11.0*).
Contribution of A. Sceglovs (70/100 %): Methodology, Validation, Formal analysis, Investigation.
4. **Sceglovs**, **A**., Siverino, C., Skadins, I., Pirsko, V., Sceglova, M., Kroica, J., Moriarty, F. T., Salma-Ancane, K. (2025). Injectable ε-Polylysine/Hyaluronic Acid Hydrogels with Resistance-Preventing Antibacterial Activity for Treating Wound Infections. *ACS Appl. Bio Mater., 8* (11), 9916–9930. https://doi.org/10.1021/acsabm.5c01252.
Contribution of A. Sceglovs (75/100 %): Conceptualisation, Writing – original draft, Visualisation, Methodology, Validation, Investigation, Writing – review & editing.
5. Rubina, A., **Sceglovs**, **A**., Ramata-Stunda, A., Pugajeva, I., Boyd, A. R., Tumilovica, A., Stipniece, L., Salma-Ancane, K. (2024). Injectable Mineralized Sr-Hydroxyapatite Nanoparticles-Loaded ε-Polylysine-Hyaluronic Acid Composite Hydrogels for Bone Regeneration. *Int. J. Biol. Macromol., 280*, 135703. https://doi.org/10.1016/j.ijbiomac.2024.135703 (*IF 8.5, Q1, CiteScore 10.3*).
Contribution of A. Sceglovs (35/100 %): Writing – review & editing, Writing – original draft, Visualisation, Investigation, Formal analysis, Conceptualisation.

Scientific conferences:

1. **Sceglovs**, **A**., Reinis, A., Salma-Ancane, K. (2021). Natural Biopolymer-Based Antibacterial Hydrogels for Tissue Engineering. *European Society for Biomaterials (ESB 2021),* 5–9 September 2021. Virtual event, virtual poster presentation.
2. **Sceglovs**, **A**., Reinis, A., Salma-Ancane, K. (2021). Synthesis and Characterization of Chemically Cross-Linked Hydrogels Based on ε-Polylysine and Hyaluronic Acid. *Materials Science and Applied Chemistry conference of RTU (MSAC 2021)*, 22 October 2021. Virtual event, virtual poster presentation.
3. **Sceglovs**, **A**., Siverino, C., Moriarty, F. T., Salma-Ancane, K. (2022). Covalently Bonded ε-Polylysine/Hyaluronic Acid Hydrogels with Enhanced Antibacterial Action. *Scandinavian Society for Biomaterials Conference (ScSB 2022)*, 13–15 June 2022, Jurmala, Latvia. Poster presentation.
4. **Sceglovs**, **A**., Siverino, C., Wychowaniec, J. K., Moriarty, F. T., 'Este, M. D., Salma-Ancane, K. (2022). Functional ε-Polylysine/Hyaluronic Acid Hydrogels with Antibacterial Activity. *Tissue Engineering and Regenerative Medicine International Society Conference (TERMIS EU 22)*, 28 June–1 July 2022, Krakow, Poland. Poster presentation.
5. **Sceglovs**, **A**., Salma-Ancane, K. (2022). Effect of Steam Sterilization Strategy on ε-Polylysine/Hyaluronic Acid Hydrogel Properties. *European Society for Biomaterials (ESB 2022),* 4–8 September 2022, Bordo, France. Poster presentation.

6. Rubina, A., Kreicberga, I., **Sceglovs**, **A**., Salma-Ancane, K. (2022). Development of Functional Composite Hydrogels for Bone Regeneration. *European Society for Biomaterials (ESB 2022)*, 4–8 September 2022, Bordo, France. Poster presentation.
7. **Sceglovs**, **A**., Salma-Ancane, K. Investigation of Impact of Steam Sterilization on ε-Polylysine/Hyaluronic Acid Hydrogel Properties. *Materials Science and Applied Chemistry Conference of RTU (MSAC 2022)*, 21 October 2022, Riga, Latvia. Poster presentation.
8. Rubina, A., Kreicberga, I., **Sceglovs**, **A**., Salma-Ancane, K. (2022). Development of Functional Composite Hydrogels for Bone Regeneration. *Materials Science and Applied Chemistry Conference of RTU (MSAC 2022)*, 21 October 2022, Riga, Latvia. Poster presentation.
9. **Sceglovs**, **A**., Skadins, I., Pirsko, V., Kroica, J., Salma-Ancane, K. (2023). Injectable Polypeptide-Based Hydrogels for Local Antibacterial Therapy. *European Society for Biomaterials (ESB 2023),* 4–8 September 2023, Davos, Switzerland. Poster presentation.
10. Rubina, A., Tumilovica, A., **Sceglovs**, **A**., Stipniece, L., Salma-Ancane, K. (2023). Injectable Hyaluronic Acid/ε-Polylysine Hydrogels Loaded with Strontium Hydroxyapatite Nanoparticles for Osteoporotic Bone Fracture Healing. *European Society for Biomaterials (ESB 2023),* 4–8 September 2023, Davos, Switzerland. Poster presentation.
11. **Sceglovs**, **A**., Skadins, I., Pirsko, V., Kroica, J., Salma-Ancane, K. (2023). Revealing Physicochemical and Antibacterial Properties of Chemically Coupled ε-Polylysine/Hyaluronic Acid Hydrogel. *Materials Science and Applied Chemistry Conference of RTU (MSAC 2023)*, 6 October 2023, Riga, Latvia. Oral presentation.
12. Rubina, A., Tumilovica, A., **Sceglovs**, **A**., Stipniece, L., Salma-Ancane, K. (2023). Injectable Nanoparticle-Hydrogel Composites for Bone Regeneration. *Materials Science and Applied Chemistry Conference of RTU (MSAC 2023)*, 6 October 2023, Riga, Latvia. Oral presentation.
13. **Sceglovs**, **A**., Skadins, I., Kroica, J., Salma-Ancane, K. (2024). Injectable Hydrogels Based on Antimicrobial Polypeptide Exhibit Enhanced In Vitro Antibacterial Activity. *4th International Biennial BioMaH Conference*, 15–18 October 2024, Rome, Italy. Poster presentation.
14. Rubina, A., **Sceglovs**, **A**., Ramat-Stunda, A., Tumilovica, A., Stipniece, L., Salma-Ancane, K. (2024). Injectable Mineralized Sr-Hydroxyapatite Nanoparticles-Loaded Composite Hydrogels for Bone Regeneration. *4th International Biennial BioMaH Conference*, 15–18 October 2024, Rome, Italy. Oral presentation.
15. **Sceglovs**, **A**., Skadins, I., Kroica, J., Salma-Ancane, K. (2025). Advanced Hydrogel Platforms: Cross-Linked Polypeptide for Non-Antibiotic Antibacterial Applications. *RSU Research Week Biennial Conference (RW 2025)*, 24–28 March 2025, Riga, Latvia. Oral presentation.
16. **Sceglovs**, **A**., Rubina, A., Skadins, I., Wychowaniec, J. K., Ramat-Stunda, A., Kroica, J., Salma-Ancane, K. Attaining Non-Antibiotic Antibacterial Hydrogels: From ε-Polylysine Networks to Composite Platforms. *Tissue Engineering and Regenerative Medicine International Society Conference (TERMIS EU 25)*, 19–23 May 2025, Freiburg, Germany. Oral presentation.

Other scientific publications developed within the Doctoral Thesis

1. Mosina, M., Severino, C., Stipniece, L., **Sceglovs**, **A**., Vasiljevs, R., Moriarty, F. T., Locs, J. (2023). Gallium-Doped Hydroxyapatite Shows Antibacterial Activity against Pseudomonas Aeruginosa without Affecting Cell Metabolic Activity. *J. Funct Biomater*., *14* (51). https://doi.org/10.3390/jfb14020051.
2. Stipniece, L., Ramata-Stunda, A., Vecstaudza, J., Kreicberga, I., Livkisa, D., Rubina, A., **Sceglovs**, **A**., Salma-Ancane, K. (2023). A Comparative Study on Physicochemical Properties and In Vitro Biocompatibility of Sr-Substituted and Sr Ranelate-Loaded Hydroxyapatite Nanoparticles. *ACS Appl. Bio Mater., 6,* 5264–5281. https://doi.org/10.1021/acsabm.3c00539.
3. Rubina, A., Tumilovica, A., **Sceglovs**, **A**., Klavins, K., Vaska, A., Stipniece, L., Sizovs, A., Novosjolova, I., Salma-Ancane, K. (2025). Injectable Hyaluronic Acid/Nanohydroxyapatite Composite Hydrogels for Localized Drug Delivery and Bone Repair. *Carbohydr. Polym. Technol. Appl., 12*, 101030. https://doi.org/10.1016/j.carpta.2025.101030 (*IF 6.5, Q1, CiteScore 11.0*).

Scientific conference presentations contributed as part of the Doctoral Thesis

1. Tumilovica, A., Rubina, A., **Sceglovs**, **A**., Stipniece, L., Salma-Ancane, K. (2023). Development of Injectable Composite Hydrogels Containing Hydroxyapatite Nanoparticles and Hyaluronic Acid. *Materials Science and Applied Chemistry conference of RTU (MSAC 2023)*, 6 October 2023, Riga, Latvia. Poster presentation.
2. Tumilovica, A., Rubina, A., **Sceglovs**, **A**., Klavins, K., Stipniece, L., Salma-Ancane, K. (2024). Development of Injectable Bioactive Composite Hydrogels for Bone Regeneration. *4th International Biennial BioMaH Conference*, 15–18 October 2024, Rome, Italy. Poster presentation.

MAIN RESULTS OF THE DOCTORAL THESIS

Potential of Naturally Derived Biopolymers (NDBs) as Alternative Antibacterials for Tissue Engineering Applications (1st Publication)

Bacterial infections have been a significant problem throughout human history. Although the development of antibiotics in the 20th century revolutionised the treatment of infections, it also initiated an ongoing evolutionary struggle against pathogenic microorganisms. As a side problem, the overuse and misuse of these lifesaving antibiotics have developed the top global public health crisis named antimicrobial resistance (AMR) occurring worldwide [33]. The dramatic report by WHO has shown that by 2050, antibiotic resistance could become as deadly as cancer and cause substantial economic damage if no action is taken [34]. The decreasing efficacy of antibiotics and the limited availability of alternative treatments underscore the urgent need for new classes of antibacterial therapeutics. Ideal alternatives should include mechanisms of action that lower the risk of resistance development.

In this context, **antibacterial naturally-derived biopolymers (aNDBs)** have attracted significant attention due to their unique antibacterial properties. Approximately two decades ago, aNDBs with intrinsic antibacterial activity were first proposed as alternatives to antibiotics for treating bacterial infections [35]. Today, aNDB-based strategies show potential for localized, non-antibiotic antibacterial applications that support the immune system and minimise impact on the natural microbiota. Such approaches could represent a sustainable innovation within modern healthcare.

Regarding aNDBs, it is crucial to reveal their antibacterial mechanism against bacteria (Figure 1). Firstly, it is worth mentioning that bacterial cell wall outer structures (adhesion and pathogenicity factors), for example, lipopolysaccharides and phospholipids of Gram-negative bacteria and teichoic and lipoteichoic acids of Gram-positive bacteria, are negatively charged. Secondly, aNDBs consist of molecules (chondroitin sulphate, o-pullulan, ε-polylysine, chitosan, antimicrobial peptides, for example, magainin-2, etc.), which contain cationic groups like primary amines, quaternary ammonium, quaternary phosphonium, guanidinium or tertiary sulfonium [36], contributing to their overall positive charge at physiological pH. As a result, interaction between aNDB and bacteria begins with mutual attachment caused by electrostatic forces [37] (Figure 1). The electrostatic interaction represents the first step towards the bactericidal effect of aNDBs. Secondly, a specific concentration of cationicity of aNDBs must be achieved to reach a multivalence effect [38] that results in the simultaneous binding of aNDB molecules to the bacterial cell structures. Further mechanisms involve pore- or micelle-forming steps (Figure 1) that describe bacteria structural integrity disruption, leading to increased permeability, physical damages, and further entry into the cytoplasm and bacteria lysis.

Besides, several reports have shown that various aNDBs have antibiofilm activity as well. Antibiofilm mechanisms rely on mechanisms of disrupting biofilm exopolysaccharides (EPS), a crucial component for biofilm stability, leading to detachment of bacterial cells or preventing bacterial adhesion at the initial stage [39], [40]. In addition, different aNDBs, for example, lactoferrin-derived peptides, neutrophil peptides, antimicrobial peptides (protegrin-1), have been found to have antibacterial activity against intracellular bacteria – *M. tuberculosis*. Antibacterial mechanism is based on disrupting the mycobacterial cell wall and enhancing membrane permeabilization [9]–[11].

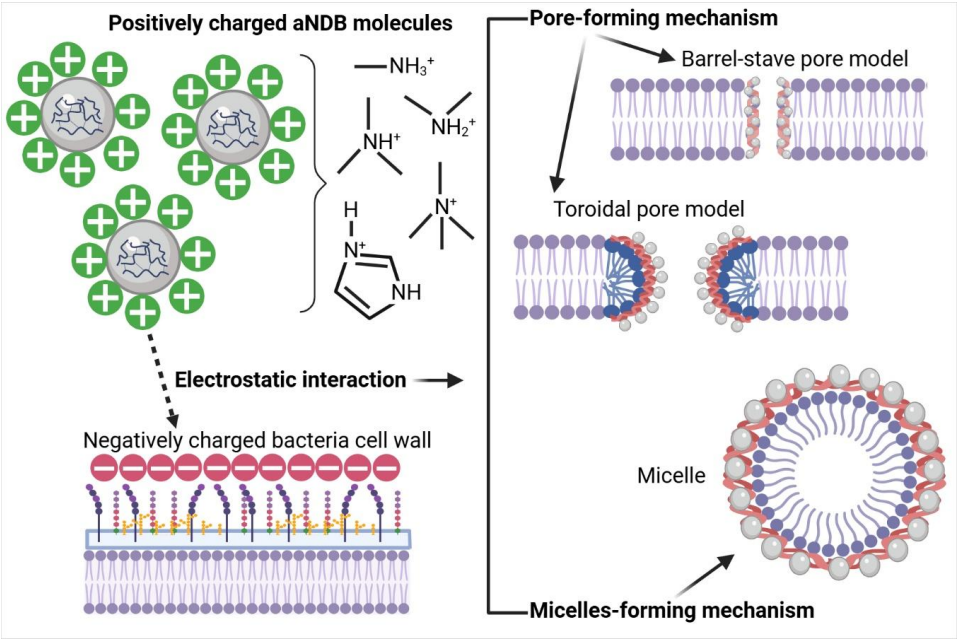

Figure 1. Biopolymer (aNDB) – bacteria cell interaction (left) and bactericidal mechanisms (right) (Created by Biorender).

Another crucial consideration is the potential for bacteria to develop resistance against aNDBs. Resistance mechanisms vary and are typically specific to the antibiotic class and its mode of action. Still, common mechanisms involve the production of specific enzymes, loss or modification of targeted molecules, activation of efflux pumps, mutations in the target sites, and alterations in cell permeability [12], [41]–[43]. It has been conventionally assumed that the development of resistance is exclusive to antibiotics, and that, theoretically, bacteria cannot develop resistance against aNDBs. On the one hand, electrostatic attraction between aNDB and bacterial outer structures seems inevitable. In addition, the aNDBs mechanism of action is not explicitly targeted. Even after penetrating the intracellular environment, aNDBs may interfere with multiple metabolic pathways [44]–[46]. Consequently, it is strongly believed that bacteria encounter challenges in impeding electrostatic interaction and developing resistance, given the biological expense associated with such a complex process.

Development of a Novel Inherently Antibacterial Chemically Crosslinked Hydrogel Matrix (2nd Publication)

Hydrogels are innovative biomaterials for tissue engineering, regenerative medicine, and drug delivery applications due to their unique characteristics, such as the ability to encapsulate and release on demand the bioactive compounds (for example, drugs or growth factors) as well as support the cell proliferation and growth [47]–[49]. In recent years, particularly aNDB-based hydrogels with inherent antibacterial activity have been investigated as promising non-antibiotic antibacterial therapeutics for infection treatment in various biomedical applications such as wound healing and tissue infection prevention [24], [50], [51]. Among short-chain antimicrobial peptides (AMP), long-chain antimicrobial polypeptides or poly(amino acids)

such as **ε-polylysine (ε-PL)** have been spotlighted as a high-performance aNDB for antimicrobial biomaterial development [2], [52]–[54]. ε-PL is a naturally occurring, linear cationic antimicrobial polypeptide produced by *Streptomyces albulus,* classified as Generally Recognised as Safe (GRAS No. 000135) by the U.S. Food and Drug Administration, and provides broad-spectrum antimicrobial activity against both Gram-positive and Gram-negative bacteria. Besides its antibacterial mechanism via membrane disruption, ε-PL has several advantages compared to other aNDBs, including a high abundance of free **ε**-amino groups (-NH_2), simple structure, low immunogenicity, low toxicity profile, ease of production and cost-effectiveness [2], [45], [55]–[57]. Until now, only a few studies have addressed the preparation and antibacterial evaluation of ε-PL-based antibacterial hydrogels. Conversely, **hyaluronic acid (HA)** is an anionic and non-sulphated glycosaminoglycan (GAG) with unique physicochemical properties and distinctive biological functions. As a critical component of the native extracellular matrix (ECM), HA is an attractive building block for designing biomimetic, cell-interactive hydrogels for tissue bioengineering applications [58]–[60]. Hydrogels are mainly fabricated using a physical or chemical crosslinking approach or combining both methods to build 3D crosslinked polymer networks [61]. While possessing biomedical safety and ease of fabrication, physically crosslinked hydrogels present low mechanical properties and limited tuneable biodegradation due to the formation of reversible intermolecular interactions and weak secondary forces, such as ionic/electrostatic interaction, hydrogen bonding, etc. [61]–[63]. However, chemically crosslinked hydrogels are usually formed by chemically stable covalent crosslinking, resulting in better mechanical properties, stability in the physiological environment, and more tuneable biodegradation dynamics than the physically crosslinked hydrogels.

In the first part of the Doctoral Thesis, novel chemically crosslinked hydrogels based on ε-PL and HA were prepared via water-soluble 1-ethyl-3-(3-dimethylaminopropyl) carbodiimide (EDC)/N-hydroxysuccinimide (NHS) mediated crosslinking between the carboxyl groups (-COOH) of HA and the primary ε-amino (-NH_2) groups of ε-PL, with constant EDC/NHS crosslinker concentration (1:1). The EDC/NHS concentration used in this study (0.24 M) was selected based on literature reports demonstrating its effectiveness in hydrogel crosslinking while maintaining non-cytotoxicity in cell culture applications [64]. Hydrogels were synthesized with varying ε-PL to HA mass ratios of 40:60, 50:50 and 60:40 wt% to introduce the non-crosslinked primary amino groups of ε-PL (Figure 2). As previously described, the non-crosslinked free amino groups of ε-PL are primarily responsible for its antibacterial activity through electrostatic attachment to the bacterial outer surface. However, an excessively high concentration of free ε-PL may increase the risk of cytotoxicity. Therefore, the main design concept was to combine antimicrobial polypeptide ε-PL with biologically active HA to develop a covalently crosslinked hydrogel matrix that ensures not only structural stability, robust mechanical properties, and viscoelastic features, but also inherent antibacterial activity while maintaining cell viability [24]. To prevent premature gelation and to ensure efficient EDC/NHS-mediated crosslinking, all reagents were pre-cooled to 0–4 °C prior to the synthesis reaction (Figure 2).

The initial results on the physicochemical properties, *in vitro* cytotoxicity, and antibacterial activity of the developed ε-PL/HA hydrogels were published in the collaborative study by Salma-Ancane et al. (2022) [24]. The aim of this study was to investigate the impact of varying ε-PL mass ratios in ε-PL/HA hydrogels on their physicochemical (Figure 3) and *in vitro*

biological properties. This included antibacterial activity against Gram-negative bacteria *E. coli* MSCL 332 (Figure 4A), as well as direct contact cytotoxicity assay to assess the cytotoxicity profile (IC_{50}) of pure ε-PL towards the Balb/c 3T3 cell line (Figure 4B–C).

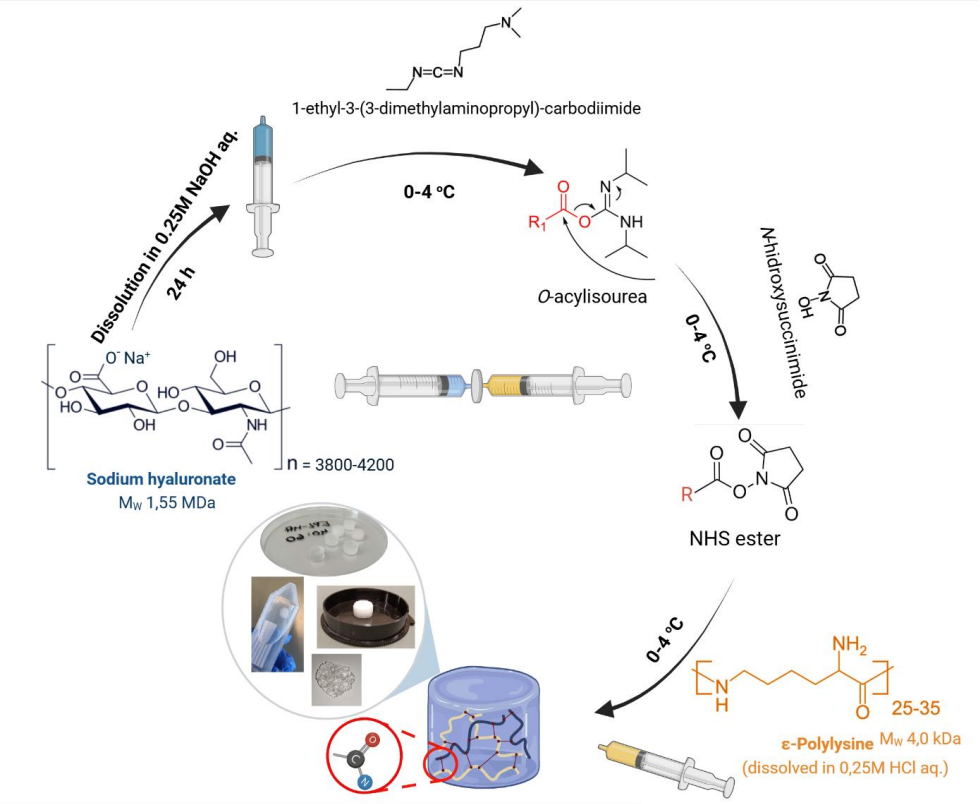

Figure 2. Schematic representation of the synthesis of chemically crosslinked ε-PL/HA hydrogels.

Physicochemical characterisation was performed to evaluate structural and functional properties (Figure 3A–D) of the developed chemically crosslinked ε-PL/HA hydrogels. X-ray diffraction (XRD) patterns (Figure 3A) revealed an amorphous structure of all prepared ε-PL/HA hydrogels with a characteristic amorphous diffraction maximum in the range of 2θ 20–23°. Additionally, diffraction peaks at 2θ 32°, 45° and 52° were observed and corresponded to the characteristic NaCl peaks. NaCl formed during the neutralisation reaction between salts of 0.25M NaOH and 0.25M HCl, in which synthesis was performed. Fourier transform infrared spectroscopy (FTIR) spectra (Figure 3B) of prepared ε-PL/HA hydrogels showed characteristic absorbance maximums that were found in pure components – ε-PL and HA. Thus, in FTIR spectra of prepared ε-PL/HA hydrogels, absorbance maximums at 1633 cm^{-1}, 1555 cm^{-1} and 1377 cm^{-1} were referred to C=O stretching vibration (Amide I), C=O-NH bond vibration (Amide II), and C-N bond vibration (Amide III). Compared to the FTIR spectra of pure ε-PL and HA, slight shifts in the Amide I, Amide II and Amide III bands could be indicative evidence of chemical interaction between the free ε-amino groups of ε-PL and the carboxylic groups of HA, indicating the formation of covalent amide bonds during crosslinking. Furthermore, the calculated Amide I/Amide II ratio from normalised spectra of ε-PL/HA hydrogels and pure component curves also revealed higher values of this ratio compared to pure ε-PL, as the values

of the three hydrogel compositions were found around 0.87, while the same band ratio for ε-PL was 0.69. The absorption bands at 3246 and 3081 cm^{-1} corresponded to unprotonated -NH_2 and protonated -NH_3^+ groups. As previously calculated, the NH_3^+/NH_2 ratios of 0.65, 0.73 and 0.89 for the 40:60, 50:50 and 60:40 wt% compositions, respectively, indicate the presence of free ε-amino groups of ε-PL, which provide inherent antibacterial activity of the ε-PL/HA hydrogels. Gel fraction test results (Figure 3C) showed similar values of gel content (51–57 %) with no statistically significant differences (p>0.05), indicating a consistent crosslinking density across the prepared hydrogels. This consistency is attributed to the fixed HA content and constant molar concentrations of EDC and NHS used during synthesis.

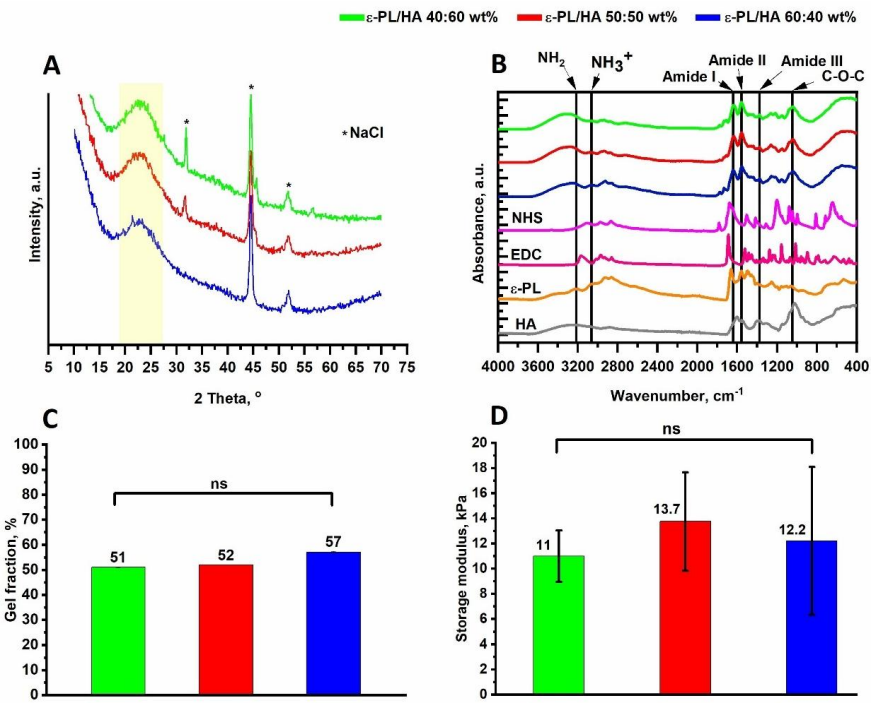

Figure 3. Summary of the main results from the investigation of the physicochemical properties of the ε-PL/HA hydrogels [24]. (A) X-ray powder diffraction (XRD) patterns of the ε-PL/HA hydrogels obtained in the 2θ range from 10 to 70. (B) Fourier transform infrared spectroscopy (FTIR) spectra of the ε-PL/HA hydrogels and the pure components used in their preparation - ε-PL, HA, EDC and NHS – recorded in a range of 400–4000 cm^{-1}. (C) Gel fraction values for three different ε-PL/HA hydrogel compositions presented as a bar chart (mean ± SD). (D) Mechanical stiffness of the ε-PL/HA hydrogel compositions, extracted from amplitude sweep curves at 1 Hz and 0.2 strain%. Three replicates were used from each experimental group.

From the *in vitro* evaluation of antibacterial activity, it was revealed that the chemically crosslinked ε-PL/HA hydrogels exhibited antibacterial effect against the Gram-negative *E. coli* MSCL 332 (Figure 4A). Antibacterial activity was evaluated using both zone of inhibition test (24 h exposure) and the broth dilution test (1 h exposure), suggesting a rapid antibacterial effect upon direct contact and the release of a certain amount of free uncrosslinked ε-PL molecules

into the agar medium, as observed in the diffusion study. Furthermore, *in vitro* direct cell studies showed sustained cell viability and cell confluence after 24 h exposure (Figure 4B–C).

A

Designation	*Diameter of inhibitory zone* ± SD [mm]*	*Log10 bacterial reduction***
ε-PL/HA 40:60 wt%	11.5 ± 0.6	1.8
ε-PL/HA 50:50 wt%	13.0 ± 1.2	2.7
ε-PL/HA 60:40 wt%	15.0 ± 0.0	3.3
Gentamicin, 10 mg/mL	30.7 ± 0.6	-

* Zone inhibition test for **24 h** against *E.coli* MSCL 332
** Broth dilution test for **1 h** against *E.coli* MSCL 332

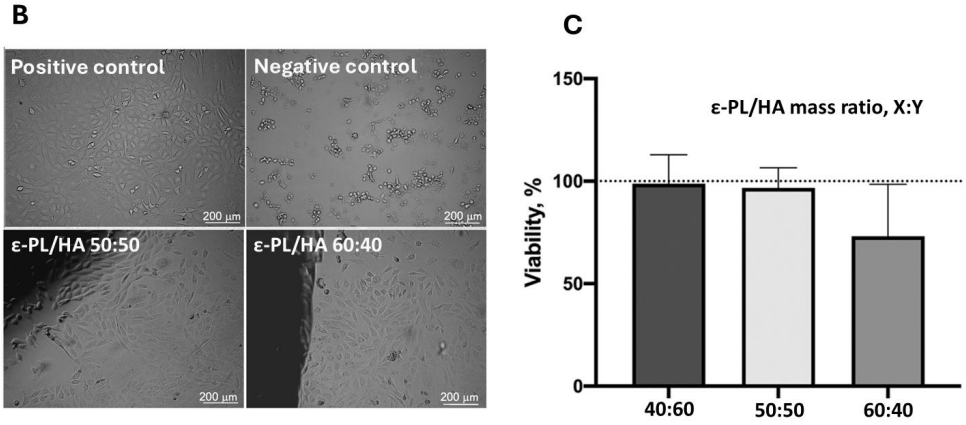

Figure 4. (A) Quantitative results from zone of inhibition test (24 h exposure) and broth dilution test (1 h exposure) against Gram-negative *E. coli* MSCL 332. (B) Microscopic images showing cell viability after 24 h of direct contact with the BALB/c 3T3 cell line. (C) Quantitative results on cell viability (expressed as %) for the prepared ε-PL/HA hydrogel compositions after 24 h of direct contact with BALB/c 3T3 cells (right).

The first part of the Doctoral Thesis demonstrated that in situ-forming, chemically crosslinked ε-PL/HA hydrogels can be successfully synthesized using an EDC/NHS-mediated polymerisation mechanism. The formation of new covalent bonds between ε-PL and HA was revealed from molecular structure analysis by characteristic FTIR spectra comparing absorbance peaks, band shifts and intensity ratios of Amide I, Amide II and Amide III regions relative to the spectra of pure components. The calculated NH_3^+/NH_2 ratios increased with higher ε-PL content I the hydrogels, indicating a higher presence of protonated ε-amino groups, which are associated with antibacterial activity. This trend was further supported by antibacterial assays. The cytotoxicity profile of pure ε-PL showed an IC50 concentration at 4.21 mg/mL, indicating potential cytotoxicity effects at higher concentrations. However, all three hydrogel compositions demonstrated no cytotoxicity effect from direct exposure to BALB/c 3T3 cell lines from direct exposure to BALB/c 3T3 cell lines, highlighting the safety of the developed hydrogel systems. Chemical crosslinking was found to be an advantageous strategy, resulting in ε-PL/HA hydrogels with enhanced structural integrity and a stable stiffness modulus in the range of 10–15 kPa, which is appropriate for musculoskeletal regeneration applications (Figure 3D) [63]. The stable covalent network also contributed to a

sustained antibacterial effect while maintaining low cytotoxicity. Furthermore, the preliminary results indicated that the chemically crosslinked ε-PL/HA hydrogels could be sterilised by steam sterilisation (at 121 °C for 20 min) without compromising mechanical integrity.

In the second part of the Doctoral Thesis, the following research tasks were implemented: (a) synthesis optimisation to reduce the risk of HA degradation; (b) optimisation of the ε-PL to HA mass ratio to achieve optimal mechanical features, high antibacterial activity, while ensuring cell viability; (c) evaluation of the hydrogels topology; (d) evaluation of the hydrogels viscoelastic properties; (e) investigation of the impact of steam sterilisation on physicochemical characteristics; and (f) assessment of *in vitro* antibacterial activity and cell viability.

Optimisation of Synthesis Method, Evaluation of Topology and Impact of Steam Sterilisation on physicochemical and Antibacterial Properties of Chemically Crosslinked ε-PL/HA Hydrogels (3rd Publication)

First, the *in situ* forming method for synthesizing ε-PL/HA hydrogels via EDC/NHS-mediated carboxyl-to-amine crosslinking was modified by using deionized water instead of 0.25M NaOH aq. (for HA) and 0.25M HCl aq. (for ε-PL) (Figure 2). This modification aimed to prevent the risk of HA degradation under alkaline conditions during synthesis. In addition, the experimental design was expanded, and ε-PL/HA hydrogels with ε-PL to HA mass ratios of 40:60, 50:50, 60:40, 70:30 and 80:20 wt% were prepared.

Secondly, small-angle X-ray scattering (SAXS) analysis was performed to examine the internal structure and network topology of all of the fabricated hydrogels [13]. Topological features play a crucial role in their biomedical applications, as they influence viscoelastic behaviour, mechanical integrity, swelling, and biological interactions. Specifically, internal surface structure affects how biomaterial interfaces with living tissue, including cell adhesion, migration, mechanotransduction, proliferation, and antibacterial activity. SAXS analysis was performed over the q-range (0.045 nm−1–0.233 nm−1), corresponding to real-space dimensions of 27–140 nm. This range includes the Porod region of the hydrogel-like structures (of real d space), thus primarily providing information about the surface features and interface smoothness of the hydrogel network. The obtained scattering data were analysed using power-law fitting to extract the decay exponent (n), which provides insight into surface topology. Results of the examined chemically crosslinked ε-PL/HA hydrogels are presented as double logarithmic plots of q-decay (Figure 5A). A highly concentrated HA solution was used as the control, and exhibited decreased scattering intensity $\sim q^{-3.9} \approx q^{-4}$, indicating typical smooth surfaces formed by large polyelectrolyte complexes (Figure 5B) [65]. The chemically crosslinked ε-PL/HA hydrogels showed similar decreased scattering intensities $\sim q^{-3.6\pm0.4}$, indicating smooth and robust network topologies, Porod surface (Figure 5B). This goes in line with the expected topological results for chemically crosslinked networks with smooth interfaces held by more robust covalent bonds. The exception, ε-PL/HA hydrogel series with 40:60 wt% mass ratio, showed significantly different scattering intensity of $\sim q^{-2.9}$ (Figure 5B), mostly typical of physically crosslinked aggregated clusters with rough interfaces [13]. As an outcome, ε-PL/HA hydrogels with ε-PL to HA mass ratios of 50:50, 60:40, 70:30 and 80:20 wt% were used in upcoming studies.

The ability of biomaterials, especially hydrogels, to withstand conventional steam sterilisation represents a significant advantage during early-stage development and clinical translation. Steam sterilisation is a highly effective, easily used and widely available sterilisation method. In the next step, the effect of steam sterilisation on the previously chosen hydrogel series was investigated to reveal in-depth physicochemical features. Then, topological evaluation was followed by scanning electron microscopy (SEM). SEM was used to observe the morphology of prepared freeze-dried hydrogel samples (Figure 5C). Both non-sterilised and sterilised samples showed a homogeneous three-dimensional network with interconnected porosity, with minimal effects visible for all hydrogels after sterilisation. Furthermore, pore size distribution after sterilisation for each ratio remained in a similar macrosize range of 66.7 ± 34.2 –193.35 ± 103.05 μm.

The gel fraction values for non-sterilised ε-PL/HA hydrogel samples with ε-PL to HA mass ratios of 50:50, 60:40, 70:30 and 80:20 wt%, were 55.6± 0.1, 56.2± 0.2, 54.7± 1.6 and 44.2± 2.9%, respectively (Figure 5D). These corresponded well to the first report values of ∼55 % [24], except for the 80:20 wt% sample, which had significantly lower gel fraction. This lower value was ascribed to the lower extent of crosslinking for this ratio. Evidently, larger amounts of free, non-crosslinked ε-PL were able to diffuse out during immersion in water, resulting in a decreased gel fraction, as a greater proportion of ε-PL dissolved relative to the initial polymer mass in the hydrogel. No significant differences in gel fraction values were observed between non-sterilised and sterilised hydrogel samples within the same ε-PL to HA mass ratio (p>0.05). This indicates that the steam sterilisation did not affect the overall extent of crosslinking in the ε-PL/HA hydrogel samples, thereby preserving the network topology established during synthesis.

During swelling behaviour studies, both non-sterilised and sterilised ε-PL/HA (ster ε-PL/HA) hydrogels demonstrated swelling capability (swelling degree >100 %) after 2 h of incubation, and maintained plateau values over the entire study period (24 h, Figure 5E). In non-sterilised hydrogel samples, the swelling capacity increased with increasing ε-PL mass ratio at 2 h, ranging from 116 % for the 50:50 wt% composition to 340 % for 80:20 wt% composition, respectively. For the 50:50, 60:40, and 80:20 wt% compositions, no significant differences were observed by 24 h (p>0.05). In contrast, the swelling capacity of ster ε-PL/HA hydrogels with ε-PL to HA mass ratio of 70:30 wt% increased from ∼215 % to ∼290 % (p<0.05), possibly indicating a reduction in mechanically active crosslinks. Despite this variation, all ster ε-PL/HA hydrogels exhibited equilibrium swelling in the range of 116–350 % (dependent on ε-PL content), achieved after 4 h of incubation under physiological conditions (37 °C), demonstrating acceptable structural stability and cohesive properties for potential tissue engineering applications.

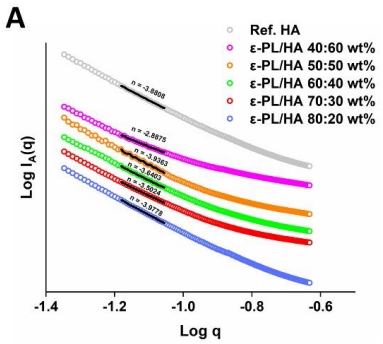

B

Sample name	Power law fitting (q^{-n}), where *n* is provided below
Ref. HA	3.9
ε-PL/HA 40:60 wt%	2.9
ε-PL/HA 50:50 wt%	3.9
ε-PL/HA 60:40 wt%	3.6
ε-PL/HA 70:30 wt%	3.5
ε-PL/HA 80:20 wt%	4.0

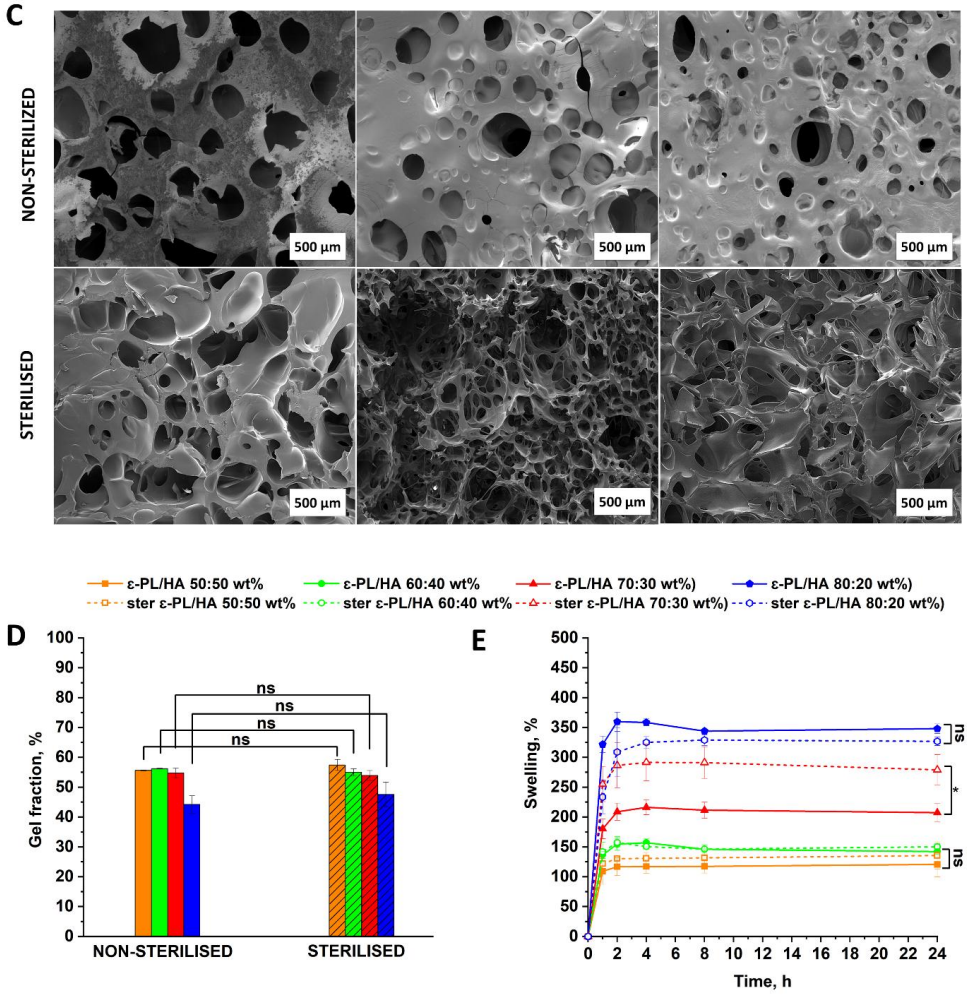

Figure 5. Investigation of the physicochemical properties of the ε-PL/HA hydrogels [13]. (A) SAXS curves of the ε-PL/HA hydrogels with mass ratios of 40:60, 50:50, 60:40, 70:30 and 80:20 wt%. (B) Calculated values of power law fitting index n from the q-decay (q^{-n}). (C) SEM micrographs of non-sterilised (top) and sterilised (bottom) hydrogels; from left to right: 60:40, 70:30 and 80:20 wt%, respectively. (D) Gel fraction values of non-sterilised and

sterilised ε-PL/HA hydrogel samples. (E) Swelling behaviour curves of non-sterilised and sterilised samples. (D–E) Data are presented as mean ± SD (n = 3).

Various rheological studies were obtained to investigate the ε-PL/HA hydrogel viscoelastic properties (Figure 6). Firstly, rheological features were observed as a function of hydrogel mass ratios and sterilisation. Amplitude sweep studies (Figure 6A–B) were performed in oscillation mode upon a strain range of 0.01 to 1000 strain% (ε), at a constant frequency of 1 Hz, equal to physiological conditions and 25 °C temperature. From the obtained curves of non-sterilised hydrogels (Figure 6A), it was concluded that hydrogels possessed soft solid-like behaviour with storage modulus (G') dominance prior to loss modulus (G'') in the linear viscoelastic region (LVR). However, ε-PL/HA hydrogels exhibited limited LVR in the range of ~ 0.1–1 % strain. In addition, observed G'' behaviour with respect to G' showed the larger G'/G'' ratio at lower strains but decreasing quite rapidly to a crossover point G' = G''. For all compositions, the crossover point remained as a $\varepsilon \approx 100$ %, highlighting hydrogel matrix resilience towards transition from solid to liquid mainly due to more stable and flexible chemical crosslinks. As for sterilised samples (Figure 6B), some minor differences were observed: (i) the crossover point (G'=G'') of all compositions changed from previously identified $\varepsilon \approx 100$ % to $\varepsilon \approx 70$ %; (ii) G'' behaviour at lower strain values (~0.01–1 %) became identical for all the compositions compared with non-sterilised samples in the same strain value range. This could be explained as an outcome of sterilisation, resulting in partial loss of physical entanglements in the hydrogel matrix raised by uncrosslinked ε-PL molecules and negatively charged HA functional groups. In the next step, storage modulus (G') values were extracted from amplitude sweep curves of both non-sterilised and sterilised hydrogel samples at $\varepsilon = 0.2$ % within the LVR (Figure 4C). Storage modulus values give insight into the mechanical stiffness of hydrogels. It was concluded that stiffness modulus for hydrogel compositions of 50:50, 60:40 and 80:20 wt% remained statistically insignificantly different (p>0.05) before and after sterilisation. However, for 70:30 wt%, this difference was significant (p<0.05), indicating that sterilisation had a higher effect on hydrogel structure and topology. Despite this finding, stiffness of ε-PL/HA hydrogel compositions of 50:50, 60:40 and 70:30 wt% before and after sterilisation remained around 10kPa, while 80:20 wt% composition showed a lower stiffness value of 8.6 kPa before sterilisation and dropped to 6.9 kPa after treatment. To sum up, these stiffness values suggest these hydrogels, after sterilisation, still address stiffness requirements (5–15 kPa) towards, for exampe, combined antibacterial and musculoskeletal regeneration applications [24].

Further rheological investigation was performed in flow mode and aimed to assess the injectability features of prepared hydrogel samples. From shear rate-dependent viscosity curves (Figure 6D), it can be seen that in case of all prepared samples, viscosity rapidly drops down as a function of increasing shear rate. This tendency suggests that prepared hydrogels are shear-thinning and can possess injectability/printability features. To answer more precisely that question, in the next step, recovery cycle studies were performed. The recovery cycles are performed to simulate the shear rate stress caused during the extrusion from a syringe/needle and to observe matrix recovery through viscosity values (Figure 6E).

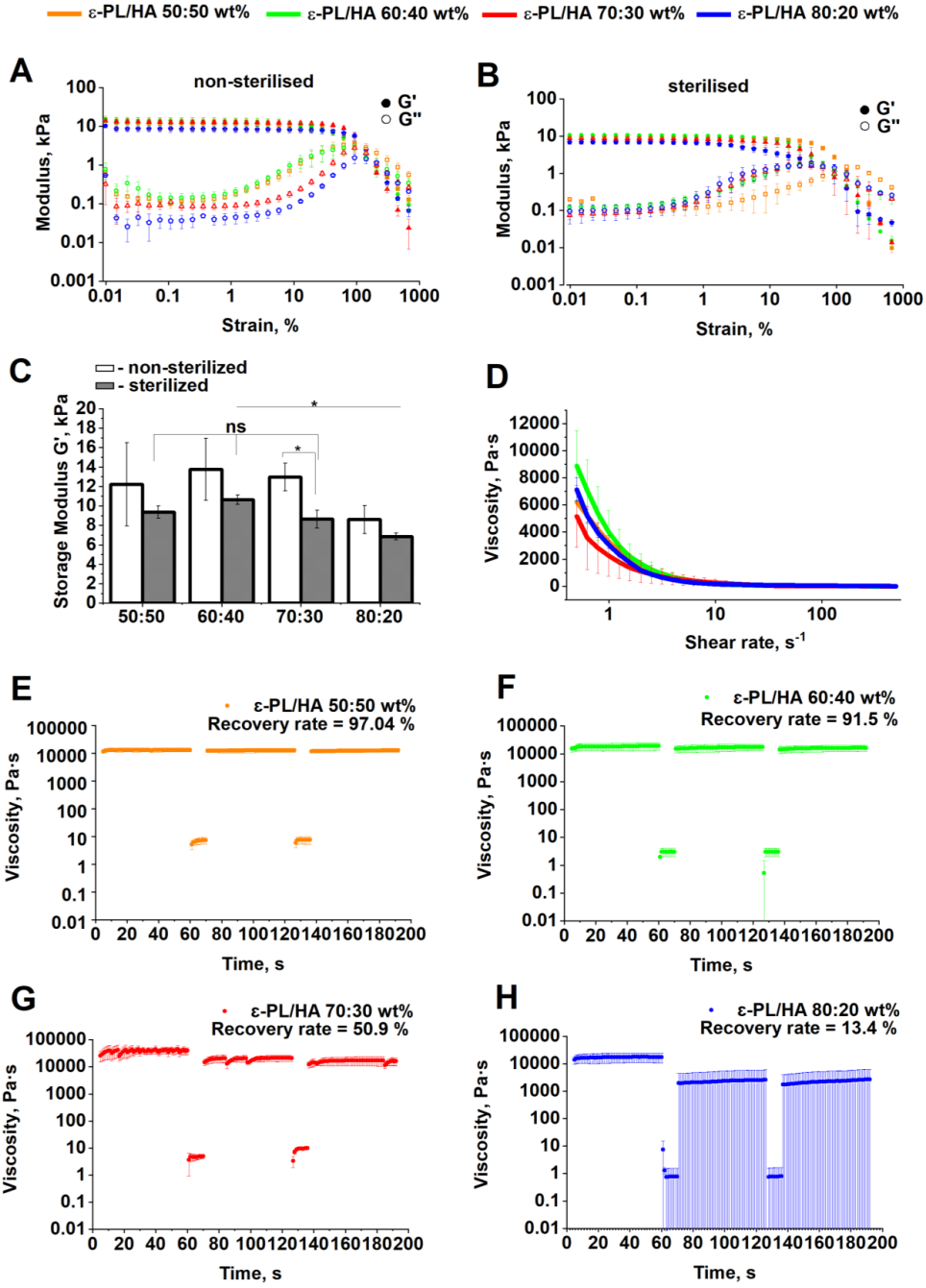

Figure 6. Rheological studies on prepared ε-PL/HA hydrogels [2], [13]. (A–B) Amplitude sweep test curves of non-sterilised (A) and sterilised (B) hydrogel samples with different compositions. (C) Extracted storage modulus (G') from amplitude sweep at ε-0.2 % strain (LVR). (D) Shear rate-dependent viscosity graph. (E–H) Recovery cycle test performed over five cycles (3+2), comprising three stress-free cycles at a shear rate of 0.1 s^{-1} for 60 s, and 2

stress-induced cycles at 200 s^{-1} for 10 s. All rheological measurements were performed in triplicate to ensure reproducibility and data reliability.

Overall, the curves showed recovery features of broken intermolecular sites after induced stress conditions, that is, high shear rate values. It was found that compositions of 50:50 and 60:40 wt% were most suitable in terms of injectable biomaterials as they possessed a stable recovery rate higher than 90 % after multiple stress-induced cycles. Lower recovery values were found for 70:30 wt% composition, suggesting lower matrix integrity and flexible chain presence. However, ε-PL/HA hydrogels with 80:20 wt% composition showed dramatically low recovery features, as only 13.4 % of the viscosity recovered compared to the initial viscosity values and possibly only due to the presence of a separate cluster in the broken hydrogel sample. As a result, three compositions of 50:50, 60:40 and 70:30 wt% were able to show recovery features. Possible difference of values between them can be explained again by structural integrity, as by increasing ε-PL mass ratio, more uncrosslinked ε-PL molecules interconnect with HA functional groups during synthesis, thereby interrupting chemical crosslinking network formation and organisation.

To sum up, physicochemical characterisation was performed for a series of ε-PL/HA hydrogels with varying ε-PL to HA mass ratios. The hydrogels showed gel fraction values, as well as swelling behaviour typical of hydrogels for tissue engineering applications. Furthermore, it was confirmed that the hydrogels could undergo steam sterilisation without significantly affecting these key properties. However, the rheological analysis revealed that 80:20 wt% composition did not meet the desired viscoelastic requirements for injectability and mechanical stiffness. Based on these findings, only 50:50, 60:40 and 70:30 wt% ε-PL/HA hydrogel compositions were selected for further *in vitro* biological evaluation within the Doctoral Thesis.

In Vitro Evaluation of Antibacterial Potential and Cytotoxicity of ε-PL/HA Hydrogels (4th Publication)

In the first part of the Doctoral Thesis, the preliminary studies confirmed the antibacterial potential of the developed ε-PL/HA hydrogels against *E. coli* MSCL 332, using zone of inhibition and broth dilution assays at short (1 h) and extended (24 h) exposure times. However, firstly, it was crucial to investigate the antibacterial profile of pure ε-PL by determining its minimum inhibitory and bactericidal concentrations (MIC/MBC), as well as assessing the potential for bacterial resistance development. The antibacterial activity of pure ε-PL and ε-PL/HA hydrogels was characterised by the broth dilution method via direct/indirect contact according to modified CLSI and EU CAST standards [66]. Antibacterial studies were performed against various Gram-negative and Gram-positive bacteria strains, including ATCC reference *Escherichia coli* (*E. coli*), *Staphylococcus aureus* (*S. aureus*) and *Staphylococcus epidermidis* (*S. epidermidis*), clinically isolated *Pseudomonas aeruginosa* (*P. aeruginosa*) and hard-to-treat clinically isolated multidrug-resistant Methicillin-resistant *Staphylococcus aureus* (MRSA), Extended spectrum β-lactamase *Escherichia coli* (ESBL *E. coli*) bacteria. MIC and MBC values of pure ε-PL are presented in Table 1. Results showed inhibitory (MIC) and bactericidal (MBC) activity against all previously mentioned bacteria strains on a microgram scale, while IC50, as previously found, was 4.21 mg/mL on the mouse fibroblast cell line

Balb/c 3T3. These results suggest that it is possible to moderate the ε-PL mass ratio in hydrogel samples to achieve a high antibacterial activity while ensuring cell viability.

Table 1

The Obtained Values of MIC/MBC Concentrations of Pure ε-PL

Bacterial strain	MIC of ε-PL, μg/mL	MBC of ε-PL, μg/mL
E. coli	37	75
P. aeruginosa	75	350
ESBL *E. coli*	18	37
S. aureus	37	75
S. epidermidis	18	37
MRSA	37	75

Furthermore, it was demonstrated that neither reference strains (*E. coli and S. aureus*) nor clinically isolated multidrug-resistant strains (ESBL *E. coli* and MRSA) developed resistance to ε-PL over the experimental timeframe of 1 month (10 passages), highlighting the strong potential of ε-PL/HA hydrogels for future antibacterial applications (Figure 7).

The results for ε-PL/HA hydrogels demonstrated a statistically significant inhibition of bacterial colony growth after 24 h of contact ($p<0.05$) compared to control samples, across all tested bacterial strains and hydrogel compositions (Figure 8A). However, several key findings were observed: (i) the inhibition rate, presented as Log_{10} reduction, was dependent on the ε-PL mass ratio in hydrogel compositions, that is, ε-PL/HA of 70:30 wt% mass ratio showed the highest inhibition rate.

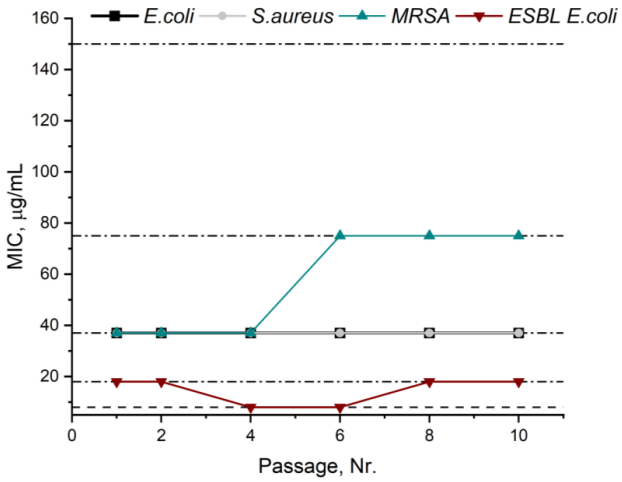

Figure 7. Bacterial resistance development studies of pure ε-PL against *E. coli*, *S. aureus*, MRSA, and ESBL *E.coli* bacteria. The experiment was performed over 10 passages, with bacterial cultures re-cultivated from sub-MIC concentrations at each step.

In the case of *S. epidermidis*, *P. aeruginosa*, and MRSA, complete bacterial eradication was achieved; (ii) for the 50:50 and 60:40 wt% hydrogel compositions, a clear trend of efficient inhibition was observed against Gram-positive strains, including the reference *S. aureus* and *S. epidermidis*, as well as the clinically isolated multidrug-resistant MRSA. In contrast, a lower

inhibition activity was achieved against Gram-negative strains (*E. coli*, *P. aeruginosa* and ESBL *E. coli*). This difference may be attributed to the unique structural features of Gram-negative bacterial cell walls, such as the presence of an outer membrane that serves as an additional barrier to penetration of polypeptide molecules, and the action of efflux systems that can reduce intracellular accumulation of antibacterial agents.

The antibacterial potential of the ε-PL/HA hydrogels over a sustained timeframe (up to 168 h) was investigated. The hydrogel samples were incubated for a week, with media refreshing cycles performed after 1 h and 24 h of incubation. This approach aimed to evaluate whether, following the initial rapid release of uncrosslinked ε-PL, expected to occur within the first 24 h, the ε-PL/HA hydrogel matrix could still provide a sustained release of ε-PL due to gradual matrix degradation. After 168 h, both direct contact and indirect test (supernatant-based) antibacterial assays were performed using 24 h exposure against Gram-negative *E. coli* and Gram-positive *S. aureus* (Figure 8B). The results showed that all compositions of hydrogels retained a statistically significant antibacterial activity ($p<0.05$) through both exposure routes: direct bacteria contact with the hydrogel matrix and indirect contact with supernatants collected at 168 h. Notably, the 50:50 wt% ε-PL/HA hydrogel composition exhibited the lowest inhibition rate compared to the other compositions in both exposure types against *S. aureus*, suggesting that its denser, and more compact matrix may have resulted in reduced degradation rate and limited availability of positively charged functional groups at the hydrogel surface.

Cytotoxicity was evaluated, using both direct and indirect contact approaches, (Figure 8C–D). In the indirect assay (Figure 8D), using Human Dermal Fibroblasts (HDFs), all ε-PL/HA hydrogels formulations exhibited no cytotoxicity at extract concentrations up to 4.35 mg/mL, as cell viability remained above 70 % (the threshold for non-cytotoxicity defined by ISO 10993-5:2009 [67]) after 48 h of exposure. Notably, at an extract concentration of 2.025 mg/mL, cell viability was significantly higher than the control, suggesting that ε-PL may promote cell proliferation when applied at appropriate concentrations. Interestingly, that 50:50 wt% ε-PL/HA composition showed no cytotoxicity (cell viability > 70 %) toward HDFs at concentrations up to 93.023 mg/mL [2]. This finding aligns with results from the long-term antibacterial study, where the same composition exhibited lower antibacterial activity, possibly due to its denser and more compact crosslinking matrix, resulting in reduced ε-PL release and lower surface charge. Furthermore, a cytotoxic effect was observed for the ε-PL/HA 60:40 wt% composition at 20.12 mg/mL, while for the 70:30 wt% composition at as low as 9.36 mg/mL, indicating a correlation between increasing ε-PL content in hydrogel samples and decreased cell viability. At concentrations $\geq$ 93.023 mg/mL, all compositions exhibited significant cytotoxicity [2]. Direct contact studies with Balb/c 3T3 cells (Figure 8C) after 24 h of exposure indicated mild cytotoxicity across all ε-PL/HA hydrogel series, with cell viability remaining close to the acceptable threshold (~70 %), 69.5±16.8, 65.3±17.4, 71.5±7.9 for 50:50, 60:40, and 70:30 wt% hydrogel compositions, respectively. No statistically significant differences were observed between the compositions.

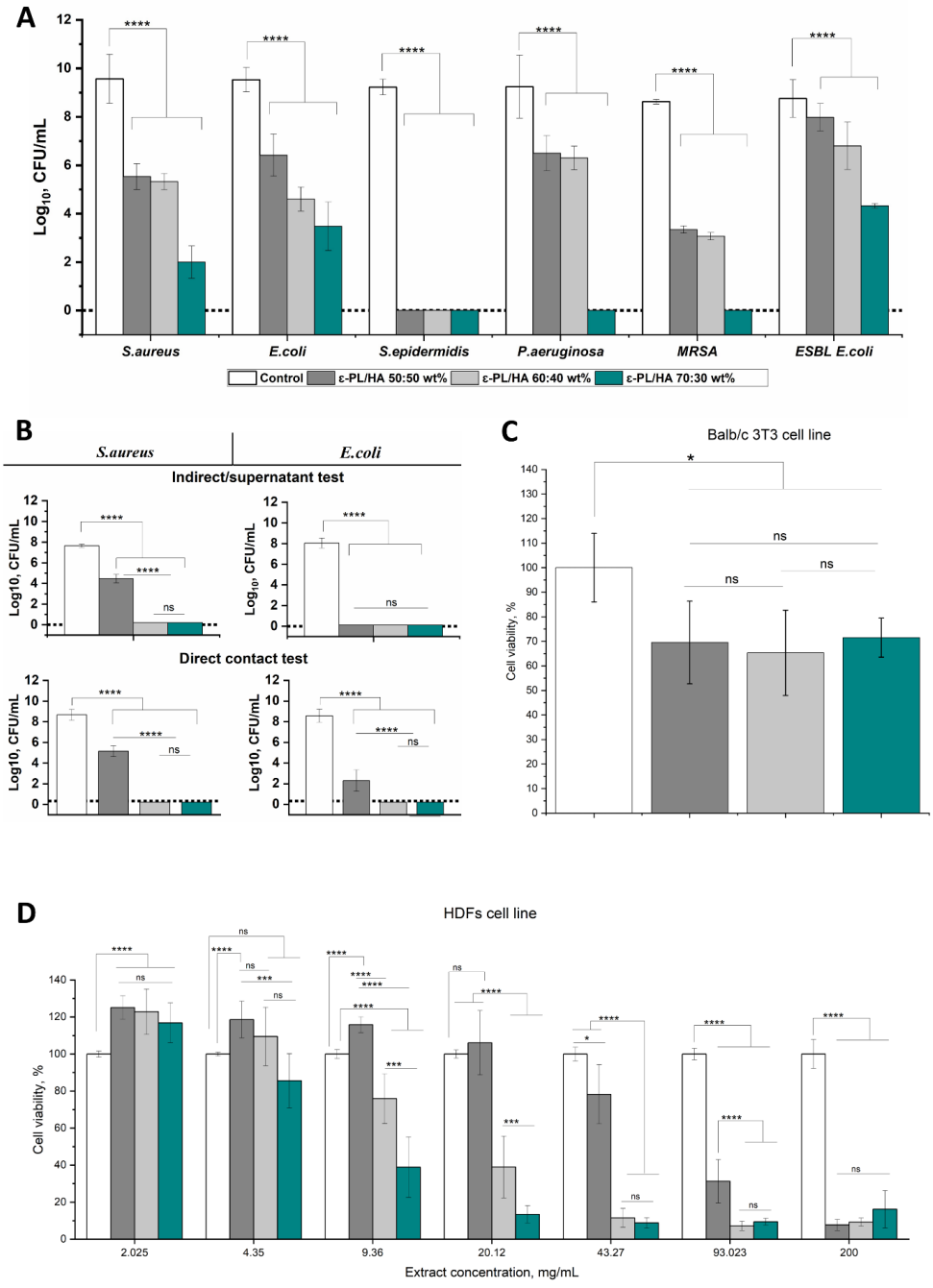

Fig. 8. *In vitro* studies on prepared ε-PL/HA hydrogels [2]. A unified colour palette was used for all ε-PL/HA hydrogels compositions across the graphs and is provided as a legend below Graph A. (A) Direct contact studies using the broth dilution method against various Gram-negative and Gram-positive bacteria strains. Results of inhibition rate are presented as Log_{10}

reduction in bacterial count. (B) Direct contact and indirect (supernatant-based) antibacterial studies after 168h incubation, with media refreshening at 1h and 24h, provided against *E.coli* **a**nd *S. aureus* . (C) Direct cell viability assay using the Balb/c cell line after 24h exposure. (D) Indirect cell viability assay using the HDF cell line after 48h exposure to various extract concentrations . Three replicates were used in each experiment, and results are presented as mean ± SD.

Figure 8. *In vitro* studies on prepared ε-PL/HA hydrogels [2]. A unified colour palette was used for all ε-PL/HA hydrogel compositions across the graphs and is provided as a legend below Graph A. (A) Direct contact studies using the broth dilution method against various Gram-negative and Gram-positive bacteria strains. Results of inhibition rate are presented as Log_{10} reduction in bacterial count. (B) Direct contact and indirect (supernatant-based) antibacterial studies after 168 h incubation, with media refreshening at 1 h and 24 h, provided against *E.coli* and *S. aureus*. (C) Direct cell viability assay using the Balb/c cell line after 24 h exposure. (D) Indirect cell viability assay using the HDF cell line after 48 h exposure to various extract concentrations. Three replicates were used in each experiment, and results are presented as mean ± SD.

Synthesis and Characterisation of Antibacterial Sr-HAp Functionalised ε-PL/HA Hydrogels (5th Publication)

Previously, the developed ε-PL/HA hydrogel composition with a 50:50 wt% showed fast-acting (up to 24 h) and sustained (up to 168 h) an antibacterial activity against a broad spectrum of pathogens, while also demonstrating favourable cell viability, ability for steam sterilisation, injectability, and smooth surface topology. Based on these properties, the 50:50 wt% ε-PL/HA hydrogel composition was selected for further development of the composite system by functionalisation of ε-PL/HA hydrogel matrix with strontium-substituted hydroxyapatite (Sr-HAp) nanoparticles. This functionalisation aimed to unite the advantageous features of both components: the viscoelastic and inherent antibacterial properties of the developed ε-PL/HA hydrogel matrix and the bone regeneration-promoting properties of Sr-HAp nanoparticles, toward the development of antibacterial and bioactive hydrogels for bone tissue engineering applications.

In this study, several compositions were developed, including a pure ε-PL/HA hydrogel matrix with 50:50 wt% composition, and Sr-HAp/ε-PL/HA composite hydrogels with varying inorganic (Sr-HAp): organic (ε-PL/HA 50:50 wt%) mass ratios of 40 %, 50 % and 60 % (Figure 9A).

As injectability is an advantageous feature for biomaterials, particularly in bone regeneration applications, the injection force of the as-prepared hydrogels was investigated (Figure 9B). The results showed that all compositions, including the pure ε-PL/HA hydrogel matrix, could be injected through a syringe with a tip inner diameter of 1.8 mm under an applied injection force of 3N. According to literature, needle gauge sizes ranging from 10 (inner diameter 2.69 mm) to 16 (inner diameter 1.19 mm) are considered suitable for orthopaedic procedures such as filling bone defects and cracks [68]. Additionally, the injection force should remain below 30 N, which is defined as the upper limit of manual injectability [69]. Based on

this criteria, the developed hydrogels can be classified as manually injectable and suitable for potential clinical applications.

To investigate viscoelastic properties of the Sr-HAp/ε-PL/HA hydrogels, compression studies were provided as part of their rheological characterisation. The compression test results (Figure 9C) revealed comparable behaviour across all tested compositions, with compression storage modulus (E') values of ~ 1000 kPa within the physiological frequency range (0.1–10 Hz). According to the literature data, the compression storage modulus (E') values of composite platforms designed for bone tissue regeneration typically range from 100 kPa to several MPa [70], [71]. Thus, the compression storage modulus values of the Sr-HAp/ε-PL/HA hydrogels fall within the expected range for bone tissue regeneration applications. However, it should be noted that these studies do not provide a comprehensive evaluation of the mechanical properties, particularly under dynamic or load-bearing conditions. Therefore, Sr-HAp/ε-PL/HA hydrogels cannot be considered suitable for load-bearing applications. However, they may still serve as promising biomaterials for providing favourable conditions for the natural bone remodelling process by maintaining nutrition transport, possessing porosity for cell migration, retaining structural integrity, and mimicking key features of the extracellular matrix [72].

To support the previously defined practical functionality, in further studies enzymatic degradation and kinetic profiles of ion release (Ca^{2+} and Sr^{2+}) were performed. Enzymatic degradation curves (Figure 9D) showed that Sr-HAp/ε-PL/HA degraded in hyaluronidase enzyme-containing PBS media over 20 weeks. While 0% Sr-HAp compositions showed a gradual degradation trend, reaching complete degradation after 20 weeks, the 40 %, 50 % and 60 % Sr-HAp compositions degraded more rapidly, achieving full degradation already after 5, 10 and 16 weeks, respectively. These results suggest that the biodegradation profile of Sr-HAp/ε-PL/HA hydrogels is a function of Sr-HAp content and could be tuned to match specific application requirement in bone regeneration. Regarding ion release curves, it was observed that Ca^{2+} and Sr^{2+} ions were released in a burst manner when loaded into hydrogels compared with the pure Sr-HAp release profile (Figure 9E–F). A reason for that could lie in the acidic nature of the ε-PL/HA hydrogel matrix, which could result in Sr-HAp dissolution, causing burst release observed within the first days of the experiments. Subsequently, the release of Ca^{2+} and Sr^{2+} ions from the Sr-HAp/ε-PL/HA hydrogels proceeded in a slow and continuous manner over three months of the experimental period. Importantly, the concentration of Sr^{2+} ions did not exceed 20–30 μM, while Ca^{2+} ions release ranged between 200 and 350 μM. Previous studies have shown that Sr^{2+} ion concentrations up to 40 μM are beneficial for the proliferation of osteoblasts in the cell culture [73], and the elevated Ca^{2+} ion concentration level up to 900 μM can further enhance the bone regenerative effects of Sr^{2+} ions [73].

Finally, the antibacterial activity of the Sr-HAp/ε-PL/HA hydrogels was evaluated in both rapid (24 h) and sustained (168 h) timeframes (Figure 10). Experimental time points were set as 24 h, 48 h, 72 h and 168 h, and studies were performed against Gram-positive bacteria: *S. aureus* (*Staphylococcus aureus*, ATCC 25923, reference), MRSA (methicillin-resistant *Staphylococcus aureus*, clinically isolated multidrug resistant strain), and Gram-negative bacteria: *E. coli* (*Escherichia coli*, ATCC 25922, reference), ESBL *E. coli* (extended spectrum β-lactamase *Escherichia coli*, clinically isolated multidrug-resistant strain). The obtained results revealed that experimental series of Sr-HAp/ε-PL/HA hydrogels were able to inhibit both reference and clinically isolated multidrug-resistant Gram-negative and Gram-positive bacterial strains. However, several tendencies and subtleties must be highlighted. First of all, a higher inhibition rate was observed against Gram-positive bacteria, both reference and resistant

strains. These results are in agreement with previous results on pure ε-PL/HA hydrogels (Figure 8A) and were similarly re-observed in the case of 0% Sr-HAp. In general, a relatively high inhibition rate was maintained for all Sr-HAp/ε-PL/HA hydrogel series throughout the entire experimental timeframe. Secondly, a sufficiently lower inhibition rate, compared to Gram-positive bacteria, was achieved against Gram-negative bacteria (both reference and clinical isolates). At the 24 h time point, the antibacterial activity of the 0% Sr-HAp composition closely matched previously obtained results for 50:50 wt% ε-PL/HA hydrogel composition (Figure 8A). Furthermore, statistically significant inhibition of *E. coli* and ESBL *E. coli* was observed for all experimental series only under short-term conditions (24 h).

A

Designation	Composition
0% Sr-HAp	100% ε-PL-HA (ε-PL:HA 50:50 wt%)
40% Sr-HAp	Sr-HAp 40 wt%, ε-PL/HA 60 wt%
50% Sr-HAp	Sr-HAp 50 wt%, ε-PL/HA 50 wt%
60% Sr-HAp	Sr-HAp 60 wt%, ε-PL/HA 40 wt%

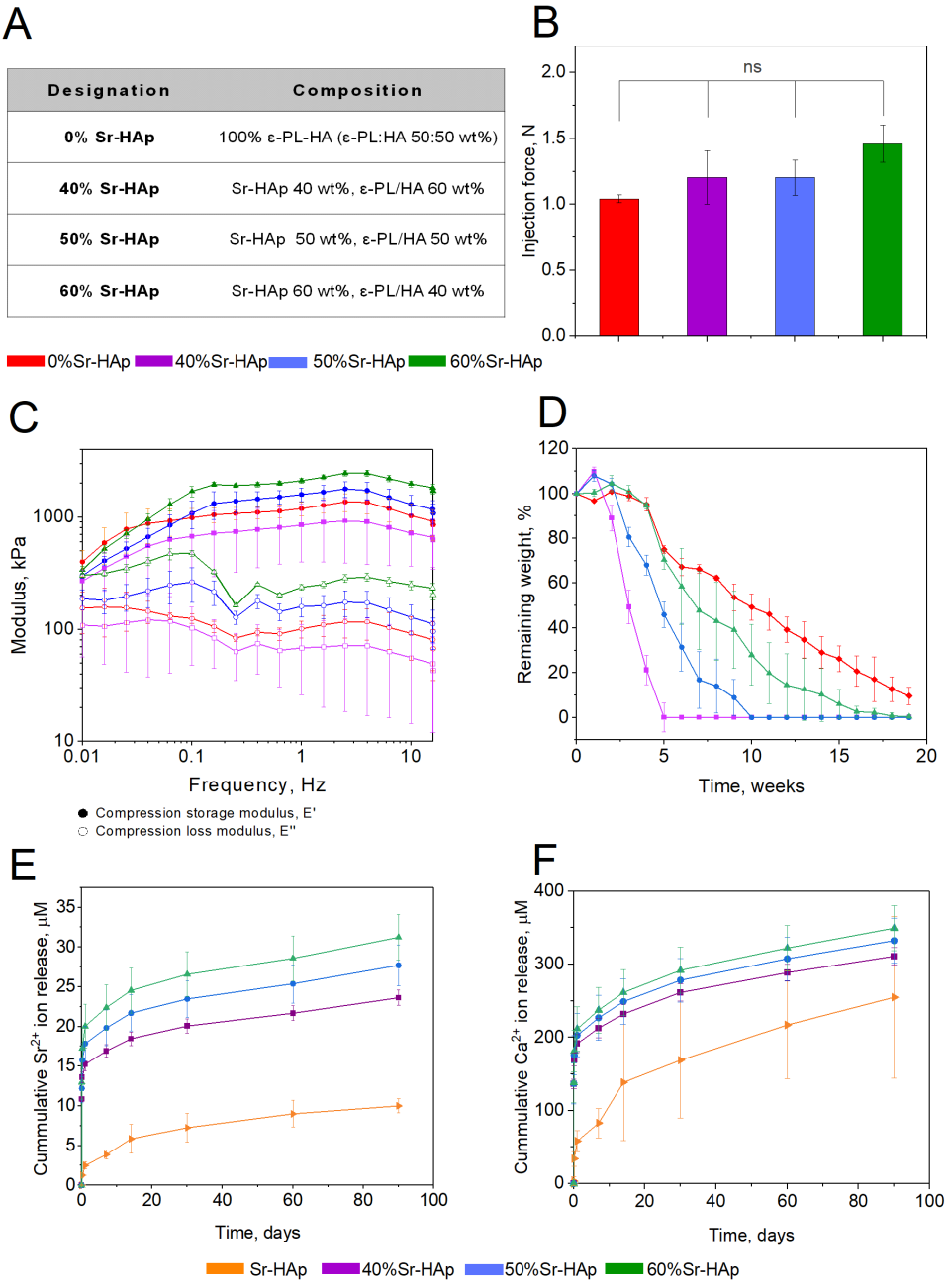

Figure 9. Physicochemical characterisation studies of the Sr-HAp/ε-PL/HA hydrogels [72]. (A) Designation and composition of the Sr-HAp/ε-PL/HA hydrogels used in subsequent experimental studies. (B) Injection force studies. No statistically significant differences (ns, p>0.05) in injection force values were found between the used compositions. (C) Compression studies within rheological investigation of the hydrogels. Compression tests were performed at 8 N axial force (axial force > dynamic force = 30 %), with 30 µm axial displacement, over a frequency range from 0.01 to 16 Hz. Compression storage modulus (E') and compression loss modulus (E'') were monitored. (D) Enzymatic degradation curves of the

Sr-HAp/ε-PL/HA hydrogels in hyaluronidase enzyme-containing PBS media over a 20-week period. (E) Sr^{2+} ion release studies. (F) Ca^{2+} ion release studies. (E–F) Ion release studies of Sr-HAp/ε-PL/HA hydrogels performed over a 90-day period, with results presented in μM concentration. Three replicates were used in each experiment. Results are presented as mean ± SD.

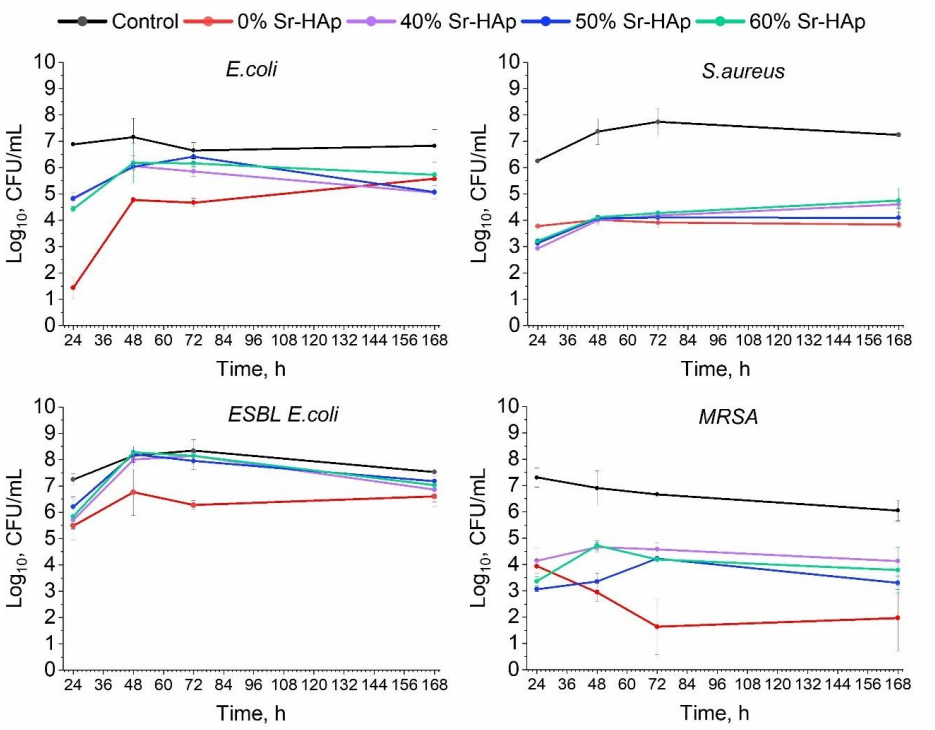

Figure 10. Antibacterial activity (24–168 h) of the as-prepared Sr-HAp/ε-PL/HA hydrogels against *E. coli*, *S. aureus*, ESBL *E. coli*, and MRSA (n = 3) [72].

As previously hypothesised, a possible explanation could rely on the unique cell wall structure of Gram-negative bacteria and their more effective efflux systems. Thirdly, it was clearly observed that 0% Sr-HAp hydrogel composition at several time points (*E. coli*: 24 h; MRSA: 72 h), and in some cases, was the only composition showing statistically significant inhibition (*E. coli*: 24 h; MRSA: 72 h; (*E. coli*: 48 h and 72 h; ESBL *E. coli*: 48 h and 72 h). This may be explained by the presence of the Sr-HAp inorganic phase in the hydrogel matrix of the 40 %, 50 % and 60 % Sr-HAp hydrogel compositions. The functionalisation with Sr-HAp nanoparticles increases physical entanglements between the ε-PL/HA hydrogel matrix and positively charged Ca^{2+}/Sr^{2+} ions, forms a physical barrier and provokes network reorganisation into a more compact configuration. This negatively affects the release kinetics of antibacterial molecules of ε-PL and results in reduced antibacterial potential of hydrogels [74]. Finally, no statistically significant difference (p>0.05) was observed between the 40 %, 50 % and 60 % Sr-HAp hydrogels at any of the tested time points, suggesting that the presence of Sr-HAp did not significantly influence the antibacterial activity of the developed Sr-HAp/ε-PL/HA hydrogels.

CONCLUSIONS

1. A reproducible synthesis methodology has been developed to fabricate chemically crosslinked, injectable ε-PL/HA hydrogels using EDC/NHS (0.24:0.24 mol) chemistry, with ε-PL to HA mass ratios of 40:60, 50:50, 60:40, 70:30, and 80:20 wt%.
2. The developed ε-PL/HA hydrogels exhibit key properties relevant for antibacterial applications in tissue engineering, including tuneable free ε-amino group content (via ε-PL mass ratio), gel fraction stability (50–60 %), mechanical stiffness within the 5–15 kPa, smooth surface topology, injectability through a 19 G needle, high recovery after injection (85–95 %), and autoclavability at 121 °C for 20 min. These features contribute to dose-dependent antibacterial activity, achieving 2 3 Log_{10} reduction in *E. coli* MSCL 332 after 1 h of contact.
3. Steam sterilisation at 121 °C for 20 min have not significantly affected gel fraction ($p > 0.05$), pore size distribution (66–200 μm), swelling (150–300 % within 2 h, swelling equilibrium after 4 h) and mechanical stiffness, while maintaining an antibacterial activity with 4–9 Log_{10} bacterial reduction after sterilisation.
4. ε-PL/HA hydrogels have demonstrated ε-PL dose-dependent antibacterial activity in both fast (up to 24 h) and sustained (up to 168 h) timeframes, via direct and indirect contact, against *E. coli*, *S. aureus*, *P. aeruginosa*, as well as clinically relevant multidrug-resistant strains MRSA, and ESBL *E. coli.* No bacterial resistance has been observed against ε-PL in reference or multidrug-resistant strains over 10 passages during a 1-month exposure period.
5. Cytotoxicity assays have demonstrated 70–90% cell viability for ε-PL/HA hydrogels in Balb/c 3T3 mouse fibroblasts, with the IC_{50} of pure ε-PL determined as 4.21 mg/mL. Indirect extract-based cytotoxicity assays on human dermal fibroblasts (HDFs) have confirmed non-cytotoxicity at extract concentrations ≤ 4.35 mg/mL, supporting the ε-PL dose-dependent biocompatibility of the developed hydrogel systems.
6. Sr-HAp/ε-PL/HA hydrogels have been successfully developed and demonstrated a synergistic effect between ε-PL/HA hydrogels and the Sr-HAp nanoparticles, resulting in sustained release of Sr^{2+} ions (20–30 μM) and Ca^{2+} ions (200–350 μM) over 90 days, retained injectability, tuneable enzymatic degradation depending on Sr-HAp content (complete degradation within 5–20 weeks). The composite hydrogels have exhibited fast-acting antibacterial activity (after 24 h) against both reference and multidrug-resistant bacteria strains, and prolonged efficacy (up to 168 h), particularly against *S. aureus* and clinically isolated multidrug-resistant MRSA.

REFERENCES

7.7 million people die from bacterial infections every year – 2022 – ReAct. https://www.reactgroup.org/news-and-views/news-and-opinions/year-2022/7-7-million-people-die-from-bacterial-infections-every-year/ (accessed 2025-02-19).

[2] Sceglovs, A.; Skadins, I.; Siverino, C.; Pirsko, V.; Sceglova, M.; Moriarty, F. T.; Kroica, J.; Salma-Ancane, K. Injectable ε-Polylysine/Hyaluronic Acid Hydrogels with Resistance-Preventing Antibacterial Activity for Treating Wound Infections. *ACS Appl. Bio Mater.*, **2025**, *8* (11), 9916–9930. https://doi.org/10.1021/acsabm.5c01252.

[3] Bilal, M.; Iqbal, H. M. N. Naturally-Derived Biopolymers: Potential Platforms for Enzyme Immobilization. *Int. J. Biol. Macromol.* **2019**, *130*, 462–482. https://doi.org/10.1016/J.IJBIOMAC.2019.02.152.

[4] Sceglovs, A.; Skadins, I.; Chitto, M.; Kroica, J.; Salma-Ancane, K. Failure or Future? Exploring Alternative Antibacterials: A Comparative Analysis of Antibiotics and Naturally Derived Biopolymers. *Front. Microbiol.* **2025**, *16*, 1526250. https://doi.org/10.3389/FMICB.2025.1526250.

[5] Sun, Y.; Bai, Y.; Yang, W.; Bu, K.; Tanveer, S. K.; Hai, J. Global Trends in Natural Biopolymers in the 21st Century: A Scientometric Review. *Front. Chem.* **2022**, *10*, 915648. https://doi.org/10.3389/FCHEM.2022.915648.

[6] Pahlevanzadeh, F.; Setayeshmehr, M.; Bakhsheshi-Rad, H. R.; Emadi, R.; Kharaziha, M.; Poursamar, S. A.; Ismail, A. F.; Sharif, S.; Chen, X.; Berto, F. A Review on Antibacterial Biomaterials in Biomedical Applications: From Materials Perspective to Bioinks Design. *Polym. 2022, Vol. 14, Page 2238* **2022**, *14* (11), 2238. https://doi.org/10.3390/POLYM14112238.

[7] Sam, S.; Joseph, B.; Thomas, S. Exploring the Antimicrobial Features of Biomaterials for Biomedical Applications. *Results Eng.* **2023**, *17*, 100979. https://doi.org/10.1016/J.RINENG.2023.100979.

[8] Coma, V. Polysaccharide-Based Biomaterials with Antimicrobial and Antioxidant Properties. *Polimeros* **2013**, *23* (3), 287–297. https://doi.org/10.4322/POLIMEROS020OV002.

[9] Khara, J. S.; Mojsoska, B.; Mukherjee, D.; Langford, P. R.; Robertson, B. D.; Jenssen, H.; Ee, P. L. R.; Newton, S. M. Ultra-Short Antimicrobial Peptoids Show Propensity for Membrane Activity Against Multi-Drug Resistant Mycobacterium Tuberculosis. *Front. Microbiol.* **2020**, *11*, 515317. https://doi.org/10.3389/FMICB.2020.00417.

[10] Jacobo-Delgado, Y. M.; Rodríguez-Carlos, A.; Serrano, C. J.; Rivas-Santiago, B. Mycobacterium Tuberculosis Cell-Wall and Antimicrobial Peptides: A Mission Impossible? *Front. Immunol.* **2023**, *14*, 1194923.

https://doi.org/10.3389/FIMMU.2023.1194923.

[11] Intorasoot, S.; Intorasoot, A.; Tawteamwong, A.; Butr-Indr, B.; Phunpae, P.; Tharinjaroen, C. S.; Wattananandkul, U.; Sangboonruang, S.; Khantipongse, J. In Vitro Antimycobacterial Activity of Human Lactoferrin-Derived Peptide, D-HLF 1-11, against Susceptible and Drug-Resistant Mycobacterium Tuberculosis and Its Synergistic Effect with Rifampicin. *Antibiot. 2022, Vol. 11, Page 1785* **2022**, *11* (12), 1785. https://doi.org/10.3390/ANTIBIOTICS11121785.

[12] C Reygaert, W. An Overview of the Antimicrobial Resistance Mechanisms of Bacteria. *AIMS Microbiol.* **2018**, *4* (3), 482–501. https://doi.org/10.3934/MICROBIOL.2018.3.482.

[13] Sceglovs, A.; Wychowaniec, J. K.; Skadins, I.; Reinis, A.; Edwards-Gayle, C. J. C.; D'Este, M.; Salma-Ancane, K. Effect of Steam Sterilisation on Physico-Chemical Properties of Antibacterial Covalently Cross-Linked ε-Polylysine/Hyaluronic Acid Hydrogels. *Carbohydr. Polym. Technol. Appl.* **2023**, *6*, 100363. https://doi.org/10.1016/J.CARPTA.2023.100363.

[14] Harvey, N.; Dennison, E.; Cooper, C. Osteoporosis: Impact on Health and Economics. *Nat. Rev. Rheumatol. 2010 62* **2010**, *6* (2), 99–105. https://doi.org/10.1038/nrrheum.2009.260.

[15] Sozen, T.; Ozisik, L.; Calik Basaran, N. An Overview and Management of Osteoporosis. *Eur. J. Rheumatol.* **2017**, *4* (1), 46–56. https://doi.org/10.5152/EURJRHEUM.2016.048.

[16] Hou, X.; Zhang, L.; Zhou, Z.; Luo, X.; Wang, T.; Zhao, X.; Lu, B.; Chen, F.; Zheng, L. Calcium Phosphate-Based Biomaterials for Bone Repair. *J. Funct. Biomater.* 2022, **2022**, *13* (4), 187. https://doi.org/10.3390/JFB13040187.

[17] Tozzi, G.; De Mori, A.; Oliveira, A.; Roldo, M. Composite Hydrogels for Bone Regeneration. *Mater. 2016,* **2016**, *9* (4), 267. https://doi.org/10.3390/MA9040267.

[18] Zhang, Y.; Shu, T.; Wang, S.; Liu, Z.; Cheng, Y.; Li, A.; Pei, D. The Osteoinductivity of Calcium Phosphate-Based Biomaterials: A Tight Interaction With Bone Healing. *Front. Bioeng. Biotechnol.* **2022**, *10*, 911180. https://doi.org/10.3389/FBIOE.2022.911180.

[19] Inzana, J. A.; Schwarz, E. M.; Kates, S. L.; Awad, H. A. Biomaterials Approaches to Treating Implant-Associated Osteomyelitis. *Biomaterials* **2016**, *81*, 58–71. https://doi.org/10.1016/J.BIOMATERIALS.2015.12.012.

[20] van Vugt, T. A. G.; Arts, J. J.; Geurts, J. A. P. Antibiotic-Loaded Polymethylmethacrylate Beads and Spacers in Treatment of Orthopedic Infections and the Role of Biofilm Formation. *Front. Microbiol.* **2019**, *10*. https://doi.org/10.3389/FMICB.2019.01626.

[21] Freischmidt, H.; Armbruster, J.; Reiter, G.; Grützner, P. A.; Helbig, L.; Guehring, T. Individualized Techniques of Implant Coating with an Antibiotic-Loaded, Hydroxyapatite/Calcium Sulphate Bone Graft Substitute. *Ther. Clin. Risk Manag.* **2020**, *16*, 689–694. https://doi.org/10.2147/TCRM.S242088.

[22] Dovedytis, M.; Liu, Z. J.; Bartlett, S. Hyaluronic Acid and Its Biomedical Applications: A Review. *Eng. Regen.* **2020**, *1*, 102–113. https://doi.org/10.1016/J.ENGREG.2020.10.001.

[23] Wang, M.; Deng, Z.; Guo, Y.; Xu, P. Designing Functional Hyaluronic Acid-Based Hydrogels for Cartilage Tissue Engineering. *Mater. Today Bio* **2022**, *17*, 100495. https://doi.org/10.1016/J.MTBIO.2022.100495.

[24] Salma-Ancane, K.; Sceglovs, A.; Tracuma, E.; Wychowaniec, J. K.; Aunina, K.; Ramata-Stunda, A.; Nikolajeva, V.; Loca, D. Effect of Crosslinking Strategy on the Biological, Antibacterial and Physicochemical Performance of Hyaluronic Acid and ε-Polylysine Based Hydrogels. *Int. J. Biol. Macromol.* **2022**, *208*, 995–1008. https://doi.org/10.1016/J.IJBIOMAC.2022.03.207.

[25] Sionkowska, A.; Kulka-Kamińska, K.; Brudzyńska, P.; Lewandowska, K.; Piwowarski, Ł. The Influence of Various Crosslinking Conditions of EDC/NHS on the Properties of Fish Collagen Film. *Mar. Drugs 2024,* **2024**, *22* (5), 194. https://doi.org/10.3390/MD22050194.

[26] Munir, M. U.; Salman, S.; Javed, I.; Bukhari, S. N. A.; Ahmad, N.; Shad, N. A.; Aziz, F. Nano-Hydroxyapatite as a Delivery System: Overview and Advancements. *Artif. Cells, Nanomedicine, Biotechnol.* **2021**, *49* (1), 717–727. https://doi.org/10.1080/21691401.2021.2016785.

[27] Lee, N. H.; Kang, M. S.; Kim, T. H.; Yoon, D. S.; Mandakhbayar, N.; Jo, S. Bin; Kim, H. S.; Knowles, J. C.; Lee, J. H.; Kim, H. W. Dual Actions of Osteoclastic-Inhibition and Osteogenic-Stimulation through Strontium-Releasing Bioactive Nanoscale Cement Imply Biomaterial-Enabled Osteoporosis Therapy. *Biomaterials* **2021**, *276*, 121025. https://doi.org/10.1016/J.BIOMATERIALS.2021.121025.

[28] Pan, H. B.; Li, Z. Y.; Lam, W. M.; Wong, J. C.; Darvell, B. W.; Luk, K. D. K.; Lu, W. W. Solubility of Strontium-Substituted Apatite by Solid Titration. *Acta Biomater.* **2009**, *5* (5), 1678–1685. https://doi.org/10.1016/J.ACTBIO.2008.11.032.

[29] Stipniece, L.; Wilson, S.; Curran, J. M.; Chen, R.; Salma-Ancane, K.; Sharma, P. K.; Meenan, B. J.; Boyd, A. R. Strontium Substituted Hydroxyapatite Promotes Direct Primary Human Osteoblast Maturation. *Ceram. Int.* **2021**, *47* (3), 3368–3379. https://doi.org/10.1016/J.CERAMINT.2020.09.182.

[30] Stipniece, L.; Ramata-Stunda, A.; Vecstaudza, J.; Kreicberga, I.; Livkisa, D.; Rubina, A.;

Sceglovs, A.; Salma-Ancane, K. A Comparative Study on Physicochemical Properties and In Vitro Biocompatibility of Sr-Substituted and Sr Ranelate-Loaded Hydroxyapatite Nanoparticles. *ACS Appl. Bio Mater.* **2023**, *6* (12), 5264–5281. https://doi.org/10.1021/ACSABM.3C00539.

[31] Kołodziejska, B.; Stępień, N.; Kolmas, J. The Influence of Strontium on Bone Tissue Metabolism and Its Application in Osteoporosis Treatment. *Int. J. Mol. Sci. 2021,* **2021**, *22* (12), 6564. https://doi.org/10.3390/IJMS22126564.

[32] Rocha Scardueli, C.; Bizelli-Silveira, C.; Adriana Marcantonio, R. C.; Marcantonio Jr, E.; Stavropoulos, A.; Spin-Neto, R. Systemic Administration of Strontium Ranelate to Enhance the Osseointegration of Implants: Systematic Review of Animal Studies. *Int. J. Implant Dent. 2018 41* **2018**, *4* (1), 1–9. https://doi.org/10.1186/S40729-018-0132-8.

[33] Akram, F.; Imtiaz, M.; Haq, I. ul. Emergent Crisis of Antibiotic Resistance: A Silent Pandemic Threat to 21st Century. *Microb. Pathog.* **2023**, *174*, 105923. https://doi.org/10.1016/J.MICPATH.2022.105923.

[34] *New report calls for urgent action to avert antimicrobial resistance crisis*. https://www.who.int/news/item/29-04-2019-new-report-calls-for-urgent-action-to-avert-antimicrobial-resistance-crisis (accessed 2024-04-02).

[35] Muñoz-Bonilla, A.; Fernández-García, M. Polymeric Materials with Antimicrobial Activity. *Prog. Polym. Sci.* **2012**, *37* (2), 281–339. https://doi.org/10.1016/J.PROGPOLYMSCI.2011.08.005.

[36] Santos, M. R. E.; Fonseca, A. C.; Mendonça, P. V.; Branco, R.; Serra, A. C.; Morais, P. V.; Coelho, J. F. J. Recent Developments in Antimicrobial Polymers: A Review. *Mater. 2016,* **2016**, *9* (7), 599. https://doi.org/10.3390/MA9070599.

[37] Haktaniyan, M.; Bradley, M. Polymers Showing Intrinsic Antimicrobial Activity. *Chem. Soc. Rev.* **2022**, *51* (20), 8584–8611. https://doi.org/10.1039/D2CS00558A.

[38] Smola-Dmochowska, A.; Lewicka, K.; Macyk, A.; Rychter, P.; Pamuła, E.; Dobrzyński, P. Biodegradable Polymers and Polymer Composites with Antibacterial Properties. *Int. J. Mol. Sci. 2023,* **2023**, *24* (8), 7473. https://doi.org/10.3390/IJMS24087473.

[39] Mishra, R.; Panda, A. K.; De Mandal, S.; Shakeel, M.; Bisht, S. S.; Khan, J. Natural Anti-Biofilm Agents: Strategies to Control Biofilm-Forming Pathogens. *Front. Microbiol.* **2020**, *11*, 566325. https://doi.org/10.3389/FMICB.2020.566325.

[40] Melander, R. J.; Basak, A. K.; Melander, C. Natural Products as Inspiration for the Development of Bacterial Antibiofilm Agents. *Nat. Prod. Rep.* **2020**, *37* (11), 1454–1477. https://doi.org/10.1039/D0NP00022A.

[41] Munita, J. M.; Arias, C. A. Mechanisms of Antibiotic Resistance. *Microbiol. Spectr.* **2016**, *4* (2). https://doi.org/10.1128/MICROBIOLSPEC.VMBF-0016-2015.

[42] Peterson, E.; Kaur, P. Antibiotic Resistance Mechanisms in Bacteria: Relationships between Resistance Determinants of Antibiotic Producers, Environmental Bacteria, and Clinical Pathogens. *Front. Microbiol.* **2018**, *9* (NOV), 426686. https://doi.org/10.3389/FMICB.2018.02928.

[43] Abushaheen, M. A.; Muzaheed; Fatani, A. J.; Alosaimi, M.; Mansy, W.; George, M.; Acharya, S.; Rathod, S.; Divakar, D. D.; Jhugroo, C.; Vellappally, S.; Khan, A. A.; Shaik, J.; Jhugroo, P. Antimicrobial Resistance, Mechanisms and Its Clinical Significance. *Dis. Mon.* **2020**, *66* (6). https://doi.org/10.1016/J.DISAMONTH.2020.100971.

[44] Chamidah, A.; Hardoko; Prihanto, A. A. Antibacterial Activities of β-Glucan (Laminaran) against Gram-Negative and Gram-Positive Bacteria. *AIP Conf. Proc.* **2017**, *1844* (1), 20011. https://doi.org/10.1063/1.4983422/748336.

[45] Hyldgaard, M.; Mygind, T.; Vad, B. S.; Stenvang, M.; Otzen, D. E.; Meyer, R. L. The Antimicrobial Mechanism of Action of Epsilon-Poly-L-Lysine. *Appl. Environ. Microbiol.* **2014**, *80* (24), 7758–7770. https://doi.org/10.1128/AEM.02204-14.

[46] Jenssen, H.; Hancock, R. E. W. Antimicrobial Properties of Lactoferrin. *Biochimie* **2009**, *91* (1), 19–29. https://doi.org/10.1016/J.BIOCHI.2008.05.015.

[47] Vedadghavami, A.; Minooei, F.; Mohammadi, M. H.; Khetani, S.; Rezaei Kolahchi, A.; Mashayekhan, S.; Sanati-Nezhad, A. Manufacturing of Hydrogel Biomaterials with Controlled Mechanical Properties for Tissue Engineering Applications. *Acta Biomater.* **2017**, *62*, 42–63. https://doi.org/10.1016/J.ACTBIO.2017.07.028.

[48] Bai, X.; Gao, M.; Syed, S.; Zhuang, J.; Xu, X.; Zhang, X. Q. Bioactive Hydrogels for Bone Regeneration. *Bioact. Mater.* **2018**, *3* (4), 401–417. https://doi.org/10.1016/J.BIOACTMAT.2018.05.006.

[49] Moreira, C. D. F.; Carvalho, S. M.; Florentino, R. M.; França, A.; Okano, B. S.; Rezende, C. M. F.; Mansur, H. S.; Pereira, M. M. Injectable Chitosan/Gelatin/Bioactive Glass Nanocomposite Hydrogels for Potential Bone Regeneration: In Vitro and in Vivo Analyses. *Int. J. Biol. Macromol.* **2019**, *132*, 811–821. https://doi.org/10.1016/J.IJBIOMAC.2019.03.237.

[50] Cross, E. R.; Coulter, S. M.; Pentlavalli, S.; Laverty, G. Unravelling the Antimicrobial Activity of Peptide Hydrogel Systems: Current and Future Perspectives. *Soft Matter* **2021**, *17* (35), 8001–8021. https://doi.org/10.1039/D1SM00839K.

[51] Qu, H.; Yao, Q.; Chen, T.; Wu, H.; Liu, Y.; Wang, C.; Dong, A. Current Status of Development and Biomedical Applications of Peptide-Based Antimicrobial Hydrogels. *Adv. Colloid Interface Sci.* **2024**, *325*, 103099. https://doi.org/10.1016/J.CIS.2024.103099.

[52] Wang, R.; Xu, D.; Liang, L.; Xu, T.; Liu, W.; Ouyang, P.; Chi, B.; Xu, H. Enzymatically

Crosslinked Epsilon-Poly-l-Lysine Hydrogels with Inherent Antibacterial Properties for Wound Infection Prevention. *RSC Adv.* **2016**, *6* (11), 8620–8627. https://doi.org/10.1039/C5RA15616E.

[53] Zou, Y. J.; He, S. S.; Du, J. Z. ε-Poly(L-Lysine)-Based Hydrogels with Fast-Acting and Prolonged Antibacterial Activities. *Chinese J. Polym. Sci. (English Ed.* **2018**, *36* (11), 1239–1250. https://doi.org/10.1007/S10118-018-2156-1.

[54] Kennedy, S. M.; Deshpande, P.; Gallagher, A. G.; Horsburgh, M. J.; Allison, H. E.; Kaye, S. B.; Wellings, D. A.; Williams, R. L. Antimicrobial Activity of Poly-Epsilon-Lysine Peptide Hydrogels Against Pseudomonas Aeruginosa. *Invest. Ophthalmol. Vis. Sci.* **2020**, *61* (10), 18–18. https://doi.org/10.1167/IOVS.61.10.18.

[55] Wang, L.; Zhang, C.; Zhang, J.; Rao, Z.; Xu, X.; Mao, Z.; Chen, X. Epsilon-Poly-L-Lysine: Recent Advances in Biomanufacturing and Applications. *Front. Bioeng. Biotechnol.* **2021**, *9*, 895. https://doi.org/10.3389/FBIOE.2021.748976.

[56] Tan, Z.; Shi, Y.; Xing, B.; Hou, Y.; Cui, J.; Jia, S. The Antimicrobial Effects and Mechanism of ε-Poly-Lysine against Staphylococcus Aureus. *Bioresour. Bioprocess.* **2019**, *6* (1). https://doi.org/10.1186/s40643-019-0246-8.

[57] Li, Y.; Wang, Y.; Li, J. Antibacterial Activity of Polyvinyl Alcohol (PVA)/ε-Polylysine Packaging Films and the Effect on Longan Fruit. *Food Sci. Technol.* **2020**, *40* (4), 838–843. https://doi.org/10.1590/FST.19919.

[58] Amorim, S.; Reis, C. A.; Reis, R. L.; Pires, R. A. Extracellular Matrix Mimics Using Hyaluronan-Based Biomaterials. *Trends Biotechnol.* **2021**, *39* (1), 90–104. https://doi.org/10.1016/J.TIBTECH.2020.06.003.

[59] Harrer, D.; Sanchez Armengol, E.; Friedl, J. D.; Jalil, A.; Jelkmann, M.; Leichner, C.; Laffleur, F. Is Hyaluronic Acid the Perfect Excipient for the Pharmaceutical Need? *Int. J. Pharm.* **2021**, *601*, 120589. https://doi.org/10.1016/J.IJPHARM.2021.120589.

[60] Guo, W.; Douma, L.; Hu, M. H.; Eglin, D.; Alini, M.; Šećerović, A.; Grad, S.; Peng, X.; Zou, X.; D'Este, M.; Peroglio, M. Hyaluronic Acid-Based Interpenetrating Network Hydrogel as a Cell Carrier for Nucleus Pulposus Repair. *Carbohydr. Polym.* **2022**, *277*, 118828. https://doi.org/10.1016/J.CARBPOL.2021.118828.

[61] Hu, W.; Wang, Z.; Xiao, Y.; Zhang, S.; Wang, J. Advances in Crosslinking Strategies of Biomedical Hydrogels. *Biomater. Sci.* **2019**, *7* (3), 843–855. https://doi.org/10.1039/c8bm01246f.

[62] Cui, H.; Zhuang, X.; He, C.; Wei, Y.; Chen, X. High Performance and Reversible Ionic Polypeptide Hydrogel Based on Charge-Driven Assembly for Biomedical Applications. *Acta Biomater.* **2015**, *11* (1), 183–190. https://doi.org/10.1016/J.ACTBIO.2014.09.017.

[63] Xue, X.; Hu, Y.; Wang, S.; Chen, X.; Jiang, Y.; Su, J. Fabrication of Physical and

Chemical Crosslinked Hydrogels for Bone Tissue Engineering. *Bioact. Mater.* **2022**, *12*, 327–339. https://doi.org/10.1016/J.BIOACTMAT.2021.10.029.

[64] Hua, J.; Li, Z.; Xia, W.; Yang, N.; Gong, J.; Zhang, J.; Qiao, C. *Preparation and Properties of EDC/NHS Mediated Crosslinking Poly (Gamma-Glutamic Acid)/Epsilon-Polylysine Hydrogels*; Elsevier B.V., 2016; Vol. 61. https://doi.org/10.1016/j.msec.2016.01.001.

[65] Porod, G. *General Theory - Small Angle X-Ray Scattering*; Glatter, O. . K. O., Ed.; Academic Press: London, 1982.

[66] *M07 Ed12 | Methods for Dilution Antimicrobial Susceptibility Tests for Bacteria That Grow Aerobically, 12th Edition*. https://clsi.org/standards/products/microbiology/documents/m07/ (accessed 2025-02-19).

[67] *ISO 10993-5:2009 - Biological evaluation of medical devices — Part 5: Tests for in vitro cytotoxicity*. https://www.iso.org/standard/36406.html (accessed 2025-02-27).

[68] Burguera, E. F.; Xu, H. H. K.; Sun, L. Injectable Calcium Phosphate Cement: Effects of Powder-to-Liquid Ratio and Needle Size. *J. Biomed. Mater. Res. Part B Appl. Biomater.* **2008**, *84B* (2), 493–502. https://doi.org/10.1002/JBM.B.30896.

[69] Jacquart, S.; Girod-Fullana, S.; Brouillet, F.; Pigasse, C.; Siadous, R.; Fatnassi, M.; Grimoud, J.; Rey, C.; Roques, C.; Combes, C. Injectable Bone Cement Containing Carboxymethyl Cellulose Microparticles as a Silver Delivery System Able to Reduce Implant-Associated Infection Risk. *Acta Biomater.* **2022**, *145*, 342–357. https://doi.org/10.1016/J.ACTBIO.2022.04.015.

[70] Baniasadi, M.; Minary-Jolandan, M.; Editor, A.; Zadpoor, A. A. Alginate-Collagen Fibril Composite Hydrogel. *Mater. 2015,* **2015**, *8* (2), 799–814. https://doi.org/10.3390/MA8020799.

[71] Liu, L.; Cooke, P. H.; Coffin, D. R.; Fishman, M. L.; Hicks, K. B. Pectin and Polyacrylamide Composite Hydrogels: Effect of Pectin on Structural and Dynamic Mechanical Properties. *J. Appl. Polym. Sci.* **2004**, *92* (3), 1893–1901. https://doi.org/10.1002/APP.20174.

[72] Rubina, A.; Sceglovs, A.; Ramata-Stunda, A.; Pugajeva, I.; Skadins, I.; Boyd, A. R.; Tumilovica, A.; Stipniece, L.; Salma-Ancane, K. Injectable Mineralized Sr-Hydroxyapatite Nanoparticles-Loaded ε-Polylysine-Hyaluronic Acid Composite Hydrogels for Bone Regeneration. *Int. J. Biol. Macromol.* **2024**, *280*, 135703. https://doi.org/10.1016/J.IJBIOMAC.2024.135703.

[73] Karvinen, J.; Kellomäki, M. Characterization of Self-Healing Hydrogels for Biomedical Applications. *Eur. Polym. J.* **2022**, *181*, 111641.

https://doi.org/10.1016/J.EURPOLYMJ.2022.111641.

[74] Murugesan, V.; Vaiyapuri, M.; Murugeasan, A. Fabrication and Characterization of Strontium Substituted Chitosan Modify Hydroxyapatite for Biomedical Applications. *Inorg. Chem. Commun.* **2022**, *142*, 109653. https://doi.org/10.1016/J.INOCHE.2022.109653.

PIELIKUMI/APPENDICES

Appendix I

1. Pielikums

Failure or Future? Exploring Alternative Antibacterials: A Comparative Analysis of Antibiotics and Naturally-Derived Biopolymers

Artemijs Sceglovs, Ingus Skadins, Marco Chitto, Juta Kroica, Kristine Salma-Ancane

Frontiers in Microbiology, **2025**, 16: 1526250. doi: 10.3389/fmicb.2025.1526250

A.S. input: Conceptualization, Writing – original draft, Writing – review & editing.

frontiers | Frontiers in Microbiology

TYPE Review
PUBLISHED 03 February 2025
DOI 10.3389/fmicb.2025.1526250

OPEN ACCESS

EDITED BY
Sebastian Guenther,
University of Greifswald, Germany

REVIEWED BY
Eugene A. Rogozhin,
Institute of Bioorganic Chemistry (RAS), Russia
Luminita Marutescu,
University of Bucharest, Romania

*CORRESPONDENCE
Kristine Salma-Ancane
kristine.salma-ancane@rtu.lv

RECEIVED 11 November 2024
ACCEPTED 13 January 2025
PUBLISHED 03 February 2025

CITATION
Sceglovs A, Skadins I, Chitto M, Kroica J and Salma-Ancane K (2025) Failure or future? Exploring alternative antibacterials: a comparative analysis of antibiotics and naturally derived biopolymers.
Front. Microbiol. 16:1526250.
doi: 10.3389/fmicb.2025.1526250

Failure or future? Exploring alternative antibacterials: a comparative analysis of antibiotics and naturally derived biopolymers

Artemijs Sceglovs[1,2], Ingus Skadins[3], Marco Chitto[4], Juta Kroica[3] and Kristine Salma-Ancane[1,2]*

[1]Institute of Biomaterials and Bioengineering, Faculty of Natural Sciences and Technology, Riga Technical University, Riga, Latvia, [2]Baltic Biomaterials Centre of Excellence, Headquarters at Riga Technical University, Riga, Latvia, [3]Department of Biology and Microbiology, Riga Stradins University, Riga, Latvia, [4]AO Research Institute Davos, Davos, Switzerland

The global crisis of antimicrobial resistance (AMR) is escalating due to the misuse and overuse of antibiotics, the slow development of new therapies, and the rise of multidrug-resistant (MDR) infections. Traditional antibiotic treatments face limitations, including the development of resistance, disruption of the microbiota, adverse side effects, and environmental impact, emphasizing the urgent need for innovative alternative antibacterial strategies. This review critically examines naturally derived biopolymers with intrinsic (essential feature) antibacterial properties as a sustainable, next-generation alternative to traditional antibiotics. These biopolymers may address bacterial resistance uniquely by disrupting bacterial membranes rather than cellular functions, potentially reducing microbiota interference. Through a comparative analysis of the mechanisms and applications of antibiotics and antibacterial naturally derived biopolymers, this review highlights the potential of such biopolymers to address AMR while supporting human and environmental health.

KEYWORDS

antibacterial naturally derived biopolymers, antibiotics, antibiotic resistance, bacterial infections, mechanism of action

1 Introduction

The World Health Organization (WHO) estimates that antimicrobial resistance (AMR) could cause up to 10 million deaths annually by 2050, with a severe impact on global healthcare costs and economic stability. Bacterial infections are among the most life-threatening healthcare challenges, accounting for approximately 13.6% of global mortality and affecting 1 in 8 individuals worldwide (Appanna, 2018). The rise of multidrug-resistant (MDR) bacteria further highlights an urgent need for alternative, next-generation antibacterial treatments. While antibiotics have historically revolutionized healthcare, their widespread use has led to substantial challenges, including disrupting human microbiota and the rise of antibiotic-resistant bacterial strains.

Beyond their pathogenic roles, bacteria are integral to human health, especially in the gut, contributing to immune modulation and digestion (Bull and Plummer, 2014; Yin et al., 2019; Arciola et al., 2018). Consequently, the modern healthcare system cannot fully eliminate infection risk, particularly in post-surgical settings (Oliva et al., 2021; Hedrick

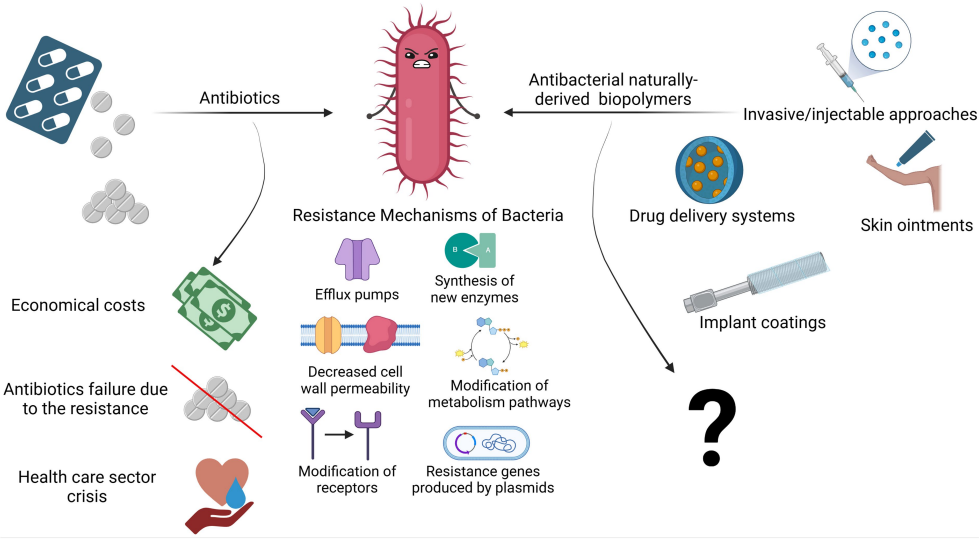

et al., 2006; van Seventer and Hochberg, 2017) and procedures involving biomaterials or medical devices (Arciola et al., 2018; Oliva et al., 2021; Hedrick et al., 2006). Infections occur when infectious agents enter human body tissues, multiply, and trigger host immune responses (van Seventer and Hochberg, 2017). Although infections cannot be entirely prevented due to inevitable interactions with environmental microbes, targeted measures can mitigate bacterial invasion and inhibit replication at potential infection sites.

The human microbiome, especially the gut microbiota, comprises numerous symbiotic bacterial species (e.g., *Lactobacillus*, *Bacillus*, *Clostridium*, *Enterococcus*, and *Ruminococcus*) that collectively represent approximately 90% of the gut flora (Rinninella et al., 2019; Martín et al., 2013; Eloe-Fadrosh and Rasko, 2013). These beneficial microorganisms are crucial in digestion, nutrient absorption, and immune defense. Importantly, they maintain a delicate balance, contributing to immune regulation and protecting against pathogens without causing harm to the host (Rinninella et al., 2019; Bogitsh et al., 2019; Hemarajata and Versalovic, 2013; Isolauri et al., 2001; Wieërs et al., 2020; Hills et al., 2019; Ding et al., 2019). However, the broad-spectrum use of antibiotics has disrupted this balance, weakening the microbiota's natural protective functions and impairing the immune response, leading to gut dysbiosis—an environment conducive to antibiotic-resistant strains (Patangia et al., 2022).

While antibiotics effectively eliminate harmful pathogens, their indiscriminate targeting also affects beneficial bacteria, reducing microbial diversity and increasing the likelihood of antibiotic resistance (Lathakumari et al., 2024). Inappropriate antibiotic use across sectors, including clinical and animal health, has further escalated the global antibiotic resistance crisis, contributing to the emergence of MDR pathogens that resist multiple antibiotic classes (Yang et al., 2024).

The decreasing efficacy of antibiotics and the limited availability of alternative treatments underscore the urgent need for new classes of antibacterial therapeutics. Ideal alternatives would incorporate mechanisms of action that lower the risk of resistance. In this context, naturally derived biopolymers (NDBs) have attracted significant attention due to their unique antibacterial properties. Although long used in biomedical applications, interest in biopolymers as antibacterial agents has surged, with publications on their use rising by approximately 400% since 2015 (Web of Science, n.d.).

Approximately two decades ago, antibacterial biopolymers, e.g., those with intrinsic antibacterial activity, were first proposed as alternatives to antibiotics for treating bacterial infections (Muñoz-Bonilla and Fernández-García, 2012). Today, biopolymer-based strategies show potential for localized, non-antibiotic antibacterial applications that support the immune system and minimize impact on the natural microbiota. Such approaches could represent a sustainable innovation within modern healthcare.

Notably, NDBs disrupt bacterial membranes instead of targeting specific metabolic pathways, a mechanism less prone to resistance development (Bustamante-Torres et al., 2022; Kamaruzzaman et al., 2019). Numerous studies have documented the use of NDBs in biomedical devices, including drug delivery systems, contact lenses, and injectable cement, where they exhibit potent antibacterial activity and biocompatibility (Pahlevanzadeh et al., 2022; Sam et al., 2023; Coma, 2013). This review provides a comprehensive examination of the potential of antibacterial NDBs, analyzing recent literature to compare their effectiveness and applications with those of conventional antibiotics. By exploring the mechanisms, advantages, and limitations of NDBs, this review assesses whether these biopolymers could serve as reliable, antibiotic-free therapeutics capable of complementing or partially replacing traditional antibiotics

in treating bacterial infections—or whether their promise remains largely theoretical.

2 Antibiotics and antibiotic resistance

In the pre-antibiotic era, more than half of deaths were attributable to infections (Aminov, 2010). Since the 20th century, antibiotics have revolutionized antibacterial therapeutics in the history of medicine, drastically changing modern medicine and extending the average human lifespan (Johnston and Badran, 2022; Cook and Wright, 2022; Sikdar et al., 2021). Several groups and generations of antibiotics have been discovered and developed with specific target mechanisms of action on bacterial cells (Kapoor et al., 2017; Coates et al., 2011) (Table 1). Conventionally, antibiotics are classified as cell wall inhibitors, protein synthesis inhibitors, nucleic acid synthesis inhibitors, antimetabolites, and cytoplasmic membrane inhibitors (Pancu et al., 2021; Ullah and Ali, 2017) (Figure 1).

Other classification principles of antibiotics rely on their origin, spectrum of action, administration strategies, chemical structure, and mechanism of action (Figure 1). Antibiotics can be administered through various routes, including oral, intravenous, intramuscular, and topical applications (Buonavoglia et al., 2021; Enenkel and Stille, 1988). The topical application is particularly relevant for localized infections, such as skin wounds or mucosal infections, where direct delivery to the affected area can enhance efficacy and minimize systemic side effects. The effectiveness of these administration strategies depends on various factors, including bioavailability, drug formulation, gastrointestinal conditions, and systemic distribution, which, if not optimized, could compromise therapeutic outcomes and limit the antibiotic's efficacy against targeted infections (McCarthy and Avent, 2020; Vinarov et al., 2021). Moreover, antibiotics exhibit specific behavioral characteristics, including whether they are bactericidal or bacteriostatic, as well as their spectrum, which can be broad or narrow. Antibiotics with a wide spectrum and bactericidal action may impact the microbiota within organisms' niches (Dubourg et al., 2014; Blaser, 2011; Yang et al., 2021), resulting in dysbacteriosis conditions post-therapy and an increasing risk of secondary disease. In addition, the systemic use of antibiotics has been documented to affect various organ systems, leading to heightened organism toxicity (Berry et al., 1995; Grill and Maganti, 2011) (Table 1).

Currently, bacteriophage therapy is the only alternative as effective as antibiotics. Phage therapy relies on using naturally occurring bacteriophages (viruses) to infect and lyse bacteria at the site of infection (Lin et al., 2017). However, phage therapy must still be licensed in the majority of countries or used under exceptional situations (Yang et al., 2023). Thus, antibiotics remain the primary treatment option in clinics to combat bacterial infections. However, the development of antibiotics has begun an endless race against pathogenic microorganisms. As a side problem, the overuse and misuse of these lifesaving drugs have developed the top global public health crisis named antibiotic resistance occurring worldwide (Akram et al., 2023). Antibiotic resistance arose from the evolutionary development of primary (antibiotic target site is not presented in bacteria strain) and secondary (genome-related and plasmid-related) resistance mechanisms in bacteria (Urban-Chmiel et al., 2022; Nilsson, 2019; Zhang and Cheng, 2022) (Table 1). The dramatic report by the WHO has shown that by 2050, drug resistance could catch up to cancer and sufficiently damage the economy if actions are not taken (World Health Organization, 2019). The uncontrolled use of antibiotics in agriculture and inappropriate therapeutic practices has provided an evolutionary advantage to bacteria, such as methicillin-resistant *Staphylococcus aureus* (MRSA), vancomycin-resistant *Enterococcus* (VRE), and others that have become resistant to one or multiple types of antibiotics, contributing to the dramatic situation in healthcare (Figure 2).

The global threat of antimicrobial resistance (AMR) necessitates collaborative action to develop and implement effective strategies (Uchil et al., 2014). Several preventative measures have been established and continue to evolve, addressing AMR at international, national, community, hospital, and individual levels (Uchil et al., 2014). At the international level, efforts focus on enhancing collaboration among governments, non-governmental organizations, professional groups, and international agencies. Key initiatives include global networks for antimicrobial use and resistance surveillance, strategies to combat counterfeit antimicrobials, and programs to foster innovation in new drugs and vaccines. Strengthening global AMR control programs remains a priority. Nationally, dedicated committees and AMR policies have been introduced to monitor and manage AMR. These policies integrate geographical, social, and economic factors to provide tailored solutions. Educational initiatives, including training programs and certification courses, aim to equip healthcare professionals and the private sector with knowledge for the rational use of antibiotics. Regulatory controls to limit over-the-counter antibiotic sales further address misuse, a key driver of resistance. For example, a review revealed that non-prescription antibiotic use varies widely, from 3% in Northern Europe to 100% in some African regions (Uchil et al., 2014; Morgan et al., 2011). In addition, efforts are directed at improving standards in healthcare systems, microbiology laboratories, and pharmaceutical companies. Protecting existing antibiotic therapies remains critical, with ongoing research focused on developing new drugs to replace outdated ones and prolonging the effectiveness of current treatments. It has already been proven that synergy and drug combinations are a winning strategy in fighting multidrug-resistant bacteria and might help protect the existing drugs through antibiotic adjuvants. For instance, β-lactamase inhibitors have been used as adjuvants for penicillin group antibiotics as they block the resistance mechanism of bacteria against these antibiotics (see Table 1). Other examples include efflux pump inhibitors and outer membrane permeabilizers (Annunziato, 2019).

3 Naturally derived biopolymers with intrinsic antibacterial properties

Naturally derived biopolymers (NDBs) are large macromolecules from living organisms such as plants and microorganisms. These polymers are formed through enzyme-catalyzed chain-growth polymerization processes of activated monomers (Sun et al., 2022). The molecular size of NDBs varies significantly based on their type and source, ranging from a few kilodaltons (kDa), as seen in polysaccharides such as chitosan (~10–50 kDa), to several megadaltons (MDa), such as cellulose and other structural polysaccharides (>1 MDa) (Moradali and Rehm, 2020; Yadav et al., 2015). This broad size range supports their diverse physicochemical

10.3389/fmicb.2025.1526250

TABLE 1 Classification of antibiotics based on the mechanism of action and chemical structure with characterization: action mechanisms, reported side effects, and bacterial resistance mechanisms.

Classification group	Chemical structure	Group example/–s	Action mechanism	Side effects	Bacterial resistance mechanism	Reference
Cell wall inhibitors	β-Lactams	Penicillins Cephalosporins Carbapenems Monobactams	Disrupt peptidoglycan synthesis in the bacterial cell wall by binding to a transpeptidase enzyme	Allergic reaction	Production of the β-lactamase enzyme. Consequently, β-lactam antibiotic therapies also include additional drugs called β-lactamase inhibitors (clavulanate, sulbactam, and tazobactam) to block this enzyme action	Majiduddin et al. (2002), Waley (1992), Castle (2007), Arer and Kar (2023), Tehrani and Martin (2018), Bush and Bradford (2016), Romano et al. (2003), Iuliano et al. (2022), Solensky (2003)
	Glycopeptides	Vancomycin				
	Bacitracin	Bacitracin				
	Fosfomycin	Fosfomycin				
Protein synthesis inhibitors (50S ribosomes)	Macrolides	Erythromycin Azithromycin Clarithromycin	Bind to 50S/30S ribosomal subunits, inhibiting their function and preventing the synthesis of new proteins. The bacteriostatic or bactericidal effects of protein synthesis inhibitors depend on the dosage.	Dysbiosis, nephrotic syndrome, aplastic anemia, and others	Transcription modification, efflux pumps, and gene mutation	Dunn and Zambraski (1980), Antibiotics Review (2010), Protein Synthesis Inhibitors-Definition (2023)
	Chloramphenicol	Chloramphenicol Levomycetin				
	Linezolid	Linezolid				
	Clindamycin	Clindamycin				
Protein synthesis inhibitors (30S ribosomes)	Aminoglycosides	Amikacin Tobramycin Neomycin Gentamicin Streptomycin				
	Tetracyclines	Tetracycline Doxycycline Minocycline				
Nucleic acid synthesis inhibitors	Quinolones	Ciprofloxacin Norfloxacin Moxifloxacin Levofloxacin	Stabilizing the enzyme–DNA complex and thus interrupting the relegation step	Aortic dissection, tendinitis, and hepatotoxicity	Modification of two enzymes: DNA gyrase and topoisomerase IV	Kapoor et al. (2017), Bhattacharjee (2016), Collin et al. (2011), Ramappa and Aithal (2013)
	Rifamycin	Rifampicin	Bind to RNA polymerases, thus blocking RNA synthesis		RNA polymerase mutation	
Antimetabolites	Sulfanilamides	Sulfamethoxazole	Inhibits folic acid synthesis in bacteria, a crucial element for DNA synthesis	Weight loss, weakness, and mouth inflammation	Efflux pumps and enzymatic inactivation	Chortkoff and Stenehjem (2019), McGee et al. (2018), Hanlon et al. (2019)
	Dihydrofolate reductase inhibitors	Trimethoprim				
Cell membrane inhibitors	Polymyxins	Colistin	Target phospholipids in the cell membrane, thus altering membranes' physical properties	No reported data, as minimal clinical applications	Increase in drug efflux, mutation, and alteration of the porin pathway	Cell Membrane Inhibitors (2023)
	Daptomycin	Daptomycin				

properties and wide-ranging applications (Troy et al., 2021; Reddy et al., 2021).

The reason is that the source of these compounds is derived from living organisms through enzymatic polymerization, forming high molecular weight macromolecules. As a result, covalently bonded repetitive monomeric units form biodegradable compounds such as polysaccharides, polyamino acids, hydroxy fatty acids, polypeptides, and glycolipids (Moradali and Rehm, 2020; Yadav et al., 2015; Troy

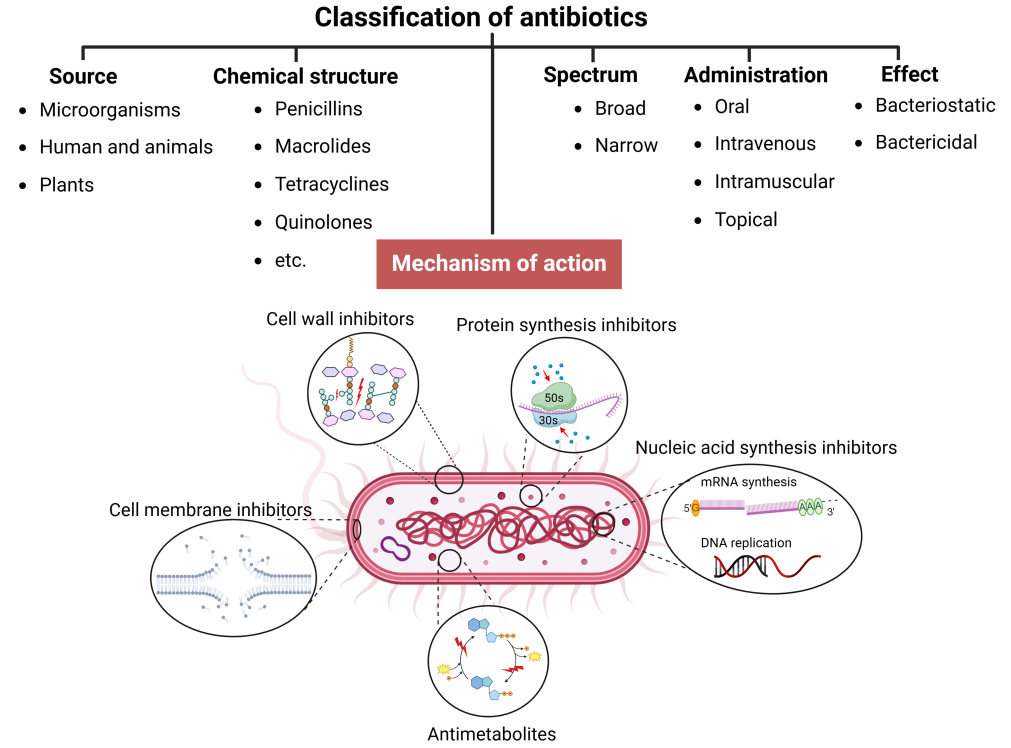

FIGURE 1
Classification of antibiotics (created by Biorender).

et al., 2021) (see Table 2). These compounds are classified as NDBs and have unique physical, chemical, and mechanical properties, which are exploited in biomedical applications. NDBs are commonly used in the development of drug delivery systems (Baranwal et al., 2022; Murali and Jayakumar, 2023; Atanase, 2021). In addition, NDBs such as collagen, gelatin, dextran, agarose/alginate, hyaluronic acid, cellulose, and fibrin are also being explored in various other biomedical applications, including open incision/wound suturing, fixing, adhesion, covering, occlusion, isolation, contact inhibition, cell proliferation, tissue guiding, and controlled drug administration (Baranwal et al., 2022). NDBs are of broad interest because of their potential to be used for developing environmentally friendly medical devices that perform high biocompatibility and serve as highly accurate biosensors, drug delivery systems, etc. (Manoukian et al., 2019). In addition to biocompatibility, biodegradation, bioadhesiveness, and biofunctionality of the NDBs, several drawbacks must be addressed, such as low stability, low melting point, high surface tension, structural complexity, and well-known immunological response from organisms (Ige et al., 2012; Jenkins et al., 1996; Reddy et al., 2021). Various NDBs such as chitosan, pectin, κ-carrageenan, alginate, ε-polylysine, and others have also been identified for their antibacterial activity (Muñoz-Bonilla et al., 2019; Li et al., 2021; Habeeb and Abdulkadhim, 2024; Hamidi et al., 2023) (see Table 2). Numerous studies have demonstrated the comparative effectiveness and potential advantages of NDBs over conventional antibiotics. For instance, Tin et al. (2009) reported that chitosan molecules with different molecular weights consistently exhibited a minimum inhibitory concentration (MIC) of 32 μg/mL against various strains of *P. aeruginosa*. In contrast, the MIC range for sulfamethoxazole was significantly broader, ranging from 64 to 2048 μg/mL (Tin et al., 2009). Similarly, Si et al. (2021) found that a chitosan derivative effectively inhibited Gram-negative and Gram-positive bacteria, with MIC values ranging from 8 to 32 μg/mL. Specifically, against *A. baumannii*, the chitosan derivative achieved an MIC of 32 μg/mL, compared to higher MIC values of 128 μg/mL for amikacin and tobramycin and 64 μg/mL for tazobactam. However, certain antibiotics outperformed NDBs in specific cases; for example, novobiocin demonstrated an MIC of 8 μg/mL, and carbenicillin and tobramycin were more effective against MRSA (Si et al., 2021). Another noteworthy example is ε-polylysine, which exhibited MIC values of 500, 800, 800, and 1,000 μg/mL against *P. aeruginosa*, *K. pneumoniae*, MSSA, and MRSA, respectively. Traditional antibiotics such as ampicillin, gentamicin, and tetracycline showed MIC values ranging from 35 to 250 μg/mL against the same bacterial strains (Sundaran et al., 2022). Importantly, combining NDBs with antibiotics has synergistic effects, significantly enhancing antibacterial activity and reducing the required antibiotic dosage (Si et al., 2021; Taheri-Araghi, 2024;

10.3389/fmicb.2025.1526250

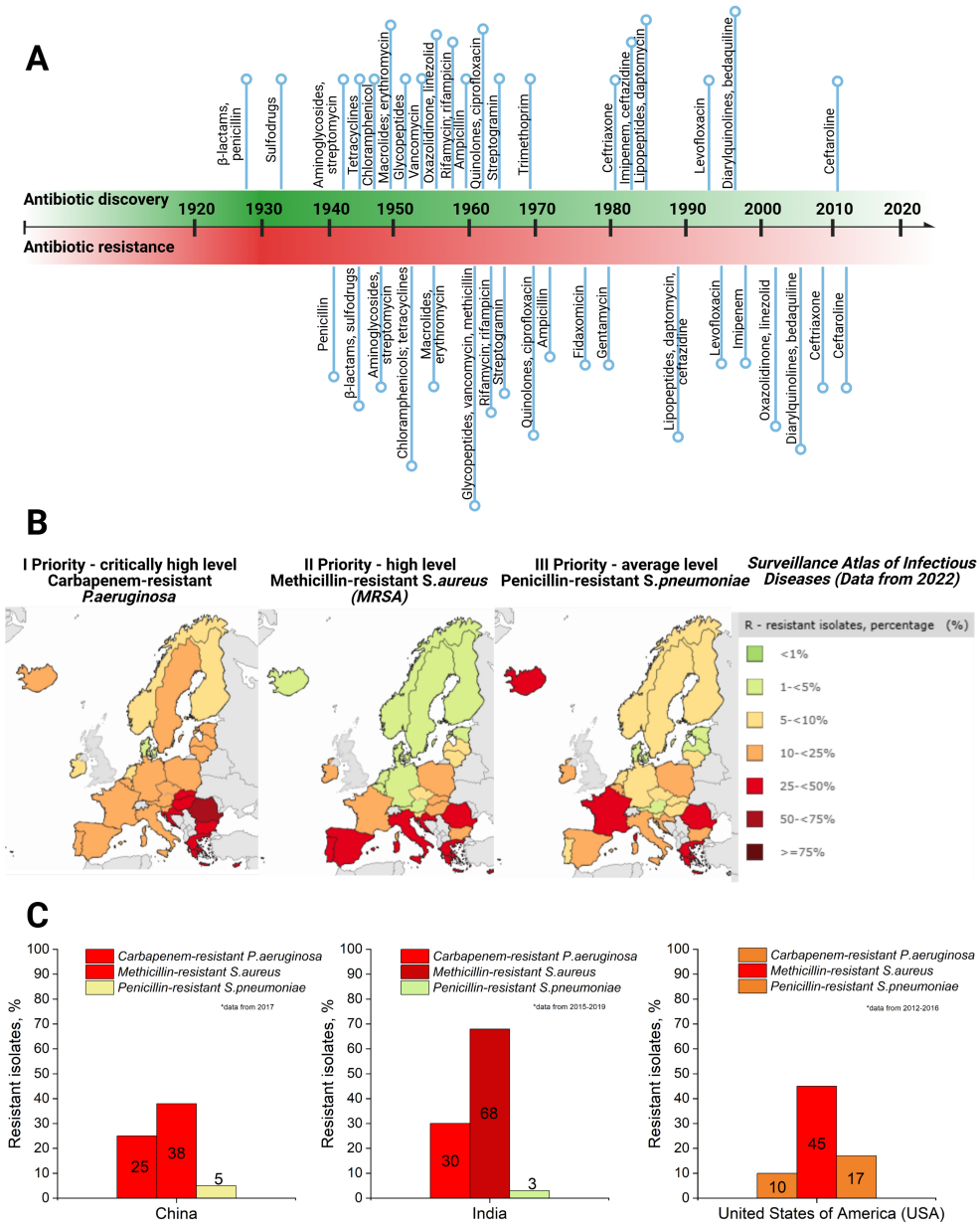

FIGURE 2
(A) Antibiotic discovery (title of antibiotics and relative point within timeline decade) and resistance reports timeline (resistance report against specific antibiotic with a title and relative point within timeline decade) (Dahal and Chaudhary, 2018). **(B)** Case map on three priority levels (I priority stands for critically high level; II priority – high level, and III – average level of resistance cases) resistant strains (carbapenem-resistant *P. aeruginosa*; methicillin-resistant *S. aureus*, and penicillin-resistant *S. pneumoniae*) in Europe, 2022, as well as a supporting table on resistant isolates' case percentage and colorful indicator for priority, with green indicating low level and dark red indicating critically high level (Surveillance Atlas of Infectious Diseases, 2022). **(C)** Comparative graphs of the same three priority resistant strains with color indication in the top three most populated world countries: China, India, and the United States of America (USA) (ResistanceMap, n.d.) (created by Biorender).

TABLE 2 Examples of naturally derived biopolymers (NDBs) and their antibacterial performance.

Class of biomolecule	Examples	Source	Intrinsic antibacterial activity (modification examples for improvement)	Antibacterial mechanism (bacteriostatic/bactericidal effect)	Reference
Polysaccharides	Chitin	Invertebrate animals (crustaceans)	+ (modified into chitosan form)	Makes the bacteria flocculate and thus kill it, presumably through lack of nutrients and oxygen (i.e., mass transfer limitation)	Kucharska et al. (2019), Benhabiles et al. (2012)
	Chitosan	Invertebrate animals (crustaceans) and certain fungi	+ (modified with quaternary ammonium)	Membrane disruption by electrostatic interaction	Muñoz-Bonilla et al. (2019), Razak and Mohamed (2021)
	Cellulose	Plants	– (modified with essential oils, metal nanoparticles, quaternary amino groups, etc.)	–	Muñoz-Bonilla et al. (2019), Nemeș et al. (2022)
	Starch	Plants	– (modified with metal oxides, antimicrobial peptides, essential oils, etc.)	–	Hou et al. (2023)
	Alginate	Macroalgae	+ (modified with essential oils, peptides, and metal nanoparticles)	Membrane disruption by electrostatic interaction	Wathoni et al. (2024), Asadpoor et al. (2021), Hegde et al. (2022)
	Pectin	Plants	+ (modified with peptides, metal nanoparticles, antibiotics, and metal ions)	Still unclear, molecules cause double oxidative stress	Muñoz-Bonilla et al. (2019), Tripathi and Mishra (2021), Daoud et al. (2013), Hassan et al. (2021)
	κ-Carrageenan	Macroalgae	+ (modified with metal oxides, metal nanoparticles, essential oils, and clay)	Damages the bacterial cell wall and cytoplasmic membrane and suppresses the growth of both Gram-positive and Gram-negative bacteria	Muñoz-Bonilla et al. (2019), Zhu et al. (2017), El-Fawal (2014)
	Chondroitin sulfate	Humans, other mammals, invertebrates, and some bacteria	+ (modified with chitosan or zinc ions)	Membrane disruption by electrostatic interaction	Unver et al. (2023), Gómez et al. (2018), Wu et al. (2022)
	β-glucans (laminaran, scleroglucan etc.)	Fungi, yeasts, and algae	+ (modified with zinc oxide, enzyme proteins, or carboxymethylated)	Penetrates bacterial cells, interfering with their metabolism and inducing cellular lysis	Chamidah and Hardoko (2017), Schwartz and Vetvicka (2021), Pino et al. (2023), Syaban et al. (2022), Song et al. (2020)
	o-Pullulan	Fungi	+ (modified with silver zinc oxide nanoparticles)	Membrane disruption by electrostatic interaction	Rai et al. (2021), Roy et al. (2023)
	Fucoidan	Brown algae	+ (modified with other molecules, e.g., chitosan and collagen)	Binds with the bacterial DNA, cytoplasmic membrane, and compounds present in the cell wall of bacteria and leads to the leakage of protein and an increase of the cytoplasmic membrane permeability, which results in the antibacterial effect of fucoidans	Habibi et al. (2024), Chmit et al. (2014), Egle et al. (2024)

(Continued)

10.3389/fmicb.2025.1526250

TABLE 2 (Continued)

Class of biomolecule	Examples	Source	Intrinsic antibacterial activity (modification examples for improvement)	Antibacterial mechanism (bacteriostatic/bactericidal effect)	Reference
Exo-polysaccharides	Hyaluronan	Bacteria	+ (modified with peptides, amino acids, and other polysaccharides, e.g., chitosan)	Neutralizes positive charge of the bacterial cell wall and so dramatically compromises bacteria adhesion ability	Zamboni et al. (2023), Hernandez-Montelongo et al. (2021)
	Xanthan	Bacteria	–(biodegraded into xanthan-oligosaccharide, modified with metal oxides)	–	Wang et al. (2020), Guo et al. (2022)
	Curdlan	Bacteria	– (modified with polyphenols and quaternary ammonium)	–	Suflet et al. (2024), Ding et al. (2024)
Proteins	Collagen	Animals and marine organisms	– (modified into oxidized form, carboxymethylated, with chitosan, alginate, antibiotics, herbal extracts, metal oxides, and peptides)	–	Valenzuela-Rojo et al. (2020), Ersanli et al. (2023)
	Silk (silk fibroin)	Silkworms	– (modified with antibiotics, inorganic nanoparticles, plant extracts, nitric oxide, and peptides)	–	Kaur et al. (2014), González-Restrepo et al. (2024), Ghalei and Handa (2022)
	Keratin	Animals	– (modified with metal nanoparticles, amides, and collagen)	–	Shanmugasundaram and Ramkumar (2018), Sun et al. (2023)
	Lactoferrin	Milk and colostrum	+ (modified with polyphenols, chitosan, and alginate)	Iron sequestering and further interaction with the bacterial surface lead to damaging the bacterial membrane, altering the outer membrane permeability	Jenssen and Hancock (2009), Wang et al. (2024)
	Lysozyme	Majority of vertebrates, including mammals	+ (modified with silica)	Cell wall disruption by hydrolyzing of 1,4-beta-linkages between *N*-acetylmuramic acid and *N*-acetylglucosamine	Khorshidian et al. (2022), van den Heuvel et al. (2018)
	Fibrin	Blood plasma of animals	– (used in combination with growth factors and other biological molecules in the form of platelet-or leukocyte-rich fibrin)	–	Moraschini et al. (2024)

(Continued)

10.3389/fmicb.2025.1526250

TABLE 2 (Continued)

Class of biomolecule	Examples	Source	Intrinsic antibacterial activity (modification examples for improvement)	Antibacterial mechanism (bacteriostatic/bactericidal effect)	Reference
Peptides (small amino acid-based biopolymers)	Magainin 2	Tailless amphibians	+ (modified with other cationic peptides)	Membrane disruption by electrostatic interaction	Kim et al. (2018), Syryamina et al. (2024)
	Defensins	Plants, insects, and mammals	+ (modified with chitosan and polylactic co-glycolic acid)	Membrane disruption by forming channels in lipid bilayer	Dong et al. (2020)
	LL-37 (Cathelin-associated antimicrobial peptide)	Neutrophils and macrophages in mammals	+ (modified with polylactic co-glycolic acid)	Membrane disruption by electrostatic interaction	Ren et al. (2024), Ridyard and Overhage (2021)
	Nisin	Bacteria	+ (modified with polysaccharides, proteins, calcium phosphates, and metal oxides)	Pore formation in the membrane and inhibition of cell wall biosynthesis by binding to lipid II	Shin et al. (2016), Li et al. (2018), Yan et al. (2024)
	Cecropin A	Insects	+ (no data)	Aggregate and assume a transbilayer orientation in membranes	Silvestro et al. (2000)
	ε-Polylysine	Bacteria	+ (modified with natural and synthetic polymers)	Membrane disruption by electrostatic interaction	Ranjbar et al. (2023), Sceglovs et al. (2023)
Other biopolymers	Suberin	Plants	+ (modified with essential oils)	Disruption of the bacterial membrane, prevention of biofilm formation, and inhibition of DNA and protein synthesis	Liakos et al. (2019), Dönmez and Önem (2024)
	Tannin	Plants	+ (used as a natural cross-linking agent for natural and synthetic polymers)	Iron chelation, inhibition of cell wall synthesis, and disruption of cell membrane	Farha et al. (2020), Baldwin and Booth (2022)

10.3389/fmicb.2025.1526250

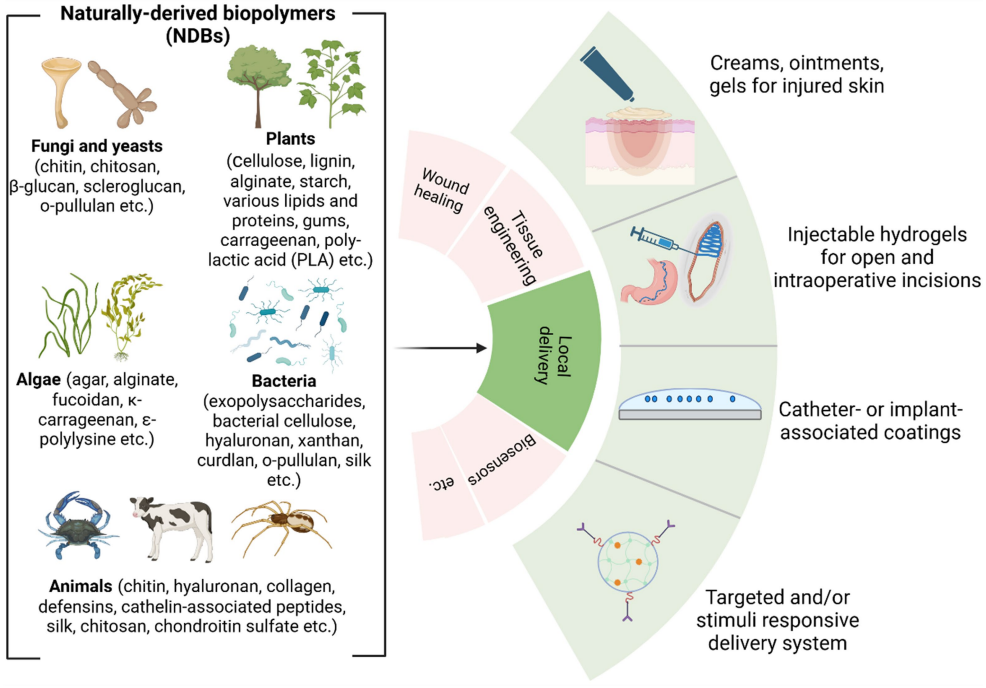

FIGURE 3
Overview of naturally derived biopolymers for local delivery applications (Biswas et al., 2022; Dimri et al., 2023; Ibrahim et al., 2019) (created by Biorender).

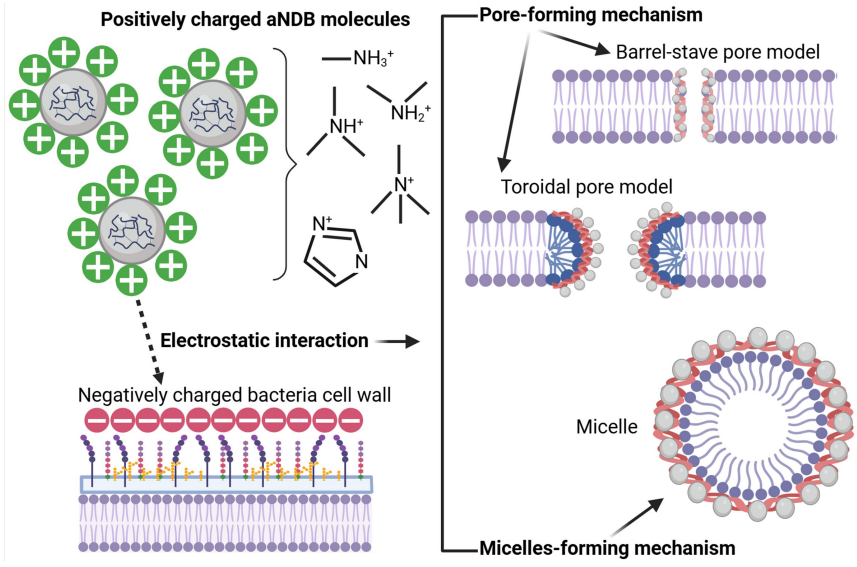

FIGURE 4
Biopolymer (aNDBs)—bacterial cell interaction (left) and bactericidal mechanisms (right) (created by Biorender).

Fayed et al., 2023; Baltimore et al., 1987; Khan et al., 2012; Kaur et al., 2022).

Considering the advantageous functionalities such as biodegradability, low immunogenicity, and non-toxicity of naturally derived biopolymer-based drug delivery systems, the antibacterial feature opens new horizons for developing local targeted antibacterial therapeutics based on antibacterial biopolymers. Countless reviews and studies have demonstrated the ability of NDBs to inhibit a broad spectrum of Gram-positive and Gram-negative bacteria, including bacterial strains currently being classified as "under urgent attention" due to their resistance to various antibiotics (Bustamante-Torres et al., 2022; Poznanski et al., 2023; Rofeal et al., 2022), as well as fungi (Poznanski et al., 2023; Ntow-Boahene et al., 2021) and viruses (Akbari et al., 2022; Bianculli et al., 2020). Several studies have highlighted that various naturally derived biopolymers (NDBs) exhibit notable antibiofilm activity (see Table 2). These antibiofilm mechanisms primarily involve disrupting biofilm exopolysaccharides (EPS), a critical component for biofilm stability. Such disruptions can lead to the detachment of bacterial cells or inhibit bacterial adhesion during the early stages of biofilm formation (Mishra et al., 2020; Melander et al., 2020). In addition, certain NDBs, such as lactoferrin-derived peptides, neutrophil peptides, and antimicrobial peptides (e.g., protegrin-1), have demonstrated antibacterial activity against intracellular pathogens, including *Mycobacterium tuberculosis*. These antibacterial effects are attributed to the disruption of the mycobacterial cell wall and enhanced membrane permeabilization (Khara et al., 2020; Jacobo-Delgado et al., 2023; Intorasoot et al., 2022). Despite these promising findings, significant challenges remain in translating NDBs into clinical applications. Key limitations include variability in their physicochemical and mechanical properties, which can impact reproducibility and reliability in therapeutic settings (Moradali and Rehm, 2020; Yadav et al., 2015). The limited physicochemical stability and difficulty tuning their biodegradation profiles further complicate their development as viable therapeutic solutions (Muñoz-Bonilla and Fernández-García, 2012; Pahlevanzadeh et al., 2022). In addition, the transition from laboratory-scale research to clinical application faces substantial barriers, including extensive preclinical testing to establish safety and efficacy, the complexities of large-scale manufacturing to ensure consistent quality, and the rigorous regulatory approval processes that demand considerable time and resources (Oliva et al., 2021; Murali and Jayakumar, 2023). Addressing these challenges will require interdisciplinary approaches and sustained efforts to optimize the properties of NDBs and streamline their development pipeline for clinical use (Arciola et al., 2018; Kong et al., 2023).

In further sections, the antibacterial potential of NDBs will be discussed to understand biopolymer interaction with bacterial cells, inhibition/bactericidal mechanism, and application specifics, to compare all these aspects with currently used conventional antibiotics, and to address the question posed in the title of this review.

4 Mode of delivery of NDBs for antibacterial treatment

Based on R&D reports, the most common local modes of delivery of antibacterial naturally derived biopolymers (aNDBs) to treat desired sites for various biomedical applications are summarized in Figure 3. Local application options and antibacterial activity are the main advantages reported in numerous studies for such biopolymers (Wu et al., 2022; Jarosz et al., 2023; Kong et al., 2023). Local delivery is preferable as it achieves the target site at the same concentration as it was prepared directly without passing through all the body barriers via the bloodstream and without losing biopolymer molecules. Such local delivery types include creams, ointments, and gels that are applied on the skin, burn or opened wounds, and surgery sites to prevent and treat infection (Zhao et al., 2023); intraoperative coatings and fillers (Ilić-Stojanović et al., 2023) are used for deeper surgical sites or dental sockets post-tooth extraction to avoid or combat already infected site; implant and catheters coating that allows preventing implant-and catheter-associated infections (Veiga and Schneider, 2013); and controlled delivery systems that achieve and bind to targeted site via different stimuli or due to specific conditions (temperature and pH), followed by antibacterial activity while providing controlled cell/ion/growth factor release from the matrix (Jacob et al., 2018) (Figure 3). This local delivery feature gives an advantage compared to conventional administration of antibiotics orally (pills and suspensions) or intravenously (in particular cases). While oral administration is convenient and suitable for at-home antibiotic therapy, it is associated with a decline in the concentration of the active compound upon reaching the infection site (Homayun et al., 2019; Kim and De Jesus, 2023). In addition, this strategy negatively impacts natural body microbiota, directly affecting the patient's immune system response to continuous or new bacteria invasion (Konstantinidis et al., 2020). Nevertheless, it is worth acknowledging the efficacy of oral drug administration in systemic or severe infections at multiple sites (Cunha, 2006). However, various studies have reported that combined device development where aNDBs served as a drug delivery system with encapsulated antibiotics might have a promising synergistic effect to achieve the exact infection site (Liu et al., 2022; Khan et al., 2021; Meng et al., 2014; Hwang et al., 2023; Schrade et al., 2022).

5 Mechanism of antibacterial action

Regarding aNDBs, it is crucial to understand that these biopolymer molecules, unlike the previously described antibiotics, do not target specific synthesis pathways or molecules. First, it is worth mentioning that bacterial cell wall outer structures serve as adhesion and pathogenicity factors; for example, lipopolysaccharides and phospholipids of Gram-negative bacteria and teichoic and lipoteichoic acids of Gram-positive bacteria are negatively charged. Second, aNDBs consist of positively charged molecules (chondroitin sulfate, o-pullulan, alginate, ε-polylysine, chitosan, magainin-2, etc.), containing cationic groups such as quaternary ammonium, quaternary phosphonium, guanidinium, or tertiary sulfonium (Santos et al., 2016), which have a positive charge. As a result, the interaction between biopolymers and bacteria begins with mutual attachment caused by electrostatic forces (Haktaniyan and Bradley, 2022). As a result, if aNDB molecules and bacteria cells are close enough, oppositely charged molecules attract each other, leading to physical binding (Figure 4). Another essential fact is that not all cationic molecules are lethal to bacteria. The electrostatic interaction represents just the first step toward the bactericidal effect of aNDBs. Second, a specific concentration of the cationicity of aNDBs must be achieved

to reach a multivalence effect (Smola-Dmochowska et al., 2023) that results in the simultaneous binding of aNDB molecules to the bacterial cell structures and moving to the next step.

In the next step, aNDB mechanisms of action on bacterial cell walls are divided into pore-forming and micelle-forming mechanisms (Qiu et al., 2020; Zhou et al., 2023). The pore-forming mechanism can be further categorized into two models: barrel-stave pore and toroidal pore (Kumar et al., 2018; Pastore et al., 2020; Mihajlovic and Lazaridis, 2010). Within the barrel-stave model, the aNDB molecules are initially oriented parallel to the membrane but eventually inserted perpendicularly in the lipid bilayer (Hegde et al., 2022) (Figure 4). This promotes lateral peptide–peptide interactions such as membrane protein ion channels. Hydrophobic regions interact with membrane lipids, and hydrophilic residues form the lumen of the channels (Brogden, 2005). On the other hand, in the toroidal pore model, peptides are also inserted perpendicularly in the lipid bilayer, but specific peptide–peptide interactions are not present (Wimley, 2010). Instead, the peptides induce a local curvature of the lipid bilayer, with the pores partly formed by peptides and partly by the phospholipid head group. The dynamic and transient lipid–peptide supramolecule is the "toroidal pore." The key distinguishing feature of this model, compared to the barrel-stave pore, is the net arrangement of the bilayer. In the barrel-stave pore, the hydrophobic and hydrophilic arrangement of the lipids is maintained, whereas, in toroidal pores, the hydrophobic and hydrophilic arrangement of the bilayer is disrupted. This provides alternate surfaces for interacting with the lipid tail and head group. As the pores are transient upon disintegration, some peptides translocate to the inner cytoplasmic leaflet, entering the cytoplasm and potentially targeting intracellular components (Kumar et al., 2018). Other features of the toroidal pores include ion selectivity and discrete size (Yeaman and Yount, 2003). Due to pore formation, joint cell wall integrity and permeability are disrupted, resulting in bacterial cell lysis.

The micelle-forming mechanism is usually called the "Carpet-like" model (Wimley, 2010; Huan et al., 2020; Shai, 2002). In this case, the aNDBs adsorb parallel to the lipid bilayer and reach a threshold concentration to cover the surface of the membrane, thereby forming a "carpet" (Figure 4). This leads to unfavorable interactions on the membrane surface. Consequently, membrane integrity is lost, producing a detergent-like effect, which eventually disintegrates the membrane by forming micelles, followed by bacterial cell death (Qiu et al., 2020; Zhou et al., 2023; Kumar et al., 2018).

6 Resistance development possibility

Another crucial consideration lies in the potential for bacteria to develop resistance to antibiotics. As previously highlighted, different bacterial strains develop resistance to commonly used antibiotics. Resistance mechanisms are unique and depend on the antibiotic group and mechanism of action specifics. Still, overall mechanisms involve specific enzyme production, loss of targeted molecules, efflux pumps, mutation of the target site, increased cell permeability, etc. (Reygaert, 2018; Munita and Arias, 2016; Peterson and Kaur, 2018; Abushaheen et al., 2020). It has been conventionally assumed that this propensity for resistance is exclusive to antibiotics, and theoretically, bacteria cannot develop resistance to aNDBs. On the one hand, electrostatic attraction between aNDBs and bacterial outer structures seems inevitable. In addition, the aNDB mechanism of action is not explicitly targeted. Even after entering the inner environment, aNDBs could enter many metabolic pathways. Based on that, it is more likely that bacteria encounter challenges in impeding electrostatic interaction and developing resistance, given the biological expense associated with such a complex process.

Although thought to be improbable, alteration of bacterial membranes has been shown as a mechanism of resistance (Epand et al., 1858; Nawrocki et al., 2014). Such alterations include incorporating components with reduced anionic charge, which leads to the inability of peptides to aggregate on bacterial membranes and prevents them from entering the cell (Baltzer and Brown, 2011). For instance, studies have shown that *Staphylococcus aureus* modifies the anionic phospholipids in the cytoplasmic membrane with L-lysine, resulting in a reduction of the net negative charge of the bacterial membrane and leading to the repulsion and subsequent resistance to aNDBs (Peschel et al., 2001). Similarly, modification of Gram-negative bacteria's lipopolysaccharides (LPS) is another bacterial mechanism contributing to resistance (Gunn, 2001; Guo et al., 1998). These modifications include incorporating fatty acids, thereby reducing the permeability of the outer membrane and increasing membrane structural stability (Peschel, 2002). Furthermore, bacteria can change the permeability of the cell wall, as is widely reported in the case of tetracyclines (Chmit et al., 2014); in addition, such non-specific structures as efflux pumps are also responsible for pumping out unfavorable molecules, and they are evidenced to work correctly against macrolides (Zhong and Shortridge, 2000).

7 Conclusion and future perspective

The highlighted findings in our review confirm that naturally occurring biopolymers with intrinsic antibacterial performance can be considered high-performance, sustainable, next-generation materials for biomedical field applications. Various studies have shown that hydrogels, biosensors, drug delivery systems, and implant coatings based on natural antibacterial biopolymers have promising physicochemical features. They possess excellent biocompatibility and are naturally derived, thus making them environmentally friendly. However, the main focus of this review was to elucidate the potential of naturally derived antibacterial biopolymers toward a specific aim—antibacterial therapy against bacterial infection in the human body—and second, to understand whether aNDBs are a future or a failure in replacing antibiotics. Multiple studies have reported these biopolymers *in vitro*; their antibacterial potential revealed action mechanisms. In addition, aNDBs have demonstrated substantial inhibitory effects against antibiotic-resistant bacteria strains. Based on the results, aNDBs could emerge as a novel weapon against bacterial infections to replace currently used antibiotics and antibiotic use approaches. Unique antibacterial action and the possibility of loading directly to the infection site (locally) open new horizons for this type of material.

However, learning from the past must be taken properly; many years ago, antibiotics were in the same situation. What is known for sure is that antibacterial biopolymers exhibit remarkable potential for combating bacteria and possess unique qualities. This material class is confined to research studies and is exclusively utilized for scientific purposes under controlled conditions. At the same time, antibiotics have already deserved the trust of medical doctors and have been

proven effective antibacterial therapy in clinical care. Bacteria possess the biological mechanisms necessary for potential evolution, raising questions about the likelihood of encountering analogous issues. The problem associated with antibiotic resistance has emerged due to prolonged global exposure to antibiotics in the medical sector, inappropriate drug misuse or overuse, and the usage of antibiotics in agriculture. It is still being determined if antibacterial biopolymers will be opened to the world as much as antibiotics and undergo the same conditions. Will we face the same problem as now? Bacteria possess the biological mechanisms necessary for potential evolution, raising questions about the likelihood of encountering similar issues. In summary, antibacterial biopolymers are promising materials with many advantages, including their antibacterial potential. However, in light of various considerations and experiences, numerous questions must be answered, particularly considering the development of bacterial resistance. It is not merely a matter of substituting one for the other but a nuanced exploration of the complexities involved.

Author contributions

AS: Conceptualization, Resources, Writing – original draft, Writing – review & editing. IS: Writing – review & editing. MC: Writing – review & editing. JK: Supervision, Writing – review & editing. KS-A: Conceptualization, Funding acquisition, Supervision, Writing – review & editing.

Funding

The author(s) declare that financial support was received for the research, authorship, and/or publication of this article. The authors acknowledge financial support for granting Open Access from the European Union's Horizon 2020 research and innovation program under grant agreement No. 857287 (BBCE—Baltic Biomaterials Centre of Excellence) and from the C316 Implementation of Consolidation and Governance Changes at Riga Technical University, LiepU, RAT, LMA, and LMC to Advance Excellence in Higher Education, Science, and Innovation program under the grant agreement C4835.Dok.1025 No. 5.2.1.1.i.0/2/24/I/CFLA/003.

Conflict of interest

The authors declare that the research was conducted in the absence of any commercial or financial relationships that could be construed as a potential conflict of interest.

Generative AI statement

The authors declare that no Generative AI was used in the creation of this manuscript.

Publisher's note

References

Abushaheen, M. A., Muzaheed, A. J., Fatani, M., Alosaimi, W., Mansy, M., George, S., et al. (2020). Antimicrobial resistance, mechanisms and its clinical significance. *Dis. Mon.* 66:100971. doi: 10.1016/J.DISAMONTH.2020.100971

Akbari, A., Bigham, A., Rahimkhoei, V., Sharifi, S., and Jabbari, E. (2022). Antiviral polymers: a review. *Polym.* 2022:1634. doi: 10.3390/POLYM14091634

Akram, F., Imtiaz, M., and ul Haq, I. (2023). Emergent crisis of antibiotic resistance: a silent pandemic threat to 21st century. *Microb. Pathog.* 174:105923. doi: 10.1016/J.MICPATH.2022.105923

Aminov, R. I. (2010). A brief history of the antibiotic era: lessons learned and challenges for the future. *Front. Microbiol.* 1:8040. doi: 10.3389/FMICB.2010.00134

Annunziato, G. (2019). Strategies to overcome antimicrobial resistance (AMR) making use of non-essential target inhibitors: a review. *Int. J. Mol. Sci.* 20:5844. doi: 10.3390/IJMS20235844

Antibiotics Review, (2010). Available at: https://errolozdalga.com/medicine/pages/OtherPages/AntibioticReview.ChanuRhee.html (Accessed April 2, 2024).

Appanna, V. D. (2018). Human microbes-the Power within, vol. *2018*. *1st* Edn: Singapore: Springer Singapore, Springer Nature Singapore Pte Ltd.

Arciola, C. R., Campoccia, D., and Montanaro, L. (2018). Implant infections: adhesion, biofilm formation and immune evasion. *Nat. Rev. Microbiol.* 2018, 397–409. doi: 10.1038/s41579-018-0019-y

Arer, V., and Kar, D. (2023). Biochemical exploration of β-lactamase inhibitors. *Front. Genet.* 13:1060736. doi: 10.3389/FGENE.2022.1060736

Asadpoor, M., Ithakisiou, G. N., van Putten, J. P. M., Pieters, R. J., Folkerts, G., and Braber, S. (2021). Antimicrobial activities of alginate and chitosan oligosaccharides against Staphylococcus aureus and group B Streptococcus. *Front. Microbiol.* 12:700605. doi: 10.3389/FMICB.2021.700605

Atanase, L. I. (2021). Micellar drug delivery systems based on natural biopolymers. *Polym.* 2021:477. doi: 10.3390/POLYM13030477

Baldwin, A., and Booth, B. W. (2022). Biomedical applications of tannic acid. *J. Biomater. Appl.* 36, 1503–1523. doi: 10.1177/08853282211058099

Baltimore, R. S., Cross, A. S., and Dobek, A. S. (1987). The inhibitory effect of sodium alginate on antibiotic activity against mucoid and non-mucoid strains of *Pseudomonas aeruginosa*. *J. Antimicrob. Chemother.* 20, 815–823. doi: 10.1093/JAC/20.6.815

Baltzer, S. A., and Brown, M. H. (2011). Antimicrobial peptides: promising alternatives to conventional antibiotics. *J. Mol. Microbiol. Biotechnol.* 20, 228–235. doi: 10.1159/000331009

Baranwal, J., Barse, B., Fais, A., Delogu, G. L., and Kumar, A. (2022). Biopolymer: a sustainable material for food and medical applications. *Polym.* 14:983. doi: 10.3390/POLYM14050983

Benhabiles, M. S., Salah, R., Lounici, H., Drouiche, N., Goosen, M. F. A., and Mameri, N. (2012). Antibacterial activity of chitin, chitosan and its oligomers prepared from shrimp shell waste. *Food Hydrocoll.* 29, 48–56. doi: 10.1016/J.FOODHYD.2012.02.013

Berry, M., Gurung, A., and Easty, D. L. (1995). Toxicity of antibiotics and antifungals on cultured human corneal cells: effect of mixing, exposure and concentration. *Eye* 9, 110–115. doi: 10.1038/eye.1995.17

Bhattacharjee, M. K. (2016). Antibiotics that inhibit nucleic acid synthesis. *Chem. Antibiot. Relat. Drugs*, 109–128. doi: 10.1007/978-3-319-40746-3_5

Bianculli, R. H., Mase, J. D., and Schulz, M. D. (2020). Antiviral polymers: past approaches and future possibilities. *Macromolecules* 53, 9158–9186. doi: 10.1021/ACS.MACROMOL.0C01273

Biswas, M. C., Jony, B., Nandy, P. K., Chowdhury, R. A., Halder, S., Kumar, D., et al. (2022). Recent advancement of biopolymers and their potential biomedical applications. *J. Polym. Environ.* 30, 51–74. doi: 10.1007/s10924-021-02199-y

Blaser, M. (2011). Stop the killing of beneficial bacteria. *Nature*. 476, 393–394. doi: 10.1038/476393a

Bogitsh, B. J., Carter, C. E., and Oeltmann, T. N. (2019). Symbiosis and parasitism. *Hum. Parasitol.*, 1–14. doi: 10.1016/B978-0-12-813712-3.00001-1

Brogden, K. A. (2005). Antimicrobial peptides: pore formers or metabolic inhibitors in bacteria? *Nat. Rev. Microbiol.* 3, 238–250. doi: 10.1038/nrmicro1098

Bull, M. J., and Plummer, N. T. (2014). Part 1: the human gut microbiome in health and disease. *Integr. Med.* 13, 17–22.

Buonavoglia, A., Leone, P., Solimando, A. G., Fasano, R., Malerba, E., Prete, M., et al. (2021). Antibiotics or no antibiotics, That is the question: An update on efficient and effective use of antibiotics in dental practice, vol. *10*. Basel, Switzerland: Antibiot.

Bush, K., and Bradford, P. A. (2016). β-Lactams and β-lactamase inhibitors: an overview. *Cold Spring Harb. Perspect. Med.* 6:5247. doi: 10.1101/CSHPERSPECT.A025247

Bustamante-Torres, M., Arcentales-Vera, B., Estrella-Nuñez, J., Yánez-Vega, H., and Bucio, E. (2022). Antimicrobial activity of composites-based on biopolymers. *Macromolecules* 2022, 258–283. doi: 10.3390/MACROMOL2030018

Castle, S. S. (2007). Beta-lactamase inhibitors. In: *xPharm: The Comprehensive Pharmacology Reference*, eds. S. J. Enna and B. David. (Netherlands: Bylund, Elsevier publisher) pp. 1–3.

Cell Membrane Inhibitors. Cell Membrane Inhibitors: Examples, Inhibition, Resistance, (2023). Available at: https://microbenotes.com/cell-membrane-inhibitors/ (Accessed December 18, 2024).

Chamidah, A., and Hardoko, A. A. P. (2017). Antibacterial activities of β-glucan (laminaran) against gram-negative and gram-positive bacteria. *AIP Conf. Proc.* 1844:20011. doi: 10.1063/1.4983422/748336

Chmit, M., Kanaan, H., Habib, J., Abbass, M., Mcheik, A., and Chokr, A. (2014). Antibacterial and antibiofilm activities of polysaccharides, essential oil, and fatty oil extracted from *Laurus nobilis* growing in Lebanon, Asian Pac. *J. Trop. Med.* 7S1, S546–S552. doi: 10.1016/S1995-7645(14)60288-1

Chortkoff, B., and Stenehjem, D. (2019). Chemotherapy, immunosuppression, and anesthesia. In: *Pharmacology and Physiology for Anesthesia*, (Second Edition), eds. H. C. Hemmings Jr and T. D. Egan. (Netherlands: Elsevier publisher) pp. 753–768.

Coates, A. R., Halls, G., and Hu, Y. (2011). Novel classes of antibiotics or more of the same? *Br. J. Pharmacol.* 163, 184–194. doi: 10.1111/J.1476-5381.2011.01250.X

Collin, F., Karkare, S., and Maxwell, A. (2011). Exploiting bacterial DNA gyrase as a drug target: current state and perspectives. *Appl. Microbiol. Biotechnol.* 92, 479–497. doi: 10.1007/S00253-011-3557-Z

Coma, V. (2013). Polysaccharide-based biomaterials with antimicrobial and antioxidant properties. *Polimeros* 20, 287–297. doi: 10.4322/POLIMEROS020OV002

Cook, M. A., and Wright, G. D. (2022). The past, present, and future of antibiotics. *Sci. Transl. Med.* 14:7793. doi: 10.1126/SCITRANSLMED.ABO7793

Cunha, B. A. (2006). Oral antibiotic therapy of serious systemic infections. *Med. Clin. North Am.* 90, 1197–1222. doi: 10.1016/J.MCNA.2006.07.009

Dahal, R. H., and Chaudhary, D. K. (2018). Microbial infections and antimicrobial resistance in Nepal: current trends and recommendations. *Open Microbiol. J.* 12, 230–242. doi: 10.2174/1874285801812010230

Daoud, Z., Sura, M., Abdel-Massih, R. M., Daoud, Z., Sura, M., and Abdel-Massih, R. M. (2013). Pectin shows antibacterial activity against *Helicobacter pylori*. *Adv. Biosci. Biotechnol.* 4, 273–277. doi: 10.4236/ABB.2013.42A037

Dimri, R., Mall, S., Sinha, S., Joshi, N. C., Bhatnagar, P., Sharma, R., et al. (2023). Role of microalgae as a sustainable alternative of biopolymers and its application in industries. *Plant Sci. Today* 10, 8–18. doi: 10.14719/PST.2460

Ding, R.-X., Goh, W. R., Wu, R.-N., Yue, X.-Q., Luo, X., Khine, W. W. T., et al. (2019). Revisit gut microbiota and its impact on human health and disease. *J. Food Drug Anal.* 27, 623–631. doi: 10.1016/J.JFDA.2018.12.012

Ding, Q., Mo, Z., Wang, X., Chen, M., Zhou, F., Liu, Z., et al. (2024). The antibacterial and hemostatic curdlan hydrogel–loading epigallocatechin gallate for facilitating the infected wound healing. *Int. J. Biol. Macromol.* 266:131257. doi: 10.1016/J.IJBIOMAC.2024.131257

Dong, Q., Guo, X., Li, L., Yu, C., Nie, L., Tian, W., et al. (2020). Understanding hyaluronic acid induced variation of water structure by near-infrared spectroscopy. *Sci. Rep.* 10, 1–8. doi: 10.1038/s41598-020-58417-5

Dönmez, İ. E., and Önem, E. (2024). Chemical composition and in vitro antibacterial activity of bark extractives and suberin monomers from Pinus brutia and *Pinus nigra*. *Eur. J. Wood Wood Prod.* 82, 231–240. doi: 10.1007/S00107-023-02004-8

Dubourg, G., Lagier, J. C., Robert, C., Armougom, F., Hugon, P., Metidji, S., et al. (2014). Culturomics and pyrosequencing evidence of the reduction in gut microbiota diversity in patients with broad-spectrum antibiotics. *Int. J. Antimicrob. Agents* 44, 117–124. doi: 10.1016/J.IJANTIMICAG.2014.04.020

Dunn, M. J., and Zambraski, E. J. (1980). Renal effects of drugs that inhibit prostaglandin synthesis. *Kidney Int.* 18, 609–622. doi: 10.1038/KI.1980.179

Egle, K., Dohle, E., Hoffmann, V., Salma, I., Al-Maawi, S., Ghanaati, S., et al. (2024). Fucoidan/chitosan hydrogels as carrier for sustained delivery of platelet-rich fibrin containing bioactive molecules. *Int. J. Biol. Macromol.* 262:129651. doi: 10.1016/J.IJBIOMAC.2024.129651

El-Fawal, G. (2014). Preparation, characterization and antibacterial activity of biodegradable films prepared from carrageenan. *J. Food Sci. Technol.* 51, 2234–2239. doi: 10.1007/S13197-013-1255-9

Eloe-Fadrosh, E. A., and Rasko, D. A. (2013). The human microbiome: from symbiosis to pathogenesis. *Annu. Rev. Med.* 64, 145–163. doi: 10.1146/ANNUREV-MED-010312-133513

Enenkel, S., and Stille, W. (1988). Administration of AntiBiotics. In: *Antibiotics in the Tropics.*, ed. Springer Berlin. Heidelberg (Springer-Varlag, Germany), 39–40.

Epand, R. M., Walker, C., Epand, R. F., and Magarvey, N. A. (1858). Molecular mechanisms of membrane targeting antibiotics. *Biochim. Biophys. Acta-Biomembr.* 1858, 980–987. doi: 10.1016/J.BBAMEM.2015.10.018

Ersanli, C., Tzora, A., Skoufos, I., Voidarou, C., and Zeugolis, D. I. (2023). Recent advances in collagen antimicrobial biomaterials for tissue engineering applications: a review. *Int. J. Mol. Sci.* 24:7808. doi: 10.3390/IJMS24097808

Farha, A. K., Yang, Q. Q., Kim, G., Bin Li, H., Zhu, F., Liu, H. Y., et al. (2020). Tannins as an alternative to antibiotics. *Food Biosci.* 38:100751. doi: 10.1016/J.FBIO.2020.100751

Fayed, B., Jagal, J., Cagliani, R., Kedia, R. A., Elsherbeny, A., Bayraktutan, H., et al. (2023). Co-administration of amoxicillin-loaded chitosan nanoparticles and inulin: a novel strategy for mitigating antibiotic resistance and preserving microbiota balance in *Helicobacter pylori* treatment. *Int. J. Biol. Macromol.* 253:126706. doi: 10.1016/J.IJBIOMAC.2023.126706

Ghalei, S., and Handa, H. (2022). A review on antibacterial silk fibroin-based biomaterials: current state and prospects. *Mater. Today Chem.* 23:100673. doi: 10.1016/J.MTCHEM.2021.100673

Gómez, M. A., Bonilla, J. M., Coronel, M. A., Martínez, J., Morán-Trujillo, L., Orellana, S. L., et al. (2018). Antibacterial activity against *Staphylococcus aureus* of chitosan/chondroitin sulfate nanocomplex aerogels alone and enriched with erythromycin and elephant garlic (*Allium ampeloprasum* L. var. ampeloprasum) extract. *Pure Appl. Chem.* 90, 885–900. doi: 10.1515/pac-2016-1112

González-Restrepo, D., Zuluaga-Vélez, A., Orozco, L. M., and Sepúlveda-Arias, J. C. (2024). Silk fibroin-based dressings with antibacterial and anti-inflammatory properties. *Eur. J. Pharm. Sci.* 195:106710. doi: 10.1016/J.EJPS.2024.106710

Grill, M. F., and Maganti, R. K. (2011). Neurotoxic effects associated with antibiotic use: management considerations. *Br. J. Clin. Pharmacol.* 72, 381–393. doi: 10.1111/J.1365-2125.2011.03991.X

Gunn, J. S. (2001). Bacterial modification of LPS and resistance to antimicrobial peptides, sage jour. *Innate Imunity* 7, 57–62. doi: 10.1177/096805190100701001

Guo, L., Lim, K. B., Poduje, C. M., Daniel, M., Gunn, J. S., Hackett, M., et al. (1998). Lipid a acylation and bacterial resistance against vertebrate antimicrobial peptides. *Cell* 95, 189–198. doi: 10.1016/S0092-8674(00)81750-X

Guo, F., Pan, F., Zhang, W., Liu, T., Zuber, F., Zhang, X., et al. (2022). Robust antibacterial activity of xanthan-gum-stabilized and patterned CeO2-x-TiO2Antifog films. *ACS Appl. Mater. Interfaces* 14, 44158–44172. doi: 10.1021/ACSAMI.2C11968

Habeeb, S. A., and Abdulkadhim, M. K. (2024). Natural biopolymer-hydrogel nanofibers for antibacterial applications. *J. Eng. Mater. Technol.* 146:3329. doi: 10.1115/1.4063329

Habibi, M., Golmakani, M. T., Eskandari, M. H., and Hosseini, S. M. H. (2024). Potential prebiotic and antibacterial activities of fucoidan from Laminaria japonica. *Int. J. Biol. Macromol.* 268:131776. doi: 10.1016/J.IJBIOMAC.2024.131776

Haktaniyan, M., and Bradley, M. (2022). Polymers showing intrinsic antimicrobial activity. *Chem. Soc. Rev.* 51, 8584–8611. doi: 10.1039/D2CS00558A

Hamidi, S., Monajjemzadeh, F., Siahi-Shadbad, M., Khatibi, S. A., and Farjami, A. (2023). Antibacterial activity of natural polymer gels and potential applications without synthetic antibiotics. *Polym. Eng. Sci.* 63, 5–21. doi: 10.1002/PEN.26184

Hanlon, J. T., Perera, S., Drinka, P. J., Crnich, C. J., Schweon, S. J., Klein-Fedyshin, M., et al. (2019). The IOU consensus recommendations for empirical therapy of cystitis in nursing home residents. *J. Am. Geriatr. Soc.* 67, 539–545. doi: 10.1111/JGS.15726

Hassan, E. A., Abou Elseoud, W. S., Abo-Elfadl, M. T., and Hassan, M. L. (2021). New pectin derivatives with antimicrobial and emulsification properties via complexation with metal-terpyridines. *Carbohydr. Polym.* 268:118230. doi: 10.1016/J.CARBPOL.2021.118230

Hedrick, T. L., Adams, J. D., and Sawyer, R. G. (2006). Implant-associated infections: an overview. *J. Long-Term Eff. Med. Implants* 16, 83–99. doi: 10.1615/jlongtermeffmedimplants.v16.i1.90

Hegde, V., Uthappa, U. T., Altalhi, T., Jung, H. Y., Han, S. S., and Kurkuri, M. D. (2022). Alginate based polymeric systems for drug delivery, antibacterial/microbial, and wound dressing applications. *Mater. Today Commun.* 33:104813. doi: 10.1016/J.MTCOMM.2022.104813

Hemarajata, P., and Versalovic, J. (2013). Effects of probiotics on gut microbiota: mechanisms of intestinal immunomodulation and neuromodulation. *Ther. Adv. Gastroenterol.* 6, 39–51. doi: 10.1177/1756283X12459294

Hernandez-Montelongo, J., Nicastro, G. G., Pereira, T. O., Zavarize, M., Beppu, M. M., Macedo, W. A. A., et al. (2021). Antibacterial effect of hyaluronan/chitosan nanofilm in the initial adhesion of *Pseudomonas aeruginosa* wild type, and IV pili and LPS mutant strains. *Surfac. Interfac.* 26:101415. doi: 10.1016/J.SURFIN.2021.101415

Hills, R. D., Pontefract, B. A., Mishcon, H. R., Black, C. A., Sutton, S. C., and Theberge, C. R. (2019). Gut microbiome: profound implications for diet and disease. *Nutrients* 2019:1613. doi: 10.3390/NU11071613

Homayun, B., Lin, X., and Choi, H. J. (2019). Challenges and recent Progress in Oral drug delivery Systems for Biopharmaceuticals. *Pharm.* 11:129. doi: 10.3390/PHARMACEUTICS11030129

Hou, X., Wang, H., Shi, Y., and Yue, Z. (2023). Recent advances of antibacterial starch-based materials. *Carbohydr. Polym.* 302:120392. doi: 10.1016/J.CARBPOL.2022.120392

Huan, Y., Kong, Q., Mou, H., and Yi, H. (2020). Antimicrobial peptides: classification, design, application and research Progress in multiple fields. *Front. Microbiol.* 11:582779. doi: 10.3389/FMICB.2020.582779

Hwang, J., Huang, H., Sullivan, M. O., and Kiick, K. L. (2023). Controlled delivery of vancomycin from collagen-tethered peptide vehicles for the treatment of wound infections. *Mol. Pharm.* 20, 1696–1708. doi: 10.1021/ACS.MOLPHARMACEUT.2C00898

Ibrahim, S., Riahi, O., Said, S. M., Sabri, M. F. M., and Rozali, S. (2019). Biopolymers from crop plants. *Ref. Modul. Mater. Sci. Mater. Eng.* doi: 10.1016/B978-0-12-803581-8.11573-5

Ige, O. O., Umoru, L. E., and Aribo, S. (2012). Natural products: a minefield of biomaterials. *ISRN Mater. Sci.* 2012, 1–20. doi: 10.5402/2012/983062

Ilić-Stojanović, S., Nikolić, L., and Cakić, S. (2023). A review of patents and innovative biopolymer-based hydrogels. *Gels.* 9:556. doi: 10.3390/gels9070556

Intorasoot, S., Intorasoot, A., Tawteamwong, A., Butr-Indr, B., Phunpae, P., Tharinjaroen, C. S., et al. (2022). In vitro antimycobacterial activity of human Lactoferrin-derived peptide, D-hLF 1-11, against susceptible and drug-resistant mycobacterium tuberculosis and its synergistic effect with rifampicin. *Antibiot.* 11:1785. doi: 10.3390/ANTIBIOTICS11121785

Isolauri, E., Sütas, Y., Kankaanpää, P., Arvilommi, H., and Salminen, S. (2001). Probiotics: effects on immunity. *Am. J. Clin. Nutr.* 73, 444s–450s. doi: 10.1093/AJCN/73.2.444S

Iuliano, S., Senn, L., Moi, L., Muller, Y. D., Ribi, C., Buss, G., et al. (2022). Management of beta-lactam antibiotics allergy: a real-life study. *Front. Allergy* 3:853587. doi: 10.3389/FALGY.2022.853587

Jacob, J., Haponiuk, J. T., Thomas, S., and Gopi, S. (2018). Biopolymer based nanomaterials in drug delivery systems: a review. *Mater. Today Chem.* 9, 43–55. doi: 10.1016/J.MTCHEM.2018.05.002

Jacobo-Delgado, Y. M., Rodríguez-Carlos, A., Serrano, C. J., and Rivas-Santiago, B. (2023). *Mycobacterium tuberculosis* cell-wall and antimicrobial peptides: a mission impossible? *Front. Immunol.* 14:1194923. doi: 10.3389/FIMMU.2023.1194923

Jarosz, K., Stadnik, D. A., Giannakoudakis, B., Barczyński, B., Barczak, M., and Kapusta, O. (2023). Antimicrobial natural hydrogels in biomedicine: properties, applications, and challenges—a concise review. *Int. J. Mol. Sci.* 24:2191. doi: 10.3390/IJMS24032191

Jenkins, A. D., Stepto, R. F. T., Kratochvíl, P., and Suter, U. W. (1996). Glossary of basic terms in polymer science (IUPAC recommendations 1996). *Pure Appl. Chem.* 68, 2287–2311. doi: 10.1351/PAC199668122287

Jenssen, H., and Hancock, R. E. W. (2009). Antimicrobial properties of lactoferrin. *Biochimie* 91, 19–29. doi: 10.1016/J.BIOCHI.2008.05.015

Johnston, C. W., and Badran, A. H. (2022). Natural and engineered precision antibiotics in the context of resistance. *Curr. Opin. Chem. Biol.* 69:102160. doi: 10.1016/J.CBPA.2022.102160

Kamaruzzaman, N. F., Tan, L. P., Hamdan, R. H., Choong, S. S., Wong, W. K., Gibson, A. J., et al. (2019). Antimicrobial polymers: the potential replacement of existing antibiotics? *Int. J. Mol. Sci.* 2019:2747. doi: 10.3390/IJMS20112747

Kapoor, G., Saigal, S., and Elongavan, A. (2017). Action and resistance mechanisms of antibiotics: a guide for clinicians. *J. Anaesthesiol. Clin. Pharmacol.* 33, 300–305. doi: 10.4103/JOACP.JOACP_349_15

Kaur, M., Cohen, Y., Poverenov, E., and Eltzov, E. (2022). Synergistic antimicrobial effect of the combination of beta-lactam antibiotics and chitosan derivative on multidrug-resistant bacteria. *Int. J. Biol. Macromol.* 223, 1107–1114. doi: 10.1016/J.IJBIOMAC.2022.11.132

Kaur, J., Rajkhowa, R., Afrin, T., Tsuzuki, T., and Wang, X. (2014). Facts and myths of antibacterial properties of silk. *Biopolymers* 101, 237–245. doi: 10.1002/BIP.22323

Khan, Y. A., Ozaltin, K., Bernal-Ballen, A., and Di Martino, A. (2021). Chitosan-alginate hydrogels for simultaneous and sustained releases of ciprofloxacin, amoxicillin and vancomycin for combination therapy. *J. Drug Deliv. Sci. Technol.* 61:102126. doi: 10.1016/J.JDDST.2020.102126

Khan, S., Tøndervik, A., Sletta, H., Klinkenberg, G., Emanuel, C., Onsøyen, E., et al. (2012). Overcoming drug resistance with alginate oligosaccharides able to potentiate the action of selected antibiotics. *Antimicrob. Agents Chemother.* 56, 5134–5141. doi: 10.1128/AAC.00525-12

Khara, J. S., Mojsoska, B., Mukherjee, D., Langford, P. R., Robertson, B. D., Jenssen, H., et al. (2020). Ultra-short antimicrobial Peptoids show propensity for membrane activity against multi-drug resistant *Mycobacterium tuberculosis*. *Front. Microbiol.* 11:515317. doi: 10.3389/FMICB.2020.00417

Khorshidian, N., Khanniri, E., Koushki, M. R., Sohrabvandi, S., and Yousefi, M. (2022). An overview of antimicrobial activity of lysozyme and its functionality in cheese. *Front. Nutr.* 9:833618. doi: 10.3389/FNUT.2022.833618

Kim, J., and De Jesus, O., Medication routes of administration, StatPearls (2023). Available at: https://www.ncbi.nlm.nih.gov/books/NBK568677/ (accessed April 2, 2024).

Kim, M. K., Kang, N., Ko, S. J., Park, J., Park, E., Shin, D. W., et al. (2018). Antibacterial and Antibiofilm activity and mode of action of Magainin 2 against drug-resistant *Acinetobacter baumannii*. *Int. J. Mol. Sci.* 19:3041. doi: 10.3390/IJMS19103041

Kong, B., Liu, R., Cheng, Y., Cai, X., Liu, J., Zhang, D., et al. (2023). Natural biopolymers derived hydrogels with injectable, self-healing, and tissue adhesive abilities for wound healing. *Nano Res.* 16, 2798–2807. doi: 10.1007/S12274-022-4936-8

Konstantinidis, T., Tsigalou, C., Karvelas, A., Stavropoulou, E., Voidarou, C., and Bezirtzoglou, E. (2020). Effects of antibiotics upon the gut microbiome: a review of the literature. *Biomed.* 8:502. doi: 10.3390/BIOMEDICINES8110502

Kucharska, M., Sikora, M., Brzoza-Malczewska, K., and Owczarek, M. (2019). Antimicrobial properties of chitin and chitosan, chitin chitosan prop. In: *Chitin and Chitosan: Properties and Applications.*, eds. L. A. M. van den and C. G. Broek Boeriu. (United States of America: John Wiley & Sons Ltd) pp.169–187.

Kumar, P., Kizhakkedathu, J. N., and Straus, S. K. (2018). Antimicrobial peptides: diversity, mechanism of action and strategies to improve the activity and biocompatibility in vivo. *Biomolecules* 8:4. doi: 10.3390/BIOM8010004

Lathakumari, R. H., Vajravelu, L. K., Satheesan, A., Ravi, S., and Thulukanam, J. (2024). Antibiotics and the gut microbiome: understanding the impact on human health. *Med. Microecol.* 20:100106. doi: 10.1016/J.MEDMIC.2024.100106

Li, Q., Montalban-Lopez, M., and Kuipers, O. P. (2018). Increasing the antimicrobial activity of nisinbased lantibiotics against gram-negative pathogens. *Appl. Environ. Microbiol.* 84:e00052-18. doi: 10.1128/AEM.00052-18

Li, J., Tian, X., Hua, T., Fu, J., Koo, M., Chan, W., et al. (2021). Chitosan natural polymer material for improving antibacterial properties of textiles. *ACS Appl. Bio Mater.* 4, 4014–4038. doi: 10.1021/ACSABM.1C00078

Liakos, I. L., Menager, C., Guigo, N., Holban, A. M., Iordache, F., Pignatelli, F., et al. (2019). Suberin/trans-cinnamaldehyde oil nanoparticles with antimicrobial activity and anticancer properties when loaded with paclitaxel. *ACS Appl. Bio Mater.* 2, 3484–3497. doi: 10.1021/ACSABM.9B00408

Lin, D. M., Koskella, B., and Lin, H. C. (2017). Phage therapy: an alternative to antibiotics in the age of multi-drug resistance. *World J. Gastrointest. Pharmacol. Ther.* 8, 162–173. doi: 10.4292/WJGPT.V8.I3.162

Liu, Y., Li, X., and Liang, A. (2022). Current research progress of local drug delivery systems based on biodegradable polymers in treating chronic osteomyelitis. *Front. Bioeng. Biotechnol.* 10:1042128. doi: 10.3389/FBIOE.2022.1042128

Majiduddin, F. K., Materon, I. C., and Palzkill, T. G. (2002). Molecular analysis of beta-lactamase structure and function. *Int. J. Med. Microbiol.* 292, 127–137. doi: 10.1078/1438-4221-00198

Manoukian, O. S., Sardashti, N., Stedman, T., Gailiunas, K., Ojha, A., Penalosa, A., et al. (2019). Biomaterials for tissue engineering and regenerative medicine, Encycl. *Biomed. Eng.* 1–3, 462–482. doi: 10.1016/B978-0-12-801238-3.64098-9

Martín, R., Miquel, S., Ulmer, J., Kechaou, N., Langella, P., and Bermúdez-Humarán, L. G. (2013). Role of commensal and probiotic bacteria in human health: a focus on inflammatory bowel disease. *Microb. Cell Factories* 12:71. doi: 10.1186/1475-2859-12-71

McCarthy, K., and Avent, M. (2020). Oral or intravenous antibiotics? *Aust. Prescr.* 43, 45–48. doi: 10.18773/AUSTPRESCR.2020.008

McGee, M., Brienesse, S., Chong, B., Levendel, A., and Lai, K. (2018). *Tropheryma whipplei* endocarditis: case presentation and review of the literature. *Open Forum Infect. Dis.* 6:330. doi: 10.1093/OFID/OFY330

Melander, R. J., Basak, A. K., and Melander, C. (2020). Natural products as inspiration for the development of bacterial antibiofilm agents. *Nat. Prod. Rep.* 37, 1454–1477. doi: 10.1039/D0NP00022A

Meng, G., He, J., Wu, Y., Wu, F., and Gu, Z. (2014). Antibiotic-loaded chitosan hydrogel with superior dual functions: antibacterial efficacy and osteoblastic cell responses. *ACS Appl. Mater. Interfaces* 6, 10005–10013. doi: 10.1021/AM502537K

Mihajlovic, M., and Lazaridis, T. (2010). Antimicrobial peptides in toroidal and cylindrical pores. *Biochim. Biophys. Acta* 1798, 1485–1493. doi: 10.1016/J.BBAMEM.2010.04.004

Mishra, R., Panda, A. K., De Mandal, S., Shakeel, M., Bisht, S. S., and Khan, J. (2020). Natural anti-biofilm agents: strategies to control biofilm-forming pathogens. *Front. Microbiol.* 11:566325. doi: 10.3389/FMICB.2020.566325

Moradali, M. F., and Rehm, B. H. A. (2020). Bacterial biopolymers: from pathogenesis to advanced materials. *Nat. Rev. Microbiol.* 18, 195–210. doi: 10.1038/s41579-019-0313-3

Moraschini, V., Miron, R. J., Mourão, C. F. A. B., Louro, R. S., Sculean, A., Fonseca, L. A. M., et al. (2024). Antimicrobial effect of platelet-rich fibrin: a systematic review of in vitro evidence-based studies. *Periodontol.* 94, 131–142. doi: 10.1111/PRD.12529

Morgan, D. J., Okeke, I. N., Laxminarayan, R., Perencevich, E. N., and Weisenberg, S. (2011). Non-prescription antimicrobial use worldwide: a systematic review. *Lancet Infect. Dis.* 11, 692–701. doi: 10.1016/S1473-3099(11)70054-8

Munita, J. M., and Arias, C. A. (2016). Mechanisms of antibiotic resistance. *Microbiol. Spectr.* 4. doi: 10.1128/MICROBIOLSPEC.VMBF-0016-2015

Muñoz-Bonilla, A., Echeverria, C., Sonseca, Á., Arrieta, M. P., and Fernández-García, M. (2019). Bio-based polymers with antimicrobial properties towards sustainable development. *Mater.* 12:641. doi: 10.3390/MA12040641

Muñoz-Bonilla, A., and Fernández-García, M. (2012). Polymeric materials with antimicrobial activity. *Prog. Polym. Sci.* 37, 281–339. doi: 10.1016/j.progpolymsci.2011.08.005

Murali, V. P., and Jayakumar, R. (eds). (2023). Natural biopolymers in drug delivery—role, challenges and clinical applications. In: *Natural Biopolymers in Drug Delivery and Tissue Engineering*, (United Kingdom: Woodhead Publishing) pp. 3–23.

Nawrocki, K. L., Crispell, E. K., and McBride, S. M. (2014). Antimicrobial peptide resistance mechanisms of gram-positive Bacteria. *Antibiot.* 3, 461–492. doi: 10.3390/ANTIBIOTICS3040461

Nemeş, N. S., Ardean, C., Davidescu, C. M., Negrea, A., Ciopec, M., Duţeanu, N., et al. (2022). Antimicrobial activity of cellulose based materials. *Polym.* 14:735. doi: 10.3390/POLYM14040735

Nilsson, A. S. (2019). Pharmacological limitations of phage therapy. *Ups. J. Med. Sci.* 124, 218–227. doi: 10.1080/03009734.2019.1688433

Ntow-Boahene, W., Cook, D., and Good, L. (2021). Antifungal polymeric materials and nanocomposites. *Front. Bioeng. Biotechnol.* 9:780328. doi: 10.3389/FBIOE.2021.780328

Oliva, A., Miele, M. C., Al Ismail, D., Di Timoteo, F., De Angelis, M., Rosa, L., et al. (2021). Challenges in the microbiological diagnosis of implant-associated infections: a summary of the current knowledge. *Front. Microbiol.* 12:750460. doi: 10.3389/FMICB.2021.750460

Pahlevanzadeh, F., Setayeshmehr, M., Bakhsheshi-Rad, H. R., Emadi, R., Kharaziha, M., Poursamar, S. A., et al. (2022). A review on antibacterial biomaterials in biomedical applications: from materials perspective to bioinks design. *Polym.* 2022:2238. doi: 10.3390/POLYM14112238

Pancu, D. F., Scurtu, A., Macasoi, I. G., Marti, D., Mioc, M., Soica, C., et al. (2021). Antibiotics: conventional therapy and natural compounds with antibacterial activity—a Pharmaco-toxicological screening. *Antibiotics* 10:401. doi: 10.3390/ANTIBIOTICS10040401

Pastore, A., Raimondi, F., Rajendran, L., and Temussi, P. A. (2020). Why does the Aβ peptide of Alzheimer share structural similarity with antimicrobial peptides? *Commun. Biol.* 3, 1–7. doi: 10.1038/s42003-020-0865-9

Patangia, D. V., Anthony Ryan, C., Dempsey, E., Paul Ross, R., and Stanton, C. (2022). Impact of antibiotics on the human microbiome and consequences for host health. *Microbiology* 11:e1260. doi: 10.1002/MBO3.1260

Peschel, A. (2002). How do bacteria resist human antimicrobial peptides? *Trends Microbiol.* 10, 179–186. doi: 10.1016/S0966-842X(02)02333-8

Peschel, A., Jack, R. W., Otto, M., Collins, L. V., Staubitz, P., Nicholson, G., et al. (2001). *Staphylococcus aureus* resistance to human defensins and evasion of neutrophil killing via the novel virulence factor MprF is based on modification of membrane lipids with l-lysine. *J. Exp. Med.* 193, 1067–1076. doi: 10.1084/JEM.193.9.1067

Peterson, E., and Kaur, P. (2018). Antibiotic resistance mechanisms in bacteria: relationships between resistance determinants of antibiotic producers, environmental bacteria, and clinical pathogens. *Front. Microbiol.* 9:426686. doi: 10.3389/FMICB.2018.02928

Pino, P., Pellegrino, G., Ronchetti, S., Mollea, C., Bosco, F., and Onida, B. (2023). Antibacterial β-glucan/zinc oxide nanocomposite films for wound healing. *BioNanoScience* 13, 426–435. doi: 10.1007/S12668-023-01079-0

Poznanski, P., Hameed, A., and Orczyk, W. (2023). Chitosan and chitosan nanoparticles: parameters enhancing antifungal activity. *Molecules* 28:2996. doi: 10.3390/MOLECULES28072996

Protein Synthesis Inhibitors-Definition. Protein Synthesis Inhibitors-Definition, Examples, Inhibition, Resistance, (2023). Available at: https://microbenotes.com/protein-synthesis-inhibitors/ (Accessed December 18, 2024).

Qiu, H., Si, Z., Luo, Y., Feng, P., Wu, X., Hou, W., et al. (2020). The mechanisms and the applications of antibacterial polymers in surface modification on medical devices. *Front. Bioeng. Biotechnol.* 8:571162. doi: 10.3389/FBIOE.2020.00910

Rai, M., Wypij, M., Ingle, A. P., Trzcińska-Wencel, J., and Golińska, P. (2021). Emerging trends in pullulan-based antimicrobial systems for various applications. *Int. J. Mol. Sci.* 22:13596. doi: 10.3390/IJMS222413596

Ramappa, V., and Aithal, G. P. (2013). Hepatotoxicity related to anti-tuberculosis drugs: mechanisms and management. *J. Clin. Exp. Hepatol.* 3, 37–49. doi: 10.1016/J.JCEH.2012.12.001

Ranjbar, H. H., Hosseini-Abari, A., Ghasemi, S. M., and Birgani, Z. H. (2023). Antibacterial activity of epsilon-poly-l-lysine produced by *Stenotrophomonas maltophilia* HS4 and *Paenibacillus polymyxa* HS5, alone and in combination with bacteriophages. *Microbiol.* 169:001363. doi: 10.1099/MIC.0.001363

Razak, N. S., and Mohamed, R. (2021). Antimicrobial sustainable biopolymers for biomedical plastics applications – an overview. *Polimery* 66, 574–583. doi: 10.14314/POLIMERY.2021.11.2

Reddy, M. S. B., Ponnamma, D., Choudhary, R., and Sadasivuni, K. K. (2021). A comparative review of natural and synthetic biopolymer composite scaffolds. *Polym.* 13:1105. doi: 10.3390/POLYM13071105

Ren, Z., Xiao, W., Song, H., and Zhou, L. (2024). Development of quantum computational model for analysis of drug delivery: loading of human beta-defensin 3 and mitoxantrone onto composite polymers. *J. Mol. Liq.* 399:124383. doi: 10.1016/J.MOLLIQ.2024.124383

ResistanceMap, (n.d.). https://resistancemap.onehealthtrust.org/Countries.php (Accessed December 18, 2024).

Reygaert, W. C. (2018). An overview of the antimicrobial resistance mechanisms of bacteria. *AIMS Microbiol.* 4, 482–501. doi: 10.3934/MICROBIOL.2018.3.482

Ridyard, K. E., and Overhage, J. (2021). The potential of human peptide LL-37 as an antimicrobial and anti-biofilm agent. *Antibiot.* 10:650. doi: 10.3390/ANTIBIOTICS10060650

Rinninella, E., Raoul, P., Cintoni, M., Franceschi, F., Miggiano, G. A. D., Gasbarrini, A., et al. (2019). What is the healthy gut microbiota composition? A changing ecosystem across age, environment, diet, and diseases. *Microorg* 7:14. doi: 10.3390/MICROORGANISMS7010014

Rofeal, M., Abdelmalek, F., and Steinbüchel, A. (2022). Naturally-sourced antibacterial polymeric nanomaterials with special reference to modified polymer variants. *Int. J. Mol. Sci.* 23:4101. doi: 10.3390/IJMS23084101

Romano, A., Mondino, C., Viola, M., and Montuschi, P. (2003). Immediate allergic reactions to β-lactams: diagnosis and therapy, *Int J Immunopathol Pharmacol*. 16, 19–23. doi: 10.1177/039463200301600103

Roy, S., Halder, M., Ramprasad, P., Dasgupta, S., Singh, Y., and Pal, D. (2023). Oxidized pullulan exhibits potent antibacterial activity against *S. aureus* by disrupting its membrane integrity. *Int. J. Biol. Macromol.* 249:126049. doi: 10.1016/J.IJBIOMAC.2023.126049

Sam, S., Joseph, B., and Thomas, S. (2023). Exploring the antimicrobial features of biomaterials for biomedical applications. *Results Eng.* 17:100979. doi: 10.1016/J.RINENG.2023.100979

Santos, M. R. E., Fonseca, A. C., Mendonça, P. V., Branco, R., Serra, A. C., Morais, P. V., et al. (2016). Recent developments in antimicrobial polymers: a review. *Mater.* 9:599. doi: 10.3390/MA9070599

Sceglovs, A., Wychowaniec, J. K., Skadins, I., Reinis, A., Edwards-Gayle, C. J. C., D'Este, M., et al. (2023). Effect of steam sterilisation on physico-chemical properties of antibacterial covalently cross-linked ε-polylysine/hyaluronic acid hydrogels. *Carbohydr. Polym. Technol. Appl.* 6:100363. doi: 10.1016/J.CARPTA.2023.100363

Schrade, S., Ritschl, L., Süss, R., Schilling, P., and Seidenstuecker, M. (2022). Gelatin nanoparticles for targeted dual drug release out of alginate-di-aldehyde-gelatin gels. *Gels.* 8:365. doi: 10.3390/gels8060365

Schwartz, B., and Vetvicka, V. (2021). Review: β-glucans as effective antibiotic alternatives in poultry. *Mol.* 26:3560. doi: 10.3390/MOLECULES26123560

Shai, Y. (2002). Mode of action of membrane active antimicrobial peptides. *Pept. Sci.* 66, 236–248. doi: 10.1002/BIP.10260

Shanmugasundaram, O. L., and Ramkumar, M. (2018). Characterization and study of physical properties and antibacterial activities of human hair keratin–silver nanoparticles and keratin–gold nanoparticles coated cotton gauze fabric. *J. Ind. Text.* 47, 798–814. doi: 10.1177/1528083716674904

Shin, J. M., Gwak, J. W., Kamarajan, P., Fenno, J. C., Rickard, A. H., and Kapila, Y. L. (2016). Biomedical applications of nisin. *J. Appl. Microbiol.* 120, 1449–1465. doi: 10.1111/JAM.13033

Si, Z., Hou, Z., Vikhe, Y. S., Thappeta, K. R. V., Marimuthu, K., De, P. P., et al. (2021). Antimicrobial effect of a novel chitosan derivative and its synergistic effect with antibiotics. *ACS Appl. Mater. Interfaces* 13, 3237–3245. doi: 10.1021/ACSAMI.0C20881

Sikdar, P., Uddin, M. M., Dip, T. M., Islam, S., Hoque, M. S., Dhar, A. K., et al. (2021). Recent advances in the synthesis of smart hydrogels. *Mater. Adv.* 2, 4532–4573. doi: 10.1039/D1MA00193K

Silvestro, L., Weiser, J. N., and Axelsen, P. H. (2000). Antibacterial and antimembrane activities of cecropin a in *Escherichia coli*. *Antimicrob. Agents Chemother.* 44, 602–607. doi: 10.1128/AAC.44.3.602-607.2000

Smola-Dmochowska, A., Lewicka, K., Macyk, A., Rychter, P., Pamuła, E., and Dobrzyński, P. (2023). Biodegradable polymers and polymer composites with antibacterial properties. *Int. J. Mol. Sci.* 24:7473. doi: 10.3390/IJMS24087473

Solensky, R. (2003). Hypersensitivity reactions to beta-lactam antibiotics. *Clin. Rev. Allergy Immunol.* 24, 201–220. doi: 10.1385/CRIAI:24:3:201

Song, J., Chen, H., Wei, Y., and Liu, J. (2020). Synthesis of carboxymethylated β-glucan from naked barley bran and its antibacterial activity and mechanism against

Staphylococcus aureus. *Carbohydr. Polym.* 242:116418. doi: 10.1016/J.CARBPOL.2020.116418

Suflet, D. M., Popescu, I., Stanciu, M. C., and Rimbu, C. M. (2024). Antimicrobial hydrogels based on cationic Curdlan derivatives for biomedical applications. *Gels* 10:424. doi: 10.3390/gels10070424

Sun, Y., Bai, Y., Yang, W., Bu, K., Tanveer, S. K., and Hai, J. (2022). Global trends in natural biopolymers in the 21st century: a scientometric review. *Front. Chem.* 10:915648. doi: 10.3389/FCHEM.2022.915648

Sun, C., Liu, W., Wang, L., Meng, R., Deng, J., Qing, R., et al. (2023). Photopolymerized keratin-PGLa hydrogels for antibiotic resistance reversal and enhancement of infectious wound healing. *Mater. Today Bio* 23:100807. doi: 10.1016/J.MTBIO.2023.100807

Sundaran, S., Kok, L. C., and Chang, H. Y. (2022). Combination effect of epsilon-poly-L-lysine and antibiotics against common bacterial pathogens. *J. Antibiot.* 75, 354–359. doi: 10.1038/s41429-022-00523-9

Surveillance Atlas of Infectious Diseases. (2022). Available at: https://atlas.ecdc.europa.eu/public/index.aspx?Dataset=27&HealthTopic=4 (Accessed April 2, 2024).

Syaban, M. F. R., Erwan, N. E., Syamsuddin, M. R. R., Zahra, F. A., and Sabila, F. L. (2022). Insilico study and analysis antibacterial activity of Beta-glucan against Beta-lactamase and protein binding penicillin-2A. *Res. J. Pharm. Technol.* 15, 1948–1952. doi: 10.52711/0974-360X.2022.00324

Syryamina, V. N., Aisenbrey, C., Kardash, M., Dzuba, S. A., and Bechinger, B. (2024). Self-assembly of spin-labeled antimicrobial peptides magainin 2 and PGLa in lipid bilayers. *Biophys. Chem.* 310:107251. doi: 10.1016/J.BPC.2024.107251

Taheri-Araghi, S. (2024). Synergistic action of antimicrobial peptides and antibiotics: current understanding and future directions. *Front. Microbiol.* 15:1390765. doi: 10.3389/FMICB.2024.1390765

Tehrani, K. H. M. E., and Martin, N. I. (2018). β-Lactam/β-lactamase inhibitor combinations: an update. *Medchemcomm* 9, 1439–1456. doi: 10.1039/C8MD00342D

Tin, S., Sakharkar, K. R., Lim, C. S., and Sakharkar, M. K. (2009). Activity of Chitosans in combination with antibiotics in *Pseudomonas aeruginosa*. *Int. J. Biol. Sci.* 5, 153–160. doi: 10.7150/IJBS.5.153

Tripathi, S., and Mishra, S. (2021). Antioxidant, antibacterial analysis of pectin isolated from Banana Peel and its application in edible coating of freshly made mozzarella cheese. *Asian Food Sci. J.* 20, 82–92. doi: 10.9734/AFSJ/2021/V20I730324

Troy, E., Tilbury, M. A., Power, A. M., and Wall, J. G. (2021). Nature-based biomaterials and their application in biomedicine. *Polym.* 13:3321. doi: 10.3390/POLYM13193321

Uchil, R. R., Kohli, G. S., Katekhaye, V. M., and Swami, O. C. (2014). Strategies to combat antimicrobial resistance. *J. Clin. Diagn. Res.* 8, ME01–ME04. doi: 10.7860/JCDR/2014/8925.4529

Ullah, H., and Ali, S. (2017). Classification of anti-bacterial agents and their functions. *Antibact. Agents*. doi: 10.5772/INTECHOPEN.68695

Unver, T., Erenler, A. S., Bingul, M., and Boga, M. (2023). Comparative analysis of antioxidant, anticholinesterase, and antibacterial activity of microbial chondroitin sulfate and commercial chondroitin sulfate. *Chem. Biodivers.* 20:e202300924. doi: 10.1002/CBDV.202300924

Urban-Chmiel, R., Marek, A., Stępień-Pyśniak, D., Wieczorek, K., Dec, M., Nowaczek, A., et al. (2022). Antibiotic resistance in Bacteria—a review. *Antibiotics* 11:1079. doi: 10.3390/antibiotics11081079

Valenzuela-Rojo, R. D., López-Cervantes, J., Sánchez-Machado, D. I., Escárcega-Galaz, A. A., and Martínez-Macias, M. R. (2020). Antibacterial, mechanical and physical properties of collagen – chitosan sponges from aquatic source. *Sustain. Chem. Pharm.* 15:100218. doi: 10.1016/J.SCP.2020.100218

van den Heuvel, D. B., Stawski, T. M., Tobler, D. J., Wirth, R., Peacock, C. L., and Benning, L. G. (2018). Formation of silica-lysozyme composites through co-precipitation and adsorption. *Front. Mater.* 5:331384. doi: 10.3389/FMATS.2018.00019

van Seventer, J. M., and Hochberg, N. S. (2017). Principles of infectious diseases: transmission, diagnosis, prevention, and control. In: *International Encyclopedia of Public Health*. (Second Edition). ed. S. R. Quah. (Singapore: Duke-NUS Medical School) 22–39.

Veiga, A. S., and Schneider, J. P. (2013). Antimicrobial hydrogels for the treatment of infection. *Biopolymers*. 100, 637–644. doi: 10.1002/bip.22412

Vinarov, Z., Abdallah, M., Agundez, J. A. G., Allegaert, K., Basit, A. W., Braeckmans, M., et al. (2021). Impact of gastrointestinal tract variability on oral drug absorption and pharmacokinetics: an UNGAP review. *Eur. J. Pharm. Sci.* 162:105812. doi: 10.1016/J.EJPS.2021.105812

Waley, S. G. (1992). ß-lactamase: mechanism of action. In: *The Chemistry of β-Lactams*., ed. M. I. Page. (Netherlands: Springer).

Wang, K., Sun, H., Cui, Z., Wang, J., Hou, J., Lu, F., et al. (2024). Lactoferrin-chitosan composite hydrogels induced by microbial transglutaminase: potential delivery systems for thermosensitive bioactive substances. *J. Agric. Food Chem.* 72, 14302–14314. doi: 10.1021/ACS.JAFC.4C01551

Wang, Z., Yang, Q., Wang, X., Li, R., Qiao, H., Ma, P., et al. (2020). Antibacterial activity of xanthan-oligosaccharide against *Staphylococcus aureus* via targeting biofilm and cell membrane. *Int. J. Biol. Macromol.* 153, 539–544. doi: 10.1016/J.IJBIOMAC.2020.03.044

Wathoni, N., Suhandi, C., Purnama, M. F. G., Mutmainnah, A., Nurbaniyah, N. S., Syafra, D. W., et al. (2024). Alginate and chitosan-based hydrogel enhance antibacterial agent activity on topical application. *Infect. Drug Resist.* 17, 791–805. doi: 10.2147/IDR.S456403

Web of Science. Journal articles on antimicrobial natural bio-polymers. (n.d.). Available at: https://www.webofscience.com/wos/woscc/summary/6ed8dab8-5b3c-4a8f-a385-af59f647f6ff-ac09097b/relevance/1 (accessed April 4, 2024)

Wieërs, G., Belkhir, L., Enaud, R., Leclercq, S., Philippart de Foy, J. M., Dequenne, I., et al. (2020). How probiotics affect the microbiota. *Front. Cell. Infect. Microbiol.* 9:454. doi: 10.3389/FCIMB.2019.00454

Wimley, W. C. (2010). Describing the mechanism of antimicrobial peptide action with the interfacial activity model. *ACS Chem. Biol.* 5, 905–917. doi: 10.1021/CB1001558

World Health Organization. New report calls for urgent action to avert antimicrobial resistance crisis, (2019). https://www.who.int/news/item/29-04-2019-new-report-calls-for-urgent-action-to-avert-antimicrobial-resistance-crisis (Accessed April 2, 2024).

Wu, G., Ma, F., Xue, Y., Peng, Y., Hu, L., Kang, X., et al. (2022). Chondroitin sulfate zinc with antibacterial properties and anti-inflammatory effects for skin wound healing. *Carbohydr. Polym.* 278:118996. doi: 10.1016/J.CARBPOL.2021.118996

Wu, J., Shaidani, S., Theodossiou, S. K., Hartzell, E. J., and Kaplan, D. L. (2022). Localized, on-demand, sustained drug delivery from biopolymer-based materials. *Expert Opin. Drug Deliv.* 19, 1317–1335. doi: 10.1080/17425247.2022.2110582

Yadav, P., Yadav, H., Shah, V. G., Shah, G., and Dhaka, G. (2015). Biomedical biopolymers, their origin and evolution in biomedical sciences: a systematic review. *J. Clin. Diagn. Res.* 9, ZE21–ZE25. doi: 10.7860/JCDR/2015/13907.6565

Yan, R., Liu, M., Zeng, X., Du, Q., Wu, Z., Guo, Y., et al. (2024). Preparation of modified chitosan-based nano-TiO2–nisin composite packaging film and preservation mechanism applied to chilled pork. *Int. J. Biol. Macromol.* 269:131873. doi: 10.1016/J.IJBIOMAC.2024.131873

Yang, L., Bajinka, O., Jarju, P. O., Tan, Y., Taal, A. M., and Ozdemir, G. (2021). The varying effects of antibiotics on gut microbiota. *AMB Express* 11, 116–113. doi: 10.1186/S13568-021-01274-W

Yang, Q., Le, S., Zhu, T., and Wu, N. (2023). Regulations of phage therapy across the world. *Front. Microbiol.* 14:1250848. doi: 10.3389/FMICB.2023.1250848

Yang, S., Qiao, J., Zhang, M., Kwok, L. Y., Matijašić, B. B., Zhang, H., et al. (2024). Prevention and treatment of antibiotics-associated adverse effects through the use of probiotics: a review. *J. Adv. Res.* [in Press]. doi: 10.1016/J.JARE.2024.06.006

Yeaman, M. R., and Yount, N. Y. (2003). Mechanisms of antimicrobial peptide action and resistance. *Pharmacol. Rev.* 55, 27–55. doi: 10.1124/PR.55.1.2

Yin, R., Kuo, H. C., Hudlikar, R., Sargsyan, D., Li, S., Wang, L., et al. (2019). Gut microbiota, dietary phytochemicals, and benefits to human health. *Curr. Pharmacol. Rep.* 5, 332–344. doi: 10.1007/S40495-019-00196-3

Zamboni, F., Wong, C. K., and Collins, M. N. (2023). Hyaluronic acid association with bacterial, fungal and viral infections: can hyaluronic acid be used as an antimicrobial polymer for biomedical and pharmaceutical applications? *Bioact. Mater.* 19, 458–473. doi: 10.1016/J.BIOACTMAT.2022.04.023

Zhang, F., and Cheng, W. (2022). The mechanism of bacterial resistance and potential bacteriostatic strategies. *Antibiot.* 2022:1215. doi: 10.3390/ANTIBIOTICS11091215

Zhao, Y., Wang, X., Qi, R., and Yuan, H. (2023). Recent advances of natural-polymer-based hydrogels for wound antibacterial therapeutics. *Polym.* 15:3305. doi: 10.3390/POLYM15153305

Zhong, P., and Shortridge, V. D. (2000). The role of efflux in macrolide resistance. *Drug Resist. Updat.* 3, 325–329. doi: 10.1054/DRUP.2000.0175

Zhou, X., Liao, F., Ye, Z., Cheng, J., Zhu, J., Chen, X., et al. (2023). Discovery and engineering of a novel peptide, Temporin-WY2, from frog skin secretion, with enhanced in vitro and in vivo antimicrobial efficacy against multi-drug resistant bacteria. *Sci Rep.* 14:18769. doi: 10.21203/RS.3.RS-3705341/V1

Zhu, M., Ge, L., Lyu, Y., Zi, Y., Li, X., Li, D., et al. (2017). Preparation, characterization and antibacterial activity of oxidized κ-carrageenan. *Carbohydr. Polym.* 174, 1051–1058. doi: 10.1016/J.CARBPOL.2017.07.029

Appendix II

2. Pielikums

Effect of Crosslinking Strategy on the Biological, Antibacterial and Physicochemical Performance of Hyaluronic Acid and ε-Polylysine Based Hydrogels

Kristine Salma Ancane, Artemijs Sceglovs, Eliza Tracuma, Jacek K. Wychowaniec, Kristine Aunina, Anna Ramata-Stunda, Vizma Nikolajeva, Dagnija Loca

International Journal of Biological Macromolecules, **2022**, 208, 995–1008.
https://doi.org/10.1016/J.IJBIOMAC.2022.03.207.

A.S. input: Methodology, Validation, Formal analysis, Investigation.

International Journal of Biological Macromolecules 208 (2022) 995–1008

Contents lists available at ScienceDirect

International Journal of Biological Macromolecules

journal homepage: www.elsevier.com/locate/ijbiomac

Effect of crosslinking strategy on the biological, antibacterial and physicochemical performance of hyaluronic acid and ε-polylysine based hydrogels

Kristine Salma-Ancane [a,b], Artemijs Sceglovs [a,b], Eliza Tracuma [a,b], Jacek K. Wychowaniec [c], Kristine Aunina [a,b], Anna Ramata-Stunda [d], Vizma Nikolajeva [d], Dagnija Loca [a,b,*]

[a] Rudolfs Cimdins Riga Biomaterials Innovations and Development Centre of RTU, Institute of General Chemical Engineering, Faculty of Materials Science and Applied Chemistry, Riga Technical University, Pulka St. 3/3, Riga LV-1007, Latvia
[b] Baltic Biomaterials Centre of Excellence, Headquarters at Riga Technical University, Riga, Latvia
[c] AO Research Institute Davos, Clavadelerstrasse 8, 7270 Davos, Switzerland
[d] Department of Microbiology and Biotechnology, Faculty of Biology, University of Latvia, Riga, Latvia

ARTICLE INFO

Keywords:
ε-Polylysine
Hyaluronic acid
Antibacterial hydrogels

ABSTRACT

The design of multifunctional hydrogels based on bioactive hyaluronic acid (HA) and antibacterial cationic polymer ε-poly-L-lysine (ε-PL) is a promising tool in tissue engineering applications. In the current study, we have designed hyaluronic acid and ε-polylysine composite hydrogel systems with antibacterial and cell attractive properties. Two distinct crosslinking approaches were used: the physical crosslinking based on electrostatic attractions and the chemical crosslinking of charged functional groups (-NH_2 and -COOH). The impact of the crosslinking strategy on fabricated hydrogel molecular structure, swelling behavior, gel fraction, morphology, porosity, viscoelastic properties, antibacterial activity, and in vitro biocompatibility was evaluated. Both chemically and physically crosslinked HA/ε-PL hydrogels demonstrated fast swelling behavior and long-term stability for at least 28 days, as well as similar order of stiffness (10–30 kPa). We demonstrated that physically crosslinked hydrogels inhibited over 99.999% of Gram-negative *E. coli*, while chemically crosslinking strategy led to the antibacterial efficiency decrease. However, cell viability was significantly improved, confirming the importance of the applied crosslinking approach to the antibacterial activity and in vitro biocompatibility. The distinct differences in the physicochemical and biological properties of the developed materials provide new opportunities to design next-generation functional composite hydrogel systems.

1. Introduction

The native extracellular matrix (ECM) is a multimolecular three-dimensional (3D) network made of a large variety of different bioactive polymers, such as peptides, proteins, and glycosaminoglycans (GAGs). It provides the structural and biochemical support for the cells across different tissues types [1–4]. The physically or chemically crosslinked 3D hydrophilic biopolymer matrices, called hydrogels, which can swell by absorbing large amounts of water or biological fluids, are highly attractive tools for mimicking the three-dimensional molecular structure of the native ECM [5]. Hydrogels are innovative biomaterials for tissue engineering, regenerative medicine, and drug delivery applications due to their unique characteristics, such as the ability to encapsulate and release on demand the bioactive compounds (e.g., drugs or growth factors) as well as support the cell proliferation and growth [6–8]. Hyaluronic acid (HA) is an anionic and non-sulfated GAG with unique physicochemical properties and distinctive biological functions. HA, as a critical element of the native ECM, is an attractive building block to design biomimetic cell-interactive hydrogels for local delivery of drugs and cells as well as for tissue bioengineering [3,9,10]. On the other hand, ε-Poly-L-lysine (ε-PL) is an L-lysine based (25–35 L-lysine residues) hydrophilic, cationic homopolyamide which is characterized by biocompatibility, biodegradability, superior tissue adhesive properties, anti-infection and anti-cancer activity and has been

* Corresponding author at: Rudolfs Cimdins Riga Biomaterials Innovations and Development Centre of RTU, Institute of General Chemical Engineering, Faculty of Materials Science and Applied Chemistry, Riga Technical University, Pulka St. 3/3, Riga LV-1007, Latvia.
E-mail address: dagnija.loca@rtu.lv (D. Loca).

https://doi.org/10.1016/j.ijbiomac.2022.03.207
Received 18 October 2021; Received in revised form 21 March 2022; Accepted 30 March 2022
Available online 1 April 2022

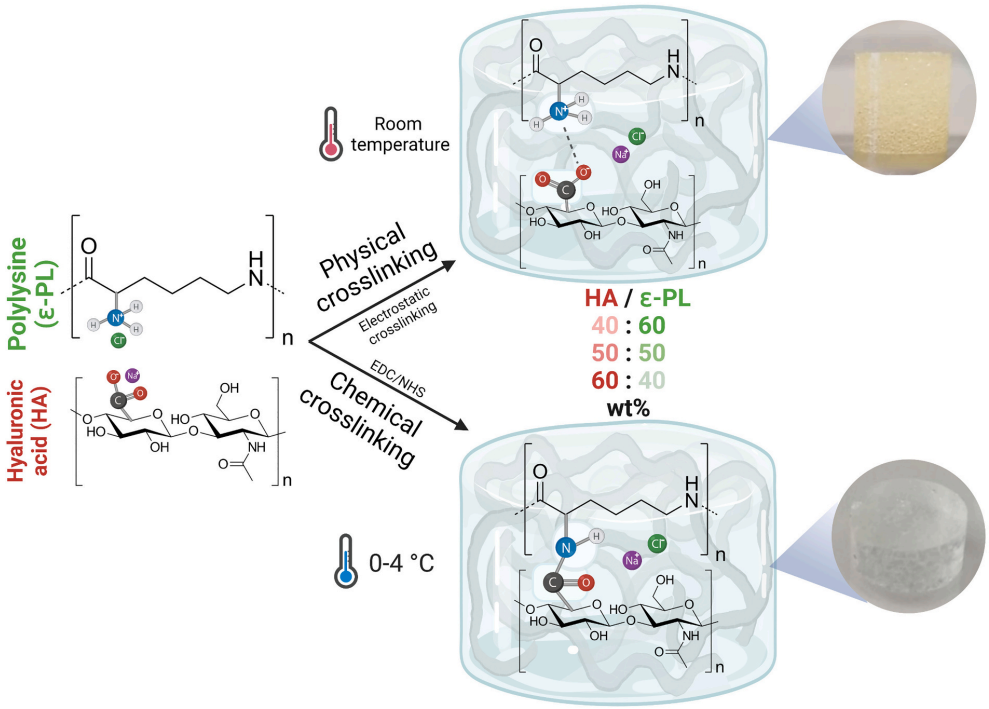

Fig. 1. Schematic illustration of the HA/ε-PL composite hydrogel fabrication process (color).

approved by the Food and Drug Administration in several countries as a commercial food preservative [11–13]. According to the recently reported studies, ε-PL-based biomaterials or hydrogels have shown a great potential to be used in numerous biomedical applications, including antimicrobial agents, targeted drug and gene delivery systems, biological adhesives, and wound healing membranes [12–15]. In the last decade, hydrogels with an anti-inflammatory and antibacterial function have been a research hotspot in the biomedical field [16].

Moreover, such hydrogels must be modified to promote tissue integration before bacterial adhesion. The main challenge is to design antibacterial hydrogels with fast-acting performance and prolonged duration. ε-PL possesses high antimicrobial activity against both Gram-negative (such as *E. coli*) and Gram-positive bacteria (such as *S. aureus*), as well as certain species of fungi and yeast [13,17]. Besides, ε-PL shows strong polycationic property and allows complexation or complementary stacking by electrostatic interactions with anionic polyelectrolytes or polymers [13].

Hydrogels are mainly fabricated using a physical or chemical crosslinking approach or a combination of both methods to build 3D crosslinked polymer networks [18]. The key advantage of the physically crosslinked hydrogels is their biomedical safety, ease of fabrication, and superior biocompatibility. Physically crosslinked hydrogels are usually formed by reversible intermolecular interactions and weak secondary forces, such as ionic/electrostatic interaction, hydrogen bonding, hydrophobic/hydrophilic interactions, crystallization/stereo complex formation, etc., avoiding the use of toxic initiators or chemical catalysts [18,19]. However, physically crosslinked hydrogels present low mechanical properties and limited tunable biodegradation [18,20]. On the other hand, chemically crosslinked hydrogels are usually formed by covalent crosslinking, resulting in better mechanical properties, stability in the physiological environment, and more tunable biodegradation dynamics than the physically crosslinked hydrogels. Up to now, the main chemical crosslinking methods include Michael type-addition, Schiff base formation, Diels-Alder "click" reaction, enzyme-induced crosslink, photo-polymerization [18,21]. Crosslinking strategy is crucial for tissue engineering applications developing hydrogels with desirable physicochemical and biological characteristics [22]. Moreover, hydrogels with the same constituents but different crosslinking structures can present completely different physicochemical performances [18,22].

In the current study, bioinspired and antibacterial composite hydrogels based on the biopolysaccharide HA and polypeptide ε-PL were designed for tissue engineering applications. Physical and chemical crosslinking strategies were chosen for the 3D network hydrogel formation by crosslinks between the carboxyl groups (-COOH) of HA and the primary ε-amino (-NH_2) groups of ε-PL [23,24]. The chemically crosslinked HA/ε-PL hydrogels were fabricated by water-soluble 1-ethyl-3-(3-dimethyl aminopropyl) carbodiimide (EDC)/N-hydroxysuccinimide (NHS) crosslinking. All chemically crosslinked HA/ε-PL hydrogels were prepared with constant EDC/NHS crosslinker concentration and variable HA to ε-PL mass ratio to introduce the non-crosslinked primary amino groups of ε-PL. Antibacterial activity of ε-PL highly depends on its cationic nature. The chemical modification of the cationic primary amino groups on the side chain of ε-PL, which provides excellent antibacterial activity and water solubility, can significantly lower the overall antibacterial activity of prepared hydrogels [14]. The physically crosslinked HA/ε-PL hydrogels were fabricated by complementary electrostatic attraction between two oppositely charged natural polyelectrolytes in the aqueous solution (see Fig. 1) [25–27]. HA acts as an anionic polyelectrolyte and ε-PL as cationic polyelectrolyte, respectively. The key benefits of this crosslinking approach include the green chemistry principles, fast fabrication process

Table 1
Designation and composition of the fabricated HA/ε-PL composite hydrogels.

Designation	Crosslinking method	Composition, wt%	Molar ratio of HA to ε-PL	HA mass (g)	ε-PL mass (g)	Total liquid volume (mL)
Phys HA/ε-PL 40:60	Physical	HA 40 wt%, ε-PL 60 wt%	1:600	0.40	0.60	2.5
Phys HA/ε-PL 50:50	Physical	HA 50 wt%, ε-PL 50 wt%	1:400	0.50	0.50	2.5
Phys HA/ε-PL 60:40	Physical	HA 60 wt%, ε-PL 40 wt%	1:270	0.60	0.40	2.5
Chem HA/ε-PL 40:60	Chemical	HA 40 wt%, ε-PL 60 wt%	1:600	0.21	0.31	4
Chem HA/ε-PL 50:50	Chemical	HA 50 wt%, ε-PL 50 wt%	1:400	0.21	0.21	4
Chem HA/ε-PL 60:40	Chemical	HA 60 wt%, ε-PL 40 wt%	1:270	0.21	0.14	4

in aqueous solutions, injectability for minimally invasive surgical procedures, and the possibility to incorporate the biologically active components [23,28]. However, bulk homogenous polyelectrolyte complex hydrogels are challenging to fabricate due to the inter-molecular flocculation effect between polyelectrolytes with opposite charges [23,29]. In the current study, the suitable experimental conditions for HA to ε-PL mixing, solid to liquid phase ratio, mixing order, and temperature to fabricate homogenous HA/ε-PL hydrogels to prevent inhomogeneous hydrogel formation were investigated.

Moreover, some recent studies have reported that ε-PL containing polyelectrolyte complexes can affect the antimicrobial efficacy of ε-PL as they prevent the cationic ε-PL interactions with the anionic surfaces of the microbial cells [13,30,31]. This study considered fabrication conditions and antibacterial functionality to design physically and chemically crosslinked antibacterial HA/ε-PL hydrogels rationally.

The combinations of HA and ε-PL mainly in polyelectrolyte HA/ε-PL multilayer films [32] and HA/ε-PL composite nanogels have previously been studied [33]. Also, ε-PL in combination with other biocompatible polymers (e.g., chitosan [34], γ-poly(glutamic acid) [26], poly(ethylene glycol) [35]) or bioactive ceramics [36] have been proposed for the antibacterial hydrogel preparation, as well as for drug delivery and tissue engineering [37]. Up to now and to our knowledge, no studies have reported polyelectrolyte complex hydrogels made via amide bond crosslinked hydrogels based on HA and ε-PL. Moreover, unlike polysaccharide-based hydrogels such as HA, relatively few reports have been devoted to polypeptide-based hydrogels such as ε-PL. Therefore, in the current research, our primary objective was to evaluate the physicochemical properties, antibacterial activity, and biocompatibility of bioinspired and antibacterial HA/ε-PL hydrogels as a function of the crosslinking strategy (physical versus chemical). By appropriate choice of the total polymer content, hydrogels in the similar stiffness range were chosen for comparison of the crosslinking methods. Finally we rationalize that by modulating mass ratio of HA to ε-PL, both the physiochemical properties (stiffness and swelling) and antibacterial properties could be tuned. For that, hydrogels with HA to ε-PL mass ratios of 60:40 wt%, 50:50 wt%, 40:60 wt%, corresponding to approximate molar ratios of HA to ε-PL of 1:270, 1:400 and 1:600, respectively, were fabricated. Specifically, by choosing consecutively higher amounts of ε-PL, the total content of the cationic groups typically associated with higher antibacterial activity is expected.

2. Materials and methods

2.1. Materials

ε-Polylysine (ε-PL·HCl, >99% purity, MW 3500–4500 Da, 25–30 L-lysine residues, water content 6.5%) was purchased from Zhengzhou Bainafo Bioengineering Co., Ltd. (China). Sodium hyaluronate (HA, cosmetic grade, >95% purity, water content 13.5%, MW 1.55 MDa) was purchased from Contipro Biotech s.r.o. (Czech Republic). 1-Ethyl-3-(3-dimethyl aminopropyl)-carbodiimide hydrochloride (EDC, 98% purity, MW 191.75 g mol^{-1}, CAS-No: 25952-53-8) was purchased from Novabiochem (USA). N-Hydroxysuccinimide (NHS, 98% purity, MW 115.09 g mol^{-1}, CAS-No: 6066-82-6) was purchased from Sigma-Aldrich. Sodium hydroxide (NaOH, CAS-No: 1310-73-2, ≥99% purity, MW 40.0 g mol^{-1}) and hydrochloric acid fuming (HCl, 37%, ACS, ISO, Reag. Ph Eur) was purchased from Emsure® (Germany). Deionized water (DI) was used throughout this study. All commercially obtained compounds were used as received.

2.2. Synthesis of electrostatically crosslinked HA/ε-PL hydrogels

The physically crosslinked HA/ε-PL hydrogels were fabricated by electrostatic attraction between two oppositely charged natural polyelectrolytes in the aqueous solution (see Fig. 1). The hydrogels were fabricated with HA to ε-PL mass ratio of 40:60 wt%, 50:50 wt%, 60:40 wt% (exact amounts of components are shown in Table 1). Hydrogels were fabricated by mixing 1 g of total polymer content and 2.5 mL of DI water 30 times in two mated syringes. Immediately after mixing, obtained samples were extruded into the custom-made 3D molds (ø = 10 mm) and left at room temperature (23 °C) for 1 h. For in vitro biological studies, prepared samples were sterilized at 105 °C for 4 min in steam under 179.5 kPa using a tabletop pre-vacuum autoclave (ELARA11, Netherlands). Obtained sterile hydrogel samples were kept in a fridge at 4 °C until the use. Prepared hydrogels were removed from the molds for all other experiments, frozen at −26 °C, and freeze-dried using a Martin Christ laboratory freeze dryer (BETA 2-8 LCSplus, Germany) −85 °C for 72 h for further investigation.

2.3. Synthesis of chemically crosslinked HA/ε-PL hydrogels

The chemically crosslinked HA/ε-PL hydrogels were fabricated by carboxyl-to-amine crosslinkers 1-ethyl-3-(3-dimethyl aminopropyl) carbodiimide (EDC) and N-hydroxysuccinimide (NHS) with EDC to NHS molar ratio of 1:1 (see Fig. 1) [38]. The hydrogels were fabricated with HA to ε-PL mass ratio of 40:60 wt%, 50:50 wt%, 60:40 wt% (exact amounts are shown in Table 1). In this case, the HA amount was always kept constant at 0.2095 g, whereas the mass of ε-PL was adjusted accordingly to 0.31425, 0.2095, 0.1397 g. HA was re-dissolved in a 0.25 M NaOH aqueous solution to induce hydrolysis of HA chains and obtain homogenous lower viscosity alkaline HA aqueous solution [39]. The prepared HA solution was rapidly mixed for 10 min at 3000 rpm at room temperature (Vortex V-1 plus, Biosan, Latvia). The HA solution was then left in the dark for 24 h for complete dissolution. Separately, ε-PL was re-dissolved in a 0.25 M HCl aqueous solution and rapidly mixed for 3 min at 1500 rpm at room temperature (Vortex V-1 plus, Biosan, Latvia). To control the gelation speed, after 24 h, the HA aqueous solution was cooled down to ~2 °C by keeping it in a laboratory freezer (−20 °C) for ~12 min (confirmed by repeated temperature measurements). The crosslinking agents, EDC and NHS, were then added to the cooled (4 °C) HA aqueous solution and mixed in by vortexing at 3000 rpm, 1 min for each added crosslinker. EDC/NHS concentration used in this study was 0.24 mol L^{-1} which is considered non-cytotoxic in hydrogel synthesis [26]. Again, separately, the ε-PL aqueous solution was cooled down to ~2 °C by keeping it in a laboratory freezer (−20 °C) for ~12 min (confirmed by repeated temperature measurements). Finally, the HA/ε-PL hydrogels were synthesized by mixing 2 mL of pre-dissolved ε-PL and 2 mL of pre-activated HA aqueous solution containing EDC/NHS in two mated syringes ~200 times (5 min). After mixing, samples were immediately extruded into the custom-made 3D molds (ø = 10 mm) and

left at room temperature (23 °C) for 24 h. For the reaction, the pH of all mixed components, as well as final pH of the fabricated hydrogels was measured and remained in the 5.5–6.5 range. Considering that the efficiency of amide bond formation or amidation in the lasts step in the presence of EDC/NHS is favored at pH 7.5–8 [25], the acidic ε-PL aqueous solution was prepared to neutralize the alkaline HA aqueous solution, resulting in the formation of a neutralization reaction by-product - crystalline phase of NaCl. Indeed, the NaCl phase was detected by X-ray powder diffractometry (XRD, PANalytical X'Pert PRO, Westborough, MA, see Section 2.4.3) in trace amounts (see results in supplementary data Fig. S1). For in vitro biological studies, prepared hydrogel samples were sterilized at 105 °C for 4 min in steam under 179.5 kPa using a tabletop pre-vacuum autoclave (ELARA11, Netherlands). The sterile hydrogel samples were then kept in a fridge at 4 °C until the use. Prepared hydrogels were removed from the molds for all other experiments, frozen at −26 °C, and freeze-dried using a Martin Christ laboratory freeze dryer (BETA 2-8 LCSplus, Germany) −85 °C for 72 h for further investigations. The fabricated HA/ε-PL hydrogel series in this study are summarized in Table 1.

2.4. Physicochemical characterization

2.4.1. Morphology

The surface and cross-section morphology of the lyophilized HA/ε-PL hydrogel samples were visualized by scanning electron microscopy (SEM) Tescan Mira\LMU (*Tescan, Brno, Czech Republic*). Secondary electrons created at an acceleration voltage of 15 kV were used for the sample image generation. The samples were fixed on standard aluminum pin stubs with an electrically conductive double-sided adhesive carbon tape for microscopy. Before examination by SEM, the samples were sputter-coated with a 15 nm thin layer of gold using Emitech K550X (*Quorum Technologies, Ashford, Kent, United Kingdom*) sputter coater. Statistical analysis of the pore size was performed manually from 50 pores per sample across several randomly chosen collected SEM images. The pore shapes were approximated by ellipses, with two radii (the meridian (Y longest) and the equatorial axis (X shortest)) being assigned for each pore, starting from the meridian and then perpendicularly drawing an equatorial line in imageJ©.

2.4.2. Molecular structure

The molecular structure of the lyophilized HA/ε-PL hydrogel samples was investigated by Fourier transform infrared spectroscopy (FTIR) using Varian FTS 800 FT-IR Scimitar Series spectrometer (Varian Inc., Palo Alto, California, USA) equipped with a GladiATR™ monolithic diamond ATR (PIKE Technologies, Madison, Wisconsin, USA). For spectra collection, the lyophilized HA/ε-PL hydrogel samples were grounded into a fine powder using a Mini-Mill PULVERISETTE 23 (*FRITCH, Idar-Oberstein, Germany*) ball mill. The spectra were collected in the mid-infrared range between 400 and 4000 cm^{-1} at a resolution of 4 cm^{-1} by co-adding 50 scans. Background air spectrum with no sample in the infrared beam was acquired before collecting the sample spectrum. Then, the background spectrum was subtracted from the sample spectrum, and the resulting spectra were normalized using Origin 2020 v9.0. Normalization was performed by setting the range 0 to 1 using the default software algorithm, where 1 was assigned to maximum and 0 to minimum values from raw absorbance intensities of all samples.

2.4.3. Phase composition

The phase composition of the lyophilized HA/ε-PL hydrogel samples was evaluated by X-ray powder diffractometry (XRD) using PANalytical X-Pert PRO MPD (Panalytical, Almelo, Netherlands) X-ray diffractometer with a Cu Kα radiation (produced at 40 kV and 30 mA). Diffraction data were collected in a 10–70°2θ range, with a step size of 0.05°2θ and time per step of 2.5 s. Phase's present in the recorded diffraction patterns was identified using a PANalytical X-Pert Highscore 2.2 software (Panalytical, Almelo, Netherlands). For recording of X-ray diffraction patterns, the lyophilized HA/ε-PL hydrogel samples were grounded into a fine powder using a Mini-*Mill PULVERISETTE 23* (*FRITCH, Idar-Oberstein, Germany*) ball mill.

2.4.4. Swelling behavior

The swelling capacity of the freeze-dried HA/ε-PL hydrogels was determined gravimetrically in DI water. The pre-weighted freeze-dried hydrogels were immersed in 20 mL of DI water and incubated under stirring at 100 rpm and 37 °C. The swollen hydrogel samples were weighed at each time interval until 672 h (28 days), removing excess water using filter paper. The corresponding swelling degree was calculated using the following equation:

$$\text{Swelling degree } (\%) = \frac{W_S - W_D}{W_D} \times 100\%$$

where W_S and W_D are the weights of the swollen and initial freeze-dried hydrogel samples, three replicate samples from each prepared hydrogel composition were analyzed, and the results were represented as an average value ± standard deviation.

2.4.5. Gel fraction

The gel fraction of the freeze-dried HA/ε-PL hydrogel samples was determined gravimetrically in deionized (DI) water. The pre-weighted freeze-dried samples were incubated in 200 mL of DI water under stirring at 100 rpm at 37 °C for 48 h. After 48 h, the swollen samples were freeze-dried, and the gel fraction was calculated using the following equation:

$$\text{Gel fraction } (\%) = \frac{W_E}{W_D} \times 100\%$$

where W_D is the initial weight of freeze-dried hydrogels, and W_E is the weight of freeze-dried hydrogel samples after extraction of DI water. Three replicate samples from each prepared hydrogel composition were analyzed, and the results were represented as an average value ± standard deviation.

2.4.6. Oscillatory rheology

The oscillatory rheology measurements were performed on the Physica MCR302 rheometer from Anton Paar. Parallel plate geometry with a 25 mm diameter top plate was used. 2 mm gap was used for the phys HA/ε-PL hydrogels, whereas a 2–2.5 mm gap was used for the chem HA/ε-PL hydrogels. Both phys and chem HA/ε-PL hydrogel samples were pre-prepared in custom-made plastic molds of inner 25 mm diameter and outer 30 mm diameter. Once samples were prepared as described in Sections 2.2 and 2.3, they were immediately placed in molds. For (i) the phys HA/ε-PL hydrogels immediately, and (ii) for the chem HA/ε-PL hydrogels 24 h later, gently placed on the bottom plate using a spatula, and subsequently the top rheometer plate was lowered slowly to minimize hydrogel disruption for each measurement. Prior to taking all measurements, all samples were equilibrated for 180 s. The humidity control hood was used to avoid sample evaporation, and silicon oil was gently spread around the sample directly before each measurement's equilibration. Amplitude sweeps were performed in an oscillatory mode at a constant frequency of 1 Hz at 37 °C, with strain varied from 0.01 to 1000%. Frequency sweeps were then performed in an oscillatory mode from 0.01 to 100 Hz at 0.2% strain within the linear viscoelastic regime, as initially established for all samples during the first amplitude measurements at 37 °C. Each measured point was held at each strain/frequency in both measurements until the instrument reported a stable reading. All measurements were repeated three times to ensure reproducibility.

2.5. Evaluation of antibacterial activity in vitro

In this study, we investigated the antibacterial properties of the

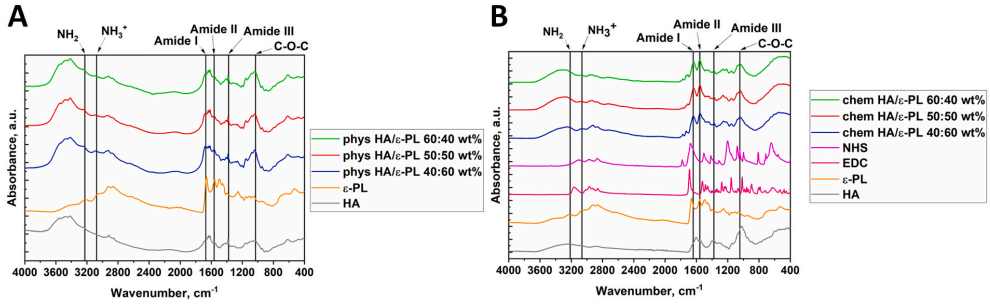

Fig. 2. FTIR normalized spectra of the phys HA/ε-PL (A) and chem HA/ε-PL (B) composite hydrogels. Vertical lines indicate the position of the characteristic bands noted above each line (color).

fabricated HA/ε-PL hydrogels against *Escherichia coli* (*E. coli*) by the zone-of-inhibition test and antimicrobial activity evaluation in bacterial suspension according to ASTM E2149-10. Fresh 18 h shake culture of *E. coli* MSCL 332 grown in a sterile Tryptic soy broth (Biolife, Italy) at 35 ± 2 °C was used in all experiments. Culture was diluted with a sterile 0.3 mM KH_2PO_4 buffer solution (pH 7.2 ± 0.1) until it reached absorbance of $A_{475} = 0.28 \pm 0.02$. This solution was then diluted 1000 times with the buffer to obtain a bacterial working suspension.

2.5.1. Procedure for the determination of leaching antimicrobial presence

Plate count agar (Sanofi Diagnostics Pasteur, France) plates were inoculated with a confluent lawn of bacteria. Eight millimeter diameter wells were bored in the agar medium. Gentamicin (KRKA, Slovenia; 10 mg mL^{-1}, 70 μL) was used as a positive control, and the HA/ε-PL hydrogel samples (diameter 7 mm) were placed in quadruplicate in agar wells. Bacteria were cultivated on an agar medium at 35 ± 2 °C for 24 h. Sterile zones of inhibition were measured using a millimeter-scale ruler.

2.5.2. Procedure for the determination of antimicrobial activity

Each HA/ε-PL hydrogel sample (surface area 3 cm^2) was placed in its tube with 5 mL of bacterial working suspension in potassium phosphate buffer. A series of dilutions were immediately prepared from the inoculum tube without HA/ε-PL hydrogel sample and inoculated into Petri plates on agar media in triplicate to determine the initial bacterial concentration in colony-forming units (CFU) mL^{-1}. All tubes were placed on the shaker at 35 ± 2 °C and mixed at 200 rpm for 1 h ± 5 min. The samples were immediately diluted in triplicate as at the beginning and inoculated into Petri plates with Plate count agar to determine the number of CFU mL^{-1}. Petri plates were incubated at 35 ± 2 °C for 24 h. Colonies were then counted, and the mean CFU mL^{-1} and bacterial reduction were calculated. Log_{10} bacterial reduction = $\text{Log}_{10}(B) - \text{Log}_{10}(A)$, where A = CFU mL^{-1} for the tube containing HA/ε-PL hydrogel sample after 1 h contact time, and B = CFU mL^{-1} in a tube with inoculum but no HA/ε-PL hydrogel sample after 1 h contact time. Three replicate samples from each prepared hydrogel composition were analyzed, and the results were represented as an average value ± standard deviation.

2.6. In vitro biocompatibility evaluation

2.6.1. Cell culture

BALB/c 3T3 cell line (ATCC) was used for all cytotoxicity assays. Cells were grown in Dulbecco's modified Eagle's medium (DMEM, Sigma) supplemented with 10% (v/v) fetal calf serum (Sigma, USA) and 100 μg $mL^{-1}$of streptomycin, and 100 μg mL^{-1} of penicillin at 37 °C within a humidified 5% CO_2 atmosphere. Cells were detached and passaged using 0.25% (w/v) of trypsin/EDTA (Sigma). For all experiments, cell seeding density was 3×10^4 cells cm^{-2}.

2.6.2. Cytotoxicity assay

The extract test was performed to assess the potentially toxic effects of the hydrogel components. Both cytotoxicities of HA/ε-PL hydrogel extracts and cytotoxicity of ε-PL solutions were assessed. BALB/c 3T3 cells were seeded in 24-well plates and incubated for 24 h to allow them to attach and start proliferating. Hydrogel samples were washed with phosphate-buffered saline (PBS, pH 7.4) and extracted with cell cultivation media (0.2 g hydrogel per 1 mL of cultivation media) for 24 h at 37 °C. Extracts were then collected, diluted with cultivation media to 12.5%, 25%, and 50% (v/v). 0.5 mL of diluted extract was then added to the corresponding cell culture wells of the 24-well plate and incubated for 24 h. Cells incubated without hydrogel samples were used as untreated controls, sodium lauryl sulfate was used as the positive (cytotoxic) control. Phase-contrast microscopy monitored cell cultures, cell confluence, and morphology changes. After incubation, cultivation media was removed, and cells were washed with PBS. Neutral red (Sigma, USA) working solution (25 μg mL^{-1}) in 5% serum-containing cultivation media was added, and cell cultures were incubated for 3 h at 37 °C and 5% CO_2. Neutral red media was removed and extracting solution (1% glacial acetic acid/50% ethanol) was added. After 20 min of incubation at $T = 21$ °C, absorption at 540 nm was measured. Changes in cell viability were calculated using the following equation:

$$\text{Cell viability } (\%) = \frac{\text{Abs}_{540\text{nm}}(\text{treatment}) - \text{Abs}_{540\text{nm}}(\text{background})}{\text{Abs}_{540\text{nm}}(\text{untreated control}) - \text{Abs}_{540\text{nm}}(\text{background})}$$

Five replicate samples of extracts from each phys HA/ε-PL hydrogel composition and at least four replicates of extracts from each chem HA/ε-PL hydrogel composition were analyzed. The results were represented as an average value ± standard deviation.

2.6.3. Direct contact assay

Balb/c 3T3 cells were seeded in 6-well plates and incubated for 24 h. Hydrogel samples were washed three times with PBS and pre-incubated for 1 h in 5 mL of cell cultivation media. Then hydrogels were transferred to cell cultures and incubated for 24 h. After incubation, media and hydrogel samples were removed, and cells were washed with PBS. The neutral red solution was added, and its uptake was measured as described before (see Section 2.6.2. *Cytotoxicity assay*). Cells incubated without samples were used as untreated controls, sodium lauryl sulfate was used as the positive (cytotoxic) control. Phase-contrast microscopy was used to monitor the cell cultures and changes in cell confluence and morphology. Five replicate samples from each prepared hydrogel composition were analyzed, and results were represented as an average value ± standard deviation.

2.7. Statistical analysis

At least three replicate samples from each prepared hydrogel

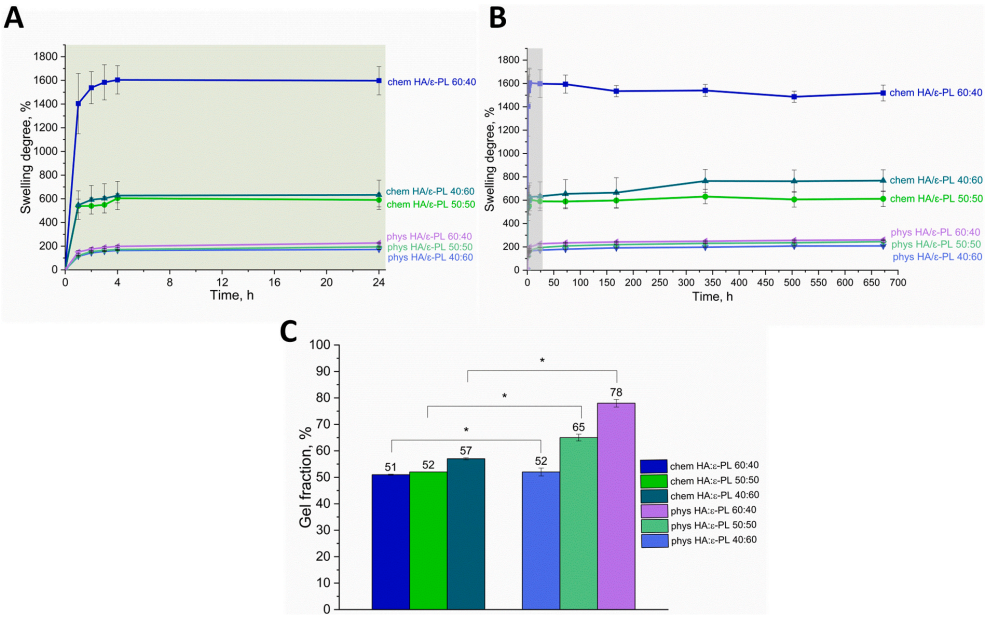

Fig. 3. Swelling degree of the phys and chem HA/ε-PL composite hydrogels (A) up to 24 h and (B) up to 672 h (28 days); (C) gel fraction of the phys and chem HA/ε-PL (color).

composition were analyzed. Average ± standard deviation (SD) was used to express the experimental values. One and two-way analysis of variance (ANOVA) with Tukey's multiple comparison test was used for statistical analysis. A p-value < 0.05 was considered to be statistically significant. (* - for $p < 0.05$; ** - for $p < 0.01$; *** - for $p < 0.001$; **** - for $p < 0.0001$). Curve-fit analysis was performed to calculate IC_{50} for ε-PL. GraphPad Prism 8 software was used for statistical analysis.

3. Results and discussion

3.1. Physicochemical characterization

3.1.1. Molecular structure

To investigate the nature of molecular interactions between HA and ε-PL using physically and chemically induced linkage, FTIR spectra of HA, ε-PL, EDC, NHS, the chem HA/ε-PL hydrogels and the phys HA/ε-PL hydrogels were evaluated (Fig. 2). The FT-IR spectra of HA showed the main characteristic bands as previously reported [40] [41]. The absorption bands at 1640 cm^{-1} (Amide I, C═O stretching vibrations), 1558 cm^{-1} (Amide II, N—H bending vibrations), 1320 cm^{-1} (Amide III), and 1157 cm^{-1} (C-O-C group) were assigned to HA, respectively [40,41]. The absorption bands at 1671 cm^{-1} 1565 cm^{-1}, 1384 cm^{-1} were assigned to the vibrational modes of Amide I (C═O stretching vibrations), Amide II (N—H bending vibrations, C—N stretching vibrations), Amide III bands from ε-PL, respectively [24,42–44]. Given that the Amide I region is also responsible for structural variations in peptides and proteins [45,46], and N—H groups in Amide II region are prone for interactions in our hydrogels, ratio of Amide I/Amide II region taken as I_{1633}/I_{1558} will dictate the type of interactions in the system. Indeed, a clear difference was observed between the types of cross-linking. Increased I_{1633}/I_{1558} ratios of 1.17, 1.33 to 1.35 were obtained for the phys HA/ε-PL hydrogels with HA to ε-PL mass ratios of 40:60 wt %, 50:50 wt%, 60:40 wt%, respectively (Fig. 2A), whereas a similar ratio of 0.87 was obtained for all chem HA/ε-PL hydrogels. The increasing ratio for the phys hydrogels directly corresponds to the mass ratio of HA to ε-PL and suppression of N—H vibrations. On the other hand, in the chem HA/ε-PL hydrogels, irrespective of the ratio of components all side N—H vibrations are suppressed due to the extensive covalent bonding.

Furthermore, the absorption bands at 3246 cm^{-1} and 3081 cm^{-1} were associated with unprotonated NH_2 (secondary amine and primary amine stretching vibrations) and protonated side-chain NH_3^+ groups in solid ε-PL, respectively [24,42,44]. Thus, the ratio between absorbance intensities of these two bands (taken from the normalized spectra (see Section 2.4.2)) is indicative of the overall charge status. NH_3^+/NH_2 ratios of 0.88, 0.83, and 0.78 for the phys HA/ε-PL hydrogels and 0.89, 0.73, 0.65 for the chem HA/ε-PL hydrogels with HA to ε-PL mass ratio of 40:60 wt%, 50:50 wt%, 60:40 wt%, respectively, were calculated from FTIR spectrum (Fig. 2A–B). Higher NH_3^+/NH_2 ratios stand for higher ε-PL content, indicating the higher concentration of free charged NH_3^+ groups. Obtained results revealed that phys HA/ε-PL hydrogels presented a higher free charged NH_3^+ groups content, suggesting other possible differences between phys HA/ε-PL and chem HA/ε-PL hydrogel antibacterial performance.

FTIR spectra of chem HA/ε-PL hydrogels with different HA to ε-PL mass ratios corresponded to the chemical interactions between the molecular structures of ε-PL and HA and formation of the covalent linkage between primary amino groups of ε-PL and carboxylic acid groups of HA via new amide bonds. This was indicated by the shifts in the Amide I, Amide II, and Amide III bands at 1633 cm^{-1}, 1555 cm^{-1} and 1377 cm^{-1}, which correspond to C═O stretching vibration, C═O—NH bond vibration, and C—N bond vibration, respectively [26,42], in comparison to FTIR spectra of pure HA and ε-PL (Fig. 2B). On the other hand, we noted no significant shifts in band positions for any physical HA/ε-PL hydrogels with different HA to ε-PL mass ratios (Fig. 2A).

3.1.2. Swelling behavior and gel fraction

It has been reported that highly swollen hydrogels with high porosity are beneficial for wound healing. They generally provide oxygen transmission, absorb excess tissue exudates, maintain a moist wound

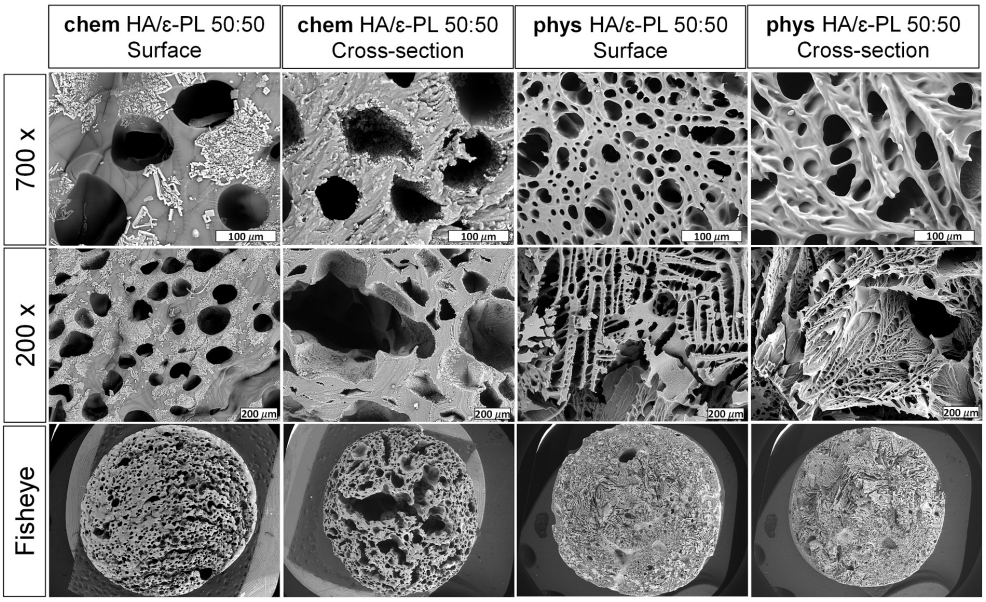

Fig. 4. SEM images of the fabricated phys and chem HA/ε-PL 50:50 wt% composite hydrogels.

environment, and insulate the invasion of external bacteria [47,48]. Hence, swelling behavior is a critical parameter for antibacterial hydrogels, mainly characterized by the swelling or water uptake capacity and the swelling kinetics to reach equilibrium [47]. Both HA and ε-PL have an excellent ability to bind the water molecules due to the highly hydrophilic functional groups in their structure, such as hydroxyl and carboxyl group of HA and primary amino groups of ε-PL [37,49,50]. The swelling degree and kinetics of the phys and chem HA/ε-PL hydrogels were assessed for up to 672 h (28 days) of incubation in DI at 37 °C (Fig. 3A–B). As expected, the crosslinking strategy significantly affected the swelling degree of the fabricated HA/ε-PL hydrogels. In general, the chem HA/ε-PL hydrogels showed a significantly higher swelling degree than the phys HA/ε-PL hydrogels, reaching the maximum at 1600% for chem HA/ε-PL 60:40 (Fig. 3A–B). With the increase of HA content, the swelling degree of the phys HA/ε-PL hydrogels increased slightly and reached 200% (for phys HA/ε-PL 60:40). The phys HA/ε-PL hydrogels exhibited relatively lower swelling degree indicating the formation of dense polyelectrolyte complex hydrogel network based on strong intermolecular electrostatic interactions between ε-PL-NH_3^+···$^-$OOC-HA. This was surprising, considering that the total HA/ε-PL concentration in the phys HA/ε-PL hydrogels was higher than in the chemically crosslinked ones (Table 1). In general, the swelling degree of hydrogels decreases with an increase of crosslinking density; the denser the hydrogel network is, the lower its water uptake capacity and swelling degree [51,52]. Higher swelling degrees of the chem HA/ε-PL hydrogels indicated lower crosslinking density of samples compared to the phys HA/ε-PL hydrogels, or higher porosity, which indeed was confirmed for the chem HA/ε-PL as described in Section 3.1.3. This was also related to the fact that ε-PL can act as a flexible crosslinker between HA chains allowing expansion of the chemically crosslinked network. Both phys and chem HA/ε-PL hydrogels exhibited fast-swelling behavior by reaching the swelling equilibrium within the first 4 h and maintaining equilibrium swelling plateau up to 672 h (Fig. 3A–B). Obtained results revealed the long-term stability and cohesion of the fabricated HA/ε-PL hydrogels under physiological conditions at 37 °C [53], which are essential parameters for functional tissue regeneration applications. Based on the obtained results, all developed HA/ε-PL hydrogels can be classified as superabsorbent or super-swelling materials since they can absorb a high amount of water (>100% of their weight) in a short amount of time [50,54].

The gel fraction of the fabricated HA/ε-PL hydrogels was significantly affected by the crosslinking strategy (Fig. 3C). Obtained results revealed that the phys HA/ε-PL hydrogels have a significantly higher gel fraction than the chem HA/ε-PL ones ($p < 0.05$). In general, the higher gel fraction is associated with a higher crosslinking degree of the hydrogel network. Thus, the phys HA/ε-PL hydrogels with lower swelling degree showed the higher gel fraction values ranged from 52 to 78%, and the gel fraction increased with an increase of HA content in samples. The chem HA/ε-PL hydrogels with higher swelling degree showed lower gel fraction values (~55%) similar for all compositions (differences were statistically insignificant, $p > 0.05$), stemming from the constant EDC/NHS crosslinker concentration used in the hydrogel preparation process.

3.1.3. Morphology

The surface and cross-section morphology of the freeze-dried Phys and chem HA/ε-PL composite hydrogels were visualized by SEM (Fig. 4). SEM images revealed a three-dimensional network with interconnected pores for all hydrogel samples. The homogenous structure was observed in the cross-section images of HA/ε-PL 50:50 wt% hydrogels with pore diameters ranging from equatorial (X) = 65 ± 47 μm to the meridian (Y) = 168 ± 65 μm and for the chem HA/ε-PL hydrogels and from equatorial (X) = 20 ± 9 μm to the meridian (Y) = 35 ± 19 for the Phys HA/ε-PL hydrogels. These trends are in good agreement with the hydrogel swelling behavior suggesting that the high swelling degree is associated with a highly porous hydrogel network, more evident for the chem HA/ε-PL hydrogels if compared to the Phys HA/ε-PL hydrogels (Fig. 3A–B). Furthermore, SEM analysis of the chem HA/ε-PL composite hydrogels revealed the formation of the NaCl crystals on the surface of hydrogels. This observation is consistent with the XRD patterns of the chem HA/ε-PL hydrogels (Fig. S1 in supplementary data). The revealed number and size ranges of pores concur with the desired characteristics of functional

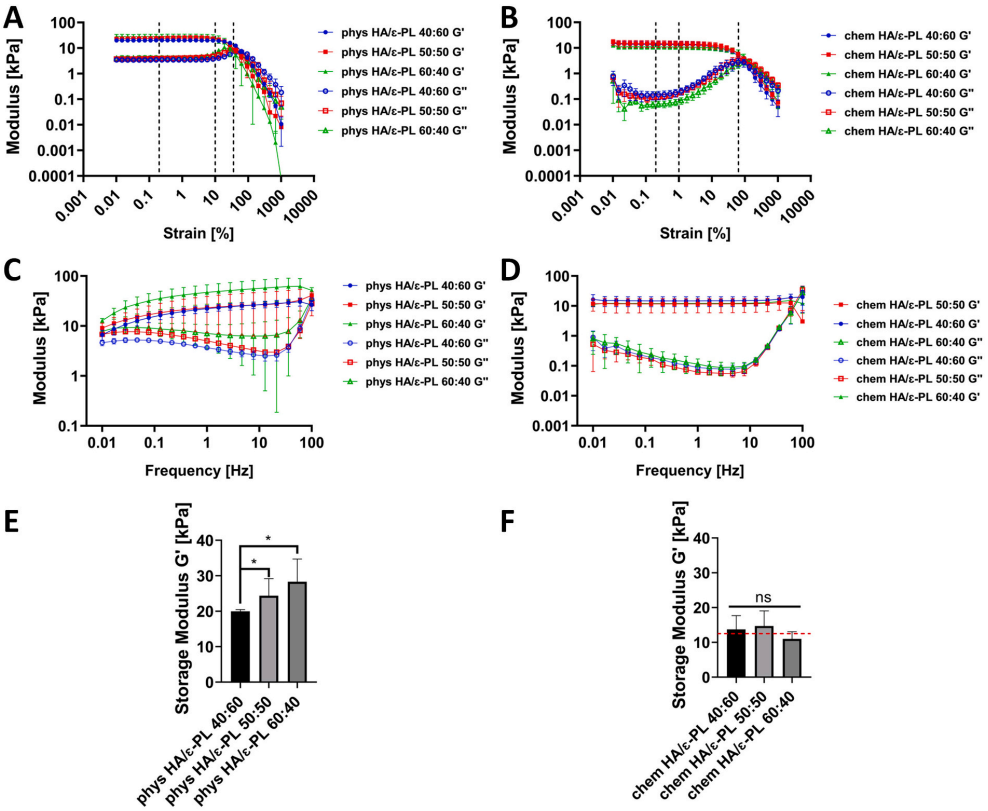

Fig. 5. Oscillatory rheology. Storage (G′ closed symbols) and loss (G″ open symbols) shear moduli vs. strain (ε) curves obtained at 1 Hz frequency of the phys HA/ε-PL (A) and chem HA/ε-PL (B) composite hydrogels. Storage (G′ closed symbols) and loss (G″ open symbols) shear moduli vs. frequency curves obtained at ε = 0.2% strain within the linear viscoelastic region of the phys HA/ε-PL (C) and chem HA/ε-PL (D) composite hydrogels. Extracted mechanical stiffness (Storage modulus, G′) of the phys HA/ε-PL (C) and chem HA/ε-PL (D) composite hydrogels from amplitude sweeps at 1 Hz and 0.2 at ε = 0.2% strain. All data is represented as average ± SD ($n = 3$, * - $p < 0.05$, ns = not significant) (color).

hydrogels for various tissue engineering applications [55,56].

3.1.4. Oscillatory rheology

The oscillatory rheology was performed to assess the mechanical properties of hydrogels. All phys and chem HA/ε-PL hydrogels were initially subjected to an amplitude sweep (Fig. 5A–B). The hydrogel storage shear moduli (G′) was observed to be an order of magnitude larger than the loss moduli (G″), confirming the typically solid-like nature of these hydrogels, irrespective of the chosen crosslinking strategy. All phys HA/ε-PL hydrogels exhibited a well-defined linear viscoelastic region (LVR) until a strain ε ≈ 10% (Fig. 5A). In contrast, the chem HA/ε-PL hydrogels exhibited limited LVR in the range of 0.1–1% strain (Fig. 5B), both marked by vertical dashed lines.

The differences in the mechanical behavior of hydrogels were observed in amplitude sweeps by the considerably different G″ behavior with respect to G′, where for chem gels larger ratio of G′/G″ was obtained at lower strains (indicating more solid-like behavior) but decreasing more rapidly to a crossover point G′ = G″ (compare Fig. 5B to A). The average crossover point has also shifted from ε ≈ 34% to ε ≈ 64% from the phys (Fig. 5A, dashed line most to the right) to chem HA/ε-PL (Fig. 5B, dashed line most to the right) hydrogels, indicating increased resilience to transition from gel to liquid for the chem HA/ε-PL hydrogels, and the ability of ε-PL acting as a flexible crosslinker between HA molecules.

The phys HA/ε-PL hydrogels exhibited behavior similar to the previously reported HA biopolymer solutions/hydrogels [57], where G′ was observed as a function of increased frequency (Fig. 5C). This typical behavior for physically entangled networks had changed for the chem HA/ε-PL, which exhibited a constant G′ across all frequency range (Fig. 5D). In contrast, instead only G″ was affected until a critical frequency of ≈10 Hz, when the transition towards liquid, and indeed hydrogel breaking, started to occur. Although the secondary relaxation time (calculated as a face value of inverse G′ = G″ crossover points in a frequency sweep) is similar for both crosslinking methods and occurs around 100 Hz; the primary relaxation time related to the crosslinking types of networks shifts from phys networks of the order of ~100 s (~0.01 Hz), by approximation and extrapolation at least 2 orders of magnitude to around 10,000 s (~0.00001 Hz) for the chem HA/ε-PL hydrogels, confirming the shift of entangled physical crosslinks to static covalent bonding type of network [58,59].

Finally, we extracted the storage modulus value to give a face value of mechanical stiffness of all hydrogels, a typical approach used for both phys and chem HA/ε-PL hydrogels towards biomedical context [56,60]. For the phys HA/ε-PL hydrogels, a significant increase of stiffness was observed ($p < 0.05$) for the increasing content of HA with G′ of 20 ± 0.5, 24.4 ± 4.8 and 28.3 ± 6.4 kPa, for 40:60 wt%, 50:50 wt%, 60:40 wt%

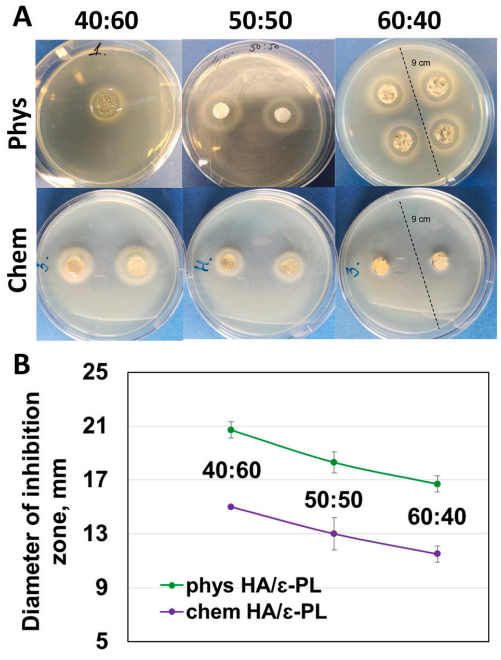

Fig. 6. (A) Representative inhibition zones of the chem and phys HA/ε-PL composite hydrogels and (B) effect of the crosslinking strategy and HA to ε-PL mass ratio on the diameter of the inhibition zone (mm) against *E. coli* (color).

HA to ε-PL mass ratio, respectively (Fig. 5E). On the other hand, irrespective of the ratio, on average, the chem HA/ε-PL hydrogels exhibited 13.2 ± 3.5 kPa G′ value, indicating the dominance of the chemical crosslinks over physical entanglements for this type of crosslinking (Fig. 5F). This is further supported by the fact that the chem HA/ε-PL hydrogels of a total 4-fold lower polymer concentration exhibited similar order of magnitude of stiffness (10–30 kPa) to the phys HA/ε-PL hydrogels. We note that although typically physically crosslinked hydrogels are associated with overall lower stiffness, in our case phys HA/ε-PL hydrogels were prepared at significantly higher HA concentrations (16–24 wt%), making stability dominant over chem gels prepared at 5.25 wt% HA content. Finally, this stiffness range suggests both types of hydrogels could in principle, be used towards e.g., combined antibacterial and musculoskeletal regeneration applications [20], as we will mention in the following sections of this manuscript.

3.2. Evaluation of antibacterial activity in vitro

According to the previous reports, ε-PL peptide shows significant antibacterial activity against Gram-positive and Gram-negative bacteria and fungi [14,61]. In general, the proposed mechanism of antibacterial action is related to the surface of ε-PL which is rich in the cationic amino groups on the side chains and responsible for the antibacterial activity [61–64]. The positively charged cationic amino groups can electrostatically adsorb to the bacteria surface and induce permeabilization of the outer bacterial cell membrane [65,66]. The antibacterial activity of the fabricated phys and chem HA/ε-PL hydrogels was investigated by the zone-of-inhibition test and antimicrobial activity evaluation in bacterial suspension using Gram-negative *E. coli* as the bacterial model organism.

3.2.1. Zone-of-inhibition test

All tested chem and phys HA/ε-PL hydrogels demonstrated antimicrobial activity (Fig. 6) against *E. coli*. The phys HA/ε-PL hydrogels with the same ε-PL mass ratio exhibited significantly ($p < 0.05$) higher antibacterial activity than the chem HA/ε-PL hydrogels, respectively. This stems from: *(i)* the amount of available charged cationic groups on phys HA/ε-PL as confirmed previously by FTIR and gel fraction experiments, *(ii)* total higher polymer content in phys HA/ε-PL, and *(iii)* the fact that the chemical modification directly involves NH_2 groups in the covalent crosslinking impairing exposition of its charge to bacteria. Thus, as expected, the highest activity was observed for phys HA/ε-PL 40:60 with highest ε-PL content and lowest activity for chem HA/ε-PL 60:40 hydrogels with lowest ε-PL content (Fig. 6). As shown in Fig. 6B, the inhibition zone was noticeable in the interface between the phys and chem HA/ε-PL hydrogels and agar, with phys HA/ε-PL hydrogels consistently showing the most significant inhibition of growth. The diameters of inhibition zones increased from 16.7 ± 0.6 to 20.7 ± 0.6 mm for the phys HA/ε-PL hydrogels and from 11.5 ± 0.6 to 15.0 ± 0.0 mm for the chem HA/ε-PL hydrogels with increasing ε-PL mass ratio, respectively.

Table 2
Diameters of sterile zones of inhibition and Log_{10} bacterial reduction after 1 h contact time. The diameter of the agar well was 8 mm. Diameter of sterile zones of inhibition are represented as average ± SD ($n = 3$, * - $p < 0.05$). Log_{10} in a tube with inoculum (without the fabricated HA/ε-PL composite hydrogels) after 1 h contact time was 5.0.

Samples	Diameter ± SD [mm]	Log_{10} bacterial reduction
phys HA/ε-PL 40:60	20.7 ± 0.6*	5.0
phys HA/ε-PL 50:50	18.3 ± 0.8*	5.0
phys HA/ε-PL 60:40	16.7 ± 0.6*	5.0
chem HA/ε-PL 40:60	15.0 ± 0.0*	3.3
chem HA/ε-PL 50:50	13.0 ± 1.2*	2.7
chem HA/ε-PL 60:40	11.5 ± 0.6*	1.8
gentamicin, 10 mg mL^{-1}	30.7 ± 0.6*	–

3.2.2. Antimicrobial activity evaluation in bacterial suspension

Bactericide effect was detected by incubating samples with *E. coli* in liquid under dynamic contact conditions. Log_{10} bacterial reduction after 1 h contact time was 5.0 (Table 2), and the corresponding killing efficiency reached 99.999% for physically crosslinked hydrogels regardless of HA to ε-PL mass ratio tested. The chem HA/ε-PL hydrogels showed significantly ($p < 0.05$) lower antibacterial activity than phys hydrogels. Its value depended on the HA to ε-PL mass ratio in the hydrogel, again confirming that the chemical modification impaired the availability of charged NH_3^+ groups and complementing results from the determination of zones of inhibition in Petri dishes experiments. These results demonstrated that the free primary amino groups of ε-PL are responsible for the antibacterial activity of the fabricated phys and chem hydrogels. Although in principle the formation of HA/ε-PL polyelectrolyte complex in phys hydrogels can affect the cationic interactions of ε-PL with anionic bacteria cells and hinder the antibacterial efficacy, the fabricated phys HA/ε-PL hydrogels maintained the highest antimicrobial activity against *E. coli*. The constant number of primary amino groups of the chem HA/ε-PL hydrogels that are crosslinked via amide bond linkage are not actively affecting bacteria. Instead, only remaining non-crosslinked free amino groups can provide moderate antibacterial effect, which is in good agreement with FTIR results (Fig. 2). In summary, it can be suggested that the fabricated phys HA/ε-PL hydrogels provide a desirable surface charge for high antibacterial activity. Thus, physical crosslinking is a more suitable approach.

3.3. In vitro biocompatibility evaluation

3.3.1. Cytotoxicity of ε-PL

Firstly, ε-PL was tested at concentrations of 3.91 to 125 mg mL^{-1} (Fig. 7A). Among tested concentrations, 7.81 mg $mL^{-1}$and higher were found cytotoxic and decreased the cell viability by more than 90%. In

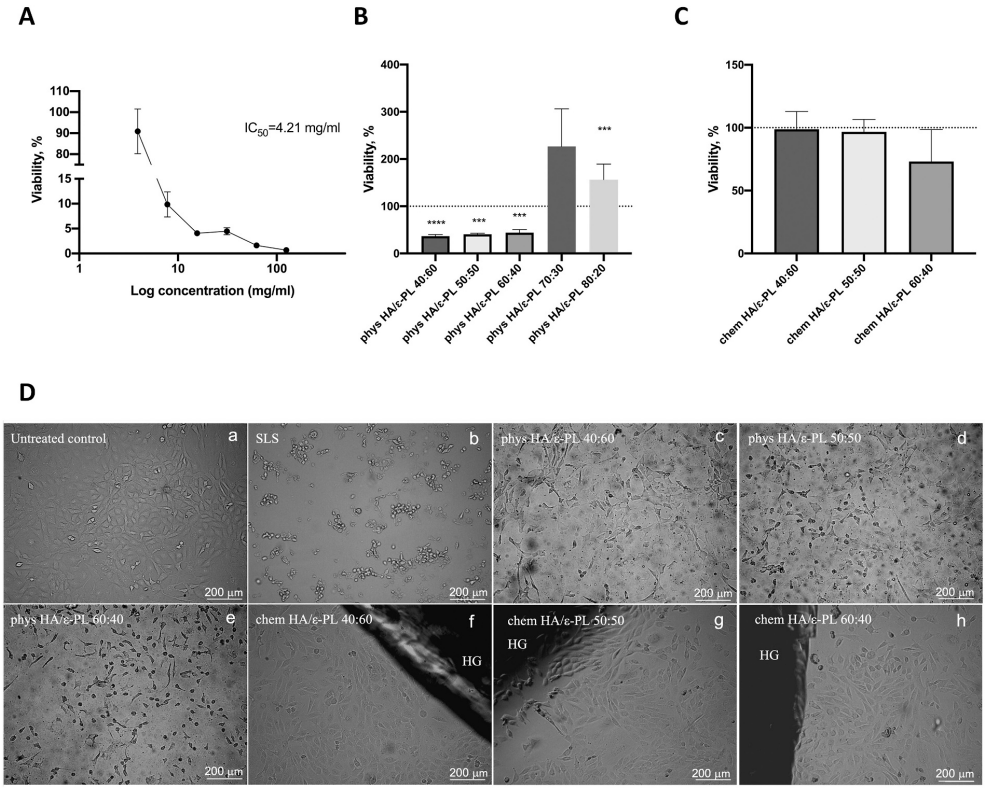

Fig. 7. (A) Cell viability after 24 h of incubation with 3.91–125 mg mL^{-1} ε-PL; (B) direct contact test with the phys HA/ε-PL hydrogel samples; (C) direct contact test with the chem HA/ε-PL hydrogel samples. Dashed lines in the graphs indicate the untreated control level (100%). (D) The representative microscopy images of BALB/c 3T3 cells after 24 h of incubation with the HA/ε-PL hydrogel samples: untreated control (a), cytotoxicity control SLS (b), the phys HA/ε-PL composite hydrogels (c–e), the chem HA/ε-PL composite hydrogels (f–h). For the chem composite hydrogels, the interface between the HA/ε-PL composite hydrogels (HG) and cell monolayer is shown. SLS - sodium lauryl sulfate (cytotoxicity control); $n = 5$; mean ± SD; *** - $p < 0.001$; **** - $p < 0.0001$.

the case of 3.91 mg mL^{-1}, no cytotoxic effects were observed, and cell viability was 90.86 ± 10.65%. Therefore, IC_{50} value for ε-PL was found to correspond to 4.21 mg mL^{-1}. Results are comparable to those observed in other studies. For example, in L929 cell line IC_{50} value (concentration that reduces cell viability by 50%) of ε-PL was 8 mg mL^{-1}, and the toxicity was significantly lower than that of the α-polylysine (α-PL) [67]. In HepG2 cell line cytotoxic effect of low concentrations (IC_{50} after 24 h incubation – 13.49 μg mL^{-1}) has been reported for ε-PL. In L-02 cell line, a reduction in cell viability by up to 40% was observed for ε-PL concentration equal to 64 μg mL^{-1} [68], overall leading to the fact that IC_{50} value depends on the cell phenotype.

3.3.2. *Cytotoxicity of hydrogel samples*

The fabricated HA/ε-PL hydrogel samples were then evaluated in both direct contact assay (Fig. 7B–D) and indirect (extract) tests (Fig. 8A–C). The phys HA/ε-PL hydrogels had a negative effect on the cell viability in the direct cytotoxicity test – all hydrogel samples reduced viability by more than 50% (Fig. 7B). The effect was statistically significant compared to untreated control, but no differences were observed between the phys HA/ε-PL hydrogels of different HA to ε-PL mass ratios (Fig. 7B). The microscopic evaluation showed reduced cell confluence and changed morphology in the presence of the phys HA/ε-PL hydrogels (Fig. 7D c–e). The chem HA/ε-PL hydrogels had a little effect on cell viability in the direct cytotoxicity test (Fig. 7C). By the microscopic evaluation, cells grew and showed normal morphology when cultivated in direct contact with the chem HA/ε-PL hydrogels (Fig. 7D f–h).

Indirect cytotoxicity test showed that extracts of the Phys HA/ε-PL hydrogel samples at the tested concentrations of 12.5%, 25%, 50% (v/v) had a negative or moderate negative effect on cell viability. The extracts of the Phys HA/ε-PL 40:60 hydrogel samples exhibited the most pronounced toxic effect compared to the other two samples (Fig. 8A). Moreover, cell viability was improved at the lower extract concentrations of 12.5% (v/v) for the Phys HA/ε-PL hydrogels (Fig. 8A, C). Among the chem HA/ε-PL hydrogels, the least toxic effect was observed for the chem HA/ε-PL 40:60 samples – at 50% (v/v) extract reduced cell viability by 13.5% (Fig. 8B). Moreover, by the lower extract concentrations of 12.5% and 25% (v/v) for chem HA/ε-PL hydrogels, cell viability was close to the untreated control level or slightly exceeded it (Fig. 8B). However, the microscopic evaluation revealed lower cell density than the untreated control (Fig. 8C). The extract concentration of 50% (v/v) of chem HA/ε-PL 50:50 and chem HA/ε-PL 60:40 samples reduced cell viability by 50% and 86%, respectively (Fig. 8B). Overall, the indirect (extract) test results showed similar trends as the direct test results of the chem HA/ε-PL hydrogels (Fig. 7C, D). Cytotoxicity assessment of the Phys HA/ε-PL hydrogels by both direct contact (Fig. 7B, D) and indirect (extract) (Fig. 8A, C) tests showed that the phys HA/ε-PL hydrogel samples with higher antimicrobial activity (Fig. 6,

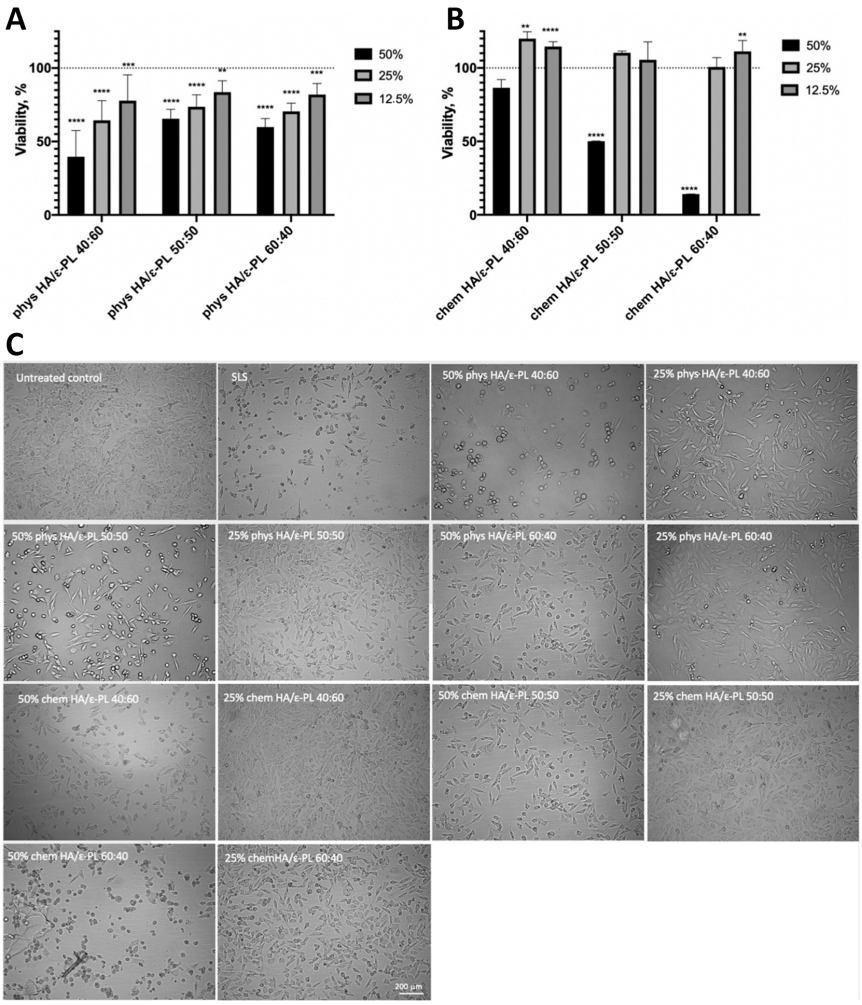

Fig. 8. (A) Cell viability after 24 h incubation with extracts of the phys HA/ε-PL hydrogels (B) and extracts of the chem HA/ε-PL hydrogels. Dashed line indicates untreated control level (100%). (C) Representative images of BALB/c 3T3 cells after 24 h incubation with the phys and chem HA/ε-PL hydrogel extracts at 50% and 25% (v/v). SLS- sodium lauryl sulfate (cytotoxicity control); $n = 5$ (for phys samples), $n = 4$ (for chem samples at 50% and 25% (v/v)) $n = 9$ (for chem samples at 12.5% (v/v)); mean ± SD; ** - $p < 0.01$; *** - $p < 0.001$; **** - $p < 0.0001$).

Table 2) had adverse effects on mammalian cell viability. In the case of the chem HA/ε-PL hydrogels, reduced cell viability was observed when extracts were tested (Fig. 8B). The increased cytotoxicity effect was found for the chem HA/ε-PL 60:40 hydrogels (Fig. 8B). We hypothesize that this effect occurred due to the release of residual non-crosslinked ε-PL primary amino groups from the hydrogel and could be supported by the highest swelling degree of chem HA/ε-PL 60:40 samples (Fig. 3B). Extracts were tested in 24-well plates with lower cultivation media volume and total seeded cell number than that used in 6-well plates performing direct contact test. This might explain the deviations between the direct and extract test results. It should be noted that in several studies where good biocompatibility of ε-PL containing composites has been shown, ε-PL concentrations lower than those used in the current study were applied [17,66,69]. On the other hand, HA as a bioactive component for tissue engineering applications is widely investigated and is considered non-cytotoxic, and shows good biocompatibility [70]. However, slight changes in cell viability have been observed in different cell lines when different HA-containing materials were assayed for cytotoxicity [71,72]. As the antimicrobial activity of hydrogels is attributable to ε-PL ability to permeabilize and disrupt the cell membranes, interactions with mammalian cell membranes might be the underlying mechanism for the composite hydrogel toxicity. Thus, further biocompatibility studies should be performed to elucidate specific effects of the fabricated Phys and chem HA/ε-PL hydrogels on cell viability, proliferation, migration, and functionality.

4. Conclusions

In this study, a series of physical and chemical crosslinked hyaluronic acid (HA)/ε-polylysine (ε-PL) hydrogels with HA to ε-PL mass ratio of 40:60 wt%, 50:50 wt%, 60:40 wt% (corresponding to molar ratios of 1:600, 1:400 and 1:270, respectively) have been prepared. The impact of

the crosslinking strategy on the physicochemical properties, antibacterial activity, and in vitro biocompatibility was evaluated. Obtained results revealed the significant impact of the crosslinking strategy on the swelling behavior, gel fraction, fast-acting antibacterial activity, and cytotoxicity of the fabricated hydrogels. The physically crosslinked hydrogels were prepared at significantly higher HA concentrations (16–24 wt%), 4-fold higher than chemically prepared gels at 5.25 wt% HA content, allowing them to exhibit similar order of magnitude of stiffness (10–30 kPa). Higher content of free charged NH_3^+ groups presented in the physically crosslinked hydrogels compared to the chemically crosslinked ones was confirmed by Fourier transform infrared spectroscopy. As such, the physically crosslinked hydrogels demonstrated a superior inhibitory effect (99.999%) on Gram-negative *E. coli*. While the chemically crosslinked hydrogels had a significantly lower inhibitory effect, related to the amount of available free charged NH_3^+ groups, lower polymer concentration, and the chemical modification directly involves NH_2 groups in covalent crosslinking, impairing its exposition and action to bacteria.

Furthermore, the obtained data confirmed the cytotoxicity of ε-PL at concentrations over 3.91 mg mL^{-1}, while this concentration was found to be favorable for antimicrobial activity. According to the cell viability tests, the chemically crosslinked hydrogels revealed superior cytocompatibility than the physically crosslinked hydrogels. The highest cell viability was observed for the chemically crosslinked HA/ε-PL 40:60 hydrogels and the physically crosslinked HA/ε-PL 60:40 hydrogel samples. Differences in the binding of amino groups of ε-PL in the physically and chemically crosslinked HA/ε-PL hydrogels and the release rate of these groups can explain the disparities in antibacterial activity and cell viability. The hypothesis that the release profile of primary amino groups of ε-PL from the fabricated HA/ε-PL hydrogels is responsible for the antibacterial and cytocompatibility performance will be tested in further studies. The distinct differences in biological and antibacterial properties of the developed chemically and physically crosslinked hydrogels provide new opportunities for the next generation functional biomaterial systems.

Supplementary data to this article can be found online at https://doi.org/10.1016/j.ijbiomac.2022.03.207.

CRediT authorship contribution statement

Kristine Salma-Arcane: Conceptualization, Supervision, Resources, Writing- Original draft preparation, Methodology, Validation, Writing - Review & Editing. **Artemis Sceglovs**: Methodology, Validation, Formal analysis, Investigation. **Eliza Trauma**: Methodology, Validation, Formal analysis, Investigation. **Jacek K. Wychowaniec**: Writing - Review & Editing, Methodology, Validation, Formal analysis, Investigation, Supervision. **Kristine Aunina**: Methodology, Validation, Formal analysis, Investigation. **Anna Ramata-Stunda**: Writing- Original draft preparation, Methodology, Validation, Formal analysis, Investigation. **Visma Nikolajeva**: Writing- Original draft preparation, Methodology, Validation, Formal analysis, Investigation. **Dagnija Loca**: Conceptualization, Supervision, Resources, Writing- Original draft preparation, Methodology, Writing - Review & Editing, Funding acquisition.

Declaration of competing interest

None.

Acknowledgements

The authors acknowledge financial support from the Latvian Council of Science research project No. lzp-2019/1-0005 “Injectable *in situ* self-crosslinking composite hydrogels for bone tissue regeneration (iBone)” and European Union's Horizon 2020 research and innovation programme under the grant agreement No. 952347 (RISEus2). J. K. W. gratefully acknowledges the European Union's Horizon 2020 (H2020-MSCA-IF-2019) research and innovation programme under the Marie Skłodowska-Curie grant agreement 893099 — ImmunoBioInks.

References

[1] D.L. Kusindarta, H. Wihadmadyatami, The Role of Extracellular Matrix in Tissue Regeneration, INTECH, 2018, https://doi.org/10.5772/intechopen.75728.
[2] J. Nicolas, L. Rabbachin, S. Sampaolesi, F. Nicotra, L. Russo, 3D extracellular matrix mimics: fundamental concepts and role of materials chemistry to influence stem cell fate, Biomacromolecules 21 (6) (2020) 1968–1994, https://doi.org/10.1021/acs.biomac.0c00045.
[3] S. Amorim, C.A. Reis, R.L. Reis, R.A. Pires, Extracellular matrix mimics using hyaluronan-based biomaterials, Trends Biotechnol. 39 (1) (2021) 90–104, https://doi.org/10.1016/j.tibtech.2020.06.003.
[4] S. Vigier, T. Fülöp, Exploring the Extracellular Matrix to Create Biomaterials, INTECH, 2016, https://doi.org/10.5772/62979.
[5] G. Jose, K.T. Shalumon, J. Chen, Natural polymers based hydrogels for cell culture applications, Curr. Med. Chem. 27 (16) (2020) 2734–2776, https://doi.org/10.2174/0929867326666190903113004.
[6] A. Vedadghavami, F. Minooei, M.H. Mohammadi, S. Khetani, A. Rezaei Kolahchi, S. Mashayekhan, A. Sanati-Nezhad, Manufacturing of hydrogel biomaterials with controlled mechanical properties for tissue engineering applications, Acta Biomater. 62 (2017) 42–63, https://doi.org/10.1016/j.actbio.2017.07.028.
[7] X. Bai, M. Gao, S. Syed, J. Zhuang, X. Xu, X. Zhang, Bioactive hydrogels for bone regeneration, Bioact. Mater. 3 (4) (2018) 401–417, https://doi.org/10.1016/j.bioactmat.2018.05.006.
[8] C.D.F. Moreira, S.M. Carvalho, R.M. Florentino, A. França, B.S. Okano, C.M. F. Rezende, H.S. Mansur, M.M. Pereira, Injectable chitosan/gelatin/bioactive glass nanocomposite hydrogels for potential bone regeneration. In vitro and in vivo analyses, Int. J. Biol. Macromol. 132 (2019) 811–821, https://doi.org/10.1016/j.ijbiomac.2019.03.237.
[9] D. Harrer, E. Sanchez Armengol, J.D. Friedl, A. Jalil, M. Jelkmann, C. Leichner, F. Laffleur, Is hyaluronic acid the perfect excipient for the pharmaceutical need? Int. J. Pharm. 601 (2021), 120589 https://doi.org/10.1016/j.ijpharm.2021.120589.
[10] W. Guo, L. Douma, M.H. Hu, D. Eglin, M. Alini, A. Šećerović, S. Grad, X. Peng, X. Zou, M. D'Este, Hyaluronic acid-based interpenetrating network hydrogel as a cell carrier for nucleus pulposus repair, Carbohydr. Polym. 277 (2022), 118828, https://doi.org/10.1016/j.carbpol.2021.118828.
[11] N.A. El-Sersy, A.E. Abdelwahab, S.S. Abouelkhiir, D.M. Abou-Zeid, S.A. Sabry, Antibacterial and anticancer activity of ε-poly-L-lysine (ε -PL) produced by a marine Bacillus subtilis sp. J. Basic Microbiol. 52 (5) (2012) 513–522, https://doi.org/10.1002/jobm.201100290.
[12] L. Cai, S. Liu, J. Guo, Y. Jia, Polypeptide-based self-healing hydrogels: design and biomedical applications, Acta Biomater. 113 (2020) 84–100, https://doi.org/10.1016/j.actbio.2020.07.001.
[13] S. Chen, S. Huang, Y. Li, C. Zhou, Recent advances in epsilon-poly-L-lysine and L-lysine-based dendrimer synthesis, modification, and biomedical applications, Front. Chem. 9 (2021), 659304, https://doi.org/10.3389/fchem.2021.659304.
[14] N.A. Patil, B. Kandasubramanian, Functionalized polylysine biomaterials for advanced medical applications: a review, Eur. Polym. J. 146 (2021), 110248, https://doi.org/10.1016/j.eurpolymj.2020.110248.
[15] R. Wang, B. Zhou, D. Xu, H. Xu, L. Liang, X. Feng, P. Ouyang, B. Chi, Antimicrobial and biocompatible ε-polylysine–γ-poly(glutamic acid)–based hydrogel system for wound healing, J. Bioact. Compat. Polym. 31 (3) (2016) 242–259, https://doi.org/10.1177/0883911515610019.
[16] S. Li, S. Dong, W. Xu, S. Tu, L. Yan, C. Zhao, J. Ding, X. Chen, Antibacterial hydrogels, Adv. Sci. 1700527 (2018), https://doi.org/10.1002/advs.201700527.
[17] R. Wang, D. Xu, L. Liang, T. Xu, W. Liu, P. Ouyang, B. Chi, H. Xu, Enzymatically crosslinked epsilon-poly-L-lysine hydrogels with inherent antibacterial properties for wound infection prevention, RSC Adv. 6 (11) (2016) 8620–8627, https://doi.org/10.1039/C5RA15616E.
[18] W. Hu, Z. Wang, Y. Xiao, S. Zhang, J. Wang, Advances in crosslinking strategies of biomedical hydrogels, Biomater. Sci. 7 (3) (2019) 843–855, https://doi.org/10.1039/C8BM01246F.
[19] H. Cui, X. Zhuang, C. He, Y. Wei, X. Chen, High performance and reversible ionic polypeptide hydrogel based on charge-driven assembly for biomedical applications, Acta Biomater. 11 (2015) 183–190, https://doi.org/10.1016/j.actbio.2014.09.017.
[20] X. Xue, Y. Hu, S. Wang, X. Chen, Y. Jiang, J. Su, Fabrication of physical and chemical crosslinked hydrogels for bone tissue engineering, Bioact. Mater. (October) (2021), https://doi.org/10.1016/j.bioactmat.2021.10.029.
[21] J.H. Lee, Injectable hydrogels delivering therapeutic agents for disease treatment and tissue engineering, Biomater. Res. 22 (1) (2018) 27, https://doi.org/10.1186/s40824-018-0138-6.
[22] N. Reddy, R. Reddy, Q. Jiang, Crosslinking biopolymers for biomedical applications, Trends Biotechnol. 33 (6) (2015) 362–369, https://doi.org/10.1016/j.tibtech.2015.03.008.
[23] S. Dakhara, C. Anajwala, Polyelectrolyte complex: a pharmaceutical review, Syst. Rev. Pharm. 1 (2) (2010) 121–127, https://doi.org/10.4103/0975-8453.75046.
[24] J. Lv, Y. Meng, Y. Shi, Y. Li, J. Chen, F. Sheng, Properties of epsilon-polylysine•HCl/high-methoxyl pectin polyelectrolyte complexes and their commercial application, J. Food Process. Preserv. 44 (2) (2020), e14320, https://doi.org/10.1111/jfpp.14320.

[25] M.P. Wickramathilaka, B.Y. Tao, Characterization of covalent crosslinking strategies for synthesizing DNA-based bioconjugates, J. Biol. Eng. 13 (1) (2019) 63, https://doi.org/10.1186/s13036-019-0191-2.
[26] J. Hua, Z. Li, W. Xia, N. Yang, J. Gong, J. Zhang, C. Qiao, Preparation and properties of EDC/NHS mediated crosslinking poly (gamma-glutamic acid)/epsilon-polylysine hydrogels, Mater. Sci. Eng. C 61 (2016) 879–892, https://doi.org/10.1016/j.msec.2016.01.001.
[27] J. Ahn, L. Kuffova, K. Merrett, D. Mitra, J.V. Forrester, F. Li, M. Griffith, Crosslinked collagen hydrogels as corneal implants: effects of sterically bulky vs. non-bulky carbodiimides as crosslinkers, Acta Biomater. 9 (8) (2013) 7796–7805, https://doi.org/10.1016/j.actbio.2013.04.014.
[28] J.Y. Seo, B. Lee, T.W. Kang, J.H. Noh, M.J. Kim, Y.B. Ji, H.J. Ju, B.H. Min, M. S. Kim, Electrostatically interactive injectable hydrogels for drug delivery, Tissue Eng. Regen. Med. 15 (5) (2018) 513–520, https://doi.org/10.1007/s13770-018-0146-6.
[29] M. He, L. Shi, G. Wang, Z. Cheng, L. Han, X. Zhang, C. Wang, J. Wang, P. Zhou, G. Wang, Biocompatible and biodegradable chitosan/sodium polyacrylate polyelectrolyte complex hydrogels with smart responsiveness, Int. J. Biol. Macromol. 155 (2020) 1245–1251, https://doi.org/10.1016/j.ijbiomac.2019.11.092.
[30] M.E. van Gent, M. Ali, P.H. Nibbering, S.N. Kłodzińska, Current advances in lipid and polymeric antimicrobial peptide delivery systems and coatings for the prevention and treatment of bacterial infections, Pharmaceutics 13 (11) (2021) 1840, https://doi.org/10.3390/pharmaceutics13111840.
[31] Y. Chang, L. McLandsborough, D.J. McClements, Antimicrobial delivery systems based on electrostatic complexes of cationic Ɛ-polylysine and anionic gum arabic, Food Hydrocoll. 35 (2014) 137–143, https://doi.org/10.1016/j.foodhyd.2013.05.004.
[32] V.Z. Prokopović, C. Duschl, D. Volodkin, Hyaluronic acid/poly-l-lysine multilayers as seservoirs for storage and release of small charged molecules, Macromol. Biosci. 15 (10) (2015) 1357–1363, https://doi.org/10.1002/mabi.201500093.
[33] E. Tračuma, D. Loca, Hyaluronic acid/polylysine composites for local drug delivery: a review, Key Eng. Mater. 850 (2020) 213–218, https://doi.org/10.4028/www.scientific.net/KEM.850.213.
[34] Y. Zou, S. He, J. Du, ε-Poly(L-lysine)-based hydrogels with fast-acting and prolonged antibacterial activities, Chin. J. Polym. Sci. 36 (11) (2018) 1239–1250, https://doi.org/10.1007/s10118-018-2156-1.
[35] R. Wang, B. Zhou, W. Liu, X. Feng, S. Li, D. Yu, J. Chang, B. Chi, H. Xu, Fast in situ generated Ɛ-polylysine-poly (ethylene glycol) hydrogels as tissue adhesives and hemostatic materials using an enzyme-catalyzed method, J. Biomater. Appl. 29 (8) (2015) 1167–1179, https://doi.org/10.1177/0885328214553960.
[36] L. Stipniece, K. Salma-Ancane, I. Narkevica, I. Juhnevica, L. Berzina-Cimdina, Fabrication of nanostructured composites based on hydroxyapatite and ε-polylysine, Mater. Lett. 163 (2016) 65–68, https://doi.org/10.1016/j.matlet.2015.10.077.
[37] S.C. Shukla, A. Singh, A.K. Pandey, A. Mishra, Review on production and medical applications of ε-polylysine, Biochem. Eng. J. 65 (2012) 70–81, https://doi.org/10.1016/j.bej.2012.04.001.
[38] A. Šćeglovs, K. Salma-Ancane, Novel hydrogels and composite hydrogels based on ε-polylysine, hyaluronic acid and hydroxyapatite, Key Eng. Mater. 850 (1) (2020) 242–248, https://doi.org/10.4028/www.scientific.net/KEM.850.242.
[39] A. Ström, A. Larsson, O. Okay, Preparation and physical properties of hyaluronic acid-based cryogels, J. Appl. Polym. Sci. 132 (29) (2015) 42194, https://doi.org/10.1002/app.42194.
[40] R. Gilli, M. Kacuráková, M. Mathlouthi, L. Navarini, S. Paoletti, FTIR studies of sodium hyaluronate and its oligomers in the amorphous solid phase and in aqueous solution, Carbohydr. Res. 263 (2) (1994) 315–326, https://doi.org/10.1016/0008-6215(94)00147-2.
[41] K. Haxaire, Y. Maréchal, M. Milas, M. Rinaudo, Hydration of polysaccharide hyaluronan observed by IR spectrometry. I. Preliminary experiments and band assignments, Biopolymers 72 (1) (2003) 10–20, https://doi.org/10.1002/bip.10245.
[42] M. Rozenberg, G. Shoham, FTIR spectra of solid poly-l-lysine in the stretching NH mode range, Biophys. Chem. 125 (1) (2007) 166–171, https://doi.org/10.1016/j.bpc.2006.07.008.
[43] J. Chen, H. Liu, Z. Xia, X. Zhao, Y. Wu, M. An, Purification and structural analysis of the effective anti-TMV compound ε-poly-l-lysine produced by Streptomyces ahygroscopicus, Molecules 24 (6) (2019) 1156, https://doi.org/10.3390/molecules24061156.
[44] R.A. Sequeira, N. Singh, M.M. Pereira, N.A. Chudasama, S. Bhattacharya, M. Sharma, D. Mondal, K. Prasad, High concentration solubility and stability of ε-poly-l-lysine in an ammonium-based ionic liquid: a suitable media for polypeptide packaging and biomaterial preparation, Int. J. Biol. Macromol. 120 (2018) 378–384, https://doi.org/10.1016/j.ijbiomac.2018.08.102.
[45] A. Barth, The infrared absorption of amino acid side chains, Prog. Biophys. Mol. Biol. 74 (3–5) (2000) 141–173, https://doi.org/10.1016/S0079-6107(00)00021-3.
[46] A. Barth, Infrared spectroscopy of proteins, Biochim. Biophys. Acta - Bioenerg. 1767 (9) (2007) 1073–1101, https://doi.org/10.1016/j.bbabio.2007.06.004.
[47] K. Yang, Q. Han, B. Chen, Y. Zheng, K. Zhang, Q. Li, J. Wang, Antimicrobial hydrogels: promising materials for medical application, Int. J. Nanomedicine 13 (2018) 2217–2263, https://doi.org/10.2147/IJN.S154748.
[48] X. Zhang, M. Qin, M. Xu, F. Miao, C. Merzougui, X. Zhang, Y. Wei, W. Chen, D. Huang, The fabrication of antibacterial hydrogels for wound healing, Eur. Polym. J. 146 (2021), 110268, https://doi.org/10.1016/j.eurpolymj.2021.110268.
[49] P. Zhai, X. Peng, B. Li, Y. Liu, H. Sun, X. Li, The application of hyaluronic acid in bone regeneration, Int. J. Biol. Macromol. 151 (2019) 1224–1239, https://doi.org/10.1016/j.ijbiomac.2019.10.169.
[50] M.J. Zohuriaan-Mehr, A. Pourjavadi, H. Salimi, M. Kurdtabar, Protein- and homo poly(amino acid)-based hydrogels with super-swelling properties, Polym. Adv. Technol. 20 (8) (2009) 655–671, https://doi.org/10.1002/pat.1395.
[51] Y. Xue, H. Chen, C. Xu, D. Yu, H. Xu, Y. Hu, Synthesis of hyaluronic acid hydrogels by crosslinking the mixture of high-molecular-weight hyaluronic acid and low-molecular-weight hyaluronic acid with 1,4-butanediol diglycidyl ether, RSC Adv. 10 (12) (2020) 7206–7213, https://doi.org/10.1039/C9RA09271D.
[52] C.E. Schanté, G. Zuber, C. Herlin, T.F. Vandamme, Chemical modifications of hyaluronic acid for the synthesis of derivatives for a broad range of biomedical applications, Carbohydr. Polym. 85 (3) (2011) 469–489, https://doi.org/10.1016/j.carbpol.2011.03.019.
[53] D. Eyrich, F. Brandl, B. Appel, H. Wiese, G. Maier, M. Wenzel, R. Staudenmaier, A. Goepferich, T. Blunk, Long-term stable fibrin gels for cartilage engineering, Biomaterials 28 (1) (2007) 55–65, https://doi.org/10.1016/j.biomaterials.2006.08.027.
[54] R.A. Batista, P.J.P. Espitia, D.M.C. Vergne, A.A. Vicente, P.A.C. Pereira, M. A. Cerqueira, J.A. Teixeira, J. Jovanovic, P. Severino, E.B. Souto, Development and evaluation of superabsorbent hydrogels based on natural polymers, Polymers (Basel) 12 (10) (2020) 2173, https://doi.org/10.3390/polym12102173.
[55] C.M. Walsh, J.K. Wychowaniec, D.F. Brougham, D. Dooley, Functional hydrogels as therapeutic tools for spinal cord injury: new perspectives on immunopharmacological interventions, Pharmacol. Ther. 108043 (2021), https://doi.org/10.1016/j.pharmthera.2021.108043.
[56] J.K. Wychowaniec, J. Litowczenko, K. Tadyszak, V. Natu, C. Aparicio, B. Peplińska, M.W. Barsoum, M. Otyepka, B. Scheibe, Unique cellular network formation guided by heterostructures based on reduced graphene oxide - Ti3C2Tx MXene hydrogels, Acta Biomater. 115 (2020) 104–115, https://doi.org/10.1016/j.actbio.2020.08.010.
[57] A. Dodero, R. Williams, S. Gagliardi, S. Vicini, M. Alloisio, M.A. Castellano, Micro-rheological and rheological study of biopolymers solutions: hyaluronic acid, Carbohydr. Polym. 203 (2019) 349–355, https://doi.org/10.1016/j.carbpol.2018.09.072.
[58] J.M. Guenet, Thermoreversible Gelation of Polymers and Biopolymers, Academic Press, 1992.
[59] J.M. Guenet, Organogels. Thermodynamics, Structure, Solvent Role, and Properties, Springer International Publishing, Cham, 2016, https://doi.org/10.1007/978-3-319-33178-2.
[60] J.K. Wychowaniec, M. Iliut, M. Zhou, J. Moffat, M.A. Elsawy, W.A. Pinheiro, J. A. Hoyland, A.F. Miller, A. Vijayaraghavan, A. Saiani, Designing peptide/graphene hybrid hydrogels through fine-tuning of molecular interactions, Biomacromolecules 19 (7) (2018) 2731–2741, https://doi.org/10.1021/acs.biomac.8b00333.
[61] T. Yoshida, T. Nagasawa, Epsilon-poly-l-lysine: microbial production, biodegradation and application potential, Appl. Microbiol. Biotechnol. 62 (1) (2003) 21–26, https://doi.org/10.1007/s00253-003-1312-9.
[62] Z. Tan, Y. Shi, B. Xing, Y. Hou, J. Cui, S. Jia, The antimicrobial effects and mechanism of ε-poly-lysine against Staphylococcus aureus, Bioresour. Bioprocess. 6 (1) (2019) 11, https://doi.org/10.1186/s40643-019-0246-8.
[63] Y. Li, Q. Han, J. Feng, W. Tian, H. Mo, Antibacterial characteristics and mechanisms of Ɛ-poly-lysine against Escherichia coli and Staphylococcus aureus, Food Control 43 (2014) 22–27, https://doi.org/10.1016/j.foodcont.2014.02.023.
[64] K. Ushimaru, T. Morita, T. Fukuoka, Bio-based, flexible, and tough material derived from ε-poly-l-lysine and fructose via the Maillard reaction, ACSOmega 5 (36) (2020) 22793–22799, https://doi.org/10.1021/acsomega.0c01813.
[65] A. Sun, X. He, L. Li, T. Li, Q. Liu, X. Zhou, X. Ji, W. Li, Z. Qian, An injectable photopolymerized hydrogel with antimicrobial and biocompatible properties for infected skin regeneration, NPG Asia Mater. 12 (1) (2020) 25, https://doi.org/10.1038/s41427-020-0206-y.
[66] C. Zhou, P. Li, X. Qi, A.R.M. Sharif, Y.F. Poon, Y. Cao, M.W. Chang, S.S.J. Leong, M. B. Chan-Park, A photopolymerized antimicrobial hydrogel coating derived from epsilon-poly-l-lysine, Biomaterials 32 (11) (2011) 2704–2712, https://doi.org/10.1016/j.biomaterials.2010.12.040.
[67] S. Hyon, N. Nakajima, H. Sugai, K. Matsumura, Low cytotoxic tissue adhesive based on oxidized dextran and epsilon-poly-L-lysine, J. Biomed. Mater. Res. Part A 102 (8) (2014) 2511–2520, https://doi.org/10.1002/jbm.a.34923.
[68] C. Shi, X. Zhao, Z. Liu, R. Meng, X. Chen, N. Guo, Antimicrobial, antioxidant, and antitumor activity of epsilon-poly-L-lysine and citral, alone or in combination, Food Nutr. Res. 60 (1) (2016) 31891, https://doi.org/10.3402/fnr.v60.31891.
[69] F. Wahid, F. Wang, Y. Xie, L. Chu, S. Jia, Y. Duan, L. Zhang, C. Zhong, Reusable ternary PVA films containing bacterial cellulose fibers and ε-polylysine with improved mechanical and antibacterial properties, Colloids Surf. B Biointerfaces 183 (September) (2019), 110486, https://doi.org/10.1016/j.colsurfb.2019.110486.
[70] J. Necas, L. Bartosikova, P. Brauner, J. Kolar, Hyaluronic acid (hyaluronan): a review, Vet. Med. (Praha) 53 (8) (2008) 397–411, https://doi.org/10.17221/1930-VETMED.
[71] D.G. Boeckel, R.S.A. Shinkai, M.L. Grossi, E.R. Teixeira, In vitro evaluation of cytotoxicity of hyaluronic acid as an extracellular matrix on OFCOL II cells by the MTT assay, Oral Surg.Oral Med. Oral Pathol. Oral Radiol. 117 (6) (2014) e423–e428, https://doi.org/10.1016/j.oooo.2012.07.486.
[72] S. Gedikli, G. Güngör, Y. Toptaş, D.E. Sezgin, M. Demirbilek, N. Yazıhan, P. Aytar Çelik, E.B. Denkbaş, V. Bütün, A. Çabuk, Optimization of hyaluronic acid production and its cytotoxicity and degradability characteristics, Prep. Biochem.

Biotechnol. 48 (7) (2018) 610–618, https://doi.org/10.1080/10826068.2018.1476885.

Appendix III

3. Pielikums

Effect of steam sterilisation on physico-chemical properties of antibacterial covalently cross-linked ε-polylysine/hyaluronic acid hydrogels

Artemijs Sceglovs, Jacek K. Wychowaniec, Ingus Skadins, Charlotte J.C. Edwards-Gayle, Matteo D'Este, Kristine Salma-Ancane

Carbohydrate Polymers Technologies and Applications, **2023**, 6: 100363.
https://doi.org/10.1016/J.CARPTA.2023.100363

A.S. input: Conceptualization, Writing – original draft, Methodology, Validation, Writing – review & editing.

Carbohydrate Polymer Technologies and Applications 6 (2023) 100363

Contents lists available at ScienceDirect

Carbohydrate Polymer Technologies and Applications

journal homepage: www.sciencedirect.com/journal/carbohydrate-polymer-technologies-and-applications

Effect of steam sterilisation on physico-chemical properties of antibacterial covalently cross-linked ε-polylysine/hyaluronic acid hydrogels

Artemijs Sceglovs [a,b], Jacek K. Wychowaniec [c], Ingus Skadins [d], Aigars Reinis [d], Charlotte J. C. Edwards-Gayle [e], Matteo D'Este [c], Kristine Salma-Ancane [a,b,*]

[a] Rudolfs Cimdins Riga Biomaterials Innovations and Development Centre of RTU, Institute of General Chemical Engineering, Faculty of Materials Science and Applied Chemistry, Riga Technical University, Pulka St. 3/3, Riga LV-1007, Latvia
[b] Baltic Biomaterials Centre of Excellence, Headquarters at Riga Technical University, Riga, Latvia
[c] AO Research Institute Davos, Clavadelerstrasse 8, Davos 7270, Switzerland
[d] Faculty of Medicine, Department of Biology and Microbiology, Riga Stradins University, Latvia
[e] Diamond Light Source, Harwell Science and Innovation Campus, Fermi Avenue, Didcot OX110DE, United Kingdom

ARTICLE INFO

Keywords:
E-polylysine
Hyaluronic acid
Hydrogels
Chemical cross-linking
Steam sterilisation
Antibacterial

ABSTRACT

Sterilisation of implantable biomaterials such as hydrogels remains a key step towards their clinical translation. Standard sterilisation methods can significantly alter hydrogels' physicochemical and biological performance. Previously, we developed composite hydrogels based on ε-polylysine (ε-PL) and hyaluronic acid (HA). The developed hydrogels demonstrated promising antibacterial activity and *in vitro* cell viability and their variable properties depending on the chosen ε-PL to HA ratio. In this study, we fabricated a series of chemically cross-linked ε-PL/HA hydrogels with expanded ε-PL to HA mass ratios.

Using small-angle X-ray scattering (SAXS), we unravelled the topological differences between physically and chemically crosslinked hydrogels. We then selected the chemically crosslinked hydrogel ε-PL/HA series of 60:40 wt%, 70:30 wt%, and 80:20 wt% ratios, with similar network topologies, to evaluate the impact of steam sterilisation on their physicochemical and viscoelastic properties. The antibacterial activity of the sterilized hydrogels was also evaluated against Gram-negative and Gram-positive bacteria. Our results showed that steam sterilisation minimally affects structure and physicochemical properties of ε-PL/HA hydrogels. Furthermore, the developed hydrogel ε-PL/HA series of 60:40 wt%, 70:30 wt%, and 80:20 wt% ratios showed pronounced antibacterial activity against Gram-negative and Gram-positive pathogenic bacteria. We expect our results will contribute to the growing understanding of using sterilisation methods for antibacterial hydrogels that have the potential for wider tissue engineering applications.

1. Introduction

Hydrogels are attractive biomaterials due to their unique biocompatibility, mechanical features similar to human tissue extracellular matrix, and tissue repair capability. In the last decade, hydrogels with an antibacterial function have been extensively studied to address the clinical challenge of infected tissue repair and healing (Li et al., 2018). One of the most effective strategies is to design hydrogels from natural biopolymers with inherent antibacterial function (Chen et al., 2023). Inherent antibacterial hydrogels limit the need of additional antibacterial agents, have simple composition, exhibits good cytocompatibility and long-lasting antibacterial activity (Jia et al., 2023). The most important parameters to design antibacterial hydrogels are the selection of biopolymers and the crosslinking strategy. In this study, ε-poly-L-lysine (ε-PL) and hyaluronic acid (HA) were selected for the development of antibacterial hydrogels, based on superior functionalities of these components, while providing antibacterial activity and mimicking the native extracellular matrix (ECM). ε-PL is an antibacterial cationic homo-polypeptide with many unique characteristics, such as non-toxicity, biodegradability, and cell surface adhesiveness (Chen et al., 2021; Zhu et al., 2023). ε-PL exhibits broad-spectrum antibacterial activity to several microorganisms, including Gram-positive and

* Corresponding author at: Rudolfs Cimdins Riga Biomaterials Innovations and Development Centre of RTU, Institute of General Chemical Engineering, Faculty of Materials Science and Applied Chemistry, Riga Technical University, Latvia
E-mail address: kristine.salma-ancane@rtu.lv (K. Salma-Ancane).

https://doi.org/10.1016/j.carpta.2023.100363

Available online 26 September 2023

Gram-negative bacteria, fungi, yeast, and bacteriophages (Wang et al., 2021; Zarrintaj et al., 2021; Zhu et al., 2023). It is known that the positively charged amino groups of ε-PL provide intrinsic antibacterial activity by disruption of the negatively charged bacterial cell membrane and cell wall (Zhu et al., 2023). Recently, several studies have focused on designing various modified ε-PL-based biomaterials with antibacterial properties for potential biomedical applications (Kennedy et al., 2020; Meng et al., 2021; Zou et al., 2018). However, this electrostatic interaction between ε-PL and negatively charged mammalian cell surfaces should be controlled to avoid the cytotoxic and haemolytic effects. HA is an essential polysaccharide of the extracellular matrix (ECM) in many tissues, which demonstrates excellent biocompatibility and plays an important biochemical role in different physiological processes (Dovedytis et al., 2020; Wang et al., 2022). Moreover, HA bears multiple functional groups that allow for numerous subsequent chemical modifications (Li et al., 2019; Liu et al., 2010). In our recent work, we developed chemically and physically cross-linked hydrogels based on HA and ε-PL with HA to ε-PL mass ratios of 60:40 wt%, 50:50 wt%, 40:60 wt% (Salma-Ancane et al., 2022). The previous study aimed to compare the physico-chemical properties and *in vitro* performance of hydrogels fabricated with two distinct cross-linking strategies. Our findings demonstrated that the developed chemically cross-linked HA/ε-PL hydrogels showed promising functionalities such as antibacterial activity and, at the same time, sufficient cell viability of BALB/c 3T3 cells for future studies. Moreover, a higher ε-PL mass ratio provided the higher antibacterial activity of the fabricated hydrogels. One of the main limitations of antibacterial hydrogels is mechanical strength (Aliakbar Ahovan et al., 2022). It is well reported that covalently cross-linked antibacterial hydrogels exhibited robust mechanical performance such as strength and stiffness which is necessary to provide mechanical support in infected wound site (Jia et al., 2023). Additionally, thanks to their hydrated nature, antibacterial hydrogels provide high permeability, good oxygen transfer, diffusion of antibacterial agent, and promote cell proliferation and tissue regeneration, respectively (Aliakbar Ahovan et al., 2022). Despite the advances development of antibacterial hydrogels with highly attractive properties and unique functions (Singh et al., 2016; Taghipour et al., 2020) for infected tissue regeneration (Catoira et al., 2019; Correa et al., 2021), the sterilisation aspect has been seldom addressed., sterilisation is still a crucial fabrication step which must be successfully introduced to achieve clinical translation (Galante et al., 2018; Huerta-ángeles et al., 2018; Peng et al., 2022). Sterilisation process is key to eliminate contamination by microorganisms such as bacteria/bacterial spores, viruses and yeast (Dai et al., 2016). The most used sterilisation methods effective to achieve high sterility assurance levels (SAL) are steam sterilisation or autoclaving, Gamma irradiation, EtO sterilisation and supercritical CO_2 sterilisation (Galante et al., 2018; Han et al., 2017; Huerta-ángeles et al., 2018; Karajanagi et al., 2011). However, due to soft nature, high water content and crosslinked 3D polymeric network structure type, hydrogels are vulnerable to all the above mentioned techniques (Han et al., 2017; Karajanagi et al., 2011; Stoppel et al., 2014; Tao et al., 2021). For example, sterilisation can lead to hydrolysis, oxidation, chain scission, depolymerization or even induce toxic effects as a result of which the developed hydrogels are no longer applicable (Galante et al., 2018; Han et al., 2017). Therefore, sterilisation methods must compromise decontamination and impact on the physicochemical and mechanical properties of the developed hydrogels. Only a few studies have been published in the last decade critically showing the effect of sterilisation methods on the properties of fabricated hydrogels with in-depth physicochemical analysis.

In this study, we aimed to develop *in situ* forming inherent antibacterial covalently cross-linked ε-PL/HA hydrogels, which can provide advantageous physico-chemical properties and long-lasting antibacterial activity after steam sterilisation. Thus, we fabricated a series of ε-PL/HA hydrogels with expanded ε-PL to HA mass ratios of 40:60 wt%, 50:50 wt%, 60:40 wt%, 70:30 wt%, 80:20 wt% using modified *in situ* forming methodology. For the first time, we used *in situ* small-angle X-ray scattering (SAXS) to explore the impact of ε-PL to HA mass ratio on the topology of the developed covalently cross-linked ε-PL/HA hydrogels in their native state. Afterwards, we selected ε-PL/HA hydrogels with ε-PL to HA mass ratios of 60:40 wt%, 70:30 wt%, 80:20 wt%, with similar network topologies and systematically evaluated the effect of steam sterilisation on their physico-chemical, viscoelastic and bactericidal effect against both Gram-negative and Gram-positive bacterial strains. Accordingly, molecular structure, phase composition, swelling behaviour, gel fraction, morphology, porosity, and rheological properties of the synthesized ε-PL/HA hydrogels were investigated before and after steam sterilisation. Our research was conducted based on the hypothesis that the developed covalently cross-linked hydrogels based on ε-PL/HA preserve physicochemical features and antibacterial activity after steam sterilisation and may potentially act as biomaterial-assisted antibacterial therapy for future biomedical applications.

2. Materials and methods

2.1. Materials

ε-Polylysine (ε-PL•HCl, 99% purity, molecular weight 3850g/mol, humidity content 6.5%) was purchased from *Zhengzhou Bainafo Bioengineering Co., Ltd* (Henan, China). Sodium hyaluronate (Na-HA, 95% purity, humidity content 13.5%, molecular weight 1.55 MDa) was purchased from *Contipro Biotech s.r.o.* (Dolní Dobrouč, Czech Republic). 1-ethyl-3-(3-dimethylaminopropyl)-carbodiimide hydrochloride (EDC, 98% purity, CAS-No: 25,952–53–8, molecular weight: 191.75g/mol) was purchased from *Novabiochem* (Burlington, USA). *N*-hydroxysuccinimide (NHS, 98% purity, CAS-No: 6066–82–6, molecular weight: 115.09g/mol) was purchased from *Sigma-Aldrich*.

For antibacterial studies: *Escherichia coli* (*E.coli)* ATCC© 25,922™ from *American Type Culture Collection* (ATCC, USA)) and, *Staphylococcus aureus* (*S.aureus)* ATCC© 25,923™ from *American Type Culture Collection* (ATCC, USA)) were used. Lysogeny broth (LB, Cat.Nr. 1102,850,500) was purchased from *Merck KGaA* (Darmstadt, Germany). Tryptone Soya Agar (TSA, casein soya bean digest agar, Code: CM0131) was purchased from *Oxoid Limited* (Hampshire, United Kingdom).

2.2. Synthesis of chemically cross-linked ε-PL/HA hydrogels

Synthesis of chemically cross-linked hydrogels based on ε-PL and HA (Fig. 1A,B) was performed according to the synthesis methodology described in the previous study (Salma-Ancane et al., 2022) with minor modifications. Hydrogels were prepared via chemical cross-linking with EDC to NHS molar ratio of 1:1 according to EDC/NHS mediated polymerization mechanism (Fig. 1C).

Firstly, HA powder was dissolved in 2mL of deionized water at a constant amount of 0.2095g. The dissolution process was performed by rapid mixing of dissolved HA in two connected syringes (Fig. 1D). Then, prepared mixture was left in a refrigerator (4 °C) overnight. The next day, EDC and NHS were added one by one, following the same mixing procedure in mated syringes. The molar concentration of EDC and NHS used in this study was 0.24 mol•L^{-1}, similarly to our previous studies (Salma-Ancane et al., 2022). Finally, ε-PL was dissolved in another 2.0mL of deionized water in quantities corresponding to the desired mass ratio (see Table 1) in the final product (0.314; 0.467; 0.786g). In the last step, pre-dissolved ε-PL was mixed with pre-activated HA for 2min. After mixing, the formed gels were directly extruded into 3D molds ($\phi = 10$mm, $H = 5$mm) and left for 24h at room temperature (23 °C).

Afterwards, for further physicochemical investigation samples were either removed from 3D molds, frozen at −26 °C and lyophilized using BETA 2–8 LCSplus *(Martin Christ, Germany)* apparatus for 72h at −85 °C, or used directly depending on the analysis protocol (see main text).

For evaluation of sterile ε-PL/HA hydrogel series (ster ε-PL/HA

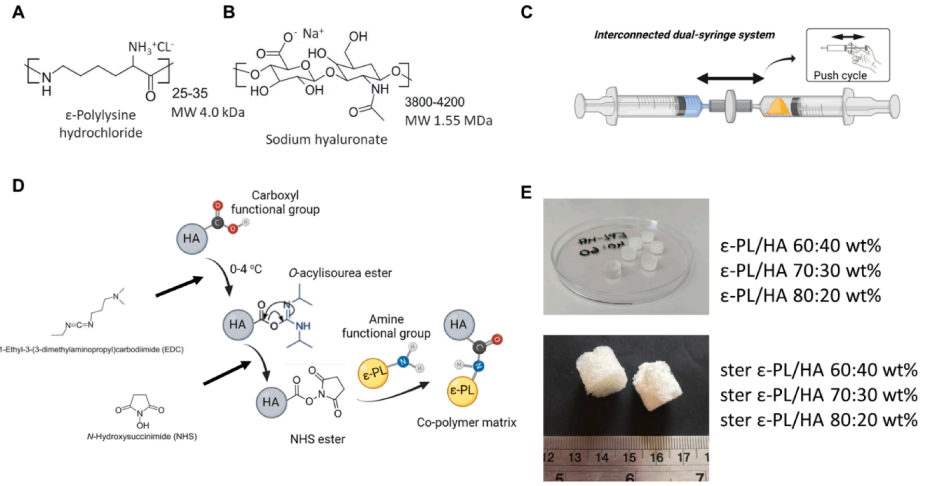

Fig. 1. Scheme depicting synthesis of chemically cross-linked ε-PL/HA hydrogels. (A) Structure of ε-PL; (B) Structure of HA; (C) Interconnected syringe technique; (D) Chemical cross-linking mechanism via EDC/NHS mediated polymerisation; (E) ε-PL/HA hydrogels photos wet (up) and freeze-dried (down) and synthesized mass ratios (Figure created with BioRender.com).

Table 1
Designation and composition of the synthesized chemically crosslinked ε-PL/HA hydrogels.

Designation	ε-PL to HA mass ratio, wt %	ε-PL (-NH_2), mmol	HA (-COOH), mmol	EDC:NHS, mmol	Liquid volume, mL
Chemically cross-linked hydrogels					
ε-PL/HA 40:60 wt%	40:60	0.0319	0.000119	0.971:0.971	4.0
ε-PL/HA 50:50 wt%	50:50	0.0479	0.000119	0.971:0.971	4.0
ε-PL/HA 60:40 wt%	60:40	0.0718	0.000119	0.971:0.971	4.0
ε-PL/HA 70:30 wt%	70:30	0.0838	0.000119	0.971:0.971	4.0
ε-PL/HA 80:20 wt%	80:20	0.0958	0.000119	0.971:0.971	4.0
Physically cross-linked hydrogels					
phys ε-PL/HA 40:60 wt%	40:60	0.0319	0.000119	–	4.0
phys ε-PL/HA 50:50 wt%	50:50	0.0479	0.000119	–	4.0
phys ε-PL/HA 60:40 wt%	60:40	0.0718	0.000119	–	4.0
phys ε-PL/HA 70:30 wt%	70:30	0.0838	0.000119	–	4.0
phys ε-PL/HA 80:20 wt%	80:20	0.0958	0.000119	–	4.0
Sterilized chemically cross-linked hydrogels					
ster ε-PL/HA 60:40 wt%	60:40	0.0718	0.000119	0.971:0.971	4.0
ster ε-PL/HA 70:30 wt%	70:30	0.0838	0.000119	0.971:0.971	4.0
ster ε-PL/HA 80:20 wt%	80:20	0.0958	0.000119	0.971:0.971	4.0

60:40, ster ε-PL/HA 70:30, ster ε-PL/HA 80:20), hydrogel samples were extracted from molds and sterilized using tabletop pre-vacuum autoclave at 121 ° C for 20min under pressure of $P = 179.5$kPa (*ELARA11, Tuttnauer Europe b.v., the Netherlands*). After sterilisation, the sterilized hydrogels were chilled and used in further experiments following the same procedure as non-sterilized samples.

The physically cross-linked ε-PL/HA hydrogels were used exclusively in the investigation by small angle X-ray scattering (SAXS), and the synthesis procedure is described in supporting information (S1.1). The fabricated HA/ε-PL hydrogel series used in this study are summarized in Table 1.

2.3. Characterization techniques

2.3.1. Topology of hydrogels by small angle X-ray scattering (SAXS)

Small Angle X-ray Scattering was performed at beamline B21, at Diamond Light Source, UK (Cowieson et al., 2020). Samples were loaded into MPS sticks enclosed with Kapton tape and loaded into the MPS sample cell (Edwards-Gayle et al., 2021). Details of experimental set up and used fitting models can be found in the Supporting Information and in the provided references (Cowieson et al., 2020; Edwards-Gayle et al., 2021).

2.3.2. The molecular structure

The molecular structure of the freeze-dried HA/ε-PL hydrogel samples was investigated by Fourier transform infrared spectroscopy (FTIR) using Varian FTS 800 FT-IR Scimitar Series spectrometer (*Varian Inc., Palo Alto, California, USA*) equipped with a GladiATR™ monolithic diamond ATR (*PIKE Technologies, Madison, Wisconsin, USA*). For spectra collection, the lyophilized ε-PL/HA hydrogel samples were grounded into a fine powder using a Mini-Mill PULVERISETTE 23 (*FRITCH, Idar-Oberstein, Germany*) ball mill. The spectra were collected in the mid-infrared range between 400 and 4000 cm^{-1} at a resolution of 4 cm^{-1} by co-adding 50 scans. Background air spectrum with no sample in the infrared beam was acquired before the collection of the sample spectrum (Salma-Ancane et al., 2022; Sceglovs & Salma-Ancane, 2020). Obtained spectra were normalized in the range from 0 (minimal value) to 1 (maximal value) by default algorithm of OriginPro 2020 v9.0 by analysing raw absorbence intensities, similar to our previous protocol (Salma-Ancane et al., 2022).

2.3.3. The phase composition

The phase composition of the lyophilized ε-PL/HA hydrogel samples was evaluated by X-ray powder diffractometry (XRD) using PANalytical X-Pert PRO MPD (*Panalytical, Almelo, the Netherlands*) X-ray diffractometer with a Cu Kα radiation (produced at 40kV and 30mA). Diffraction data were collected in a 10–70 °2θ range, with a step size of 0.05 °2θ and time per step of 2.5s. For a recording of X-ray diffraction patterns, the lyophilized ε-PL/HA hydrogel samples were grounded into a fine powder using a Mini-Mill PULVERISETTE 23 *(FRITCH, Idar-Oberstein, Germany)* ball mill (Salma-Ancane et al., 2022).

2.3.4. Morphology

The morphology of ε-PL/HA hydrogels was obtained by scanning electron microscopy (SEM) method. Micrographs at different magnifications were obtained using field emission SEM apparatus TESCAN "Mira/LMU" *(Tescan Orsey Holding, Czech Republic)* at an acceleration voltage of 3–7kV. For microscopy, the samples were fixed on a standard aluminium pin stub with electrically conductive double-sided adhesive carbon tape. Each sample was sputter coated with a 15nm thin gold layer before imaging using Emitech K550X (*Quorum Technologies, Ashford, Kent, United Kingdom*) sputter coater. To analyse pore size distributions in all obtained hydrogels, ImageJ® software was used.

2.3.5. Gel fraction

To determine insoluble/hydrogel content in obtained samples, the initial weight was measured directly after lyophilization. The hydrogel sample was soaked in 200mL of deionized water for 48h at room temperature and freeze-dried. Then hydrogel weight was determined, and gel fraction value was measured according to Eq. (1) (Gulrez et al., 2011; Salma-Ancane et al., 2022; Sceglovs & Salma-Ancane, 2020):

$$\mathbf{GF}\% = \left(\frac{\boldsymbol{Wi}}{\boldsymbol{Wd}}\right) \times 100(\%) \quad (1)$$

where W_d is the weight of the dried initial sample and W_i is the weight of the dried insoluble part after extraction. Three replicates from each group of hydrogels were used in this experiment and results are presented as average value ± standard deviation.

2.3.6. Swelling behaviour

The swelling behaviour of fabricated hydrogels was determined in deionized water (DI). Hydrogel samples were used in wet form without freeze-drying. After 24h at room temperature according to preparation protocol, hydrogels were taken out of 3D molds and used for further experimental steps. Firstly, the hydrogel sample was weighed to obtain the initial wet sample weight of W_0. In the next step, the pre-weighed hydrogel sample was immersed in 100mL DI and incubated under stirring at 60 RPM and 37°C. At different time points (1; 2; 4; 8; 24h) weight of swollen hydrogel (W_s) was measured. An excess amount of water was gently removed from swollen hydrogel surface with filter paper. The swelling capacity ($Sw_{\%}$) of hydrogel was calculated using the equation below Eq. (2) (Gulrez et al., 2011):

$$\mathbf{Sw}\% = \frac{\boldsymbol{Wo} - \boldsymbol{Ws}}{\boldsymbol{Wo}} \times 100\% \quad (2)$$

Three replicates from each ε-PL/HA hydrogel composition were used for described study and results are presented as the mean value ± standard deviation.

2.3.7. Oscillatory rheology

To perform oscillatory rheology, Thermo HR-20 Hybrid rheometer from TA Instruments (*USA*) was used. For rheological studies of sterilized and non-sterilized ε-PL/HA hydrogel samples with different mass ratios, amplitude and frequency sweep tests were chosen. In both cases, a 25mm parallel plate with a gap in the range 2.5–2.7mm was used. To avoid sample evaporation, silicone oil was gently applied around the sample, and a humidity control trap was used. Before each measurement, each sample was left to relax for 180s. For sample loading, following steps were used: firstly, after synthesis, samples were immediately extruded into custom molds ($\phi = 25$mm, $H = 2$mm) and pressed with a 25mm flat metal tablet under its own weight. Secondly, obtained hydrogel samples with a 25mm diameter were left for 24 h Finally, for rheological studies, non-sterilized samples were carefully placed under a parallel plate with a spatula, and then a parallel plate was moved towards the hydrogel sample slowly to avoid sample disruption. As for sterilized samples, the previously described steam sterilisation approach was used, then samples were left for 30min to cool down at 25°C, and further steps were kept as for the non-sterilized samples. Amplitude sweep studies were done in oscillatory mode at a constant frequency of 1Hz and temperature of 25°C. During the test, amplitude strain modulus changed logarithmically in the range from 0.01 to 1000%. As for frequency sweep, tests were performed in oscillatory mode at constant temperature of 25°C and at an amplitude strain at 0.2% within the linear viscoelastic regime, as originally established for all samples during the first amplitude measurements. In both measurements, each measured point was held at each strain/frequency until a stable reading was reported by the instrument. All measurements were repeated three times to ensure reproducibility.

2.3.8. Sterilisation efficiency test

To prove the steam sterilisation approach's efficiency used in this study, a broth microdilution study was used against Gram-positive (Gram+) ATCC© 25,923™ *Staphylococcus aureus* (*S.aureus*) and Gram-negative (Gram-) ATCC© 25,922™ *E. coli* (*E.coli*) bacteria strains. The experiment was designed based on modified CLSI and EUCAST standard protocols. ε-PL/HA hydrogels with a mass ratio of 70:30 wt% were prepared using the methodology described in section 1.2. Bacterial suspensions of McFarland 0.5 (corresponds to 1.5×10^8 CFU•mL^{-1}) were prepared with densitometer DEN-1 (*Biosan Ltd., Latvia*) in saline solution with the addition of lysogeny broth (LB) 1:1 and ε-PL/HA hydrogel. The final concentration of bacteria after repeated calculation of dilution was 7.5×10^7 CFU•mL^{-1}. Three replicates were used in each experimental group. Experimental groups consist of positive control (LB media + sterilisation), hydrogels group (suspension of LB media/bacteria + hydrogel sample + sterilisation) and negative control (suspension LB media/bacteria). After the preparation of solutions, tubes were placed in an autoclave under the temperature and pressure conditions described previously. After the sterilisation cycle, suspensions were inoculated on TSA plates and placed in CO_2 incubator ICO-150 (*Memmert GmbH + Co.KG, Germany*) for 24h at 37°C. The next day, plates were removed from the incubator, and remaining bacteria colonies were counted using the automatic colony counter SCAN-300 (*Interscience, France*).

2.3.9. Determination of antibacterial activity by plate counting method

The experimental procedure was performed according to the protocol as described in section 1.3.8. Bacterial suspensions of *E.coli* and *S. aureus* were prepared in 10mL glass tubes with saline solution and lysogeny broth at a concentration corresponding to McFarland 0.5 (1.5×10^8 CFU•mL^{-1}). Sterilized ε-PL/HA hydrogel samples of different compositions were placed in tubes with 2.0mL of bacteria suspension and incubated at 60 RPM for 24h at 37°C. After 24h 10 μL of bacterial suspension *inoculum* from each tested tube were transferred on separate TSA plates and distributed on agar surfaces. Afterwards, TSA plates were repeatedly incubated using the same conditions. In the last step, TSA plates were removed from the incubator and surviving colonies were counted. Three replicates were used from each hydrogel composition. The results are presented as the logarithmic reduction ($Log_{10}A - Log_{10}B$) ± standard deviation, where $Log_{10}A$ is the logarithmic value of initial bacteria concentration and $Log_{10}B$ is the logarithmic value of the concentration of bacteria after 24h contact with sample.

2.3.10. Statistical analysis

For all experiments, unless otherwise stated, three replicates were used from each ε-PL/HA hydrogel mass ratios in each experiment. Results are shown as average value ± standard deviation (SD). To perform statistical significance one- or two-way analysis of variance (Anova) with Tukey's multiple comparisons were used during the proceeding process. A statistically significant results were considered as of $p<0.05$ (ns - >0.05, * - <0.05, ** - <0.01, *** - <0.005 and **** - <0.001). To obtain statistical analysis IBM SPSS Statistics 23 software was used.

3. Results and discussion

3.1. Topological differences in physically versus chemically crosslinked hydrogels

Initially SAXS was used to examine the cross-linked structure and topology of all of the fabricated hydrogels, in the q-range (0.045 nm^{-1} - 0.233 nm^{-1}) covering only the Porod region of the hydrogel-like structures (27 – 140nm of real *d* space). Thus, only surface information on the gel structure could be obtained from this method, as evaluated from power law fits. In Fig. S1A,B, the SAXS patterns obtained for physically (Fig. S1A) and chemically (Fig. S1B) crosslinked hydrogels at various ε-PL to HA ratios are presented as double logarithmic plots. The calculated q-decay (Table S1) was used to examine the surface changes due to either physical or chemical cross linking. For high concentration HA control solution, scattering intensity decreased $\sim q^{-3.9} \approx q^{-4}$, indicating behaviour typical of large clusters with smooth interfaces for polyelectrolyte complexes (Porod, 1982). For all physically crosslinked gels, scattering intensities decrease $\sim q^{-2.9\pm0.6}$ behaviour typical of aggregated clusters with rough interfaces (Porod, 1982), whereas for chemically crosslinked hydrogels scattering intensities decreases $\sim q^{-3.6\pm0.4}$, indicating smoother Porod surface. This goes in line with the expected topological results for chemically crosslinked networks with smooth interfaces held by more robust covalent bonds, as compared to propagating roughness due to occurrence of the physical interactions in physical hydrogels. For both physically and chemically crosslinked hydrogels, we observed that as the proportion of ε-polylysine increased in both gels, the *n* exponent decreased with lowest values reported for 60:40 wt% (in chemically crosslinked gels) and 70:30 wt% (in physically crosslinked gels) and then returned to a highest value at ε-PL/HA 80:20 wt% ratio (Table S1). For chemically crosslinked hydrogels with mass ratios of 60:40, 50:50 and 80:20 wt% the *n* exponent was relatively close ($n = 3.7\pm0.3$), indicating overall similar types of crosslinked structures. As such and based on the fact that chemically crosslinked hydrogels

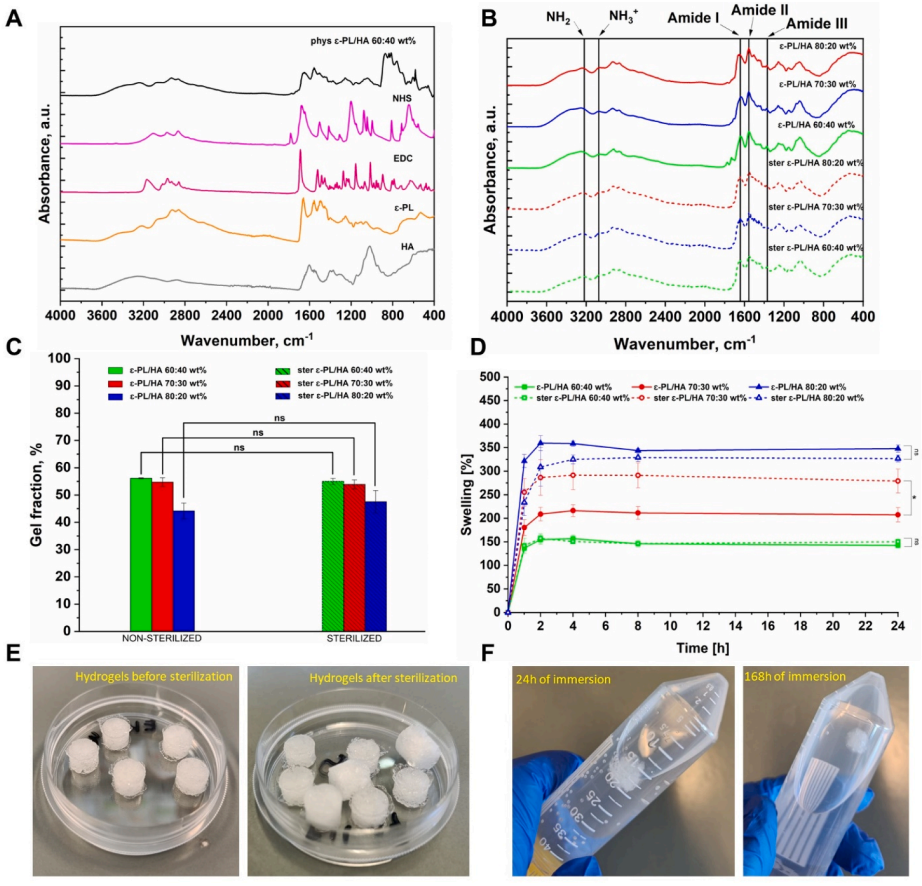

Fig. 2. Characterization of ε-PL/HA hydrogels. (A) FT-IR spectra of phys ε-PL/HA hydrogel and starting materials; (B) FT-IR spectra of sterilized and non-sterilized ε-PL/HA hydrogels; (C) Gel fraction values and (D) Swelling behaviour curves of the ε-PL/HA hydrogels. (E-F) Photographs represent hydrogels prepared in different, as specified, conditions.

constitute interesting stable antimicrobial materials (Salma-Ancane et al., 2022), we selected a series of ε-PL to HA hydrogels with mass ratios of 60:40, 70:30 and 80:20 wt% to further investigate the exact effects on molecular and structural aspects as a function of applied sterilisation.

3.2. Physicochemical characterization of chemically crosslinked hydrogels

3.2.1. Molecular structure

The effect of steam sterilisation on the composite hydrogels was investigated with FT-IR (Fig. 2A and B). Besides, FT-IR was taken for pure ε-PL, HA, EDC, NHS, as well as physically cross-linked ε-PL/HA 60:40 wt% hydrogels prepared in the same way as chemically cross-linked but without the addition of EDC and NHS crosslinking agents (see supporting methods S1.1. and Table1). The primary data processing showed similar trends as described in our previous study (Salma-Ancane et al., 2022). The absorption bands at 1640–1650 cm^{-1} (Amide I, C = O stretching vibrations), 1558–1605 cm^{-1} (Amide II, N—H bending vibrations), 1320–1325 cm^{-1} (Amide III) and 1157–1205 cm^{-1} (C—O-C group) were assigned to HA, respectively (Gilli et al., 1994; Haxaire et al., 2003). The absorption bands at 1671 cm^{-1}, 1565 cm^{-1}, 1384 cm^{-1} were assigned to the vibrational modes of Amide I (C = O stretching vibrations), Amide II (N—H bending vibrations, C—N stretching vibrations), and Amide III bands from ε-PL, respectively (Chen et al., 2019; Lv et al., 2020; Rozenberg & Shoham, 2007; Sequeira et al., 2018).

Overall, for all ε-PL/HA hydrogel samples, the higher values of calculated ratios of absorbence intensities between Amide I to Amide II (I_{1645}/I_{1558}) and Amide I to Amide III (I_{1645}/I_{1398}) bands, as well the indicative shifts corresponding to C = O stretching vibration, C = O—NH bond vibration, and C—N bond vibration, in comparison to phys ε-PL/HA 60:40 wt%, were associated with the covalent linkage formation (Table. 2 The I_{1645}/I_{1558} ratio remained similar for all ε-PL/HA samples, with values 0.85± 0.02, similar to the ratio obtained in our previous work of 0.87 for all chemically functionalized ε-PL/HA hydrogels (Salma-Ancane et al., 2022). The calculated lower values of I_{1645}/I_{1558} ratios of all ε-PL/HA hydrogels in comparison with phys ε-PL/HA 60:40 wt% indicate that all side N–H vibrations are suppressed and reveal formation of covalent bonding. The fact that these ratios slightly increase to 0.88± 0.01 upon sterilisation, indicates minimal changes occur to the formed covalent bonding and overall structural features are preserved (Fig. 2B).

The NH_3^+/NH_2 ratio (I_{3062}/I_{3228}), indicative of the number of free lysine residues, was calculated from normalized FT-IR data. It was found that ratio has been consistently increasing as a function of feeding ratio of ε-PL, with similar values of 0.85 for ε-PL/HA 60:40 wt% and 0.83 for ε-PL/HA 70:30 wt%, and higher value of 1.03 for ε-PL/HA 80:20 wt%. However, these ratios have considerably increased for all three studied ε-PL/HA hydrogel samples upon sterilisation (Table 2). The increase of NH_3^+/NH_2 ratio most probably might be associated rather with hydrolysis or with partial depolymerization of free-uncrosslinked HA chains which are highly sensitive to heating (Caspersen et al., 2014; Reháková et al., 1994; Szabó et al., 2013). Furthermore, it is reported that high thermal stability was observed for covalently crosslinked hydrogels via EDC/NHS chemistry (Skopinska-Wisniewska et al., 2021; Usha et al., 2012). As we will discuss later, the fact that molecularly more NH_3^+ groups are present after steam sterilisation does not significantly impede the structural properties of the formed gels. However, it arguably

Table 2
Comparison of calculated absorbence ratios from FT-IR curves.

Sample	I_{1645}/I_{1558} (Amide I to Amide II)	I_{1645}/I_{1398} (Amide I to Amide III)	I_{3062}/I_{3228}(NH_3^+ to NH_2)
Current work			
ε-PL/HA 60:40 wt%	0.87	1.62	0.85
ε-PL/HA 70:30 wt%	0.83	1.72	0.83
ε-PL/HA 80:20 wt%	0.83	1.64	1.03
ster ε-PL/HA 60:40 wt%	0.88	1.31	1.1
ster ε-PL/HA 70:30 wt%	0.89	1.43	1.03
ster ε-PL/HA 80:20 wt%	0.87	1.39	1.05
phys ε-PL/HA 60:40 wt%	1.08	1.44	0.86
Previous work (Salma-Ancane et al., 2022)			
chem ε-PL/HA 60:40 wt%	0.87	1.58	0.88
phys ε-PL/HA 60:40 wt%	1.17	1.39	0.89

contributes to the more pronounced antimicrobial properties, as we and others discussed before (Cardoso et al., 2021; Salma-Ancane et al., 2022), and as we will show in later sections.

3.2.2. X-ray diffraction

X-ray diffraction patterns (Fig. S2) revealed the characteristic of polymer amorphous "halo" for all ε-PL/HA hydrogel samples. For ε-PL/HA hydrogel samples at 32° and 45° additional crystalline phase of NaCl was detected as a result of a neutralization reaction between Na-HA and ε-PL•HCl, similarly to our previous work (Salma-Ancane et al., 2022). We further note that after sterilisation, we did not observe any remaining NaCl peaks, indicating that sterilisation helps with purifying the content, possibly due to solubilisation of remaining salts into the water phase.

3.2.3. Gel fraction

The gel fraction values for non-sterilized ε-PL/HA hydrogel samples with ε-PL to HA mass ratios of 60:40, 70:30 and 80:20 wt%, were 56.2± 0.2, 54.7± 1.6 and 44.2± 2.9%, respectively (Fig. 2C). These corresponded well to previously reported values of ~55% by us (Salma-Ancane et al., 2022), except the 80:20 wt% sample, which had significantly lower gel fraction. We ascribe this lower value to the lower extent of crosslinking for this ratio. Evidently, the larger amounts of free non-crosslinked ε-PL present (as observed by FTIR, Fig. 2B), were able to diffuse during immersion in water leading to decreasing gel fraction value as larger fraction of ε-PL dissolved compared to the total initial mass of the polymer content in the gel. The obtained gel fraction values for ster ε-PL/HA hydrogel samples with ε-PL to HA mass ratios of 60:40, 70:30 and 80:20 wt% were 55.0± 1.1, 53.9± 1.7 and 47.6± 4.1%, respectively (Fig. 2C). We observed no significant changes in gel fraction values between non-sterilized and sterilized hydrogel samples within the same ε-PL to HA mass ratio ($p>0.05$). This indicates that the steam sterilisation did not affect the overall extent of crosslinking in our samples, retaining original types of network topologies after synthesis.

3.2.4. Swelling capacity

Both non-sterilized and sterilized ε-PL/HA hydrogels demonstrated swelling higher than 100% after 2 h incubation time, and maintained the reached plateau values over the studied period (24 h, Fig. 2D). The swelling capacity increased with an increasing mass ratio of ε-PL in the non-sterilized hydrogel samples at 2 h, going from ~ 150% for the mass ratio of 60:40 wt%, to ~ 210% and 340% for 70:30 wt% and 80:20 wt%, respectively. These results complemented well the obtained gel fraction values and amounts of free non-crosslinked NH_3^+ groups, with higher gel fraction values relating to the higher crosslinking state and consequently to lower swelling capacity. The ster 60:40 wt% ε-PL/HA hydrogels showed the same swelling behaviour as non-sterilized ε-PL/HA hydrogel sample, while ster 80:20 wt% ε-PL/HA hydrogels showed some minimal changes in the swelling during first 8 h, as compared to the non-sterilized sample. For both formulations however, no significant differences were noted by 24 h ($p>0.05$). In contrast, the swelling capacity of ster ε-PL/HA hydrogels with ε-PL to HA mass ratio of 70:30 wt% increased from ~215% to ~290% ($p<0.05$), possibly indicating decreasing in mechanically active crosslinks. As variations were not detected with other characterization techniques, it is likely that the decrease is limited. Despite this noted difference, all ster ε-PL/HA hydrogels exhibited equilibrium swelling in the range 150–350% (ε-PL content dependant), achieved after 4 h incubation time under physiological conditions (37°C), demonstrating acceptable structural stability and cohesion properties for potential tissue engineering applications.

3.2.5. Morphology

Next, we used SEM to evaluate the impact of steam sterilisation on the morphology of the freeze-dried ε-PL/HA hydrogels (Fig. 3). All samples showed a homogeneous three-dimensional network with interconnected porosity, with minimal effects visible for all hydrogels after sterilisation. General obtained pore size ranges fitted well our previously obtained values with overall pore ranges plotted as log normal distributions and noted in graph insets in Fig. 3. Furthermore, pore sizes after sterilisation for each ratio remained in the similar range, except the 60:40 wt% ε-PL/HA (Table 3.). We also noted that distribution of pores was a function of the ε-PL to HA ratio, with largest pores observed for 60:40 wt% ε-PL/HA hydrogels (193± 103μm), and similar lower distribution of pores for 70:30 (69± 34μm) and 80:20 wt% (84± 61μm) ε-PL/HA hydrogels. Finally, we note that the measurements utilising SEM method are prone to hold artefacts due to drying effects and hence should be taken with cautious.

3.2.6. Oscillatory rheology

The rheological properties of the prepared ε-PL/HA hydrogels as a

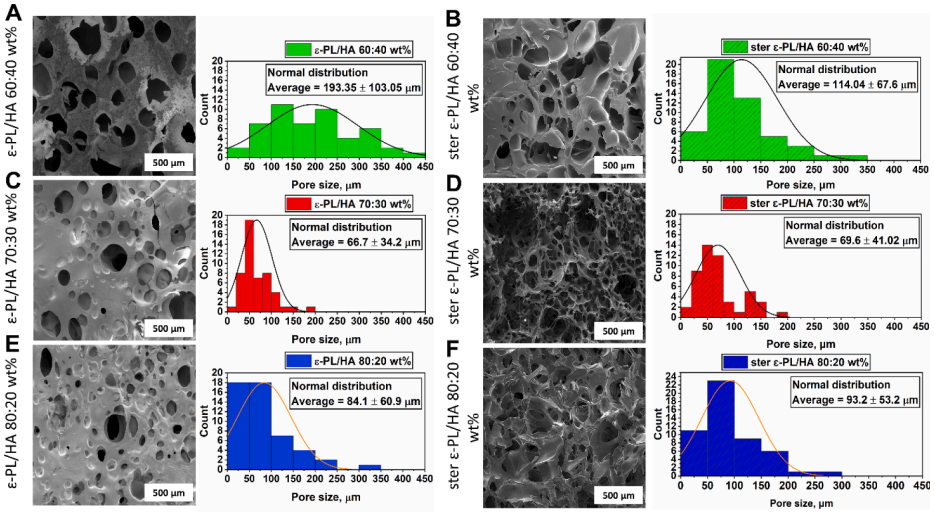

Fig. 3. (A–F) SEM microphotographs and analysis of pore distribution of freeze-dried non-sterilized (A, C, E) and sterilized ε-PL/HA hydrogels (B, D, F).

Table 3
Results of ANOVA with Tukey's multiple comparison test of pore distribution between experimental groups presented in Fig. 3. Results are presented as p values of statistical significance (ns - >0.05, * - <0.05, ** - <0.01, *** - <0.005 and **** - <0.001). Grey shaded parts were either self-pairs or pairs excluded from the statistical comparison.

Sample	ε-PL/HA 70:30 wt%	ε-PL/HA 80:20 wt%	ster ε-PL/HA 60:40 wt%	ster ε-PL/HA 70:30 wt%	ster ε-PL/HA 80:20 wt%
ε-PL/HA 60:40 wt%	****	****	****		
ε-PL/HA 70:30 wt%		*		NS	
ε-PL/HA 80:20 wt%	*				NS
ster ε-PL/HA 60:40 wt%				****	NS
ster ε-PL/HA 70:30 wt%	NS		****		*

function of different mass ratios and sterilisation are illustrated in Fig. 4. Firstly amplitude sweeps were carried out on non-sterilized (Fig. 4A) and sterilized ε-PL/HA hydrogels (Fig. 4B). Indeed, all studied hydrogel ratios, 60:40, 70:30 and 80:20 wt%, showed soft solid-like behaviour with G' > G" in the linear viscoelastic regime (LVR) of strain up until ~ 1%, in both non-sterilized and sterilized cases. Upon sterilisation, two phenomena were observed: (i), the crossover and transition point (G' = G") has shifted from a strain of ε ≈ 90% for non-sterilized samples to ε ≈ 70% for sterilized samples, and (ii) the apparent ε-PL/HA ratio dependant values of G" in non-sterilized case have all come together to display similar behaviour in the sterilized samples, irrespective of the sample composition. This implies that sterilisation has partly affected the overall hydrogel structure and its network topology, driven by the partial loss of physical entanglements in hydrogel structure that were formed by free and non-cross-linked ε-PL with remaining negatively charged HA functional groups.

The frequency dependant behaviour of non-sterilized gels matched the data previously obtained by us (Fig. 4C, (Salma-Ancane et al., 2022)). As we previously noted and here as well, G" of non-sterilized samples started to increase above a critical $f \approx 10$Hz, until finally reaching a crossover (G' = G") point around $f = 100$Hz (Fig. 5C, (Salma-Ancane et al., 2022)). Sterilisation has amended this behaviour in all formulations, affecting primarily the G" response of all tested gels at higher frequencies (> 10Hz, Fig. 4D). The observed major changes in G" upon sterilisation relate to the shift of interactions between water molecules and polymer chains. It could be that higher availability of free NH_3^+ functional side groups after sterilisation may lead to increased H-bonding with surrounding water molecules, and thus lesser extent of

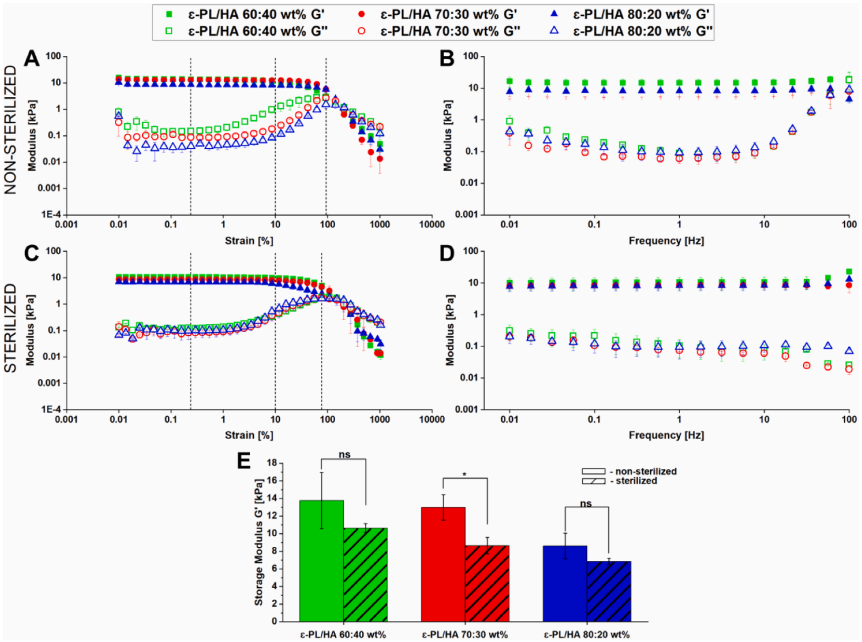

Fig. 4. Oscillatory rheology. A.C. Amplitude sweep; B.D. Frequency sweep of sterilized/non-sterilized ε-PL/HA hydrogels; E. Comparison of extracted storage modulus from amplitude sweep curves at 1Hz and 0.2% strain.

dissipated energy via polymer-water interactions (hence lower loss moduli G" at both lower strains (Fig. 4B) and at higher frequencies (Fig. 4D). Finally, we noted no significant differences between the extracted G' of both non-sterilized and sterilized hydrogels at 1Hz and at ε=0.2% for 60:40 and 80:20 wt% mass ratio ε-PL/HA ($p>0.05$), however there was significant difference for the 70:30 wt% sample ($p<0.05$) (Fig. 4E). In this case, the stiffness values went from 13.0± 1.4 to 8.6± 0.9kPa and correlated well to the significant change in swelling capacity for this ratio. Overall the properties of all sterilized hydrogels were largely similar to the non-sterilized. Overall structure of sterilized hydrogels remains stable in both viscous and elastic regions. We also note that the storage modulus in the range of 5–15kPa is within requirements for different applications in tissue engineering (Salma-Ancane et al., 2022; Xu et al., 2022; Xue et al., 2022).

3.2.7. Sterilisation efficiency test

To validate efficiency of the chosen steam sterilisation method, we purposely inoculated two bacteria strains (separately into independent tubes with lysogeny broth): *E.coli* as Gram-negative and *S.aureus* as Gram-positive bacteria, then placed the ε-PL/HA 70:30 wt% hydrogel samples of prior to the test and counted the bacteria colonies after further inoculation and 24h of incubation time. We noted that the sterilisation approach used in this work successfully eradicated all used Gram-negative and Gram-positive bacteria (Table 4), giving the same result as positive control, *i.e.* non-bacteria contaminated lysogeny broth (LB) subjected to the sterilisation. As expected, without sterilisation, bacteria started to grow in prepared suspension (negative control) and expanded in their colonies within 24h after inoculation on TSA plate. Given the effectiveness of sterilisation protocol, in next section we will describe direct contact between bacteria and sterilized hydrogels to evaluate their antibacterial efficiency.

3.2.8. Determination of antibacterial activity by plate counting method

To prove the antibacterial capability of the developed ε-PL/HA hydrogels, the bactericidal activities were studied using plate counting method for 24h against the same Gram+ and Gram- bacteria as mentioned in the previous section (again, in separately cultured strains with each hydrogel). As shown in Table 5, the sterilized ε-PL/HA hydrogels with all ε-PL to HA mass ratios led to 3–4 log bacteria reduction after 24 h As expected, for both Gram+ and Gram-, the extent of bacterial culture reduction was increased for the hydrogels with the increased amount of ε-PL. ε-PL has been reported to irreversibly form complexes with Gram- bacteria (*e.g. E.coli*) cell wall molecules, thus increasing cell membrane permeability and decreasing cell wall integrity (Hyldgaard et al., 2014; Zarrintaj et al., 2021). In the case of Gram+ bacteria (*S.aureus*), it is hypothesized, that the bactericidal effect is achieved by endocytosis of ε-PL molecules and further involvement in several metabolic pathways of bacteria (Tan et al., 2019; Zarrintaj et al., 2021). Due to many limitations and intracellular nature of the pathways, the ε-PL effects are less pronounced, but still evident for the 70:30 and 80:20 wt% hydrogels as compared to the 60:40% one (Table 6). The overall extent of the log reduction indeed exceeded those reported by us previously (Salma-Ancane et al., 2022), indicating that generating sterile and functioning 80:20 wt% ε-PL/HA hydrogels with higher antimicrobial efficiency is possible and offers a viable biomaterial that could be implemented in various future tissue engineering applications.

Table 5
Evaluation of antibacterial activity of the ster ε-PL/HA hydrogels. Initial seeded bacteria concentration was 1.5×10^8 CFU•mL^{-1} in each case.

Hydrogel sample	Log_{10}(CFU) Initial	ΔLog_{10}(CFU) Reduction bacteria reduction ± standard deviation	
		E.coli	*S.aureus*
ster ε-PL/HA 60:40 wt%	8.18	3.77± 0.22	3.33± 0.28
ster ε-PL/HA 70:30 wt%	8.18	4.22± 0.18	3.95± 0.31
ster ε-PL/HA 80:20 wt%	8.18	6.16± 0.95	4.06± 0.19

4. Conclusions

In summary, here we developed a series of covalently cross-linked and antibacterial hydrogels from ε-polylysine and hyaluronic acid. Steam sterilisation showed minimal impact on physico-chemical features of prepared hydrogels samples, including molecular make-up as revealed by the absorbence intensities between Amide I to Amide II (I_{1645}/I_{1558}). However, values of calculated ratios of absorbence intensities between the protonated side-chain NH_3^+ groups and unprotonated NH_2 groups of ε-polylysine NH_3^+/NH_2 (I_{3062}/I_{3228}) ratio increased in the sterilized samples, indicating higher amount of inherent antibacterial NH_3^+ side groups in the sterilized hydrogels. Gel fraction values between non-sterilized and sterilized hydrogel samples remained similar, indicating that the overall extent of crosslinking and network was preserved after sterilisation. All sterilized hydrogels reached swelling equilibrium within the first 4h under physiological conditions at 37°C and demonstrated high swelling capacity in the range of 150–350%. Interconnected porosity for all hydrogel samples were largely unaffected after steam sterilisation. Oscillatory rheology results revealed that steam sterilisation decreased loss moduli G" at lower strains and at higher frequencies for all sterilized samples, confirming higher availability of free NH_3^+functional side groups after sterilisation and an increase in H-bonding with surrounding water molecules. Overall, the mechanical properties of all sterilized hydrogels were almost unaffected, with storage modulus in the range of 5–15kPa. With antibacterial studies, we validated the steam sterilisation efficiency on the developed hydrogels, as well as confirmed that hydrogels provided pronounced antibacterial activity against Gram-negative and Gram-positive bacterial strains.

Here, for the first time, we confirmed that steam sterilisation minimally affected the molecular make-up and structure of the covalently cross-linked ε-polylysine/hyaluronic acid hydrogels. By controlling the feeding ratio of two components (ε-polylysine to hyaluronic acid) and their overall polymer content, we demonstrated possibilities of tuning final physicochemical and *in vitro* antibacterial properties. The presented research is a step forward for the clinical translation of the developed inherent antibacterial ε-PL/HA hydrogels for various tissue engineering applications. Our research study brings an expanded methodology of evaluating soft biomaterials after sterilisation, highlighting the importance of evaluating the effects of sterilization in developing new soft biomaterials.

Table 4
Experimental groups and results for microbiology studies.

Group	Bacteria	Initial bacteria concentration, CFU•mL^{-1}	ε-PL/HA 70:30 wt% hydrogel	Sterilisation	Survived bacteria concentration, CFU•mL^{-1}
Positive control (LB media)	–	0	No	Yes	0
ε-PL/HA 70:30 wt% hydrogel	*E.coli*	7.5×10^7	Yes	Yes	0
	S.aureus				
Negative control (LB+bacteria)	*E.coli*	7.5×10^7	No	No	$2.0–4.0\times 10^8$
	S.aureus				

Table 6
Results of ANOVA with Tukey's multiple comparison test of antibacterial activity between experimental groups presented in Table 6. Red colour refers to E.coli and blue colour refers to S.aureus. Results are presented as p values of statistical significance (ns - >0.05, * - <0.05, ** - <0.01, *** - <0.005 and **** - <0.001). Grey shaded parts represent self-pair excluded from the statistical comparison.

Sample	ster ε-PL/HA 70:30 wt%	ster ε-PL/HA 80:20 wt%
ster ε-PL/HA 60:40 wt%	*	**
	*	*
ster ε-PL/HA 70:30 wt%		*
		NS

Funding sources and acknowledgments

The authors acknowledge financial support from the Latvian Council of Science research project No. lzp-2020/1–0072 "Injectable bioactive biocomposites for osteoporotic bone tissue regeneration (inBioBone)" and the European Union's Horizon 2020 research and innovation programme under the grant agreement No. 857287 (BBCE – Baltic Biomaterials Centre of Excellence). J. K. W. gratefully acknowledges the European Union's Horizon 2020 (H2020-MSCA-IF-2019) research and innovation programme under the Marie Skłodowska-Curie grant agreement 893099 — ImmunoBioInks, as well as the Diamond Light Source for the award of beamtime SM29767.

CRediT authorship contribution statement

Artemijs Sceglovs: Conceptualization, Resources, Writing – original draft, Methodology, Validation, Writing – review & editing. **Jacek K. Wychowaniec:** Writing – review & editing, Methodology, Validation, Formal analysis, Investigation, Supervision. **Ingus Skadins:** Methodology, Validation, Formal analysis, Investigation. **Aigars Reinis:** Methodology, Validation, Formal analysis, Investigation. **Charlotte J.C. Edwards-Gayle:** Methodology, Validation, Writing – review & editing. **Matteo D'Este:** Supervision, Resources, Methodology, Writing – review & editing. **Kristine Salma-Ancane:** Conceptualization, Supervision, Writing – review & editing, Funding acquisition.

Declaration of competing interest

The authors declare that they have no known competing financial interests or personal relationships that could have appeared to influence the work reported in this paper.

Data availability

Data will be made available on request.

Supplementary materials

Supplementary data associated with this article can be found, in the online version, at 10.1016/j.carpta.2023.100363.

References

Aliakbar Ahovan, Z., Esmaeili, Z., Eftekhari, B. S., Khosravimelal, S., Alehosseini, M., Orive, G., et al. (2022). Antibacterial smart hydrogels: New hope for infectious wound management. *Materials Today Bio, 17*. https://doi.org/10.1016/J.MTBIO.2022.100499

Cardoso, P., Glossop, H., Meikle, T. G., Aburto-Medina, A., Conn, C. E., Sarojini, V., et al. (2021). Molecular engineering of antimicrobial peptides: Microbial targets, peptide motifs and translation opportunities. *Biophysical Reviews, 13*(1), 35–69. https://doi.org/10.1007/S12551-021-00784-Y. *2021 13:1*.

Caspersen, M. B., Roubroeks, J. P., Liu, Q., Huang, S., Fogh, J., Zhao, R., et al. (2014). Thermal degradation and stability of sodium hyaluronate in solid state. *Carbohydrate Polymers, 107*(1), 25–30. https://doi.org/10.1016/J.CARBPOL.2014.02.005

Catoira, M. C., Fusaro, L., Di Francesco, D., Ramella, M., & Boccafoschi, F. (2019). Overview of natural hydrogels for regenerative medicine applications. *Journal of Materials Science: Materials in Medicine, 30*(10), 1–10. https://doi.org/10.1007/S10856-019-6318-7

Chen, J., Liu, H., Xia, Z., Zhao, X., Wu, Y., & An, M. (2019). Purification and structural analysis of the effective anti-TMV compound ε-Poly-L-lysine produced by streptomyces ahygroscopicus. *Molecules, 24*(6). https://doi.org/10.3390/MOLECULES24061156. Basel, Switzerland.

Chen, Q., He, Y., Li, Q., Yang, K., Sun, L., Xu, H., et al. (2023). Intelligent design and medical applications of antimicrobial hydrogels. *Colloid and Interface Science Communications, 53*, Article 100696. https://doi.org/10.1016/J.COLCOM.2023.100696

Chen, S., Huang, S., Li, Y., & Zhou, C. (2021). Recent Advances in Epsilon-Poly-L-Lysine and L-Lysine-Based Dendrimer Synthesis, Modification, and Biomedical Applications. *Frontiers in Chemistry, 9*, 169. https://doi.org/10.3389/FCHEM.2021.659304

Correa, S., Grosskopf, A. K., Lopez Hernandez, H., Chan, D., Yu, A. C., Stapleton, L. M., & Appel, E. A. (2021). Translational Applications of Hydrogels. *Chemical Reviews, 121*(18), 11385–11457. https://doi.org/10.1021/ACS.CHEMREV.0C01177

Cowieson, N. P., Edwards-Gayle, C. J. C., Inoue, K., Khunti, N. S., Doutch, J., Williams, E., et al. (2020). Beamline B21: High-throughput small-angle X-ray scattering at diamond light source. *Journal of Synchrotron Radiation, 27*(5), 1438–1446. https://doi.org/10.1107/S1600577520009960/HTTPS://JOURNALS.IUCR.ORG/SERVICES/RSS.HTML

Dai, Z., Ronholm, J., Tian, Y., Sethi, B., & Cao, X. (2016). Sterilisation techniques for biodegradable scaffolds in tissue engineering applications. *Journal of Tissue Engineering, 7*. https://doi.org/10.1177/2041731416648810

Dovedytis, M., Liu, Z. J., & Bartlett, S. (2020). Hyaluronic acid and its biomedical applications: A review. *Engineered Regeneration, 1*, 102–113. https://doi.org/10.1016/j.engreg.2020.10.001

Edwards-Gayle, C. J. C., Khunti, N., Hamley, I. W., Inoue, K., Cowieson, N., & Rambo, R. (2021). Design of a multipurpose sample cell holder for the Diamond Light Source high-throughput SAXS beamline B21. *Journal of Synchrotron Radiation, 28*, 318–321. https://doi.org/10.1107/S1600577520013831

Galante, R., Pinto, T. J. A., Colaço, R., & Serro, A. P. (2018). Sterilisation of hydrogels for biomedical applications: A review. *Journal of Biomedical Materials Research Part B: Applied Biomaterials, 106*(6), 2472–2492. https://doi.org/10.1002/JBM.B.34048

Gilli, R., Kacuráková, M., Mathlouthi, M., Navarini, L., & Paoletti, S. (1994). FTIR studies of sodium hyaluronate and its oligomers in the amorphous solid phase and in aqueous solution. *Carbohydrate Research, 263*(2), 315–326. https://doi.org/10.1016/0008-6215(94)00147-2

Gulrez, S. K. H., Al-Assaf, S., Phillips, G. O., Gulrez, S. K. H., Al-Assaf, S., & Phillips, G. O. (2011). Hydrogels: Methods of preparation, characterisation and applications. *Progress in Molecular and Environmental Bioengineering - From Analysis and Modeling to Technology Applications*. https://doi.org/10.5772/24553

Han, X., Hung, H. C., Jain, P., Sun, F., Xu, X., Yang, W., et al. (2017). Sterilisation, hydration-dehydration and tube fabrication of Zwitterionic hydrogels. *Biointerphases, 12*(2), 02C411. https://doi.org/10.1116/1.4983502

Haxaire, K., Maréchal, Y., Milas, M., & Rinaudo, M. (2003). Hydration of polysaccharide hyaluronan observed by IR spectrometry. I. Preliminary experiments and band assignments. *Biopolymers, 72*(1), 10–20. https://doi.org/10.1002/BIP.10245

Huerta-ángeles, G., Nešporová, K., Ambrožová, G., Kubala, L., & Velebný, V. (2018). An effective translation: The development of hyaluronan-based medical products from the physicochemical, and preclinical aspects. *Frontiers in Bioengineering and Biotechnology, 6*(MAY), 62. https://doi.org/10.3389/FBIOE.2018.00062/BIBTEX

Hyldgaard, M., Mygind, T., Vad, B. S., Stenvang, M., Otzen, D. E., & Meyer, R. L. (2014). The antimicrobial mechanism of action of epsilon-poly-L-lysine. *Applied and Environmental Microbiology, 80*(24), 7758–7770. https://doi.org/10.1128/AEM.02204-14

Jia, B., Li, G., Cao, E., Luo, J., Zhao, X., & Huang, H. (2023). Recent progress of antibacterial hydrogels in wound dressings. *Materials Today Bio, 19*, Article 100582. https://doi.org/10.1016/J.MTBIO.2023.100582

Karajanagi, S. S., Yoganathan, R., Mammucari, R., Park, H., Cox, J., Zeitels, S. M., et al. (2011). Application of a dense gas technique for sterilizing soft biomaterials.

Biotechnology and Bioengineering, 108(7), 1716–1725. https://doi.org/10.1002/BIT.23105

Kennedy, S. M., Deshpande, P., Gallagher, A. G., Horsburgh, M. J., Allison, H. E., Kaye, S. B., & Williams, R. L. (2020). Antimicrobial Activity of Poly-epsilon-lysine Peptide Hydrogels Against Pseudomonas aeruginosa. *Investigative Ophthalmology & Visual Science, 61*(10). https://doi.org/10.1167/IOVS.61.10.18

Li, S., Dong, S., Xu, W., Tu, S., Yan, L., Zhao, C., et al. (2018). Antibacterial hydrogels. *Advanced Science, 5*(5). https://doi.org/10.1002/ADVS.201700527. Weinheim, Baden-Wurttemberg, Germany.

Liu, H., Chen, X. F., & Zhou, C. R. (2010). Preparation and Properties of Injectable Hydroxyapatite for Bone Repair Materials. *Key Engineering Materials, 434–435*, 590–593. https://doi.org/10.4028/www.scientific.net/kem.434-435.590

Li, H., Qi, Z., Zheng, S., Chang, Y., Kong, W., Fu, C., … Pan, S. (2019). The Application of Hyaluronic Acid-Based Hydrogels in Bone and Cartilage Tissue Engineering. *Advances in Materials Science and Engineering, 2019*, Article 3027303. https://doi.org/10.1155/2019/3027303

Lv, J. M., Meng, Y. C., Shi, Y. G., Li, Y. H., Chen, J., & Sheng, F. (2020). Properties of epsilon-polylysine·HCl/high-methoxyl pectin polyelectrolyte complexes and their commercial application. *Journal of Food Processing and Preservation, 44*(2), e14320. https://doi.org/10.1111/JFPP.14320

Meng, Z., He, Y., Wang, F., Hang, R., Zhang, X., Huang, X., & Yao, X. (2021). Enhancement of Antibacterial and Mechanical Properties of Photocurable ε-Poly- l -lysine Hydrogels by Tannic Acid Treatment. *ACS Applied Bio Materials, 4*(3), 2713–2722. https://doi.org/10.1021/ACSABM.0C01633

Peng, W., Lu, X., Wu, J., Wang, Y., Zhu, X., Ouyang, H., … Bao, J (2022). Autoclaving pHEMA-Based Hydrogels Immersed in Deionized Water has No Effect on Physicochemical Properties and Cell Behaviors. *ACS Omega, 7*(36), 32038–32045. https://doi.org/10.1021/ACSOMEGA.2C03096

Porod, G. (1982). General theory - small angle X-ray scattering. O.. K. O. Glatter. *Academic press*. Academic Press. https://doi.org/10.1021/jp106578f.

Reháková, M., Bakoš, D., Soldán, M., & Vizárová, K. (1994). Depolymerization reactions of hyaluronic acid in solution. *International Journal of Biological Macromolecules, 16*(3), 121–124. https://doi.org/10.1016/0141-8130(94)90037-X

Rozenberg, M., & Shoham, G. (2007). FTIR spectra of solid poly-L-lysine in the stretching NH mode range. *Biophysical Chemistry, 125*(1), 166–171. https://doi.org/10.1016/J.BPC.2006.07.008

Salma-Ancane, K., Sceglovs, A., Tracuma, E., Wychowaniec, J. K., Aunina, K., Ramata-Stunda, A., et al. (2022). Effect of crosslinking strategy on the biological, antibacterial and physicochemical performance of hyaluronic acid and ε-polylysine based hydrogels. *International Journal of Biological Macromolecules, 208*, 995–1008. https://doi.org/10.1016/J.IJBIOMAC.2022.03.207

Sceglovs, A., & Salma-Ancane, K. (2020). Novel hydrogels and composite hydrogels based on ε-polylysine, hyaluronic acid, and hydroxyapatite. *Key Engineering Materials*, 242–248. https://doi.org/10.4028/www.scientific.net/KEM.850.242, 850 KEM.

Sequeira, R. A., Singh, N., Pereira, M. M., Chudasama, N. A., Bhattacharya, S., Sharma, M., et al. (2018). High concentration solubility and stability of ε-poly-L-lysine in an ammonium-based ionic liquid: A suitable media for polypeptide packaging and biomaterial preparation. *International Journal of Biological Macromolecules, 120*, 378–384. https://doi.org/10.1016/J.IJBIOMAC.2018.08.102

Singh, M. R., Patel, S., & Singh, D. (2016). Natural polymer-based hydrogels as scaffolds for tissue engineering. *Nanobiomaterials in Soft Tissue Engineering: Applications of Nanobiomaterials*, 231–260. https://doi.org/10.1016/B978-0-323-42865-1.00009-X

Skopinska-Wisniewska, J., Tuszynska, M., & Olewnik-Kruszkowska, E. (2021). Comparative study of gelatin hydrogels modified by various cross-linking agents. *Materials, 14*(2), 396. https://doi.org/10.3390/MA14020396, 2021, Vol. 14, Page 396.

Stoppel, W. L., White, J. C., Horava, S. D., Henry, A. C., Roberts, S. C., & Bhatia, S. R. (2014). Terminal sterilisation of alginate hydrogels: Efficacy and impact on mechanical properties. *Journal of Biomedical Materials Research Part B: Applied Biomaterials, 102*(4), 877–884. https://doi.org/10.1002/JBM.B.33070

Szabó, A., Szabó, B., Balogh, E., Zelkó, R., & Antal, I. (2013). Structural elucidation of hyaluronic acid gels after heat sterilisation. *Polymer Testing, 32*(8), 1322–1325. https://doi.org/10.1016/J.POLYMERTESTING.2013.08.006

Taghipour, Y. D., Hokmabad, V. R., Del Bakhshayesh, Asadi, N., Salehi, R., & Nasrabadi, H. T. (2020). The Application of Hydrogels Based on Natural Polymers for Tissue Engineering. *Current Medicinal Chemistry, 27*(16), 2658–2680. https://doi.org/10.2174/0929867326666190711103956

Tan, Z., Shi, Y., Xing, B., Hou, Y., Cui, J., & Jia, S. (2019). The antimicrobial effects and mechanism of ε-poly-lysine against Staphylococcus aureus. *Bioresources and Bioprocessing, 6*(1), 1–10. https://doi.org/10.1186/S40643-019-0246-8/FIGURES/5

Tao, M., Ao, T., Mao, X., Yan, X., Javed, R., Hou, W., et al. (2021). Sterilisation and disinfection methods for decellularized matrix materials: Review, consideration and proposal. *Bioactive Materials, 6*(9), 2927–2945. https://doi.org/10.1016/J.BIOACTMAT.2021.02.010

Usha, R., Sreeram, K. J., & Rajaram, A. (2012). Stabilization of collagen with EDC/NHS in the presence of L-lysine: A comprehensive study. *Colloids and Surfaces B: Biointerfaces, 90*(1), 83–90. https://doi.org/10.1016/j.colsurfb.2011.10.002

Wang, L., Zhang, C., Zhang, J., Rao, Z., Xu, X., Mao, Z., & Chen, X. (2021). Epsilon-poly-L-lysine: Recent Advances in Biomanufacturing and Applications. *Frontiers in Bioengineering and Biotechnology, 9*, 895. https://doi.org/10.3389/FBIOE.2021.748976

Wang, M., Deng, Z., Guo, Y., & Xu, P. (2022). Designing functional hyaluronic acid-based hydrogels for cartilage tissue engineering. *Materials Today Bio, 17*, 100495. https://doi.org/10.1016/J.MTBIO.2022.100495

Xu, F., Dawson, C., Lamb, M., Mueller, E., Stefanek, E., Akbari, M., et al. (2022). Hydrogels for tissue engineering: addressing key design needs toward clinical translation. *Frontiers in Bioengineering and Biotechnology, 10*, 696. https://doi.org/10.3389/FBIOE.2022.849831/BIBTEX

Xue, X., Hu, Y., Wang, S., Chen, X., Jiang, Y., & Su, J. (2022). Fabrication of physical and chemical crosslinked hydrogels for bone tissue engineering. *Bioactive Materials, 12*, 327–339. https://doi.org/10.1016/J.BIOACTMAT.2021.10.029

Zarrintaj, P., Ghorbani, S., Barani, M., Singh Chauhan, N. P., Khodadadi Yazdi, M., Saeb, M. R., et al. (2021). Polylysine for skin regeneration: A review of recent advances and future perspectives. *Bioengineering & Translational Medicine, 7*(1). https://doi.org/10.1002/BTM2.10261

Zhu, H., Liu, R., Shang, Y., & Sun, L. (2023). Polylysine complexes and their biomedical applications. *Engineered Regeneration, 4*(1), 20–27. https://doi.org/10.1016/J.ENGREG.2022.11.001

Zou, Y. J., He, S. S., & Du, J. Z. (2018). ε-Poly(L-lysine)-based Hydrogels with Fast-acting and Prolonged Antibacterial Activities. *Chinese Journal of Polymer Science (English Edition), 36*(11), 1239–1250. https://doi.org/10.1007/S10118-018-2156-1

Appendix IV

4. Pielikums

Injectable ε-polylysine/hyaluronic acid hydrogels with resistance-preventing antibacterial activity for treating wound infections

Artemijs Sceglovs, Claudia Siverino, Ingus Skadins, Marika Sceglova, Valdis Pirsko, Thomas F. Moriarty, Juta Kroica, Kristine Salma-Ancane

ACS Applied Bio Materials, **2025**, 8 (11), 9916–9930.
https://doi.org/10.1021/acsabm.5c01252

A.S. input: Conceptualization, Writing – original draft, Visualisation, Methodology, Validation, Investigation, Writing – review & editing.

ACS APPLIED BIO MATERIALS

www.acsabm.org
Article

Injectable ε-Polylysine/Hyaluronic Acid Hydrogels with Resistance-Preventing Antibacterial Activity for Treating Wound Infections

Artemijs Sceglovs, Claudia Siverino, Ingus Skadins, Marika Sceglova, Valdis Pirsko, Thomas Fintan Moriarty, Juta Kroica, and Kristine Salma-Ancane*

Cite This: ACS Appl. Bio Mater. 2025, 8, 9916−9930
Read Online

ABSTRACT: The growing threat of antimicrobial resistance has created an urgent demand for nonantibiotic biomaterials capable of preventing infections without promoting bacterial resistance. In this study, we developed injectable, covalently cross-linked hydrogels composed of ε-poly-L-lysine (ε-PL) and hyaluronic acid (HA) for localized wound infection treatment. These hydrogels combine the inherent antibacterial properties of ε-PL with the biocompatibility of HA, forming a shear-thinning, self-recovering system suitable for syringe-based administration. We first evaluated the antibacterial activity of pure ε-PL, determining minimum inhibitory and bactericidal concentrations (MIC/MBC) and evaluating resistance development against ATCC and clinically isolated multidrug-resistant strains (MRSA, ESBL-*E. coli*, *P. aeruginosa*). Notably, no resistance emerged in any strain after the serial passages. Hydrogels formed at varying ε-PL/HA ratios demonstrated strong immediate and long-term bactericidal activity while maintaining high cytocompatibility with murine and human fibroblasts. The hydrogels significantly reduced biofilm formation of *S. aureus* and MRSA within 24 h, achieving reductions comparable to or greater than vancomycin-gentamicin controls. Rheological analysis confirmed injectability, stability, and tunable stiffness. This study presents the first demonstration that ε-PL-based hydrogels can prevent resistance development in multidrug-resistant pathogens, offering a safe and antibiotic-free approach for infection control. The combination of antibacterial efficacy, resistance prevention, and biocompatibility makes these hydrogels promising candidates for wound infection management.

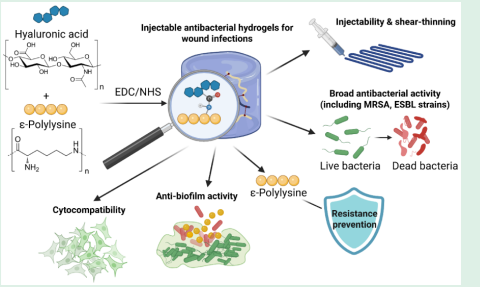

KEYWORDS: *antibacterial hydrogels, ε-polylysine, hyaluronic acid, multidrug-resistant bacteria, resistance prevention, antibiofilm*

1. INTRODUCTION

Bacterial infections account for 13.6% of global mortality, and the rise of antimicrobial resistance (AMR) represents a major global health crisis due to the growing prevalence of multidrug-resistant pathogens.[1−3] In 2019, six priority AMR pathogens (including extended-spectrum β-lactamase-producing *Escherichia coli* (ESBL *E. coli*), methicillin-resistant *Staphylococcus aureus* (MRSA), etc.) were linked to ∼930,000 direct deaths and associated with 3.57 million deaths.[4,5] By 2050, AMR is projected to be associated with more than 30 million deaths worldwide.[6] The WHO Global Action Plan has emphasized the urgent need to develop alternative, nonantibiotic therapies.[7,8] Healthcare-associated infections (e.g., surgical sites, infected wounds, implants) often require systemic antibiotic therapy, which is ineffective due to biofilm formation and poor antibiotic penetration.[9,10] Antibiotic-loaded commercial biomaterials for wound infection treatment are available in clinics and can enhance the local drug concentration. However, they may still promote resistance and adverse tissue responses.[10] Commercially available nonantibiotic wound dressings, including silver- or iodine-based products, are also used for tissue infection treatment, but their long-term effectiveness is limited and may cause cytotoxicity. This highlights the urgent need to develop safe, sustained nonantibiotic therapies for localized treatment. Injectable hydrogels have been extensively explored for localized infection treatment, as they can be applied directly into wounds or deep tissues and provide sustained, targeted release of antibacterial agents.[11] A range of nonantibiotic antibacterial agents have been incorporated into such hydrogels, including metal and metal oxide nanoparticles,[12,13] enzymes,[14] bacteriophages,[15] and especially antimicrobial peptides (AMPs). AMPs, from both natural and synthetic sources, are particularly attractive due to their broad-spectrum activity against multidrug-resistant bacteria.[16] They kill bacteria primarily by

Received: July 2, 2025
Revised: September 26, 2025
Accepted: October 3, 2025
Published: October 30, 2025

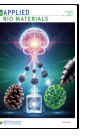

https://doi.org/10.1021/acsabm.5c01252
ACS Appl. Bio Mater. 2025, 8, 9916−9930

disturbing membranes through electrostatic interactions, along with additional mechanisms, which makes resistance development less likely than with conventional antibiotics.[15,16] However, their precise modes of action are not yet fully understood.[17]

Biomaterial-based AMP delivery systems have shown promise for infection prevention and treatment, including applications in wound healing,[17−21] implant coatings,[22] and advanced carriers such as microneedles,[23] dressings,[22,24] nanoparticles,[24,25] and hydrogels.[21,22] However, these systems face several functional challenges, including limited loading capacity, burst release, and reduced long-term efficacy and safety.[11,25] A promising alternative is to integrate AMPs directly into a 3D hydrogel network, creating inherent antibacterial properties through surface chemistry and molecular design.[22,23] This strategy provides stable, localized, and sustained activity, including inhibition of bacterial growth, membrane disruption, and biofilm prevention,[11,16,24] while allowing cross-linking and AMP content to be tuned to balance biodegradation, efficacy, and biological safety.

In recent years, naturally derived AMP (nAMP)-based hydrogels (e.g., LL-37, β-defensins, hLF1−11, magainin) have emerged as promising nonantibiotic therapeutics for wound healing and tissue infection prevention.[26,27] Their evolutionary origin contributes to lower cytotoxicity, higher biocompatibility, reduced resistance potential, and multifunctional activity compared to synthetic alternatives.[28] While most nAMPs are short-chain, long-chain antimicrobial polypeptides such as ε-polylysine (ε-PL) are of special interest. ε-PL is a naturally occurring cationic poly(amino acid) produced by *Streptomyces albulus*, is FDA-recognized as GRAS and has been used safely for decades as a food preservative. More recently, it has attracted attention as a broad-spectrum antibacterial biopolymer for tissue engineering applications, including wound dressings, scaffolds, coatings and hydrogels.[29−32] Its strong positive charge and simple lysine-based structure provide biocompatibility, low toxicity, low immunogenicity, and biodegradability.[29−32] At physiological pH, the ε-amino side groups of lysine residues are protonated to $-NH_3^+$, giving ε-PL its strong polycationic character. These positively charged groups interact electrostatically with bacterial surface components, such as lipopolysaccharides in Gram-negative and lipo-/teichoic acids in Gram-positive bacteria, resulting in bacterial membrane disruption, metabolic interference, and reactive oxygen species (ROS) induction.[33,34] Despite promising preclinical data, no ε-PL-based medical products exist, and only a few hydrogels have been tested in preclinical studies.[14,35,36] Examples include polyglutamic acid/ε-PL composites,[37] silk fibroin/ε-PL hydrogels,[38] and polyacrylamide/gelatin/ε-PL hydrogels,[39] among others.[40,41] However, no previous studies have systematically evaluated the antibacterial activity of ε-PL-based hydrogels against clinically relevant multidrug-resistant pathogens nor investigated their potential for resistance development or biofilm inhibition, key translational benchmarks addressed in the present study. To date, no clinically available ε-PL-based dressings exist and HA-based hydrogels alone are inefficient for infected wounds. This study of ε-PL/HA hydrogels directly addresses this gap by combining the inherent antibacterial activity of ε-PL with the wound healing activity of HA, thereby advancing the translational potential of nonantibiotic therapeutics for treating multidrug-resistant infections. In our previous studies, covalently cross-linked ε-PL/HA hydrogels were developed using EDC/NHS-mediated carbodiimide chemistry.[42,43] These hydrogels exhibited bactericidal activity against ATCC reference strains of *E. coli* and *S. aureus*, assessed by the agar diffusion method.

The aim of this study was to evaluate the clinically relevant antibacterial potential of ε-PL and antibacterial activity, cytocompatibility, rheology/injectability, and antibiofilm performance of covalently cross-linked ε-PL/HA hydrogels for minimally invasive, syringe-based delivery to infection sites. To systematically investigate the impact of ε-PL content on *in vitro* cytocompatibility and antibacterial efficacy, three ε-PL/HA hydrogel series 50:50, 60:40, and 70:30 wt % were selected. These series were chosen based on our previous studies, where they demonstrated a validated balance between inherent antibacterial activity and mechanical robustness, making them suitable for local infection treatment applications.[42,43]

The antibacterial performance of pure ε-PL was first evaluated through minimum inhibitory concentration (MIC) and minimum bactericidal concentration (MBC) testing and the evaluation of bacterial resistance development against ATCC reference *E. coli*, *Staphylococcus aureus* (*S. aureus*), and *S. epidermidis*, clinically isolated *P. aeruginosa* and the multidrug-resistant pathogens MRSA and ESBL *E. coli*. Subsequently, the bactericidal activity of the hydrogels was evaluated against the same ATCC reference strains and clinically isolated multidrug-resistant bacterial strains. In addition, the antibiofilm activity of the hydrogels was evaluated against *S. aureus* and *MRSA*. The cytocompatibility was evaluated by using human dermal fibroblasts (HDFs) and Balb/c 3T3 fibroblasts. This study provides the first evidence that ε-PL/HA hydrogels exhibit strong bactericidal performance and antibiofilm activity, while pure ε-PL does not induce bacterial resistance, highlighting their potential in bacterial wound infection treatment.

2. MATERIALS AND METHODS

2.1. Materials. ε-PL (ε-PL·HCl, 99% purity, molecular weight 3850 g/mol, humidity content 6.5%) was purchased from Zhengzhou Bainafo Bioengineering Co., Ltd. (Henan, China). Sodium hyaluronate (Na-HA, 95% purity, humidity content 13.5%, molecular weight 1.55 MDa) was purchased from Contipro Biotech s.r.o. (Dolní Dobrouč, Czech Republic). 1-Ethyl-3-(3-(dimethylamino)propyl)-carbodiimide hydrochloride (EDC, 98% purity, CAS No.: 25952-53-8, molecular weight: 191.75 g/mol) was purchased from Novabiochem (Burlington, USA). *N*-Hydroxysuccinimide (NHS, 98% purity, CAS No.: 6066-82-6, molecular weight: 115.09 g/mol) was purchased from Sigma-Aldrich.

E. coli ATCC 25922, Methicillin-sensitive *S. aureus* ATCC 25923, and *S. epidermidis* ATCC 35984 were acquired from the *American Type Culture Collection* (ATCC, USA). *P. aeruginosa* was a clinical isolate cultured from a patient with a biofilm-related infection (St. Gallen Kantonsspital, Switzerland). Methicillin-resistant *S. aureus* (*MRSA*) was isolated from a patient pus sample (Riga Stradins Hospital, Latvia). *ESBL E. coli* was clinically isolated from patients (Riga Stradins Hospital, Latvia). Tryptone soy broth (TSB, CM0129) was purchased from Oxoid Limited (Hampshire, United Kingdom). Lysogeny broth (LB, Cat. Nr. 1102850500) was purchased from *Merck KGaA* (Darmstadt, Germany). Tryptone Soya Agar (TSA, casein soybean digest agar, Code: CM0131) was purchased from *Oxoid Limited* (Hampshire, United Kingdom).

For the cell culture experiments, human dermal fibroblasts (HDFs) from Thermo Fisher Scientific Inc. (Waltham, USA) were used. The Balb/c 3T3 mouse fibroblast cell line was obtained from the American Type Culture Collection (CCL-163, ATCC, USA). Dimethyl sulfoxide was purchased from *Labochema* (Latvia). Phosphate-buffered saline (PBS, liquid, pH 7.2) was obtained from *Sigma-*

https://doi.org/10.1021/acsabm.5c01252
ACS Appl. Bio Mater. 2025, 8, 9916−9930

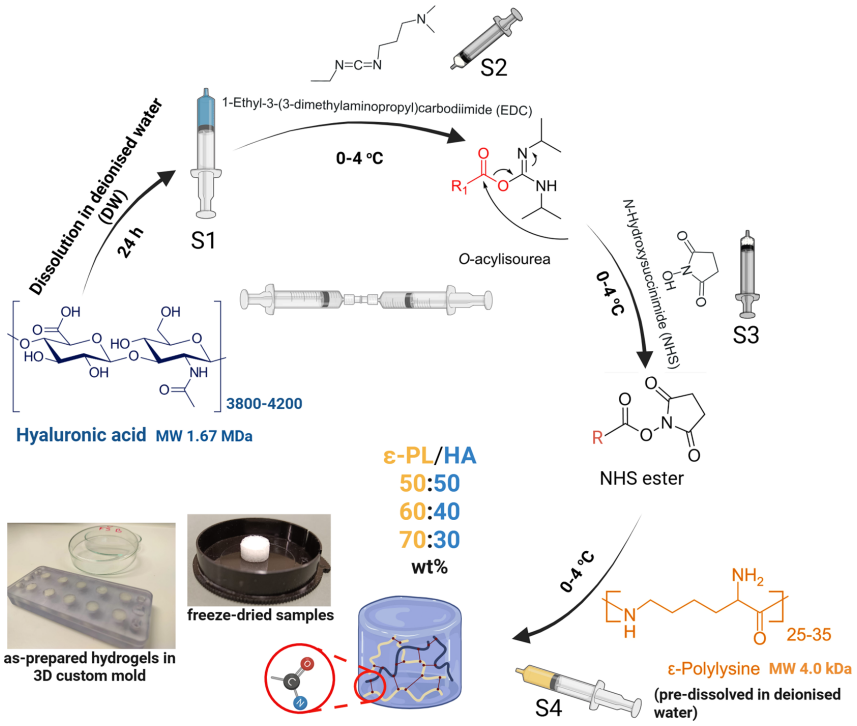

Figure 1. Schematic representation of the synthesis route of chemically cross-linked ε-PL/HA hydrogels.

Aldrich. Trypsin (Trypsin-EDTA (0.25%), phenol red); Penicillin-Streptomycin (PenStrep, 10,000 U/mL); Dulbecco's Modified Eagle Medium/Nutrient Mixture F-12 (DMEM/F12; Cat# 11320033); Fetal Bovine Serum (FBS); Calcein (AM, cell-permanent dye); and Dulbecco's Modified Eagle Medium (DMEM) were purchased from *Thermo Fisher Scientific Inc.* (Waltham, USA); The CellTiter Blue cell viability assay was purchased from *Promega Corporation* (Madison, USA); LIVE/DEAD staining with Hoechst 33342 was purchased from *Sigma-Aldrich* (5 μg/mL, Cat# 14533), and propidium iodide was purchased from *Invitrogen* (1 μg/mL, Cat# P1304MP)

2.2. Fabrication of Chemically Cross-Linked ε-PL/HA Hydrogels. The *in situ* forming covalently cross-linked ε-PL/HA hydrogel series with ε-PL to HA mass ratios of 50:50, 60:40, and 70:30 wt % were prepared via EDC/NHS-mediated carboxyl-to-amine cross-linking, step-by-step, following the synthesis methodology as previously described[43] (Figure 1). EDC acts as an activator by reacting with the carboxyl groups (−COOH) of HA and forms an unstable O-acylisourea intermediate, which is stabilized by NHS through the formation of NHS esters. These activated esters are attacked by the primary ε-amino ($-NH_2$) groups of ε-PL, leading to the formation of stable covalent amide bonds and a chemically cross-linked ε-PL/HA hydrogel network.[42,43] The EDC to NHS molar ratio was 1:1 for all HA to ε-PL mass ratios of ε-PL/HA hydrogel series to introduce the uncross-linked primary ε-amino ($-NH_2$) groups of ε-PL. Hydrogels were synthesized by mixing and homogenization components via an interconnected syringe technique (Fisher Scientific, BD PlastiPak Syringe with Luer Lock, 5 mL) at room temperature (23 °C) following the order described as follows: 1) preparation of the starting components in syringes: syringe No. 1 (S1) was prepared by rapid mixing of 0.21 g of Na-HA powder with 2 mL of deionized water (DW); the S2 and S3 contained 0.19 g of EDC and 0.11 g of NHS, respectively; the S4 was prepared by rapid mixing of the appropriate amount of ε-PL − 0.19, 0.29, and 0.46 g with 2 mL DW, corresponding to the desired ε-PL to HA composition of 50:50, 60:40 and 70:30 wt %, respectively. All prepared syringes (S1−S4) were stored in the refrigerator at 4 °C for 24 h; 2) synthesis of chemically cross-linked the ε-PL/HA hydrogels: after 24 h, the S1 containing Na-HA aqueous solution was mixed with the S2 containing EDC powder by using the same interconnected syringes. Then, the preactivated aqueous solution was mixed with the S3 containing NHS. Finally, the S4 containing ε-PL solution was rapidly mixed with the preactivated HA/EDC/NHS syringe for 1 min; 3) fabrication of as-prepared hydrogel 3D samples: as-prepared hydrogels were cast into cylindrical molds (Ø 10 mm, H 5 mm) and left for complete cross-linking for 24 h at room temperature (23 °C). For *in vitro* studies, as-prepared hydrogel samples were steam-sterilized in an autoclave at 121 °C for 20 min under 215 kPa pressure. The designation and composition of the ε-PL/HA hydrogel series are summarized in Table 1.

2.3. Rheological Studies. Temperature-dependent viscosity, shear rate-dependent viscosity, and recovery cycle tests, as well as time and amplitude sweep studies, were chosen for rheological studies to evaluate the injectability, shear-thinning, and self-healing features of the ε-PL/HA hydrogels. These rheological studies were performed to investigate whether the hydrogels could be applied by minimally invasive delivery to bacterial infection sites via syringe extrusion. Time sweep measurements were conducted to determine the gelation time of the as-prepared ε-PL/HA hydrogels, which is a critical parameter for injectable biomaterials. Gelation time was evaluated by monitoring changes in the storage modulus and axial force over time. The experiment was carried out for 215 min under LVR conditions (0.2% strain and 1 Hz) and physiological temperature (37 °C). Unlike subsequent rheological studies, the hydrogel samples in this test were loaded into the rheometer immediately after syringe mixing, using a 25 mm geometry plate and a 1300 μm gap, without allowing any relaxation time. Amplitude sweep studies were conducted to reveal

https://doi.org/10.1021/acsabm.5c01252
ACS Appl. Bio Mater. 2025, 8, 9916−9930

Table 1. Designation and Composition of the Synthesized Chemically Crosslinked ε-PL/HA Hydrogels

Designation	ε-PL to HA mass ratio, wt %	ε-PL (−NH_2), mmol	HA (−COOH), mmol	EDC:NHS, molar ratio	Liquid volume, mL
ε-PL/HA 50:50 wt %	50:50	0.0479	0.000119	1:1	4
ε-PL/HA 60:40 wt %	60:40	0.0718	0.000119	1:1	4
ε-PL/HA 70:30 wt %	70:30	0.0838	0.000119	1:1	4

the cross-linking degree of the prepared hydrogels by extracting the storage modulus from the linear viscoelastic region (LVR) of amplitude sweep curves of the ε-PL/HA hydrogel series. Extracted storage modulus values were added to the equation. Finally, cross-linking densities (q, mol·m^{-3}) were obtained: $q = Mw/Mc$, where Mw is the molecular weight of the cross-linked monomer calculated as follows: $Mw = Mw(HA) + Mw(\varepsilon\text{-}PL)$, where $Mw(HA)$ is the molecular weight of a HA monomer, and $Mw(\varepsilon\text{-}PL)$ is the molecular weight of an ε-PL monomer. In turn, Mc, e.g., molecular weight between cross-links of the prepared hydrogels was calculated as $Mc = RTd/G'$, where R is the universal gas constant (8.314 $m^3 \times Pa \times K^{-1} \times mol^{-1}$), T is the absolute temperature (298 K), and d is the density of the polymer (found experimentally as $d = m/V = m/\pi r^2 h$), G' is a storage modulus at 0.2% strain and 1 Hz frequency according to the defined LVR.[44] The Thermo HR-20 Hybrid rheometer from TA Instruments (USA) was used to perform rheological characterization. A 25 mm parallel plate with a gap of 2.0−3.0 mm was used in all cases. Silicone oil was gently applied around the sample to avoid evaporation, and a humidity control trap was used. Before each measurement, each sample was left to a relaxation time of 180 s. The sample loading procedure was followed step-by-step according to the methodology described in a previous report.[43,44] Temperature-dependent viscosity tests were done in flow mode at a temperature range of 4 to 37 °C. Viscosity values were measured at each 1 °C step change. During shear rate-dependent viscosity tests, shear rate values were changed logarithmically from 0.5 to 500 s^{-1}. Finally, in recovery tests, the viscosity values were measured over five cycles. The cycle parameters were as follows: first, third, and fifth cycles—constant shear rate of 0.1 s^{-1} for 60 s; second and fourth cycles—rapidly increased constant shear rate of 200 s^{-1} for 10 s. To obtain amplitude sweep curves of the prepared ε-PL/HA hydrogels, studies were performed in oscillation mode at a constant frequency (1 Hz) and temperature (25 °C). Amplitude strain modulus values were changed logarithmically during the test from 0.01% to 1000%. All measurements were repeated three times to ensure reproducibility.

2.4. *In Vitro* Antibacterial Activity Assay. A series of antibacterial tests was designed to investigate the antibacterial performance of the ε-PL/HA hydrogels and the pure antimicrobial polypeptide ε-PL. First, the minimum inhibitory concentration (MIC), minimum bactericidal concentration (MBC), and bacterial resistance development against ε-PL were evaluated. Additionally, antibiofilm studies, as well as both direct bactericidal activity and indirect assessments of antibacterial activity, were performed for the as-prepared (hydrated form) ε-PL/HA hydrogels. The results of these investigations are detailed in the following sections.

2.4.1. Minimum Inhibitory/Bactericidal Concentration Studies of ε-PL. The MIC and MBC studies were performed for ε-PL aqueous solutions against target *E. coli*, *S. aureus*, *S. epidermidis*, *P. aeruginosa*, *ESBL E. coli*, and *MRSA* listed in Section 2.1 The bacteria were cultured overnight in 20 mL of TSB at 37 °C with agitation at 60 rpm. Overnight cultures were diluted in TSB to an optical density at 600 nm (OD_{600}) of 0.1, corresponding to a bacterial concentration of approximately 1−2 × 10^8 colony-forming units (CFUs). Bacteria (10 μL from the OD = 0.1 corresponding to 1 × 10^6 CFU/mL) were then incubated for 24 h (60 rpm and 37 °C) at a range of concentrations of ε-PL aqueous solution (4, 8, 18, 37, 75, 150, 200, 350, 400, 500, and 600 μg/mL). After incubation with hydrogels, bacterial suspensions were collected from each well and serially diluted 10-fold (10^0 to 10^{-6}) in sterile PBS. Aliquots of 10 μL from each dilution were spotted onto tryptic soy agar (TSA) plates and incubated at 37 °C for 24 h under static conditions. Colony-forming units (CFUs) were then enumerated from the dilution, yielding countable colonies.

2.4.2. Evaluation of Bacterial Resistance Development against ε-PL. *E. coli*, including ESBL *E. coli*, as well as *S. aureus*, including MRSA, were used in this study. In the beginning, the bacteria were cultured overnight, then diluted to an OD of 0.1 and incubated with the experimental range of ε-PL aqueous solution exactly as described above for MIC studies. The experimental concentration range of the ε-PL aqueous solutions was chosen based on MIC values for each strain ±1−2 fold concentrations and turned out to be the same (control, 8, 18, 37, 75, and 150 μg/mL). To assess resistance development, each strain was passaged twice weekly in the presence of subinhibitory concentrations of ε-PL. The passaging process included inoculating surviving bacterial colonies into 20 mL of broth media for 24 h at 37 °C and 60 rpm. Afterward, bacteria were transferred, streaked on a TSA plate, and incubated for 24 h at 37 °C. MICs were determined using the broth microdilution method according to CLSI guidelines.[45] MICs were recorded as the lowest concentration of ε-PL that prevented visible growth after 24 h (37 °C) of incubation, and MIC determination was performed after passages 1, 2, 4, 6, and 10 to track the development of resistance. Three parallel replicates from each concentration were studied to ensure result validation.

2.4.3. Antibiofilm Activity of ε-PL/HA Hydrogels. In order to investigate the antibiofilm activity of the prepared ε-PL/HA hydrogels, two studies were performed: antibiofilm activity via biofilm biomass quantification using the crystal violet assay and antibiofilm activity with the Live/Dead assay and quantitative viability.

2.4.3.1. Biofilm Biomass Quantification via Crystal Violet Assay. The antibiofilm activity of the ε-PL/HA hydrogels was evaluated using the crystal violet assay[46−48] against two of the most common healthcare-associated biofilm-forming bacteria, *S. aureus* and *MRSA*.[49−51] Overnight bacterial cultures were diluted 1:50 in TSB (corresponding to a bacterial concentration of 6−7 × 10^7 CFU/mL), and 24-well plates were inoculated with 1 mL of the suspension and incubated for 24 h at 37 °C under static conditions to allow biofilm formation. Following incubation, the medium was removed and wells were assigned to three groups: (i) untreated controls (1 mL of fresh b suspension, n = 4); (ii) antibiotic-treated controls (1 mL of vancomycin/gentamicin mixture, 3 and 2 mg/mL, respectively; n = 4); (iii) hydrogel-treated wells (one hydrated hydrogel disc, h = 5 mm, ø = 10 mm, ∼0.4 g, immersed in 1 mL of 0.9% NaCl, n = 4). All plates were sealed with parafilm and incubated for an additional 24 h at 37 °C under static conditions. After treatment, hydrogels were removed, and wells were washed three times with 1 mL of 0.9% NaCl. Biofilms were stained with 1 mL of 0.1% crystal violet for 20 min, rinsed once with 0.9% NaCl, and decolorized with 1 mL of 96% ethanol. Three 100 μL aliquots per well were transferred to a 96-well plate, and absorbance was measured at 570 nm using a Tecan microplate reader (*Tecan Trading AG*, Switzerland).

2.4.3.2. Antibiofilm Activity of ε-PL/HA Hydrogels via Live/Dead and Viability Assay. For proof-of-concept antibiofilm studies, Live/Dead assay experiments were performed against *S. aureus* due to its clinical relevance and biofilm-forming ability, as described in Section 2.4.3.1. Overnight bacterial cultures were diluted 1:50 in TSB, and two parallel 24-well plates were inoculated with 1 mL of the suspension and one hydrogel sample per well (dimensions as described in Section 2.4.3.1, with three replicates per composition). Plates were incubated for 24 and 72 h at 37 °C under static conditions to allow biofilm formation on the hydrogel surface. Titanium (Ti) discs of identical size were used as positive controls in each plate. For the 72 h experiment, hydrogel samples and Ti discs were transferred daily into fresh wells containing newly added TSB to support continuous biofilm growth and to remove planktonic bacteria.

https://doi.org/10.1021/acsabm.5c01252
ACS Appl. Bio Mater. 2025, 8, 9916−9930

After 24 h, hydrogels and Ti discs were transferred into empty wells, washed twice with 1 mL of 0.9% NaCl, and stained with 1 mL of Live/Dead dye (BacLight Bacterial Viability Kit, Component A − 1.67 mM SYTO 9 and 1.67 mM PI; Component B − 1.67 mM SYTO 9 and 18.3 mM PI; Invitrogen, Thermo Fisher, USA). Samples were incubated for 15 min in the dark to avoid photobleaching. Biofilms were then analyzed by confocal microscopy (LSM900, Zeiss AG, Feldbach, Switzerland) using two channels: Ex/Em 480/635 nm (green) and Ex/Em 535/617 nm (red). After imaging, hydrogel samples and Ti discs were placed in 2 mL Eppendorf tubes containing 1 mL of 0.9% NaCl, vortexed for 1 min at 3000 rpm, sonicated for 10 min (Bandelin electronic GmbH & Co. KG, Germany), and vortexed again for 1 min. Aliquots were transferred into 96-well plates, serially diluted 6-fold, and plated on TSA for viable bacteria enumeration, as described in Section 2.4.1. The same procedure was followed for the 72 h samples.

2.4.4. Direct Test of Antibacterial Activity of ε-PL/HA Hydrogels. Bactericidal activity of the ε-PL/HA hydrogels was performed according to CLSI and EUCAST standards,[45,52] with minor modifications in order to adjust the protocol procedure for hydrogel testing up to 24 h. Bacterial suspensions of the target bacterial strains of *E. coli*, *S. aureus*, *S. epidermidis*, clinically isolated *P. aeruginosa*, and clinically isolated multidrug-resistant *ESBL E. coli* and *MRSA* were prepared in a glass tube with 0.9% NaCl until they reached McFarland = 1.0, corresponding to approximately 3×10^8 CFU/mL. Experimental 6-well plates were prepared for each bacterial strain, including: (i) three replicates of sterilized hydrogel samples (one scaffold (*h* 5 mm, ø 10 mm, ∼0.4 g) per well) from each series, immersed in 2 mL of bacterial suspension; (ii) a positive control contained 2 mL of pure 0.9% NaCl; and (iii) a negative control contained −2 mL of bacterial suspension in 0.9% NaCl. The prepared six-well plates were tightly tied with parafilm and incubated for 24 h at 60 rpm and 37 °C. Afterward, six-stage dilutions were prepared, and the surviving bacterial colonies were counted according to the previous description in Section 2.4.1.

2.4.5. Long-Term Antibacterial Activity of ε-PL/HA Hydrogels. Long-term antibacterial studies included both direct contact tests on prepared ε-PL/HA hydrogels and indirect/supernatant studies on collected supernatants after an incubation period of 168 h implemented within the stability testing of ε-PL/HA hydrogels (Section 2.4.5.1). The hydrogels ε-PL/HA 50:50 wt %, ε-PL/HA 60:40 wt %, and ε-PL/HA 70:30 wt % were incubated in 50 mL DW (0.8% v/v) at 60 rpm and 37 °C for 168 h (with media refreshing at 1 h and 24 h).

For long-term indirect/supernatant studies: after 168 h, the supernatants were collected. Briefly, 1 mL of supernatant and 1 mL of prepared bacterial suspension (*E. coli* and *S. aureus*) in 0.9% NaCl with McFarland 1.0 (approximately 3×10^8 CFU/mL) were mixed, and antibacterial activity was evaluated after 24 h at 37 °C of incubation according to the methodology described in Section 2.4.4.

For long-term direct studies: ε-PL/HA hydrogel samples (50:50, 60:40, 70:30 wt %) were extracted after 168 h incubation in DW and used for the direct test with *E. coli* (Gr−) and *S. aureus* (Gr+). Extracted hydrogel samples (one scaffold ∼0.6 g per well, triplicates from each series were used) were immersed in 2 mL of bacterial suspension of McFarland 1.0 (3×10^8 CFU/mL), and the procedure following incubation for 24 h at 37 °C was followed according to the steps described in Section 2.4.4.

2.4.5.1. Swelling Behavior and Structural Stability Studies of ε-PL/HA Hydrogels. In order to prepare ε-PL/HA hydrogel samples for long-term antibacterial activity studies as well as to collect supernatants for indirect testing, stability studies were conducted to reveal what happens to hydrogels in physicochemical aspects and how it affects their further antibacterial performance. Three replicates in hydrated form without freeze-drying from the hydrogels ε-PL/HA 50:50 wt %, ε-PL/HA 60:40 wt %, and ε-PL/HA 70:30 wt % series were weighed first to obtain the initial weight (W_0) and incubated in 50 mL DW (0.8% v/v) at 60 rpm and 37 °C for 168 h (with media refreshing at 1 and 24 h). Stability testing was performed by weighing hydrogel samples (W_s) at different time points of 1, 2, 3, 4, 24, 48, 72, 96, and 168 h. Results and observations were based on the remaining weight of the samples, calculated by the equation used in swelling behavior studies (eq 1):

$$R_w = \frac{W_s - W_0}{W_0} \times 100\% \quad (1)$$

2.5. *In Vitro* Cytotoxicity Assay. *2.5.1. Cell Culture.* The HDFs and Balb/c 3T3 cells were used to evaluate the effects of the different ε-PL/HA hydrogels on cell viability. HDF cells were cultured in DMEM/F12 supplemented with 10% FBS at 37 °C in a humidified 5% CO_2 atmosphere. Balb/c 3T3 cells were cultured in DMEM with 10% FBS under the same conditions. Both cell types were subcultured at least twice prior to experiments.

2.5.2. Indirect Cytotoxicity Assay on HDFs. Each hydrogel sample (200 mg) was washed three times with DPBS (pH 7.1−7.7; Sigma-Aldrich, cat. no. D1408) and allowed to swell for 4 h at 37 °C in DPBS. Afterward, the swollen hydrogel was cultured in DMEM for 24 h at 37 °C under 5% CO_2 atmosphere. The culture media containing the released products from the hydrogel were collected and diluted with fresh growth medium using a dilution factor of 2.15 (200, 93.023, 43.27, 20.12, 9.36, 4.35, 2.025 mg/mL). The experimental approach was consistent with the OECD GD 129 standard procedure.[53] HDF cells were seeded in 96-well plates at 1.75×10^3 cells/100 μL/well (∼5500 cells/cm^2) and allowed to reach 50−60% confluence before treatment. Hydrogel extracts were added and incubated for 48 h. One untreated plate was retained at $t = 0$ to normalize growth rates. Cell viability was assessed using LIVE/DEAD staining with Hoechst 33342 and propidium iodide (PI), followed by fixation in 4% paraformaldehyde. High-content imaging (InCell 2200, *GE HealthCare, USA*) was used to capture five fields/well with a 10× lens (DAPI (from 4′,6-diamidino-2-phenylindole) channel: Ex 390 nm/Em 432.5 nm, PI channel: Ex 542 nm/Em 597 nm). CellProfiler (v4.2.5) was used for automated nuclei segmentation and PI intensity quantification. Cells were classified as live (none to low PI) or dead (high PI), and viability values were normalized to negative control wells. Controls included the following: untreated cells (negative, 100% viability), Geneticin (G418, positive cytotoxic control), and medium-only controls. Each condition was tested in triplicate wells across three independent experiments ($n = 3$).

2.5.3. Direct Cytotoxicity Assay on Balb/c 3T3 Cell Line. First, hydrogels were preswelled, as described in Section 2.5.2. Then, the swollen hydrogel samples were incubated with 1 mL DMEM/10% FBS (this volume of media does not cover the upper surface of the hydrogel). Then, 10 μL of Balb/c 3T3 (3×10^4 cells/cm^2) was pipetted on top of the hydrogel, and an additional 100 μL of cell culture media was added to fully cover the hydrogel. After 24 h, cell metabolic activity was measured using CellTiter Blue, according to the manufacturer's recommendations.[54] Fluorescence was measured using the Tecan plate reader (Männedorf, Switzerland), at 560Ex/590Em ($n = 3$ measurements per well). The resulting data were converted into cell viability (%) using eq 1:

$$\text{Cell Viability, \%} = \left(\frac{\text{Average Fluorescence}_{560\text{Ex}/590\text{Em}} - \text{Negative control}}{\text{Positive control} - \text{Negative control}}\right) \times 100 \quad (2)$$

The morphology of the cells in contact with the hydrogel was assessed by using calcein staining. After 24 h of culture, 500 μL of 0.001 v/v% of calcein/DMEM solution was added to each well containing the hydrogel. After 20 min of incubation, cell morphology was evaluated using an OPTIKA ECO IM-5 fluorescent microscope (OPTIKA Srl, Italy). Experiments were performed in triplicate wells across three independent replicates.

2.6. Statistical Analysis. All results were expressed as the mean value ± standard deviation (SD) of at least three independent samples from ε-PL and each ε-PL/HA hydrogel series. One- or two-way analysis of variance (ANOVA) with Tukey's multiple comparisons was used during the data analysis to determine statistical significance.

https://doi.org/10.1021/acsabm.5c01252
ACS Appl. Bio Mater. 2025, 8, 9916−9930

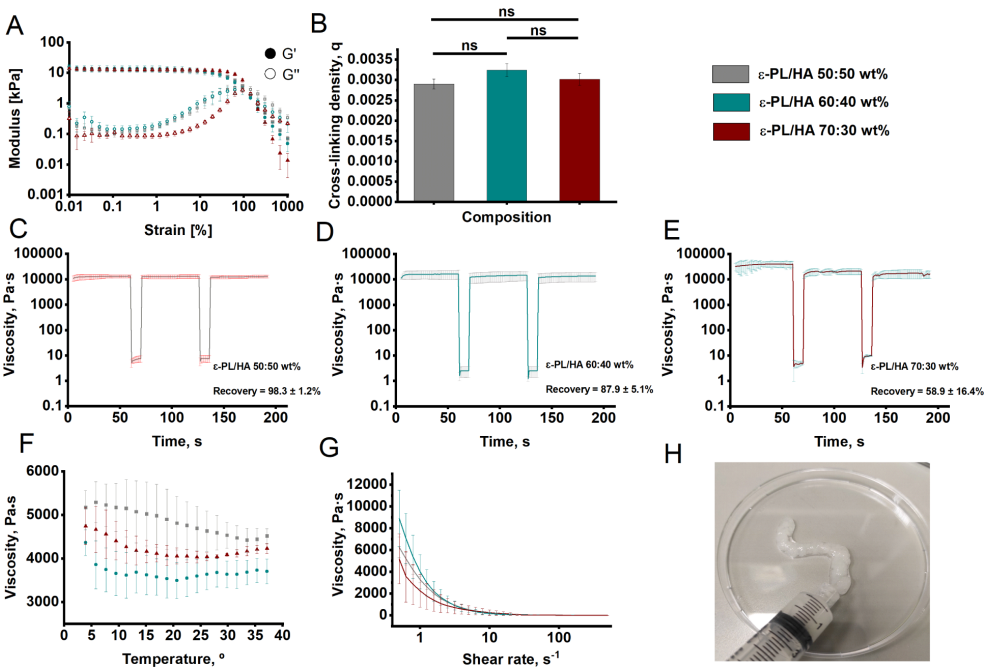

Figure 2. Rheological characterization of the ε-PL/HA hydrogels.ε-PL/HA 50:50 wt % colored as gray, 60:40 wt % -— dark green and 70:30 wt % -— dark red. (**A**,**B**) Amplitude sweep and cross-linking density. Amplitude sweep studies were obtained at a constant temperature of 25 °C and frequency of 1 Hz. Amplitude strain ranged from 0.01 to 1000%. (**C**−**E**) Recovery cycle tests done in flow mode under constant temperature of 25 °C, within 5 (3 + 2) cycles corresponding to 3*x*—shear rate at 0.1 s^{-1} for 60 s within LVR, and 2*x*—stress-induced cycles at 200 s^{-1} for 10 s; (**F**) Temperature-dependent viscosity test performed in flow mode at a constant frequency of 1 Hz, within temperature range from 4 to 37 °C with 1 °Cstep (T = 4 °C; ns for all hydrogel series: ε-PL/HA 50:50 wt %, ε-PL/HA 60:40 wt %, ε-PL/HA 70:30 wt %; T = 25 °C; ns for all hydrogel series; T = 37 °C; ns for all hydrogel series); (G) Shear rate dependent viscosity studies performed in flow mode under constant temperature of 25 °C within the range 0.1−500 s^{-1} shear rate with logarithmic step; (**H**) Illustration of the ε-PL/HA hydrogel sample extruded from the syringe with an inner diameter of 2.1 mm. Three replicates were used to ensure qualitative measurement results..

Statistically significant results were considered as of $p < 0.05$ (ns − >0.05, * − <0.05, ** − <0.01, *** − <0.005, and **** − <0.001). Statistical analysis was performed by using IBM SPSS Statistics 23 software.

3. RESULTS AND DISCUSSION

3.1. Rheological Studies. A temperature-dependent viscosity test was performed on all ε-PL/HA hydrogels to evaluate their thermoresponsive behavior and viscosity stability across a temperature range of 4 to 37 °C (Figure 2F). The viscosity of each hydrogel remained stable between 3500 and 5500 Pa·s across the tested temperature range (4−37 °C), with no statistically significant differences ($p > 0.05$). This thermal stability supports hydrogel consistency at both room temperature (23 °C) and physiological temperature (37 °C), indicating their suitability for clinical use. The comparable viscosity profiles across all hydrogel series are attributed to the constant molar concentration of high molecular weight (HMW) HA (Table 1), which, through chain entanglement and hydrogen bonding, stabilizes the hydrogel network.[43,55] As seen in Figure 2F, three distinct rheological regions were observed: Region I (4−15 °C), recognized as typical Newtonian behavior, with slight viscosity reduction as temperature increased; Region II (15−30 °C), where temperature-dependent behavior reverses upon the shear-dependent divergence point; and Region III (>30 °C), where a slight increase in viscosity could be observed, as from this point, the viscosity value changes as a function of the shear rate.[56]

To further evaluate the flow behavior and injectability of the ε-PL/HA hydrogels, shear rate-dependent viscosity tests were performed (Figure 2G). These tests confirmed that all hydrogel series exhibit pronounced shear-thinning behavior, a key property for syringe-injectable biomaterials. The viscosity remained high at low shear rates (<1 s^{-1}), particularly for the ε-PL/HA 50:50 wt %, suggesting a more entangled polymer network and stronger intermolecular interactions. In contrast, the ε-PL/HA 60:40 wt % and ε-PL/HA 70:30 wt % exhibited progressively lower viscosity, likely due to reduced cross-linked density and polymer interactions. All hydrogel formulations reached a viscosity plateau at higher shear rates (>10 s-1), indicating smooth syringeability and fluid-like behavior under injection-relevant conditions.[57] The cyclic strain time sweep studies were performed to simulate the shear rate stress caused during extrusion from a syringe and to observe matrix recovery through viscosity values (Figure 2C−E). All ε-PL/HA hydrogel formulations exhibited rapid viscosity self-recovery within 15 s after high shear, indicating the ability to restore their structural state postdeformation.[58,59] However, it was observed that ε-PL/HA 70:30 wt % hydrogels exhibited

https://doi.org/10.1021/acsabm.5c01252
ACS Appl. Bio Mater. 2025, 8, 9916−9930

Table 2. Crosslinking Characteristics of ε-PL/HA Hydrogels

Designation	NH_3^+/NH_2 ratio (I_{3062}/I_{3228})[42,43]	Gel fraction, %[42,43]	Swelling capacity, %[a]	Cross-linking density (q, mol·m^{-3})	Gelation time, min[b]
ε-PL/HA 50:50 wt %	0.73	52 ± 0.05	166.07± 34.8	0.003 ± 0.0001	34
ε-PL/HA 60:40 wt %	0.85	56.2 ± 0.2	277.2 ± 13.6	0.003 ± 0.0001	41
ε-PL/HA 70:30 wt %	0.83	54.7 ± 1.6	441.5 ± 41.8	0.003 ± 0.0001	46

[a]See Figure S2. [b]See Figure S1.

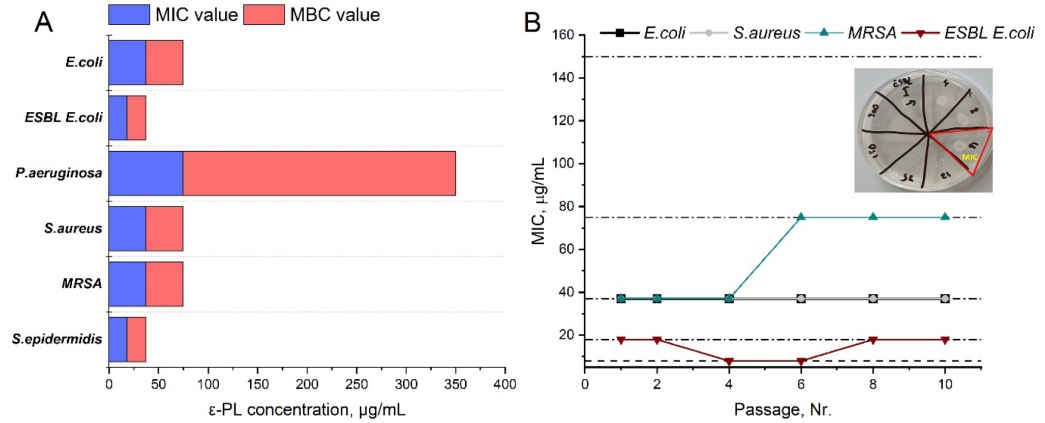

Figure 3. Antibacterial activity of pure ε-PL. **(A)** Minimum inhibitory/bactericidal concentration (MIC/MBC) studies against different bacterial species: *E. coli*, *P. aeruginosa*, ESBL *E. coli*, *S. aureus*, *S. epidermidis*, and MRSA (blue bars indicate obtained MIC values and red bars − MBC values); **(B)** Resistance development studies against *S. aureus*, MRSA, *E. coli* and ESBL *E. coli* within 10 passages and plotted curves reveal changes of MIC value within 1, 2, 4, 6, and 10 passages.

significantly reduced recovery capability, with a measured recovery rate of 58.9 ± 16.4%, compared to 98.3 ± 1.2% for ε-PL/HA 50:50 wt % and 87.9 ± 5.1% for ε-PL/HA 60:40 wt %, respectively. This significantly lower recovery in the 70:30 wt % hydrogel may be attributed to excess free, uncross-linked ε-PL chains, which can interfere with network cohesion and hinder viscosity restoration. Similar effects have been reported in other polymer systems, such as CMC-based hydrogels, where free polymer chains negatively impact flow and recovery behavior.[60]

Further insights were obtained from amplitude sweep tests (Figure 2A) and cross-linking density calculations (Figure 2B), which showed no significant differences among the hydrogel compositions. Besides the viscoelastic behavior described in our previous work,[42,43] extracted storage modulus (G′) values were used to calculate the cross-linking density of prepared ε-PL/HA hydrogels (Figure 2A,B). The cross-linking density (q) was obtained as 0.0029 ± 0.00012, 0.0032 ± 0.00015, and 0.003 ± 0.00014 mol·m^{-3} for ε-PL/HA hydrogels with 50:50, 60:40, and 70:30 wt %, respectively. A nonsignificant difference was found between cross-linking density values within all hydrogel series, suggesting that ε-PL and HA cross-linked equally. To sum up, these uncross-linked ε-PL chains were introduced during the fabrication process, where all ε-PL/HA hydrogel series were prepared with a constant EDC/NHS cross-linker concentration, while varying the ε-PL to HA mass ratios.

Overall, rheological characterization confirmed that ε-PL/HA hydrogels possess key properties for syringe-based delivery, including shear-thinning behavior, rapid self-recovery, temperature stability, and tunable viscosity. These attributes ensure consistent performance before and after injection and support the potential of the hydrogels for clinical applications, such as wound infection treatment and 3D bioprinting.

To support the rheological data, additional indicators of cross-linking efficiency were analyzed, including the NH_3^+/NH_2 ratio,[42,43] gel fraction,[42,43] swelling capacity, cross-linking density, and gelation time. These results are summarized in Table 2. With increasing ε-PL content, FTIR analysis showed a shift in the amide bands and an increase in the NH_3^+/NH_2 absorbance ratio, reflecting more free ε-PL residues at higher ε-PL mass ratios. This trend is consistent with the rheological results, confirming that higher ε-PL content leads to less dense networks with higher swelling capacity.

3.2. Minimum Inhibitory/Bactericidal Concentration of ε-PL.

The antibacterial activity of pure ε-PL was evaluated by determining the MIC and MBC values against both the Gram-positive and Gram-negative bacterial species, including multidrug-resistant isolates. This property is particularly important, as the bacterial strains selected for this study are among the most common pathogens associated with postsurgical, skin, oral, and implant-related infections.[61,62] The MIC/MBC experiments (Figure 3A) demonstrated the potent inhibitory capability of ε-PL against a wide range of bacterial species. The results revealed that ε-PL at a concentration of 100 μg/mL effectively inhibited the growth of both Gram-negative and Gram-positive bacteria, including multidrug-resistant strains. Remarkably, a lower concentration of ε-PL, such as 75 μg/mL, was sufficient to achieve a

https://doi.org/10.1021/acsabm.5c01252
ACS Appl. Bio Mater. 2025, 8, 9916−9930

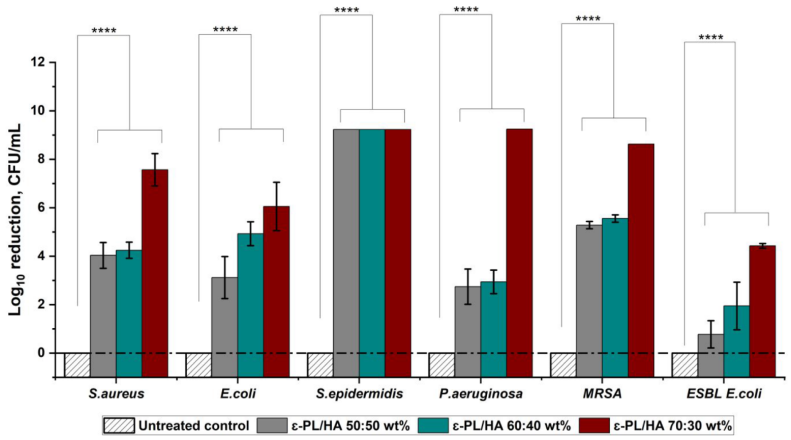

Figure 4. Direct antibacterial activity of ε-PL/HA hydrogels against *S. aureus*, *E. coli*, *S. epidermidis*, *P. aeruginosa*, *MRSA*, and *ESBL E. coli* after 24 h. Data are expressed as log reduction in CFU (mean ± SD, $n = 3$), and statistical analysis was performed by one-way ANOVA: ns − >0.05, * − <0.05, ** − <0.01, *** − <0.005, and **** − <0.001. Dash-dotted lines indicate compositions where complete eradication was achieved.

bactericidal effect against *E. coli*, *ESBL E. coli*, *S. epidermidis*, *S. aureus*, and *MRSA*.

However, for Gram-negative *P. aeruginosa*, significantly higher concentrations of ε-PL (∼350 μg/mL) were required to achieve a bactericidal effect. This observation may be attributed to the unique structural and functional characteristics of *P. aeruginosa* compared to other representatives of the Gram-negative family (e.g., *E. coli*), including its robust outer membrane, multiple efflux pumps, and highly adaptive gene expression system.[63] These characteristics and well-developed resistance mechanisms contribute to its classification as a high-risk opportunistic pathogen in clinical settings.[63] In addition to the general structural barriers common to Gram-negative bacteria, several studies have explored how these intrinsic and acquired features interfere with the mechanisms of action of even the most potent antibiotics.[63] Computational studies have shown that divalent cations and their interaction with anionic lipopolysaccharides (LPS) increase the stiffness of the outer membrane, enhancing membrane integrity and reducing the cell surface anionicity.[63] This structural rigidity is a critical factor that may significantly hinder the antibacterial action of ε-PL, as previously described.

3.3. Evaluation of Bacterial Resistance Development against ε-PL. For the first time, a comprehensive evaluation was conducted to assess the potential of the antimicrobial polypeptide ε-PL to induce bacterial resistance, including in multidrug-resistant isolates. The MIC values were measured after passages in the presence of a range of ε-PL concentrations to track the resistance development. Bacterial suspensions were inoculated with ε-PL (8, 18, 37, 75, and 150 μg/mL) and incubated for 24 h at 37 °C on TSA plates (illustration provided in Figure 3B). The results (Figure 3B) demonstrated that *E. coli* and *S. aureus* remained consistently sensitive to ε-PL, as the MIC values did not change compared with initial results (Figure 3A). Similarly, the MIC value for *ESBL E. coli* remained stable at 18 μg/mL over 10 passages, indicating no resistance development. A slight MIC increase was observed for MRSA after 10 passages. However, this shift was within one 2-fold dilution, which corresponds to the expected biological and technical variability of MIC assays,[64] and therefore does not indicate actual resistance development. Tan et al. previously described the inhibition mechanism of ε-PL against *S. aureus* as a dual-action process: membrane disruption via the classical carpet-like model and participation in the tricarboxylic acid cycle, affecting aconitase and succinate dehydrogenase enzymes.[65] It is hypothesized that the minor MIC fluctuation observed for MRSA may be due to suppression of the secondary metabolic mechanism of ε-PL, thereby requiring slightly higher concentrations to maintain inhibitory efficacy.

3.4. Direct Studies of Antibacterial Activity of Prepared Hydrogels. The bactericidal activity of the ε-PL/HA hydrogels with ε-PL:HA mass ratios of 50:50, 60:40, and 70:30 wt % was evaluated using a direct contact test (Figure 4). All tested hydrogels demonstrated statistically significant ($p < 0.05$) antibacterial activity, expressed as log reduction in CFU compared to the untreated control. Complete eradication of *S. epidermidis* was achieved by all hydrogel series, while significant log reductions were also observed for *S. aureus*, *E. coli*, *P. aeruginosa*, *MRSA*, and *ESBL E. coli*. These findings are consistent with the high sensitivity observed in MIC/MBC tests of pure ε-PL. The bactericidal effect was most pronounced in hydrogels with a higher ε-PL content, reflecting the increased availability of free, primary ε-amino ($-NH_2$) groups that become protonated [NH_3^+] in aqueous conditions, contributing to improved antibacterial activity (Figure 4). These positively charged groups enable electrostatic interactions with negatively charged bacterial membranes, enhancing bactericidal efficacy. As shown in Figure 1B, the cross-linking density (q, mol·m^{-3}) remained consistent across all hydrogel series, indicating that differences in antibacterial performance were related to the number of free, uncross-linked ε-amino ($-NH_2$) groups rather than the cross-linking degree. Our previous reports[42,43] confirmed this relationship, showing that increasing ε-PL mass ratios led to higher NH_3^+/NH_2 values (0.73, 0.85, and 0.83 for ε-PL/HA 50:50, 60:40, and 70:30 wt %, respectively), consistent with FTIR analysis. These data demonstrate that a higher ε-PL content correlates with a greater concentration of positively charged NH_3^+ groups, critical for antibacterial efficacy. Polymers containing positively charged functional groups, such as amines, are known to

https://doi.org/10.1021/acsabm.5c01252
ACS Appl. Bio Mater. 2025, 8, 9916−9930

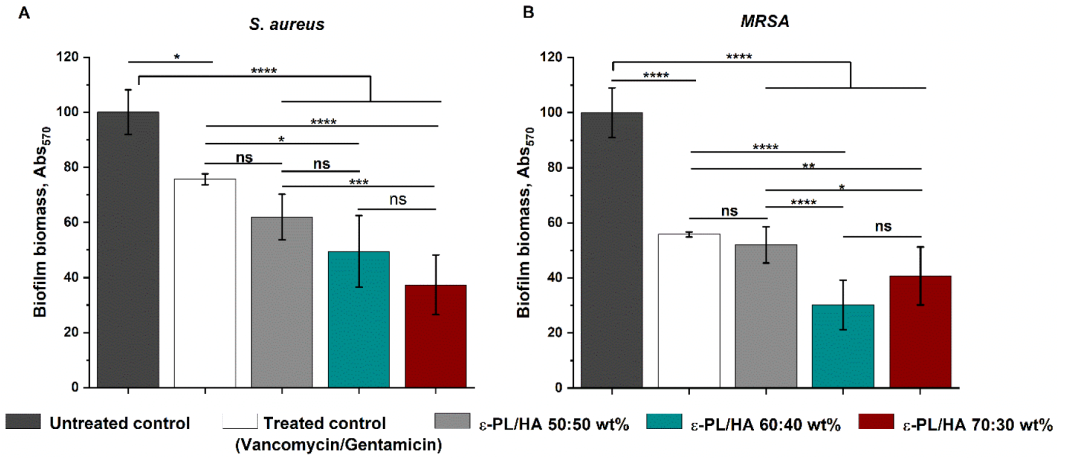

Figure 5. Antibiofilm activity of ε-PL/HA hydrogels was tested by crystal violet biofilm biomass quantification testing against (A) *S. aureus* and (B) *MRSA* bacteria. Untreated controls consisted of a 1:50 diluted overnight bacterial suspension in TSB. A vancomycin (3 mg/mL) and gentamicin (2 mg/mL) mixture served as the antibiotic control. Each group was tested in quadruplicate ($n = 4$). Biofilm biomass was quantified by absorbance at 570 nm. Data are presented as mean ± SD, and statistical analysis was performed by one-way ANOVA: ns – >0.05, * – <0.05, ** – <0.01, *** – <0.005, and **** – <0.001.

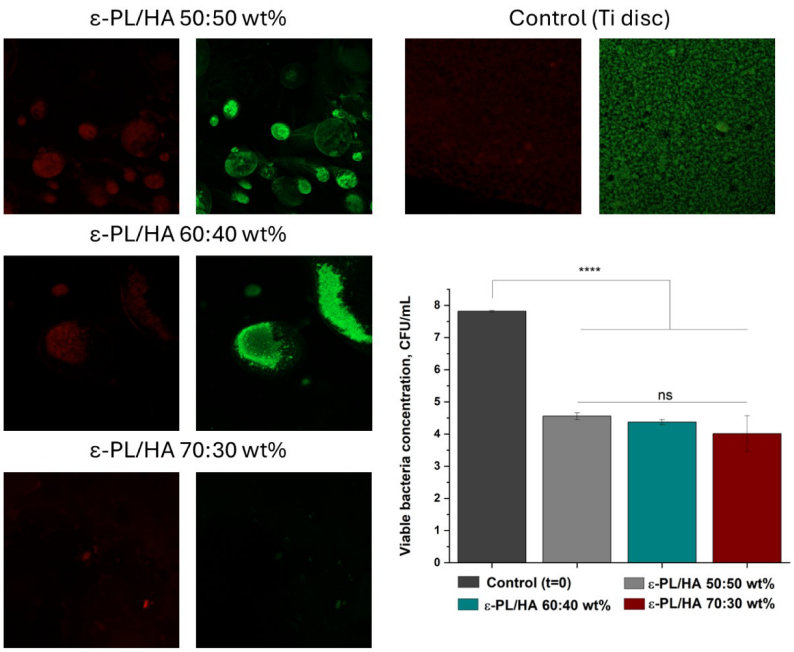

Figure 6. Live/Dead and viability assay for ε-PL/HA hydrogels against *S. aureus*. Live/Dead microscopical images (scale 200 μm) illustrating bacteria attaching after 24 h of incubation on hydrogel surface. Red fluorescent dye represents dead bacteria, while Green dye represents viable bacteria found on the hydrogel surface. Quantitative graph represents viable bacteria concentration after 24 h compared with initial bacteria suspension concentration. Data are expressed as log viable bacteria in CFU (mean ± SD, $n = 3$). Statistical analysis was performed by one-way ANOVA: ns – >0.05, * – <0.05, ** – <0.01, *** – <0.005 and **** – <0.001.

disrupt bacterial membranes via electrostatic attraction, particularly when cationic charge reaches a critical threshold (multivalence effect).[66] In line with the MIC/MBC results, all hydrogels also demonstrated statistically significant inhibition

https://doi.org/10.1021/acsabm.5c01252
ACS Appl. Bio Mater. 2025, 8, 9916–9930

of *P. aeruginosa* growth. However, complete eradication was observed only for the ε-PL/HA 70:30 wt % hydrogel containing the highest free NH_3^+ content. For the other isolates (*S. aureus*, *E. coli*, *MRSA*, *ESBL E. coli*), log reduction was comparable across the hydrogel series, suggesting that hydrogel composition primarily influences *P. aeruginosa* susceptibility. These findings indicate that a sufficient concentration of free, uncross-linked primary ε-amino ($-NH_2$) groups is essential for effective electrostatic interactions, which promote bacterial membrane disruption and may interfere with the metabolic pathways, thereby enhancing bactericidal efficacy.

3.5. Biofilm Biomass Quantification via Crystal Violet Assay. The antibiofilm activity of ε-PL/HA hydrogels was evaluated using the conventional crystal violet assay to comprehensively assess their antibacterial performance. The activity was tested against two clinically relevant bacterial strains, *S. aureus* and *MRSA*, which are frequently associated with healthcare- and medical device-related biofilm infections. Bacterial biofilms are complex microbial communities encased in extracellular polymeric substances, representing a significant challenge in treating infections and contributing significantly to their persistence.[49] The ability of ε-PL/HA hydrogels to inhibit or reduce biofilms would further strengthen their antibacterial performance and highlight their potential biomedical applications. This is particularly important as conventional antibiotics often display reduced efficacy against biofilms due to several factors, including: (i) metabolic alterations of bacteria within the biofilm, (ii) limited penetration of antibiotics through the extracellular matrix, (iii) inactivation of antibiotics by matrix components, (iv) inoculum effects related to the high bacterial density, and (v) enhanced horizontal transfer of resistance mechanisms due to close cell-to-cell proximity.[51] Results on the antibiofilm activity of ε-PL/HA hydrogels are shown in Figure 5. The obtained results revealed that all ε-PL/HA hydrogel compositions achieved a statistically significant reduction ($p < 0.001$) in biofilm biomass formed by *S. aureus* and *MRSA* within 24 h compared to untreated controls (Figure 5). For the treated control, a vancomycin/gentamicin mixture was used. This choice was based on literature evidence identifying vancomycin as a first-line clinical antibiotic against *S. aureus*, including *MRSA* infections, and demonstrating the synergistic activity of vancomycin−gentamicin combinations against *S. aureus* biofilms.[67,68] Consistent with these reports, the applied antibiotic mixture (3 mg/mL vancomycin and 2 mg/mL gentamicin) also produced a significant reduction ($p < 0.05$) in established biofilms of both bacterial strains. No significant difference was observed between the antibiotic mixture and the 50:50 wt % hydrogel composition, indicating that this formulation was equally effective as clinically used antibiotics. However, the 60:40 and 70:30 wt % hydrogel formulations showed significantly greater biofilm reduction ($p < 0.05$) than the treated control for both *S. aureus* and *MRSA*. These findings demonstrate the strong antibiofilm properties of ε-PL/HA hydrogels and underline the influence of increasing ε-PL content on their antibacterial efficacy.

3.6. Antibiofilm Activity of ε-PL/HA Hydrogels via Live/Dead and Viability Assay. Live/Dead staining and viability assays against *S. aureus* supported previous findings. After 24 h, fewer bacteria were able to attach to the surface of the prepared hydrogels and form biofilms compared to Ti discs, as observed in the Live/Dead images (Figure 6). Quantitative analysis of viable *S. aureus* bacteria confirmed a significant reduction ($p < 0.05$) in bacterial colonies across all ε-PL/HA hydrogel compositions compared to the initial concentration ($t = 0$, Figure 6).

In contrast, after 72 h, Live/Dead staining revealed a markedly higher presence of *S. aureus* (Figure S3), which was further confirmed by increased viable bacterial concentrations (Figure S3). These results indicate that while ε-PL/HA hydrogels effectively reduce initial bacterial attachment and early biofilm formation, their antibiofilm activity is less pronounced against mature biofilms over longer incubation periods.

3.7. Long-Term Indirect and Direct Antibacterial Potential of ε-PL/HA Hydrogels. The sustained antibacterial performance of ε-PL/HA hydrogels (50:50, 60:40, and 70:30 wt %) was assessed over 168 h (7 days) using two complementary approaches: an indirect test (supernatants collected) to measure antibacterial activity mediated by released, free ε-amino groups of ε-PL (Figure 7A), and a direct contact test to evaluate bactericidal effects during prolonged exposure to the hydrogel surface (Figure 7B). Antibacterial efficacy was expressed as a log reduction in CFU compared to the untreated control. In the indirect test, the 70:30 wt % hydrogel achieved the most significant log reduction in CFU for both *S. aureus* and *E. coli*, followed closely by the 60:40 wt % formulation. The 50:50 wt % hydrogel produced only moderate inhibition, with no statistically significant difference compared to higher ε-PL ratio hydrogels.

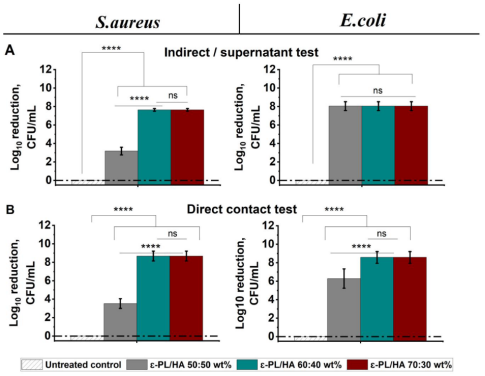

Figure 7. Long-term antibacterial activity of ε-PL/HA hydrogels against *S. aureus* and *E. coli*. (A) Indirect antibacterial test (supernatants collected after 168 h); (B) Direct antibacterial activity after 168 h direct contact with hydrogels. Data are expressed as log reduction in CFU (mean ± SD, $n = 3$). Statistical analysis was performed by one-way ANOVA: ns − >0.05, * − <0.05, ** − <0.01, *** − <0.005, and **** − < 0.001. Dash-dotted lines indicate compositions where complete eradication was achieved.

In the direct contact test, all hydrogels maintained antibacterial activity over 168 h, but the 60:40 and 70:30 wt % hydrogels were markedly more effective, achieving complete eradication of *S. aureus* and a substantial log reduction in *E. coli* CFU. In contrast, the 50:50 wt % hydrogel exhibited lower bactericidal efficacy.

These findings indicate that a higher ε-PL content increases the availability of free, uncross-linked ε-amino ($-NH_2$) groups, which sustain electrostatic interactions with bacterial mem-

https://doi.org/10.1021/acsabm.5c01252
ACS Appl. Bio Mater. 2025, 8, 9916−9930

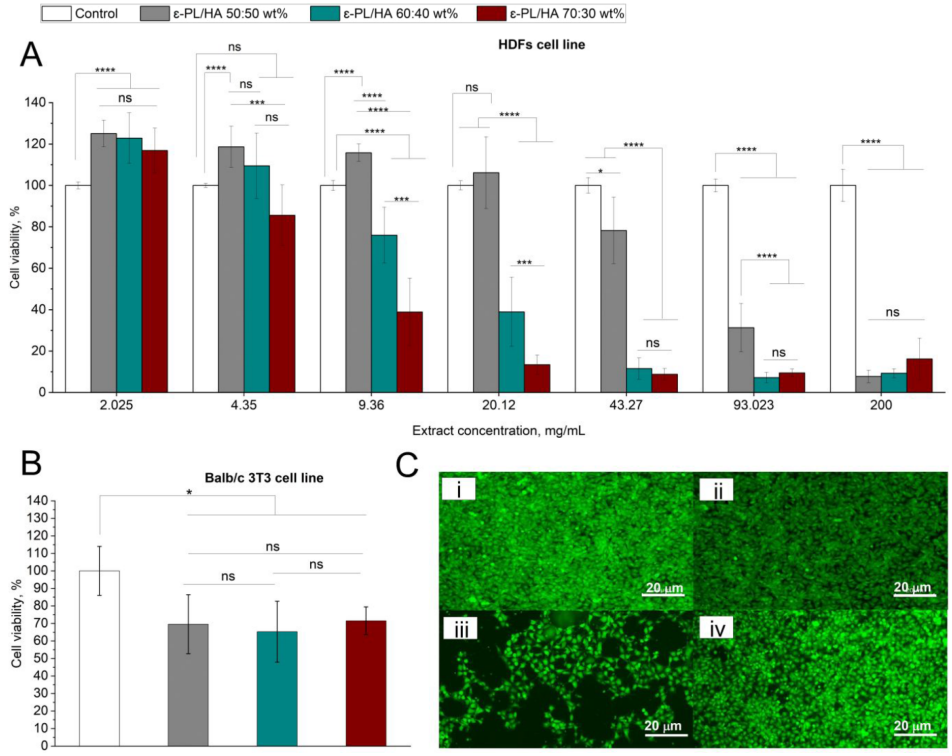

Figure 8. Cytotoxicity assay of ε-PL/HA hydrogels on HDFs and Balb/c 3T3 cells via indirect and direct tests. (A) Indirect assay on HDFs exposed to hydrogel extracts at concentrations ranging from 2.025 to 200 mg/mL for 48 h; (B) Direct assay on Balb/c 3T3 fibroblasts cultured on ε-PL/HA hydrogels (50:50, 60:40, 70:30 wt %) for 24 h; (C) Representative microscopic images of Balb/c 3T3 cells after 24 h direct culture: (i), (ii) cells in contact with ε-PL/HA 50:50 wt % hydrogel; (iii) negative control; (iv) positive control. Data are represented as mean ± SD (n = 3). Statistical analysis was performed by one-way ANOVA: ns >0.05, * <0.05, ** <0.01, *** <0.005, **** <0.001.

branes over time. The presence of free NH_3^+ groups appears crucial for maintaining the multivalence effect, particularly against Gram-negative bacteria such as *E. coli*. However, excessive cross-linking can reduce the number of free NH_3^+ groups, potentially compromising antibacterial action. Overall, the results highlight the importance of balancing cross-linking density with the availability of functional groups to achieve a long-term antibacterial performance. While the present study confirms sustained bactericidal potential for at least 7 days, extended evaluations (≥5 weeks) are needed to verify durability. Previous reports by A. Smola-Dmochowska et al. with *P. aeruginosa* support that maintaining high local concentrations of antibacterial molecules is essential for sustained efficacy.[66] Notably, our earlier work by K. Salma-Ancane et al. also revealed that increasing the ε-PL ratio improves antibacterial potency but may reduce mammalian cell viability,[42] underscoring the need to optimize formulations for both efficacy and cytocompatibility.

3.8. Swelling Behavior and Structural Stability Studies of ε-PL/HA Hydrogels. Stability studies were performed on ε-PL/HA hydrogels to investigate structural changes during incubation under dynamic conditions for 168 h. This could also help interpret results from the long-term antibacterial activity studies (Section 3.7). As described in Section 3.7, hydrogels and supernatants showed significant bacterial colony reduction compared to controls. The stability test results are shown in Figure S2 as the remaining hydrogel weight over 168 h, with measurements at 1, 2, 3, 4, 24, 48, 72, 96, and 168 h.

Within the first 24 h, the swelling curves of the prepared ε-PL/HA hydrogels with different compositions closely reproduced the swelling behavior observed in our previous study.[43] In the first hour, the hydrogels rapidly absorbed water, followed by network reorganization, reaching swelling capacities of 175%, 280%, and 440% for 50:50, 60:40, and 70:30 wt % compositions, respectively. After this initial phase, the hydrogel weight remained stable, indicating that the hydrogels did not degrade within this time frame. These results agree with our recent study by Rubina et al., where ε-PL/HA hydrogels maintained their weight in PBS containing hyaluronidase for up to 5 weeks, followed by gradual weight loss and complete degradation by 20 weeks.[44]

Based on our stability studies and previously reported enzymatic degradation profiles, it can be concluded that the hydrogels are stable for at least 168 h under dynamic conditions in both water and physiological-like environments. These findings and the long-term antibacterial studies indicate that although the bulk degradation was not detectable, trace

https://doi.org/10.1021/acsabm.5c01252
ACS Appl. Bio Mater. 2025, 8, 9916−9930

releases of uncross-linked ε-PL occurred at levels sufficient to sustain antibacterial activity in the hydrogel and its supernatant up to 168 h.

3.9. Cell Viability Assay. The indirect cytotoxicity of ε-PL/HA hydrogels was first assessed on HDFs using hydrogel extracts after 48 h of exposure (Figure 8A). Cell viability remained above 70% up to 4.35 mg/mL extract concentration for all hydrogel compositions, indicating no cytotoxicity. Notably, at the lowest concentration of 2.025 mg/mL, the ε-PL/HA 50:50 wt % hydrogels enhanced HDF viability compared to the controls, suggesting that low concentrations of ε-PL may support cell viability. This observation aligns with previous findings by Tan et al., where low doses of ε-PL were shown to increase intracellular amino acid levels, indicating a self-protective mechanism against environmental stressors.[65] This effect may arise from metabolic modulation rather than cytotoxicity, implying that careful dosing can exploit the beneficial properties of ε-PL while minimizing cytotoxic effects. Therefore, at lower concentrations, ε-PL may promote cell survival, particularly in designing highly biocompatible hydrogels. At higher concentrations, differences between compositions became evident: the ε-PL/HA 50:50 wt % maintained cell viability >70% up to 93.023 mg/mL, while the ε-PL/HA 60:40 wt % showed cytotoxic effects starting from 20.12 mg/mL, and the ε-PL/HA 70:30 wt % exhibited significant cytotoxicity at 9.36 mg/mL. All hydrogel series exhibited significant cytotoxicity at the highest tested concentration (≥93.023 mg/mL). Among the tested series, ε-PL/HA 50:50 wt % hydrogels displayed the most favorable balance between maintaining cell viability and minimizing cytotoxic effects. Direct cytotoxicity testing on Balb/c 3T3 cells (Figure 8B) revealed that all hydrogel series exhibited mild cytotoxicity, with cell viability decreasing to approximately 70% compared to the untreated control ($p < 0.05$). No significant differences were observed between hydrogel series (ns), indicating that the type of hydrogel series did not significantly influence cell viability. Comparing both results, it could be observed that HDF cells exposed to hydrogel extracts exhibited higher viability compared to Balb/c 3T3 cells directly cultured on the hydrogels. This is a common observation previously noticed in several studies.[42,69] The difference in results directly relies on the testing approach, as indirect exposure limits the contact of cells with the hydrogel network. In contrast, a direct culture imposes both chemical and physical stress.

Representative microscopy images of Balb/c 3T3 cells after direct contact with hydrogels (Figure 8C, i–iv) confirmed that the cells maintained normal morphology and attachment, comparable to the negative control, whereas the positive control showed cell death. This suggests that although viability decreased slightly, overall cell integrity and morphology remained unaffected. Furthermore, the observed cytotoxicity of the hydrogels can be attributed to the antibacterial activity of ε-PL, which disrupts bacterial membranes but may also interact with mammalian cell membranes. This is consistent with the mechanism of polycationic hydrogels, which can induce electrostatic interactions with negatively charged cell membranes. However, by microscopic evaluation, cells grew and showed normal morphology when cultivated directly with the ε-PL/HA hydrogels. In the context of developing antibacterial hydrogels for tissue engineering, achieving a balance between antimicrobial efficacy and cytocompatibility is crucial.[70,71] Although increasing the ε-PL content enhances bactericidal activity, it also raises the risk of cytotoxicity, underscoring the need for careful composition optimization. This balance often depends on both the concentration and the type of antimicrobial agents incorporated into the hydrogel network.[72] These findings indicate that while a higher ε-PL content enhances antibacterial action, achieving a formulation with optimal cytocompatibility is essential for practical biomedical applications. The ε-PL/HA 50:50 wt % hydrogel demonstrated the most favorable balance, making it a promising candidate for tissue engineering.

4. CONCLUSIONS

This study demonstrated the development and evaluation of *in situ* forming, covalently cross-linked ε-polylysine/hyaluronic acid hydrogels with tunable ε-PL content (50:50, 60:40, and 70:30 wt %) for minimally invasive, syringe-based delivery to infection sites. Rheological characterization confirmed that the hydrogels exhibit favorable mechanical properties, including shear-thinning behavior, self-recovery capability, and consistent injectability across a physiologically relevant temperature range, supporting their practical use in clinical settings. *In vitro,* antibacterial assays revealed that the hydrogels provided intense bactericidal activity against a broad panel of clinically relevant Gram-positive and Gram-negative bacteria, including multidrug-resistant bacterial strains. They also demonstrated strong antibiofilm activity within 24 h and retained prolonged antibacterial efficacy, while ε-PL contributed intrinsic antibacterial activity without promoting bacterial resistance development. Cytocompatibility assessments showed a dose-dependent response of fibroblasts to the ε-PL concentration included in the hydrogels, highlighting the importance of ε-PL concentration in modulating cell viability. This study presents the first comprehensive evaluation of injectable ε-PL/HA hydrogels that exhibit favorable rheological features (shear-thinning behavior, injectability, self-recovery), sustained antibacterial efficacy, and biocompatibility. Combining the membrane-disruptive action of ε-PL with the biologically active properties of HA, these hydrogels represent a promising nonantibiotic strategy for localized treatment of bacterial wound infections, including those caused by antibiotic-resistant and biofilm-associated pathogens.

■ ASSOCIATED CONTENT

Supporting Information

The Supporting Information is available free of charge at https://pubs.acs.org/doi/10.1021/acsabm.5c01252.

S.1.1. Time sweep studies: results and discussion, as well as gelation time values summarized in Table 2. Figure S1 within Section S.1.1. supporting Section 3.1. Figures S2 supporting Section 3.8. Figure S3 supporting Section 3.6 (PDF)

■ AUTHOR INFORMATION

Corresponding Author

Kristine Salma-Ancane − *Institute of Biomaterials and Bioengineering, Faculty of Natural Sciences and Technology, Riga Technical University, Riga lv-1048, Latvia; Baltic Biomaterials Centre of Excellence, Headquarters at Riga Technical University, Riga lv-1048, Latvia;* orcid.org/0000-0001-9215-0097; Email: kristine.salma-ancane@rtu.lv

https://doi.org/10.1021/acsabm.5c01252
ACS Appl. Bio Mater. 2025, 8, 9916−9930

Authors

Artemijs Sceglovs − *Institute of Biomaterials and Bioengineering, Faculty of Natural Sciences and Technology, Riga Technical University, Riga lv-1048, Latvia; Baltic Biomaterials Centre of Excellence, Headquarters at Riga Technical University, Riga lv-1048, Latvia*

Claudia Siverino − *AO Research Institute Davos, Davos 7270, Switzerland*

Ingus Skadins − *Department of Biology and Microbiology, Riga Stradins University, Riga lv-1007, Latvia*

Marika Sceglova − *Institute of Biomaterials and Bioengineering, Faculty of Natural Sciences and Technology, Riga Technical University, Riga lv-1048, Latvia; Baltic Biomaterials Centre of Excellence, Headquarters at Riga Technical University, Riga lv-1048, Latvia*

Valdis Pirsko − *Institute of Microbiology and Virology, Riga Stradins University, Riga lv-1067, Latvia*

Thomas Fintan Moriarty − *AO Research Institute Davos, Davos 7270, Switzerland;* orcid.org/0000-0003-2307-0397

Juta Kroica − *Department of Biology and Microbiology, Riga Stradins University, Riga lv-1007, Latvia*

Complete contact information is available at: https://pubs.acs.org/10.1021/acsabm.5c01252

Author Contributions

A.S.: Conceptualization, Resources, Writing—Original draft preparation, Methodology, Validation, Writing—Review and Editing. C.S.: Writing—Review and Editing, Methodology, Validation, Formal analysis, Investigation, Supervision. I.S.: Methodology, Validation, Formal analysis, Investigation. M.S.: Methodology, Investigation. V.P.: Methodology, Validation, Formal analysis, Investigation. F.T.M.: Supervision, Resources, Methodology, Writing—Review and Editing. J.K.: Supervision, Resources, Methodology, Writing—Review and Editing. K.S.-A.: Conceptualization, Supervision, Resources, Methodology, Writing—Review and Editing, Funding acquisition.

Funding

The authors acknowledge financial support from the European Union's Horizon 2020 research and innovation program under the grant agreement No. 857287 (BBCE). The authors acknowledge financial support from the C316 Implementation of Consolidation and Governance Changes at Riga Technical University, LiepU, RAT, LMA, and LMC to Advance Excellence in Higher Education, Science, and Innovation program under the grant agreement C4835.Dok.1025 No. 5.2.1.1.i.0/2/24/I/CFLA/003. The authors confirm using Biorender for creating Graphical abstract and Figure 1, and hereby confirm that Science Suite Inc. dba BioRender ("BioRender") has granted the following BioRender user: Kristine Salma-Ancane ("User") a BioRender Academic Publication License in accordance with BioRender's Terms of Service and Academic License Terms ("License Terms") to permit such User to do the following on the condition that all requirements in this Confirmation are met: 1) publish their Completed Graphics created in the BioRender Services containing both User Content and BioRender Content (as both are defined in the License Terms) in publications (journals, textbooks, Web sites, etc.); and 2) sublicense such Completed Graphics under "open access" publication sub-licensing models such as CC-BY 4.0 and more restrictive models, so long as the conditions set forth herein are fully met.

The authors thank Lauma Ievina (Institute of Biomaterials and Bioengineering, Faculty of Natural Sciences and Technology, Riga Technical University; Baltic Biomaterials Centre of Excellence) for her excellent help in confocal microscopy analysis.

Notes

•ε-PL/HA hydrogels are shear-thinning and injectable •Strong antibacterial effect against multidrug-resistant strains •ε-PL prevents resistance and kills MRSA and ESBL-producing *E. coli* •Hydrogels reduce *S. aureus* and MRSA biofilms, matching antibiotic controls •Hydrogels maintain high fibroblast cytocompatibility

The authors declare no competing financial interest.

REFERENCES

(1) *7.7 million people die from bacterial infections every year − 2022 − ReAct.* https://www.reactgroup.org/news-and-views/news-and-opinions/year-2022/7-7-million-people-die-from-bacterial-infections-every-year/ (accessed 2025−02−19).

(2) *WHO updates list of drug-resistant bacteria most threatening to human health.* https://www.who.int/news/item/17-05-2024-who-updates-list-of-drug-resistant-bacteria-most-threatening-to-human-health (accessed 2025−06−04).

(3) Oliveira, M.; Antunes, W.; Mota, S.; Madureira-Carvalho, Á.; Dinis-Oliveira, R. J.; Dias da Silva, D. An Overview of the Recent Advances in Antimicrobial Resistance. *Microorganisms* **2024**, *12* (9), 1920.

(4) Ventola, C. L. The Antibiotic Resistance Crisis: Causes and Threats. *Pharm. Ther.* **2015**, *40* (4), 277−283.

(5) *Antimicrobial resistance.* https://www.who.int/news-room/fact-sheets/detail/antimicrobial-resistance (accessed 2025−06−04).

(6) Naghavi, M.; Vollset, S. E.; Ikuta, K. S.; Swetschinski, L. R.; Gray, A. P.; Wool, E. E.; Robles Aguilar, G.; Mestrovic, T.; Smith, G.; Han, C.; et al. Global burden of bacterial antimicrobial resistance 1990−2021: a systematic analysis with forecasts to 2050. *Lancet* **2024**, *404* (10459), 1199−1226.

(7) *WHO releases report on state of development of antibacterials.* https://www.who.int/news/item/14-06-2024-who-releases-report-on-state-of-development-of-antibacterials (accessed 2025−02−19).

(8) *WHO outlines 40 research priorities on antimicrobial resistance.* https://www.who.int/news/item/22-06-2023-who-outlines-40-research-priorities-on-antimicrobial-resistance (accessed 2025−02−19).

(9) *Healthcare-associated infections.* https://www.ecdc.europa.eu/en/healthcare-associated-infections (accessed 2025−06−11).

(10) Hu, Y.; Yu, L.; Dai, Q.; Hu, X.; Shen, Y. Multifunctional Antibacterial Hydrogels for Chronic Wound Management. *Biomater. Sci.* **2024**, *12* (10), 2460−2479.

(11) Liang, J.-Y.; Li, Q.; Feng, L.B.; Hu, S.X.; Zhang, S.Q.; Li, C.X.; Zhang, X.B. Injectable Antimicrobial Hydrogels with Antimicrobial Peptide and Sanguinarine Controlled Release Ability for Preventing Bacterial Infections. *Am. J. Transl. Res.* **2021**, *13* (11), 12614−12625.

(12) Boonkaew, B.; Suwanpreuksa, P.; Cuttle, L.; Barber, P. M.; Supaphol, P. Hydrogels Containing Silver Nanoparticles for Burn Wounds Show Antimicrobial Activity without Cytotoxicity. *J. Appl. Polym. Sci.* **2014**, *131* 9. .

(13) Mohandas, A.; Kumar Pt, S.; Raja, B.; Lakshmanan, V.-K.; Jayakumar, R. Exploration of alginate hydrogel/nano zinc oxide composite bandages for infected wounds [Corrigendum]. *Int. J. Nanomed.* **2019**, *14* (1), 2607−2608.

(14) Kalelkar, P. P. Biomaterial-Based Antimicrobial Therapies for the Treatment of Bacterial Infections. *Nat. Rev. Mater.* **2021**, *7* (1), 39−54.

(15) Chen, B.; Ponce Benavente, L.; Chittò, M.; Post, V.; Constant, C.; Zeiter, S.; Nylund, P.; D'Este, M.; González Moreno, M.; Trampuz, A. Combination of Bacteriophages and Vancomycin in a

Co-Delivery Hydrogel for Localized Treatment of Fracture-Related Infections. *Npj Biofilms Microbiomes* **2024**, *10* (1), 77.
(16) Xuan, J.; Feng, W.; Wang, J.; Wang, R.; Zhang, B.; Bo, L.; Chen, Z.-S.; Yang, H.; Sun, L. Antimicrobial Peptides for Combating Drug-Resistant Bacterial Infections. *Drug Resist. Update* **2023**, *68*, 100954.
(17) Lebaudy, E.; Guilbaud-Chéreau, C.; Frisch, B.; Vrana, N. E.; Lavalle, P. The High Potential of ε-Poly-l-Lysine for the Development of Antimicrobial Biomaterials. *Adv. nanobiomed Res.* **2023**, *3* (12), 2300080.
(18) Sceglovs, A.; Skadins, I.; Chitto, M.; Kroica, J.; Salma-Ancane, K. Failure or Future? Exploring Alternative Antibacterials: A Comparative Analysis of Antibiotics and Naturally Derived Biopolymers. *Front. Microbiol.* **2025**, *16*, 1526250.
(19) Qiu, H.; Si, Z.; Luo, Y.; Feng, P.; Wu, X.; Hou, W.; Zhu, Y.; Chan-Park, M. B.; Xu, L.; Huang, D. The Mechanisms and the Applications of Antibacterial Polymers in Surface Modification on Medical Devices. *Front. Bioeng. Biotechnol.* **2020**, *8*, 910.
(20) Li, G.; Lai, Z.; Shan, A. Advances of Antimicrobial Peptide-Based Biomaterials for the Treatment of Bacterial Infections. *Adv. Sci* **2023**, *10* (11), 2206602.
(21) Copling, A.; Akantibila, M.; Kumaresan, R.; Fleischer, G.; Cortes, D.; Tripathi, R.S.; Carabetta, V.J.; Vega, S.L. Recent Advances in Antimicrobial Peptide Hydrogels. *Int. J. Mol. Sci.* **2023**, *24* (8), 7563.
(22) Drexelius, M. G.; Neundorf, I. Application of Antimicrobial Peptides on Biomedical Implants: Three Ways to Pursue Peptide Coatings. *Int. J. Mol. Sci.* **2021**, *22* (24), 13212.
(23) Wang, B.; Zhao, D.; Li, Y.; Zhou, X.; Hui, Z.; Lei, X.; Qiu, L.; Bai, Y.; Wang, C.; Xia, J.; et al. Antimicrobial Peptide Nanoparticle-Based Microneedle Patches for the Treatment of Bacteria-Infected Wounds. *ACS Appl. Nano Mater.* **2023**, *6* (8), 6891−6900.
(24) Sultana, A.; Luo, H.; Ramakrishna, S. Antimicrobial Peptides and Their Applications in Biomedical Sector. *Antibiot* **2021**, *10* (9), 1094.
(25) Moretta, A.; Scieuzo, C.; Petrone, A.M.; Salvia, R.; Manniello, M.D.; Franco, A.; Lucchetti, D.; Vassallo, A.; Vogel, H.; Sgambato, A. Antimicrobial Peptides: A New Hope in Biomedical and Pharmaceutical Fields. *Front. Cell. Infect. Microbiol.* **2021**, *11*, 668632.
(26) Sousa, M. G. C.; Rezende, T. M. B.; Franco, O. L. Nanofibers as Drug-Delivery Systems for Antimicrobial Peptides. *Drug Discovery Today* **2021**, *26* (8), 2064−2074.
(27) Fadaka, A. O.; Sibuyi, N.R.S.; Madiehe, A.M.; Meyer, M. Nanotechnology-Based Delivery Systems for Antimicrobial Peptides. *Pharm* **2021**, *13* (11), 1795.
(28) Huan, Y.; Kong, Q.; Mou, H.; Yi, H. Antimicrobial Peptides: Classification, Design, Application and Research Progress in Multiple Fields. *Front. Microbiol.* **2020**, *11*, 582779.
(29) Zou, Y. J.; He, S.S.; Du, J.Z. ε-Poly(L-Lysine)-Based Hydrogels with Fast-Acting and Prolonged Antibacterial Activities. *Chin. J. Polym. Sci.* **2018**, *36* (11), 1239−1250.
(30) Kennedy, S. M.; Deshpande, P.; Gallagher, A. G.; Horsburgh, M. J.; Allison, H. E.; Kaye, S. B.; Wellings, D. A.; Williams, R. L. Antimicrobial Activity of Poly-Epsilon-Lysine Peptide Hydrogels Against Pseudomonas Aeruginosa. *Invest. Ophthalmol. Vis. Sci.* **2020**, *61* (10), 18.
(31) Chen, Y.; Miao, W.; Li, X.; Xu, Y.; Gao, H.; Zheng, B. The Structure, Properties, Synthesis Method and Antimicrobial Mechanism of ε-Polylysine with the Preservative Effects for Aquatic Products. *Trends Food Sci. Technol.* **2023**, *139*, 104131.
(32) Hyldgaard, M.; Mygind, T.; Vad, B. S.; Stenvang, M.; Otzen, D. E.; Meyer, R. L. The Antimicrobial Mechanism of Action of Epsilon-Poly-L-Lysine. *Appl. Environ. Microbiol.* **2014**, *80* (24), 7758−7770.
(33) Shima, S.; Matsuoka, H.; Iwamoto, T.; Sakai, H. Antimicrobial action of.EPSILON.-poly-L-lysine. *J. Antibiot.* **1984**, *37* (11), 1449−1455.
(34) Ye, R.; Xu, H.; Wan, C.; Peng, S.; Wang, L.; Xu, H.; Aguilar, Z. P.; Xiong, Y.; Zeng, Z.; Wei, H. Antibacterial Activity and Mechanism of Action of ε-Poly-l-Lysine. *Biochem. Biophys. Res. Commun.* **2013**, *439* (1), 148−153.
(35) Wang, L. Epsilon-Poly-L-Lysine: Recent Advances in Biomanufacturing and Applications. *Front. Bioeng. Biotechnol.* **2021**, *9*, 748976.
(36) Tan, Z.; Shi, Y.; Xing, B.; Hou, Y.; Cui, J.; Jia, S. The Antimicrobial Effects and Mechanism of ε-Poly-Lysine against Staphylococcus Aureus. *Bioresour. Bioprocess* **2019**, *6* (1), 1−10.
(37) Wei, R.; Chen, T.; Wang, Y.; Xu, Q.; Feng, B.; Weng, J.; Peng, W.; Wang, J. By Endowing Polyglutamic Acid/Polylysine Composite Hydrogel with Super Intrinsic Characteristics to Enhance Its Wound Repair Potential. *Macromol. Biosci* **2021**, *21* (5), 2000367.
(38) Sundaran, S.; Kok, L.C.; Chang, H.Y. Combination Effect of Epsilon-Poly-L-Lysine and Antibiotics against Common Bacterial Pathogens. *J. Antibiot.* **2022**, *75* (6), 354−359.
(39) Liu, H.; Li, Z.; Zhao, Y.; Feng, Y.; Zvyagin, A.V.; Wang, J.; Yang, X.; Yang, B.; Lin, Q. Novel Diabetic Foot Wound Dressing Based on Multifunctional Hydrogels with Extensive Temperature-Tolerant, Durable, Adhesive, and Intrinsic Antibacterial Properties. *ACS Appl. Mater. Interfaces* **2021**, *13* (23), 26770−26781.
(40) Qi, X.; Pan, W.; Tong, X.; Gao, T.; Xiang, Y.; You, S.; Mao, R.; Chi, J.; Hu, R.; Zhang, W.; et al. ε-Polylysine-stabilized agarose/polydopamine hydrogel dressings with robust photothermal property for wound healing. *Carbohydr. Polym* **2021**, *264*, 118046.
(41) Lopez Mora, N.; Owens, M.; Schmidt, S.; Silva, A. F.; Bradley, M. Poly-Epsilon-Lysine Hydrogels with Dynamic Crosslinking Facilitates Cell Proliferation. *Materials* **2020**, *13* (17), 3851.
(42) Salma-Ancane, K.; Sceglovs, A.; Tracuma, E.; Wychowaniec, J. K.; Aunina, K.; Ramata-Stunda, A.; Nikolajeva, V.; Loca, D. Effect of Crosslinking Strategy on the Biological, Antibacterial and Physicochemical Performance of Hyaluronic Acid and ε-Polylysine Based Hydrogels. *Int. J. Biol. Macromol.* **2022**, *208*, 995−1008.
(43) Sceglovs, A.; Wychowaniec, J. K.; Skadins, I.; Reinis, A.; Edwards-Gayle, C. J. C.; D'Este, M.; Salma-Ancane, K. Effect of Steam Sterilisation on Physico-Chemical Properties of Antibacterial Covalently Cross-Linked ε-Polylysine/Hyaluronic Acid Hydrogels. *Carbohydr. Polym. Technol. Appl.* **2023**, *6*, 100363.
(44) Rubina, A.; Sceglovs, A.; Ramata-Stunda, A.; Pugajeva, I.; Skadins, I.; Boyd, A. R.; Tumilovica, A.; Stipniece, L.; Salma-Ancane, K. Injectable Mineralized Sr-Hydroxyapatite Nanoparticles-Loaded ε-Polylysine-Hyaluronic Acid Composite Hydrogels for Bone Regeneration. *Int. J. Biol. Macromol.* **2024**, *280*, 135703.
(45) *M07 Ed12 | Methods for Dilution Antimicrobial Susceptibility Tests for Bacteria That Grow Aerobically*, https://clsi.org/standards/products/microbiology/documents/m07/ (accessed 2025−02−19).
(46) Wilson, C.; Lukowicz, R.; Merchant, S.; Valquier-Flynn, H.; Caballero, J.; Sandoval, J.; Okuom, M.; Huber, C.; Brooks, T.D.; Wilson, E., et al. Quantitative and Qualitative Assessment Methods for Biofilm Growth: A Mini-Review. *Res. Rev. J. Eng. Technol.*. **2017**, *6*(4), PMID: 30214915; PMCID: PMC6133255.
(47) Kanematsu, H.; Ikigai, H.; Yoshitake, M. Evaluation of Various Metallic Coatings on Steel to Mitigate Biofilm Formation. *Int. J. Mol. Sci.* **2009**, *10* (2), 559−571.
(48) *Biofilm testing for antibacterial bacteriophage | BMG LABTECH*. https://www.bmglabtech.com/en/application-notes/testing-novel-bacteriophages-for-antibacterial-properties-with-a-crystal-violet-biofilm-quantification-assay/ (accessed 2025−09−02).
(49) Zhao, A.; Sun, J.; Liu, Y. Understanding Bacterial Biofilms: From Definition to Treatment Strategies. *Front. Cell. Infect. Microbiol.* **2023**, *13*, 1137947.
(50) Grari, O.; Ezrari, S.; El Yandouzi, I.; Benaissa, E.; Ben Lahlou, Y.; Lahmer, M.; Saddari, A.; Elouennass, M.; Maleb, A. A Comprehensive Review on Biofilm-Associated Infections: Mechanisms, Diagnostic Challenges, and Innovative Therapeutic Strategies. *Microbe* **2025**, *8*, 100436.
(51) Schulze, A.; Mitterer, F.; Pombo, J. P.; Schild, S. Biofilms by bacterial human pathogens: Clinical relevance - development, composition and regulation - therapeutical strategies. *Microb. Cell* **2021**, *8* (2), 28.

(52) *eucast: SOPs*. https://www.eucast.org/eucastsops (accessed 2025−02−19).
(53) *Guidance Document on Using Cytotoxicity Tests to Estimate Starting Doses for Acute Oral Systematic Toxicity Tests | OECD* https://www.oecd.org/en/publications/guidance-document-on-using-cytotoxicity-tests-to-estimate-starting-doses-for-acute-oral-systematic-toxicity-tests_d77a7e39-en.html (accessed 2025−02−19).
(54) *CellTiter-Blue® Cell Viability Assay Protocol*. https://worldwide.promega.com/resources/protocols/technical-bulletins/101/celltiter-blue-cell-viability-assay-protocol/ (accessed 2025−08−20).
(55) Borzacchiello, A.; Russo, L.; Malle, B. M.; Schwach-Abdellaoui, K.; Ambrosio, L. Hyaluronic Acid Based Hydrogels for Regenerative Medicine Applications. *BioMed. Res. Int.* **2015**, *2015* (1), 871218.
(56) Shriky, B.; Kelly, A.; Isreb, M.; Babenko, M.; Mahmoudi, N.; Rogers, S.; Shebanova, O.; Snow, T.; Gough, T. Pluronic F127 Thermosensitive Injectable Smart Hydrogels for Controlled Drug Delivery System Development. *J. Colloid Interface Sci.* **2020**, *565*, 119−130.
(57) Tang, Y.; Hu, M.; Tang, F.; Huang, R.; Wang, H.; Wu, D.; Lan, P. Easily-Injectable Shear-Thinning Hydrogel Provides Long-Lasting Submucosal Barrier for Gastrointestinal Endoscopic Surgery. *Bioact. Mater.* **2022**, *15*, 44−52.
(58) Chen, M. H.; Wang, L. L.; Chung, J. J.; Kim, Y.-H.; Atluri, P.; Burdick, J. A. Methods to Assess Shear-Thinning Hydrogels for Application As Injectable Biomaterials. *ACS Biomater. Sci. Eng.* **2017**, 3 (12), 3146−3160.
(59) Li, L.; Li, H. Rheological properties and 3D printability of alginate-based hydrogels for biofabrication. *Front. Bioeng. Biotechnol. Conference Abstract: 10th World Biomaterials Congress* **2016**, DOI: 10.3389/CONF.FBIOE.2016.01.01814
(60) Enoch, K.; Somasundaram, A. A. Rheological Insights on Carboxymethyl Cellulose Hydrogels. *Int. J. Biol. Macromol.* **2023**, *253*, 127481.
(61) Ribeiro, M. Infection of Orthopedic Implants with Emphasis on Bacterial Adhesion Process and Techniques Used in Studying Bacterial-Material Interactions. *Biomatter* **2012**, *2* (4), 176.
(62) Masters, E. A.; Ricciardi, B.F.; Bentley, K.L.D.M.; Moriarty, T.F.; Schwarz, E.M.; Muthukrishnan, G. Skeletal Infections: Microbial Pathogenesis, Immunity and Clinical Management. *Nat. Rev. Microbiol.* **2022**, *20* (7), 385−400.
(63) López, C. A.; Zgurskaya, H.; Gnanakaran, S. Molecular Characterization of the Outer Membrane of Pseudomonas Aeruginosa. *Biochim. Biophys. Acta - Biomembr.* **2020**, *1862* (3), 183151.
(64) Kadeřábková, N.; Mahmood, A.J.; Mavridou, D.A. Antibiotic Susceptibility Testing Using Minimum Inhibitory Concentration (MIC) Assays. *Npj Antimicrob Resist* **2024**, *2* (1), 1−9.
(65) Tan, Z.; Shi, Y.; Xing, B.; Hou, Y.; Cui, J.; Jia, S. The Antimicrobial Effects and Mechanism of ε-Poly-Lysine against Staphylococcus Aureus. *Bioresour. Bioprocess.* **2019**, *6* (1), 11.
(66) Smola-Dmochowska, A.; Lewicka, K.; Macyk, A.; Rychter, P.; Pamuła, E.; Dobrzyński, P. Biodegradable Polymers and Polymer Composites with Antibacterial Properties. *IJMS* **2023**, *24* (8), 7473.
(67) Borges, N. H.; Suss, P.H.; Ortis, G.B.; Dantas, L.R.; Tuon, F.F. Synergistic Activity of Vancomycin and Gentamicin Against Staphylococcus Aureus Biofilms on Polyurethane Surface. *Microorganisms* **2025**, *13* (5), 1119.
(68) Pedroni, M. A.; Ribeiro, V. S. T.; Cieslinski, J.; Lopes, A. P. D. A.; Kraft, L.; Suss, P. H.; Tuon, F. F. Different Concentrations of Vancomycin with Gentamicin Loaded PMMA to Inhibit Biofilm Formation of Staphylococcus Aureus and Their Implications. *J. Orthop. Sci.* **2024**, *29* (1), 334−340.
(69) Guarnieri, R.; Reda, R.; Di Nardo, D.; Miccoli, G.; Zanza, A.; Testarelli, L. In Vitro Direct and Indirect Cytotoxicity Comparative Analysis of One Pre-Hydrated versus One Dried Acellular Porcine Dermal Matrix. *Materials* **2022**, *15* (5), 1937.
(70) Zhu, J.; Cheng, H.; Zhang, Z.; Chen, K.; Zhang, Q.; Zhang, C.; Gao, W.; Zheng, Y. Antibacterial Hydrogels for Wound Dressing Applications: Current Status, Progress, Challenges, and Trends. *Gels* **2024**, *10* (8), 495.
(71) Tang, Y.; Xu, H.; Wang, X.; Dong, S.; Guo, L.; Zhang, S.; Yang, X.; Liu, C.; Jiang, X.; Kan, M.; Wu, S. Advances in Preparation and Application of Antibacterial Hydrogels. *J. Nanobiotechnol.* **2023**, *21* (1), 1−20.
(72) Jablonská, E.; Kubásek, J.; Vojtěch, D.; Ruml, T.; Lipov, J. Test Conditions Can Significantly Affect the Results of in Vitro Cytotoxicity Testing of Degradable Metallic Biomaterials. *Sci. Rep.* **2021**, *11* (1), 1−9.

https://doi.org/10.1021/acsabm.5c01252
ACS Appl. Bio Mater. 2025, 8, 9916−9930

Appendix V

5. Pielikums

Injectable mineralized Sr-hydroxyapatite nanoparticles-loaded ε-polylysine-hyaluronic acid composite hydrogels for bone regeneration

Anna Rubina, Artemijs Sceglovs, Anna Ramata-Stunda, Iveta Pugajeva, Adrian R. Boyd, Anastasija Tumilovica, Liga Stipniece, Kristine Salma-Ancane

International Journal of Biological Macromolecules, **2024**, 280: 135703.
https://doi.org/10.1016/j.ijbiomac.2024.135703

A.S. input: Writing – review & editing, Writing – original draft, Visualization, Investigation, Formal analysis, Conceptualization.

International Journal of Biological Macromolecules 280 (2024) 135703

Contents lists available at ScienceDirect

International Journal of Biological Macromolecules

journal homepage: www.elsevier.com/locate/ijbiomac

Injectable mineralized Sr-hydroxyapatite nanoparticles-loaded ε-polylysine-hyaluronic acid composite hydrogels for bone regeneration

A. Rubina [a,b], A. Sceglovs [a,b], A. Ramata-Stunda [c], I. Pugajeva [d], I. Skadins [e], A.R. Boyd [f], A. Tumilovica [a,b], L. Stipniece [a,b,*], K. Salma-Ancane [a,b,*]

[a] Institute of Biomaterials and Bioengineering, Faculty of Natural Sciences and Technology, Riga Technical University, Pulka St. 3/3, Riga LV-1007, Latvia
[b] Baltic Biomaterials Centre of Excellence, Headquarters at Riga Technical University, Riga, Latvia
[c] Department of Microbiology and Biotechnology, Faculty of Biology, University of Latvia, Jelgavas St. 1, Riga LV-1004, Latvia
[d] Institute of Food Safety, Animal Health and Environment "BIOR", Lejupes Street 3, Riga LV-1076, Latvia
[e] Department of Biology and Microbiology, Riga Stradins University, Dzirciema St. 16, Riga LV-1007, Latvia
[f] Nanotechnology and Integrated Bioengineering Centre (NIBEC), School of Engineering, Ulster University, Shore Road, Newtownabbey, Co. Antrim, BT37 0QB, United Kingdom of Great Britain and Northern Ireland

ARTICLE INFO

Keywords:
Sr-substituted hydroxyapatite nanoparticles
Injectable nanocomposite hydrogels
Sr ion delivery
Antibacterial hydrogels
Osteogenic potential

ABSTRACT

In this study, multifunctional injectable mineralized antibacterial nanocomposite hydrogels were prepared by a homogenous distribution of high content of (up to 60 wt%) Sr-substituted hydroxyapatite (Sr-HAp) nanoparticles into covalently cross-linked ε-polylysine (ε-PL) and hyaluronic acid (HA) hydrogel network. The developed bone-targeted nanocomposite hydrogels were to synergistically combine the functional properties of bioactive Sr-HAp nanoparticles and antibacterial ε-PL-HA hydrogels for bone tissue regeneration. Viscoelasticity, injectability, structural parameters, degradation, antibacterial activity, and *in vitro* biocompatibility of the fabricated nanocomposite hydrogels were characterized. Physical performances of the ε-PL-HA hydrogels can be tailored by altering the mass ratio of Sr-HAp. The nanocomposite hydrogels revealed good stability against enzymatic degradation, which increased from 5 to 19 weeks with increasing the mass ratio of Sr-HAp from 40 % to 60 %. The loading of the Sr-HAp at relatively high mass ratios did not suppress the fast-acting and long-term antibacterial activity of the ε-PL-HA hydrogels against *S. aureus* and *E. coli*. The cell studies confirmed the cytocompatibility and pre-collagen I synthesis-promoting activity of the fabricated nanocomposite hydrogels.

1. Introduction

Bone defects and fracture regeneration remain a major medical challenge in modern clinical practice [1]. One of the main reasons is the global silent epidemic - osteoporosis. According to the World Health Organization (WHO), metabolic bone disease - osteoporosis, is the second most prevalent illness globally, after cardiovascular diseases [2]. Osteoporosis can cause complex fragility fractures and critical-size bone defects (defects involving 50 % of the cortical diameter with a minimum length of 1 cm [3]), which need complex surgical intervention and reconstruction. The costs of healthcare systems attributed to osteoporotic fractures in the European Union are around €37 billion per year, predicted to double by 2050 [4]. Thus, there is an urgent need for multifunctional bone-targeted biomaterials with promising therapeutic and regeneration capabilities [5].

The current treatment protocols for complex osteoporotic fractures involve the use of auto/allografts [6], inert metallic implants [7], or bioactive ceramic implants [8], but their use is associated with various limitations. The gold standard, autografts, are expensive and of low availability, while allografts also have limited availability and possess infection risks [9]. Inert metallic implants offer high mechanical strength but lack bioactivity and bioresorbability and cannot fully integrate with bone tissues. In turn, bioactive calcium phosphate (CaP) bone biomaterials demonstrate excellent biocompatibility and bioactivity in physiological conditions due to their similarity with the major inorganic component of bone tissue and can form intimate functional interfaces with bone tissue. However, CaP biomaterials have low mechanical strength, uncertain degradation rate, lack of cohesiveness, and

* Corresponding authors at: Institute of Biomaterials and Bioengineering, Faculty of Natural Sciences and Technology, Riga Technical University, Pulka St. 3/3, Riga LV-1007, Latvia.
E-mail addresses: liga.stipniece@rtu.lv (L. Stipniece), kristine.salma-ancane@rtu.lv (K. Salma-Ancane).

https://doi.org/10.1016/j.ijbiomac.2024.135703
Received 9 April 2024; Received in revised form 11 September 2024; Accepted 14 September 2024
Available online 16 September 2024

mechanical integrity [9,10]. Moreover, the commercially available bone biomaterials have limited regeneration potential for bone-related disease treatment and are still far from those of the unique composite structure of bone.

Bone is a complex inorganic-organic nanocomposite composed of extracellular matrix (ECM) and several types of cells [11]. The bone ECM consists of 20–40 % organic matrix, 50–70 % minerals, mostly hydroxyapatite (HAp) nanocrystallites between and within the length of collagen fibers, and 5–10 % water. The organic matrix is composed of type I collagen (90 %) and over 200 different non-collagenous proteins (~10 %), of which proteoglycans and glycosaminoglycans, including non-sulfated glycosaminoglycan hyaluronic acid (HA), play a significant role in physiological bone remodeling [12,13].

Injectable natural biopolymer-based hydrogels have been extensively explored as versatile biomaterials for bone tissue engineering applications due to their advantageous functionalities such as biocompatibility and non-toxicity, ability to mimic three-dimensional (3D) ECM, intrinsic cellular interactions, rheological properties, and biodegradability [14,15]. Moreover, the main advantages of the injectable hydrogels as bone-targeted biomaterials include the ability to mimic the bone ECM, provide a functionalized microenvironment for bone defect regeneration, form the desired shape to fill internal large and irregular defects, locally administrate drugs or biologically active molecules directly to the bone defect site over a long period, improve therapeutic efficiency, and decrease toxic effects [16–19]. Among the variety of naturally derived biopolymers, hyaluronic acid (HA) is one of the most versatile biopolymers for bone regeneration, providing an extracellular environment for osteogenesis-related cells and initiating many cellular signaling pathways in bone regeneration [20,21]. Extensively researched injectable HA-based hydrogels have shown their superior potential to mimic the natural extracellular matrix of bone tissue and provide a suitable microenvironment for cell support and tissue regeneration [22], such as osteogenesis, tunable rheological/mechanical properties, biocompatibility, biodegradability, and mass transferability [23]. Recently, ε-poly-L-lysine (ε-PL) as an antimicrobial polypeptide has been extensively researched as a high-performance component for developing antibacterial biomaterials due to its antifungal and antibacterial properties, solubility, biodegradability, and non-toxicity to humans and the environment [24]. In our earlier studies, ε-PL was used to achieve an inherent antibacterial activity of the ε-PL-HA hydrogels. We reported the biomedical potential of the developed *in situ* forming covalently cross-linked hydrogel scaffolds based on ε-PL and HA for use as novel antibacterial biomaterials for tissue engineering applications, owing to its biocompatibility, sterilizability, and flourishing antibacterial activity against Gram-negative *E. coli* and Gram-positive *S. aureus* strains [25,26].

Despite the promising characteristics, injectable natural biopolymer-based hydrogels still need to be improved as a bone-filling material, as they cannot provide the critical bone-forming capability necessary to promote bone repair and healing and need better structural integrity and mechanical properties [19]. The injectable polymer hydrogels require a suitable bioactive filler to promote osteogenesis effectively [27,28]. Considering that bone is a natural hierarchical biocomposite, there has been a growing trend to develop novel injectable nanocomposite hydrogels by biofunctionalization of injectable conventional hydrogel networks with bioactive inorganic nanofillers such as CaP particles to introduce specialized functional properties (support mesenchymal stem cell differentiation, influence ECM protein adsorption, enhance cell adhesion and tissue formation), mimic the bone's unique nanostructure and composition, thus enhancing bone regeneration capability [29]. Moreover, incorporating CaP nanofillers into conventional hydrogels improves structural integrity, porosity, viscoelastic properties, and degradation rate of the material, making it more efficient as a biomaterial for bone regeneration [29]. Several studies have explored incorporating bioactive HAp nanoparticles into silk fibroin [30], chitosan/alginate [31], bio-mimetic polysaccharide [32] hydrogel networks to form 3D porous scaffolds, and injectable composite hydrogels with enhanced bone tissue regeneration capability and improved mechanical properties. While CaP can initiate bone formation, bioactive CaP fillers-loaded hydrogels are more compatible with biological systems, and the highly swollen 3D hydrogel networks can provide nutrient diffusion to cells, thereby promoting cell adhesion and attachment [33,34]. Moreover, the osteoimmunomodulatory potential of CaP-based bone biomaterials can be further improved by substituting calcium (Ca^{2+}) ions with other biologically relevant ions, such as strontium (Sr^{2+}) ions [35]. As a bioactive element, Sr has gained attention for its capability to promote new bone formation and inhibit bone resorption through Ca-sensing receptor activation and RANKL expression inhibition. It also has angiogenic properties, making it a promising osteoporosis treatment [36]. Introducing Sr^{2+} ions into the HAp structure enhances its bioactivity and osteogenesis ability [37].

To the best of our knowledge, few reports address the development of non-antibiotic nanocomposite hydrogels for multifunctional bone tissue regeneration, which can simultaneously provide bioactivity, biomolecule delivery, and inherent antibacterial activity. For example, *Wang* et al. prepared injectable antibacterial Ag-containing HAp/gelatin methacryloyl hydrogels [38], *Shin* et al. prepared injectable calcium fluoride/alginate nanocomposite hydrogels [39], *Douglas* et al. prepared injectable Zn- and Sr-enriched bioactive glass gellan gum composite hydrogels [40]. So far, there are no studies found on the development and evaluation of injectable nanocomposite hydrogels based on bioactive Sr-substituted HAp (Sr-HAp) and HA and antimicrobial ε-PL for bone tissue engineering applications.

In a recent study, we synthesized Sr-HAp nanoparticles as local delivery vehicles of osteogenic factors. We systemically evaluated its physicochemical properties, *in vitro* Sr^{2+} ion release, and cellular effects on pre-osteoblastic and osteoblastic cell lines [41]. In this study, we used the Sr-HAp as the bioactive inorganic nanofiller for injectable nanocomposite hydrogel fabrication.

This work aims to develop multifunctional injectable nanocomposite hydrogels based on Sr-HAp-loaded covalently crosslinked ε-PL-HA hydrogel network. First, the optimal mass ratios of the Sr-HAp were selected for further systematic investigation based on the nanocomposite hydrogels' injection force and syneresis behavior. Next, we systematically evaluated the impact of the Sr-HAp at various mass ratios of 40 wt%, 50 wt%, and 60 wt% on the physicochemical properties, rheological properties, *in vitro* antibacterial performance, and *in vitro* osteogenic capability of the injectable Sr-HAp-loaded ε-PL-HA nanocomposite hydrogels (Sr-HAp/ε-PL-HA). For the first time, our results demonstrate the developed Sr-HAp biofunctionalized ε-PL-HA hydrogels with the successful incorporation of the Sr-HAp nanofiller up to 60 wt% to create a stiffer hydrogel microenvironment for bone cells synergistically and to provide biocompatibility and cell adhesion while exhibiting prominent *in vitro* inhibitory effect against *S. aureus* and *E. coli.*

2. Materials and methods

2.1. Materials

For the synthesis of Sr-HAp: deionized water (DW, *Adrona Crystal E,* 0.055 μS), calcium carbonate ($CaCO_3$, *Schaefer Kalk*, M = 100.09 g/mol, CAS Nr. 471–34-1), phosphoric acid (H_3PO_4, *"Latvijas ķīmija"*, 75 %, M = 97.99 g/mol, CAS Nr. 7664-38-2), strontium carbonate ($SrCO_3$, *Sigma Aldrich*, ≥ 98 %, M = 147.63 g/mol, CAS 1633-05-2).

For the preparation of hydrogels: hyaluronan (HA, *Contipro*, M = 1.71 MDa, CAS Nr. 9067-32-7), ε-polylysine (ε-polylysine hydrochloride (ε-PL·HCl) *Zhengzhou Bainafo Bioengineering Co., Ltd* (Henan, China), 99 % purity, MW 3500–4500 Da, 25–30 l-lysine residues, water content 6.5 %), N-hydroxysuccinimide (NHS, *Sigma-Aldrich*, 98 %, M = 115.09 g/mol, CAS Nr.6066-82-6), 1-ethyl-3-(3-dimethyl aminopropyl)carbodiimide hydrochloride (EDC, *fluorochem*, 99 %, M = 191.70, CAS Nr. 25,952–53-8).

For the physicochemical characterization: phosphate-buffered saline (PBS tablets, *Sigma-Aldrich*), hyaluronidase (hyaluronidase from bovine tests, 400–1000 units/mg solid, *Sigma Aldrich,* CAS Nr. 37,326–33-3), proteinase K (proteinase K from Tritirachium album, ≥30 units/mg protein, *Sigma Aldrich*, CAS Nr. 39,450–01-6), nitric acid (HNO_3, *ChemLab,* 65 %, M = 63.01 g/mol, CAS Nr. 7697-37-2), multielement standard solution 5 for ICP (Sr = 10.00 ± 0.03 mg/L, *Sigma Aldrich*, lot No. BCCB7069).

For the antibacterial studies: *Escherichia coli* (*E. coli*, American Type Culture Collection (ATCC©) 25922™) methicillin-sensitive *Staphylococcus aureus* (*S. aureus*, ATCC© 25923™), extended-spectrum β-lactamase *E. coli* (ESBL *E. coli*, clinically isolated from patients at Riga East Clinical University Hospital, Latvia; ethical committee approval ID: 2-PĒK-4/462/2022), methicillin-resistant *S. aureus* (MRSA, clinically isolated from patients at Riga East Clinical University Hospital, Latvia; ethical committee approval ID: 2-PĒK-4/462/2022), tryptone soya broth (TSB, CM0129, *Oxoid Limited*, Hampshire, United Kingdom), tryptone soya agar (TSA, casein soya bean digest agar, Code: CM0131, *Oxoid Limited*, Hampshire, United Kingdom).

For the cell culture studies: human osteoblast line MG-63 (Cat.No CRL-1427) and mouse preosteoblast cell line MC3T3-E1 subclone 4 (Cat. No CRL-2593) were purchased from American Type Culture Collection (ATCC, Manassas, Virginia, USA), Dulbecco's modified Eagle's medium (DMEM, *Sigma*, Irvine, UK), fetal bovine serum (FBS, *Sigma*, St. Louis, MO, USA), penicillin/streptomycin solution (*Sigma*, St. Louis, MO, USA), alpha-modified Eagle's medium with nucleosides and without vitamin C (α-MEM, without L-ascorbic acid, *Gibco*, Grand Island, NY, USA), trypsin/EDTA (*Sigma*, St. Louis, MO, USA), phosphate-buffered saline (PBS, *Sigma*, Irvine, UK), 3-[4,5-dimethylthiazol-2-yl]-2,5 diphenyl tetrazolium bromide (MTT, *Sigma*, St. Louis, MO, USA), dimethyl sulfoxide (DMSO, Sigma, St. Louis, MO, USA), Alkaline Phosphatase Assay Kit (*Sigma*, St. Louis, MO, USA), Triton X-100 (*Sigma*, St. Louis, MO, USA), bovine serum albumin (BSA, *Sigma*, Irvine, UK), QuickStart Bradford 1× Dye Reagent (*BioRad*, Hercules, CA, USA), human procollagen I DuoSet ELISA kit (*R&D Systems,* Minneapolis, *MN*, USA), human matrix metalloproteinase 1 DuoSet ELISA kit (MMP-1, *R&D Systems,* Minneapolis, MN, USA). Cell viability dyes, SYTO 9 and propidium iodide were supplied by *Life Technologies Corp*. (Eugene, OR, USA).

2.2. Synthesis of Sr-HAp

The Sr-HAp was chemically precipitated in a laboratory reactor (*Power Control-Visc P7, IKA Eurostar, WERKE,* Germany) following the procedure described previously in [41]. Before the synthesis, $CaCO_3$ and $SrCO_3$ were calcined at 1100 °C for 1 h to obtain CaO and SrO, respectively. The amount of added SrO was calculated to yield 3 wt% Sr to the total Sr-HAp synthesis yield. The 0.3 M $Ca(OH)_2$/$Sr(OH)_2$ aqueous suspension was prepared by dispersing the CaO and SrO in DW. The 2 M H_3PO_4 aqueous solution was added to the $Ca(OH)_2$/$Sr(OH)_2$ suspension using an automated dosing system (*TITRONIC® universal, Schott,* Germany). Synthesis temperature (45 °C) and agitator speed (100 rpm) were kept constant throughout the synthesis. By adding the 2 M H_3PO_4 aqueous solution, the pH of the synthesis was reduced to 8. After settling for approximately 20 h, the precipitates were vacuum-filtered through a paper filter. Finally, the Sr-HAp wet precipitates were collected as a paste and stored in a refrigerator at 4 °C until further use. The moisture content of the Sr-HAp paste was determined in a moisture analyzer (*Humidity Analyzer MRS 120–3, Kern,* Germany*)* at 120 °C. The Sr-HAp paste with 3 wt% Sr and a moisture content of 80 % was used to fabricate nanocomposite hydrogels. A detailed physicochemical characterization and *in vitro* biological evaluation of the Sr-HAp containing 3 wt% Sr is provided in our recent study [41].

Table 1
Designation and composition of the tested samples.

Designation	Composition
0 % Sr-HAp	100 % ε-PL-HA (where ε-PL:HA 50:50 wt%)
10 % Sr-HAp	Sr-HAp 10 wt%, ε-PL-HA 90 wt%
20 % Sr-HAp	Sr-HAp 20 wt%, ε-PL-HA 80 wt%
30 % Sr-HAp	Sr-HAp 30 wt%, ε-PL-HA 70 wt%
40 % Sr-HAp	Sr-HAp 40 wt%, ε-PL-HA 60 wt%
50 % Sr-HAp	Sr-HAp 50 wt%, ε-PL-HA 50 wt%
60 % Sr-HAp	Sr-HAp 60 wt%, ε-PL-HA 40 wt%
70 % Sr-HAp	Sr-HAp 70 wt%, ε-PL-HA 30 wt%
80 % Sr-HAp	Sr-HAp 80 wt%, ε-PL-HA 20 wt%
Sr-HAp	Sr-HAp 100 wt%

2.3. Fabrication of injectable Sr-HAp loaded ε-PL-HA nanocomposite hydrogels

The *in situ* forming nanocomposite hydrogels were synthesized *via* EDC/NHS-mediated carboxyl-to-amine cross-linking. The designation and composition of the fabricated Sr-HAp/ε-PL-HA hydrogels are summarized in Table 1.

ε-PL, HA, EDC, and NHS amounts were kept constant for fabricated nanocomposite hydrogels (Table S1). The mass ratio of ε-PL and HA were kept at 50:50 wt% for all Sr-HAp/ε-PL-HA series. The as-synthesized Sr-HAp paste was added to the synthesis media at a mass ratio of 10 wt% to 80 wt% (exact amounts of components for each series are summarized in Table S1). All components were mixed and homogenized using an interconnected syringe technique (*Fisher Scientific*, *BD PlastiPak*™ Syringe with *Luer* Lock, 5 mL) at room temperature (23 °C) following the order depicted in Fig. 1.

The nanocomposite hydrogel fabrication step-by-step process: a) preparation of the first syringe: 0.105 g of the HA powder was dissolved in 2 mL of the DW by rapidly mixing using interconnected syringes. HA aqueous solution, EDC, and NHS were stored in the refrigerator at 4 °C for 24 h; b) preparation of the second syringe: 0.098 g of the ε-PL powder was dissolved in DW by rapidly mixing using interconnected syringes. The amount of the DW added to the ε-PL powder varied depending on the mass ratio of the Sr-HAp paste (Table S1), so the total amount of water in the first syringe was 2 mL; Sr-HAp paste was homogenously dispersed into the as-prepared ε-PL aqueous solution using the same interconnected syringes. The second syringe with ε-PL/Sr-HAp aqueous suspension was stored in the refrigerator at 4 °C for 24 h; c) After 24 h, 0.093 g of the EDC was added into the first syringe (as-prepared HA aqueous solution) and mixed using the same interconnected syringes. Afterward, 0.056 g of the NHS was mixed into the first syringe. The molar ratio of EDC to NHS was set at 1:1. Finally, the aqueous mixture of the pre-activated HA/EDC/NHS in the first syringe and the homogenous aqueous suspension of the ε-PL/Sr-HAp in the second syringe were connected and rapidly mixed for 1 min. The molar ratio of ε-PL to HA was set at 1:0.0026.

2.4. Characterization

Depending on the characterization method, the as-prepared and lyophilized nanocomposite hydrogels were characterized.

The as-prepared nanocomposite hydrogels were fabricated as follows: the precursor mixtures were cast into cylindrical molds (diameter 10 mm, height 5 mm) for uniformity and left to crosslink for 24 h at room temperature (23 °C).

The lyophilized nanocomposite hydrogels were prepared as follows: the as-prepared hydrogels were frozen at −26 °C and lyophilized using a lyophilizer *BETA 2–8 LSCplus* (*Martin Christ*, Germany) at 75 mtorr for 72 h.

For the antibacterial and *in vitro* cell studies, the as-prepared nanocomposite hydrogels were steam-sterilized in an autoclave at 121 °C for 20 min.

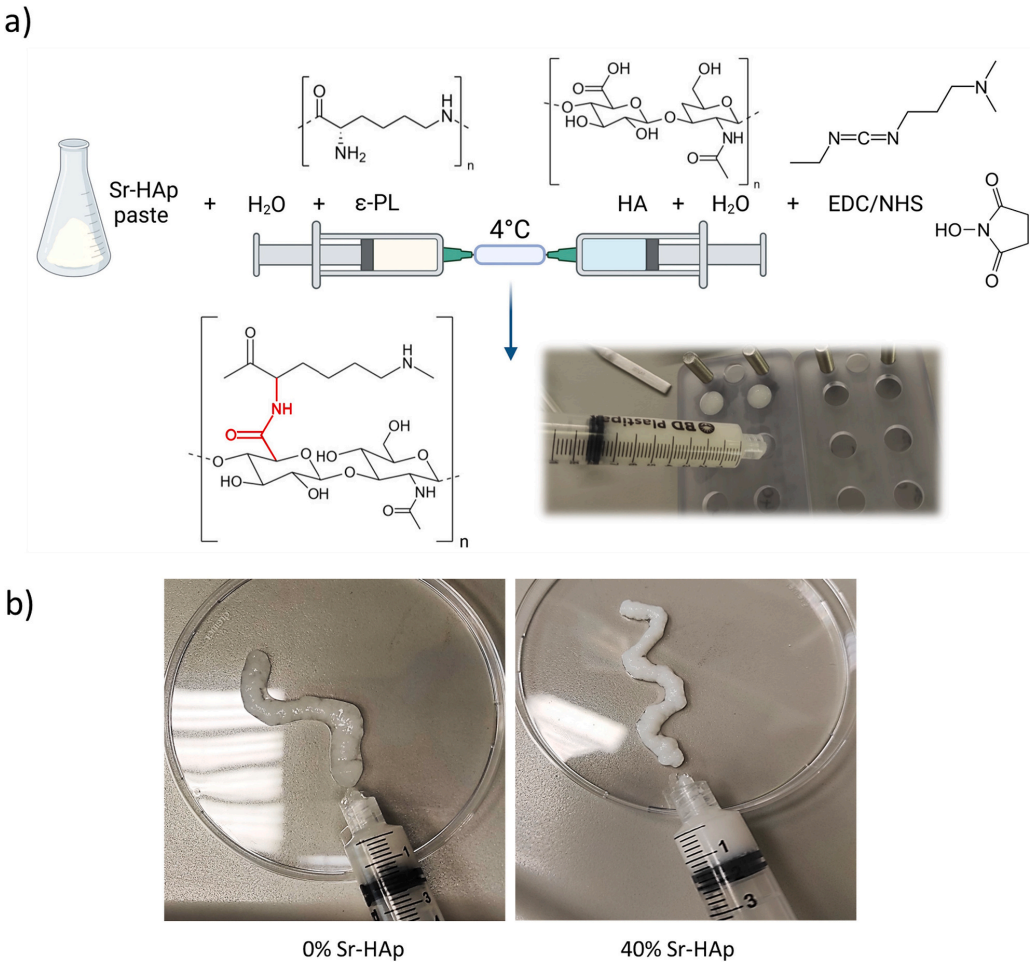

Fig. 1. a) Schematic representation of the synthesis of the nanocomposite hydrogels, b) - digital photos of the as-prepared (on the left) and 3D-molded (on the right) nanocomposite hydrogels (COLOR).

2.4.1. Injection force

The injection force of the as-prepared nanocomposite hydrogels was measured by mechanical testing following an analogous method described in [42]. The measurements were performed on an electromechanical universal testing machine (*Model 25ST, Tinius Olsen,* USA). The setup used to determine injection force is shown in Fig. S1. Briefly, the 5 mL syringe (the inner diameter of the tip 1.8 mm) with the as-prepared nanocomposite hydrogel was inserted vertically in a custom-made stand that was inserted into the electromechanical universal testing machine. The syringe plunger was pressed down at a set rate, 1 mm/s, while the applied force was recorded. All measurements were done in triplicate.

2.4.2. Syneresis

The syneresis, namely liquid exudation from the gel network during gelation, was determined by placing the as-prepared nanocomposite hydrogels in pre-weighed test tubes (W_E), weighed (W_I) and incubated in a table-top environmental shaker-incubator (*ES-20, Biosan,* Latvia) at 37 °C providing orbital shaking at 100 rpm. After 24 h, the test tubes were opened, the separated water was decanted, and the tubes with the nanocomposite hydrogel were weighed again (W_F). Syneresis was calculated as follows: Syneresis $= (W_I - W_F)/(W_I - W_E) \times 100$ %. All measurements were done in triplicate.

2.4.3. Rheology

Time, amplitude, frequency sweep tests, shear rate dependent viscosity, compression, and cyclic strain time sweep tests were chosen for rheological studies. The *Thermo HR-20 Hybrid* rheometer (*TA Instruments,* USA), a 25 mm parallel plate with a gap of 1 mm, was used. Silicone oil was gently applied around the sample to avoid evaporation, and a humidity control trap was used. All tests were performed at 25 °C. The precursor mixture was extruded directly on the rheometer plate for the time sweep tests before complete gelation occurred: a) the precursor mixtures of the nanocomposite hydrogels were extruded on the Peltier plate of the rheometer; b) a parallel plate was slowly lowered toward the nanocomposite hydrogel sample.

The time sweep analysis was performed for 180 min at 0.2 % strain and 1 Hz frequency. For the amplitude and frequency sweep and

compression tests, the precursor mixtures of the nanocomposite hydrogels were extruded into a custom mold (diameter 25 mm) and left to crosslink for 3 min. The amplitude sweep tests were performed in oscillatory mode with a shear strain logarithmically changing range from 0.01 to 1000 % at a constant frequency of 1 Hz. The frequency sweep tests were performed in oscillatory mode varying from 0.01 to 100 Hz at a constant strain of 0.2 % within the linear viscoelastic region (LVR), as experimentally observed for all samples during amplitude sweep experiments. The stiffness of the nanocomposite hydrogels was determined from the amplitude sweep tests as the *G'* value at 0.2 % strain and 1 Hz frequency. The viscosity-shear rate tests were performed at shear rate values, logarithmically increasing from 0.1 to 500 s^{-1}. The compression tests were performed at 8 N axial force (axial force > dynamic force = 30 %), axial displacement 30 μm, in the frequency range from 0.01 to 16 Hz, and compression storage modulus (*E'*) and compression loss modulus (*E''*) were monitored. The molecular weight between crosslinks (M_c) of the composite hydrogels was calculated as follows: $M_c = RTd/G'$, where R is the universal gas constant, T is the absolute temperature, and d is the density of the polymer (found experimentally by dividing sample mass with the volume ($d = m/V = m/\pi r^2 h$)), G' is storage module at 1 Hz frequency. Afterward, crosslinking density (q) was calculated: $q = M_w/M_c$, where M_w is the molecular weight of the monomer calculated as follows: $M_w = M_w(HA) + M_w(\varepsilon\text{-}PL)$, where $M_w(HA)$ is the molecular weight of a HA monomer, and $M_w(\varepsilon\text{-}PL)$ is the molecular weight of an ε-PL monomer [43]. The cyclic recovery tests were performed to evaluate nanocomposite hydrogels' recovery after extrusion-like conditions. One cyclic recovery test duration was 130 s, divided into three stages, of which the duration of the first and third was 60 s at a shear rate of 0.1 s^{-1} and the second - 10 s at a shear rate of 350 s^{-1}. All measurements were done in triplicate.

2.4.4. Swelling degree and gel fraction

The swelling degree of the lyophilized and as-prepared nanocomposite hydrogels and the gel fraction of lyophilized nanocomposite hydrogels were determined gravimetrically using an analytical scale (*Kern 770, Kern,* Germany).

To determine the swelling degree, the as-prepared hydrogel cylinders (7 replicates) were weighed (W_D), immersed in 20 mL PBS (pH = 7.4), and incubated at 37 °C with 100 rpm agitation. At specific time points (1, 2, 4, 5, 6, 24, 48 h), the samples were removed from the PBS, the excess liquid was gently shaken off, and the samples were weighed (W_S). The swelling degree (SW) was calculated as follows: $SW = (W_S - W_D)/W_D \times 100$ %.

To determine the gel fraction, the lyophilized nanocomposite hydrogels (5 replicates) were weighed (W_D), immersed in 20 mL PBS (pH = 7.4), and incubated at 37 °C with 100 rpm agitation. After 24 h, the samples were removed from the PBS and lyophilized again. The lyophilized samples were weighed again (W_G), and the gel fraction (GF) was calculated as follows: $GF = W_G / W_D \times 100$ %.

2.4.5. Phase composition

To analyze the phase composition (Fig. S6(a)), the nanocomposite hydrogels were lyophilized as described above, and the Sr-HAp paste was dried at 105 °C for 24 h. Further, the dried Sr-HAp paste, and the lyophilized nanocomposite hydrogels were ground into a fine powder using a pestle. The Sr-HAp and nanocomposite hydrogels' phase composition was evaluated by X-ray powder diffractometry (XRD, *PANalytical AERIS,* Almelo, Netherlands) with Cu Kα radiation (produced at 40 kV and 15 mA). The diffraction data were collected in a 10–70° 2θ range, with a step size of 0.044° 2θ and time per step of 99.45 s. Phases present in the recorded diffraction patterns were identified using a *PANalytical X-Pert Highscore 2.2* software (*Panalytical, Almelo,* Netherlands) and the International Centre for Diffraction Data PDF-2 (ICDD, *Newtown Square,* Pennsylvania, USA) database.

2.4.6. Molecular structure

To analyze the molecular structure (Fig. S6(b) and Fig. S7), the nanocomposite hydrogels were lyophilized as described above, and the Sr-HAp paste was dried at 105 °C for 24 h. Further, the dried Sr-HAp paste, and the lyophilized nanocomposite hydrogels were ground into a fine powder using a pestle. The Sr-HAp and nanocomposite hydrogels' molecular structure was analyzed using the Fourier transform infrared spectroscopy (FT-IR, *Nicolet IS50 FT-IR, Thermo Fisher,* USA) in the attenuated reflectance mode (ATR, *IS50 ATR Nicolet, Thermo Fisher,* USA). Absorbance was measured in the wavenumber range of 400 to 4000 cm^{-1} and at 4 cm^{-1} resolution, 64 scans per sample. In addition, Raman spectroscopy was undertaken using a *Renishaw inVia™ Qontor® Confocal* Raman Microscope (*Renishaw Ltd.*, Gloucestershire, UK) using a Raman 'point and shoot' method. Before beginning measurements, the Raman system was calibrated using an internal silicon reference to 520 cm^{-1}. In acquisition mode, the laser was operated at 10 % power (equal to 5 mW) and focused through an x20 objective over an extended wavenumber scan, 200–1800 cm^{-1}, with 60 s integration time (averaged over 6 collections). Averaged spectra were data-processed by cosmic ray removal.

2.4.7. Microstructure and morphology

This study used micro-computed tomography (μ-CT) as a non-destructive imaging technique to analyze samples. Before scanning, samples were lyophilized. The scans were conducted using a μCT50 cabinet cone-beam μ-CT system (*Scanco Medical AG*, Switzerland) with the following parameters: 55 kVp energy, 109 μA tube current, 1100 ms integration time, and a 4 μm voxel size. Each sample was scanned for approximately 5.4 h. After the scanning process, automated reconstruction of 3D datasets from μ-CT projection data was performed. The visualization module utilized advanced 3D data reproduction techniques, employing high-quality beam tracking algorithms to enhance the analysis of large datasets.

The morphology of lyophilized nanocomposite hydrogels was analyzed by scanning electron microscopy (SEM) *Verios 5 XHR SEM* (*Verios, Thermo Scientific*, USA). The images were generated using secondary electrons at an acceleration voltage of 2 kV. The samples were fixed on aluminum pin stubs with electrically conductive carbon tape.

2.4.8. Enzymatic degradation and ion release

Enzymatic degradation of the as-prepared nanocomposite hydrogels was determined by measuring the remaining weight of the samples upon hyaluronidase treatment (0.025 mg/mL equal to 100 U/sample) over a five-month incubation period. Biodegradation media was prepared by dissolving hyaluronidase powder in PBS (25 mg hyaluronidase added to 100 mL PBS solution) and then diluting the solution 10 times. All samples (5 replicates) were weighed (W_0) before immersion in 10 mL biodegradation media at 37 °C with 100 rpm agitation. The biodegradation media was changed daily, and the weight of the incubated samples was recorded once a week (W_R). The remaining weight (RW) was expressed as a percentage of the sample's initial weight: $RW = W_R / W_0 \times 100$ %.

Enzymatic degradation of the as-prepared nanocomposite hydrogels was also studied in the presence of proteinase K (0.05 mg/mL equal to 12.5 U/sample) over a twelve-day incubation period. Biodegradation media was prepared by dissolving proteinase K powder in PBS (60 mg proteinase K added to 120 mL PBS solution) and diluting the solution 10 times. 5 replicates were weighed (W_0) before immersion in 10 mL biodegradation media at 37 °C with 100 rpm agitation. The biodegradation media was changed daily, and the weight of the incubated samples was recorded once a day (W_R). The remaining weight (RW) was expressed as a percentage of the sample's initial weight: $RW = W_R / W_0 \times 100$ %.

The as-prepared hydrogel cylinders and the Sr-HAp paste were used for ion release measurements. The 5 replicates of each nanocomposite hydrogel series, as well as Sr-HAp paste (20 mg of dry mass), were

weighed in the plastic sample containers, poured over with 20 mL PBS (pH = 7.4), and incubated at 37 °C with 100 rpm agitation. At 1 h, 4 h, 24 h, 1 day, 7 days, 14 days, 30 days, 60 days, and 90 days, in the case of hydrogels, all the PBS, and in the case of Sr-HAp paste - 10 mL of the PBS was removed and replaced with fresh PBS. The amount of released Sr^{2+} and Ca^{2+} ions in the PBS after incubation of the hydrogels and the Sr-HAp paste was measured by an inductively coupled plasma mass spectrometry (ICP-MS; *Agilent 7700×, Agilent Technologies,* Tokyo, Japan). The ICP-MS method was validated before sample analysis regarding the limit of quantification (LOQ), precision, trueness, recovery, uncertainty, stability, and carry-over. The validation results are summarized in Table S2. The stock solution of 0.25 mL concentrated nitric acid (HNO_3, 65 %) was diluted to 50 mL with DW (*A* 0.055 μS/cm, *Adrona Crystal*) was used. The experimental PBS samples were dissolved in 0.5 % HNO_3 aqueous solution and diluted with deionized water. The degree of dilution was optimized before the analysis of each series of samples to ensure that the measured concentration was within the linear range of the calibration curve. The sample measuring parameters were as follows: plasma mode – regular, robust, RF forward power 1300 W, sampling depth 8.0 mm, plasma gas flow 15.0 L/min, carrier gas flow 0.6 L/min, dilution gas flow 0.4 L/min, spray chamber temperature 2 °C, extraction lens 0 *V*, kinetic energy discrimination 3 V.

2.4.9. In vitro antibacterial activity

The long-term antibacterial activity of the sterilized as-prepared nanocomposite hydrogels was assessed using a plate counting method according to CLSI and EUCAST standards with minor modifications, as described in an earlier study [26]. The experiment was performed against four bacterial strains: Gram-negative *E. coli* (reference (ATCC) and clinically isolated antibiotic-resistant (ESBL *E. coli*)) and Gram-positive *S. aureus* (reference (ATCC) and clinically isolated antibiotic-resistant (MRSA)). The tests were performed for extended periods with time control points at 24, 48, 72, and 168 h. First, the bacterial suspensions were prepared in glass tubes with PBS until they reached *McFarland* = 0.5, corresponding to a bacterial concentration of $1.5 \cdot 10^8$ CFU/mL. In the second step, experimental 6-well plates were prepared for each bacterium with positive/negative and three replicates of the sterilized as-prepared nanocomposite hydrogels from each composition. The positive control consisted of 2 mL PBS, and the negative control consisted of 2 mL bacteria suspension in PBS equal to $3 \cdot 10^8$ CFU/mL. The sterilized as-prepared nanocomposite hydrogels were inserted in 2 mL bacterial suspension (at $3 \cdot 10^8$ CFU/mL final concentration). Prepared 6-well plates were tightly sealed with parafilm and incubated for 24 h at 37 °C with 60 rpm agitation. For pre-determined control time points, supernatants were completely extracted from wells, and samples were poured with 2 mL of a freshly prepared bacteria suspension. Finally, surviving bacterial colonies were counted by preparing 6-fold dilutions (1:10 to 1:1000000) and applying the dilution bands on the TSA plate. The TSA plates were dried at room temperature and then incubated at 37 °C for 24 h. The bacterial colonies were counted manually from dilution bands.

2.4.10. In vitro cell studies

Three to five replicate samples of each nanocomposite hydrogel series were analyzed using *in vitro* cell assays. The cylindrical samples of the as-prepared 0 % Sr-HAp, 40 % Sr-HAp, 50 % Sr-HAp, and 60 % Sr-HAp hydrogels with an average weight of 0.055 ± 0.009 g, 0.074 ± 0.008 g, 0.082 ± 0.007 g, and 0.082 ± 0.009 g, respectively, were used for the *in vitro* cell studies.

2.4.10.1. Cell cultures. Human osteoblast line MG-63 (Cat.No CRL-1427) and mouse preosteoblast cell line MC3T3-E1 subclone 4 (Cat.No CRL-2593) were purchased from American Type Culture Collection (ATCC, Manassas, Virginia, USA) and used for biocompatibility testing. MG-63 cells were grown in DMEM supplemented with 100 μg/mL of streptomycin, 100 μg/mL of penicillin, and 10 % (*v*/v) FBS. MC3T3-E1 cells were cultivated in α-MEM cell culture media supplemented with 100 μg/mL of streptomycin, 100 μg/mL of penicillin, and 10 % (v/v) FBS. Cell cultivation was done at 37 °C within a humidified 5 % CO_2 atmosphere. Cells were detached and passaged using 0.25 % trypsin/EDTA. Both cell lines were used for proliferation and alkaline phosphatase (ALP) activity assays. Collagen production and MMP-1 secretion were assessed for MG-63 cells.

2.4.10.2. Cell proliferation assay. A proliferation assay was performed in the human osteoblast cell line MG-63 and mouse preosteoblasts MC3T3-E1. The as-prepared hydrogels were washed two times with sterile PBS (pH 7.4) and once with cell culture media and placed in 48-well cultivation plates. MG-63 osteoblasts and MC3T3-E1 preosteoblasts ($5 * 10^3$ cells per well) were seeded on the hydrogels. Plates were incubated for 2, 5, and 7 days. After incubation, the media was removed, and the hydrogels were transferred to a new cultivation plate. The cell proliferation, both in the hydrogels and on the cultivation plate surface surrounding the hydrogels, was quantified using an MTT reduction assay: (a) 0.5 mL of 0.5 mg/mL MTT solution in 5 % serum-containing medium was added to each well, (b) plates were incubated for 3 h at 37 °C and 5 % CO_2 to allow the formation of insoluble formazan precipitates due to the metabolic activity of viable cells, (c) 0.45 mL of DMSO was added, (d) the plate was incubated for 30 in case of cells grown on the plate surface in presence of biomaterial and 2 h in case of hydrogel samples at room temperature with gentle shaking to dissolve the formazan precipitate, (e) the absorption was measured at 570 nm using an *Infinite Pro 200* microplate reader (*Tecan,* Austria). Blank wells without cells were used for the background measurement. Cells grown on the cultivation plate surface without the biomaterials were used as controls.

2.4.10.3. Alkaline phosphatase assay. The alkaline phosphatase (ALP) activity after 3, 5, and 7 days in the osteoblast and the pre-osteoblast cultures was measured using The Alkaline Phosphatase Assay Kit. Cells were seeded on the hydrogels in the 48-well plates as described in Section 2.4.10.2. Cells cultivated on the surface of a 48-well cultivation plate were used as controls. The plates were incubated at 37 °C, 5 % CO_2 for 3, 5, and 7 days; half of the culture media was changed every 3 days. After the incubation, the media was aspirated. The hydrogels were washed with 0.5 mL of PBS and transferred to the new 48-well plate to prepare lysates from cells grown in the hydrogels and on the cultivation plate in the presence of the hydrogels. Cells were lysed with 0.5 mL of 0.2 % Triton X-100 aqueous solution for 20 min with shaking at room temperature. ALP activity was measured according to the manufacturer's protocol: (a) a reaction working reagent containing 200 μL assay buffer, 5 μL 0.2 M Mg acetate, and 2 μL 1 M pNPP was prepared, (b) 30 μL of cell lysate was mixed with 170 μL of the working reagent, (c) optical density (*OD*) at 405 nm was measured immediately after mixing (OD_{0min}) and after 50 min incubation (OD_{50min}) using the microplate reader. Incubation time was prolonged compared to standard ALP activity assay protocol due to the relatively low activity in the cell lysates. Tartrazine supplied with the kit was used as a calibrator (OD_{cal}), and water was used as the blank (OD_{blank}). The following equation was used to calculate *ALP* (IU/mL):

$$ALP = ((OD_{50min} - OD_{0min}) \times RnxVol \times 35.3)/((OD_{cal} - OD_{blank}) \times SampleVol \times T),$$

where *RnxVol* is the reaction volume, *SampleVol* is the sample volume, and *T* is the incubation time. The total protein content in the cell lysates was determined using *QuickStart Bradford* 1× Dye Reagent and BSA as a standard. ALP activity was expressed as IU/mg protein.

2.4.10.4. Secretion of pre-collagen I and MMP-1. MG-63 osteoblasts were seeded on the hydrogels in the 48-well plates as described in

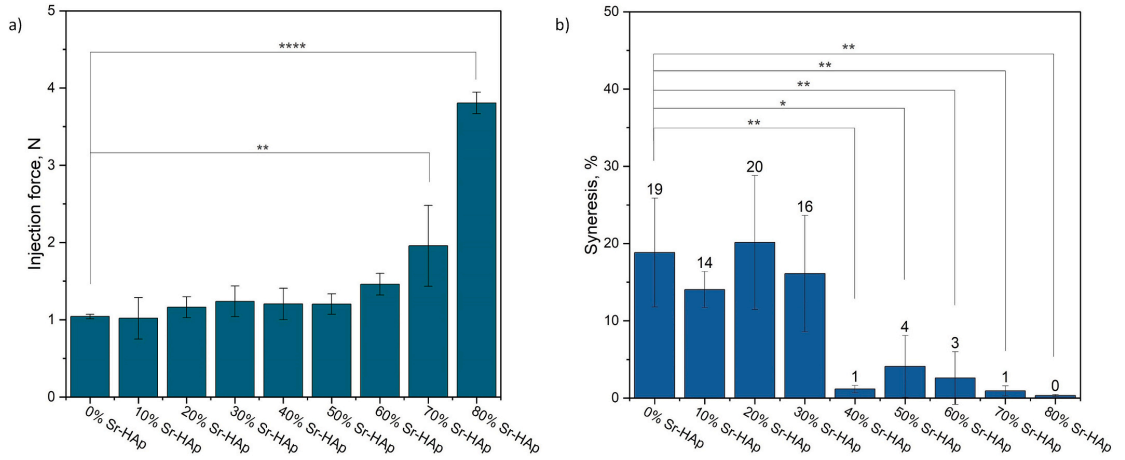

Fig. 2. The injection force (a) and the syneresis level (b) of the Sr-HAp-loaded ε-PL-HA nanocomposite hydrogels (ANOVA: * - for $p < 0.05$, ** - for $p < 0.01$, *** - for $p < 0.001$, **** - for $p < 0.0001$, $n = 3$) (COLOR).

Section 2.4.10.2. Cells cultivated on the surface of a 48-well cultivation plate were used as controls. The plates were incubated at 37 °C, 5 % CO_2 for 7 days, and half of the culture media was changed every 3 days. Media were collected for analysis after 2, 5, and 7 days of hydrogel cultivation. The secretion of pro-collagen I and MMP-1 in the culture media was quantified using ELISA immunoassays employing *DuoSet Human* pro-collagen I alpha 1 and MMP-1 ELISA kits (*R&D Systems*, USA), following the manufacturer's recommendations. Standard dilutions of pro-collagen I and MMP-1 were used to generate the standard curve and calculate the concentrations of both analytes in the culture media. The pre-collagen I to MMP-1 ratios were calculated for all formulations.

2.4.10.5. Live/dead staining. Cells were seeded on the hydrogels in the 48-well plates as described in Section 2.4.10.2. Cells cultivated on the surface of a 48-well cultivation plate were used as controls. The plates were incubated at 37 °C, 5 % CO_2 for 5 and 7 days. After cultivation, the media was discarded, and samples were washed with PBS. A mixture of fluorescent cell viability dyes (5 μM SYTO 9 dye and 30 μM propidium iodide) was added to the samples and incubated for 15 min at 37 °C, 5 % CO_2 in the dark. After incubation, samples were washed with PBS and imaged using *Leica DMI400B* inverted fluorescence microscope.

2.4.11. Statistical analysis

All results were expressed as the mean value ± standard deviation (SD) of at least three independent samples. The significance of the results was evaluated using One-way ANOVA with the significance level set at $p < 0.05$ (ns - > 0.05, * - for $p < 0.05$; ** - for $p < 0.01$; *** - for $p < 0.001$; **** - for $p < 0.0001$). Cell studies data processing, visualization, and statistical analysis were performed using GraphPad Prism 9 software.

3. Results and discussion

3.1. Injection force and syneresis

For hydrogels to be injectable, transporting the sol or the pre-gel to a target site through an injection device is required [44]. Thus, injectability is related to the ease of administration. Knowing how much force (injection force) is needed to push the hydrogel out at a given injection rate is essential. As discussed, we aimed to replicate bone composition, namely, the polymeric phase intercalated by the inorganic phase [16]. Thus, the addition of the inorganic filler, the Sr-HAp, was expected to affect the injection force of the ε-PL-HA hydrogels due to the change in the viscous properties [45]. Therefore, the injection force was measured for each series of the fabricated Sr-HAp/ε-PL-HA to define the appropriate amount of the Sr-HAp without compromising the injectability of the nanocomposite hydrogels. The results are shown in Fig. 2(a).

The force measured at the syringe plunger depends on the syringe and needles employed [46]. It has been reported that gauge sizes from 10 (inner diameter 2.69 mm) to 16 (inner diameter 1.19 mm) are appropriate for orthopedic procedures such as filling bone lesions and cracks [47]. Since the inner diameter of the syringe tip (1.8 mm) corresponds to these dimensions, the injection force measurements were done without a needle. As described in the literature, the injection force should be below the acceptable limit of manual injectability for subcutaneous injection, which is 30 N [48]. The measured injection forces for all the fabricated Sr-HAp/ε-PL-HA series are under 5 N. Therefore, we can assume all tested nanocomposite hydrogels are manually injectable in a clinical setting. The measurements show a slight increase in injection force while increasing the Sr-HAp mass ratio from 0 % to 70 % and a steep increase for 80 % Sr-HAp.

The phenomenon of syneresis means macroscopic shrinkage and liquid exudation from the gel network after gelation [49]. This is an undesirable feature for injectable biomaterials. It can lead to gel size and shape changes and, thus, to the inefficient filling of bone defects [50]. The degree of syneresis of the fabricated nanocomposite hydrogel series is summarized in Fig. 2(b). The degree of syneresis of the Sr-HAp/ε-PL-HA decreased with increasing the Sr-HAp mass ratio. Thus, Sr-HAp enhanced the nanocomposite hydrogel stability and acted as the syneresis inhibitor. To explain the decrease of the syneresis by increasing the Sr-HAp mass ratio, the hydrophilicity of the Sr-HAp particles due to the surface [OH] groups should be considered [51,52]. The [OH] groups can form hydrogen bonds, thus limiting the movement of polymer chains and lowering the syneresis of the nanocomposite hydrogels. The most optimal Sr-HAp/ε-PL-HA ratios were selected for further studies based on the described injectability and syneresis results. The syneresis results indicate that the hydrogels with a higher Sr-HAp mass ratio (≥40 %) could be more favorable for use as injectable biomaterials. On the other hand, the injectability results show that increasing the Sr-HAp mass ratio in the nanocomposite hydrogels to 80 % requires a higher injection force, which is undesirable. Thus, the nanocomposite

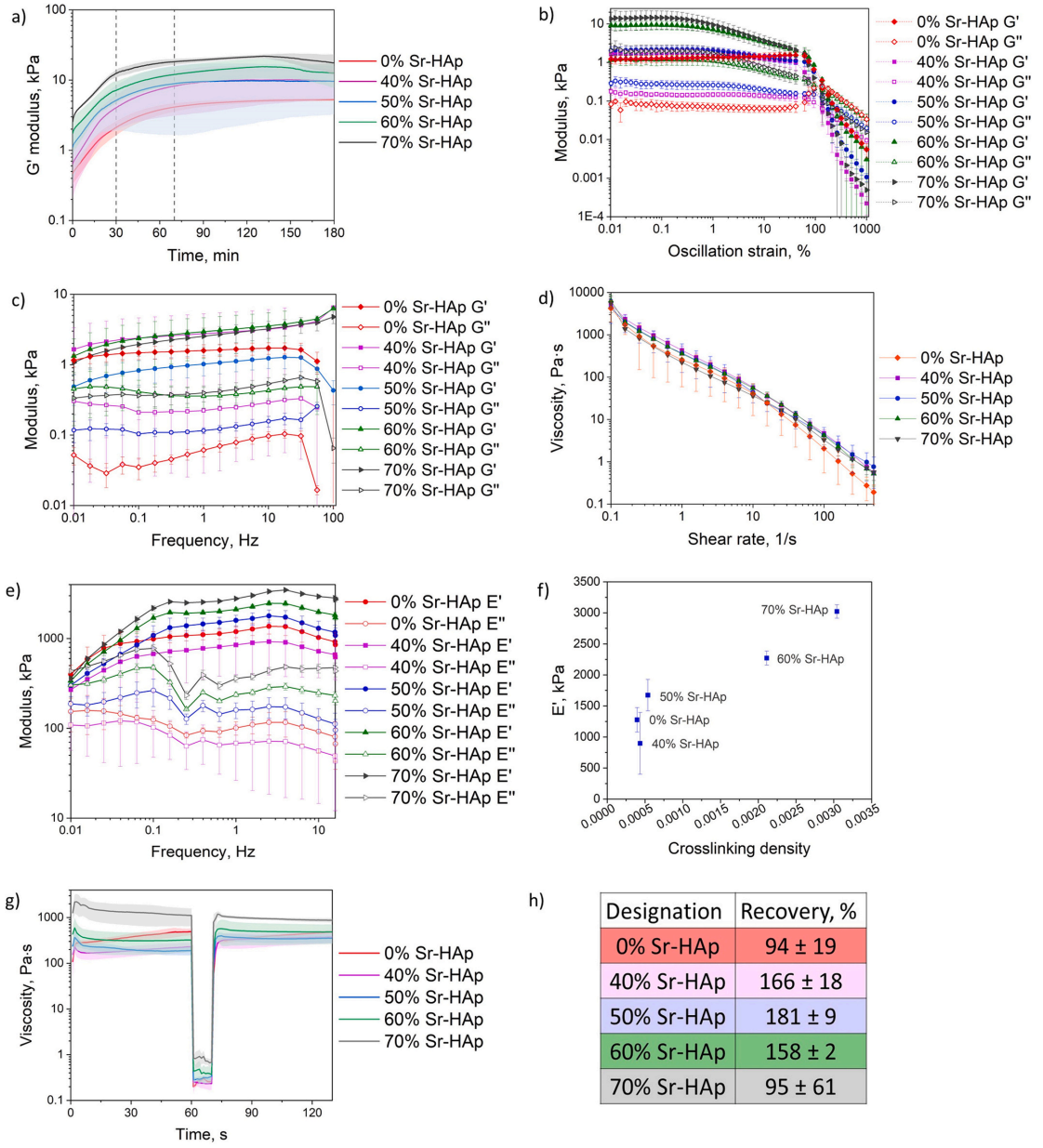

h)

Designation	Recovery, %
0% Sr-HAp	94 ± 19
40% Sr-HAp	166 ± 18
50% Sr-HAp	181 ± 9
60% Sr-HAp	158 ± 2
70% Sr-HAp	95 ± 61

Fig. 3. The rheological characterization of the nanocomposite hydrogels: a) time sweep curves, b) amplitude sweep curves, c) frequency sweep curves, d) viscosity – shear rate curves, e) compression curves, f) correlation between compression storage moduli (E') (extracted from compression curves at 1 Hz) and calculated crosslinking density values, g) cyclic strain time sweep curves, and h) calculated viscosity recovery rates (COLOR).

hydrogels with 40, 50, 60, and 70 % of the Sr-HAp were chosen for further evaluation.

3.2. Rheology

The rheological properties of injectable hydrogels are essential to predict their viscoelastic performance during and after injection and whether they resist tension forces due to movements in the injected area [53]. Optimally, the viscosity of the injectable gel should be low in the initial stage but increase rapidly with time to ensure an easy injection and, subsequently, a quick formation of bulk hydrogel to avoid its outflow to the surrounding tissues [54]. Gelation time is one of the most

critical parameters when applying hydrogels as injectable biomaterials. The dynamic process of gelation time should include mixing the components, injection, and complete filling of the target sites and the final gelation of the hydrogel [55]. Rheological oscillation time sweep analysis shows the storage moduli (G') dependence on time. This allows us to predict the time needed for the hydrogels to transit from fluid flow-like behavior to solid elastic behavior, namely, the total gelation time. The time sweep curves are summarized in Fig. 3(a).

Usually, the G' and G'' curve crossover point indicates the gelation point of the hydrogels [56]. However, throughout the tests, G' was greater than that of G'' for all formulations, indicating the elastic nature of the hydrogels over their viscous nature. This can be explained by forming a gel-like structure while mixing the reagents. As the EDC and NHS are added to the HA solution, the [COOH] groups of the HA are activated, forming an O-acylisourea active ester that reacts with nearby [OH] groups, generating intermolecular cross-links [57,58]. Consequentially, we used this test to determine the stability of the hydrogels. Namely, the hydrogels were considered stable when the G' value reached a plateau. The time sweep tests were performed for 3 h to observe the onset of the stable value of G'. It can be argued that the formulations were completely gelled within 30–70 min, depending on the Sr-HAp mass ratio. It has been claimed that the optimal gelation time for injectable hydrogels for bone-filling applications is 5 min [59]. Although this time is significantly longer in our case, the gelation or curing time, in our case, gives sufficient time for mixing the components before injection.

Determination of the LVR plateau region and its limits is crucial for further rheological studies and inferring interconnections and dominance in the sample structure. Thus, the amplitude sweep tests within a constant frequency value of 1 Hz were performed [60]. The amplitude sweep curves are summarized in Fig. 3(b). For all Sr-HAp/ε-PL-HA series, $G' > G''$ indicating solid-like material characteristics, namely, the dominance of elasticity over viscous nature, is valid until the crossover point, *i.e.,* until matrix transition occurs [61,62]. This is true for all Sr-HAp/ε-PL-HA series and is mainly predetermined by intermolecular cross-links in the composite structure [56]. The amplitude sweep curves of the 0 % Sr-HAp hydrogels coincide with our earlier study [25]. A relatively high ratio between storage (G') and loss (G'') moduli and narrow LVR from 0.1 to 0.5 % and crossover points at an oscillatory strain of ~200 % indicates chemical entanglement dominance in the hydrogel matrix. The curves of the Sr-HAp/ε-PL-HA hydrogels show that adding Sr-HAp has tipped the balance where physical interactions dominate and well-defined LVR regions (0.01–1 %) were observed. Moreover, the addition of the Sr-HAp nanoparticles caused an increase in storage modulus (G'). The formation of the physically crosslinked network through electrostatic interactions between the Sr-HAp and the functional groups of ε-PL and HA could explain this. Namely, electrostatic bonds might have been formed either by the SrHAp *a(b)*-planes (Ca^{2+} ions) interaction with negatively charged dissociated carboxyl groups [COO^-] of the HA or through the SrHAp *c*-planes (PO_4^{3-} ions and OH^- ions) interaction with positively charged amino groups [NH_3^+] of the ε-PL [63]. Furthermore, it has been reported that adding and the mass ratio of the inorganic phase might affect stiffness moduli at lower strain values within LVR [25]. The stiffness moduli values in the LVR region increased with increasing the Sr-HAp mass ratio. Up to 50 % Sr-HAp, no statistically significant effect was observed on the stiffness moduli, and the value remained at 1–2 kPa. However, when the mass ratio of the Sr-HAp reached 60 % and 70 %, the stiffness moduli increased to 9 ± 2 kPa and 14 ± 7 kPa, respectively (Fig. S2). A rapid decrease in storage moduli (G') at ~200 % indicates the final matrix transition from solid-like to liquid-like.

The frequency sweep tests were performed at a constant strain value of 0.2 % (defined as a stable strain value within the LVR for all tested samples) (Fig. 3(c)). The nanocomposite hydrogels did not break down within the experimental frequency range. For all compositions, storage (G') and loss (G'') moduli remained at the same level, suggesting that the G' and G'' values were relatively independent of the frequency [56]. No transitions or crossover points were observed for the fabricated hydrogels, indicating permanent chemical crosslinking, which correlates with the time sweep test results (Fig. 3(a)).

The shear rate-dependent viscosity tests assessed the dependency of the viscosity of the hydrogels on the applied shear rate to determine the tendency of the hydrogels to flow [56]. Shear-thinning behavior plays a crucial role in the injectability and syringeability of the viscous system. For all tested compositions, viscosity values rapidly decreased as the shear rate increased, confirming that the fabricated hydrogels have shear-thinning behavior and possess injectability (Fig. 3(d)).

Overall, the rheology results suggest that the obtained nanocomposite hydrogels are at least partly characterized by the "gelation first and injection later" features, which offer advantages such as minimization of leakage after injection and efficient adaptation to complex irregular bone defect sites [55]. As described, HA partially intermolecular cross-links upon adding EDC and NHS and forms a gel before injection, which meets the conditions of shear-thinning hydrogels. However, complete cross-linking to create a stable covalently crosslinked hydrogel occurs after injection, *i.e.*, *in situ* gelation. Thus, the hydrogels show the *in-situ* gelation and the shear-thinning characteristics.

The compression tests assessed the dependency of the compression storage (E') and compression loss (E'') moduli as a function of frequency under constant axial force compression to simulate the physiological conditions of the human body and to examine the viscoelastic properties of the composite hydrogels in such conditions (Fig. 3(e)). Similar E' and E'' curves were obtained for all tested compositions. However, slightly higher E' and E'' values for the hydrogels with higher Sr-HAp mass ratios could be related to higher resistance to spread in the lateral direction. The E' and E'' curves did not cross over the entire frequency range, indicating a stable, strong, chemically crosslinked polymer network. Generally, the hydrogels proposed for bone tissue regeneration have compression storage modulus ranging from 100 kPa to several MPa [64–66]. Regardless of the composition, the measured compression storage moduli of the nanocomposite hydrogels fall within this region. Thus, we can conclude that the developed hydrogels are suitable for bone tissue regeneration. It should be noted that they are not aimed for load-bearing bone application. Still, they should maintain nutrition transport, possess porosity for cell migration, retain structural integrity, and mimic the extracellular matrix. In addition, the compression storage moduli (E') are plotted as a function of cross-linking density (q) (Fig. 3(f)). The E' increased with the q, which is higher for nanocomposite hydrogels with a higher Sr-HAp mass ratio. A higher cross-linking density leads to lower chain flexibility and, thus, lower uptake and swelling degree. Moreover, these results show that adding Sr-HAp nanoparticles can increase the cross-linking density of composite hydrogels through interaction with the hydrogel matrix, *e.g.*, forming hydrogen bonds and, thus, enhancing the stiffness of the hydrogel [67,68].

Next, the cyclic strain time sweep studies were performed (Fig. 3(g)). This is crucial for extrusion and injectability applications, as the material should overcome stress and retrieve the before-stress properties [61]. The nanocomposite hydrogels were alternately subjected to low and high shear rates to simulate the injection through a syringe. As a result, viscosity recovery rates of the hydrogels with and without Sr-HAp showed recovery ability in the 94–181 % range (Fig. 3(h)). Thus, the hydrogels can survive injection/extrusion-like conditions and recover their structure. An increase in the viscosity over 100 % occurs because the hydrogels are still undergoing gelation, so the viscosity continues to increase throughout the test. However, nanocomposite hydrogels with 70 % Sr-HAp showed the lowest recovery rate of 95 ± 61 % (excluding 0 % Sr-HAp, which is used as a reference). They do not fully recover their structure after the applied stress. The significant standard deviation (61 %) indicates that the 70 % Sr-HAp nanocomposite hydrogel recovery is relatively unpredictable and can be as low as 34 %. Therefore, further studies were conducted only on the 40 % Sr-HAp, 50 % Sr-HAp, and 60

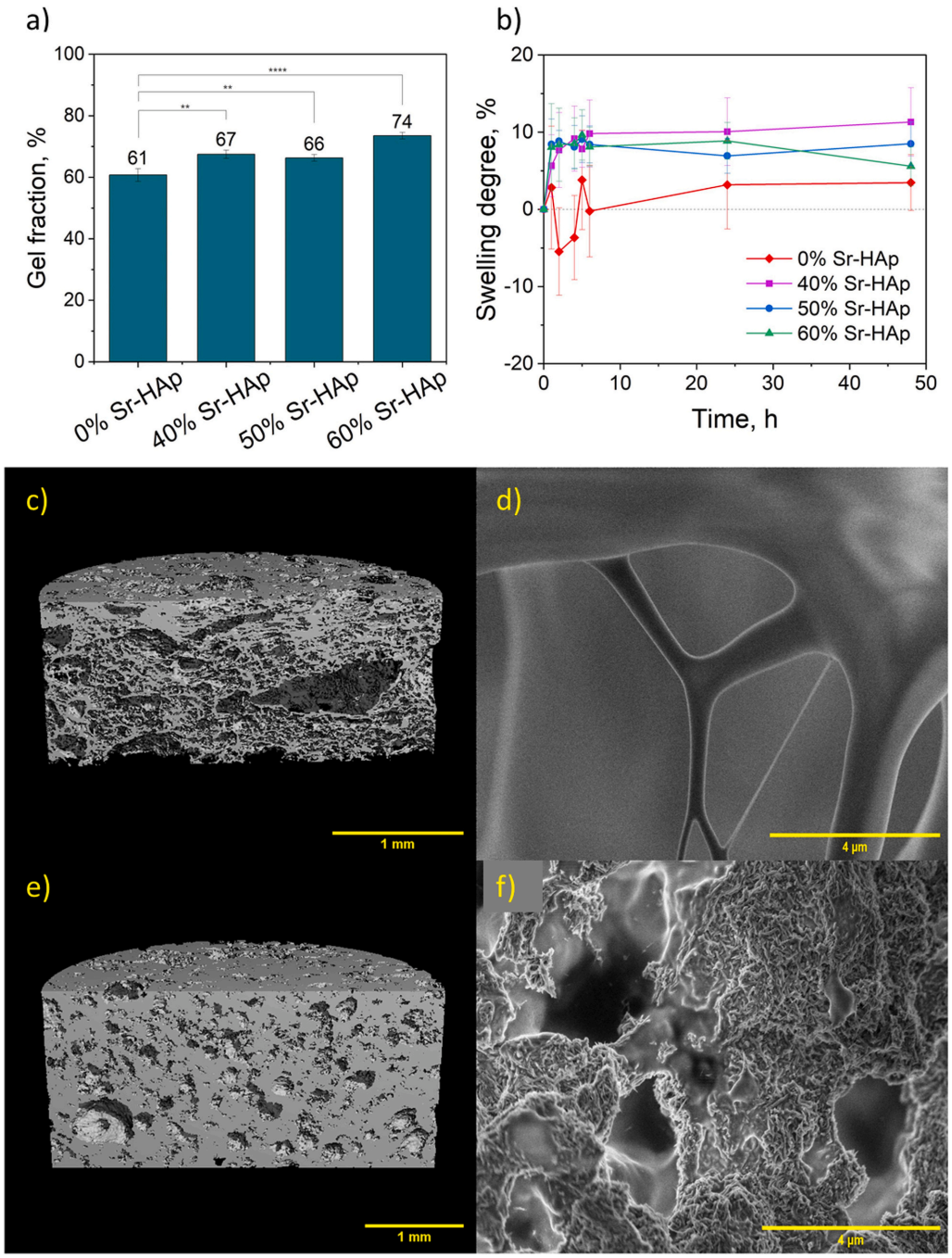

Fig. 4. The gel fraction (a) and the swelling degree (b) of the Sr-HAp-loaded ε-PL-HA nanocomposite hydrogels (ANOVA: * - for $p < 0.05$, ** - for $p < 0.01$, *** - for $p < 0.001$, **** - for $p < 0.0001$, $n = 5$), μ-CT cross-section images of the (c) 0 % Sr-HAp and (e) 60 % Sr-HAp, and the SEM images of the (d) 0 % Sr-HAp and (f) 60 % Sr-HAp at 25 kX magnification (COLOR).

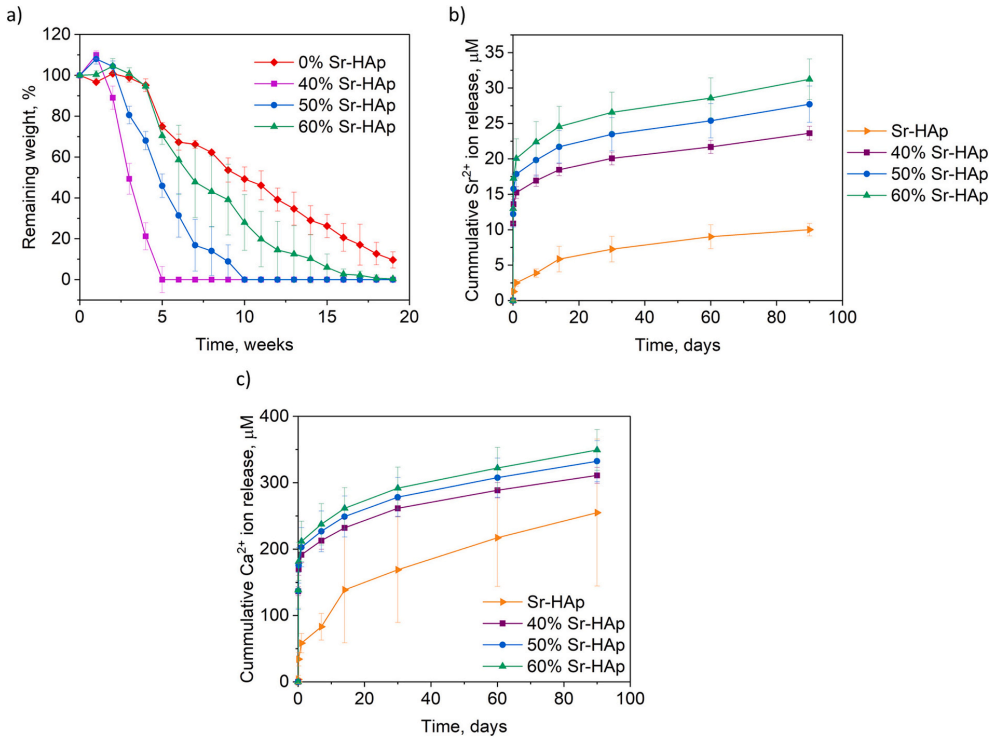

Fig. 5. The enzymatic degradation of the Sr-HAp-loaded ε-PL-HA nanocomposite hydrogels by hyaluronidase (a) and cumulative Sr^{2+} (b) and Ca^{2+} (c) ion release from the as-prepared Sr-HAp-loaded ε-PL-HA nanocomposite hydrogels and the Sr-HAp paste in PBS for up to 90 days ($n = 5$) (COLOR).

% Sr-HAp hydrogels, and the 0 % Sr-HAp hydrogels were used as the reference.

3.3. Gel fraction and swelling degree

The cross-linked fraction of hydrogel is the gel fraction, providing information on cross-linking efficiency and degree. The unreacted fraction can be dissolved and removed, while the crosslinked part, namely the gel fraction, remains. As shown in Fig. 4(a), the gel fraction of the lyophilized nanocomposite hydrogels increased with increasing the Sr-HAp mass ratio. According to synthesis parameters, all nanocomposite hydrogel series were fabricated with constant crosslinking agent concentrations (Table S1). We assume that the slight increase in the crosslinked gel fraction is associated with the Sr-HAp interaction with ε-PL and HA macromolecules. Thus, during the *in-situ* formation of the chemically crosslinked nanocomposite hydrogels, the physically crosslinked network was simultaneously formed *via* electrostatic interactions between charged Sr-HAp and free non-crosslinked functional groups of ε-PL and HA. *Svarca* et al. observed the same effect of CaP addition on the crosslinking efficiency of the HA hydrogels [69]. They attributed this to the influence of the added CaP particles on the distances between the HA chains. Namely, as the particles fill the empty spaces between the polymer chains, the chains are brought closer to each other, allowing crosslinking to occur more effectively. Moreover, the increase in the mass ratio of Sr-HAp was at the expense of the total ε-PL-HA mass ratio (Table S1). Thus, the hydrogels with a higher Sr-HAp mass ratio contain less polymer, which remains free. Accordingly, by removing this unreacted part of the polymers, the total hydrogel weight is less altered. As demonstrated in Fig. S3, the swelling degree of the lyophilized Sr-HAp/ε-PL-HA hydrogels decreases with increasing the Sr-HAp mass ratio, and these results are in good agreement with the gel fraction analysis (Fig. 4(a)). Thus, higher swelling capacity is associated with a lower gel fraction and crosslinking density. The lyophilized nanocomposite hydrogels exhibited fast-swelling ability, reaching an equilibrium swelling degree of ~500–750 % after 1 h. The 0 % Sr-HAp hydrogels reveal a significantly higher swelling degree, reaching the equilibrium swelling rate at 2000 % after 4 h. In general, the chemical composition, the network structure, and the crosslinking density determine the swelling degree of the hydrogels [70]. The high binding affinity of the water molecules of the ε-PL-HA hydrogels and the Sr-HAp/ε-PL-HA nanocomposite hydrogels are primarily associated with the presence of polar hydrophilic functional groups such as primary [NH_2] groups of the ε-PL, [OH] and [COOH] groups of the HA, and [OH] groups of the Sr-HAp. We assume that the increase of Sr-HAp mass ratio in hydrogels introduces new hydrogen bonds and physical crosslinking networks through electrostatic interactions into the hydrogel network, which can limit the free movement of the non-crosslinked part of ε-PL-HA hydrogel. As the Sr-HAp mass ratio is relatively high, the spacings between the crosslinks of the nanocomposite hydrogel network become significantly smaller. In other words, Sr-HAp particles limit the movement of polymer chains and reduce swelling. Accordingly, hydrogels with a smaller mesh size exhibit a lower swelling degree [69]. Moreover, in the case of lyophilized hydrogels, the microstructure significantly influences the degree of swelling. Namely, the amount of retained liquid is related to the porosity of the hydrogels. As shown in Fig. 4(c-f) and described in Section 3.4, the porosity of the ε-PL-HA hydrogels significantly decreases with the addition of the Sr-HAp.

Considering that the hydrogels will be used non-lyophilized, the

degree of swelling of the as-prepared hydrogels was determined and is shown in Fig. 4(b). The as-prepared hydrogels were pre-swollen due to the water added during the preparation. Thus, the degree of swelling is low (up to 10 %). After 5 h, the hydrogels reached a swelling equilibrium, indicating the dimensional and structural stability of the hydrogels due to their pre-swollen form. This observation is beneficial, as in the case of injectable hydrogels, the swelling must be controlled to avoid undesirable compression on the surrounding tissues [71]. Hydrogels without the Sr-HAp did not swell. The swelling degree increased with the addition of the Sr-HAp. However, no changes were observed when the Sr-HAp mass ratio was increased. This could be explained by the differences in the water content of the as-prepared hydrogels (Table S1). The as-prepared 0 % Sr-HAp hydrogel has the highest water content and exhibits a lower swelling degree than the Sr-HAp-loaded nanocomposite hydrogels.

3.4. Microstructure and morphology

A recent review article emphasizes the importance of physically incorporated pores for medical applications of hydrogels. Generally, tissue engineering scaffolds mimic normal tissue development processes, allowing cells to formulate their microenvironment. Ideally, scaffolds have a 3D, highly porous structure with an interconnected pore network to facilitate the diffusion of cells/tissues, nutrients, metabolic wastes, and paracrine factors [72].

Thus, the μ-CT and SEM were used to evaluate the microstructure of the fabricated hydrogels (Fig. 4(c-f)). The pores in the ε-PL-HA hydrogels are formed *in situ* by bubbles trapped in the hydrogel. As the HA and ε-PL are chemically crosslinked with EDC/NHS, the CO_2 bubbles are formed during the activation of the HA carboxyl groups [25]. The hydrogel gelation time is too short for the bubbles to escape the hydrogel matrix, leaving a porous structure (macropores up to 1 mm) [73]. Since these are closed pores, such porosity is undesirable, as it can adversely affect mechanical properties and lead to incomplete bone defect filling. However, it should be noted that before analysis, the samples were lyophilized, and the drying process may have caused artifacts in the hydrogel structure, giving false information [74]. In the case of lyophilization, the primary cause of artifacts is the formation of ice crystals upon freezing [75]. Still, the tendency for porosity and pore sizes to decrease with increasing the Sr-HAp mass ratio was observed. According to μ-CT measurements, the porosity of the hydrogels decreased in the following order: 0 % Sr-HAp (approx. 82 %) > 40 % Sr-HAp (approx. 49 %) > 50 % Sr-HAp (approx. 45 %) > 60 % Sr-HAp (approx. 39 %). Adding the Sr-HAp improves the structural and mechanical integrity of the ε-PL-HA hydrogels.

The SEM images reveal that the Sr-HAp is homogeneously dispersed throughout the hydrogel as a few hundred nm long needle-shaped particles (Fig. 4(f)). However, since the Sr-HAp nanoparticles are embedded in a polymer matrix, they are exposed to the surrounding environment, such as physiological solutions, cell environment, *etc.*, in separate areas.

3.5. Enzymatic degradation and ion release

HA hydrogels in physiological environments degrade by hydrolysis and enzymatic hydrolysis due to naturally occurring hyaluronidase and reactive oxygen species [76]. In turn, ε-PL is degraded by hydrolytic or proteolytic enzymes (proteases), which cleave the peptide bonds between the lysine residues in ε-PL [77]. Thus, the weight loss of the hydrogels by the enzymatic degradation as a function of soaking time in PBS containing hyaluronidase and proteinase K was evaluated, and the results are reported in Fig. 5(a) and Fig. S4, respectively.

The hydrogels swell and degrade concurrently when exposed to the degradation media, accompanied by disruption of their original structure as observed by SEM analysis (Fig. S5). Namely, as the hydrogel swells, the mesh size becomes larger, allowing liquid to diffuse in and out of the hydrogel [78]. However, as the as-prepared hydrogels were pre-swollen upon synthesis, all samples underwent mass loss over time without significant swelling. Hyaluronidase (Fig. 5(a)) treatment promoted little to no degradation of the nanocomposite hydrogels during the first weeks. The 0 % Sr-HAp hydrogels were degraded at a lower rate than the nanocomposite hydrogels. The nanocomposite hydrogels with the lowest Sr-HAp mass ratio (40 % Sr-HAp) showed the fastest enzymatic degradation and degraded fully in 5 weeks. This could be explained by the lower fraction of the polymer used to prepare the hydrogels [58]. Furthermore, the higher Sr-HAp mass ratio led to a lower degradation rate of the nanocomposite hydrogels. This could be due to lower porosity with an increased Sr-HAp mass ratio. Higher porosity favors water absorption (higher swelling degree) and, thus, increases the degradation rate. Another explanation could be related to the acidic nature of the ε-PL-HA hydrogels (approx. pH 5). Degradation of the hydrogels is expected to be accompanied by the release and accumulation of acidic degradation products [79]. This autocatalytic effect can contribute to the dissolution of the Sr-HAp. In turn, the dissolution of the Sr-HAp is associated with a local pH increase. It has been reported that even a slight increase in the pH value enhances the hydrogels' stability, significantly prolonging the degradation rate [80]. The 50 % Sr-HAp and 60 % Sr-HAp hydrogels were degraded within 10 and 19 weeks.

In the case of the proteinase K treatment (Fig. S4), weight loss was observed after the first day, suggesting rapid degradation of the hydrogels. The initial weight loss was higher for the 0 % Sr-HAp hydrogels (approx. 20 %), while it was about the same level for the Sr-HAp-loaded nanocomposite hydrogels (5–10 %). The weight loss differences among various compositions might be explained by simultaneous degradation and water uptake or swelling. As described in Section 3.3., in the case of the as-prepared hydrogels, swelling (swelling degree in PBS up to 10 % at 24 h) was observed only in the case of the Sr-HAp-loaded nanocomposite hydrogels. Hence, the Sr-HAp-loaded nanocomposite hydrogels have a lower degradation rate than their Sr-HAp-free counterparts. In addition, the higher porosity of 0 % Sr-HAp hydrogels enables more efficient diffusion of liquids inside the samples, which may also contribute to their degradation. Afterward, a slight increase in weight was observed, followed by a plateau for the rest of the experiment (up to twelve days) for all compositions. Given that proteinase K hydrolyzes peptide bonds, it is expected that the mass loss mainly resulted from the degradation of ε-PL [77].

Ideally, injectable biomaterials for bone regeneration should degrade at a rate that matches the growth rate of new bone tissue to ensure proper structural integrity throughout the healing process. Optimally, the biomaterial should fully resorb over several months to years [81].

Degradation of the nanocomposite hydrogels is expected to be accompanied by ion release from the Sr-HAp. Biomaterials, which can ensure the long-term (months to years) local supply of the Sr^{2+} ions, have been proposed to be suitable for patients with osteoporotic fractures or bone defects [82]. Since we intended the nanocomposite hydrogels to be carriers of Sr^{2+} ions, the cumulative ion release under physiological conditions was analyzed for 3 months (Fig. 5(b,c)). Generally, the higher the mass ratio of the Sr-HAp, the higher the amount of released ions. However, the amount of released ions from the Sr-HAp paste was lower. The amount of the released ions from the Sr-HAp/ε-PL-HA hydrogels significantly increased due to the burst release of the Sr^{2+} and Ca^{2+} ions in the first few days. It is well known that the dissolution of HAp is inversely related to pH. The dissolution of nanocrystalline HAp at pH 5 (pH of the ε-PL-HA hydrogels) is accompanied by a rapid initial increase in the Ca^{2+} and PO_4^{3-} ions concentrations, followed by a gradual decrease as the pH increases [83]. Thus, the significant burst release from the nanocomposite hydrogels could be related to their acidic nature. Namely, partial dissolution of Sr-HAp particles may have occurred in the hydrogel matrix, creating free ions. The free ions were most likely released during the first days, thus causing burst release. The burst release can cause an adverse effect as the high local concentration of the Sr^{2+} ions can result in cytotoxicity [82].

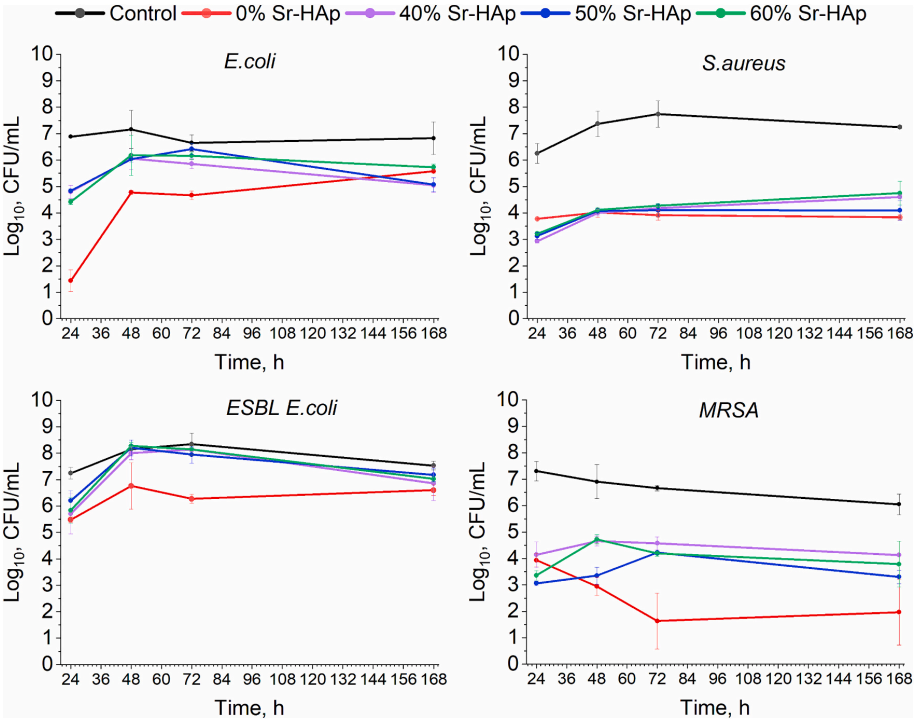

Fig. 6. Antibacterial activity of the as-prepared Sr-HAp-loaded ε-PL-HA nanocomposite hydrogels on *E. coli*, *S. aureus, ESBL E. coli,* and *MRSA* bacteria strains (n = 3) (COLOR).

However, the concentration of Sr^{2+} ions released from the nanocomposite hydrogels does not exceed 20–30 μM. Our earlier study suggests that up to 40 μM of Sr^{2+} ions in the cell culture is beneficial for the proliferation of MG-63 osteoblasts [41]. In addition, the simultaneous release of Ca^{2+} ions in relatively high concentrations should also be considered. Up to 200 μM of Ca^{2+} ions were burst-released in the first days. According to the literature, elevated Ca^{2+} ions concentration (up to 900 μM) enhances the bone regeneration effects of Sr^{2+} ions [84]. The burst release was followed by slow and continuous release of Sr^{2+} and Ca^{2+} ions over 3 months.

3.6. Antibacterial properties

The ε-PL with a cationic surface because of its positively charged amino acid residues is expected to act as an antibacterial component in the Sr-HAp/ε-PL-HA nanocomposite hydrogels. Thus, the antibacterial activity of the as-prepared Sr-HAp/ε-PL-HA hydrogels against *E. coli*, *ESBL E. coli* (Gram-negative) and *S. aureus*, MRSA (Gram-positive) was assessed using the standard plate counting microdilution method (Fig. 6).

To evaluate the long-term antibacterial activity, the bacteria were subjected to direct contact with the hydrogels, and experimental time points were 24 h, 48 h, 72 h, and 168 h. At all experimental time points, it was observed that the nanocomposite hydrogels induced statistically significant (statistical analysis is shown in Fig. S8) reduction in the number of bacterial colonies of Gram-positive reference and clinically isolated antibiotic-resistant *S. aureus* strains. All experimental series showed fast-acting and long-term antibacterial activity against both *S. aureus* strains. In the case of Gram-negative *E. coli* and ESBL *E. coli* strains, the hydrogels showed a significant reduction in bacterial colonies only in a fast-acting perspective, *i.e.*, after 24 h. Structural features of Gram-negative bacteria cell walls could explain this tendency. The presence and polarity of the outer membrane of Gram-negative bacteria prevent the achievement of cationic on the bacterial membrane surface, resulting in reduced antibacterial action [85]. Furthermore, the presence of the inorganic phase, namely, the Sr-HAp, might compromise the antibacterial profile of the composite hydrogels [86] by affecting the release of the antibacterial component or creating a physical barrier in the matrix. Statistically significant differences were found between the 0 % Sr-HAp hydrogels and Sr-HAp-loaded nanocomposite hydrogels at different experimental stages. For example, in the case of *E. coli* at the 24 h point, the 0 % Sr-HAp series showed significantly higher inhibition than other compositions. As for 48 h and 72 h, 0 % Sr-HAp hydrogels were the only ones to maintain antibacterial activity against *E. coli.* This difference might arise because the Sr-HAp increases physical entanglements in the polypeptide network and slows the release of antibacterial ε-PL. As mentioned above, such deacceleration of ε-PL release leads to a decreased concentration of ε-PL molecules on the bacterial surface below its' antibacterial effect. No significant differences were found between Sr-HAp/ε-PL-HA nanocomposite hydrogels with different Sr-HAp mass ratios, suggesting that the Sr-HAp does not have an impact on the antibacterial activity of the ε-PL-HA hydrogels.

Overall, the Sr-HAp/ε-PL-HA nanocomposite hydrogels possess fast-acting and long-term antibacterial activity against Gram-positive bacteria and can inhibit Gram-negative bacteria in a fast-acting perspective. Although the antibacterial activity provided by the ε-PL is desirable, they might be hampered by the risk of cytotoxicity. To evaluate whether the addition of the Sr-HAp improves the biocompatibility of the ε-PL-HA hydrogels, *in vitro* cell tests were performed.

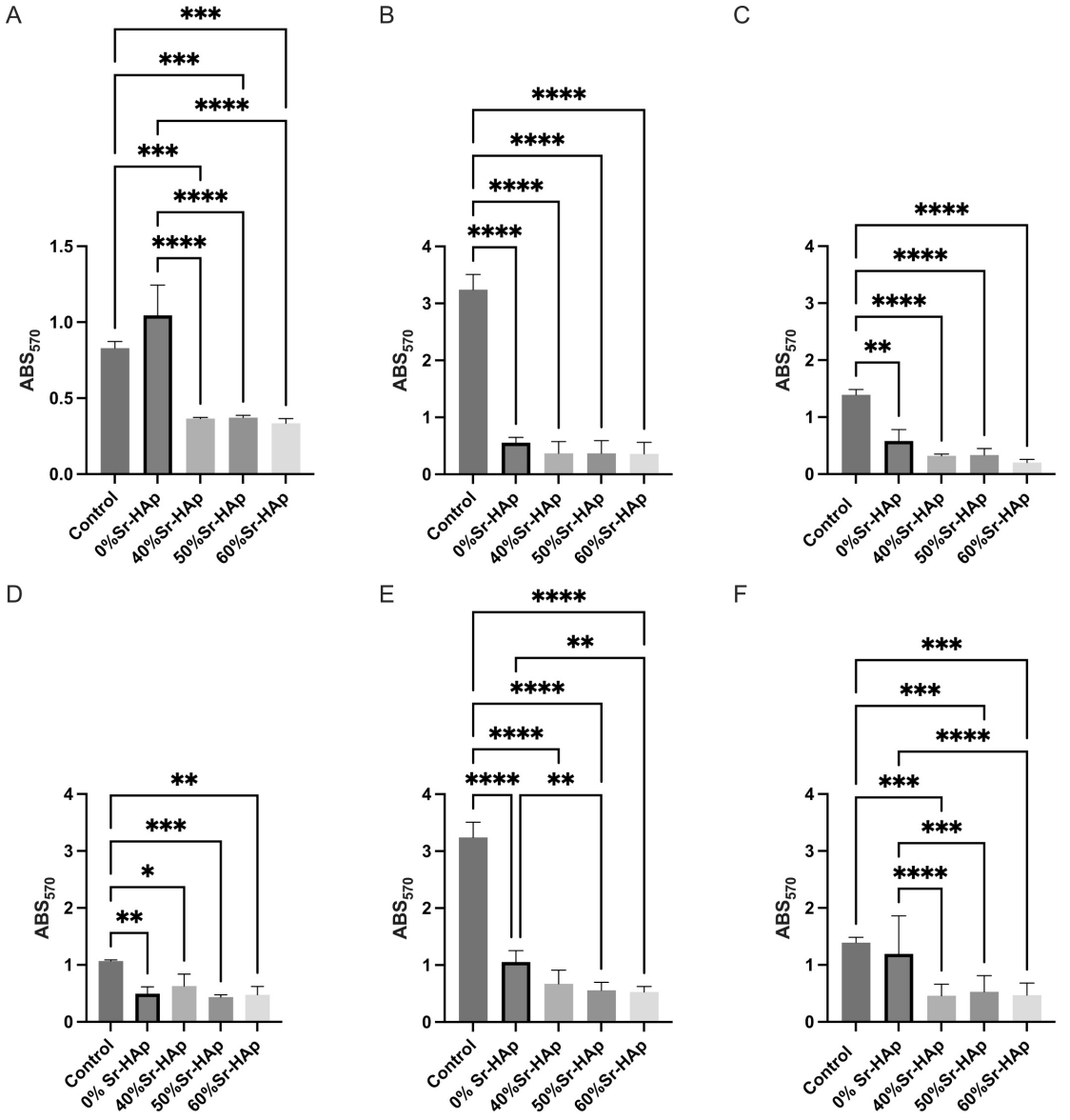

Fig. 7. Effect of the Sr-HAp-loaded ε-PL-HA nanocomposite hydrogels on the proliferation of MG-63 osteoblasts in the hydrogels (A, B, C) and on the cultivation plate surface surrounding the hydrogel (D, E, F) after 2 (A, D), 5 (B, E), and 7 (C, F) days of cultivation, control – cells grown in standard cultivation conditions (ANOVA: * for $p < 0.05$, ** - for $p < 0.01$, *** - for $p < 0.001$ **** for $p < 0.0001$, $n = 3$).

3.7. *In vitro biocompatibility*

3.7.1. *Proliferation of osteoblasts and pre-osteoblasts*

The proliferation of MG-63 osteoblasts (Fig. 7) and MC3T3-E1 pre-osteoblast (Fig. 8) was evaluated on days 2, 5, and 7. It was observed that some of the cells seeded onto the hydrogels tend to migrate, attach, and proliferate on the cultivation plate surface surrounding the hydrogels. The samples and the corresponding plate wells were assayed separately to assess the proportion of cells growing around the hydrogel *versus* those in the hydrogel samples.

The proliferation of MG-63 cells was lower in the hydrogels (Fig. 7 (A-C)) than on the cultivation plate (Fig. 7(D—F)), especially on days 5 and 7. This could be explained by dissolution of the hydrogels in the culture medium. As the hydrogel dissolves, the released components are evenly distributed in the culture media and over the surface of the cultivation plate. Thus, cell migration and proliferation outside the hydrogels could be promoted.

In the case of 0 % Sr-HAp, the highest MG-63 cell proliferation in the

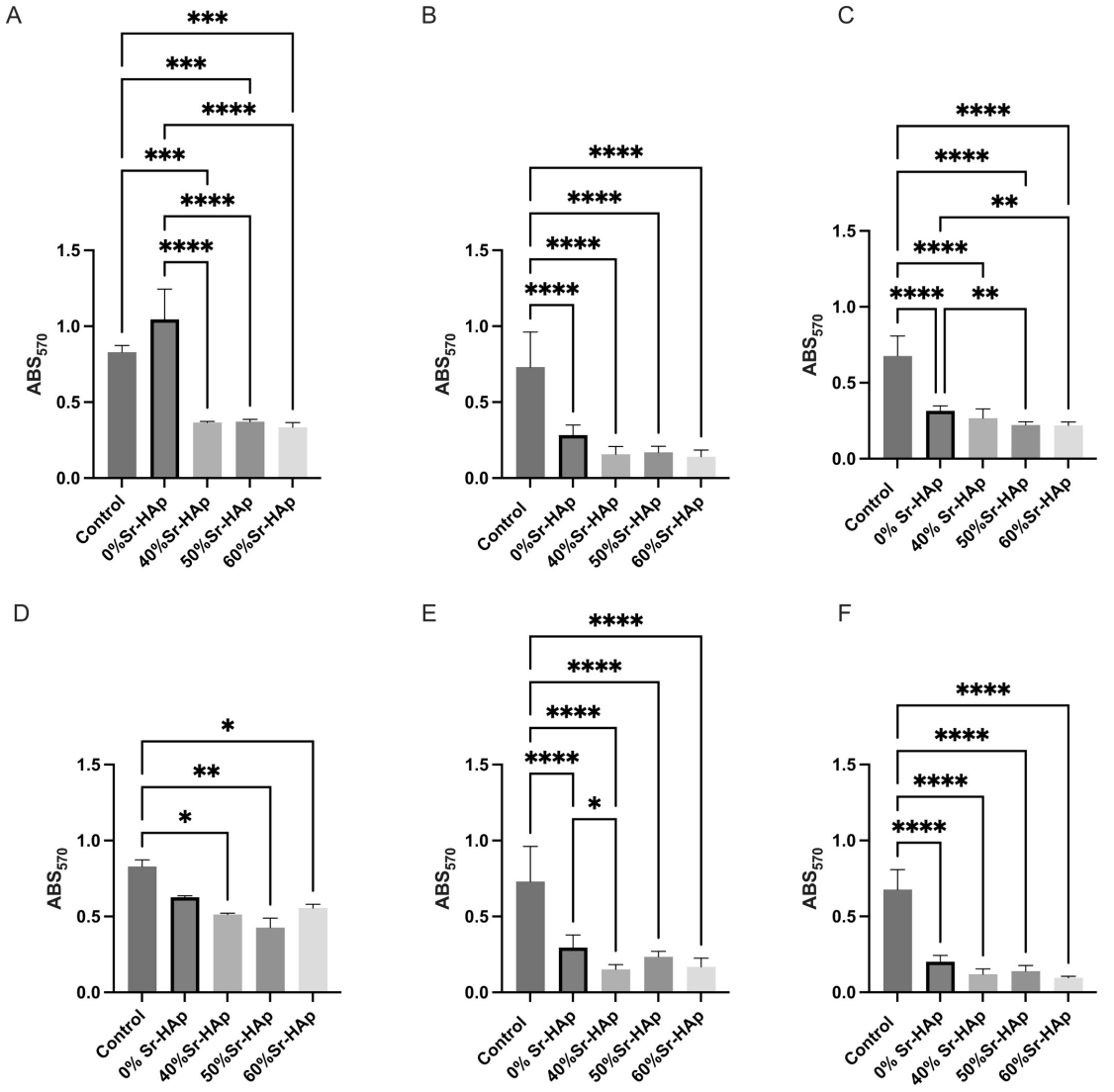

Fig. 8. Effect of the Sr-HAp-loaded ε-PL-HA nanocomposite hydrogels on the proliferation of the MC3T3-E1 pre-osteoblasts in the hydrogels (A, B, C) and on the cultivation plate surface surrounding the hydrogel (D, E, F) after 2 (A, D), 5 (B, E), and 7 (C, F) days of cultivation, control – cells grown in standard cultivation conditions (ANOVA: * for $p < 0.05$, ** - for $p < 0.01$, *** - for $p < 0.001$, **** for $p < 0.0001$, $n = 3$).

hydrogels and on the cultivation plate surface was observed. At 2 days after seeding, cell proliferation in 0 % Sr-HAp even slightly exceeded that of the control cells. Moreover, the superiority of 0 % Sr-HAp compared to the hydrogels containing Sr-HAp increased with incubation time. Moreover, no significant differences were observed among the hydrogels with various mass ratios of the Sr-HAp, and the proliferation of the MG-63 cells in the hydrogels decreased on day 5 and day 7. A similar tendency was observed on the cultivation plate surface. This is contrary to information in the literature suggesting that adding HAp to the polymer composites [87] and the presence of Sr in the biomaterials [88,89] leads to higher osteogenic activity, including the proliferation of the osteoblasts. This could be due to the influence of the microstructure of hydrogels. The 0 % Sr-HAp hydrogels are significantly more porous than the nanocomposite hydrogels (Fig. 4(c,e)) and, thus, more favorable to cell migration inside the samples [72]. At the same time, differences in the proliferation of the MG-63 cells on the cultivation plate could be related to the differences in degradation (*i.e.*, the released components (ions, polymers)) of the hydrogels. Up to 0.250 mM of Ca^{2+} and 0.025 mM Sr^{2+} ions were released from all the Sr-HAp/ε-PL-HA hydrogels in 7 days (Fig. 5). Regarding released Ca^{2+} ion concentration, it has been suggested that 2–4 mM is optimal for the survival and proliferation of osteoblasts, 6–8 mM favor osteoblast differentiation and matrix mineralization, and concentrations above 10 mM are considered cytotoxic [90]. According to the literature, the Sr^{2+} ions therapeutic

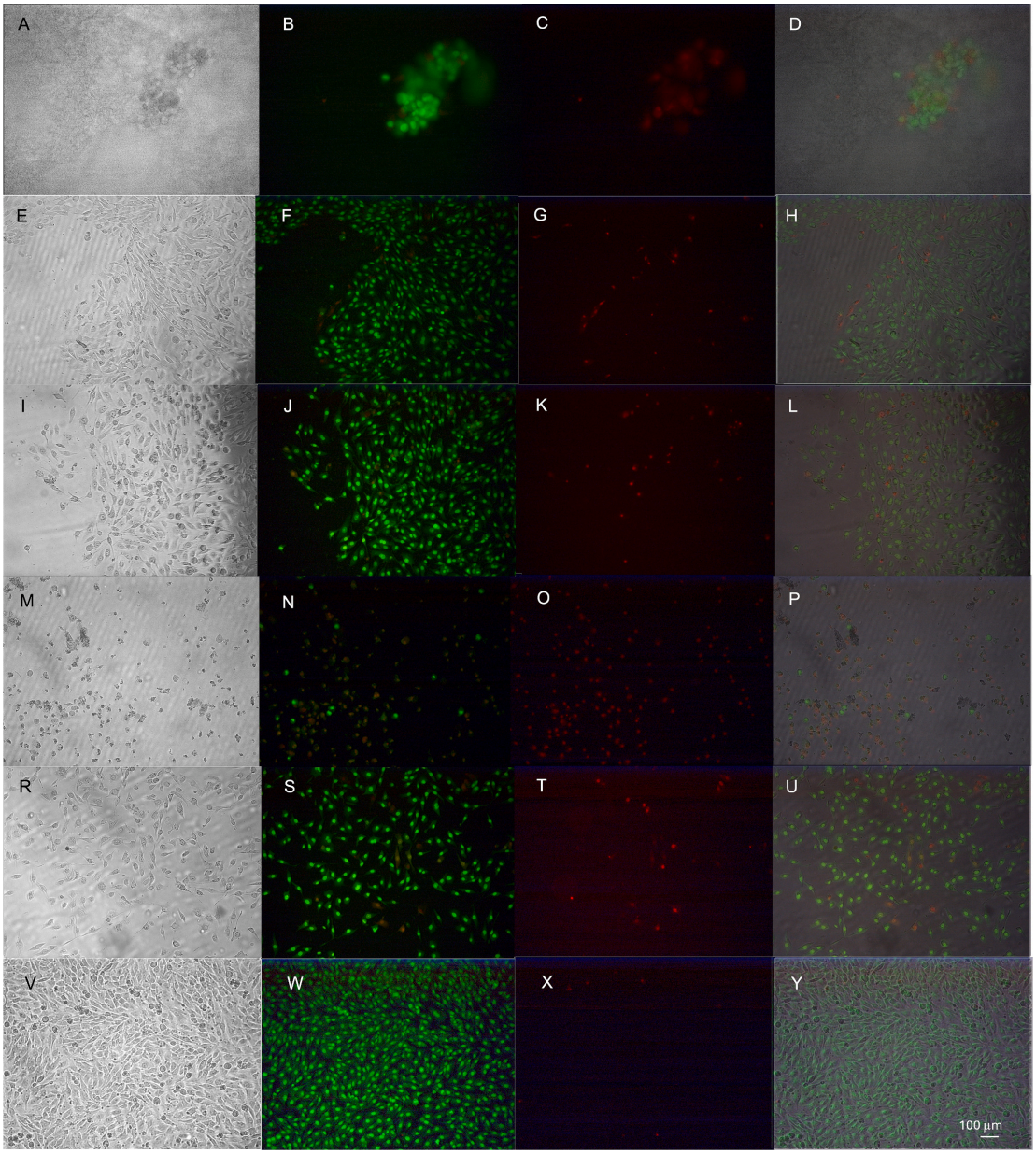

Fig. 9. Live/dead staining of MG-63 osteoblasts after 5 days of cultivation. MG-63 osteoblasts A - D – in the 0 % Sr-HAp hydrogel, and on the cultivation plate surface surrounding E - H – the 0 % Sr-HAp, I - L – 40 % Sr-HAp, M - P –50 % Sr-HAp, R - U - 60 % Sr-HAp hydrogels, *V*—Y – control cells grown on the surface (A, E, I, M, R, V – brightfield; B, F, J, N, S, W– SYTO 9 (green); C, G, K, O, T, X – propidium iodide (red); D, H, L, P, U, Y – merged images; the scale bar represents 100 μm).

level is 2–45 ppm (0.02–0.52 mM) [91]. Thus, the concentrations of Ca^{2+} and Sr^{2+} ions released in 7 days can be considered safe. However, the Sr-HAp/ε-PL-HA hydrogels are more susceptible to enzymatic degradation than the ε-PL-HA hydrogels. This could have resulted in a higher initial release of organic substances from the polymers upon incubation in the cell culture media, affecting cell behavior.

In the case of the MC3T3-E1 cells, the proliferation was slightly higher in the hydrogels (Fig. 8(A-C)) than on the cultivation plate surface surrounding the hydrogels (Fig. 8(D—F)). MC3T3-E1 proliferation in the hydrogels and on the cultivation plate surface decreased over time. This indicates the different sensitivity of the MG-63 and MC3T3-E1 cell lines to the components of the hydrogels. It has been reported that

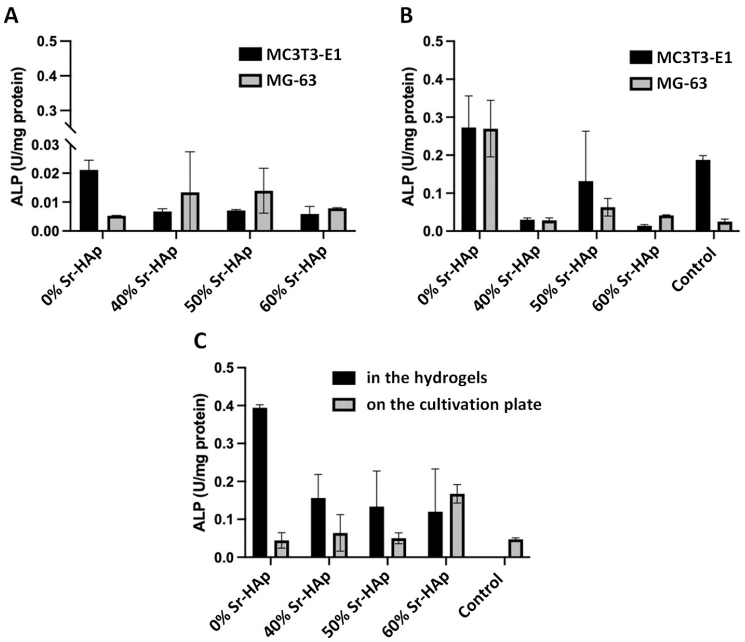

Fig. 10. The ALP activity in the lysates from the MC3T3-E1 and the MG-63 cells (A) grown in the hydrogels, (B) on the cultivation plate in the presence of the hydrogels for 5 days, and (C) in the lysates from the MG-63 cells grown in the hydrogels and on the cultivation plate in the presence of the hydrogels for 7 days ($n = 3$).

low concentrations (up to 0.18 mM) of Sr^{2+} ions have MC3T3-E1 proliferation and osteogenesis-stimulating activity, while high concentrations (above 24 mM) have been shown to reduce cell viability [92,93]. Like MG-63 osteoblasts, MC3T3-E1 pre-osteoblasts showed higher proliferation in the 0 % Sr-HAp hydrogel, with the most pronounced differences observed on day 2.

To further characterize the growth and morphology of the cells, live/dead staining was performed after 5- and 7-day cultivation of MG-63 and MC3T3-E1 cells on the hydrogels. Detecting live cells using live/dead dyes proved challenging due to the hydrogel structure. Single cells or small clusters were found in all hydrogels, but cell densities were generally low, with both live and dead cells present (Fig. S9 – Fig. S12). MG-63 cells grew more noticeably outside the hydrogel, *i.e.*, on the cultivation plate surface surrounding the hydrogels, which aligns with the MTT assay results. Growth on the cultivation plate surface indicates that cells prefer to grow on standard cell cultivation plastic compared to the nanocomposite hydrogels. Still, the presence of hydrogels and the potential leakage of components from them did not significantly affect cell viability and morphology. More viable cells were observed in the 0 % Sr-HAp hydrogels compared to the Sr-HAp-loaded nanocomposite hydrogels. Cells predominantly were localized at the edges of the material (Fig. 9, Fig. S9(A-H), Fig. S10(A-C), Fig. S11(A-C)). Interestingly, less viable MG-63 cells were observed in the presence of the 50 % Sr-HAp samples compared to other nanocomposite hydrogels. Higher density and viability were observed in control cells. However, cell density and viability after 5 days and 7 days also increased in the presence of hydrogels, indicating that the potential cytotoxic effect is weak and during continuous cultivation, cells continue to grow and proliferate (Fig. S9(M-P), Fig. S10(M-P)). All hydrogels supported live MC3T3-E1 cells after 5 and 7 days of culture. Cell numbers observed in the hydrogels were low; however, normal cell morphology was observed (Figs. S10-S11).

In general, both cell lines showed viability in the hydrogels and on the cultivation plate surface surrounding the hydrogels, indicating that the hydrogels are not cytotoxic. However, the proliferation rates varied depending on the cell line. Although the Sr-HAp loading in the ε-PL-HA nanocomposite hydrogels did not show proliferation-stimulating activity, it should be noted that a substantial part of the Sr-HAp is embedded in the hydrogel matrix as observed from the SEM analysis (Fig. 4(f)) and, thus, not in direct contact with the cells upon initial stages of incubation. Therefore, the significant effect from the Sr-HAp would be observed upon the dissolution of the nanocomposite hydrogels in the cell culture medium.

3.7.2. Alkaline phosphatase activity

ALP activity is generally used as an early marker for osteodifferentiation *in vitro*. Thus, the ALP activity in both cell lines was measured in the lysates from cells grown in the hydrogels and on the cultivation plate in the presence of the hydrogels (Fig. 10).

Regarding the cells grown in the hydrogels for 5 days, the highest ALP activity of the MC3T3-E1 was observed in the case of the 0 % Sr-HAp hydrogels (Fig. 10(A)). In turn, the ALP activity of the MC3T3-E1 cells grown in the Sr-HAp/ε-PL-HA hydrogels did not differ significantly. Meanwhile, the ALP activity of the MG-63 cells grown in the hydrogels for 5 days was equal for all hydrogel compositions. However, after 7 days of cultivation, the ALP activity of the MG-63 cells grown in the hydrogels increased, the highest being in the case of the 0 % Sr-HAp (Fig. 10(C)). In general, the ALP activity of the lysates from cells grown in the hydrogels was lower than for cells grown on the cultivation plate (Fig. 10(B)). According to the literature, ALP expression can be down-regulated when grown in 3D cultures compared to plastic-surface cultivation [94]. Also, for the cells grown on the cultivation plate in the presence of hydrogels for 5 days, the highest ALP activity for both cell lines was observed in the case of 0 % Sr-HAp (Fig. 10(B)). Moreover, for the MC3T3-E1, the ALP activity in the case of 0 % Sr-HAp was higher than those grown on the cultivation plate without the hydrogels

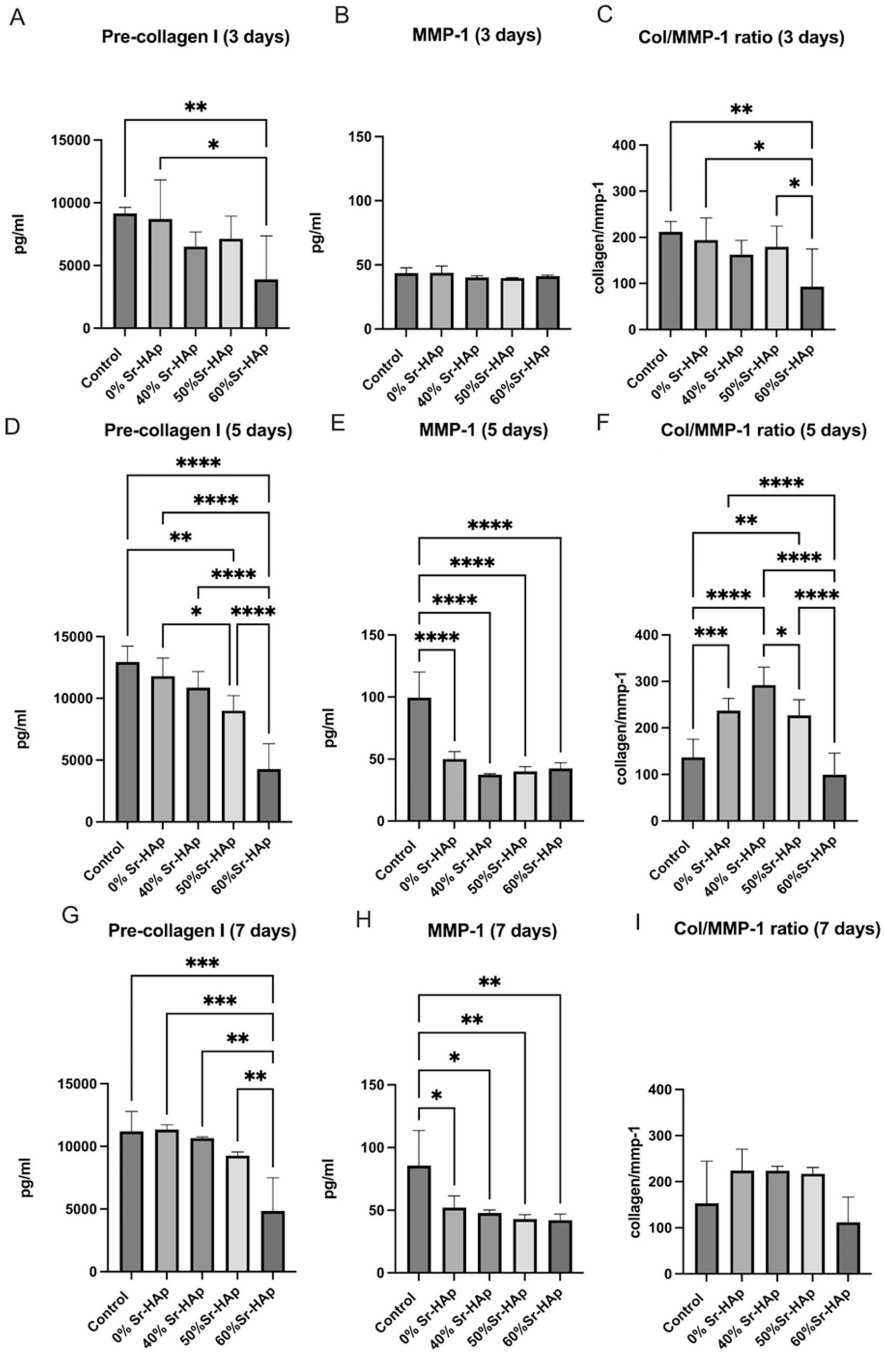

Fig. 11. Secretion of pre-collagen I (A, D, G) and MMP-1 (B, E, H) and ratio between pre-collagen I and MMP-1 (Col/MMP-1 ratio, C, F, I) after 3, 5, and 7 days of MG-63 cultivation on the Sr-HAp-loaded nanocomposite hydrogels (ANOVA: * for $p < 0.05$; ** $p < 0.01$, for *** - for $p < 0.001$, **** for $p < 0.0001$, $n = 3$).

(control), indicating the stimulating activity of the 0 % Sr-HAp. In the case of MG-63, the ALP activity higher than the control was in the lysates of the cells grown in the presence of 0 % Sr-HAp, 50 % Sr-HAp, and 60 % Sr-HAp hydrogels. These observations correlate with cell proliferation assays (Fig. 7 and Fig. 8). Upregulation of ALP production is more pronounced at higher cell densities [95,96]. Thus, the lower proliferation of MG-63 and MC3T3-E1 cells in the Sr-HAp/ε-PL-HA hydrogels compared to the 0 % Sr-HAp could explain the observed tendencies of ALP activities. Interestingly, the lysates of the MG-63 osteoblasts grown for 7 days on the cultivation plate in the presence of the 0 % Sr-HAp hydrogels showed significantly lower ALP activity than after 5 days of cultivation (Fig. 10(C)). A similar effect was observed in cell studies of Sr-incorporated HAp bioceramics using bone marrow mesenchymal cells. Namely, the ALP activity after 7 days of cultivation increased compared to 4-day cultivation [97]. In addition, *Tsai* et al. observed that the MG-63 ALP activity was the highest after 3 days of cultivation in the presence of Sr-substituted HAp nanofibrous matrix and decreased during prolonged cultivation [88]. Also, changes in ALP activity in the lysates from cells grown on the cultivation plate could be explained by the release of Sr^{2+} and other hydrogel components. The studies found in the literature show that ALP activity highly depends on the concentration of Sr in the tested materials and the release of Sr^{2+} ions in the culture medium. Generally, it has been reported before that Sr^{2+} ions released from various biomaterials stimulate osteogenesis [98,99]. Even low Sr ratios in composite materials are reported to positively affect ALP activity in MC3T3-E1 cells; however, increasing Sr content leads to lower ALP activity [99]. *Xie* et al. reported that stimulation of ALP activity by Sr^{2+} ions released from biomaterials depends on Ca^{2+} concentrations [84].

3.7.3. Secretion of pre-collagen and MMP-1

The organic part of bone ECM is composed mainly of collagen type I, primarily synthesized by osteoblasts. Collagen acts as the scaffold for bone cells, promotes bone formation, and provides mechanical support and bone strength [100]. ECM is dynamic, and it continuously undergoes remodeling mediated by enzymes MMPs. MMPs are involved in bone tissue regeneration and repair. Regulation of matrix formation and remodeling is crucial for tissue homeostasis [101]. Increased levels of MMPs are characteristic of inflammatory bone diseases and infections. Elevated levels of MMP-1 and mutations in corresponding genes lead to increased degradation of collagen I and are associated with the development of osteoporosis [102].

In this study, the pre-collagen I and MMP-1 levels secreted by MG-63 cells grown in the Sr-HAp-loaded nanocomposite hydrogels for 3, 5, and 7 days were measured (Fig. 11).

At all cultivation times, the cells grown in the 0 % Sr-HAp hydrogels produced pre-collagen I at a similar level to the control. On days 5 and 7, the pre-collagen I level decreased with increasing the mass ratios of Sr-HAp in the hydrogels. The most pronounced increase in the pre-collagen I was observed for the 40 % Sr-HAp hydrogels. From day 3 to day 7, the pre-collagen I concentration in the presence of 40 % Sr-HAp hydrogels increased by an average of 4143 pg/mL, while in the control - an average of 2056 pg/mL. No correlation between collagen production and cell proliferation was observed. This allows us to assert that even if the nanocomposite hydrogels do not stimulate cell proliferation, they promote pre-collagen I synthesis in osteoblasts and ECM production.

After 3 days of cultivation, the MMP-1 secretion for all hydrogels was similar to the control level. Still, after 5 and 7 days, the MMP-1 secretion of the cells in the presence of 0 % Sr-HAp hydrogels increased.

The pre-collagen I to MMP-1 (Col/MMP-1) ratios were calculated to evaluate if the hydrogels in the cultivation media promote collagen production or degradation. Higher Col/MMP-1 ratios indicate a predominance of collagen synthesis over degradation. After 5 and 7 days of cultivation, the 0 % Sr-HAp, 40 % Sr-HAp, and 50 % Sr-HAp hydrogels provided conditions where collagen synthesis exceeds degradation compared to the control. The highest Col/MMP- ratios were observed on day 5. In the case of 60 % Sr-HAp, the Col/MMP-1 ratios were lower than the control's, indicating lower ECM synthesis-promoting activity.

A study with murine osteoblasts showed that collagen matrix is required for cell differentiation and increased ALP expression [103]. This was partly observed in our research. The highest pre-collagen I concentrations were achieved after 7 days of cultivation in the 0 % Sr-HAp hydrogels. The lysates from cells grown in the 0 % Sr-HAp hydrogels also had the highest ALP activity after the same cultivation period. High average ALP activity was obtained in the lysate of MG-63 cells grown for 5 days in the 40 % Sr-HAp hydrogels, and the highest Col/MMP-1 ratio was calculated, indicating a correlation between collagen production and ALP activity. A correlation between collagen production and ALP activity was not observed for the rest of the nanocomposite hydrogels.

4. Conclusions

The Sr-hydroxyapatite loaded ε-polylysine-hyaluronic acid hydrogels that can be manually injected, set *in situ*, and offer structural support and temporary scaffold for bone defect filling were successfully prepared. The physical properties, including injectability, syneresis, swelling, gel fraction, and degradation kinetics, can be optimized by changing the mass ratio of the Sr-HAp. The nanocomposite hydrogels slowly release Sr^{2+} and Ca^{2+} ions at therapeutic bone regeneration concentrations. Furthermore, they show outstanding antibacterial activity and collagen synthesis-promoting activity.

CRediT authorship contribution statement

A. Rubina: Writing – original draft, Visualization, Validation, Methodology, Investigation, Formal analysis, Data curation, Conceptualization. **A. Sceglovs:** Writing – review & editing, Writing – original draft, Visualization, Investigation, Formal analysis, Conceptualization. **A. Ramata-Stunda:** Writing – original draft, Visualization, Validation, Methodology, Investigation, Formal analysis. **I. Pugajeva:** Writing – review & editing, Visualization, Methodology, Investigation. **I. Skadins:** Writing – review & editing, Methodology, Investigation. **A.R. Boyd:** Writing – review & editing, Methodology, Investigation. **A. Tumilovica:** Visualization, Methodology, Investigation. **L. Stipniece:** Writing – review & editing, Writing – original draft, Visualization, Validation, Supervision, Methodology, Conceptualization. **K. Salma-Ancane:** Writing – review & editing, Writing – original draft, Validation, Supervision, Resources, Methodology, Funding acquisition, Conceptualization.

Declaration of competing interest

The authors declare that they have no known competing financial interests or personal relationships that could have appeared to influence the work reported in this paper.

Data availability

Data will be made available on request.

Acknowledgments

The authors acknowledge financial support from the European Union's Horizon 2020 research and innovation programme under the grant agreement No. 857287.

The authors thank Anastasija Borisova (Institute of Food Safety, Animal Health and Environment "BIOR") for her excellent help in ICP-MS analysis.

Appendix A. Supplementary data

Supplementary data to this article can be found online at https://doi.

org/10.1016/j.ijbiomac.2024.135703.

References

[1] T. Winkler, F.A. Sass, G.N. Duda, K. Schmidt-Bleek, A review of biomaterials in bone defect healing, remaining shortcomings and future opportunities for bone tissue engineering: the unsolved challenge, Bone Joint Res. 7 (2018) (2018) 232–243, https://doi.org/10.1302/2046-3758.73.BJR-2017-0270.R1.

[2] Osteoporosis: A Global Health Crisis - NBI. https://www.nbihealth.com/osteoporosis-global-health-crisis/, 2023 (Accessed 24 January, 2023).

[3] E.H. Schemitsch, Size matters: defining critical in bone defect size!, J. Orthop. Trauma 31 (2017) S20–S22, https://doi.org/10.1097/bot.0000000000000978.

[4] E. Hernlund, A. Svedbom, M. Ivergård, J. Compston, C. Cooper, J. Stenmark, E. V. McCloskey, B. Jönsson, J.A. Kanis, Osteoporosis in the European Union: medical management, epidemiology and economic burden, Arch. Osteoporos. 8 (2013), https://doi.org/10.1007/s11657-013-0136-1.

[5] M. Fontcuberta-Rigo, M. Nakamura, P. Puigbò, Phylobone: a comprehensive database of bone extracellular matrix proteins in human and model organisms, Bone Res. 11 (2023), https://doi.org/10.1038/s41413-023-00281-w.

[6] P.J. Meeder, C. Eggers, The history of autogenous bone grafting, Injury 25 (1994) A2–A3, https://doi.org/10.1016/0020-1383(94)90254-2.

[7] J. Adhikari, P. Saha, A. Sinha, Surface modification of metallic bone implants-polymer and polymer-assisted coating for bone in-growth, in: P. Balakrishnan, S. M.S. Sabu Thomas (Eds.), Fundamental Biomaterials: Metals, Woodhead Publishing, 2018, pp. 299–321, https://doi.org/10.1016/B978-0-08-102205-4.00014-3.

[8] G. Kaur, V. Kumar, F. Baino, J.C Mauro, G. Pickrell, I. Evans, O. Bretcanu, Mechanical properties of bioactive glasses, ceramics, glass-ceramics and composites: state-of-the-art review and future challenges, Mater. Sci. Eng. C Mater. Biol. Appl. 104 (2019) 109895. doi:https://doi.org/10.1016/j.msec.2019.109895.

[9] J. Zhang, W. Liu, V. Schnitzler, F. Tancret, J.M. Bouler, Calcium phosphate cements for bone substitution: chemistry, handling and mechanical properties, Acta Biomater. 10 (2014) 1035–1049, https://doi.org/10.1016/j.msec.2019.109895.

[10] G. Tozzi, A. De Mori, A. Oliveira, M. Roldo, Composite hydrogels for bone regeneration, Materials (Basel) 9 (2016), https://doi.org/10.3390/ma9040267.

[11] X. Ren, X. Chen, Z. Geng, J. Su, Bone-targeted biomaterials: strategies and applications, Chem. Eng. J. 446 (2022) 137133, https://doi.org/10.1016/j.cej.2022.137133.

[12] R. Menezes, R. Vincent, L. Osorno, P. Hu, T.L. Arinzeh, Biomaterials and tissue engineering approaches using glycosaminoglycans for tissue repair: lessons learned from the native extracellular matrix, Acta Biomater. 163 (2023) 210–227, https://doi.org/10.1016/j.actbio.2022.09.064.

[13] Y.M. Coulson-Thomas, V.J. Coulson-Thomas, A.L. Norton, T.F. Gesteira, R. P. Cavalheiro, M.C.Z. Meneghetti, J.R. Martins, R.A. Dixon, H.B. Nader, The identification of proteoglycans and glycosaminoglycans in archaeological human bones and teeth, PloS One 10 (2015) e0131105, https://doi.org/10.1371/journal.pone.0131105.

[14] J.M. Anderson, J.L. Patterson, J.B. Vines, A. Javed, S.R. Gilbert, H.W. Jun, Biphasic peptide amphiphile nanomatrix embedded with hydroxyapatite nanoparticles for stimulated osteoinductive response, ACS Nano 5 (2011) 9463–9479, https://doi.org/10.1021/nn203247m.

[15] K. Phogat, S.B. Ghosh, S. Bandyopadhyay-Ghosh, Recent advances on injectable nanocomposite hydrogels towards bone tissue rehabilitation, J. Appl. Polym. Sci. 140 (2023) e53362, https://doi.org/10.1002/app.53362.

[16] L. Huang, Y.Y. Cheng, P.L. Koo, K.M. Lee, L. Qin, J.C.Y. Cheng, S.M. Kumta, The effect of hyaluronan on osteoblast proliferation and differentiation in rat calvarial-derived cell cultures, J. Biomed. Mater. Res. 66A (2003) 880–884, https://doi.org/10.1002/jbm.a.10535.

[17] C.B. Highley, G.D. Prestwich, J.A. Burdick, Recent advances in hyaluronic acid hydrogels for biomedical applications, Curr. Opin. Biotechnol. 40 (2016) 35–40, https://doi.org/10.1016/j.matpr.2022.12.208.

[18] P. Ghandforoushan, M. Alehosseini, N. Golafshan, M. Castilho, A. Dolatshahi-Pirouz, J. Hanaee, S. Davaran, G. Orive, Injectable hydrogels for cartilage and bone tissue regeneration: a review, Int. J. Biol. Macromol. 246 (2023) 125674, https://doi.org/10.1016/j.ijbiomac.2023.125674.

[19] M. Liu, X. Zeng, C. Ma, Y. Huan, Z. Ali, X. Mou, S. Li, Y. Deng, N. He, Injectable hydrogels for cartilage and bone tissue engineering, Bone Res. 5 (2017) 17014, https://doi.org/10.1038/boneres.2017.14.

[20] G. Kogan, L. Šoltés, R. Stern, P. Gemeiner, Hyaluronic acid: a natural biopolymer with a broad range of biomedical and industrial applications, Biotechnol. Lett. 29 (2007) 17–25, https://doi.org/10.1007/s10529-006-9219-z.

[21] S. Li, M. Pei, T. Wan, H. Yang, S. Gu, Y. Tao, X. Liu, Y. Zhou, W. Xu, P. Xiao, Self-healing hyaluronic acid hydrogels based on dynamic Schiff base linkages as biomaterials, Carbohydr. Polym. 250 (2020) 116922, https://doi.org/10.1016/j.carbpol.2020.116922.

[22] X. Yu, X. Tang, S.V. Gohil, C.T. Laurencin, Biomaterials for bone regenerative engineering, Adv. Healthc. Mater. 4 (2015) 1268–1285, https://doi.org/10.1002/adhm.201400760.

[23] H. Zhang, S. Wu, W. Chen, Y. Hu, Z. Geng, J. Su, Bone/cartilage targeted hydrogel: strategies and applications, Bioact. Mater. 23 (2022) 156–169, https://doi.org/10.1016/j.bioactmat.2022.10.028.

[24] L. Wang, C. Zhang, J. Zhang, Z. Rao, X. Xu, Z. Mao, X. Chen, Epsilon-poly-L-lysine: recent advances in biomanufacturing and applications, Front. Bioeng. Biotechnol. 9 (2021) 748976, https://doi.org/10.3389/fbioe.2021.748976.

[25] K. Salma-Ancane, A. Sceglovs, E. Tracuma, J.K. Wychowaniec, K. Aunina, A. Ramata-Stunda, V. Nikolajeva, D. Loca, Effect of crosslinking strategy on the biological, antibacterial and physicochemical performance of hyaluronic acid and ε-polylysine based hydrogels, Int. J. Biol. Macromol. 208 (2022) 995–1008, https://doi.org/10.1016/j.ijbiomac.2022.03.207.

[26] A. Sceglovs, J.K. Wychowaniec, I. Skadins, A. Reinis, C.J.C. Edwards-Gayle, M. D'Este, K. Salma-Ancane, Effect of steam sterilisation on physico-chemical properties of antibacterial covalently cross-linked ε-polylysine/hyaluronic acid hydrogels, Carbohydr. Polym. 6 (2023) 100363, https://doi.org/10.1016/j.carpta.2023.100363.

[27] X. Bai, M. Gao, S. Syed, J. Zhuang, X. Xu, X.Q. Zhang, Bioactive hydrogels for bone regeneration, Bioact. Mater. 3 (2018) 401–417, https://doi.org/10.1016/j.bioactmat.2018.05.006.

[28] Y.Y. Chun, J.K. Wang, N.S. Tan, P.P. Chan, T.T. Tan, C. Choong, A periosteum-inspired 3D hydrogel-bioceramic composite for enhanced bone regeneration, Macromol. Biosci. 16 (2016) 276–287, https://doi.org/10.1002/mabi.201500258.

[29] J. Jeong, J.H. Kim, J.H. Shim, N.S. Hwang, C.Y. Heo, Bioactive calcium phosphate materials and applications in bone regeneration, Biomat. Res. 23 (2019) 1839–1851, https://doi.org/10.1186/s40824-018-0149-3.

[30] K. Wang, W. Cheng, Z. Ding, G. Xu, X. Zheng, M. Li, G. Lu, Q. Lu, Injectable silk/hydroxyapatite nanocomposite hydrogels with vascularization capacity for bone regeneration, J. Mater. Sci. Technol. 63 (2021) 172–181, https://doi.org/10.1016/j.jmst.2020.02.030.

[31] Z. Zou, L. Wang, Z. Zhou, Q. Sun, D. Liu, Y. Chen, H. Hu, Y. Cai, S. Lin, Z. Yu, B. Tan, W. Guo, Z. Ling, X. Zou, Simultaneous incorporation of PTH(1-34) and nano-hydroxyapatite into chitosan/alginate hydrogels for efficient bone regeneration, Bioact. Mater. 6 (2021) 1839–1851, https://doi.org/10.1016/j.bioactmat.2020.11.021.

[32] Y. Pan, Y. Zhao, R. Kuang, H. Liu, D. Sun, T. Mao, K. Jiang, X. Yang, N. Watanabe, K.H. Mayo, Q. Lin, J. Li, Injectable hydrogel-loaded nano-hydroxyapatite that improves bone regeneration and alveolar ridge promotion, Mater. Sci. Eng. C 116 (2020) 111158, https://doi.org/10.1016/j.msec.2020.111158.

[33] O. Faruq, B. Kim, A.R. Padalhin, G.H. Lee, B.T. Lee, A hybrid composite system of biphasic calcium phosphate granules loaded with hyaluronic acid-gelatin hydrogel for bone regeneration, J. Biomater. Appl. 32 (2017) 433–445, https://doi.org/10.1177/0885328217773068.

[34] J.A. Burdick, K.S. Anseth, Photoencapsulation of osteoblasts in injectable RGD-modified PEG hydrogels for bone tissue engineering, Biomaterials 23 (2002) 4315–4323, https://doi.org/10.1016/S0142-9612(02)00176-X.

[35] M. Fosca, A. Streza, I.V. Antoniac, G. Vadalà, J.V. Rau, Ion-doped calcium phosphate-based coatings with antibacterial properties, J. Funct. Biomater. 14 (2023) 250, https://doi.org/10.3390/jfb14050250.

[36] R. Zhao, S. Chen, W. Zhao, L. Yang, B. Yuan, V.S. Ioan, A.V. Iulian, X. Yang, X. Zhu, X.A. Zhang, A bioceramic scaffold composed of strontium-doped three-dimensional hydroxyapatite whiskers for enhanced bone regeneration in osteoporotic defects, Theranostics 10 (2020) 1572–1589, https://doi.org/10.7150/thno.40103.

[37] X. Ding, X. Li, C. L, M. Qi, Z. Zhang, X. Sun, L. Wang, Y. Zhou, Chitosan/dextran hydrogel constructs containing strontium-doped hydroxyapatite with enhanced osteogenic potential in rat cranium, ACS Biomater Sci. Eng. 5 (2019) 4574–4586, https://doi.org/10.1021/acsbiomaterials.9b00584.

[38] J. Wang, X. Wang, Z. Liang, W. Lan, Y. Wei, Y. Hu, L. Wang, Q. Lei, D. Huang, Injectable antibacterial Ag-HA/GelMA hydrogel for bone tissue engineering, Front. Bioeng. Biotechnol. 11 (2023) 1219460, https://doi.org/10.3389/fbioe.2023.1219460.

[39] Y. Shin, K.-H. Cheon, E.-H. Song, Y.-J. Seong, J.-U. Park, H.-E. Kim, S.-H. Jeong, Fluorine-ion-releasing injectable alginate nanocomposite hydrogel for enhanced bioactivity and antibacterial property, Int. J. Biol. Macromol. 123 (2019) 866–877, https://doi.org/10.1016/j.ijbiomac.2018.11.108.

[40] T.E.L. Douglas, M. Dziadek, S. Gorodzha, J. Liskova, G. Brackman, V. Vanhoorne, C. Vervaet, L. Balcaen, M. del Rosario Florez, A.R. Garcia, V. Boccaccini, T. Weinhardt, F. Baumbach, T. Vanhaecke, L. Coenye, M.A. Bacakova, R. A. Surmeneva, K. Surmenev, A.G. Skirtach Cholewa-Kowalska, Novel injectable gellan gum hydrogel composites incorporating Zn- and Sr-enriched bioactive glass microparticles: high-resolution X-ray microcomputed tomography, antibacterial and *in vitro* testing, J. Tissue Eng. Regen. Med. 12 (2018) 1313–1326, https://doi.org/10.1002/term.2654.

[41] L. Stipniece, A. Ramata-Stunda, J. Vecstaudza, I. Kreicberga, D. Livkisa, A. Rubina, A. Sceglovs, K. Salma-Ancane, A comparative study on physicochemical properties and *in vitro* biocompatibility of Sr-substituted and Sr ranelate-loaded hydroxyapatite nanoparticles, ACS Appl. Bio Mater. 6 (2023) 5264–5281, https://doi.org/10.1021/acsabm.3c00539.

[42] T.E. Robinson, E.A.B. Hughes, N.M. Eisenstein, L.M. Grover, S.C. Cox, The quantification of injectability by mechanical testing, J. Vis. Exp. 159 (2020) e61417, https://doi.org/10.3791/61417.

[43] T.T. Chen, Quantifying polymer crosslinking density using rheology and DMA. https://www.tainstruments.com/applications-notes/quantifying-polymer-crosslinking-density-using-rheology-and-dma/ (Accessed 16th August, 2024).

[44] J.M. Alonso, J. Andrade Del Olmo, R. Perez Gonzalez, V. Saez-Martinez, Injectable hydrogels: from laboratory to industrialization, Polymers (Basel) 13 (2021) 650, https://doi.org/10.3390/polym13040650.

[45] T. Levingstone, B. Ali, C. Kearney, N. Dunne, Hydroxyapatite sonosensitization of ultrasound-triggered, thermally responsive hydrogels: an on-demand delivery system for bone repair applications, J. Biomed. Mater. Res. 109 (2021) 1622–1633, https://doi.org/10.1002/jbm.b.34820.
[46] P. Bertsch, M. Diba, D.J. Mooney, S.C.G. Leeuwenburgh, Self-healing injectable hydrogels for tissue regeneration, Chem. Rev. 123 (2023) 834–873, https://doi.org/10.1021/acs.chemrev.2c00179.
[47] E.F. Burguera, H.H. Xu, L. Sun, Injectable calcium phosphate cement: effects of powder-to-liquid ratio and needle size, J. Biomed. Mater. Res. B Appl. Biomater. 84 (2008) 493–502, https://doi.org/10.1002/jbm.b.30896.
[48] S. Jacquart, S. Girod-Fullana, F. Brouillet, C. Pigasse, R. Siadous, M. Fatnassi, J. Grimoud, C. Rey, C. Roques, C. Combes, Injectable bone cement containing carboxymethyl cellulose microparticles as a silver delivery system able to reduce implant-associated infection risk, Acta Biomater. 145 (2022) 342–357, https://doi.org/10.1016/j.actbio.2022.04.015.
[49] M. Haghighi, K. Rezaei, General analytical schemes for the characterization of pectin-based edible gelled systems, ScientificWorldJournal 2012 (2012) 967407, https://doi.org/10.1100/2012/967407.
[50] A. Prince, Development of In Situ Forming Hydrogels for Intra-Articular Drug Delivery, Doctoral dissertation,, The University of Western Ontario, Canada, 2019, https://ir.lib.uwo.ca/etd/6077.
[51] K. Bouiahya, A. Oulguidoum, A. Laghzizil, M. Shalabi, J.M.M. Nunzi, S. Masse, Hydrophobic chemical surface functionalization of hydroxyapatite nanoparticles for naphthalene removal, Colloids Surf. A Physicochem. Eng. Asp. 595 (2020) 124706, https://doi.org/10.1016/j.colsurfa.2020.124706.
[52] X. Ran, X. Yu, J. He, Z. Xiao, Molecular mechanism of nano-hydroxyapatite surface changes from hydrophilic to hydrophobic, Asian J. Chem. 26 (2014) 5355–5359, https://doi.org/10.14233/ajchem.2014.18110.
[53] G. Kaya, F. Oytun, Rheological properties of injectable hyaluronic acid hydrogels for soft tissue engineering applications, Biointerface Res. Appl. Chem. 11 (2020) 8424–8430, https://doi.org/10.33263/BRIAC111.84248430.
[54] Y. Zhao, Z. Cui, B. Liu, J. Xiang, D. Qiu, Y. Tian, X. Qu, Z. Yang, An injectable strong hydrogel for bone reconstruction, Adv. Healthc. Mater. 8 (2019) 1900709, https://doi.org/10.1002/adhm.201900709.
[55] H. Zhou, C. Liang, Z. Wei, Y. Bai, S.B. Bhaduri, T.J. Webster, L. Bian, L. Yang, Injectable biomaterials for translational medicine, Mater. Today 28 (2019) 81–97, https://doi.org/10.1016/j.mattod.2019.04.020.
[56] G. Stojkov, Z. Niyazov, F. Picchioni, R.K. Bose, Relationship between structure and rheology of hydrogels for various applications, Gels 7 (2021) 255, https://doi.org/10.3390/gels7040255.
[57] B.M. Hong, G.L. Hong, M.A. Gwak, K.H. Kim, J.E. Jeong, J.Y. Jung, S.A. Park, W. H. Park, Self-crosslinkable hyaluronate-based hydrogels as a soft tissue filler, Int. J. Biol. Macromol. 185 (2021) 98–110, https://doi.org/10.1016/j.ijbiomac.2021.06.047.
[58] E. López-Ruiz, G. Jiménez, L. Álvarez de Cienfuegos, C. Antic, R. Sabata, J. A. Marchal, P. Gálvez-Martín, Advances of hyaluronic acid in stem cell therapy and tissue engineering, including current clinical trials, Eur. Cell. Mater. 37 (2019) 186–213, https://doi.org/10.22203/ecm.v037a12.
[59] K. Flegeau, O. Gauthier, G. Rethore, F. Autrusseau, A. Schaefer, J. Lesoeur, J. Veziers, A. Bresin, H. Gaitier, P. Weiss, Injectable silanized hyaluronic acid hydrogel/biphasic calcium phosphate granule composites with improved handling and biodegradability promote bone regeneration in rabbits, Biomater. Sci. 9 (2021) 5640–5651, https://doi.org/10.1039/D1BM00403D.
[60] H. Bakhtiari, A. Nouri, M. Khakbiz, M. Tolouei-Rad, Fatigue behaviour of load-bearing polymeric bone scaffolds: a review, Acta Biomater. 172 (2023) 16–37, https://doi.org/10.1016/j.actbio.2023.09.048.
[61] M.H. Chen, L.L. Wang, J.J. Chung, Y.H. Kim, P. Atluri, J.A. Burdick, Methods to assess shear-thinning hydrogels for application as injectable biomaterials, ACS Biomater Sci. Eng. 3 (2017) 3146–3160, https://doi.org/10.1021/acsbiomaterials.7b00734.
[62] S. Bashir, M. Hina, J. Iqbal, A.H. Rajpar, M.A. Mujtaba, N.A. Alghamdi, S. Wageh, K. Ramesh, S. Ramesh, Fundamental concepts of hydrogels: synthesis, properties, and their applications, Polymers (Basel) 12 (2020) 2702, https://doi.org/10.3390/polym12112702.
[63] K. Farbod, M.R. Nejadnik, J.A. Jansen, S.C.G. Leeuwenburgh, Interactions between inorganic and organic phases in bone tissue as a source of inspiration for design of novel nanocomposites, Tissue Eng. Part B Rev. 20 (2014) 173–188, https://doi.org/10.1089/ten.teb.2013.0221.
[64] M. Baniasadi, M. Minary-Jolandan, Alginate-collagen fibril composite hydrogel, Materials 8 (2) (2015) 799–814, https://doi.org/10.3390/ma8020799.
[65] L. Liu, P.H. Cooke, D.R. Coffin, M.L. Fishman, K.B. Hicks, Pectin and polyacrylamide composite hydrogels: effect of pectin on structural and dynamic mechanical properties, J. Appl. Polym. Sci. 92 (2004) 1893–1901, https://doi.org/10.1002/app.20174.
[66] R. Kocen, M. Gasik, A. Gantar, S. Novak, Viscoelastic behaviour of hydrogel-based composites for tissue engineering under mechanical load, Biomed. Mater. 12 (2) (2017) 025004, https://doi.org/10.1088/1748-605X/aa5b00.
[67] B.Y.S. Kumar, A.M. Isloor, G.C.M. Kumar, A.A.M. Inamuddin, Nanohydroxyapatite reinforced chitosan composite hydrogel with tunable mechanical and biological properties for cartilage regeneration, Sci. Rep. 9 (2019) 15957, https://doi.org/10.1038/s41598-019-52042-7.
[68] J.A. Sanchez-Fernandez, G. Presbitero-Espinosa, L. Pena-Paras, E.I.R. Pizana, K.P. V. Galvan, M. Vopalensky, I. Kumpova, L.E. Elizalde-Herrera, Characterization of sodium alginate hydrogels reinforced with nanoparticles of hydroxyapatite for biomedical applications, Polymers 13 (2021) 2927, https://doi.org/10.3390/polym13172927.
[69] A. Svarca, A. Grava, A. Dubnika, A. Ramata-Stunda, R. Narnickis, K. Aunina, E. Rieksta, M. Boroduskis, I. Jurgelane, L. Locs, D. Loca, Calcium phosphate/hyaluronic acid composite hydrogels for local antiosteoporotic drug delivery, Front. Bioeng. Biotechnol. 10 (2022) 917765, https://doi.org/10.3389/fbioe.2022.917765.
[70] W.A. Laftah, S. Hashim, A.N. Ibrahim, Polymer hydrogels: a review, Polym. - Plast. Technol. Eng. 50 (2011) 1475–1486, https://doi.org/10.1080/03602559.2011.593082.
[71] W. Feng, Z. Wang, Tailoring the swelling-shrinkable behavior of hydrogels for biomedical applications, Adv. Sci. 10 (2023) 2303326, https://doi.org/10.1002/advs.202303326.
[72] R. Foudazi, R. Zowada, I. Manas-Zloczower, D.L. Feke, Porous hydrogels: present challenges and future opportunities, Langmuir 39 (2023) 2092–2111, https://doi.org/10.1021/acs.langmuir.2c02253.
[73] L. Wang, S. Dong, Y. Liu, Y. Ma, J. Zhang, Z. Yang, W. Jiang, Y. Yuan, Fabrication of injectable, porous hyaluronic acid hydrogel based on an in-situ bubble-forming hydrogel entrapment process, Polymers (Basel) 12 (2020) 1138, https://doi.org/10.3390/polym12051138.
[74] J. Karvinen, M. Kellomaki, Characterization of self-healing hydrogels for biomedical applications, Eur. Polym. J. 181 (2022) 111641, https://doi.org/10.1016/j.eurpolymj.2022.111641.
[75] Z. Kaberova, E. Karpushkin, M. Nevoralová, M. Vetrík, M. Šlouf, M. Dušková-Smrčková, Microscopic structure of swollen hydrogels by scanning electron and light microscopies: artifacts and reality, Polymers 12 (2020) 578, https://doi.org/10.3390/polym12030578.
[76] A. Borzacchiello, L. Russo, B.M. Malle, K. Schwach-Abdellaoui, L. Ambrosio, Hyaluronic acid based hydrogels for regenerative medicine applications, Biomed. Res. Int. 2015 (2015) 242378, https://doi.org/10.1155/2015/871218.
[77] H. He, E. Luedke, X. Zhang, B. Yu, A. Schmitt, B. McClarren, V. Grignol, W. E. Carson, L.J. Lee, A naonoporous cell-therapy device with controllable biodegradation for long-term drug release, J. Control. Release 165 (3) (2013) 226–233, https://doi.org/10.1016/j.jconrel.2012.11.020.
[78] G.G. de Lima, L. Campos, A. Junqueira, D.M. Devine, M.J.D. Nugent, A novel pH-sensitive ceramic-hydrogel for biomedical applications, Polym. Adv. Technol. 26 (2015) 1439–1446, https://doi.org/10.1002/pat.3593.
[79] Y. Zhu, H. Jiang, S.H. Ye, T. Yoshizumi, W.R. Wagner, Tailoring the degradation rates of thermally responsive hydrogels designed for soft tissue injection by varying the autocatalytic potential, Biomaterials 53 (2015) 484–493, https://doi.org/10.1016/j.biomaterials.2015.02.100.
[80] S. Utech, A.R. Boccaccini, A review of hydrogel-based composites for biomedical applications: enhancement of hydrogel properties by addition of rigid inorganic fillers, J. Mater. Sci. 51 (2016) 271–310, https://doi.org/10.1007/s10853-015-9382-5.
[81] S. Wei, J.X. Ma, L. Xu, Biodegradable materials for bone defect repair, Military Med. Res. 7 (2020) 54, https://doi.org/10.1186/s40779-020-00280-6.
[82] X. Sheng, C. Li, Z. Wang, Y. Xu, Y. Sun, W. Zhang, H. Liu, J. Wang, Advanced applications of strontium-containing biomaterials in bone tissue engineering, Mater. Today Bio. 20 (2023), https://doi.org/10.1016/j.mtbio.2023.100636.
[83] L.C. Chow, L. Sun, B. Hockey, Properties of nanostructured hydroxyapatite prepared by a spray drying technique, J. Res. Natl. Inst. Stand. Technol. 109 (2004) 543–551, doi:10.6028%2Fjres.109.041.
[84] H. Xie, Z. Gu, Y. He, J. Xu, C. Xu, L. Li, Q. Ye, Microenvironment construction of strontium–calcium-based biomaterials for bone tissue regeneration: the equilibrium effect of calcium to strontium, J. Mater. Chem. B 6 (2018) 2332–2339, https://doi.org/10.1039/C8TB00306H.
[85] T.J. Silhavy, D. Kahne, S. Walker, The bacterial cell envelope, Cold Spring Harb. Perspect. Biol. 2 (5) (2010) a000414, https://doi.org/10.1101/cshperspect.a000414.
[86] V. Murugesan, M. Vaiyapuri, A. Murugeasan, Fabrication and characterization of strontium substituted chitosan modify hydroxyapatite for biomedical applications, Inorg. Chem. Comm. 142 (2022) 109653, https://doi.org/10.1016/j.inoche.2022.109653.
[87] E. Filova, T. Suchy, Z. Sucharda, M. Supova, M. Zaloudkova, K. Balik, V. Lisa, M. Slouf, L. Bacakova, Support for the initial attachment, growth and differentiation of MG-63 cells: a comparison between nano-size hydroxyapatite and micro-size hydroxyapatite in composites, Int. J. Nanomedicine 9 (2014) 3687–3706, https://doi.org/10.2147/IJN.S56661.
[88] S.-W. Tsai, Y.-W. Hsu, W.-L. Pan, F.-Y. Hsu, The effect of strontium-substituted hydroxyapatite nanofibrous matrix on osteoblast proliferation and differentiation, Membranes 11 (2021) 624, https://doi.org/10.3390/membranes11080624.
[89] Y. Hao, H. Yan, X. Wang, B. Zhu, C. Ning, S. Ge, Evaluation of osteoinduction and proliferation on nano-Sr-HAP: a novel orthopedic biomaterial for bone tissue regeneration, J. Nanosci. Nanotechnol. 12 (2012) 207–212, https://doi.org/10.1166/jnn.2012.5125.
[90] S. Maeno, Y. Niki, H. Matsumoto, H. Morioka, T. Yatabe, A. Funayama, Y. Toyama, T. Taguchi, J. Tanaka, The effect of calcium ion concentration on osteoblast viability, proliferation and differentiation in monolayer and 3D culture, Biomaterials 26 (2005) 4847–4855, https://doi.org/10.1016/j.biomaterials.2005.01.006.
[91] L. Gritsch, M. Maqbool, V. Mourino, F.E. Ciraldo, M. Cresswell, P.R. Jackson, C. Lovell, A.R. Boccaccini, Chitosan/hydroxyapatite composite bone tissue engineering scaffolds with dual and decoupled therapeutic ion delivery: copper and strontium, J. Mater. Chem. B 7 (2019) 6109–6124, https://doi.org/10.1039/C9TB00897G.

[92] J. Liu, S.C.F. Rawlinson, R.G. Hill, F. Fortune, Strontium-substituted bioactive glasses in vitro osteogenic and antibacterial effects, Dent. Mater. 32 (2016) 412–422, https://doi.org/10.1016/j.dental.2015.12.013.
[93] Y. Cheng, L. Huang, Y. Wang, Q. Huo, Y. Shao, H. Bao, Z. Li, Y. Liu, X. Li, Strontium promotes osteogenic differentiation by activating autophagy via the AMPK/mTOR signaling pathway in MC3T3-E1 cells, Int. J. Mol. Med. 44 (2019) 652–660, https://doi.org/10.3892/ijmm.2019.4216.
[94] F. Boukhechba, T. Balaguer, J.-F. Michiels, K. Ackermann, D. Quincey, J.-M. Bouler, W. Pyerin, G.F. Carle, N. Rochet, Human primary osteocyte differentiation in a 3D culture system, J. Bone Miner. Res. 24 (2009) 1927–1935, https://doi.org/10.1359/jbmr.090517.
[95] G. Nasello, P. Alaman-Diez, J. Schiavi, M.A. Perez, L. McNamara, J.M. Garcia-Aznar, Primary human osteoblasts cultured in a 3D microenvironment create a unique representative model of their differentiation into osteocytes, Front. Bioeng. Biotechnol. 8 (2020) 336, https://doi.org/10.3389/fbioe.2020.00336.
[96] M. Izumiya, M. Haniu, K. Ueda, H. Ishida, C. Ma, H. Ideta, A. Sobajima, K. Ueshiba, T. Uemura, N. Saito, H. Haniu, Evaluation of MC3T3-E1 cell osteogenesis in different cell culture media, Int. J. Mol. Sci. 22 (2021) 7752, https://doi.org/10.3390/ijms22147752.
[97] Y. Zhuang, A. Liu, S. Jiang, U. Liaqat, K. Lin, W. Sun, C. Yuan, Promoting vascularized bone regeneration via strontium-incorporated hydroxyapatite bioceramic, Mater. Des. 234 (2023) 112313, https://doi.org/10.1016/j.matdes.2023.112313.
[98] D. Marx, A.R. Yazdi, M. Papini, M. Towler, A review of the latest insights into the mechanism of action of strontium in bone, Bone Rep. 12 (2020) 100273, https://doi.org/10.1016/j.bonr.2020.100273.
[99] H.W. Kim, Y.J. Kim, Fabrication of strontium-substituted hydroxyapatite scaffolds using 3D printing for enhanced bone regeneration, J. Mater. Sci. 56 (2021) 1673–1684, https://doi.org/10.1007/s10853-020-05391-y.
[100] X. Lin, S. Patil, Y.-G. Gao, A. Qian, The bone extracellular matrix in bone formation and regeneration, Front. Pharmacol. 11 (2020) 757, https://doi.org/10.3389/fphar.2020.00757.
[101] R. Fattahi, F. Mohebichamkhorami, N. Taghipour, S.H. Keshel, The effect of extracellular matrix remodeling on material-based strategies for bone regeneration: review article, Tissue Cell 76 (2022) 101748, https://doi.org/10.1016/j.tice.2022.101748.
[102] L. Liang, D.-P. Zhu, S.-S. Guo, D. Zhang, T. Zhang, MMP-1 gene polymorphism in osteoporosis, Eur. Rev. Med. Pharmacol. Sci. 23 (2019) 67–72, https://doi.org/10.26355/eurrev_201908_18631.
[103] R.J. Wenstrup, J.L. Fowlkes, D.P. Witte, J.B. Florer, Discordant expression of osteoblast markers in MC3T3-E1 cells that synthesize a high turnover matrix, J. Biol. Chem. 271 (1996) 10271–10276, https://doi.org/10.1074/jbc.271.17.10271.

Artemijs Ščeglovs dzimis 1996. gadā Rīgā. Rīgas Tehniskajā universitātē (RTU) ieguvis bakalaura grādu ķīmijā (2019), Rīgas Stradiņa universitātē – maģistra grādu biomedicīnā (2021). Patlaban ir RTU pētnieks. Iesaistījies nacionālo un starptautisko projektu īstenošanā, kuru ietvaros piedalās starptautiskās konferencēs Eiropā, pilnveidojot profesionālo pieredzi apmācībās un mobilitātes braucienos. Zinātniskās intereses saistītas ar biomateriālu izstrādi, fokusējoties uz antibakteriālo aktivitāti pret dažādām slimību izraisošām, tostarp antibiotiku rezistentām, baktērijām.

Artemijs Ščeglovs was born in 1996 in Riga, Latvia. In 2019, he obtained a Bachelor's degree in Chemistry from Riga Technical University (RTU), and a Master's degree in Biomedicine – from Riga Stradiņš University in 2021. At present, Artemijs is as a Researcher at RTU. He is involved in the implementation of national and international projects, participating in international conferences across Europe and enhancing his professional experience through training and mobility visits. Research interests are related to the development of biomaterials with a focus on antibacterial activity against various disease-causing, including antibiotic-resistant, bacteria.